Technical Report Documentation Page

1. Report No. FHWA/TX-11/0-5701-1	2. Government Accession No.	3. Recipient's Catalog No.
4. Title and Subtitle Cross-Frame Connection Details for Skewed Steel Bridges		5. Report Date October 31, 2010 6. Performing Organization Code
7. Author(s) Craig Quadrato, Weihua Wang, Anthony Battistini, Andrew Wahr, Todd Helwig, Karl Frank, and Michael Engelhardt		8. Performing Organization Report No. 0-5701-1
9. Performing Organization Name and Address Center for Transportation Research The University of Texas at Austin 1616 Guadalupe, Suite 4.202 Austin, TX 78701		10. Work Unit No. (TRAIS) 11. Contract or Grant No. 0-5701
12. Sponsoring Agency Name and Address Texas Department of Transportation Research and Technology Implementation Office P.O. Box 5080 Austin, TX 78763-5080		13. Type of Report and Period Covered Technical Report August 2008 through August 2010 14. Sponsoring Agency Code
15. Supplementary Notes Project performed in cooperation with the Texas Department of Transportation and the Federal Highway Administration.		

16. Abstract

This report documents a research investigation on connection details and bracing layouts for stability bracing of steel bridges with skewed supports. Cross-frames and diaphragms play an important role in stabilizing steel girders, particularly during construction. The commonly used bent plate connection between skewed braces and steel girders can introduce flexibility that can have detrimental effects on the bracing behavior. An alternative detail investigated in this study is a split pipe stiffener used to connect cross-frames to girders at a skew. The split pipe stiffener allows perpendicular connections to the cross-frame connection tab, regardless of the skew angle. The split pipe provides a stiffer connection between the cross-frame and the girder. More importantly, the split pipe stiffener increases the torsional stiffness of the girder by introducing substantial warping restraint. This increases the lateral torsional buckling capacity of the girder and allows the first line of intermediate cross-frames to be moved farther from the support. Overall, the increase in girder torsional stiffness and buckling capacity that results from the use of the split pipe stiffener will enhance the safety of the girder at all stages of construction: during transportation, lifting, erection, and placement of the concrete deck. This study also examined layout patterns for intermediate cross-frames in skewed bridges. Results showed that staggering the intermediate cross-frames reduces live load induced forces in the cross-frame members and mitigates the potential for associated fatigue cracking. This report also provides design recommendations for the split pipe stiffener and provides a procedure for computing the buckling capacity of girders with split pipe stiffeners.

17. Key Words	18. Distribution Statement
Skewed steel bridges, bracing, lateral torsional buckling, connection details, bracing layout	No restrictions. This document is available to the public through the National Technical Information Service, Springfield, Virginia 22161; www.ntis.gov.

19. Security Classif. (of report)	20. Security Classif. (of this page)	21. No. of pages	22. Price
Unclassified	Unclassified	412	

Form DOT F 1700.7 (8-72) Reproduction of completed page authorized

Cross-Frame Connection Details for Skewed Steel Bridges

Craig Quadrato
Weihua Wang
Anthony Battistini
Andrew Wahr
Todd Helwig
Karl Frank
Michael Engelhardt

CTR Technical Report:	0-5701-1
Report Date:	October 31, 2010
Project:	0-5701
Project Title:	Cross-Frame and Diaphragm Layout and Connection Details
Sponsoring Agency:	Texas Department of Transportation
Performing Agency:	Center for Transportation Research at The University of Texas at Austin

Project performed in cooperation with the Texas Department of Transportation and the Federal Highway Administration.

Center for Transportation Research
The University of Texas at Austin
1616 Guadalupe
Austin, TX 78701

www.utexas.edu/research/ctr

Disclaimers

Author's Disclaimer: The contents of this report reflect the views of the authors, who are responsible for the facts and the accuracy of the data presented herein. The contents do not necessarily reflect the official view or policies of the Federal Highway Administration or the Texas Department of Transportation (TxDOT). This report does not constitute a standard, specification, or regulation.

Patent Disclaimer: There was no invention or discovery conceived or first actually reduced to practice in the course of or under this contract, including any art, method, process, machine manufacture, design or composition of matter, or any new useful improvement thereof, or any variety of plant, which is or may be patentable under the patent laws of the United States of America or any foreign country.

Notice: The United States Government and the State of Texas do not endorse products or manufacturers. If trade or manufacturers' names appear herein, it is solely because they are considered essential to the object of this report.

Engineering Disclaimer

NOT INTENDED FOR CONSTRUCTION, BIDDING, OR PERMIT PURPOSES.

Project Engineer: Michael D. Engelhardt
Professional Engineer License State and Number: Texas P.E. #88934
P. E. Designation: Research Supervisor

Acknowledgments

The authors gratefully acknowledge the financial support provided for this project by the Texas Department of Transportation. The authors extend a special thanks to Yongqian Lin, Kenneth Ozuna, Michael Hyzak, and Duncan Stewart of the Texas Department of Transportation for their support, assistance, and advice throughout the course of this project.

Table of Contents

List of Figures

List of Tables

Chapter 1. Introduction

1.1 Problem Description

Cross-frames serve an important role in steel bridges by causing adjacent girder lines to resist applied loads as a unit, thereby enhancing torsional stiffness of the system and providing overall stability. The critical stage for cross-frames is generally during construction before the concrete deck has cured, because at this stage the steel girders must support all of the applied loads. After the concrete deck has cured, cross-frames help resist lateral loads during the service life of the bridge. The cross-frame spacing is typically controlled by the construction loading case prior to the concrete deck curing. While the American Association of State Highways and Transportation Officials (AASHTO) design guidelines (American Association of State Highway and Transportation Officials 2010) allow a rational analysis to determine cross-frame spacing, many states and jurisdictions use rules based on previous experience to set intermediate cross-frame spacing.

Although the primary purpose of the majority of the cross-frames is served for just a few short weeks while the bridge is under construction, their fabrication and erection represent substantial cost in materials and labor. Additionally, each cross-frame attached to the girder must be periodically inspected for fatigue cracking, which causes additional cost and risk during the bridge service life.

Cross-frames in skewed bridges present additional challenges. A skewed bridge is one with supporting elements across the width of the bridge that intersect the bridge cross section at an angle other than 90° (see Figure 1.1 and Figure 1.2). The necessity of the skewed supports is typically related to geometric issues with intersecting roadways or the surrounding terrain. The skewing of a bridge requires that the abutments not be perpendicular to the girder's longitudinal axis. This causes an offset to the support in each adjacent girder. This offset is shown in Figure 1.3 for a bridge with a nearly 60° skew angle. The left exterior girder has a 70' offset to the support while the right exterior girder has no offset at the highlighted intermediate cross-frame line.

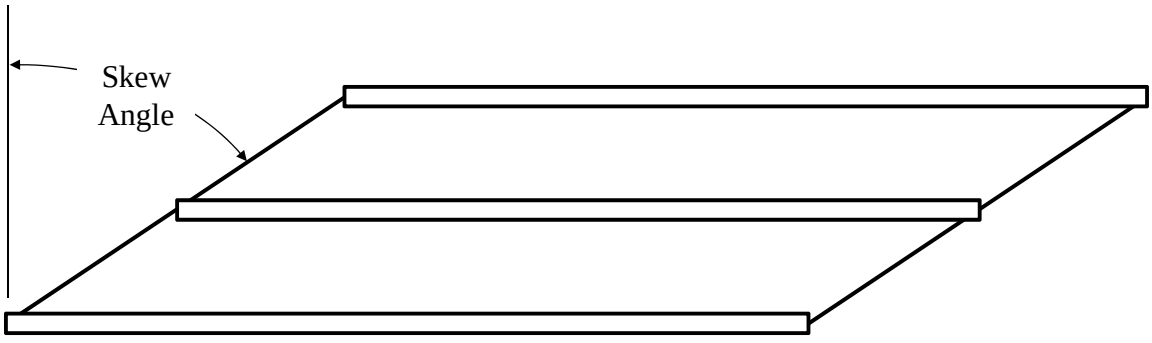

Figure 1.1: Skewed bridge plan view showing positive skew angle

Figure 1.2: Skewed straight steel girder bridge

As trucks pass over the bridge, the support offset causes differential deflections between the adjacent girders and makes the bridge twist along the contiguous line of intermediate cross-frames inducing live load forces in the cross-frame members. In turn, these cyclic live load forces cause additional fatigue risk not experienced in unskewed bridges.

Figure 1.3: Skewed bridge support offset

Additionally, because the girders are generally connected through a series of end cross-frames, the skewed end brace has components directed along both the longitudinal and transverse direction on the girder end. As the girders experience a strong axis rotation at the skewed support, forces are induced in the cross-frame that produce girder end twist (Figure 1.4). Accounting for this end twist complicates both the fabrication and erection of cross-frames. Also, excessive girder end twist is likely to reduce the buckling capacity of the girder.

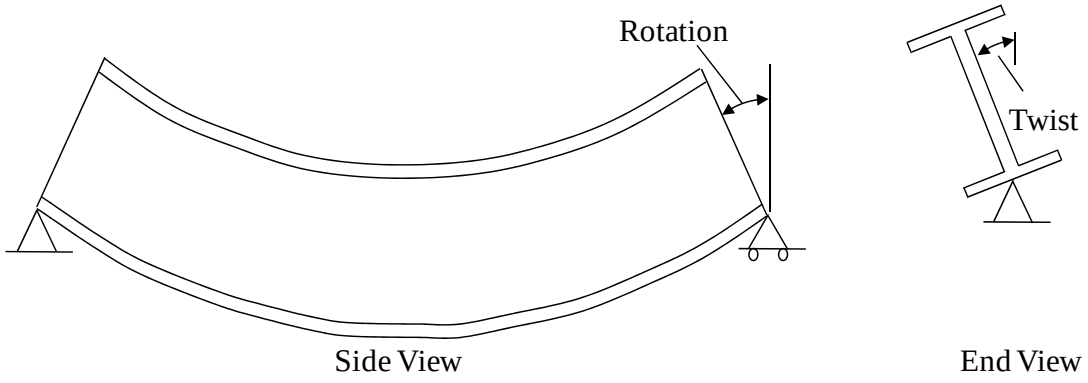

Figure 1.4: Girder rotation and end twist

1.2 Previous and Proposed Solutions

Several methods may be taken to mitigate the live load induced cross-frame fatigue issues. First, the intermediate cross-frame line may be skewed to match the bridge skew angle. However, AASHTO only allows this for skew angles less than or equal to 20° because the cross-frame stiffness perpendicular to the girder drops significantly as the skew increases. The lower stiffness reduces the effectiveness of the cross-frame and may result in dangerous conditions on the bridge. This was the case in the Churchman Road Bridge in Delaware where skewed intermediate cross-frames at an angle of approximately 60° (significantly larger than the 20° limit in AASHTO) were used as shown in Figure 1.5. The subsequent reduction in stiffness caused excessive girder twist under steel dead load alone. This twist required significant retrofit before the concrete slab could be placed (Winterling 2007).

Figure 1.5: Churchman Road Bridge Delaware skewed intermediate cross-frames

Another method to mitigate the intermediate live load forces is to use a lean-on bracing system as pictured in Figure 1.3. In the lean-on bracing system, the diagonal members of some cross-frames are removed so the cross-frame no longer represents a rigid support line across the width of the bridge. Therefore, as the bridge twists, the intermediate cross-frames attract less live load force and thus reduce the associated fatigue issues (Herman, Helwig and Chong 2007) (Wang 2002).

Finally, another mitigation measure may be to make the cross-frames at the abutments and intermediate piers more efficient in stabilizing the girder end so the first row of intermediate cross-frames may be moved farther from the abutment and intermediate piers. By doing this, the intermediate cross-frames will be moved to a region that has less differential deflection which will reduce the live load forces they attract. Additionally, if the end cross-frames are stiffened; they will be more effective in limiting the girder end twist previously described. This will make cross-frame fit up easier and aid in keeping the girder webs plumb after concrete deck placement.

However, making the end cross-frames more efficient cannot be done by adjusting their skew angle because AASHTO requires that the end cross-frames be parallel to the bridge skew

angle to support the slab edge and transfer any lateral forces to the bearings (American Association of State Highway and Transportation Officials 2010). Therefore another method must be found to stiffen the end cross-frames.

1.3 Skewed End Cross-frame Connections

In order to most efficiently stiffen the skewed end cross-frames, the least stiff component of the cross-frame should be identified because stiffening this component will have the greatest effect. While previous research has quantified the stiffness of the brace members, girder in-plane stiffness, and the girder cross sectional stiffness, only limited research exists on the stiffness of the cross-frame to girder connection.

Many states, like Texas, have allowed a bent plate to connect the cross-frame to the girder parallel to the skew angle (AASHTO/NSBA Steel Bridge Collaboration 2003) as shown in Figure 1.6 and Figure 1.7. The bent plate and the connection plate it attaches to appear to be relatively flexible and, if they represent the least stiff component in the cross-frame system, will be the limiting factor in the cross-frame stiffness.

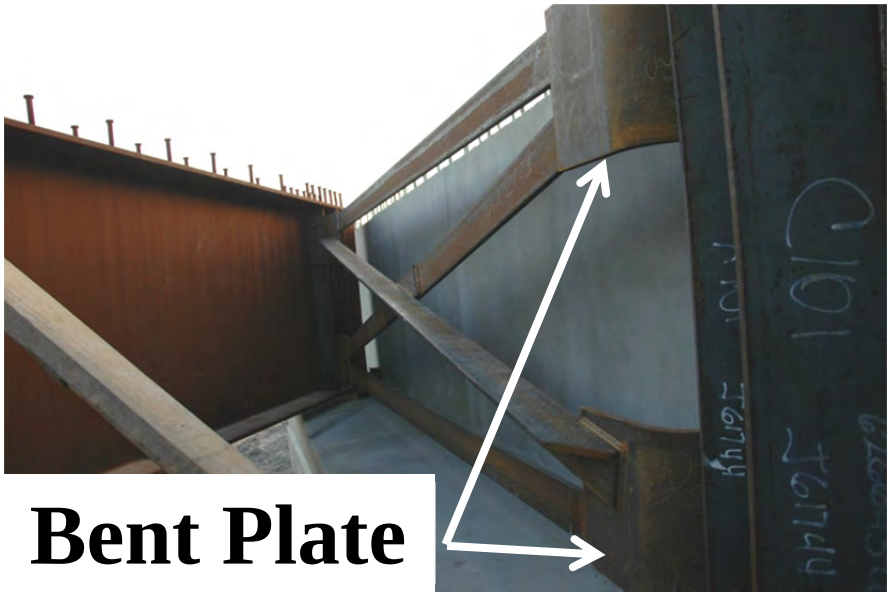

Figure 1.6: Bent plate end cross-frame connection elevation view

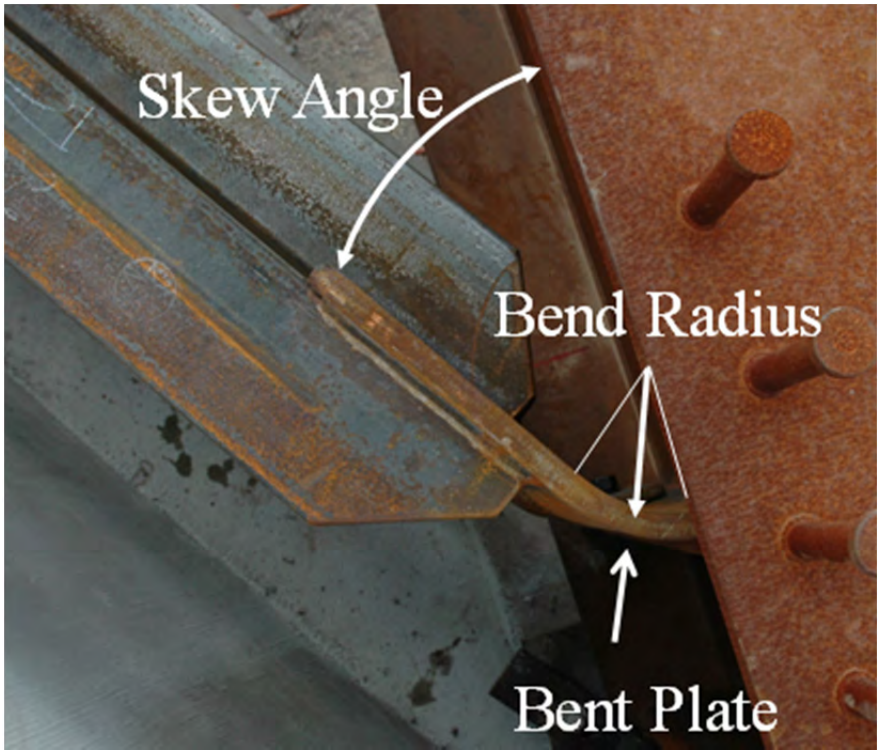

Figure 1.7: Bent plate end cross-frame connection plan view

If the bent plate connection is the least stiff cross-frame component, then it will limit the force the cross-frame attracts. This effect was investigated during concrete deck placement of a nearly 60° skewed bridge in Lubbock, Texas. One end cross-frame was instrumented with strain gages so the brace member forces could be monitored during the concrete deck placement.

The results for the top strut of the end cross-frame are shown in Figure 1.8. The results show that the axial force never exceeded 4 kips in the cross-frame member. Additionally, no end cross-frame member's axial force exceeded 4 kips during the concrete placement (Battistini 2009). One of the reasons for this may have been the bent plate's flexibility. By limiting the cross-frame's stiffness, the bent plate keeps the end cross-frame from attracting higher forces. It therefore may also allow the girder to rotate an excessive amount relative to the support. If the bent plate connection could be stiffened, then the end cross-frame would attract more force and therefore be used more efficiently in the skewed bridge bracing system.

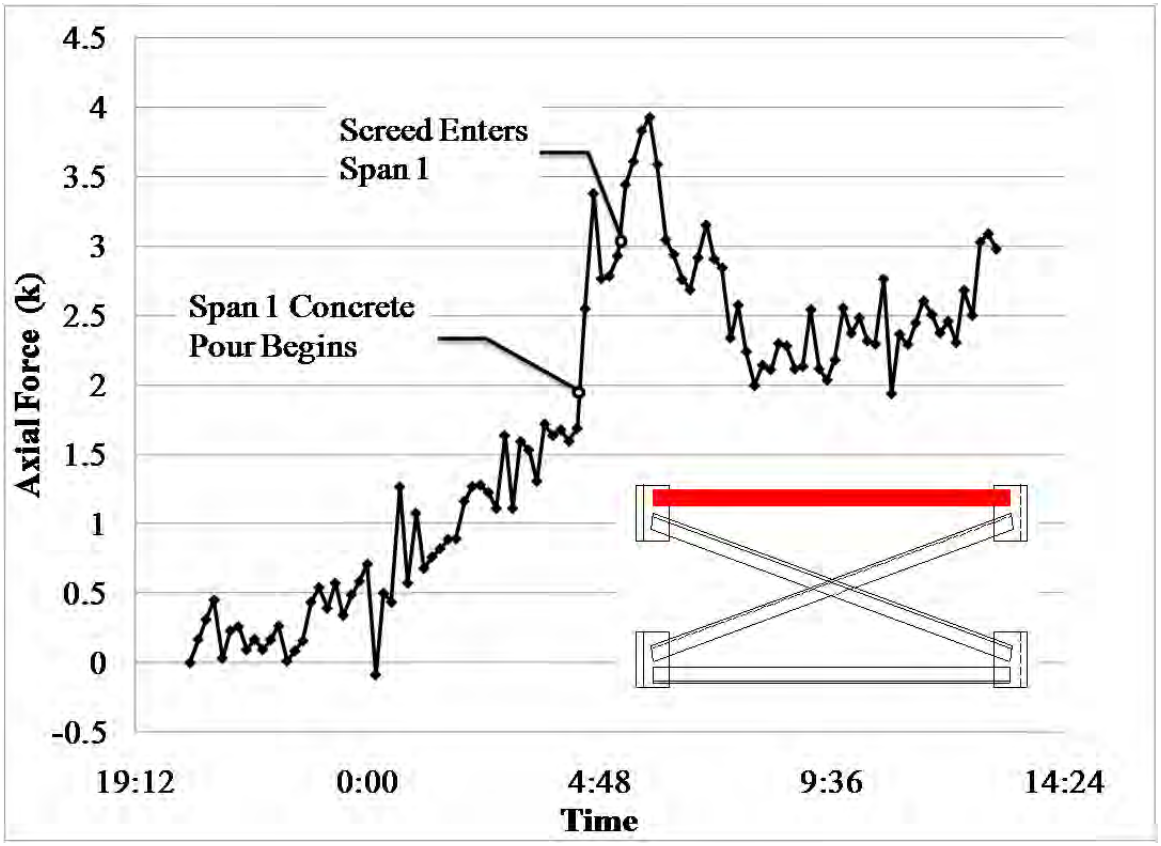

Figure 1.8: Top strut axial force during concrete placement

1.4 Research Purpose

The purpose of this research is to propose methods to make the end cross-frames more structurally efficient so they reduce girder end twist and allow the first row of intermediate cross-frames to be moved further from the abutment region. Moving the first row of intermediate cross-frames farther from the abutment is likely to decrease live load induced fatigue forces and to mitigate fatigue cracking.

The research outlined in this report primarily focuses on stiffening the end cross-frame connection to the girder. In addition to recommending measures to stiffen the existing bent plate connection, a new connection has been proposed consisting of a pipe, split in half, with each half welded to the girder web and flanges as shown in Figure 1.9. Besides offering the possibility of a stiffer connection, the split pipe also offers warping restraint that has been shown to significantly increase girder elastic buckling capacity (Ojalvo and Chambers, Effects of Warping Restraints on I-Beam Buckling 1977). Increasing the girder buckling strength will result in larger permissible unbraced lengths and allow the first row of intermediate cross-frames to be moved farther from the abutment region.

Figure 1.9: Split pipe end frame connection (53° skew)

1.5 Research Methods

The methods used in this study include laboratory tests, finite element modeling, and parametric studies. The laboratory tests consisted of small scale connection testing, fatigue testing, and large scale single girder lateral load tests, as well as large scale two and three girder buckling tests.

The laboratory tests in this study were used to directly compare the impact of varying key parameters used in the experiments. In addition to demonstrating the fundamental behavior of cross-frames in skewed bridges, the laboratory results provided valuable data that could be used to validate the finite element models created with the three-dimensional finite element program ANSYS® Academic Research, Release 11.0. This model was then used, in conjunction with the laboratory results, to conduct parametric studies that formed the basis for design guidance and recommendations.

1.6 Report Organization

This report is organized into seven chapters. An overview of previous research along with pertinent background information that is used in the subsequent chapters is provided in Chapter 2. A description of the experimental program including the connection, fatigue, and large scale

girder lateral and buckling tests is provided in Chapter 3. Chapter 4 covers the modeling techniques used to create the finite element model as well as the analytic and experimental results used to validate the model. A description of the parametric studies performed as well as the analytic equations and conclusions derived from the parametric studies and laboratory experiments is provided in Chapter 5. Chapter 6 presents the test program, results and finite element parametric studies for fatigue behavior of different details. Finally, the summary and conclusions are provided in Chapter 7 along with design recommendations.

Chapter 2. Background

2.1 Introduction

The flexural strength of a girder can be controlled by several limit states, including the cross sectional yield strength (typically expressed as a yield or fully plastic moment capacity) or local or global instability of the girder. Local instabilities include local flange or web buckling, both of which are controlled by the respective plate slenderness. The global stability is governed by lateral torsional buckling of the girders, which consists of a simultaneous twist and lateral deflection of the girder as depicted in Figure 2.1. The global buckling strength is a function of the boundary conditions of the girder as well as the spacing between braces. To stabilize a girder and allow an increase in the buckling strength, a variety of bracing schemes may be employed to limit the laterally or torsionally unsupported length.

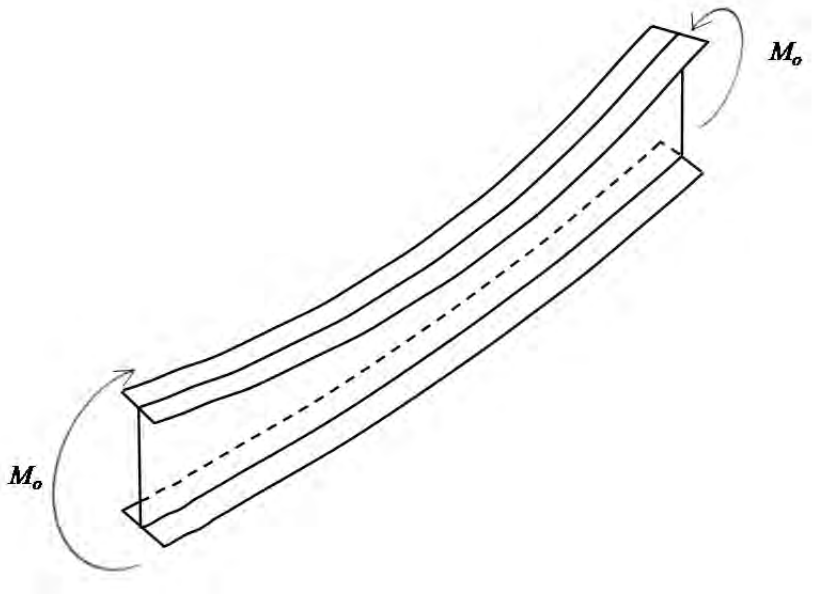

Figure 2.1: Girder lateral torsional buckling (Zhou, 2006).

For most boundary conditions, the compression flange of a girder experiences the largest lateral deformation as the beam buckles. Regions of the beam in tension do not tend to drive the buckling, and therefore the cross section also experiences torsional deformations. A beam's resistance to lateral torsional buckling can be improved by providing restraints at the ends of the beam or at locations along the length of the beam. The primary focus of the research documented in this report is the role of bracing at the ends of the girder.

2.2 Basic Elastic Beam Buckling Strength

Timoshenko and Gere (1961) used equilibrium and elastic theory to derive the critical lateral torsional buckling moment for an unbraced doubly symmetric beam under uniform moment with simple supports, no twist at the ends, and no warping restraint at the ends (Figure 2.2).

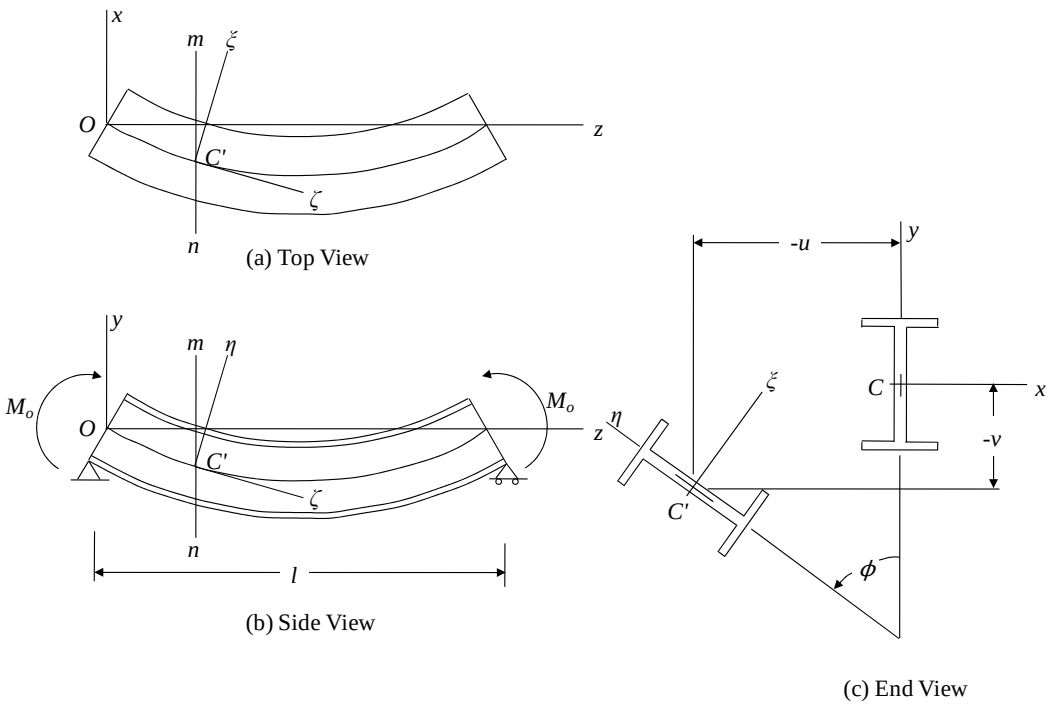

Figure 2.2: (a) Top, (b) side, and (c) end view of buckled beam.

For small deflections and rotations, Timoshenko and Gere transformed the moment about the *x*-axis (M_o) into the rotated coordinate system giving the moment components shown below.

$$M_\xi = M_o \tag{2.1}$$

$$M_\eta = \phi M_o \tag{2.2}$$

$$M_\zeta = -\frac{du}{dz} M_o \tag{2.3}$$

Then by using the equation for elastic curvature about each axis and the equation for twist of an open thin walled cross section, they found the following governing differential equations for vertical deflection (v), lateral translation (u), and twist (ϕ).

$$EI_\xi \frac{d^2v}{dz^2} - M_o = 0 \tag{2.4}$$

$$EI_\eta \frac{d^2u}{dz^2} - \phi M_o = 0 \tag{2.5}$$

$$GJ\frac{d\phi}{dz} - EC_w \frac{d^3\phi}{dz^3} + \frac{du}{dz} M_o = 0 \tag{2.6}$$

where

E = elastic modulus
I_ξ = strong-axis moment of inertia for the rotated cross section
I_η = weak-axis moment of inertia for the rotated cross section
G = shear modulus of elasticity
J = torsional constant
C_w = torsional warping constant

Equation 2.4 defines the bending behavior of a beam about the strong axis. Equations (2.5) and (2.6) contain cross terms of the lateral deformation (u) and angle of twist of the beam (ϕ). By differentiating Equation (2.6) with respect to the z-axis and using Equation (2.5), the differential equation for the angle of twist becomes:

$$EC_w \frac{d^4\phi}{dz^4} - GJ\frac{d^2\phi}{dz^2} - \frac{{M_o}^2}{EI_\eta}\phi = 0 \tag{2.7}$$

Equation (2.7) is a fourth order homogenous equation with constant coefficients that can be solved using the differential operator technique to find two real and two complex roots. To perform this operation Equation (2.7) can be recast to simplify the final result.

$$\frac{d^4\phi}{dz^4} - 2\alpha\frac{d^2\phi}{dz^2} - \beta\phi = 0 \tag{2.8}$$

where

$$\alpha = \frac{GJ}{2EC_w} \tag{2.9}$$

$$\beta = \frac{{M_o}^2}{EI_\eta EC_w} \tag{2.10}$$

Then using the differential operator (D) Equation (2.8) becomes

$$D^4 - D^2 2\alpha - \beta = 0 \tag{2.11}$$

The roots for the auxiliary equation for Equation (2.11) are, respectively,

$$m_1, m_2 = \pm i\sqrt{-\alpha + \sqrt{\alpha^2 + \beta}} \tag{2.12}$$

$$m_3, m_4 = \pm\sqrt{\alpha + \sqrt{\alpha^2 + \beta}} \tag{2.13}$$

So the solution becomes

$$\phi = A_1 e^{m_1 z} + A_2 e^{m_2 z} + A_3 e^{m_3 z} + A_4 e^{m_4 z} \quad (2.14)$$

Using Euler's formula the complex roots can be rewritten in terms of trigonometric functions giving the solution to the angle of twist as

$$\phi = A_1 \sin(m_1 z) + A_2 \cos(m_2 z) + A_3 e^{m_3} + A_4 e^{m_4} \quad (2.15)$$

The boundary conditions Timoshenko used at the end of the beam consisted of a simply supported beam free to warp with no twist. Applying these boundary conditions of no twist shown in Equation (2.16) provides a solution for the constants (A_1, A_2, A_3, and A_4) and the resulting solution for M_o in Equation (2.17).

$$\phi = \frac{d^2\phi}{d\phi^2} = 0 \quad (2.16)$$

$$M_{ocr} = \pi / L_b \sqrt{E I_y G J + \pi^2 E^2 C_w I_y / L_b^2} \quad (2.17)$$

where

M_{ocr} = buckling moment
L_b = unbraced length
I_y = weak-axis moment of inertia

Timoshenko's solution in Equation (2.17) is applicable to uniform moment loading on simply supported beams with twist prevented at the ends. However, depending on the bracing details that are used in practice, significant twist may occur at the ends of the beam. For example, in girders with skewed supports, the ends will twist to some degree and some warping restraint will be provided to the girder from the bracing. The amount of warping restraint depends on the cross-frame-to-girder connection used. A discussion of how these two departures from the assumptions in Equation (2.17) may impact the basic girder buckling strength in skewed steel bridges is provided in the following two sections.

2.3 Girder End Rotation in Skewed Bridges

The elastic buckling strength equation discussed in the preceding section was developed with the assumption that the girder ends do not twist. However, in a bridge with skewed supports, the girder ends are likely to twist. This twist occurs because the girder is part of the end cross-frame system. As the girder deflects vertically, it induces a rotation perpendicular to its web. However, at the girder ends, the girder cannot rotate perpendicular to its web due to the high in-plane stiffness of the cross-frame system. Instead, the cross-frame twists about the abutment center line and induces a twist on the girder end (Ude, 2009). The rotation vectors for this system are shown in Figure 2.3.

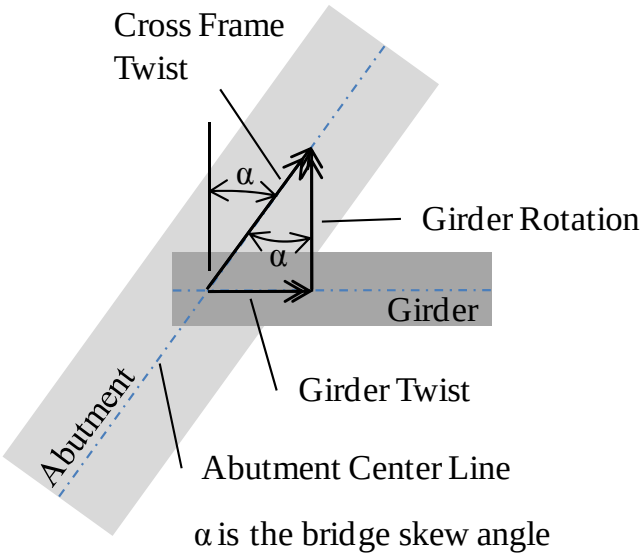

Figure 2.3: Cross-frame twist induced by strong axis girder rotation.

One purpose of the end cross-frames on a skewed bridge is to resist twist, but they will not completely prevent twist as assumed in Timoshenko's solution. The cross-frame will prevent twist of the girder end by the couple imposed by the braces' axial stiffness and by the individual braces' flexural stiffnesses.

2.4 End Cross-frame Stiffness

To accurately account for the impact of end cross-frames as well as intermediate frames on girder buckling capacities, equations quantifying the cross-frame stiffness must be developed. Cross-frames are a series of component stiffnesses and the overall cross-frame stiffness can be calculated by adding, in series, the stiffness contribution of each component (Yura, 2001) as shown in Equation (5.1). An explanation for each cross-frame component stiffness (brace, girder web, and girder in-plane stiffness) is given below. Additionally a proposed solution to quantify the connection stiffness is given.

$$\frac{1}{\beta_T} = \frac{1}{\beta_{br}} + \frac{1}{\beta_{sec}} + \frac{1}{\beta_g} \tag{2.18}$$

where

β_{br} = stiffness of attached brace
β_T = discrete brace system stiffness
β_{sec} = web stiffness including any stiffeners
β_g = attached girder stiffness

2.4.1 Brace Stiffness (β_{br})

2.4.1.1 Introduction

The torsional resistance of the braces making up the cross-frame system consists of an axial component and a bending component. The axial component comes from the brace's axial stiffness acting on the girder cross section with a separation typically described as the height of brace. The axial stiffnesses and related forces separated by the height of brace exert a stabilizing couple resisting the twist of the cross section. Additionally, the flexural stiffness of each brace member in the cross-frame system will also resist the twist of the cross section as long as they are connected to the cross section with a connection capable of transferring moment. So, in order for the girder cross section to twist, each connected brace must bend. The deflected shape of such a cross-frame is shown in Figure 2.4.

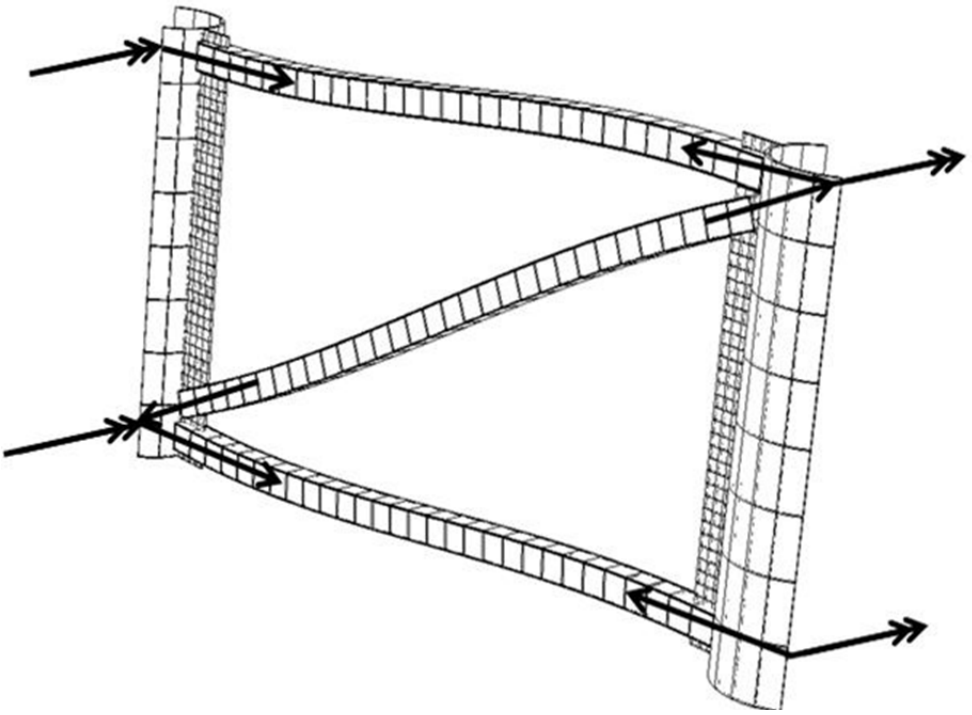

Figure 2.4: Cross-frame with brace member axial force and moment vectors

2.4.1.2 Brace Axial Component of Torsional Stiffness

The equation describing the torsional restraint of the cross-frame system due to the axial stiffnesses of its braces can be found in previous research for several different cross-frame configurations (Yura, 2001). The complete derivation for a single diagonal cross-frame is given below. The derivation begins with the free body diagram of a cross-frame shown in Figure 2.5. Although most conventional cross-frames have two diagonals, these diagonals are often composed of angles that have a relatively low buckling strength compared to the tensile strength. Therefore, the cross-frames are often modeled as a tension-only system, which is why the cross-frame in Figure 2.5 only has a single diagonal.

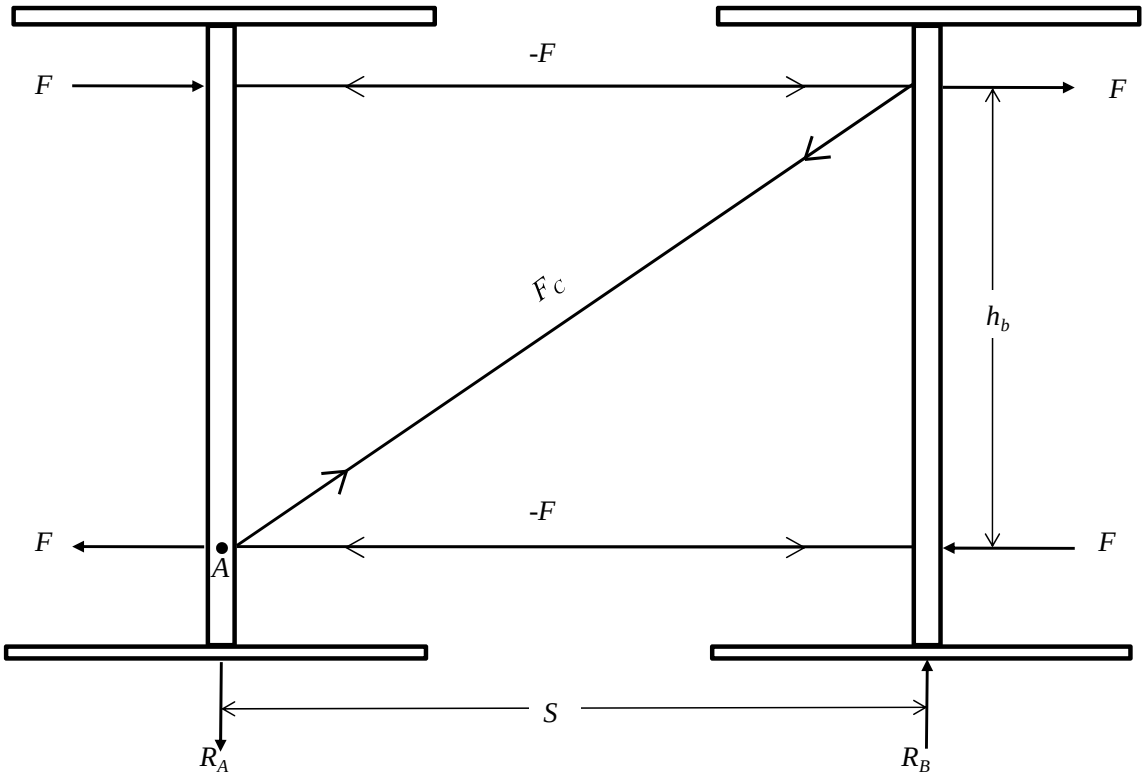

Figure 2.5. Single diagonal cross-frame free body diagram

Using equilibrium the reactions at *A* and *B* (R_A and R_B) are solved by summing moments about point *A* then summing vertical forces using the free body diagram of joint *A* gives the force in the diagonal member (F_c).

$$R_A = R_B = \frac{2Fh_b}{S} \tag{2.19}$$

$$F_C = \frac{2FL_c}{S} \tag{2.20}$$

Then to find deflections in terms of the forces above, the deflected shape of the cross-frame is drawn with all deflections taken on one side of the cross-frame as shown in Figure 2.6.

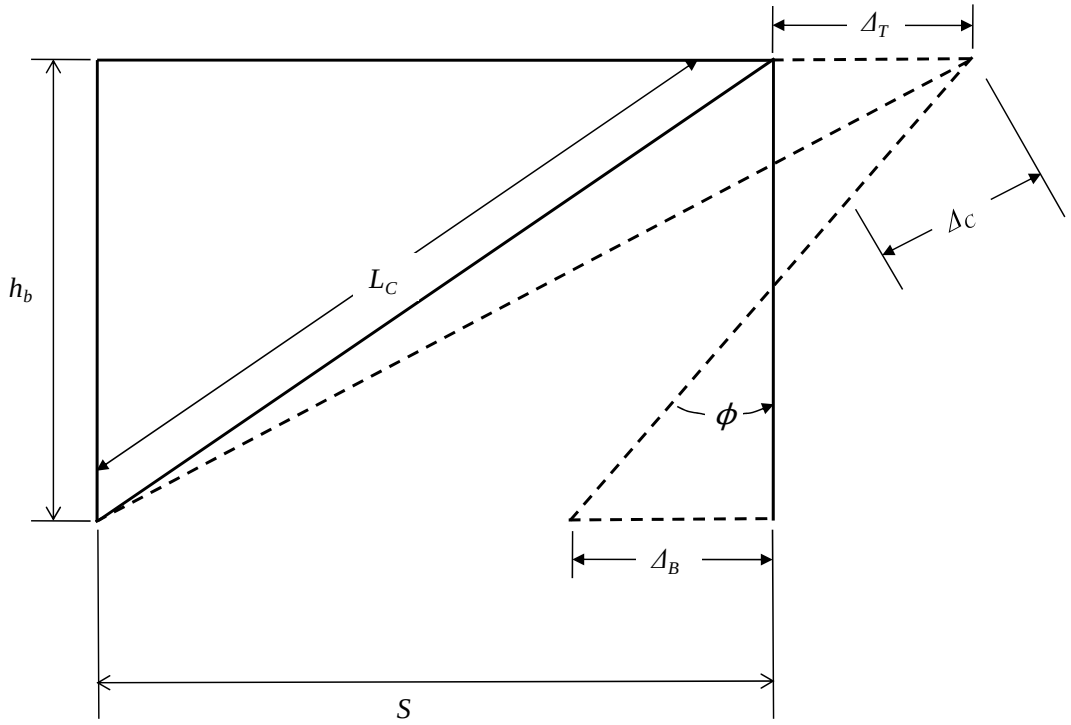

Figure 2.6: Tension-only cross-frame deflected shape

The deflected shape in Figure 2.6 is used to find the deflections in terms of forces. First the deflection of the diagonal (Δ_C) is found in terms of the top horizontal deflection (Δ_T) using similar triangles. Then the top and bottom (Δ_B) deflections are found in terms of the strut force (F).

$$\Delta_C = \frac{S}{L_C}\Delta_T \tag{2.21}$$

$$F_C = k_C\Delta_C = \left(\frac{AE}{L}\right)_C \Delta_C = \left(\frac{AE}{L}\right)_C \frac{S}{L_C}\Delta_T \tag{2.22}$$

Setting Equation (2.22) equal to Equation (2.20) yields the top deflection in terms of the strut force. A similar procedure is used to find the bottom deflection in terms of the strut force.

$$\Delta_T = \frac{2FL_C^3}{(AE)_c S^2} \tag{2.23}$$

$$\Delta_B = \frac{FS}{(AE)_S} \tag{2.24}$$

Defining the girder twist in terms of the top and bottom deflection gives the following relationship.

$$\phi = \frac{\Delta_T + \Delta_B}{h_b} \tag{2.25}$$

Now substituting Equations (2.23) and (2.24) gives:

$$\phi = \frac{2FL_C^3}{h_b S^2 (AE)_c} + \frac{FS}{h_b (AE)_S} \tag{2.26}$$

Then defining the axial portion of the cross-frame stiffness in terms of the moment the cross-frame imposes on the girder gives:

$$\beta_{braxial} = \frac{M}{\phi} \tag{2.27}$$

where

$$M = Fh_b \tag{2.28}$$

And now substituting Equations (2.26) and (2.28) into Equation (2.27) gives:

$$\beta_{braxial} = \frac{Eh_b^2}{\frac{2L_C^3}{A_c S^2} + \frac{S}{A_S}} \tag{2.29}$$

Finally by multiplying the second term in the denominator by $(S/S)^2$ and simplifying gives the final result for the tension-only cross-frame stiffness due to the axial stiffness of the braces as:

$$\beta_{braxial} = \frac{Eh_b^2 S^2}{\frac{2L_C^3}{A_c} + \frac{S^3}{A_S}} \tag{2.30}$$

Equation (2.30) is valid if the cross-frame is normal to the girder. A skewed cross-frame with skew angle α is shown in Figure 2.7. From the figure the relationships between the normal and skewed cross-frame members and forces are shown below.

$$F' = \frac{F}{cos\ \alpha} \tag{2.31}$$

$$L'_C = \frac{L_C}{\cos \alpha} \tag{2.32}$$

$$S' = \frac{S}{cos\,\alpha} \tag{2.33}$$

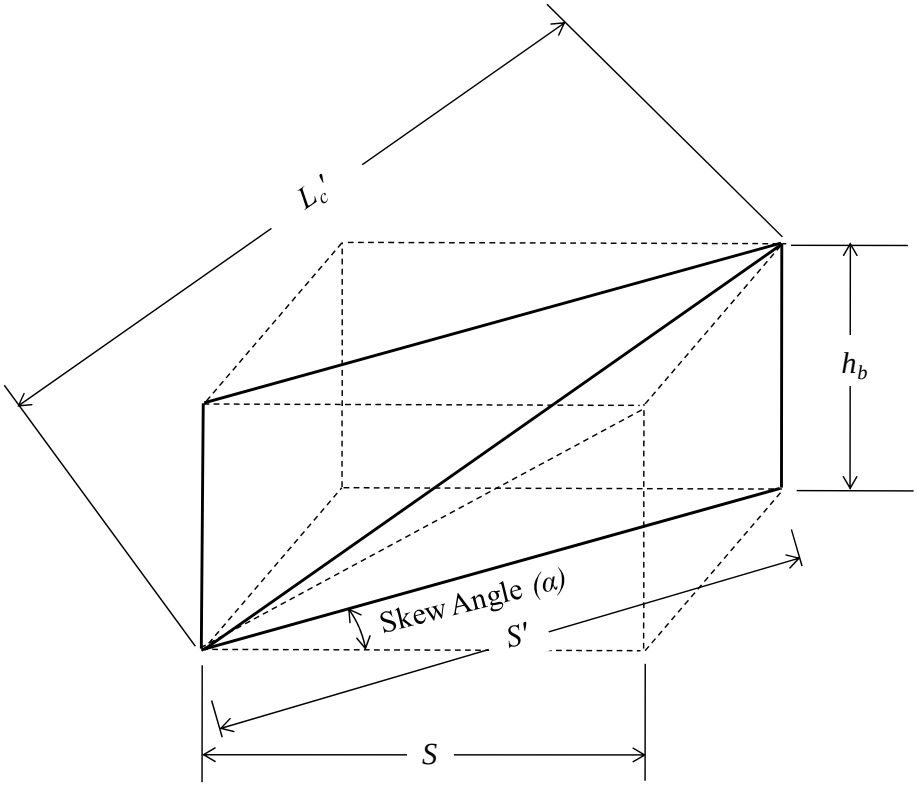

Figure 2.7: Skewed cross-frame

Now the top and bottom cross-frame deflections in Equations (2.23) and (2.24) can be written including the skew angle α.

$$\Delta'_T = \frac{2F'L'^3_C}{(AE)_c S'^2} = \frac{2FL^3_C \cos^2\alpha}{(AE)_c S^2\, cos^4\,\alpha} = \frac{2FL^3_C}{(AE)_c S^2\, cos^2\,\alpha} \tag{2.34}$$

$$\Delta'_B = \frac{F'S'}{(AE)_S} = \frac{FS}{(AE)_S\, cos^2\,\alpha} \tag{2.35}$$

And the girder twist given by Equation (2.26) is used with the deflections of Equations (2.34) and (2.35) giving the girder twist in the skewed coordinate system.

$$\phi' = \left[\frac{2FL^3_C}{h_b S^2 (AE)_c} + \frac{FS}{h_b (AE)_S}\right]\frac{1}{\cos^2\alpha} = \frac{\phi}{cos^2\,\alpha} \tag{2.36}$$

Now using the final result of Equation (2.36) the skewed cross-frame stiffness can be written as (Wang & Helwig, 2008):

$$\beta_{braxialskew} = \frac{M}{\phi'} = \frac{M}{\phi} cos^2\,\alpha = \beta_{braxial}\, cos^2\,\alpha \tag{2.37}$$

2.4.1.3 Brace Bending Component of Torsional Stiffness

As the girder cross section twists, it will cause the cross-frame members to bend in reverse curvature if the braces are connected to the girder with a moment resisting connection (Figure 2.4) and the brace height extends above midheight of the girder. From basic mechanics the bending stiffness of a brace in the plane of the cross-frame is described in Equation (2.38).

$$\beta_{brbend} = \frac{6EI_{br}}{L_{br}} \tag{2.38}$$

where

I_{br} = Brace moment of inertia in plane of the cross-frame
L_{br} = Brace member length

The inclusion of the bending stiffness of the braces simply requires that the bending stiffness of each brace be added to the result of Equation (2.30) giving the brace stiffness shown in Equation (2.39).

$$\beta_{br} = \frac{Eh_b^2S^2}{\frac{2L_C^3}{A_c} + \frac{S^3}{A_S}} + 2\frac{6EI_{strut}}{S} + \frac{6EI_{diagonal}}{L_c} \tag{2.39}$$

To account for the impact of support skew on the bending stiffness of the braces, a similar procedure to that for the brace axial stiffness is followed as described below.

The girder twist shown in Figure 2.3 is resisted by a corresponding cross-frame twist and brace rotation. The twist and rotation vector triangle for the girder twist and cross-frame resistance are shown in Figure 2.8. The geometry from this vector triangle leads to the transformation of the girder twist to the brace rotation.

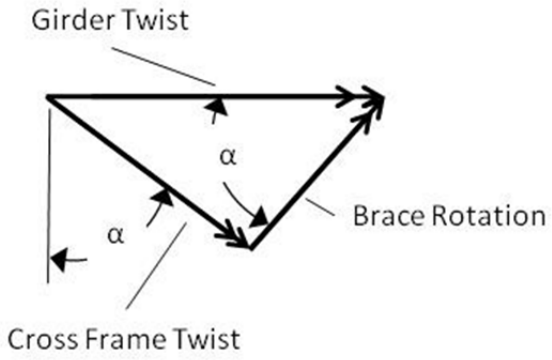

Figure 2.8: Girder and brace twist/rotation triangle (α is the bridge skew angle)

$$\theta_{brace\ rotation} = \theta_{girder\ twist} \cos\alpha \tag{2.40}$$

Therefore,

$$M_{brace} = \beta_{brbend}\theta_{girder\ twist} \cos\alpha \tag{2.41}$$

where

M_{brace} = bending moment applied to brace in cross-frame plane

Additionally, the length of the brace is also impacted by the skew angle as shown in Equation (2.32). Combining this skew impact into Equation (2.38) and substituting into Equation (2.41) gives

$$M_{brace} = \beta_{brbend}\theta_{girder\ twist} \cos^2\alpha \tag{2.42}$$

Therefore

$$\beta_{brbendskew} = \beta_{brbend} \cos^2\alpha \tag{2.43}$$

And finally, combining Equations (2.43) and (2.37) yields

$$\beta_{brskew} = \left[\frac{Eh_b^2S^2}{\frac{2L_C^3}{A_c} + \frac{S^3}{A_S}} + 2\frac{6EI_{strut}}{S} + \frac{6EI_{diagonal}}{L_c}\right]\cos^2\alpha \tag{2.44}$$

2.4.2 Web Stiffness (β_{sec})

If the cross-frame attaches directly to the girder web, then web distortion (normal to the plane of the web) will reduce the overall stiffness of the cross-frame stiffness. The contribution of the web to the cross-frame stiffness is calculated using Equation (2.45) (Yura, Phillips, Raju, & Webb, 1992). If the cross-frame attaches at a full depth web stiffener, then the web stiffness typically may be taken as infinite as there will be insignificant web distortion. Similarly, when modeling a cross-frame in a finite element program, connecting the cross-frame directly to the web-flange interface allows the web stiffness to be taken as infinite.

$$\beta_{sec} = \frac{3.3E}{h}\left(\frac{(\mathrm{N} + 1.5h)t_w^3}{12} + \frac{t_s b_s^3}{12}\right) \tag{2.45}$$

where

E = Young's Modulus
h = web depth
N = brace contact area with flange
t_w = web thickness
t_s = stiffener thickness
b_s = stiffener width

2.4.3 Attached girder stiffness (β_g)

As the girders begin to twist during buckling, the cross-frame is forced to resist the couple created. In turn, the cross-frame's resisting moment is countered by vertical reactions on the girders. These vertical reactions cause the girder to deflect in the girder's strong plane and the girder's in-plane flexibility will also affect the stiffness of the cross-frame system. The impact of the girder's in-plane flexibility is given by Equation (2.46) (Helwig, Yura, & Frank, 1993).

$$\beta_g = \frac{12S^2EI_x}{L^3} \tag{2.46}$$

where

S = spacing between girders
E = Young's modulus
I_x = girder moment of inertia about its strong axis
L = girder length

2.4.4 Connection Stiffness ($\beta_{conntors}$)

The stiffness of the cross-frame will also be affected by its connections. This component is not yet reflected in Equation (5.1). The development of connection stiffness parallels that of the brace stiffness because the force and geometry are the same for each and is given below. The derivation begins with Equation (2.22) and then substitutes the connection stiffness rather than the brace's axial stiffness. Of course this assumes the axial stiffness of the connection perpendicular to the girder is known.

Using the same deflected geometry as in the brace stiffness derivation (Figure 2.6) the top and bottom connection displacements are given below.

$$\Delta_{Tconn} = \frac{2FL_C^2}{\beta_{conn}S^2} \tag{2.47}$$

$$\Delta_{Bconn} = \frac{F}{\beta_{conn}} \tag{2.48}$$

where

β_{conn} = axial connection stiffness perpendicular to the girder

Using these deflections and substituting them into Equation (2.25) then simplifying gives the connection torsional stiffness perpendicular to the girder shown below.

$$\beta_{conntors} = \frac{\beta_{conn}\, h_b^2}{\frac{2L_c^2}{S^2} + 1} \tag{2.49}$$

Equation (2.49) assumes that the axial connection stiffness perpendicular to the girder is known. As outlined in Chapter 1, a common connection that is used to simplify fabrication for

cross-frame connections at skewed supports is the bent plate detail. To develop the connection stiffness perpendicular to the girder web for a bent plate, the axial and lateral stiffness of the bent plate must be quantified and then transformed into a component perpendicular to the girder. These quantities are explored through laboratory testing and finite element modeling and developed in Chapter 5 (Parametric Studies and Design Guidance).

2.5 Impact of Girder End Twist on Elastic Buckling Strength

Previous research has shown that as a girder's end is allowed to twist due to support rotation, its buckling strength is reduced (Flint, 1951) (Schmidt, 1965) (Bose, 1982). The relationship between support rotation and buckling strength is given by Flint (1951) as

$$\frac{M_{cr}}{M_o} = 1 - \frac{4}{3}\left[\frac{\left(\theta/T\right)_{support}}{\left(L/JG\right)_{girder}}\right] \tag{2.50}$$

where
M_{cr} = girder buckling strength with support rotation
M_o = girder buckling strength with no support rotation
θ = support rotation due to torque (T)

Rearranging the terms and using the cross-frame stiffness rather than the support stiffness parameters, Equation (2.50) can be recast to account for the girder cross section torsional stiffness relative to the cross-frame stiffness. This formulation is shown in Equation (2.51).

$$n = 1 - \frac{4}{3}\left(\frac{GJ}{L}\right)_{girder}\left(\frac{1}{\beta_T}\right) \tag{2.51}$$

While subsequent analytical studies have shown that the reduction in buckling capacity is negligible if the support stiffness is 20 times the girder's torsional stiffness (Schmidt, 1965), Equation (2.50) has been found to overestimate the girder buckling capacity when end twist is allowed (Bose, 1982). Additionally it is not specific to cross-frames; rather, its derivation comes from support twist. Therefore, Equation (2.51) will be investigated in Chapter 5 using a parametric study to determine its accuracy when end cross-frame stiffnesses rather than support stiffnesses are used.

2.6 Tipping Effect

When analyzing the buckling strength of a girder, the vertical load and reaction forces at the supports are assumed to pass through the plane of web. However, in actual bridges, the load is applied to the girder through secondary members or slabs, and the girder is supported through bearings. Due to the twist of the cross section of the girder, the loading position tends to shift away from the web plane. The resulting restoring torque will provide beneficial tipping effect as illustrated in Figure 2.1(a).

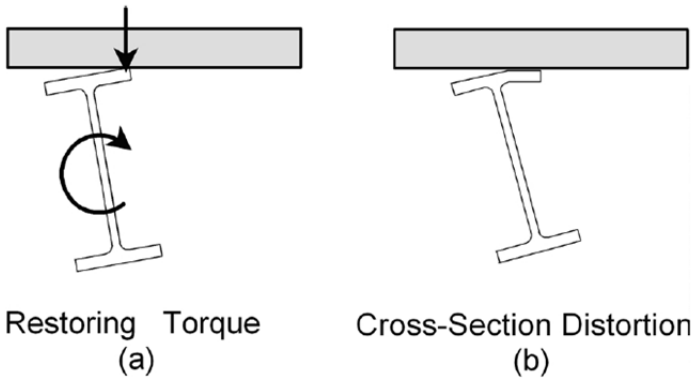

Figure 2.9: Tipping Effect

Previous research (Flint, 1951) (Fisher, 1970) (Linder, 1982) has indicated that cross section distortion severely limits the beneficial effects of tipping, as illustrated in Figure 2.1(b). Therefore, the tipping effect is recommended to be considered only when cross section distortion is prevented by stiffeners.

The tipping effect will be studied in this report in order to provide better prediction of the girder behavior due to buckling and to the skew effect. In the laboratory, the tipping effect under top flange loading can be avoided by loading through a knife edge. The tipping effect at the support will be investigated by supporting the girders with different bearings in the laboratory tests and also in finite element modeling. The details of the test setup and modeling will be described in Chapter 4 and Chapter 5, respectively.

2.7 Girder Warping Restraint in Skewed Bridges

Typical end cross-frames are connected to girders via connection plates or bearing stiffeners (AASHTO/NSBA Steel Bridge Collaboration, 2003) that offer negligible restraint to girder end warping. However, the integration of a warp restraining device into the girder-end frame connection can provide significant warping restraint and dramatically increase the girder's buckling capacity.

Such warp restraining devices have previously been studied (Hunt, 1973). One analytical study found that the use of a pipe connecting the girder flanges (Figure 2.10) can provide as much as a 70% increase in the buckling capacity (Ojalvo & Chambers, 1977).

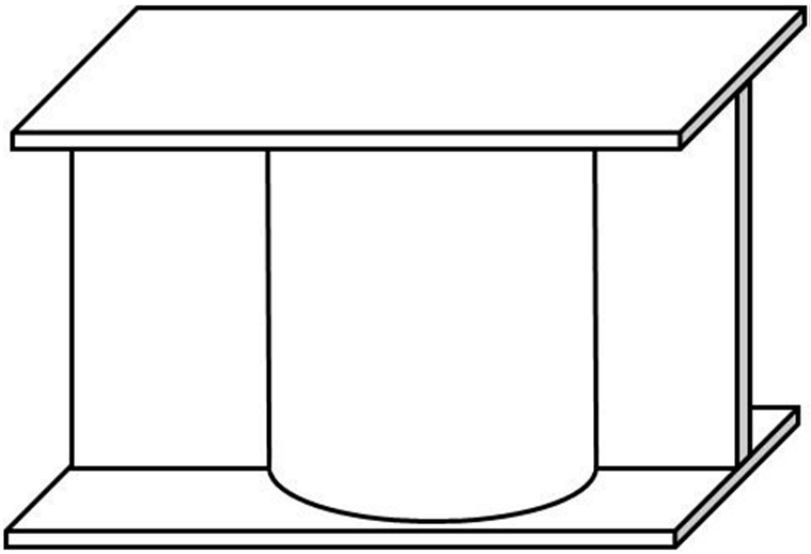

Figure 2.10: Wide flange shape with pipe stiffener

The reason a pipe stiffener is effective in increasing the girder buckling capacity is shown in Figure 2.11. As the girder twists during buckling, the flanges undergo differential twist about the vertical axis through the web. The differential twist of the flanges is often referred to as warping deformation. The relative flange twist is represented in the figure by the flange ends rotating in opposite directions. For the flanges to twist relatively to one another, they must twist the pipe that connects them. Because the pipe is a closed shape, it is torsionally stiff and provides a significant source of warping restraint that adds to the stability of the girder.

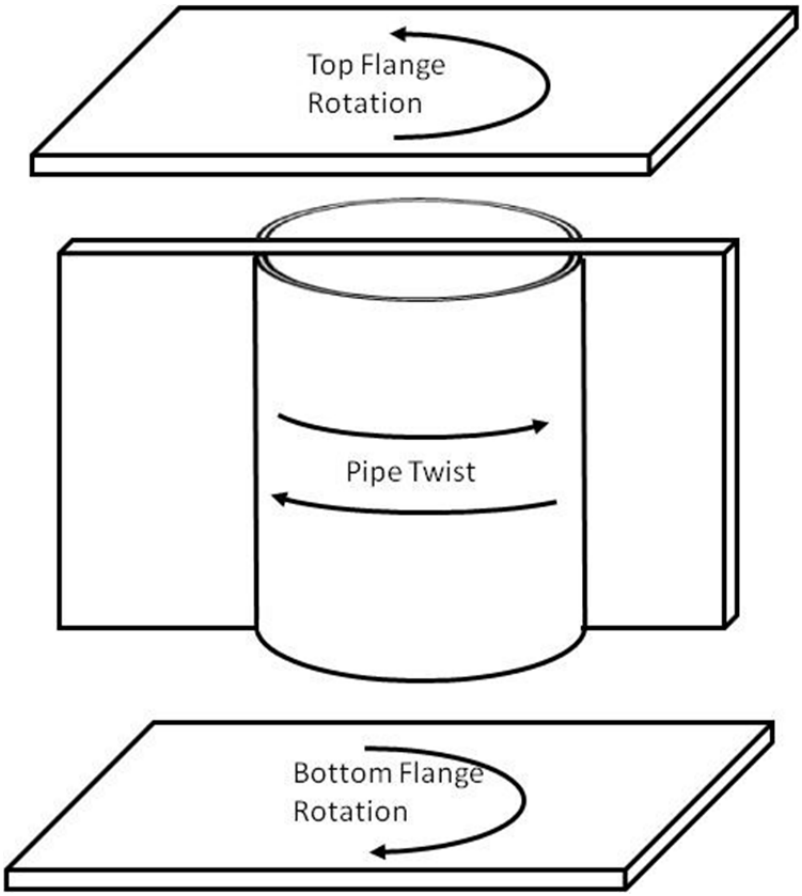

Figure 2.11: Pipe stiffener twist due to girder flange end rotation

Ojalvo and Chambers (1977) analytically investigated the increase in buckling strength due to pipe stiffeners at the ends of girders and developed a method to calculate this contribution. By incorporating the resistance the pipe provides to each flange into the boundary conditions for Equation (2.15), an iterative numerical integration can be used to calculate the increase in buckling strength. This procedure is described below.

Using the coordinate system shown in Figure 2.2 and equating the rotation of the bottom flange plus the angle of twist in the tube to the rotation of the top flange Ojalvo and Chambers (1977) derive the following compatibility equation:

$$u' + \frac{d}{2}\phi' - \frac{d^2}{2}\frac{E}{GJ}I_f\phi'' = u' - \frac{d}{2}\phi' \tag{2.52}$$

where

d = distance between flange centroids
I_f = flange strong axis moment of inertia

From Equation (2.52) and the simply supported end conditions, the following boundary conditions for the simply supported beams with warping restraint are developed.

$$\phi = u = u'' = 0 \tag{2.53}$$

$$\phi' - \left(EI_f/2GJ\right)d\phi'' = 0 \tag{2.54}$$

With the above boundary conditions, Ojalvo and Chambers used a numerical integration technique to solve Equations (2.5) and (2.6) as an initial value problem for the critical buckling moment for six rolled shapes using both an infinitely stiff tube and a tube with a ¼" thick wall as the warping restraint. While this analysis produces accurate results and shows that such a warping restraint device provides a near warping fixed end condition, this method is not user-friendly as it requires an iterative solution of four simultaneous equations to converge on a buckling solution.

Another possibility in calculating the girder buckling strength due to warping restraint provided by a pipe stiffener is to consider the two sources of stability defined in Equation (4.1). An examination shows that the terms under the radical define both components of the girder's resistance to lateral torsional buckling. The first term defines the uniform (St. Venant) torsional resistance and the second term defines the torsional warping resistance. Therefore, the warping resistance provided by a pipe stiffener can be incorporated into the second term as an effective torsional length factor (K_z) as shown in Equation (2.55). Such a method has previously been employed to calculate the impact of warping restraint provided by adjacent unbraced girder lengths (Structural Stability Research Council, 1988). Of course a suitable selection for K_z must be made.

$$M_{cr} = \mathrm{C_b}\pi/L_b\sqrt{EI_yGJ + \pi^2E^2C_wI_y/(K_zL_b)^2} \tag{2.55}$$

where

C_b = moment gradient coefficient
K_z = effective length factor for torsion

The critical parameter in determining K_z for a pipe stiffener lies in the relative rotational stiffness of the girder's compression flange about its strong axis ($2EI_f/L$ where I_f is the flange's strong axis moment of inertia) to the torsional stiffness of the pipe (GJ/L). If the torsional stiffness of the pipe is much greater than that of the girder flange then K_z will approach 0.5 with no intermediate bracing and 0.7 with intermediate bracing (torsionally fixed). For the case with intermediate bracing, the warping restraint is taken as zero to maintain consistency with typical design specifications. Likewise if the stiffness of the pipe is much smaller than the stiffness of the flange then K_z will approach 1.0 (torsionally free). This is analogous to a sidesway inhibited column where the torsional stiffness of the pipe is considered as the flexural stiffness of a girder framing into the end of the column. Approaching the problem in this way allows the sidesway inhibited alignment chart (American Institute of Steel Construction, 2001) for columns to be used to select an appropriate K_z where the relative rotational stiffness of the girder flange to the torsional stiffness of the pipe is used to calculate G_A or G_B at the pipe stiffened end of the girder.

In order to use the alignment chart, the assumption that the stiffening girders bend in single curvature with $2EI/L$ stiffness must be considered in terms of the pipe stiffener. If the pipe is much stiffer than the girder flanges, then as the flanges attempt to warp in opposite directions the very rigid pipe will limit the flange warping to a very small amount. This condition will

result in a very high effective torsional stiffness similar to the *6EI/L* of beams bent in reverse curvature which is three times the assumed value of *2EI/L* in the chart. Likewise as the stiffness of the pipe declines relative to the flange flexural stiffness, the pipe will allow more flange rotation thereby reducing its effectiveness in increasing girder buckling strength. So, in general *G* may be defined as:

$$G_{A\ or\ B} = \left(\frac{EI}{L_b}\right)_{flange} \Big/ m\left(\frac{GJ}{L}\right)_{pipe} \tag{2.56}$$

where

I = flange strong axis moment of inertia
m = pipe stiffness multiplier based on relative stiffness of pipe to flange
L = pipe length

The difficulty in assessing the value of *m* comes from the indeterminate nature of the pipe boundary conditions. Because the boundary conditions depend on the relative torsional stiffness of the pipe to the flexural stiffness of the flange and in turn the flexural stiffness of the flange depends on the torsional stiffness of the pipe there is no simple solution to define *m*. Therefore, to determine a value for *m* based on the pipe to flange stiffness a finite element parametric study will be used to establish values of *m* for corresponding ratios of the pipe torsional stiffness to the girder flange flexural stiffness. This study is described in Chapter 5 (Parametric Studies and Design Guidance).

2.8 Estimation of Girder Buckling Strength with Initial Imperfections

Equation (4.1) considers only a linear elastic solution to the girder buckling problem; however, real girders have initial imperfections that will affect the buckling strength. To incorporate the impact of initial imperfections, a large deflection analysis can be used rather than an eigenvalue buckling analysis, but determining the buckling load then becomes a challenge because the deflections continue to increase as the load increases and approaches, but never reaches the eigenvalue buckling load.

Meck (1977) built on the method Southwell proposed to solve such a problem for columns in 1932 (Southwell, 1932). By solving for equilibrium on an Euler column with an initial imperfection, Southwell was able to develop an explicit relationship between critical load, deflection, and initial imperfection shown in Equation (2.57).

$$P_{cr}\left(\frac{x_c}{P}\right) = x_c + x_{oc} \tag{2.57}$$

where

x_c = lateral deflection at midspan of column under load P
x_{oc} = initial lateral imperfection at midspan of column.

By putting Equation (2.57) into slope-intercept form and plotting x_c/P versus x_{oc} a straight line plot is found whose slope is the critical buckling load and y-intercept is the initial imperfection.

Following a similar pattern, Meck used Timoshenko's equilibrium equations for beam buckling and then applied an energy method to solve them for buckling under a point load at mid-span which produced the following simultaneous equations.

$$\alpha \frac{\emptyset_c}{P} = u_c + \overline{u_c} \tag{2.58}$$

$$\beta \frac{u_c}{P} = \emptyset_c + \overline{\emptyset_c} \tag{2.59}$$

where

$$\alpha = \frac{2\left(GJ + \frac{\pi^2 E C_w}{L}\right)}{\left(\frac{1}{4} + \frac{1}{\pi^2}\right) L} \tag{2.60}$$

ϕ_c is the twist at girder midspan
u_c is the lateral deflection of the girder centroid at midspan
$\overline{u_c}$ is the initial lateral imperfection of the girder centroid at midspan
P is the load applied to the centroid of the cross section

$$\beta = \frac{2\pi^2 E I_y}{\left(\frac{1}{4} + \frac{1}{\pi^2}\right) L^3} \tag{2.61}$$

Similar to Southwell's column procedure, two plots are produced and their slopes are α and β. Then setting the initial lateral and twist imperfections to zero in Equations (2.58) and (2.59) and solving for P_{cr} yields the following relationship.

$$P_{cr}{}^2 = \alpha\beta \tag{2.62}$$

So, the product of the slopes of the two graphs becomes the buckling load. However, few girders have point loads applied at their centroids. So to account for top flange loading, Meck recommended that Equation (2.58) becomes

$$\alpha \frac{\emptyset_c}{P} = (u_c + e\emptyset_c) + \left(\overline{u_c} + e\overline{\emptyset_c}\right) \tag{2.63}$$

where

e is the vertical distance from the centroid to the point of load application.

Then ϕ_c/P is plotted against $u_c+e\phi_c$ and the slope of the straight line plot is α. Then finally the critical buckling load is found by solving the following quadratic equation.

$$P_{cr}^2 + \beta e P_{cr} - \alpha\beta = 0 \tag{2.64}$$

2.9 Current Code Provisions and Construction Practices

The preceding theoretical discussion forms the basis for skewed steel bridge girder end cross-frame design as codified in a number of national and Texas state specific publications. These provisions are summarized below.

2.9.1 2007 AASHTO Bridge Design Provisions (American Association of State Highway and Transportation Officials, 2010)

2.9.1.1 Section 6.7.4.1 Diaphragms and Cross-Frames—General

In the first edition of the LRFD Specification, AASHTO removed the arbitrary requirement that diaphragms be spaced at no more than 25 feet (AASHTO LRFD 1994). Instead a rational analysis is recommended to establish acceptable diaphragm spacing. While not directly specified in AASHTO, a rational analysis should ensure that the brace has both adequate stiffness and strength to provide girder stability as well as meeting other requirements that the braces provide to the bridge. The specification requires that cross-frames be spaced to provide:

- Transfer of lateral wind loads to the bearings
- Stability of the bottom flange when in compression
- Stability of the top flange when in compression
- Consideration of any flange lateral bending effects
- Distribution of vertical dead and live loads

Additionally, where there is a discontinuity in the slab or at the edge of the slab, the slab is required to be supported by diaphragms or other edge supports (Section 9.4.4) to stiffen the deck for wheel loads at the edge of the slab.

2.9.1.2 Section 6.6.1.3 Distortion Induced Fatigue

The AASHTO specification requires transverse connection plates to be bolted or welded to both the girder web and flange when the connection plates are attached to diaphragms or cross-frames. Attaching the connection plate to the flanges reduces the problems with distortional fatigue around the cross-frame regions. The commentary states that for skewed bridges, the diaphragm forces should be determined by analysis and references Keating, et al., (1990).

For lateral connection plates (such as a bent plate), the specification limits the placement of plates to a vertical distance not less than one-half the width of the flange above or below the flange on stiffened webs and at least six inches above or below the flanges on unstiffened webs. These provisions are intended to minimize the effect of weld terminations on fatigue strength and prevent distortion induced fatigue on the web to flange weld.

2.9.1.3 Section 6.7.4.2 Diaphragms and Cross-Frames—I-Section Members

The specification allows intermediate diaphragms or cross-frames on bridges with supports skewed 20° or less to be placed parallel to the skew. However, when the supports are

skewed more than 20° the intermediate diaphragms or cross-frames are required to be placed normal to the girders. The braces can be placed either along a continuous bracing line or can also be staggered along a line parallel to the skew angle. End diaphragms are required to be designed for forces and distortions transmitted by the deck to the bearings.

2.9.2 2004 AASHTO Bridge Construction Specification (American Association of State Highway and Transportation Officials, 2010)

2.9.2.1 Section 11.4.3.3 Bent Plates

AASHTO Specification listed the minimum bend radii of cold bent plates. The table is presented here in Table 2.1. The specification recommends that the bend line be oriented perpendicular to the final rolling directions. If this is not possible the minimum radius should be multiplied by 1.5. If a smaller radius than that allowed by cold bending is required, then hot bending is required in accordance with the specification provisions.

Table 2.1: Minimum Cold Bend Radii [Table 11.4.3.3.2-1, AASHTO 2010]

AASHTO M 270M/M270 (ASTM A 709/A 709M) Grades, ksi	Thickness, in. (*t*)			
	Up to 0.75	Over 0.75 to 1.0, incl.	Over 1.0 to 2.0, incl.	Over 2.0
36	1.5*t*	1.5*t*	1.5*t*	2.0*t*
50, 50S 50W, or HPS 50W	1.5*t*	1.5*t*	2.0*t*	2.5*t*
HPS 70W	1.5*t*	1.5*t*	2.5*t*	3.0*t*
100	1.75*t*	2.25*t*	4.5*t*	5.5*t*
100W	1.75*t*	2.25*t*	4.5*t*	5.5*t*

2.9.3 2003 AASHTO/NSBA Guidelines for Design for Constructability (AASHTO/NSBA Steel Bridge Collaboration, 2003)

2.9.3.1 Section1.6.1 Deflections for Straight Structures on Skewed Piers and Abutments

The guidelines point out that differential girder deflections and twist on bridges with highly skewed supports must be evaluated for the load under which diaphragms must fit (no-load, steel only, or non-composite dead load). The differential deflections are caused by the differing distance to the supports for adjacent girders. Girder twist becomes an issue because the twist is normal to the skewed pier and not the web causing the top flange to deflect away from the bottom flange resulting in the web being out of plumb and the flanges to be unlevel.

2.9.4 2007 TxDOT LRFD Bridge Design Manual (TxDOT, 2007)

2.9.4.1 Chapter 3 Section 12 Straight Plate Girders

Guidelines for TxDOT bridges on bracing permit the cross-frame spacing to be a maximum of 30 feet and at least two interior bearings must have a diaphragm intersecting them at each bent. The manual also confirms the AASHTO provisions on aligning diaphragms with a skew 20° or less and normal to girders for larger skews.

2.9.5 2007 TxDOT Preferred Practices for Steel Bridge Design, Fabrication, and Erection (Texas Steel Quality Council, 2007)

2.9.5.1 Section 2.6 Diaphragms and Cross-frames

TxDOT has preferred field welding to connect diaphragms and cross-frames to girders due to erection tolerances. TxDOT plans utilize standard drawings for cross-frames and diaphragms that are published on the Miscellaneous Details Steel Girders and Beams (SGMD) sheets (Texas Department of Transportation, 2006). These standard details cover bridge skews up to 45° and any skew over 45° requires additional details to show the girder to cross-frame connections. Cross-frames are allowed to be spaced more than 25 feet if this spacing can be attained without temporary bracing and all other limit states are satisfied.

According to TxDOT preferred practices, fabricators prefer single equal leg angles to all other types of members for cross-frames. Also, due to the use of Dart welders, welding stiffener and connection plates at more than a 20° to the girder is problematic.

2.9.6 Current Texas Cross-frame Connection Fabrication Practices

Based on the preceding national and state guidance, Texas bridge fabricators are given significant leeway in creating end cross-frame connections on steel girder bridges. The connection found in the TxDOT SGMD plan sheet (Texas Department of Transportation, 2006) uses an integral bearing stiffener connection plate to connect bent plates that support the cross-frame brace members for skew angles between 20° and 45° and straight connection plates for skews 20° and under (Figure 2.12).

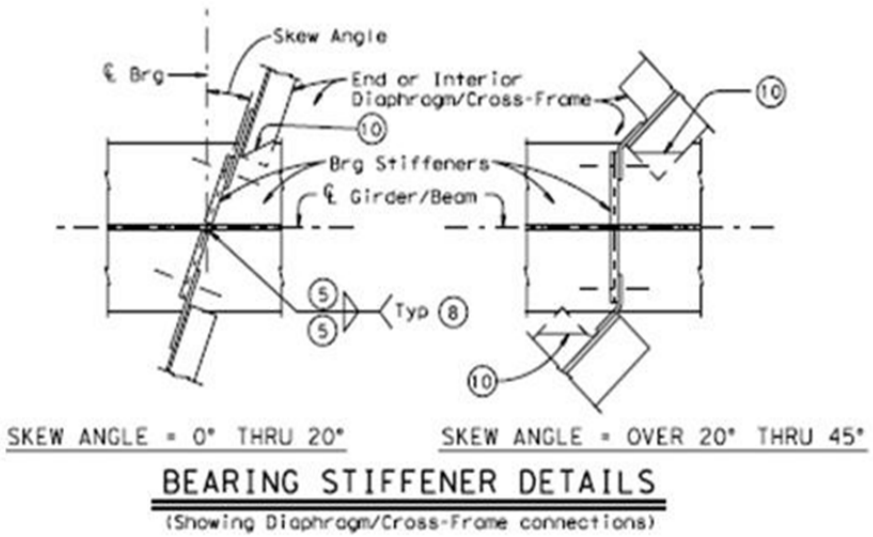

Figure 2.12: TxDOT standard skewed cross-frame connection (from SGMD sheet 1)

However, fabricators have used other connection details successfully. One of the most common departures from the standard plans is to use separate cross-frame connection plates and bearing stiffeners (Figure 2.13) so the cross-frame forces are collinear.

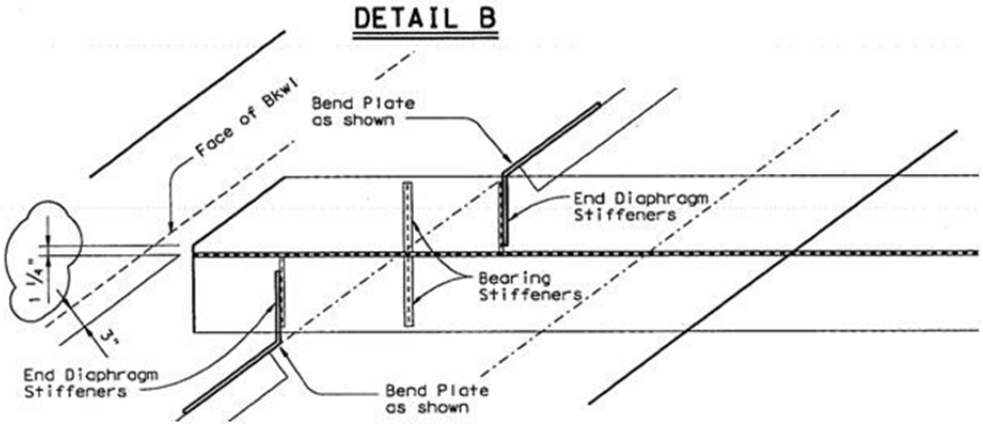

Figure 2.13: Cross-frame connection for US 82 at 9th St. underpass Lubbock, TX

In addition to using bent plates to account for the bridge skew angle, additional connections such as those utilizing pipes for the web stiffeners have been tried (Figure 2.14 and Figure 2.15). The pipe stiffener allows a connection plate to be welded at any angle thereby standardizing the connection no matter what the skew angle. It can also provide warping restraint as previously described in this chapter.

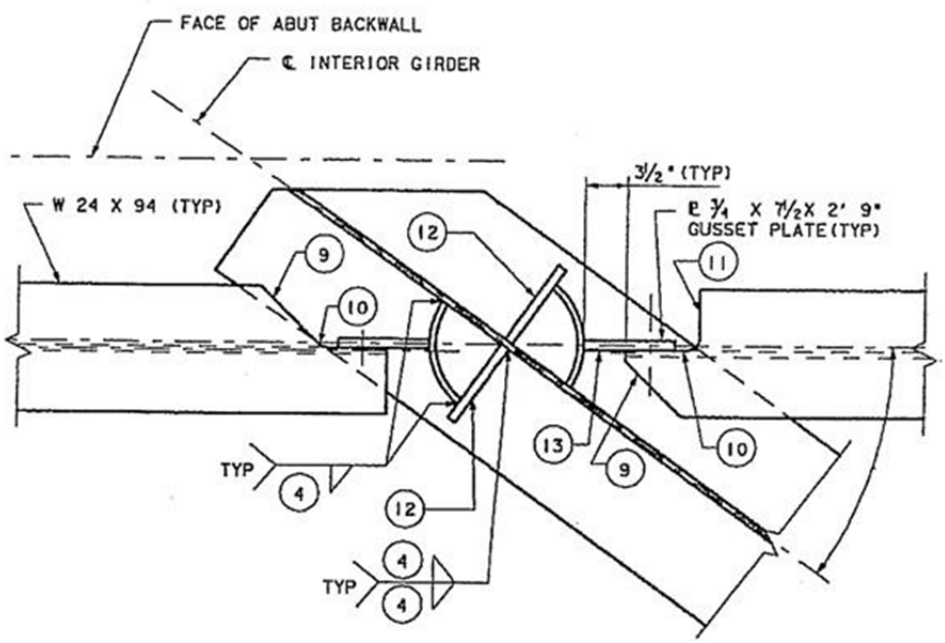

Figure 2.14: Quarter pipe end cross-frame connection

Figure 2.15: Full pipe end cross-frame connection

2.10 Background Summary

This chapter has described the current state of research and code provisions for skewed steel girder bridge bracing. Most of this research has focused on intermediate cross-frame bracing perpendicular and parallel to the bridge skew angle. The past research also assumes a rigid connection between the cross-frame and girder and that the girder ends are free to warp and

do not twist. These assumptions have been adopted into the current codes and standard practices outlined in this chapter.

In Chapter 3 (Experimental Program), several series of connection and large scale experiments will be described that tested the impact of these assumptions on girder buckling strength, end twist and cross-frame forces. These experimental results will then be used to validate the finite element modeling techniques developed in Chapter 4 (Finite Element Modeling), and in Chapter 5 (Parametric Studies and Design Guidance) the validated model will be used in several parametric studies to extend the experimental results. Additionally Chapter 6 describes pipe stiffener fatigue test results comparing the pipe stiffener to the currently used plate stiffener detail.

Chapter 3. Experimental Program

3.1 Introduction

The experimental program consisted of three different series of laboratory tests. First, small scale connection testing was performed for the bent plate and split pipe stiffener connections. Next, a fatigue test was run on several split pipe and plate stiffeners to compare the fatigue performance of each. Then, large scale buckling and lateral load tests were performed on various girder systems using plate and split pipe stiffeners at the supports. The buckling tests were conducted on single, twin, and three girder systems. In addition to varying the connection details at the end cross-frames, intermediate cross-frame details and support conditions were also considered.

The primary purpose of the small and large scale tests was to validate the finite element modeling techniques used in the parametric studies. Additionally, each specimen was compared to the others to show the impact of the varying parameters in the laboratory tests. These comparisons are described in this chapter. A discussion of the validation of the finite element model using the laboratory results is provided in Chapter 4.

This chapter will not discuss the fatigue study. Instead, the fatigue test setup and results, along with finite element analysis with respect to fatigue will be presented in Chapter 6 of this report for the wholeness of this topic.

3.2 Connection Testing

The small-scale connection testing program is covered in detail in a related research report (Battistini 2009). The key results and conclusions are summarized here.

2.10.1 Small Scale Connection Test Setup

The connection test frame with a bent plate connection assembly is shown in Figure 3.1. The test frame was designed to accept a W135x55 girder segment with a bent plate or split pipe stiffener connection assembly at skew angles of 0°, 15°, 30°, 45°, or 60°. Once in the frame, a loading ram was used to deliver a tension load to a single angle attached to the connection assembly.

2.10.2 Connection Specimens

There were six different bent plate specimens tested with differing skew angles and bend radii and two split pipe stiffeners tested with different skew angles. The bent plates were 5/16" thick and the pipe had a 10.75" outside diameter with a 0.34" wall thickness. Each connection assembly was welded to a W135x55 girder segment. Four of the bent plate specimens are shown in Figure 3.2 and the 45° split pipe specimen is shown in Figure 3.3. The specimens tested are summarized in Table 3.1.

Figure 3.1: Small scale test set up—south (left) and east (right)

Figure 3.2: Bent plate connection specimens

Figure 3.3: 45° Split pipe connection specimen

Table 3.1 Small scale test specimens

Connection	Skew Angle	Bend Radius
Bent Plate	15°	0.50"
Bent Plate	30°	0.84"
Bent Plate	45°	0.59"
Bent Plate	45°	0.94"
Bent Plate	45°	2.41"
Bent Plate	60°	0.63"
Split pipe	0°	N/A
Split pipe	45°	N/A

During the test, a tension load was applied to each specimen and the lateral and vertical deflections of the bent plate and split pipe connection plate were measured so the deflections could be used to validate the finite element model of each connection. The results were also directly compared and some key conclusions were made based on the laboratory tests. In each of the graphs shown below, the error bars show the minimum and maximum values for each test while the line plotted is the average value.

2.10.3 Connection Testing Key Results

The results of the vertical and lateral deflections measured at the top of bent plate specimens top are shown in Figure 3.4 and Figure 3.5, respectively. The 45° skew specimen data shown are for the 0.59" bend radius. The vertical deflection results clearly show that despite the varying bend radius, larger skew angles increase the plate flexibility. These results are not quite as clear for the lateral deflection data due to the small deflections of the 45° specimen. The reasons for these small deflections were a result of the specimen imperfection, relatively small bend radius, and ram offset in the test frame. These anomolies are explained in the previously mentioned research report (Battistini 2009). However, all other specimens show that similar to the vertical deflection, larger skew angles resulted in an increase in lateral deflection. Finally, the larger variability in the 30° specimen was due to not carefully aligning the loading ram, connection clevis and specimen. These were the first tests run and initially it was thought that the applied load would align the ram, clevis, and specimen, but the friction between the parts did allow some small offset. In subsequent tests this condition was monitored more closely to ensure the proper alignment occurred, resulting in less variablity in the data.

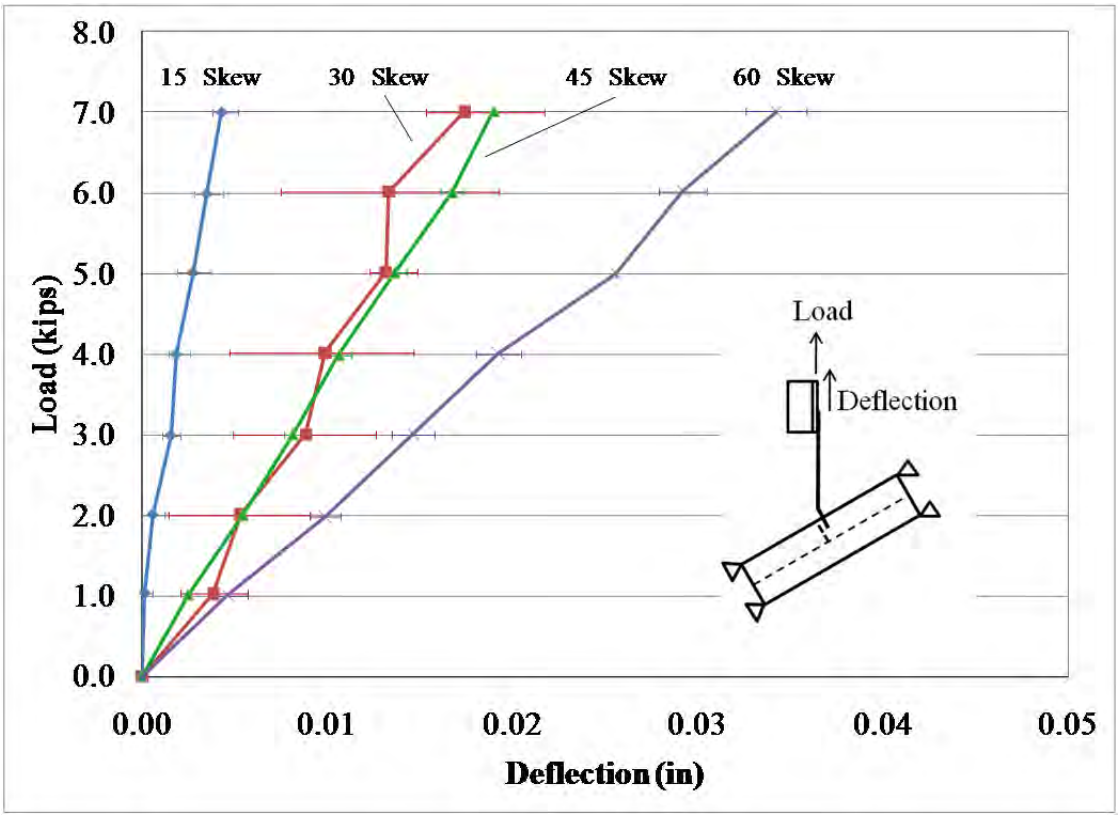

Figure 3.4: Bent plate top vertical deflection

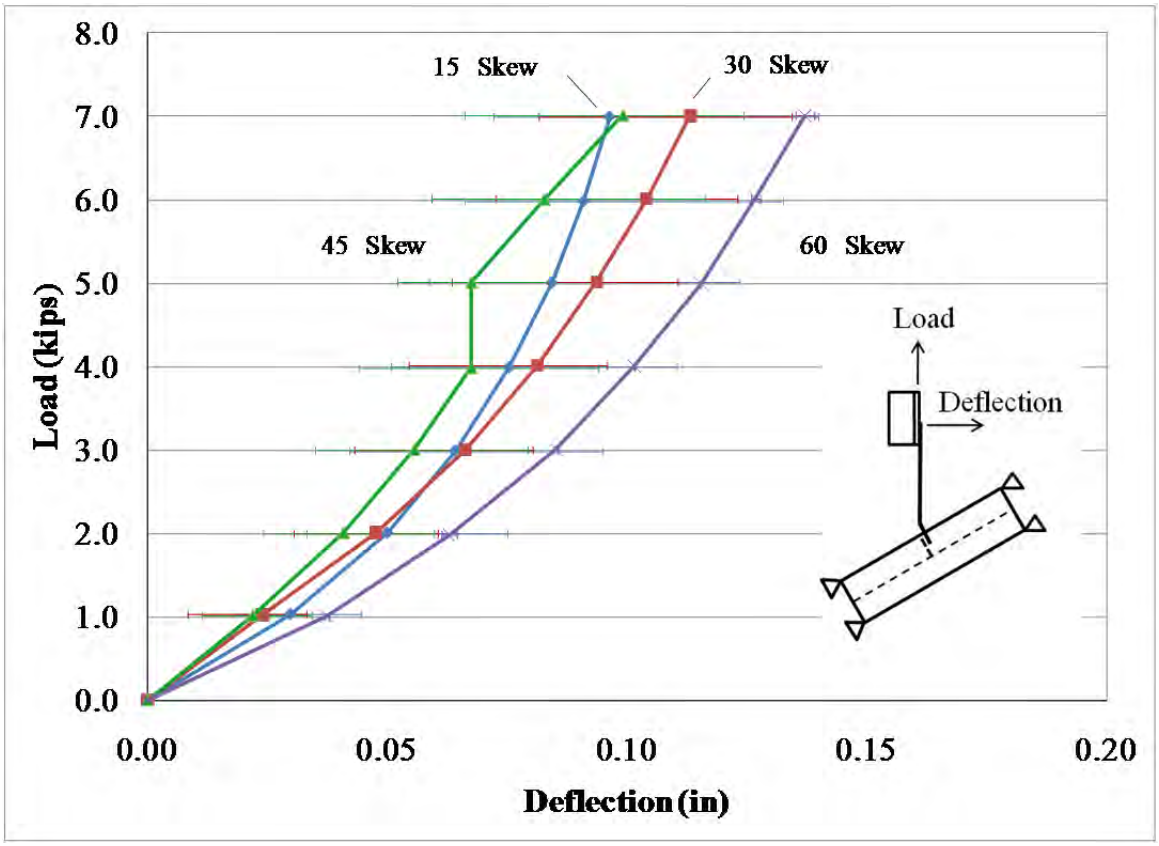

Figure 3.5: Bent plate top lateral deflection

The impact of the bend radii on the vertical deflection for the 45° specimens is shown in Figure 3.6 and Figure 3.7. The specimens with the larger bend radius had larger axial deflections for a given load level. Therefore, in addition to the impact of skew angle on the stiffness of the plate, the bend radius also affects the plate axial flexibility. The lateral deflection results do not show this same pattern as the 2.41" radius specimen deflects less than the 0.94" radius specimen as shown in Figure 3.7. It was unclear whether this difference was due to the previously mentioned anomalies in the specimen and test setup or if it was a result of the difference in bend radius.

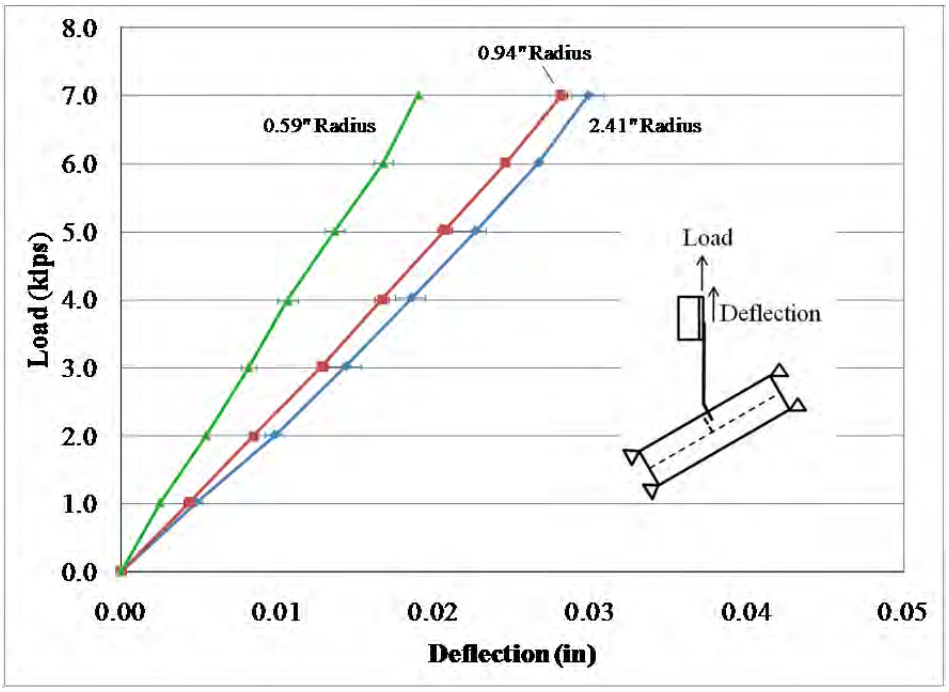

Figure 3.6: 45° skew bent plate vertical deflection

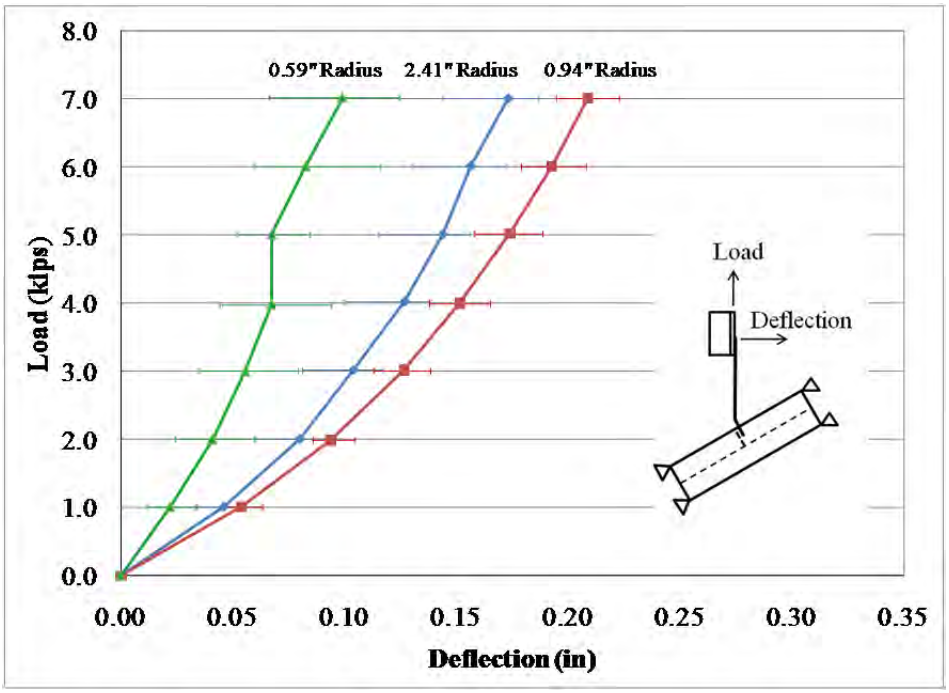

Figure 3.7: 45° skew bent plate lateral deflection

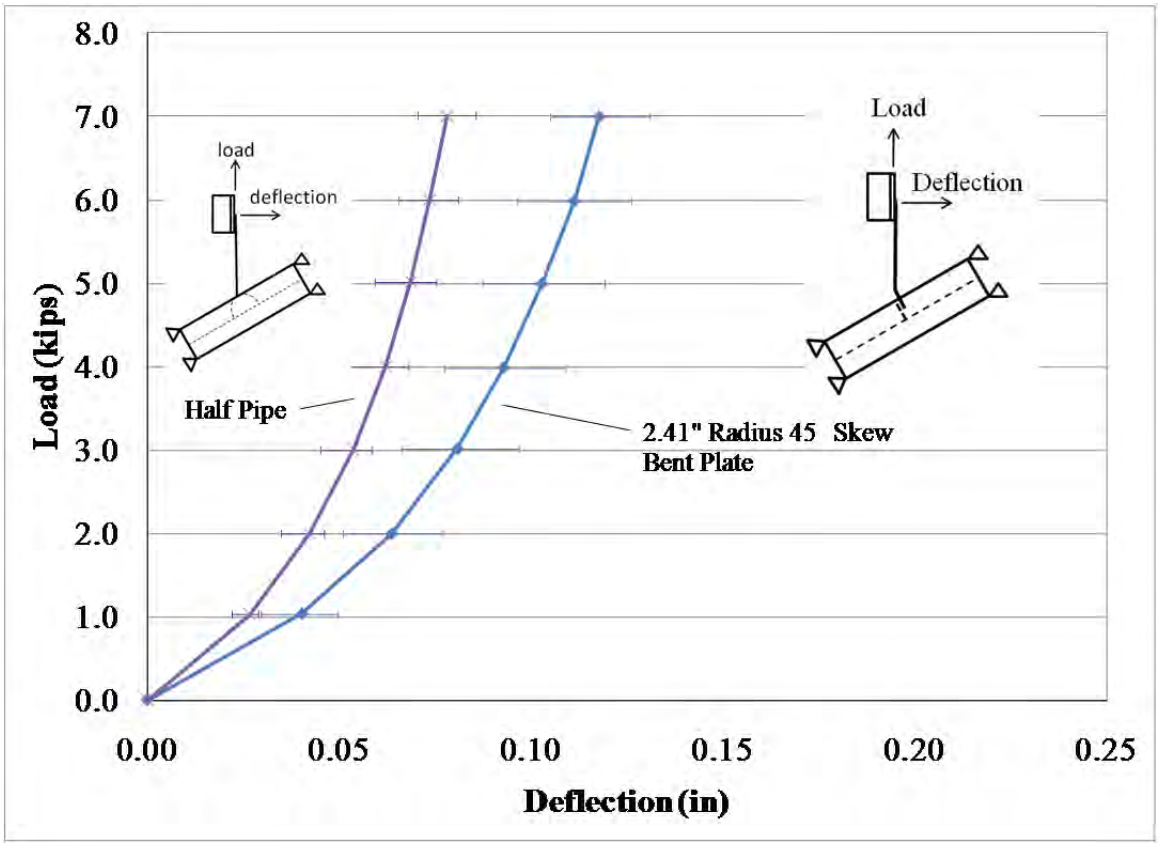

Figure 3.8: 45° skew lateral deflection comparison

The comparison between the 45° skew bent plate and split pipe stiffener connection are shown in Figure 3.8. From the figure it can be seen that the split pipe specimen had significantly smaller deflections than the bent plate detail. The results shown are typical of all of the bent plate and split pipe stiffener tests that were conducted. The difference between the bent plate and split pipe stiffener vertical deflections were found to be negligible. The tests showed that the split pipe stiffeners were stiffer than the bent plate details and that the difference in the stiffness increased with larger skew angles.

3.3 Large Scale Testing

The large scale testing program consisted of single, two, and three girder tests. The purpose of the testing was to validate the finite element modeling as well as compare the performance of the split pipe stiffener and bent plate connection under a variety of support and bracing conditions.

2.10.4 Single and Twin Girder Testing

The purpose of the tests on the single and twin girder systems was to validate the finite element modeling of the girder as well as the plate and split pipe bearing stiffeners. Additionally, the tests were used to measure the impact of the split pipe stiffener warping resistance on the girder buckling strength.

3.3.1.1 Single and Twin Girder Testing Program

Four total girders were tested in two pairs. The first girder pair had plate bearing stiffeners as shown in Figure 3.9. These two girders were named Girder Bent Plate (GBP) 1 and 2. The second girder pair had split pipe bearing stiffeners as shown in Figure 3.10 and were named Girder Split Pipe (GSP) 1 and 2. A plan view of the whole test specimen is shown in Figure 3.11. A picture of a typical twin girder buckling test setup is shown in Figure 3.12.

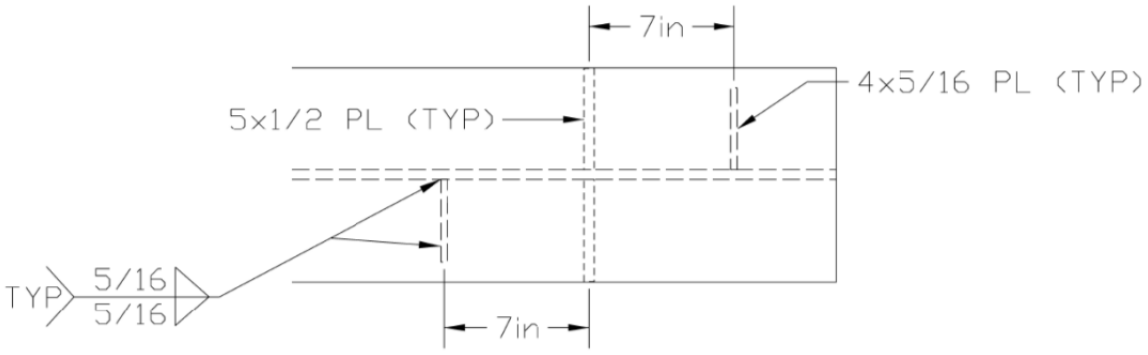

Figure 3.9: Bent plate connection plate stiffener detail

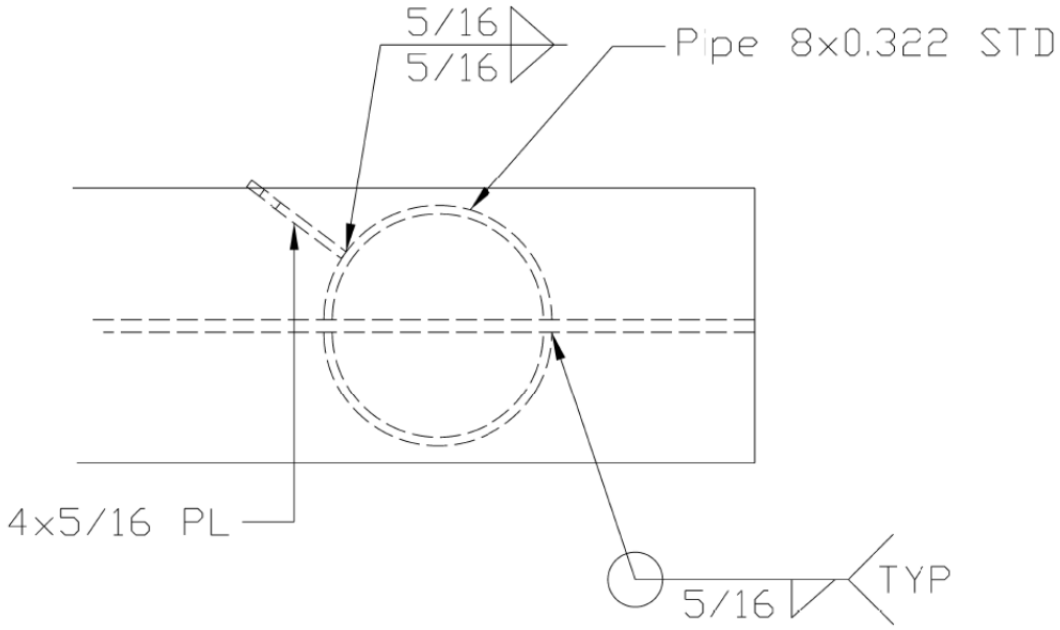

Figure 3.10: Split pipe stiffener connection detail

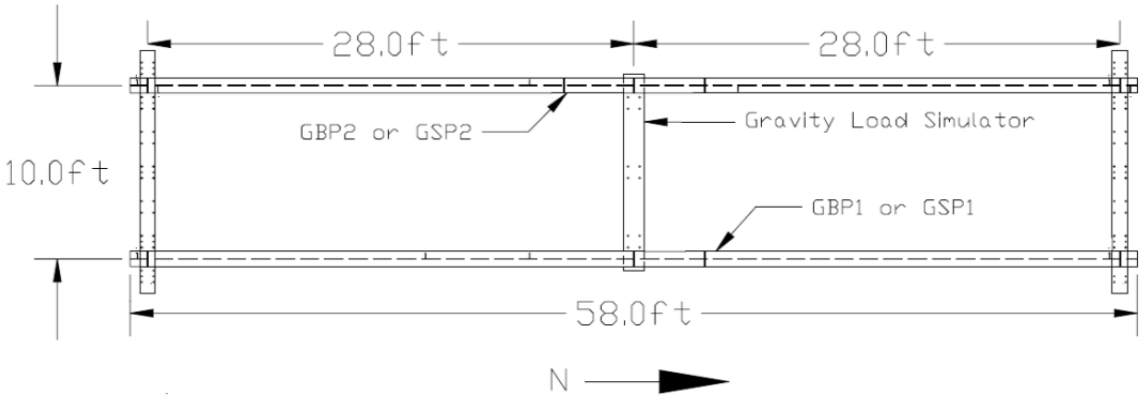

Figure 3.11: Twin girder test specimen plan view (plate stiffened specimen shown)

Figure 3.12: GBP1 and GBP2 in the twin girder buckling test frame (looking north)

In addition to the basic tests used to measure the girders buckling strength and strong axis flexural resistance, tests were conducted with lateral loads applied to gain a measure of the lateral and torsional stiffness of the girder system. The lateral loads were applied with and without vertical loads to assess the degree of restraint that may have been provided by the gravity load simulator. Additionally, a series of lateral and torsional tests were run on GBP2 and GSP2 individually to compare with the twin girder lateral and torsional tests. A summary of all twin and single girder testing is provided in Table 3.2.

Table 3.2 Single and twin girder tests

Girders Tested	Test Type	Number of Tests
GSP1 and 2	Buckling	2
GSP1 and 2	Lateral With No Vertical Load	2
GSP1 and 2	Lateral With 2k Vertical Load	2
GSP1 and 2	Lateral Eccentric With 2k Vertical Load	2
GSP2	Lateral With No Vertical Load	2
GSP2	Lateral Eccentric With No Vertical Load	2
GBP1 and 2	Buckling	2
GBP1 and 2	Lateral With No Vertical Load	2
GBP1 and 2	Lateral With 2k Vertical Load	2
GBP1 and 2	Lateral Eccentric With 2k Vertical Load	2
GBP2	Lateral With No Vertical Load	2
GBP2	Lateral Eccentric With No Vertical Load	2

3.3.1.2 Specimen Fabrication

Each specimen was fabricated from a 58' long W30x90 girder. The span length was 56' with a 1' overhang on each end. The plate bearing and load point stiffeners were fabricated from 5"x1/2" plate and all connection plates were fabricated from 4"x5/16" plate. All welds used to connect the plates were 5/16" fillet welds. The connection plates for the end and intermediate cross-frame connection locations were welded to the girders prior to the twin girder tests in anticipation of the three girder tests when cross-frames were to be installed.

Split Pipe Stiffener Fabrication

The split pipe stiffener detail is shown in Figure 3.10. The split pipe stiffener was fabricated at Ferguson Structural Laboratory from a standard 8" x 0.322" pipe purchased from a local pipe supplier. For larger skew angles and smaller pipe diameters, the connection plate will be very near the girder web making the web side weld difficult if not done prior to attaching the pipe to the girder. Each connection plate was positioned so the cross-frame would overlap the connection plate on the side away from the girder web, again to ensure weld access for future cross-frame connection.

Fabricating the split pipe stiffener consisted of splitting the pipe in half with a track torch, saw cutting the pipe to length, grinding it to fit, then welding the connection plate to the pipe, and finally welding the pipe to the girder. The following figures show the key steps in this process.

Figure 3.13 shows the pipe splitting process. To prevent the pipe from expanding after cutting the first side, the torch was started before the beginning of the pipe and ended prior to the end of the pipe leaving a short uncut portion on each end of the pipe (as seen on the left pipe in Figure 3.13). The pipe was then rotated 180° and the opposite side was then completely split with the torch (as seen on the right pipe in Figure 3.13). Finally the pipe was rotated again and the first cut was completed to sever the pipe into two halves. This process kept the cuts even and maintained a uniform cross section throughout the pipe length after the cuts were completed.

Figure 3.13: Splitting the pipe stiffener with a track torch

Figure 3.14 shows a completed split pipe with connection plate prepared for welding to the girder. To achieve the appropriate fit, each split pipe was ground to match the fillet area of the girder. This process usually took less than one-half hour for each split pipe. During welding, the girder was rotated so each weld could be made in the horizontal position. Each split pipe was welded by hand with a continuous feed welder and took approximately 20 minutes of welding time (not including time to rotate the girder). All welds were 5/16" fillet welds based on the typical weld size specified by TxDOT to connect cross-frames to girders (Texas Department of Transportation 2006).

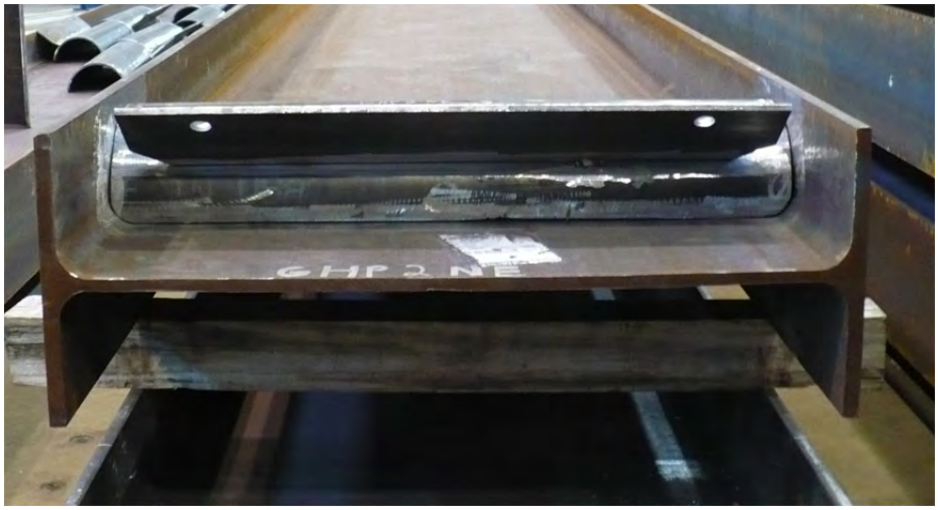

Figure 3.14: Split pipe stiffener prepared for welding

Plate Stiffener Fabrication

The plate stiffener detail is shown in Figure 3.9. The detail consists of four plates. The two offset plates are for the bent plate cross-frame connections and the central plates are the bearing stiffeners. While TxDOT allows the bearing stiffener to be used as the bent plate cross-frame connection plate, most Texas fabricators prefer to offset the cross-frame connection plates to align the cross-frame forces. Therefore, this method was selected for the test specimens. The amount of connection plate offset is determined by the skew angle and distance between adjacent girders. Figure 3.9 shows the detail for a 53° skew with approximately 7" between the bearing stiffeners and cross-frame connection plates.

3.3.1.3 Twin and Single Girder Test Frame Setup

An end view of the test setup prior to testing was shown in Figure 3.12. Figure 3.15 shows the twin girder test frame during a buckling test. The test setup used for all single and twin girder tests was essentially the same. Only the method of load application differed between the lateral load tests and the buckling tests. The basic boundary conditions used were simple supports with no twist and unrestrained warping at the girder ends. Vertical loads were delivered via a gravity load simulator while lateral loads were imparted using a rod and turnbuckle system. The following sections describe these aspects of the test setup.

Figure 3.15: Twin girder buckling test (looking north)

Test Frame Boundary Conditions

The wide flange sections shown in Figure 3.12 that were used to support the girders provide a good model of simply supported conditions because the web flexibility of the supports allows movement in the longitudinal direction of the girders. The girders rested on 4" diameter thrust washers as shown in Figure 3.16, to minimize warping restraint. The thrust washer allows the girder flange to rotate in its strong plane, but because it has a small diameter relative to the flange width, it provides only modest tipping restraint.

To prevent twist at the girder ends, threaded rods were used on both sides of the top and bottom flange. After the girders were set in place, the rods were advanced until they came into contact with the flanges. The rods were then adjusted to plumb the girder ends prior to testing. The ends of the rods in contact with the girder flanges were rounded to minimize any warping restraint they may have provided to the girder. Figure 3.17 shows the threaded rods prior to plumbing the girders (note the top rod is not yet in contact with the left flange) and the thrust washer bearing at the south end of GBP1.

Figure 3.16: Thrust washer bearing

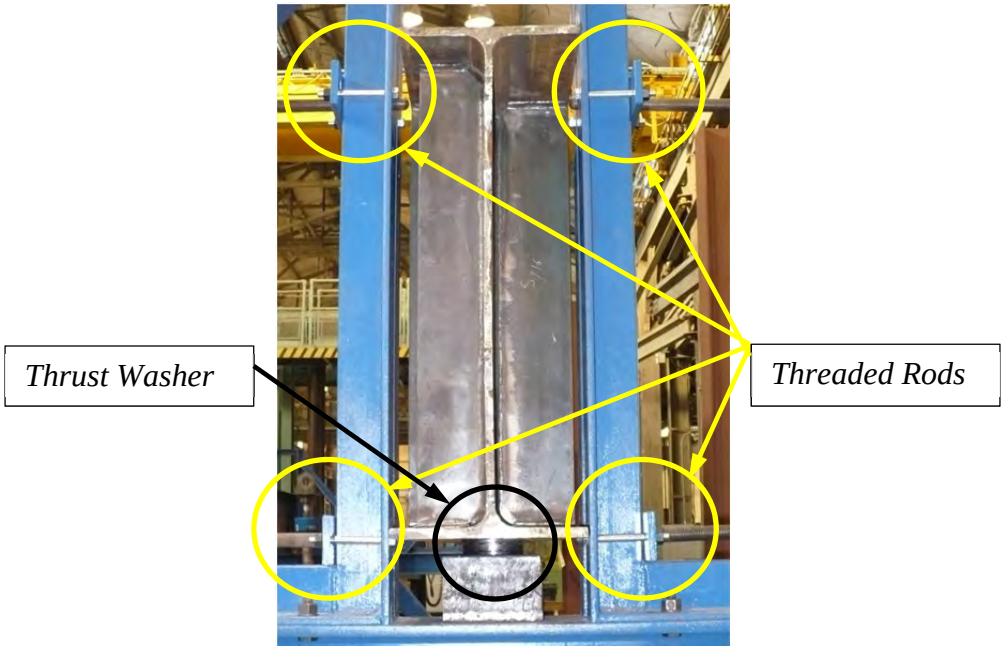

Figure 3.17: Threaded rods and thrust washer

Load Application

The vertical loads were applied via a gravity load simulator as shown in Figure 3.18. The gravity load simulator delivers load and then translates with the specimens as they buckle in order to keep the applied load vertical. In doing so, the gravity load simulator does not impart a restoring force on the specimen and should therefore not add any stability to the specimens. The displacement of the gravity load simulator while the loading ram maintains its vertical orientation is evident in Figure 3.18. More information about the gravity load simulator may be found in Yarimici, et al. (1966).

In the twin girder buckling tests, the gravity load simulator was centered between the beams, so its total load was delivered evenly to the two specimens and was measured via a load cell positioned between the loading ram and load beam. Because the gravity load simulator is a mechanism, two adjustable struts are used to keep the apparatus stable with no load is applied. Once load is applied to the beams, the gravity load simulator displaces laterally with the girder. In the buckling tests, the gravity load simulator was loaded with 1 kip prior to the removal of the lateral stops. This procedure allowed the simulator to remain stable until enough friction developed between the knife edges and the top flanges of the beams to essentially link the apparatus to the beams.

Figure 3.18: Gravity load simulator applying vertical load (looking south)

The concentrated load from the gravity load simulator was delivered to each specimen at its mid-span through a knife edge. A thrust washer was placed between the knife edge and the loading beam to minimize warping restraint from the point of load contact. The use of the knife edge minimized any torsional restraint provided to the girder from the load point. This assembly was loosely held in place by four bolts which acted to prevent the knife edge from shifting under low loads, but still allowed the loading assembly to rotate as required. Figure 3.19 shows a picture of the knife edge and thrust washer assembly.

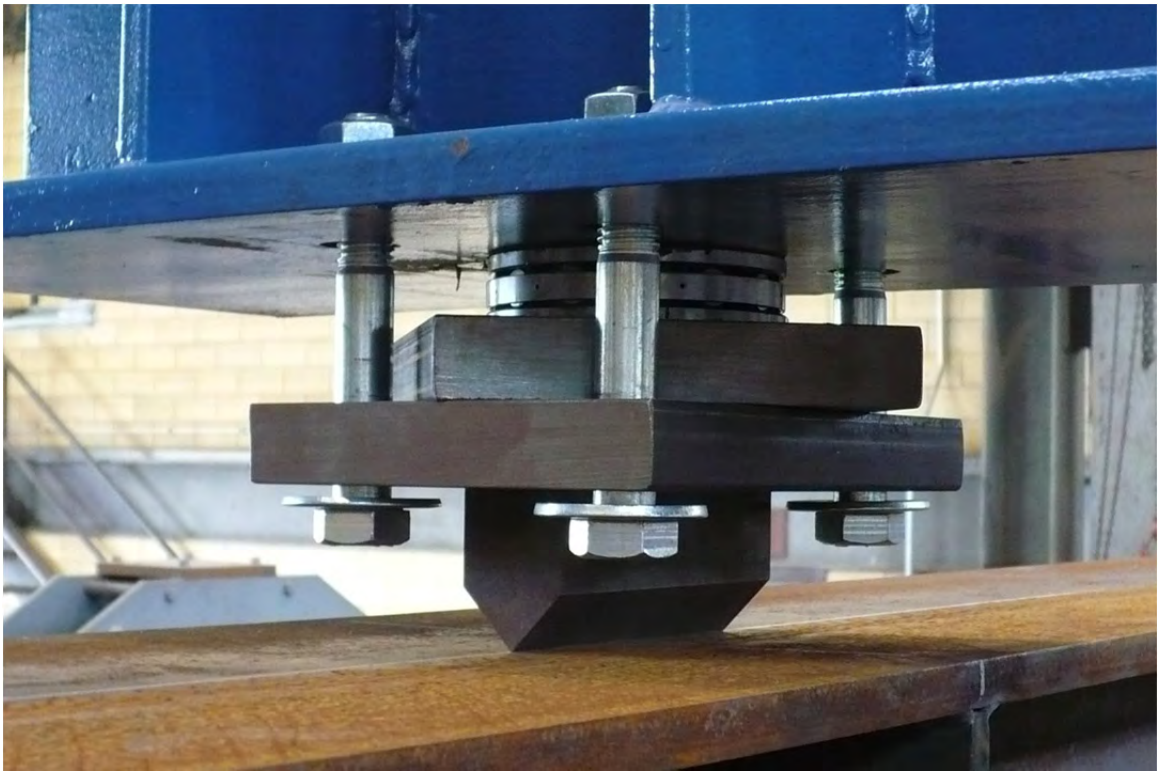

Figure 3.19: Knife edge and thrust washer assembly

The loads for the lateral load tests were applied to the mid-span of girders GBP2 and GSP2 (the western girders). Two load positions on the cross section were used. In the first case, the load was applied at the cross section mid-height, while in the second case, the load was applied at 25.75" above the centroid of the bottom flange (a point just below the top flange). The first load case resulted in weak axis bending while the second case resulted in bending and twisting. The loads were delivered via a turnbuckle and rod system shown in Figure 3.20. As the turnbuckle was rotated by hand, the lateral load on the girder increased and was read by a load cell reacting against the web of the reaction column.

Strain and Deflection Measurements

Strain gages, string potentiometers, linear potentiometers, and tilt sensors were used to gather specimen data. Measurements were taken at mid-span, and the ends of the girders were also instrumented to monitor the twist and lateral deformations. Although the supports are assumed to rigidly prevent lateral deformation and twist, the effects of realistic support details on the deformational behavior at the supports was of interest in the project.

Figure 3.20: Torsional load test turnbuckle loading system

Buckling Test Measurements

At girder mid-span, four strain gages, one at each flange edge, were used so that flange bending stresses could be calculated. This also allowed the calculation of load delivered to each girder to check that the gravity load simulator was delivering the same load to each girder. Additionally at mid-span, the top and bottom flange lateral deflections were measured using 6" linear potentiometers. This data was used to monitor mid-span deflections and to calculate the girder mid-span twist. The calculated twist was checked by a tilt sensor that was mounted to the mid-depth of the web at the girder mid-span. Finally a 4" linear potentiometer was mounted below the girder bottom flange to measure vertical deflection. In order to minimize friction between the linear potentiometers and the specimen, glass or Teflon plates were mounted to the specimen to ensure the specimen deformations did not disturb the alignment of the linear potentiometer.

Girder end twist was monitored by measuring the top and bottom flange lateral translations. The top flanges were instrumented with string potentiometers while the bottom flanges were instrumented with 2" linear potentiometers. No significant end twist was detected during any of the testing when the end brackets were used. When cross-frames were used on the three girder systems, deformation at the supports did occur.

Lateral Load Test Measurements

During the lateral load testing, girder twist and lateral translations were measured at mid-span. Also, as in the buckling tests, the girder ends were monitored for twist. The lateral translations were measured using a linear potentiometer at mid-height of the cross section, and twist was measured at the same location using a tilt sensor. This instrumentation configuration is shown in Figure 3.21.

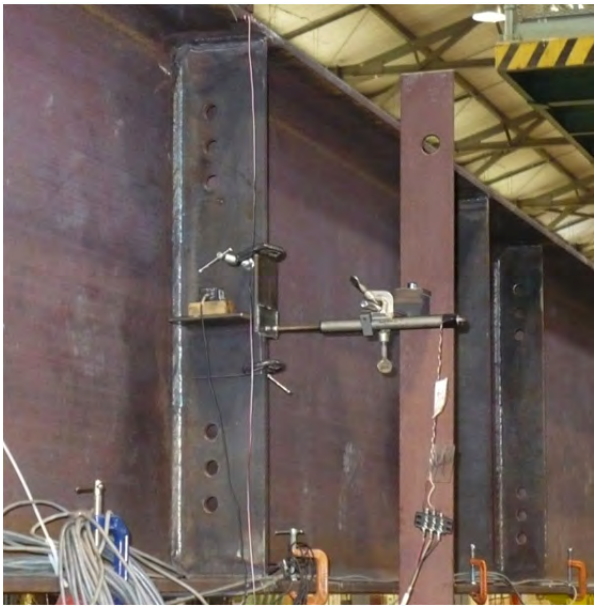

Figure 3.21 Lateral load test instrumentation

Initial Imperfection Measurements

To model the girder buckling behavior, an initial imperfection measurement was taken for each specimen. To capture both the initial twist and sweep of the girder, the lateral deviations from the girder bottom flange end points were measured for both sides of the top and bottom flanges. The two side measurements for each flange were then averaged to arrive at the initial imperfection for each flange.

Figure 3.22 shows the calculations used to arrive at the initial imperfections on the east and west side of the girders. The reference line used to measure the flange imperfections was a music wire strung along each side of the girder's bottom flange. The wire passed over threaded rods clamped to the ends of the girder. Weights were hung from the wire to keep it taut during the measurements. The bottom flange deviations from the wire (d_{BFLW} and d_{BFLE}) were measured directly using calipers. A plumb bob and calipers were then used to measure the deviation of the top flange from the bottom flange of the girder ($d_{TFLW\text{-}BFLW}$ and $d_{TFLE\text{-}BFLE}$). The top flange deviations (d_{TFLW} and d_{TFLE}) were then calculated as shown in Figure 3.22. After the top and bottom flange deviations were measured and calculated, they were linearly adjusted to account for the offset in the wire from each end of the girder. Graphs of the initial imperfections used during testing can be found in Appendix A (Large Scale Experimental Results).

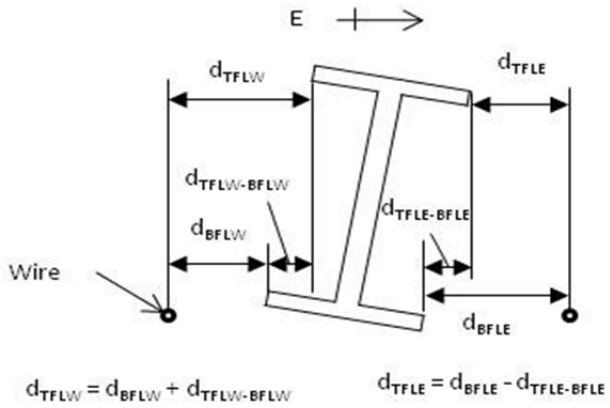

Figure 3.22: Initial imperfection calculations

3.3.1.4 Single and Twin Girder Test Results

Single girder testing consisted of lateral load tests, while the twin girder tests consisted of both lateral load tests and buckling tests as listed in Table 3.2. The results for each of these tests are reported below. Each of the laboratory results are depicted by a series of error bars showing the minimum, average, and maximum values at the reported load levels for each of the two tests. Where analytic solutions are available they are plotted with dotted lines. Where no analytical solutions exist, the average of each test specimen is plotted with a solid line.

Single Girder Lateral and Torsional Test Results

A picture of a typical single girder lateral load test is shown in Figure 3.23. The results of the lateral load tests for the plate stiffened girder (GBP2) and split pipe stiffened girder (GSP2) are shown in Figure 3.24.

Figure 3.23: Typical single girder lateral load test

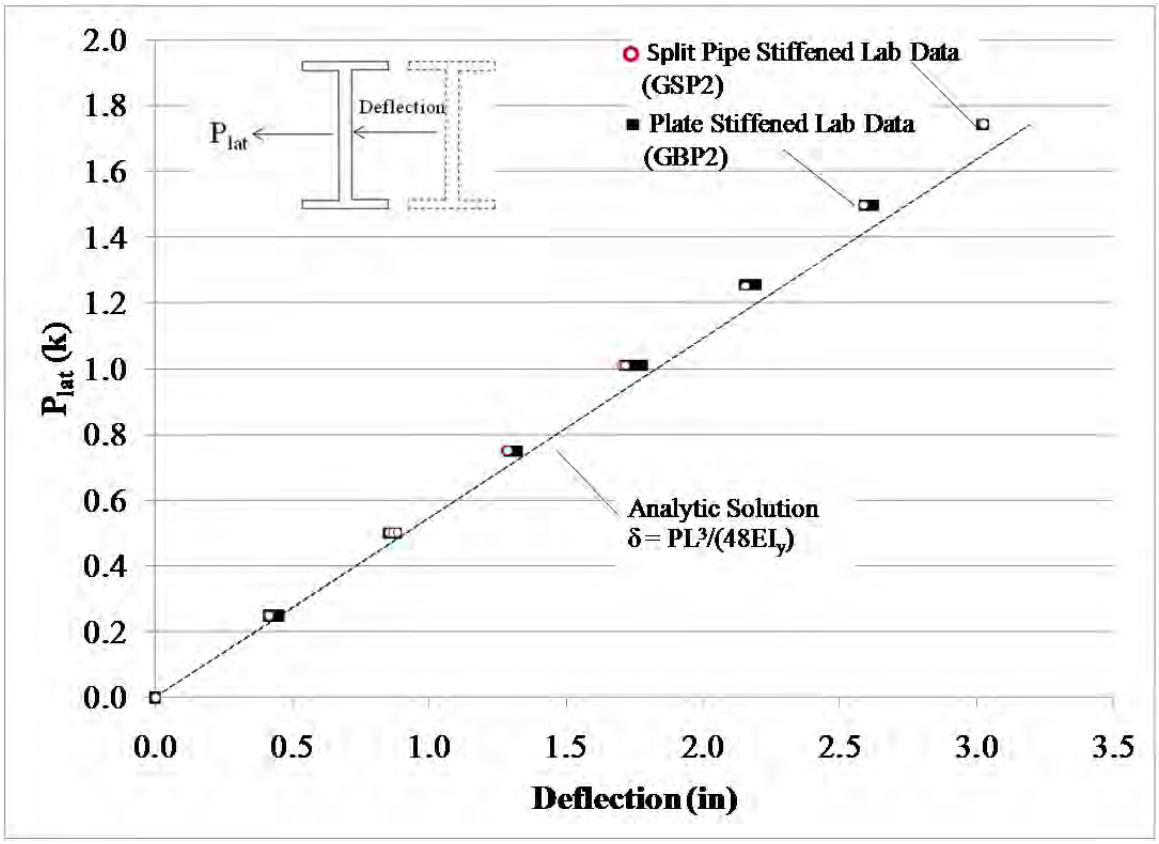

Figure 3.24: Single girder lateral load test results

From Figure 3.24 it can be seen that there is negligible difference between the plate and split pipe stiffened girder lateral stiffness. This is to be expected as both the top and bottom flanges rotate the same amount at their ends during the test causing the stiffeners to undergo only a rigid body rotation (no twist). Therefore the type of stiffener does not change the girder's behavior. When compared to the analytic solution, both girders appear to be stiffer by a small amount. The most likely reason is the friction generated between the threaded rods at the girder ends. As the lateral load increases, the friction between the girder flanges and the threaded rods increase which adds restraint to the girders.

The results for the lateral load tests with the eccentric load are shown in Figure 3.25. From the figure it can be seen that the split pipe stiffened girder (GSP2) is nearly 50% stiffer than the plate stiffened girder. This is due to the warping restraint provided by the split pipe. The variability in the plate stiffened data was due to the tilt sensor registering the vibrations of the turnbuckle being hand tightened. Because the data was gathered continuously, it was being recorded as the turnbuckle was being turned to increase the load. This procedure was changed to record data discretely during the split pipe stiffened data gathering so the specimen was static during data collection. This resulted in a much smaller variability in the split pipe stiffened specimen data.

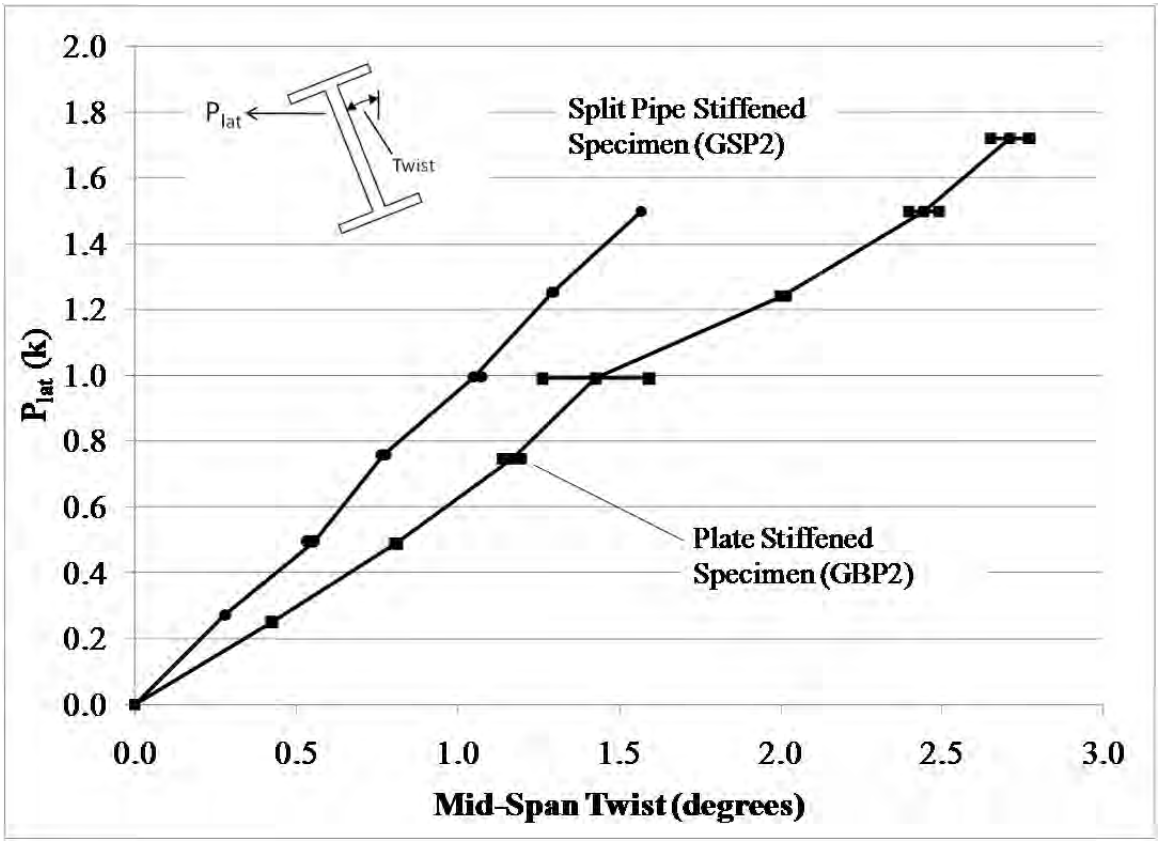

Figure 3.25: Single girder torsional test results

Twin Girder Lateral and Torsional Test Results

The twin girder lateral load tests were conducted with and without vertical loads applied by the gravity load simulator. For the twin girder lateral tests, flexible single angle members were clamped to each girder's top and bottom flange so the lateral load applied through a turn buckle on one side of the test setup was distributed to both girders. A picture of the typical test set up with vertical load is shown in Figure 3.26.

A gravity load of two kips was applied to the two girders. A comparison of the systems with and without applied vertical loads for the plate stiffened girders is shown in Figure 3.27. These results show that the presence of the gravity load simulator and vertical load does not add any significant lateral stiffness to the system.

Figure 3.26: Twin girder lateral load test under vertical load

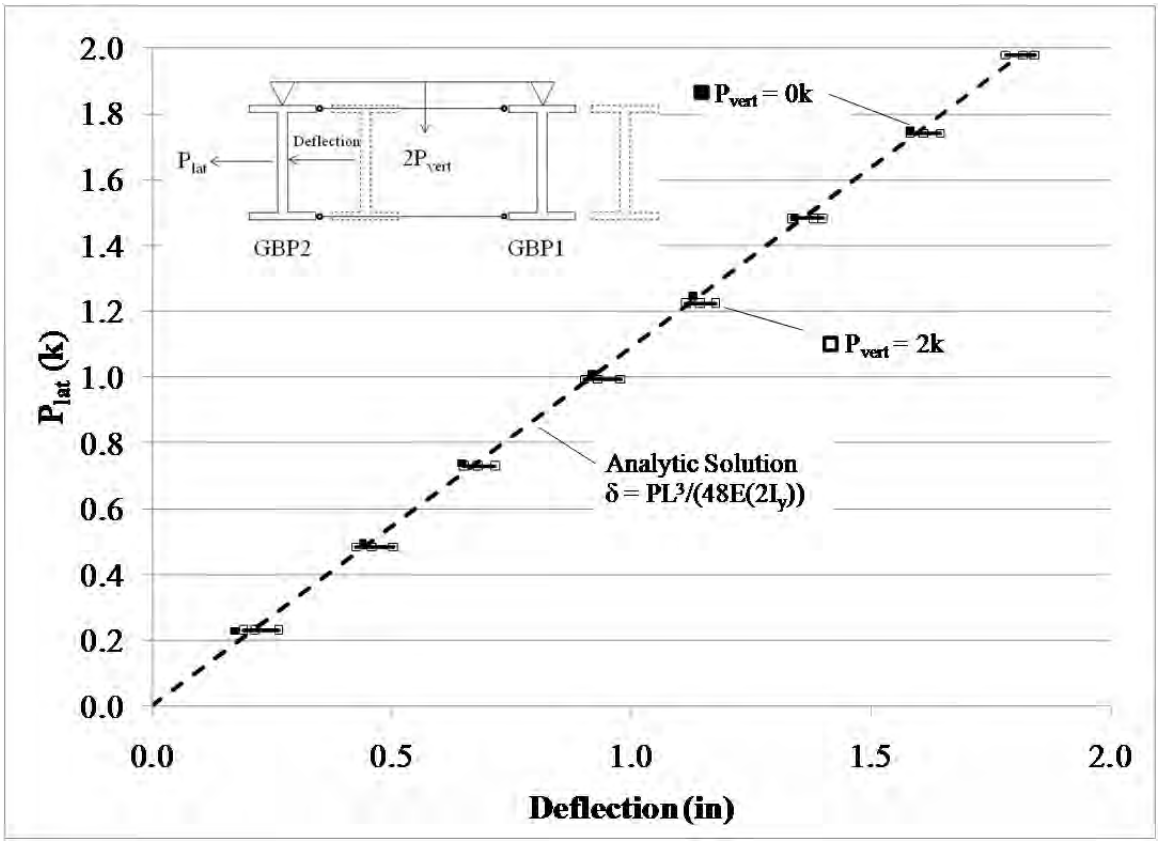

Figure 3.27: Plate stiffened twin girder lateral load test mid-span results

The data for the split pipe stiffened girders with and without vertical load is shown in Figure 3.28. These results show that under vertical load, the split pipe stiffened section is about 17% stiffer than under no vertical load. This goes against expectations because the presence of the compressive stresses associated with the strong axis bending moment would tend to reduce the stiffness of the girders. In this case, the effect on the stiffness would be very small because the applied load was less than 11% of the buckling capacity. One possible reason for the larger stiffness has to do with the initial twist of GSP2. It is the only girder in the tests that has a twist in the direction of the applied lateral load. Therefore when vertical load is applied, it will begin to displace laterally in this direction giving it a larger initial imperfection in the lateral load direction and increase the reaction against the threaded rods. The increased reaction will increase the friction between the girder and the lateral supports and stiffen the system resulting in the higher stiffness seen in Figure 3.28.

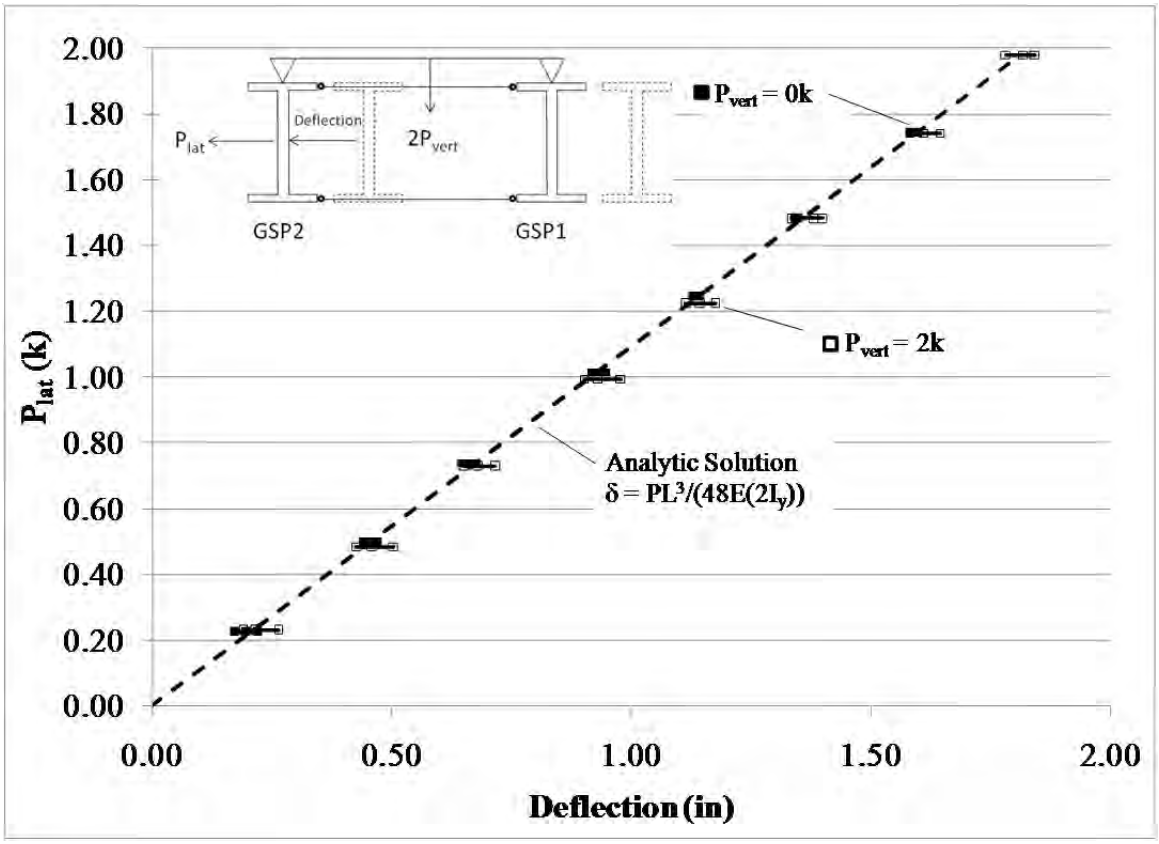

Figure 3.28: Split pipe stiffened twin girder lateral load test results

The eccentric lateral load tests on the twin girders were conducted with two kips of vertical load on each girder. Additionally, the single angles fastened to the girder flanges in the lateral tests were removed so they would not act as torsional restraints between the girders. The results for these tests are shown in Figure 3.29.

The variability in the plate stiffened data was caused by the tilt sensor reading data continuously during the manual turning of the turnbuckle (the same issue as in the single girder torsional test). This procedure was corrected during the split pipe stiffener specimen data collection resulting in a much smaller variability. As with the single girder torsional test, the split pipe stiffened girders are over 70% torsionally stiffer than the plate stiffened girders.

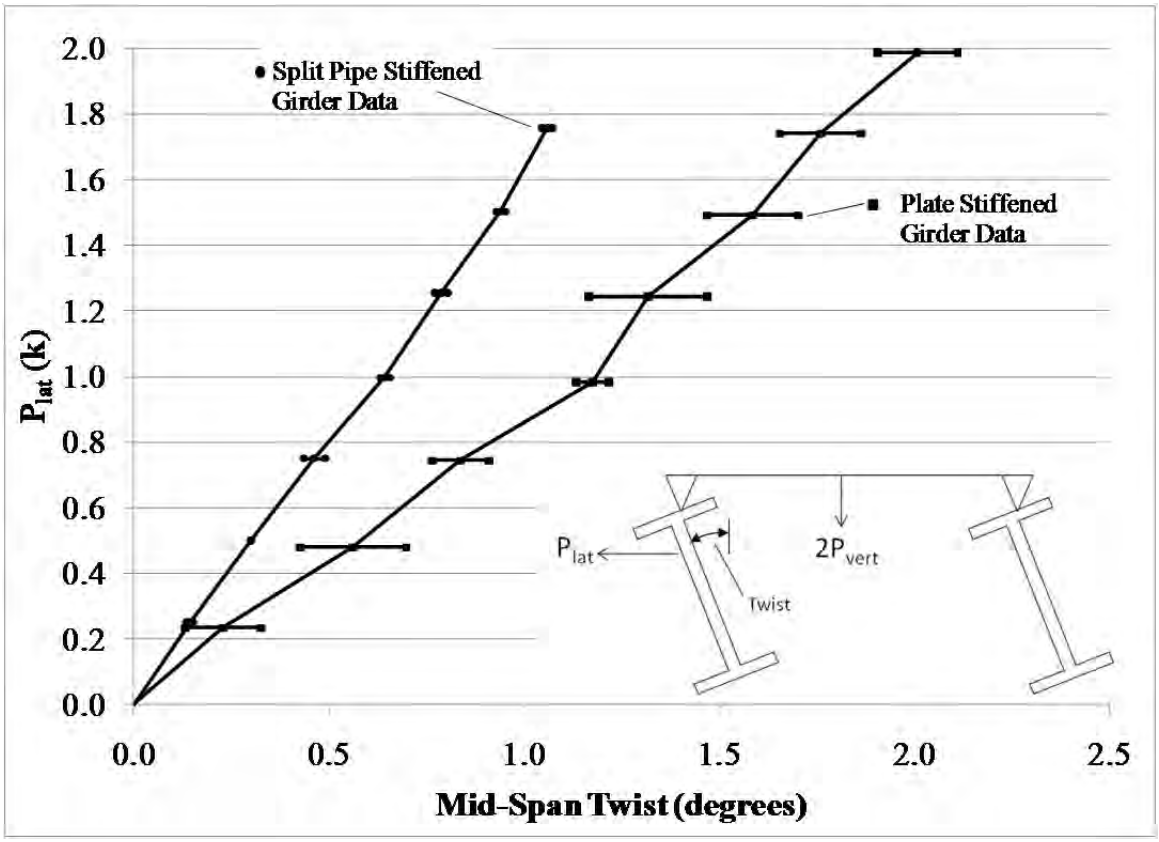

Figure 3.29: Twin girder torsional mid-span test results

Twin Girder Buckling Test Results

The top flange lateral deflection results for the split pipe and plate stiffened girder are shown in Figure 3.30. The deflections shown in the figure are the absolute values so that both specimens could be compared directly. The results show that the buckling capacity of the split pipe stiffened section increased the buckling capacity by over 50% relative to the plate stiffened specimens. This is due to the warping restraint provided by the split pipe. Graphs of all the deflections, twist, and stresses for each specimen are provided in Appendix A (Large Scale Experimental Results).

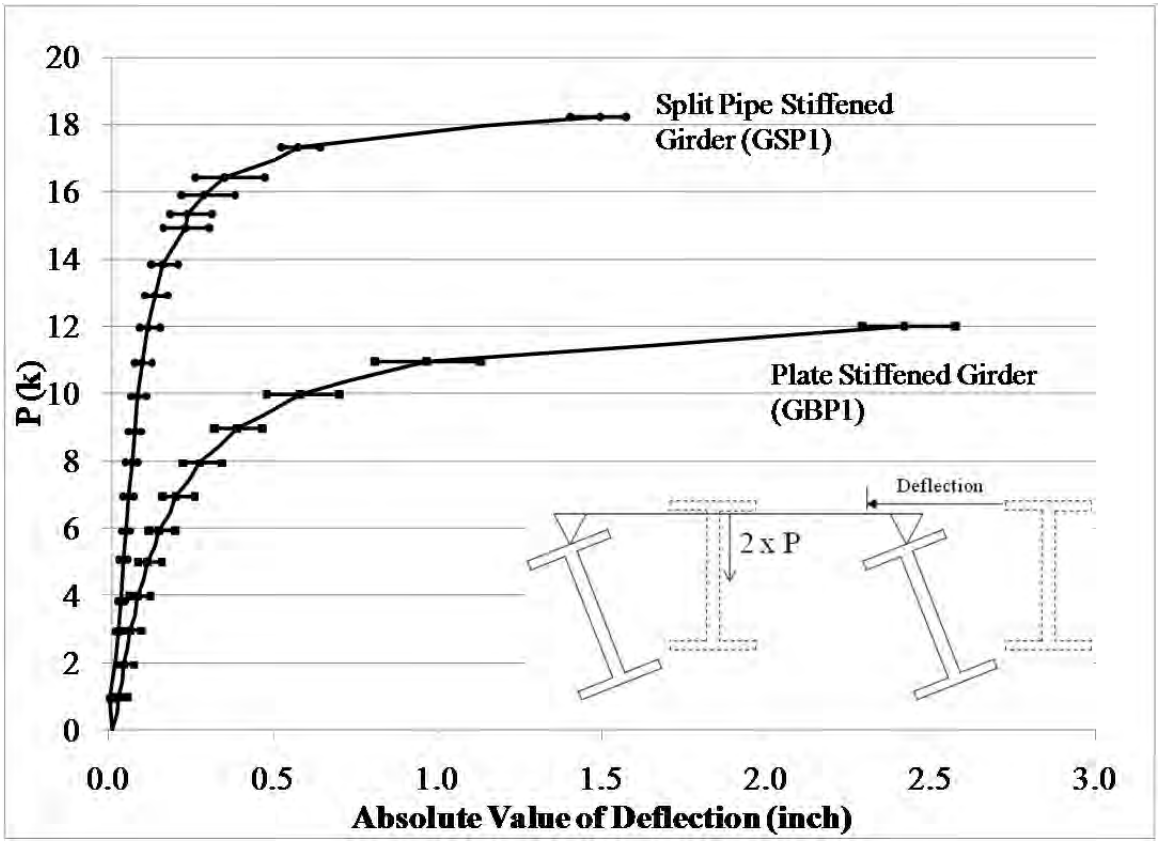

Figure 3.30: Twin girder buckling test mid-span top flange deflections

3.3.2 Three Girder Testing

The purpose of the three girder test program was to measure the buckling capacity, brace forces, and girder end twist for girders with realistic details for the bracing and support conditions. Both split pipe stiffeners and plate stiffeners with bent plate connections were considered in order to compare the specimen responses and validate the cross-frame finite element model. The tests were developed to measure the effects of the support skew as well as the bracing details for both intermediate and support cross-frames. The results from the split pipe stiffened cross-frame specimen and plate stiffened specimen are included in this report.

A picture of the typical test setup is shown in Figure 3.31. In the figure, three split pipe stiffened W30x90 girders GSP1, GSP2, and GSP3 were placed from right to left. A plan view of the test specimen with the key components labeled is shown in Figure 3.32. The tests with three plate stiffened W30x90 girders GBP1, GBP2, and GBP3 were set up in the same layout. Both sets of specimens were constructed along a 53° skew angle.

The testing program, measurements taken, and results are described below. The same girder specimens used for the two girder tests were used again in the three girder tests. The fabrication and the initial imperfection measurements were performed in the same manner as the twin girder testing, so it is not described in this section again.

Figure 3.31: Three girder test (53° skew and no intermediate frames- looking south)

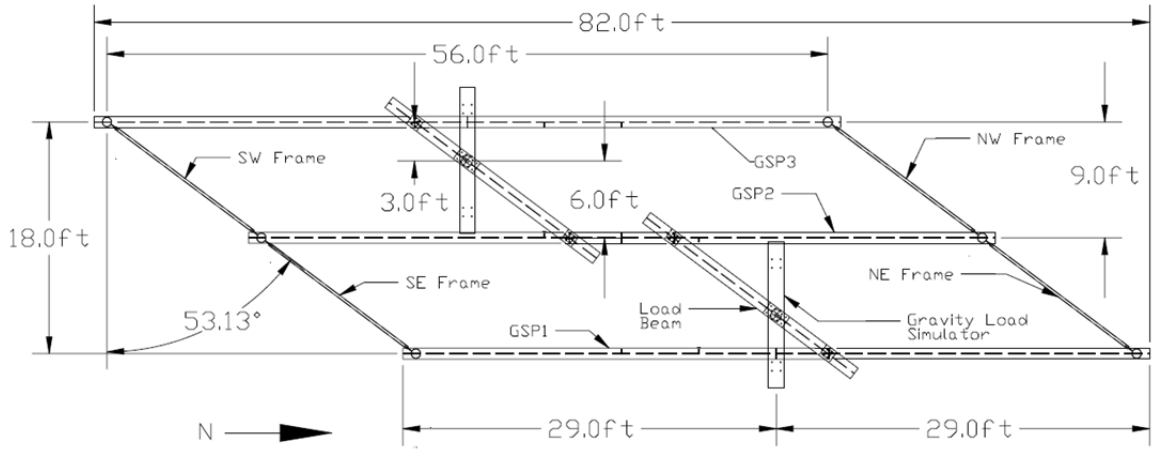

Figure 3.32: Three girder test specimen plan view (no intermediate frames)

3.3.2.1 Three Girder Testing Program

The parameters varied for the three girder testing were the end cross-frame connection details, the placement of intermediate cross-frames and the bearing types. Tests were performed with no intermediate frames, with intermediate frames continuous across the width of the girders

(centered at midspan of GSP2), and with intermediate frames staggered along the skew angle. The cross-frame locations were varied to determine the effects of their placement on the end and intermediate cross-frame forces and on girder end twist. Other support conditions besides the thrust washer were tested to investigate the effect of tipping restraint provided by the bearing pads. The tests conducted are listed in Table 3.3.

Table 3.3: Three girder test program

Stiffener/Connection Type	Intermediate Cross-frames	Bearing Type	Number of Tests
Split Pipe	None	Thrust Washer	3
Split Pipe	Staggered	Thrust Washer	2
Split Pipe	Continuous	Thrust Washer	2
Split Pipe	None	Rubber Pad	2
Split Pipe	None	Rubber Pad with Shims	3
Bent Plate	None	Thrust Washer	3
Bent Plate	Staggered	Thrust Washer	7 [1]
Bent Plate	Continuous	Thrust Washer	10 [1]
Bent Plate	None	Rubber Pad	3
Bent Plate	None	Rubber Pad with Shims	4

Note: [1]Number of test includes the tests with full and partial loading.

3.3.2.2 Cross-frame Fabrication

The cross-frames that were used at the supports and intermediate locations were fabricated at The Ferguson Structural Engineering Laboratory at The University of Texas at Austin. The cross-frames had single diagonals with two struts, which were all constructed from HSS2.5x2.5x1/4 tubes. Although cross-frame members are often composed of angles, the use of tubular members had two benefits: 1) higher axial buckling strength and 2) concentric connections that made member force measurement easier. The two diagonal cross-frames made from angle systems are usually modeled as tension only systems due to the low buckling strength of angles. With the higher buckling strength, the cross-frames composed from the tubes only required a single diagonal. The intermediate frames were bolted to connection plates perpendicular to the girders while the end frames were welded to the connection plate on the split pipe stiffener parallel to the skew angle.

In a one-diagonal cross-frame, the change of the diagonal direction causes the reversal in the sign of the forces in all members: all tension members become compression member and vice versa, but the absolute value of the forces in members remains the same. In the large scale test, the directions of cross-frame diagonals were installed opposite for the split pipe girder and the bent plate girder specimens. So opposite signs of forces can be observed in our test results.

The details used to construct the end cross-frames are shown in Figure 3.33, and a picture of a completed split pipe end cross-frame is shown in Figure 3.34. The details used to construct the intermediate cross-frames are shown in Figure 3.35, and a picture of a completed intermediate cross-frame is shown in Figure 3.36.

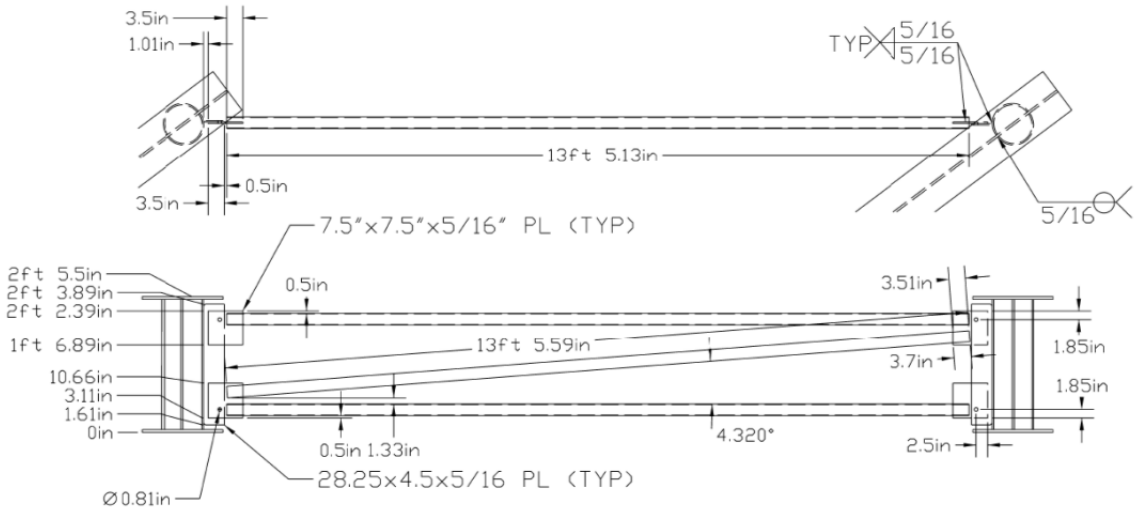

Figure 3.33: Split pipe end cross-frame detail

Figure 3.34: Split pipe end cross-frame (SE cross-frame shown)

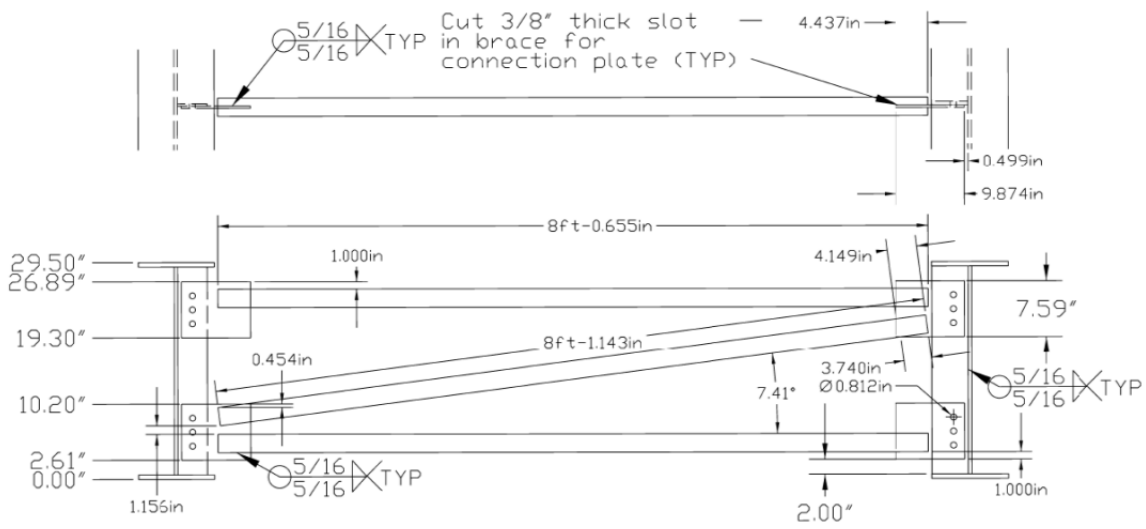

Figure 3.35: Intermediate cross-frame detail

Figure 3.36: Intermediate cross-frame (western frame shown)

3.3.2.3 Test Frame Setup

The three girder test setup is shown in Figure 3.31. As previously discussed, many of the aspects of the three girder test setup are the same as the two girder test setup. The similarities and differences are covered below.

Test Frame Boundary Conditions

The bearing boundary conditions of one girder and twin girder tests were already covered in Section 3.3.1.3 of this chapter, as was the load point boundary conditions using the knife edge bearing surface.

A major difference of the three girder tests was the source of the girder end twist restraint. In the single and twin girder tests, twist was restrained at the ends of the girders by a set of rigid threaded rods connected to a bracket anchored to the supports. As noted earlier in this chapter, the end restraints were very stiff and the one- and two- girder systems experienced no

significant translation. In the three girder test, the twist restraint was provided by the end cross-frames. The supports were also skewed, which can lead to significant out of plane deformations.

Load Application

The load was delivered to the girders via gravity load simulators in a similar fashion in the twin girder test (see Section 3.3.1.3). As shown in Figure 3.32, the load beams were offset four feet either side of the center of GSP2 (or GBP2) so they would not interfere with their placement on GSP2 (or GBP2). Finally, each gravity load simulator was placed between the girders they loaded and offset 1/3 of the girder spacing toward the exterior girder. Because the load beams was essentially simply supported on top of the girders, 2/3 of the gravity load simulators force was applied to the exterior girder and 1/3 of the force was applied to GSP2 (or GBP2). Therefore each of the girders received essentially the same magnitude of the total load.

Strain and Deflection Measurements

The girders and cross-frames were instrumented to gather the required structural responses. As in the twin girder test each girder was monitored at mid-span for vertical deflection, top flange lateral deflection, bottom flange lateral deflection, twist, and the strains on both sides of the top and bottom flange. In addition to these measurements the girder end twist was measured with tilt sensors and by measuring the top and bottom flange translation with a string and linear potentiometers.

Each cross-frame brace was instrumented with a strain gage on the top and bottom of each member at the ¼ and ¾ points along the member lengths. This allowed the axial force to be calculated in two locations and allowed the calculation of the maximum and minimum moment in each brace member. Typical cross-frame strain gage locations are indicated in Figure 3.37.

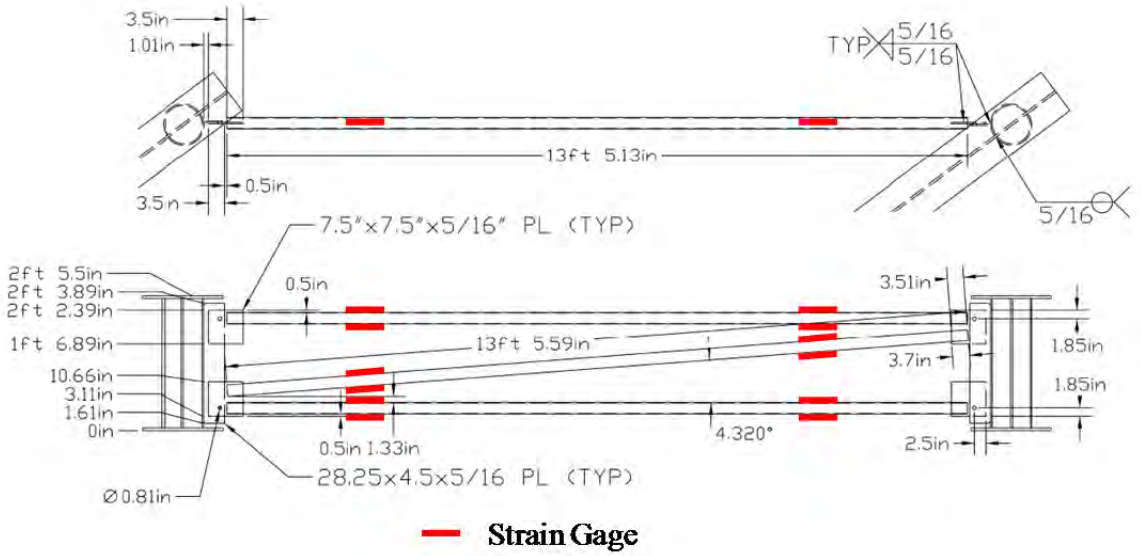

Figure 3.37: Cross-frame strain gage locations

3.3.2.4 Three Girder Specimen Test Results

The results for the three-girder split pipe (GSP) and three-girder bent plate (GBP) specimen tests are presented below. A complete series of graphs of all the structural responses recorded for each test are provided in Appendix A (Large Scale Experimental Results).

Thrust Washer Bearing and No Intermediate Cross-frames

The vertical deflection results for GSP2 and GBP2 are shown in Figure 3.38 and Figure 3.39 along with the analytic solution for the mid-span vertical deflection of a simply supported beam. The figures show that the girder with either connection is slightly stiffer than the analytic solution. This is to be expected as the cross-frames provide a small amount of rotational support to the girder ends and help stiffen the girder against vertical deflection.

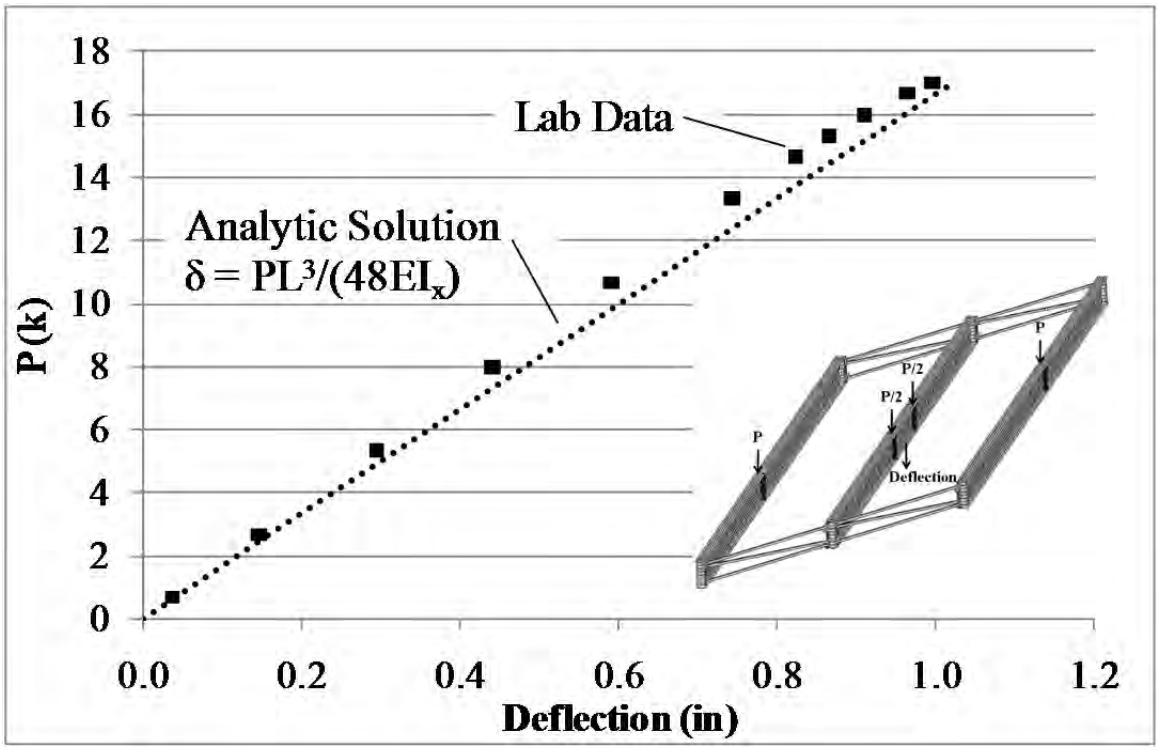

Figure 3.38: GSP2 mid-span vertical deflection laboratory results

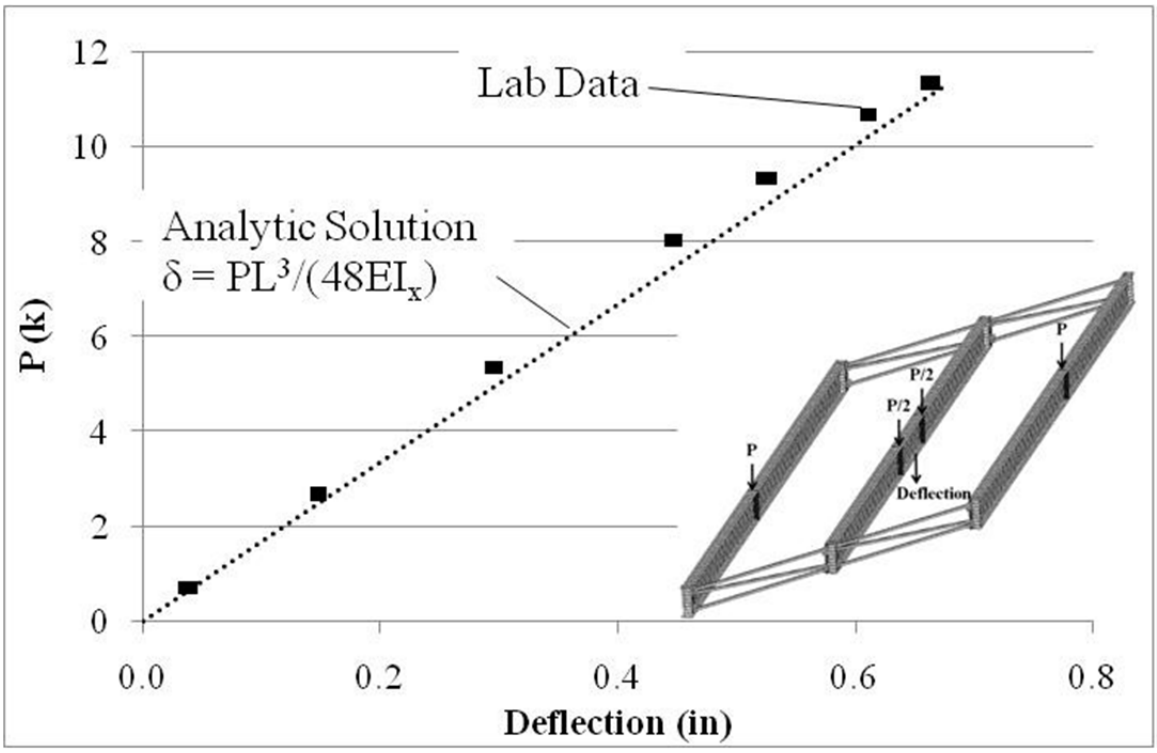

Figure 3.39: GBP2 mid-span vertical deflection laboratory results

A comparison plot for GSP2 mid-span top flange lateral deflection is shown in Figure 3.40. As discussed in Chapter 2, the impact of allowing twist at the girder end does decrease the girder strength. Using the apparent buckling capacities from Figure 3.40, allowing end twist reduces the girder buckling strength by only about 7%. Such a small decrease in strength is consistent with the previous research discussed in Chapter 2 (Background). The small difference in the loading conditions between the twin and three girder tests may also contribute to some of the difference.

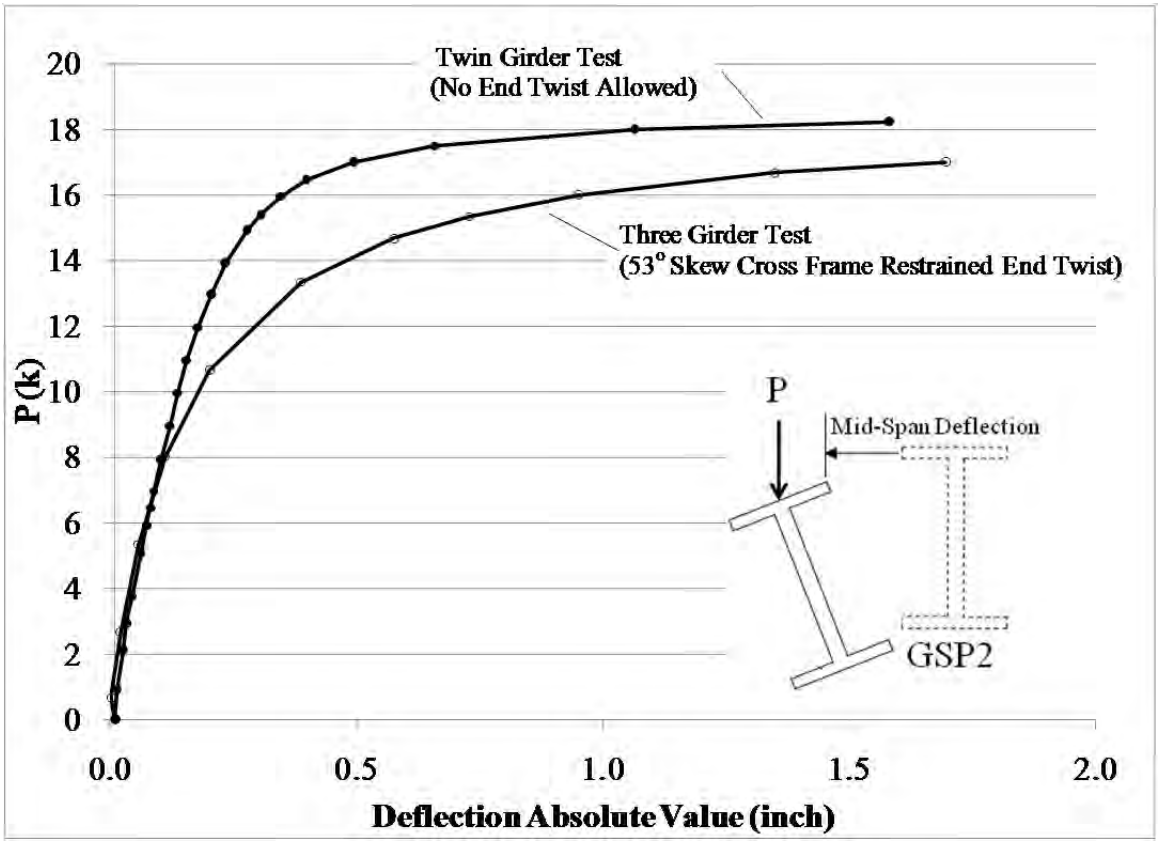

Figure 3.40: GSP2 mid-span top flange lateral deflection with and without end twist

A comparison of the mid-span buckling twist of the girders is shown in Figure 3.41. Similar to what was seen in twin girder test, the girder stiffened with the split pipes has approximately 50% more buckling strength than the plate stiffened girder.

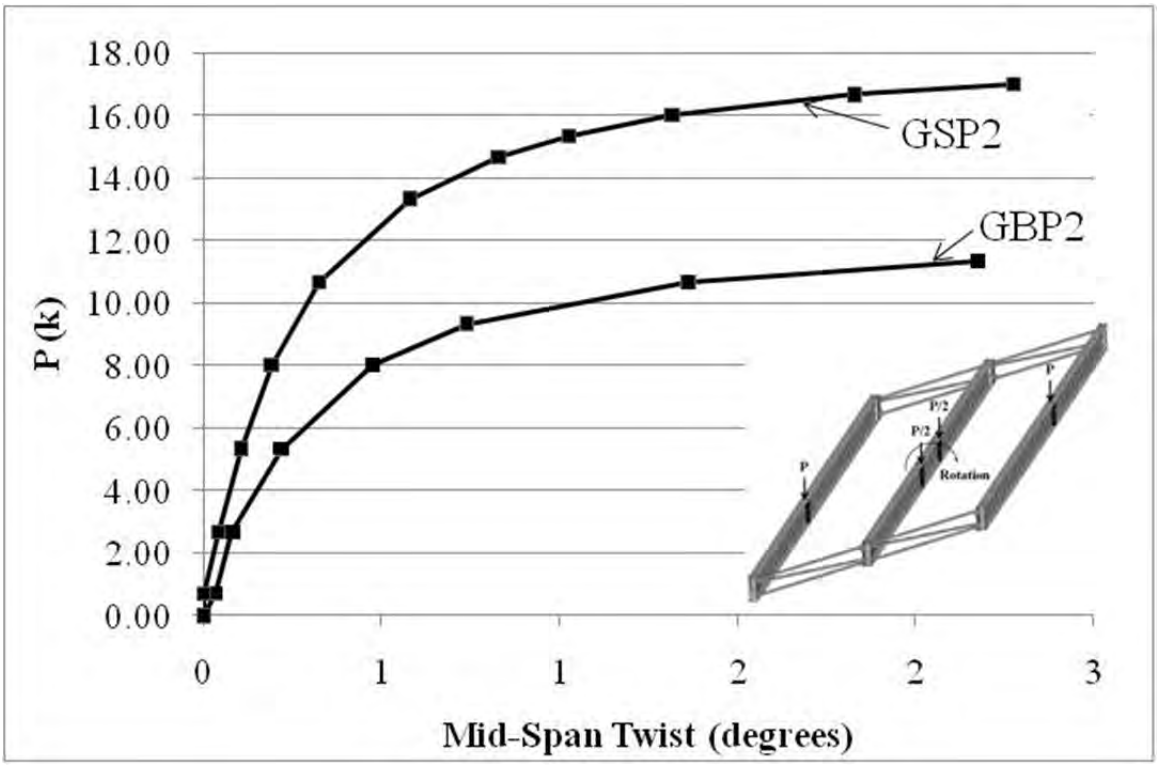

Figure 3.41: GSP2 and GBP2 mid-span twist

The end twists from the north and south ends of GSP2 and GBP2 are shown in Figure 3.42. A comparison of the result shows that at the north end, the girder with the split pipes will twist less than the girder with the bent plates. However, a comparison of twist at the south end is more complicated. As explained in Chapter 2 (Background) the girder twist due to the skewed abutments are opposite one another on each girder end. In addition, the girder lateral buckling will cause end twist. In our laboratory specimens, the buckling twist on the north end is in the same direction as the skew twist, but on the south end, they are opposite one another. As a result, the plot at the south end shows the development of twist at the beginning of loading and a reduction later when the girder nears the buckling capacity. A similar response is seen in the cross-frame forces.

The axial brace forces for the southwest and northwest cross-frames of both GSP and GBP specimens are shown in Figure 3.43 through Figure 3.46. The skew and stability force interaction can be seen in the graphs. For the south end cross-frame forces, the skew and stability forces are additive so the forces do not change direction. However, on the north end, the skew and stability forces work against each other and as the specimen load increases the stability forces increase and cause a force reversal in the braces.

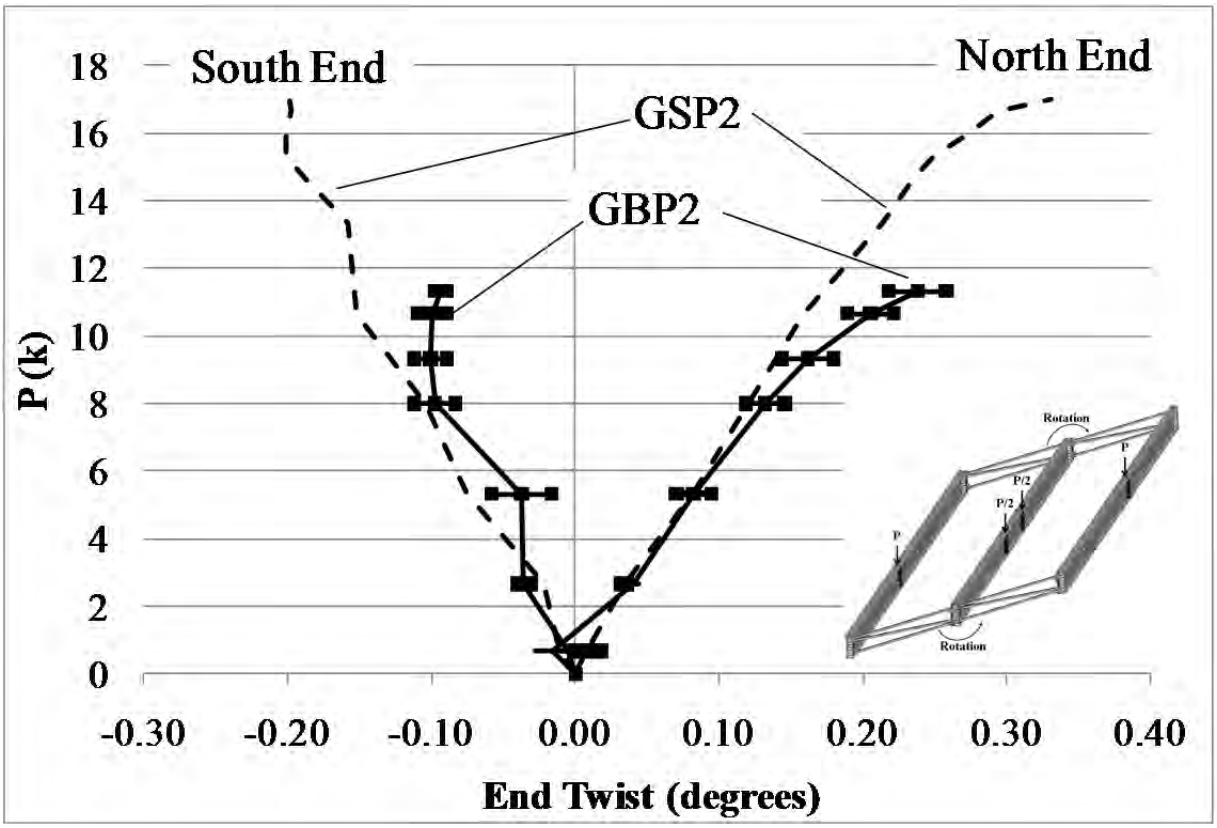

Figure 3.42: GSP2 and GBP2 north and south end twists

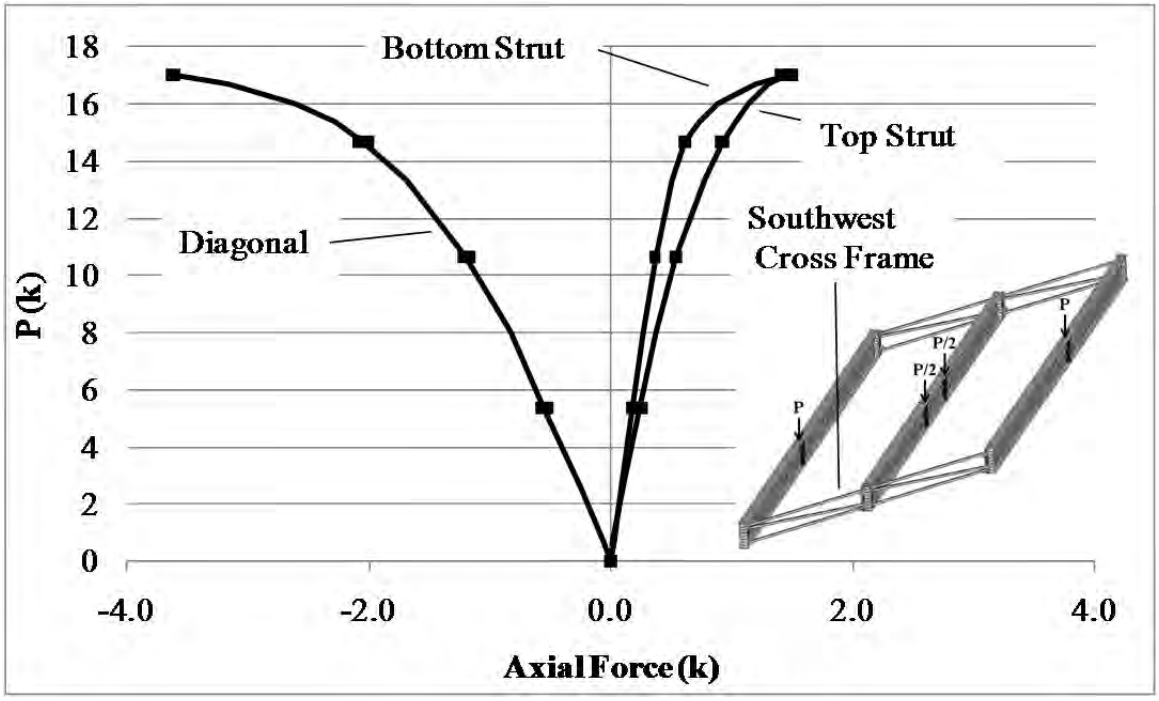

Figure 3.43: GSP Specimen southwest cross-frame axial brace forces

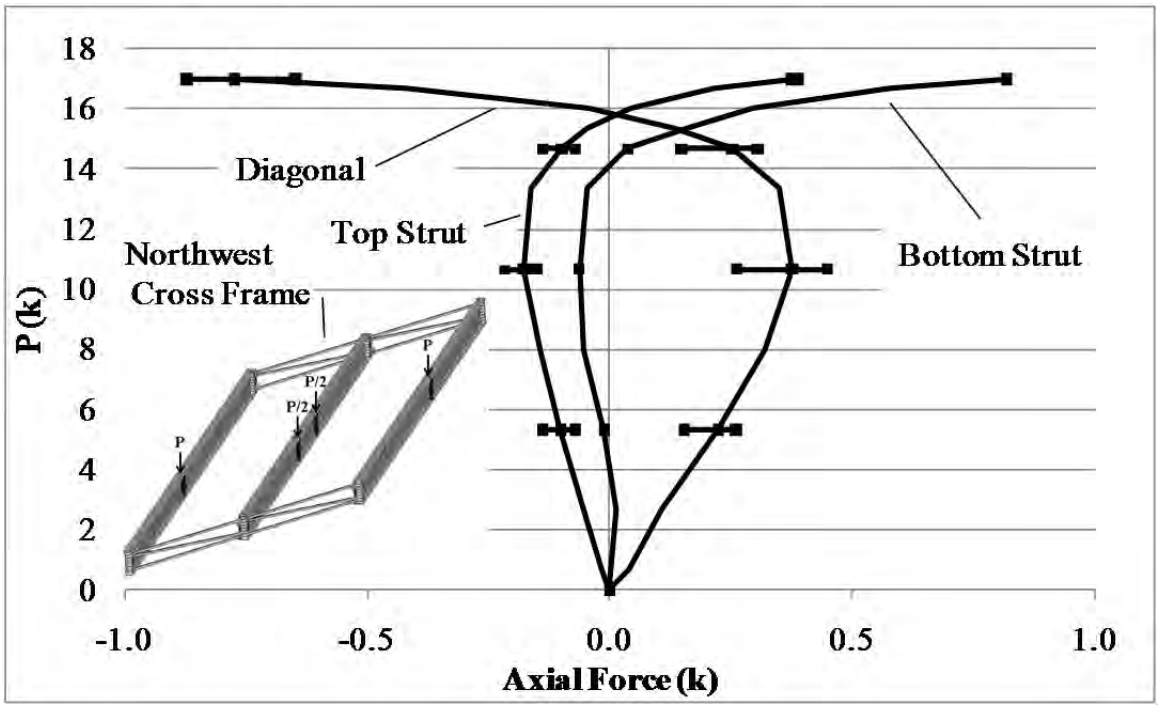

Figure 3.44: GSP Specimen northwest cross-frame axial brace forces

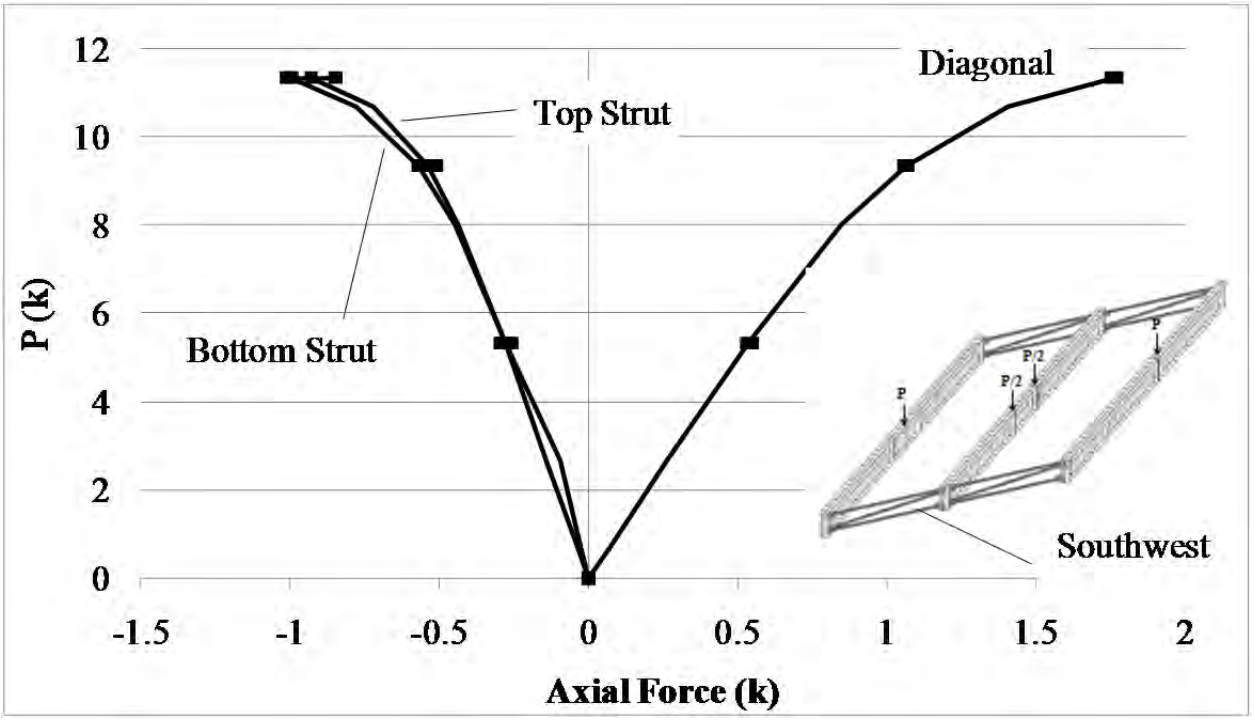

Figure 3.45: GBP Specimen southwest cross-frame axial brace forces

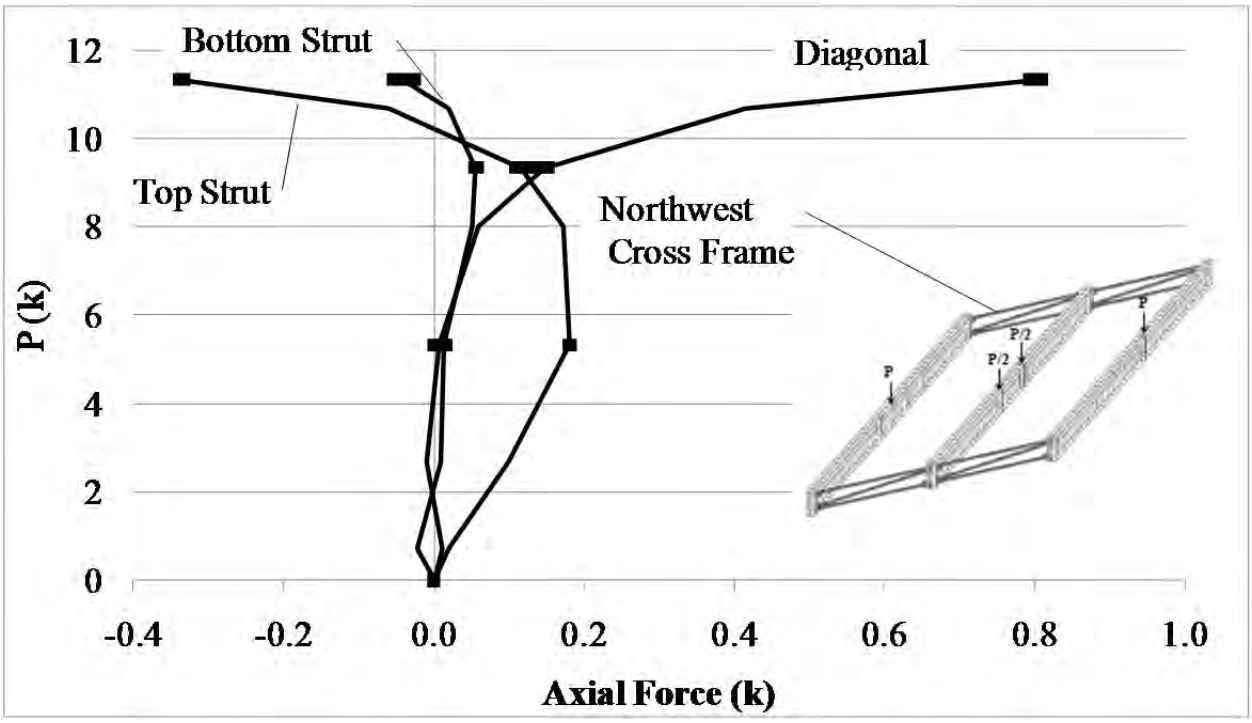

Figure 3.46: GBP Specimen northwest cross-frame axial brace forces

Thrust Washer Bearing and Staggered Intermediate Cross-frames

Tests were performed on both GSP and GBP specimens with intermediate cross-frames. Two different layout patterns of intermediate cross-frame were used: staggered and continuous. A picture of the staggered intermediate cross-frame in GSP specimen is shown in Figure 3.47, and a plan view drawing is shown in Figure 3.48. The same layout was also used for GBP specimen. The intermediate cross-frames were staggered parallel to the skew angle which positioned them 6' to either side of the center of GSP2.

Figure 3.47: 53° Skew GSP specimen with staggered intermediate cross-frames (looking south)

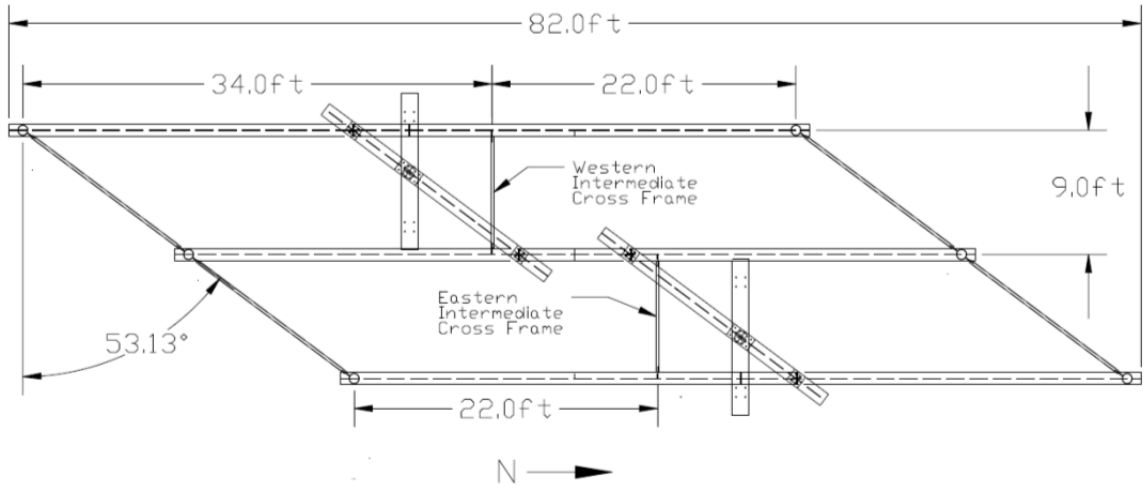

Figure 3.48: Plan view of 53° skew GSP specimen with staggered intermediate cross-frames

One of the purposes of the test was to compare the end cross-frame forces and girder end twist with and without intermediate cross-frames. Figure 3.49 shows a comparison of the southwest end cross-frame forces without intermediate cross-frames and with staggered intermediate cross-frames. The only difference between the end cross-frame forces in the two bracing schemes is the magnitude of the stability forces in the case without intermediate cross-

frames. Because the intermediate cross-frames reduce the unbraced length, the end cross-frames do not attract significant stability forces at the applied load level.

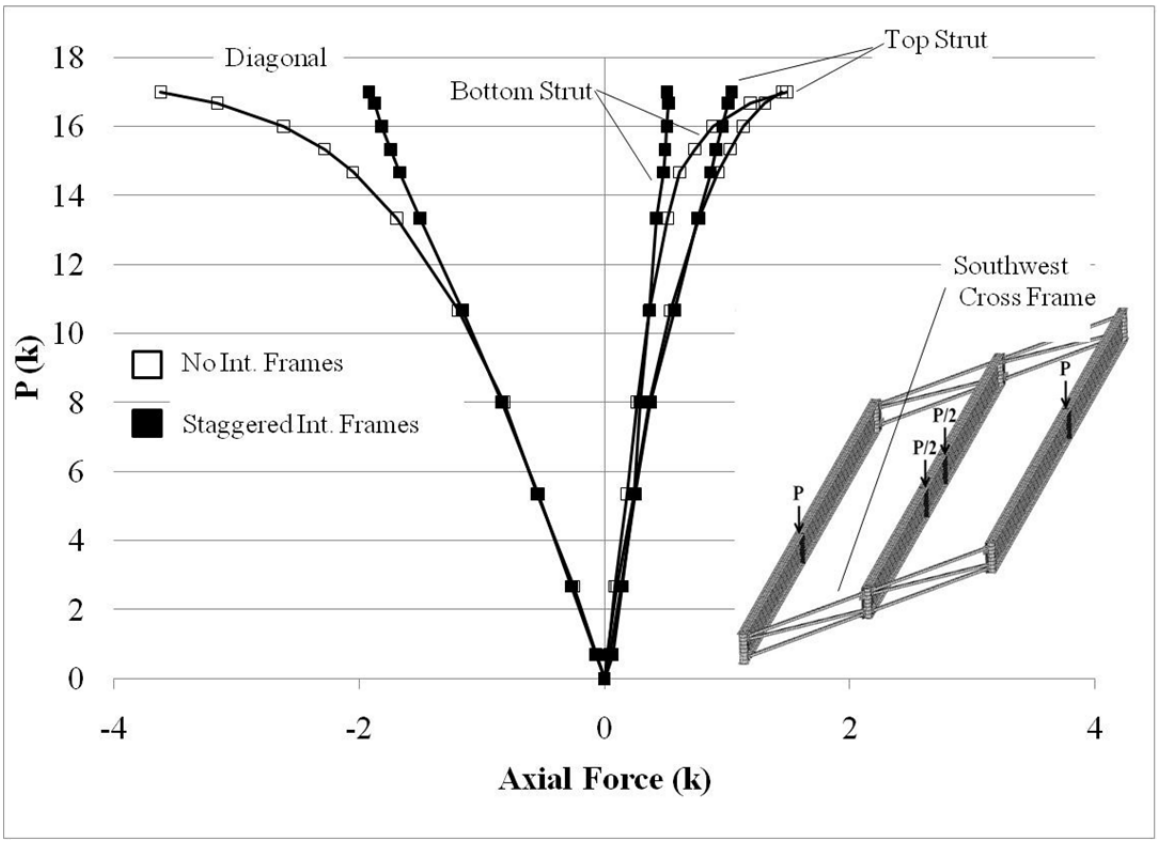

Figure 3.49: Southwest cross-frame forces with and without staggered intermediate frames

A similar pattern can be seen in the girder end twist for GSP2 shown in Figure 3.50. The specimen with the staggered intermediate bracing shows a nearly equal and opposite twist at the girder ends, while the unbraced specimen shows the previously mentioned impact of stability forces causing the end twist to be unequal. Therefore, these laboratory results show that adding intermediate cross-frames reduces the stability forces in the end cross-frames, but the skew forces remain relatively unchanged. The complete series of graphs showing the cross-frame forces and girder end twist for the staggered cross-frame layout are given in Appendix A (Large Scale Experimental Results). The mid-span lateral deflections and twist were negligible and are therefore not included in this paper.

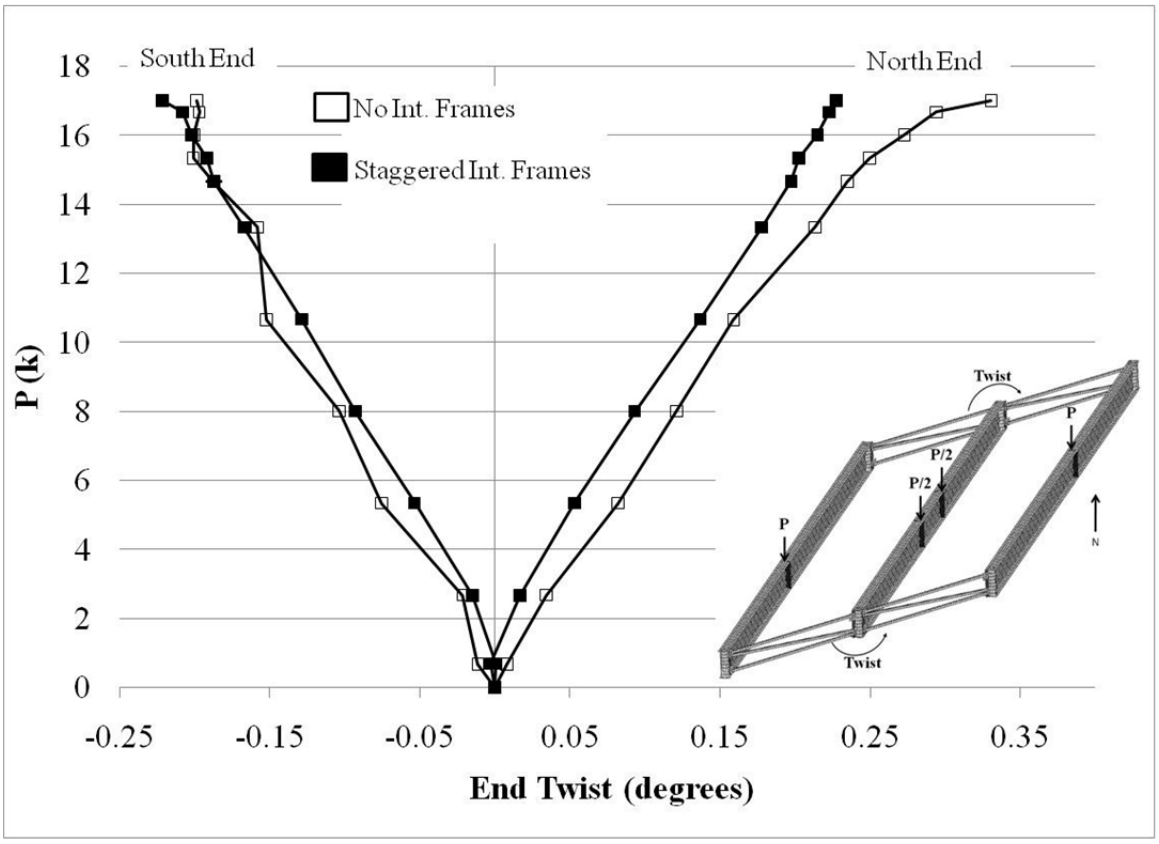

Figure 3.50: GSP2 end twist with and without staggered intermediate cross-frames

Thrust Washer Bearing and Continuous Intermediate Cross-frames

A plan view drawing of the continuous intermediate cross-frame layout is shown in Figure 3.51. As noted earlier, the braces were positioned so that they framed into GSP2 at mid-span but were offset by 12 feet from the middle of the other two girders for the case of a 53° skew angle.

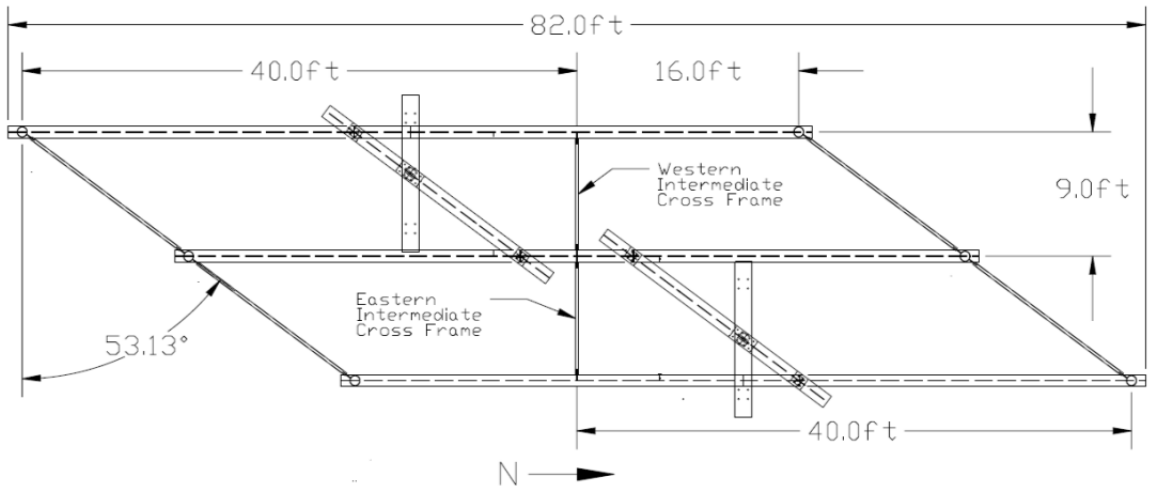

Figure 3.51: Plan view 53° skew specimen with continuous intermediate cross-frames

Staggering the intermediate cross-frames is done in an attempt to reduce the cross-frame forces. The graphs in Figure 3.52 and Figure 3.53 demonstrate the comparison. Staggering the intermediate cross-frames parallel to the skew angle resulted in a significant reduction in the cross-frame forces relative to the case where the braces were continuous across the bridge width.

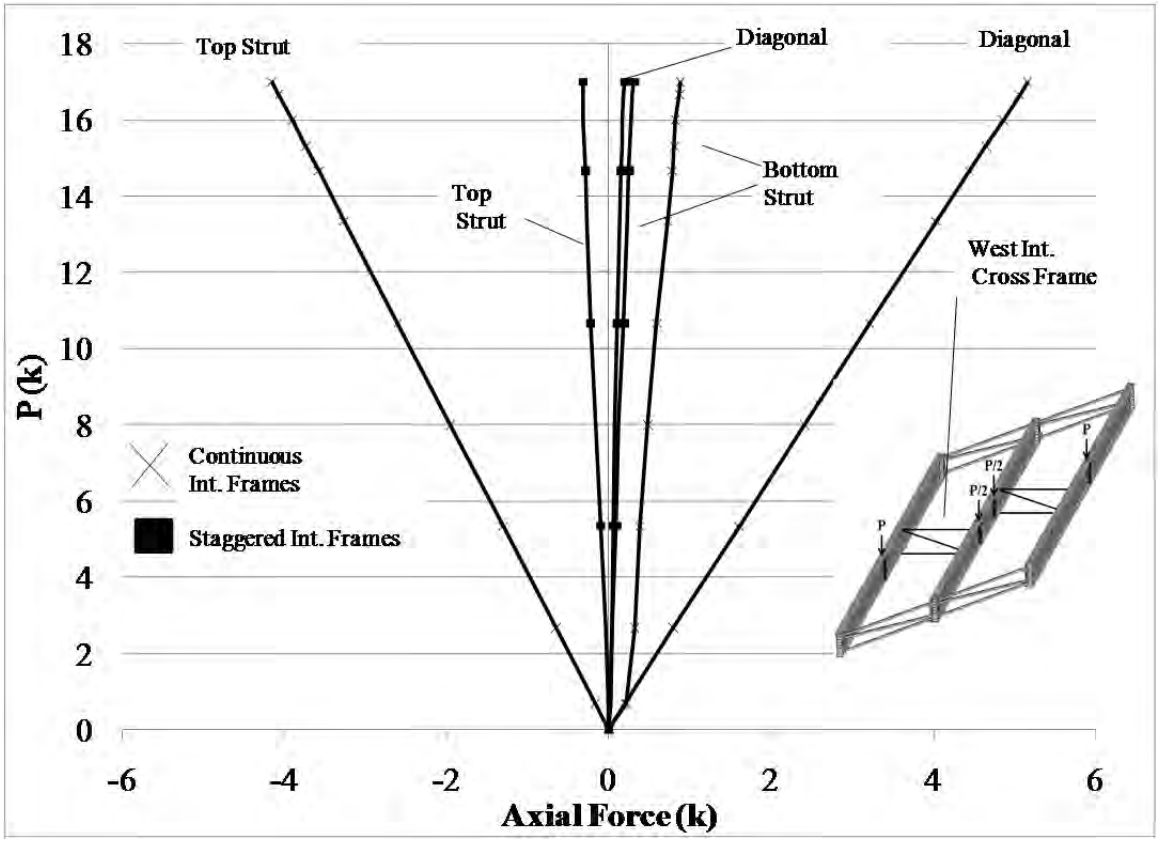

Figure 3.52: Staggered and continuous intermediate cross-frame forces in GSP specimen

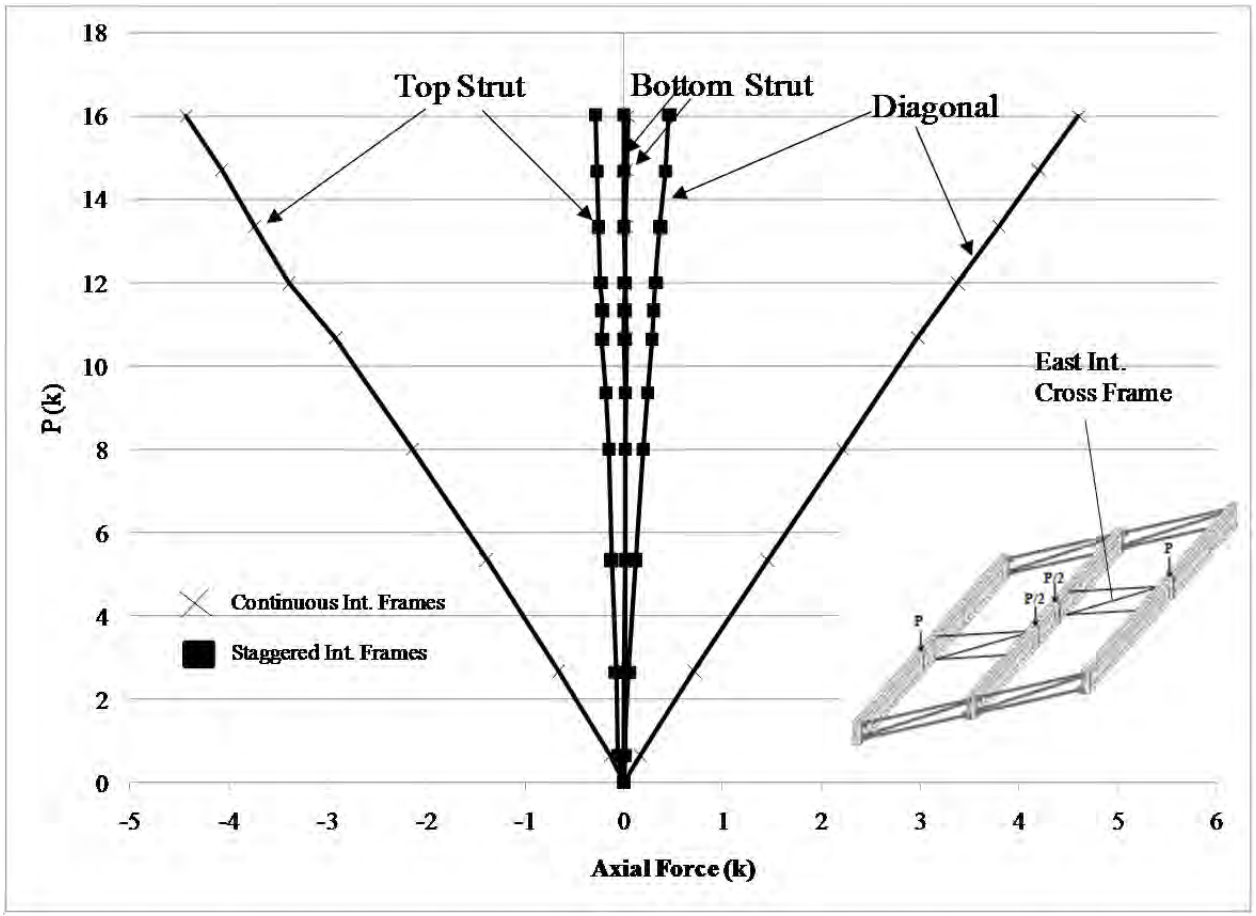

Figure 3.53: Staggered and continuous intermediate cross-frame forces in GBP specimen

However, as shown in Figure 3.54, the staggering of the cross-frames does not appear to change the skew induced girder end twist. With the unbraced length used in this experiment, staggering the cross-frames has no apparent effect on the girder end twist. Of course, it may be expected this result would change as the intermediate frames are moved closer to the abutment.

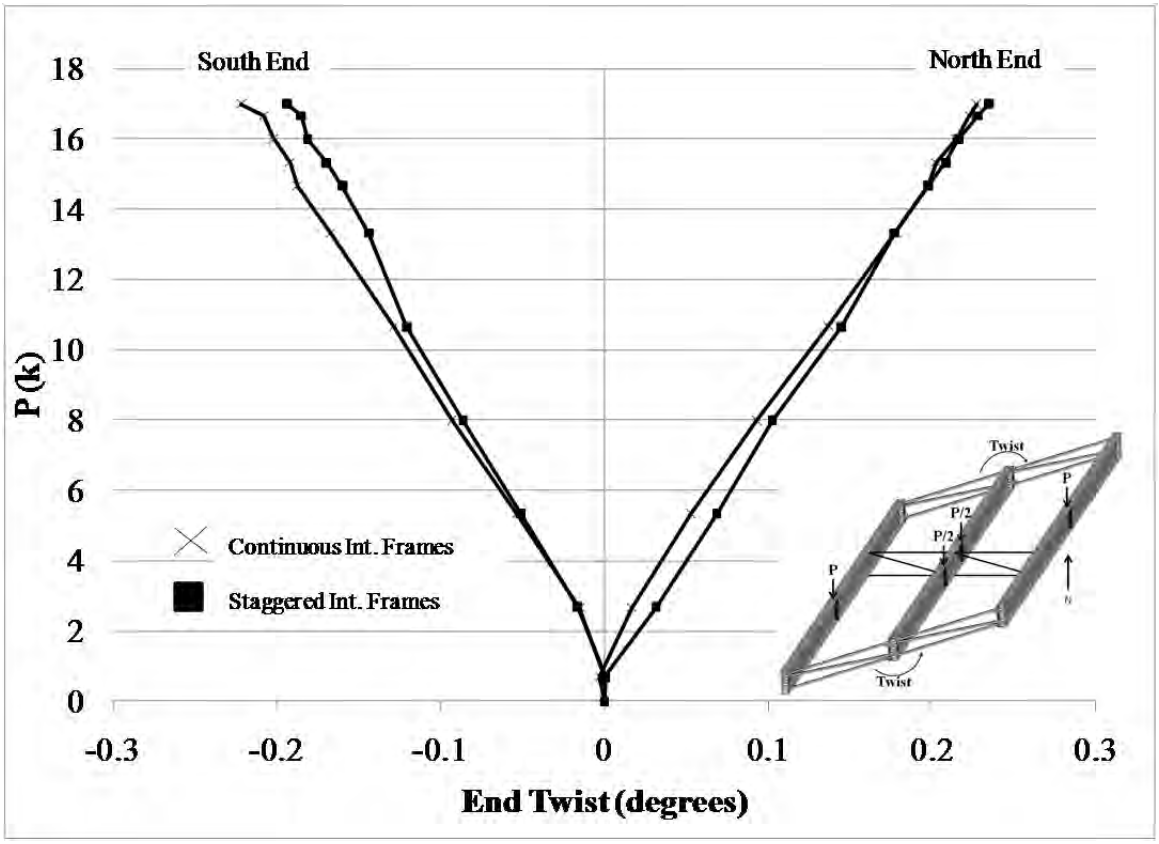

Figure 3.54: GSP2 end rotations for staggered and continuous intermediate cross-frames

Partial Loading on Staggered and Continuous Cross-frame Specimens

During the test of the GBP specimen with intermediate cross-frames, additional sets of tests were performed with partial loading on girders. In these test setups, the load beam in the east bay was removed and only GBP2 and GBP3 were loaded during the test. Because the gravity load simulator was placed closer to GBP3, the applied force on GBP3 was two times that on GBP2. A picture of this setup is shown in Figure 3.55. The plots in Figure 3.56 demonstrate a reduction in brace forces by staggering the cross-frames, similar to that seen under full loading. This asymmetrical loading condition is similar to a truck live load on a bridge.

Figure 3.55: 53° Skew GBP specimen with staggered intermediate cross-frames, partially loaded

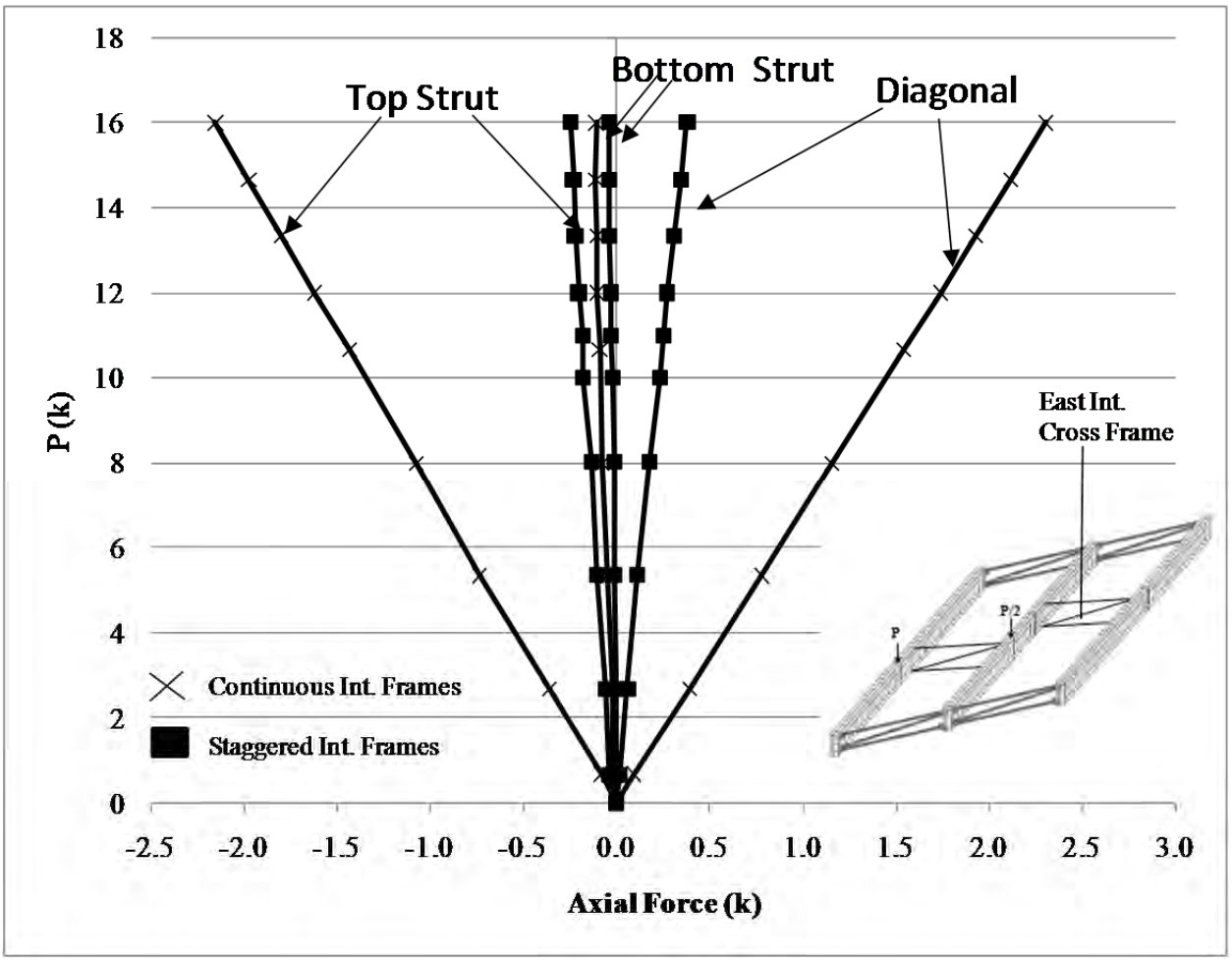

Figure 3.56: Staggered and continuous intermediate cross-frame forces, partially loaded

Bearing Pads and No Intermediate Cross-frames

As discussed in Chapter 2, the tipping effect at the support will potentially reduce the girder end twist and increase buckling capacity. In order to investigate the tipping effect, tests were conducted with two different bearing pads other than the thrust washer supporting the three-girder specimen. Pictures of a rubber bearing pad without shims and a rubber bearing pad with shims used in the tests are shown in Figure 3.57 and Figure 3.58 respectively. Dimensions of all bearing pads are 15″x9.25″x3.625″.

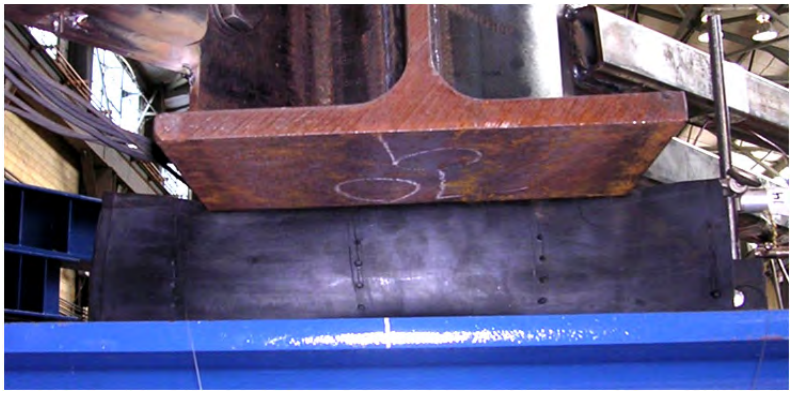

Figure 3.57: Rubber bearing pad without shims

Figure 3.58: Rubber bearing pad with shims

Deformation of the bearing pad was measured by a linear potentiometer attached to the bottom flange near the bearing pad, as illustrated in Figure 3.59. Figure 3.60 shows the deformation of the bearing pads under the north and south ends of GBP3. It is seen that the deformation of the bearing pad can approximately be considered as linear. Furthermore, the stiffness of rubber pad with shims is much higher than rubber pad without shims. Accordingly, the average axial stiffness of the bearing pads can be calculated by dividing the total applied load on the frame by the sum of all deformations from six bearings. The calculated average axial deformation stiffness for both types of bearing pad is listed in Table 3.4: Bearing pad axial stiffness.

Table 3.4: Bearing pad axial stiffness

Bearing Type	Axial Stiffness (kips/in)
Rubber Pad	22.1
Rubber Pad with Shims	178.6

Figure 3.59: Measurement of bearing pad deformation

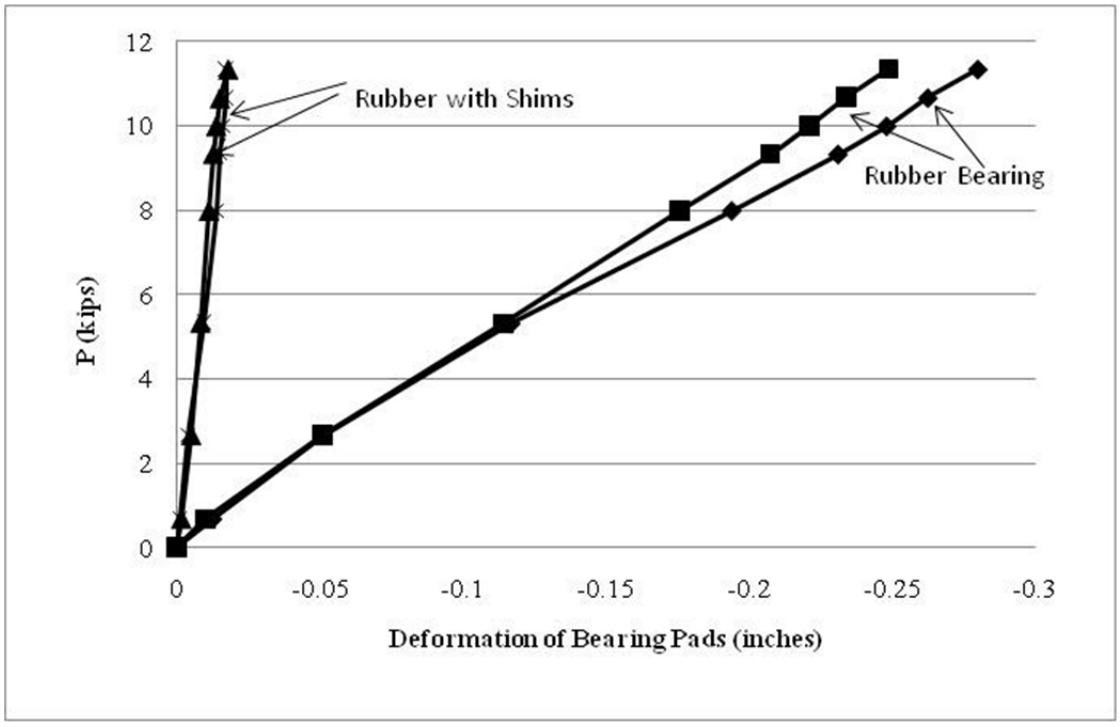

Figure 3.60: Deformation of bearing pads supporting GBP3

Mid-span twist results of GSP3 supported by the two types of bearing pads along with results of a test with the thrust washer are plotted in Figure 3.61. End twist results of the same girder are plotted in Figure 3.62. The comparison shows that the buckling capacity of the girders is not greatly affected by the different bearing conditions, but the girders do experience different end twists when different bearing pads are used. Evidently, the tipping effect plays a role in

reducing the end twist of girders. Because the rubber pad with shims has much more stiffness than the pure rubber pad, it provides more tipping effect (end twist of girders is smaller under the same load). The rubber pad with shims also showed more tipping effect than thrust washer even though the stiffness of thrust washer is nearly infinite. However, the size of the bearing pad (10.6″ x 9.25″) is greater than that of thrust washer (4″ in diameter), and therefore the reaction force on the bearing pads can shift further from the plane of the web than for the thrust washer resulting in a higher restoring moment.

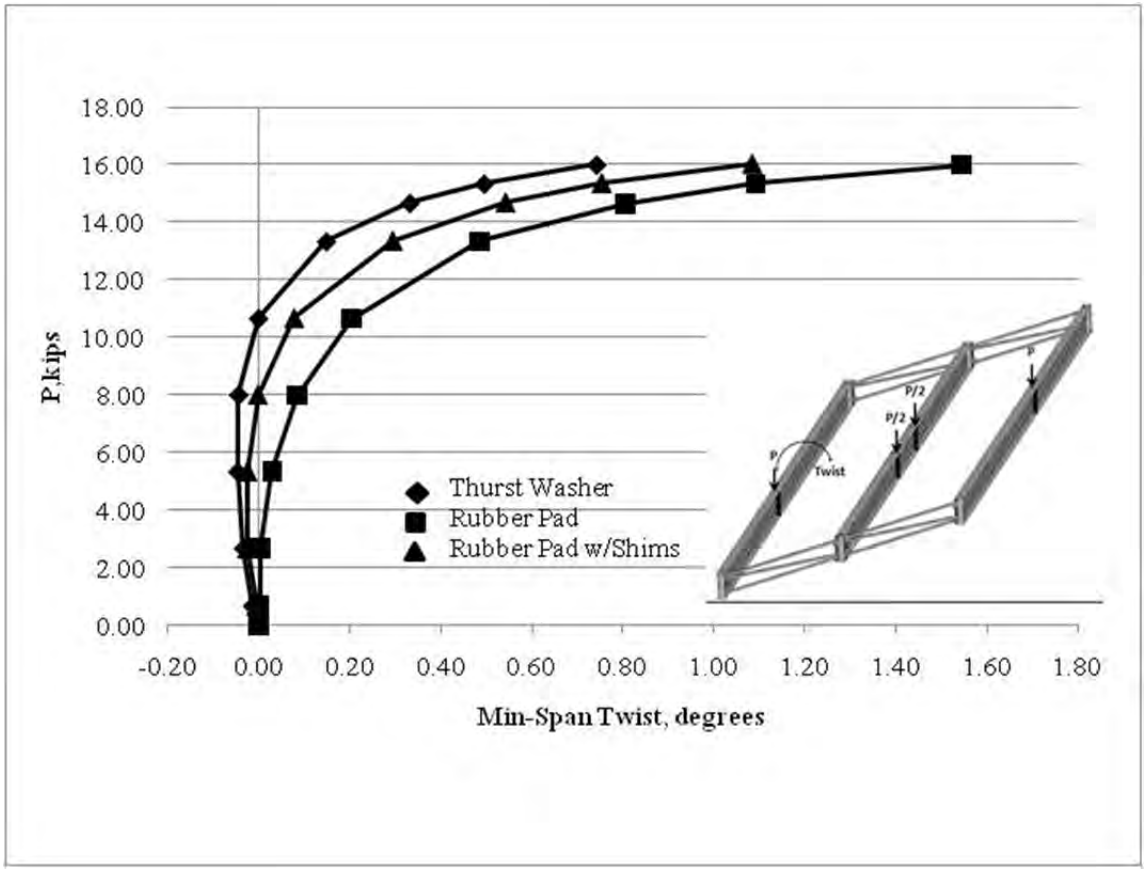

Figure 3.61: Girder mid-span twist comparison of different bearing types

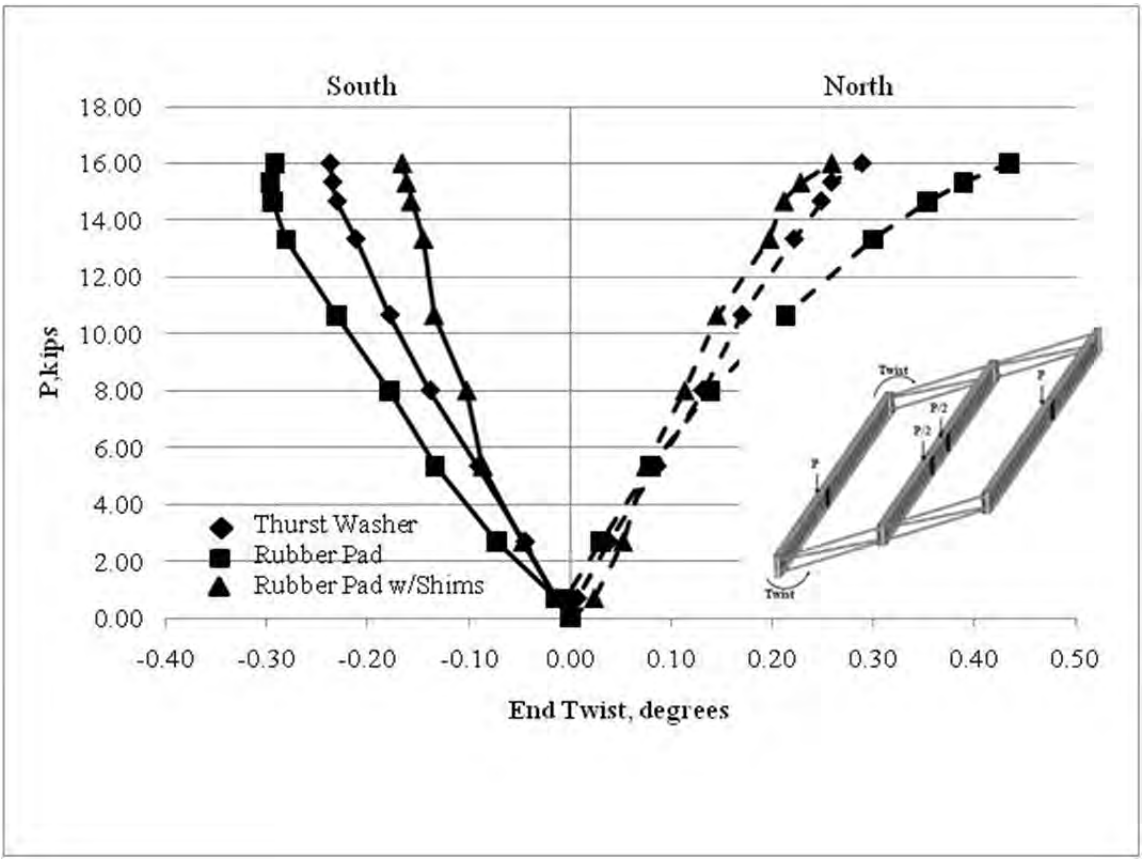

Figure 3.62: Girder end twist comparison of different bearings

3.4 Experimental Program Summary

3.4.1 Small Scale Test

The experimental program has given several important results. First the connection tests demonstrated that the split pipe stiffener is stiffer than the bent plate connection when a simple tension load is applied. Vertical deflections, which provide the main indication of stiffness in the cross-frame direction, were 63–75% less for the split pipe than the bent plate. Additionally, no rotation of the connection plate was measured with the split pipe detail (Battistini 2009).

Data collected on the effect of skew angle for the bent plate detail show the stiffness of the connection decreases with increasing skew angle. The main reason for this behavior is the component of force perpendicular to the stiffener causing bending of the stiffener. This component increases with the skew angle, leading to larger deflections and lower stiffness (Battistini 2009). With increasing bend radius, the deflections also increased. Larger bend radii create larger eccentricities from the connection, increasing the moment arm on the stiffener. The stiffness, therefore, also decreases with increasing bend radius (Battistini 2009).

3.4.2 Large Scale Test

Several important lessons were also learned during the large scale testing.

First, the split pipe adds warping restraint to the girder ends and can significantly increases the elastic buckling capacity.

Second, forces induced by skewed supports twist the ends of a girder in equal but opposite directions. The stability forces will interact with these skew forces limiting the skew induced twist when it is opposite to the buckling twist and increasing the skew induced twist when it is in the same direction as the buckling twist. As a result, the split pipe detail can reduce the end twist when the forces are in the same direction in comparison with bent plate connection, but no decisive conclusion can be made when the two forces counteracting each other. However in general, it can be concluded that as far as the maximum absolute end twist of a bridge is concerned, the split pipe connection will result in lower end twists in girders than when bent plate connection is used.

Third, the impact of staggering intermediate cross-frames significantly decreases the intermediate cross-frame forces as seen in the laboratory specimen, while the skew induced girder end twist appears to be insensitive to intermediate cross-frame stagger. Finally, the bearing pad can significantly affect the end twist of girders but not the buckling strength of the girders.

The above mentioned results are specific to the test parameters described in this chapter. In Chapter 4 (Finite Element Modeling) the laboratory results from this chapter are used to validate the finite element modeling techniques used to create a skewed bridge substructure finite element model. This validated model can then be used to extend the experimental results in this chapter to a wider array of geometric and loading parameters.

Chapter 4. Finite Element Modeling

4.1 Introduction

This chapter includes a description of the finite element modeling techniques used to develop models of laboratory specimens described in Chapter 3 (Experimental Program). The purpose for developing these models was to validate the modeling techniques used in order to employ these techniques in the parametric studies described in Chapter 5 (Parametric Studies and Design Recommendations). The three-dimensional finite element program ANSYS® Academic Research, Release 11.0 was used to create these models. Using the ANSYS Parametric Design Language (APDL) allowed a computer code to be developed that was used to conduct the parametric studies.

This chapter begins with a general discussion of the modeling and analysis techniques used and then describe the specific components used to build the connection, cross-frame, and bridge substructure models. Where analytic solutions and laboratory results were used to validate the modeling techniques, they are covered in the applicable section describing the component. Additional validation results can be found in Appendix B (Finite Element Modeling Validation Results).

4.2 General Modeling and Analysis Techniques

Most of the girder and cross-frame components investigated in this study were modeled as steel plates connected at their mid-thicknesses (such as a web-flange interface) or overlapped at their surfaces (such as a basic tension splice). Once these basic plates and connections were created to form the finite element model, three different types of analyses were conducted. These were a first order elastic analysis, an elastic critical load analysis (eigenvalue buckling analysis), and a second-order elastic analysis (non-linear geometric analysis). The basic plate and connection components are described in the following sections.

4.2.1 Steel Plate Modeling

The element used to create the steel plates for the models was the 8-node shell element (ANSYS SHELL93). This element has been successfully used in previous girder buckling research to model the flat plates that make up most girders (Helwig 1994) (Wang 2002) (Whisenhunt 2004). In this current study, this element was also used to model curved surfaces. Because the element has mid-side nodes, it models curved shells well and supports non-linear geometric analysis (ANSYS Inc. 2010).

The SHELL93 element has 6° of freedom at each node and allows the user to define its thickness at each corner. Because it does not require multiple rows of nodes to define its thickness, it is much more computationally efficient than using a solid element to model the components in this study. Additionally, its aspect ratio is defined in two dimensions rather than three, which eases maintaining an element aspect ratio near unity. Providing an aspect ratio near unity can be important in maintaining accuracy in the finite element solution. Because the shape functions in a quadrilateral element are derived for a square element in isoperimetric coordinates, excessive deviations from this assumed aspect ratio can result in significant error.

In this study, the finite element analytical (FEA) model was not formed directly by initially creating nodes and elements, but was instead derived from meshing geometric entities, such as key points, lines, and areas created to represent the component geometry. This meant that the SHELL93 element aspect ratios took on the underlying aspect ratios of the areas from which they were meshed. To ensure an element aspect ratio as near unity as possible, and accurately represent the component geometry, an algorithm in the APDL code was used that formed nearly square areas for every component.

The algorithm computed the number of square areas required to construct the underlying plate. Any overage or underage along the length of the plate was then calculated. This overage or underage was then distributed among each of the areas along the length so all areas had the same aspect ratio. The aspect ratio was always less than two and usually very near unity. Once the areas were created, they were then meshed with a user-provided mesh density to create the number of elements per line requested. A mesh density of two creates four elements in each area because the elements were created along the length and the height of the area.

4.2.2 Plate Connections

The method of connection between the different components was a primary concern in the development of the FEA model. Due to complex curved and angled geometries in this study as well as the offset between the shell nodes at its outer surface, these connections presented a significant challenge. Three different methods were used to connect the shell elements. They were coincident nodes, constraint equations, and multipoint constraint elements. The primary factors in deciding which method was used were the component mesh density, the point of contact between the elements, and the relative deformation expected between the elements.

Coincident nodes were used where plates intersected at their mid-thicknesses and the component mesh densities were the same. An example of this was the web-flange interface of an I-shaped girder like the one shown in Figure 4.1. Of course this assumes the mesh density of the flange is the same as the web along the length of the girder. In this study the mesh density of the web was used to control the mesh density of the flange in order to enforce the nodal coincidence for both plates. A major advantage of this method is that the elements share the same nodes and have the same degrees of freedom, and as a result, no further measures are needed to create an accurate representation of the plate connections. A disadvantage of the method is that the flange density is set by the web. The previously described algorithm to create near unity element aspect ratios was not directly applied to the flange. To mitigate this, two areas were used along the web depth, which allowed the flange elements to have aspect ratios between one and two for the girder geometries used in the study.

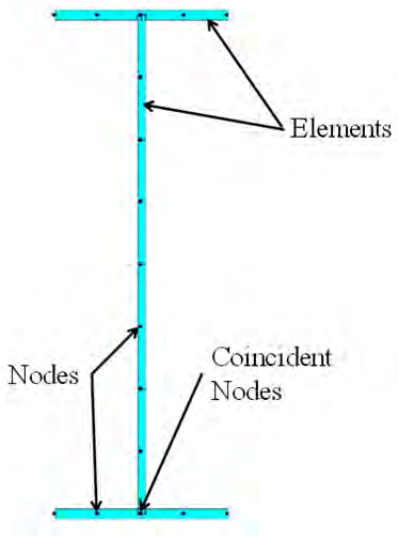

Figure 4.1: Girder cross section nodes and elements

Constraint equations were used where the plates intersected at their mid-thickness, had different mesh densities, and where little relative deformation was expected between the connected components. An example was where the braces intersected the connection plates. Constraint equations are equations that constrain nodes between two elements. Therefore the constrained node's response is governed by the shape functions of the constraining element. This means the constraint equation is generated based on the location of the constrained node relative to the constrained element. The advantages of this connection method is that it is computationally efficient (no additional elements or nodes are generated), it allows the mesh densities of the connected components to be different, and ANSYS has built in functions that allow these equations to be easily developed.

The major disadvantage of the constraint equation connection is the equation is not updated as the relative position of the node changes with respect to its constraining element during a non-linear analysis. For this reason, the constraint equations were only used on this project where little relative deformation was expected between elements. Another disadvantage is that if the constraining node does not lie along the constraining element's mid-thickness, when the constraining element undergoes a rigid body rotation a virtual reaction can develop between the constraining element's nodes and the constrained node. This may cause the structure to appear not to be in equilibrium. Therefore another criterion employed for the use of constraint equations in the modeling was to limit their use only to cases where plate components intersected at their mid-thicknesses.

If large relative deformation was expected between plates with differing mesh densities not intersecting at their mid-thickness, then a multi-point constraint element with 6°of freedom at each end node (ANSYS MPC184 – rigid beam) was used to model the connection. This element does have non-linear capabilities (therefore it updates the geometric relationship between its nodes during a non-linear analysis) and does not impose virtual reactions if rigid body rotation occurs. This element was particularly well suited to model welds in cases where the size of the weld was an important consideration. Table 4.1 summarizes the types of connections and when they were used.

Table 4.1: Model plate connection parameters

Connection Type	Plate Intersection		Mesh Density		Relative Deformation	
	Mid-thickness	Not Mid-thickness	Same	Different	Little	Significant
Coincident Node	X		X		X	X
Constraint Equation	X			X	X	
Multi-Point Constraint Element		X		X		X

4.3 Connection Modeling and Validation

One of the purposes of the study was to compare the stiffnesses of the bent plate and split pipe stiffener connections. To do this computationally, finite element models of the bent plate and split pipe connections were created and then validated with laboratory results. The laboratory data used was from the connection tests described in Chapter 3 (Experimental Program). This section describes the creation and validation of the models for both the bent plate and split pipe stiffener models.

4.3.1 Bent Plate Connection Modeling

The bent plate connection model was created based on the geometry of the laboratory specimen and the general modeling techniques previously described in this chapter. A picture of the model with some of the key aspects called out is shown in Figure 4.2.

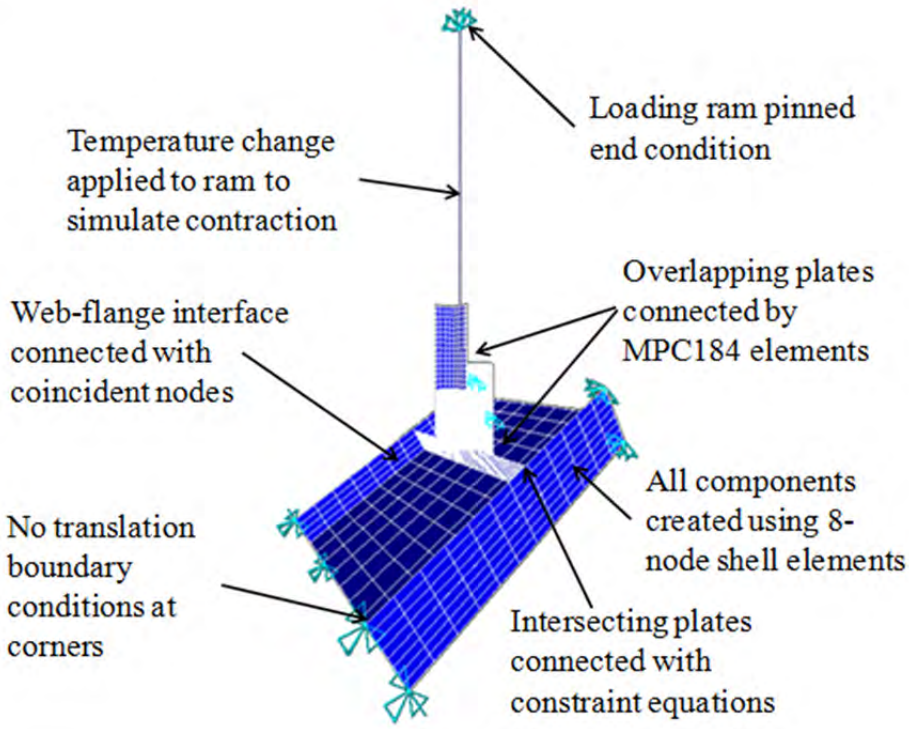

Figure 4.2: Bent plate connection finite element model

Figure 4.2 indicates the locations were the connection methods outlined in the last section were used in the model. The line marked as the "ram" in the figure consisted of a truss element connected to the angle in the model. To simulate the ram applying the tension load to the specimen, a temperature contraction was supplied to the ram with the end of the ram being pinned as it was in the specimen test frame. This allowed the model to account for the restoring force the ram applied to the specimen as the angle and bent plate experienced lateral deflection.

A critical feature in the model was accurately capturing the weld between the connection plate and bent plate at the bend in the plate. Comparisons between the model and the FEA solutions, demonstrated that the weld provided significant stiffening to the connection because it increased the effective thickness at the bend in the plate. Including the weld into the model resulted in good agreement between the laboratory test results and the FEA solution. A picture of the multi-point constraint elements used to model the weld at the bend and the constraint equations connecting the connection plate and girder are shown in Figure 4.3. Additional lessons learned during model validation are covered in the small scale testing validation section of this chapter.

The bend in the bent plate was spanned by four elements as seen in Figure 4.3. This was done to ensure that there was at least one element per 15° of arc in accordance with the recommendation found in the ANSYS documentation for modeling curved surfaces (ANSYS Inc. 2010).

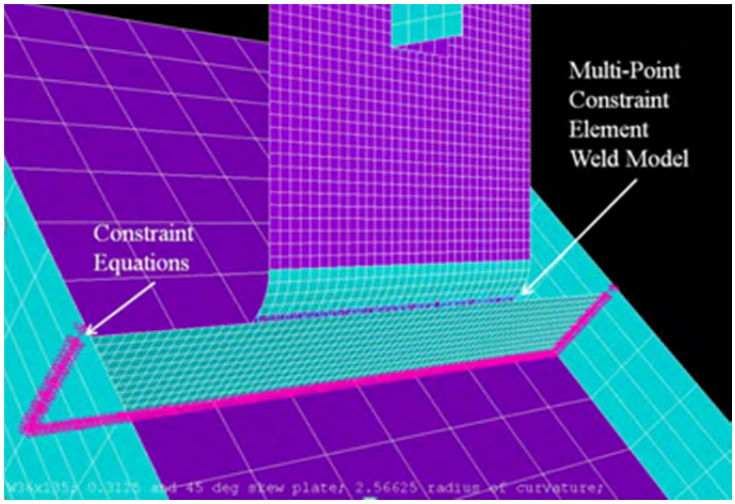

Figure 4.3: Bent plate connection weld models

4.3.2 Bent Plate Connection Modeling Validation

The laboratory results from the bent plate connection tests were used to validate the bent plate finite element model. Both the vertical and lateral deflections of the plate were compared to assure the behavior of the bent plate, connection plate to the girder web, as well as the connections between the plates were being appropriately modeled. All specimens listed in the connection testing section of the previous chapter were used to validate the bent plate connection modeling techniques.

One parameter that was identified to be particularly important was the ratio of the bend radius to element thickness of the bend in the bent plate. ANSYS allows this ratio to be 0.5 or larger, but issues a warning if this ratio is below five because this approaches the limit of the plate theory on which ANSYS SHELL93 element is based. Therefore the three 45° skew specimens were used to find how small the ratio could be and still have good agreement between the model and test results.

The results of the validation showed that as long as the bend radius to element thickness was greater than three, the model had good agreement with the specimen lateral translation. An example of this is shown in Figure 4.4 where the bend ratio to element thickness is 3.2 (the bent plate was 5/16" thick with a 1" bend radius) and there is good agreement.

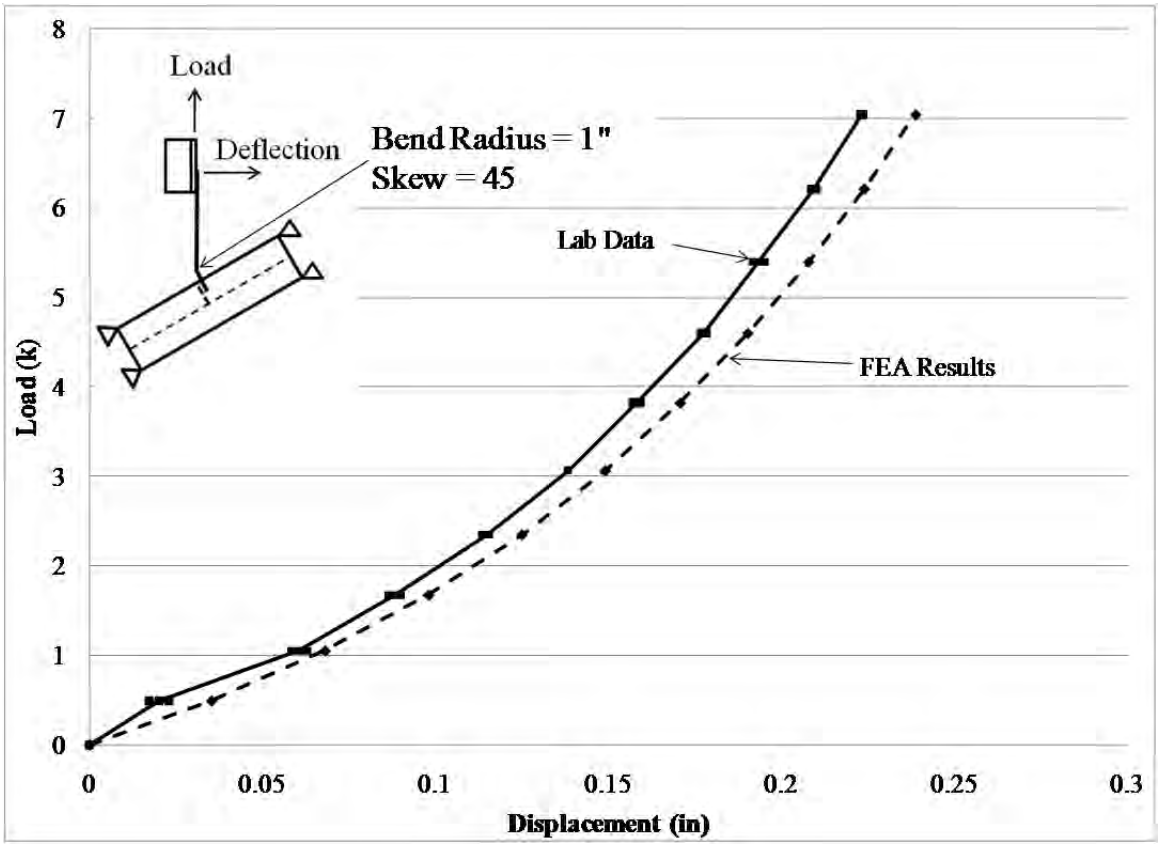

Figure 4.4: 45° specimen lateral results with 3.2 bend radius to thickness ratio

However, if the bend ratio to element thickness ratio was below three, poor agreement between the specimen and model lateral deflection generally resulted as shown in Figure 4.5 for a bend ratio to element thickness of 1.9. An additional case where this occurred was with the 60° specimen that can be found in Appendix B (Finite Element Model Validation Results).

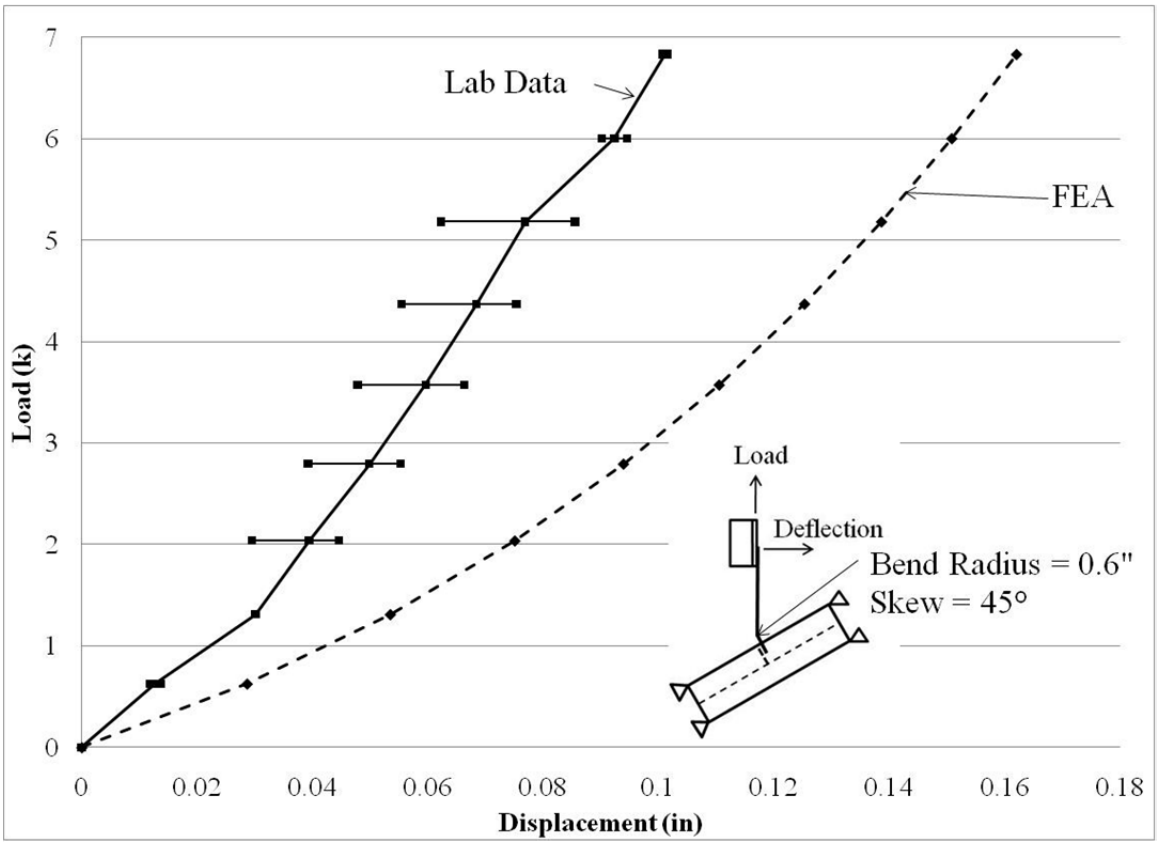

Figure 4.5: 45° specimen lateral results with 1.9 bend radius to thickness ratio

Finally, if the bend radius to element thickness was larger than three then the vertical deflections also showed good agreement demonstrated by the graph of results in Figure 4.6.

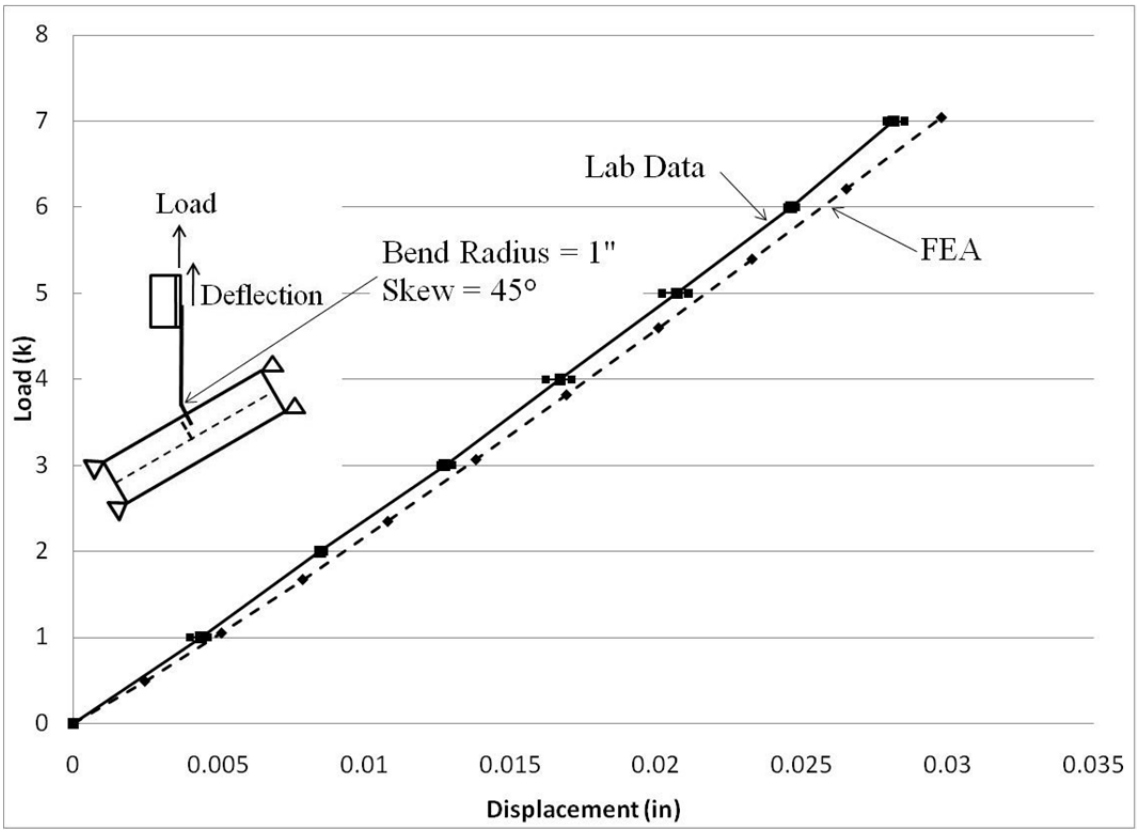

Figure 4.6: 45° specimen vertical results with 3.2 bend radius to thickness ratio

All other cases showed good agreement between the model and specimen deflections except for the axial deformation in the 15° skew specimen. The poor comparison in this case was likely due to fact that the deflections were relatively small (less than five-thousandths of an inch) therefore measuring them was extremely difficult. Charts of this case as well as all others can be found in Appendix B (Finite Element Model Validation Results).

4.3.3 Split Pipe Connection Modeling and Validation

The 0° and 45° split pipe specimens described in the previous chapter were used to validate the split pipe connection model. A picture of the model and specimen is shown in Figure 4.7. The same techniques used in the bent plate model were again used in the split pipe model. This section provides an overview of the comparisons between the test results and computational solutions used to validate the FEA modeling techniques.

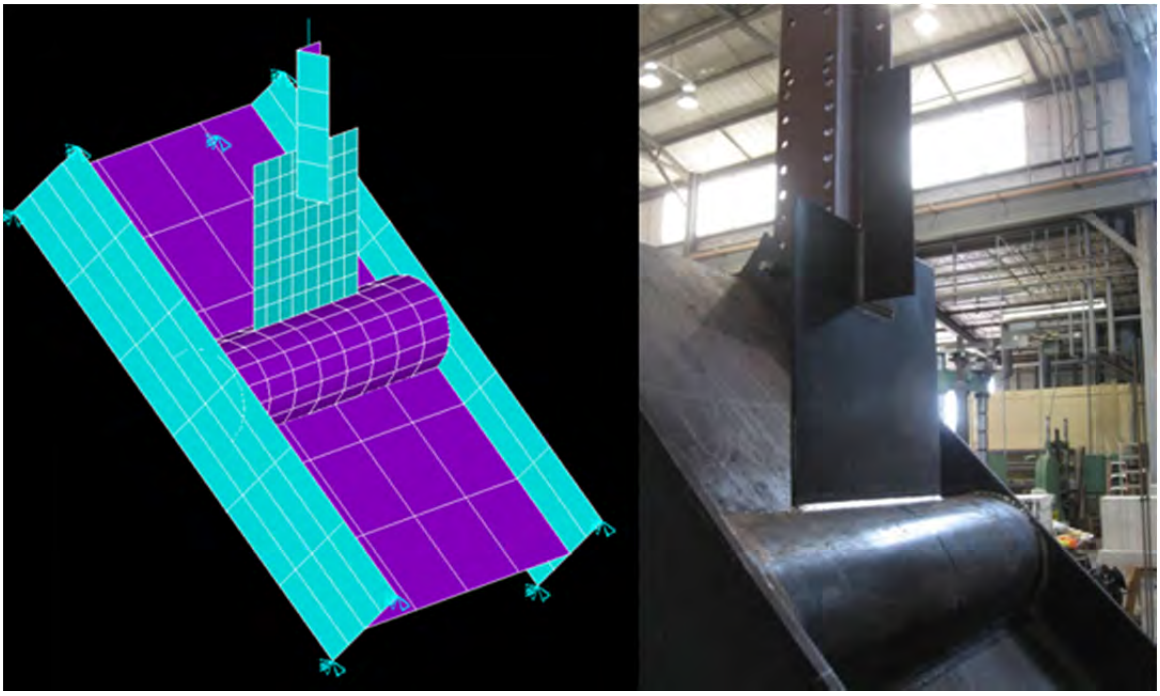

Figure 4.7: 45° connection model (left) and specimen (right)

The 0° skew lateral deflection results are shown in Figure 4.8. The lateral deflection in this case primarily occurred due to the eccentricity in the connection between the angle and the plate welded to the split pipe. Although there was difference between the FEA solution and the measurements, the model did have a similar shape to the measurements. The 45° lateral deflection results are shown in Figure 4.9. The 45° specimen deflected less than the 0° specimen because the connection plate was closer to the pipe–web interface. The model reflects this as well and shows good agreement with the laboratory specimen. While the model results between the two skew cases may seem inconsistent because it predicts a stiffer connection than the lab results in the 0° skew case and a more flexible connection than the lab results in the 45° case, two factors must be considered. First, the differences between the laboratory results are only 0.02" which is near the expected error of the measuring device and test frame. Secondly, the model assumes no imperfections, while there is certainly some imperfection in the laboratory specimens that most likely would account for a majority of the difference between the laboratory results. The vertical deflection results are provided in Appendix B (Finite Element Validation Results).

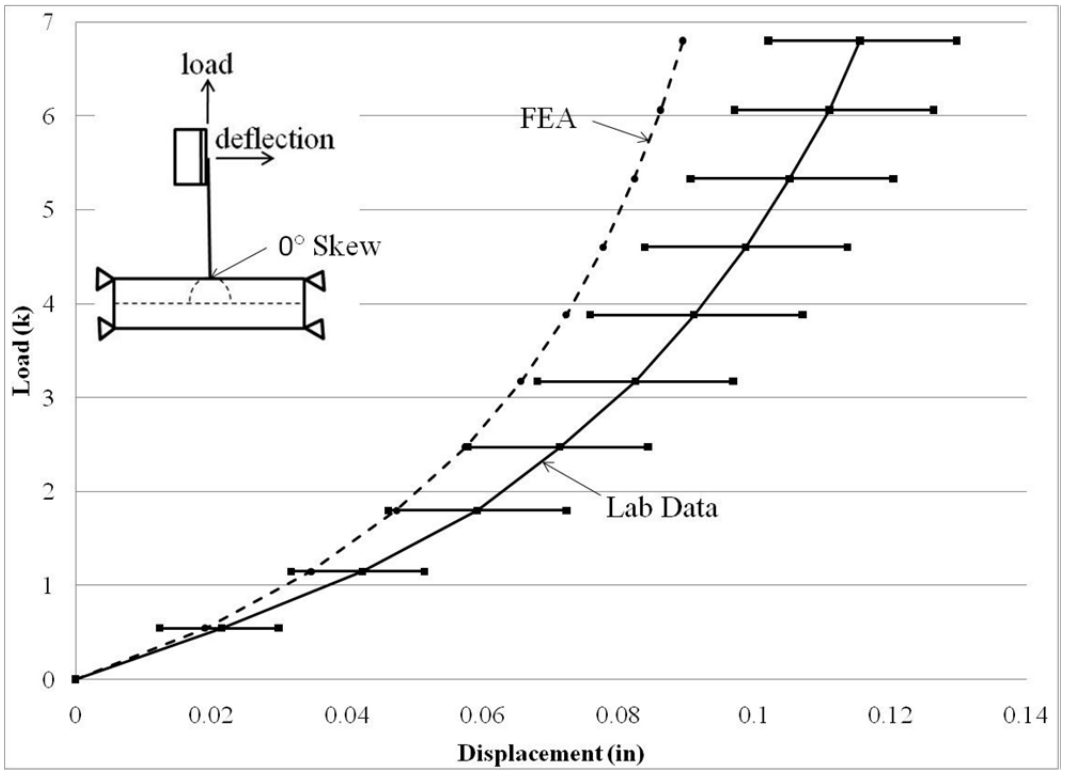

Figure 4.8: 0° skew split pipe lateral deflection FEA and specimen results

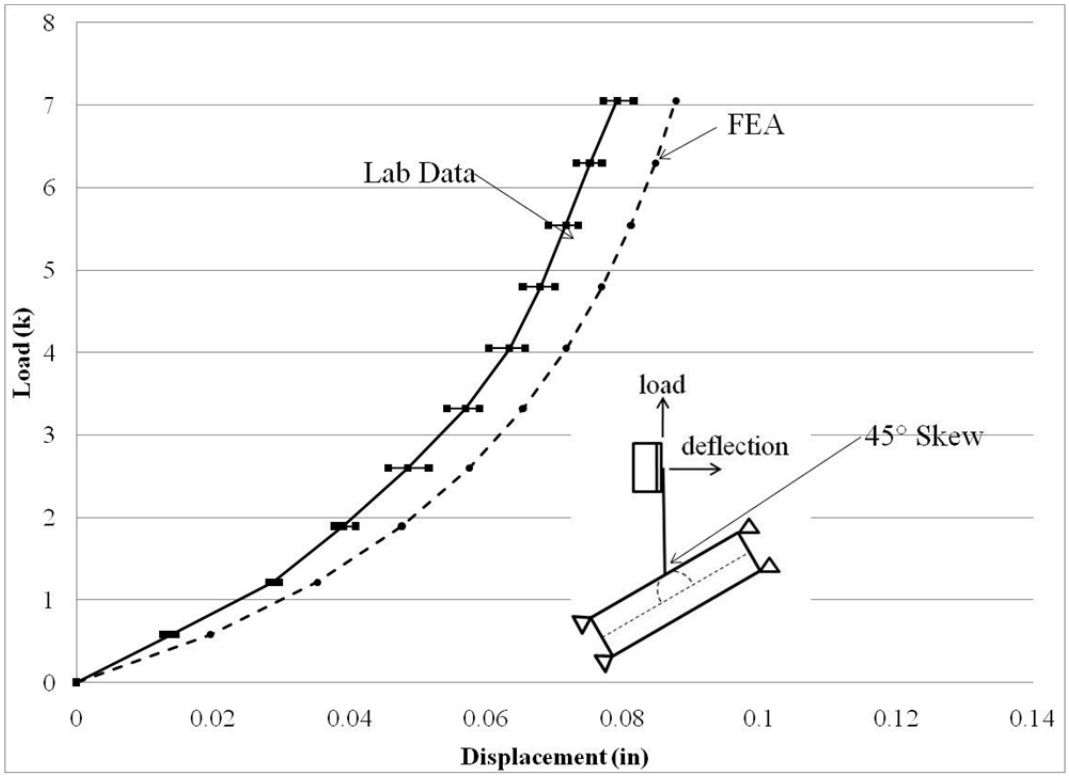

Figure 4.9: 45° skew split pipe lateral deflection FEA and specimen results

4.4 Single Girder Modeling

After confidence had been gained in the modeling of the bent plate and split pipe connection models, the next step in the modeling was to create a finite element model of the full girder system. Validation comparisons were conducted by comparing the model with eigenvalue and non-linear geometric buckling results from both analytic solutions and laboratory test results. This section describes the modeling techniques used to create the girder model, stiffeners, connection plates, and split pipe stiffener as well as the analytic and laboratory validation data.

4.4.1 Girder Cross Section

The girder cross section was constructed using the basic techniques described in Section 4.2 by considering the girder cross section to be composed of three plate elements including the top flange plate, the bottom flange plate, and the web plate. As previously mentioned the plates were connected using coincident nodes. Figure 4.10 shows a W30x90 girder segment model. In the left part of the figure are the areas used to create the model. The right side of the figure shows the model elements when a web mesh density per area of two is used. Note there are four elements along the depth of the web because two areas make up the web depth.

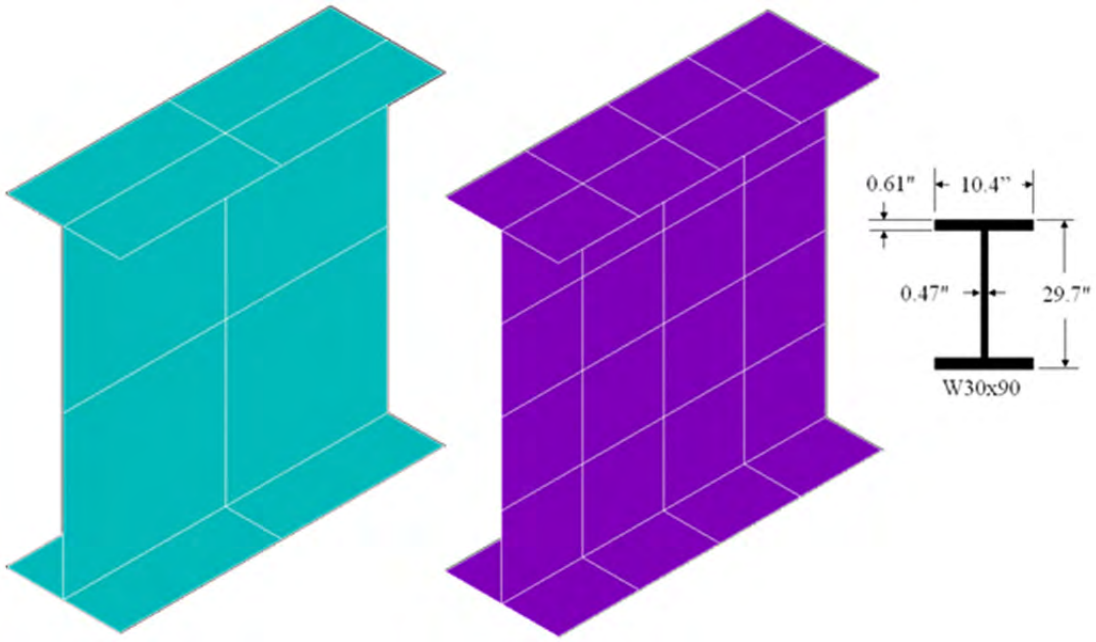

Figure 4.10: W30x90 finite element model girder segment areas (left) elements (right)

Accounting for the fillets in a rolled shape must be accomplished to get an accurate model of the laboratory specimen. While the model uses plates to build the girders, the geometric properties of the fillet between the flange and web are modeled by using beam elements (ANSYS BEAM4) connected between each node along the length of the web-flange interfaces. The geometric properties of the beam elements (area, torsional constant, etc.) are assigned by calculating the properties as if the rolled shape were a plate girder and then subtracting them from the rolled shape values as given in the AISC Steel Construction Manual (American Institute of Steel Construction 2005).

4.4.2 Plate Stiffeners

Plate stiffeners were used in several different applications in this study, including bearing stiffeners, concentrated load stiffeners, and cross-frame connection plates. They are all modeled in the same way using the plate modeling technique previously discussed with the stiffeners intersecting the web and flange plates at their mid-thicknesses. The most important consideration was found to be the method of attaching the stiffeners to the girder cross section.

Two different stiffener-to-girder connections were used depending on whether the FEA solution was being compared to analytic solutions or to actual conditions. The plate stiffeners do actually provide some warping restraint; however, the analytic solutions that were used to validate the model accuracy did not account for the warping restraint provided by the plate stiffeners. Therefore, if minimal warping restraint was desired then constraint equations were used to connect the stiffeners to the girders. This was the typical application if an eigenvalue buckling analysis was being used to compare with an analytic solution.

However, in the case of comparisons between the FEA models and test results, the test data included the increased warping stiffness provided by the plate stiffeners. To obtain an estimate of the actual warping restraint provided by the stiffener, multi-point constraint elements were used to model the welds that attached the stiffeners to the girders. The multipoint constraint equations were used to connect nodes on the stiffeners and girders that were connected via fillet welds. The lengths of the multipoint constraint equations were set by the half thicknesses of the plates they connected and the size of the weld. Figure 4.11 shows both connection types. The left side shows the constraint equation connection and the right depicts the weld modeled by multi-point constraint elements.

When using element welds, their size was set by the connected component mesh densities. Therefore, an adequate mesh density had to be selected to ensure the weld element sizes and orientations were accurate. In some cases, a denser mesh was required than typically used, which added to the computational time on larger models.

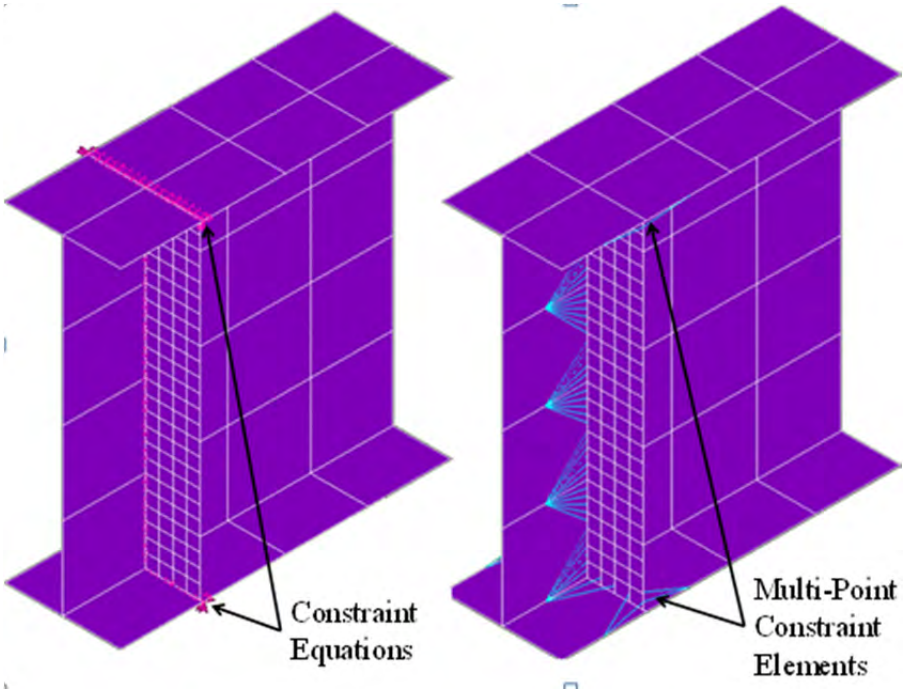

Figure 4.11: Plate stiffener connections

4.4.3 Split Pipe Stiffeners

The split pipe stiffeners were modeled using the basic steel plate modeling techniques previously described in Section 4.2.1 with the additional curved surface modeling considerations as described in Section 4.3.1. The split pipes were connected to the girder web and flanges using constraint equations. Figure 4.12 shows split pipe bearing stiffeners connected to a girder segment.

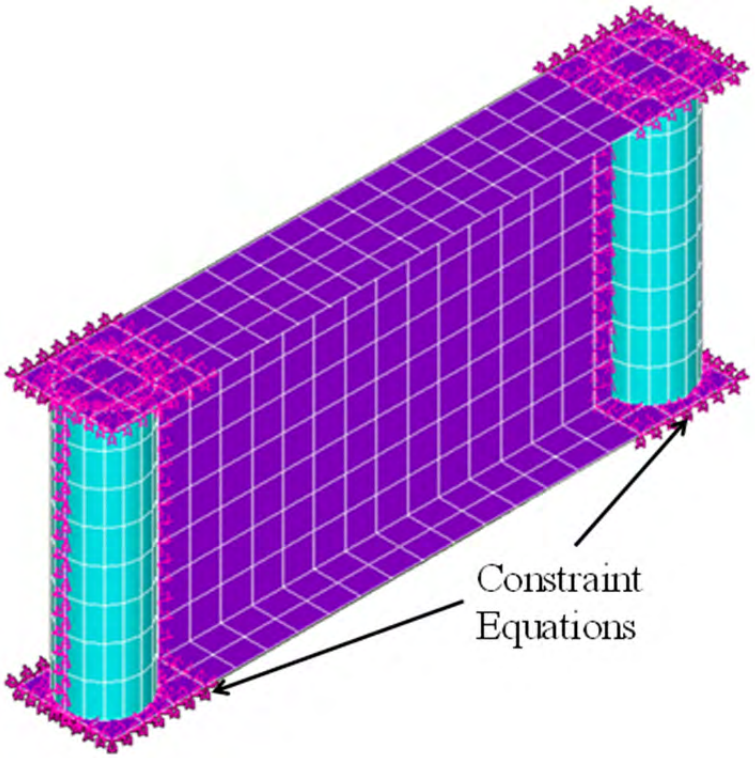

Figure 4.12: Split pipe stiffener model

4.4.4 Steel Self-Weight

The self-weight of the steel was accounted for by applying a gravitational acceleration to the model. The density of the steel was included as one of the material properties that ANSYS used to formulate a lumped mass matrix for each element that was included in the analysis via the inertial loads it created.

One exception to this was the self-weight of the loading beam. Its self-weight was accounted for by using a concentrated mass element (MASS21) at the point of contact between the load beam and girder. The reason for this is explained in the next section. A picture of the load beam in the twin girder model is shown in Figure 4.13.

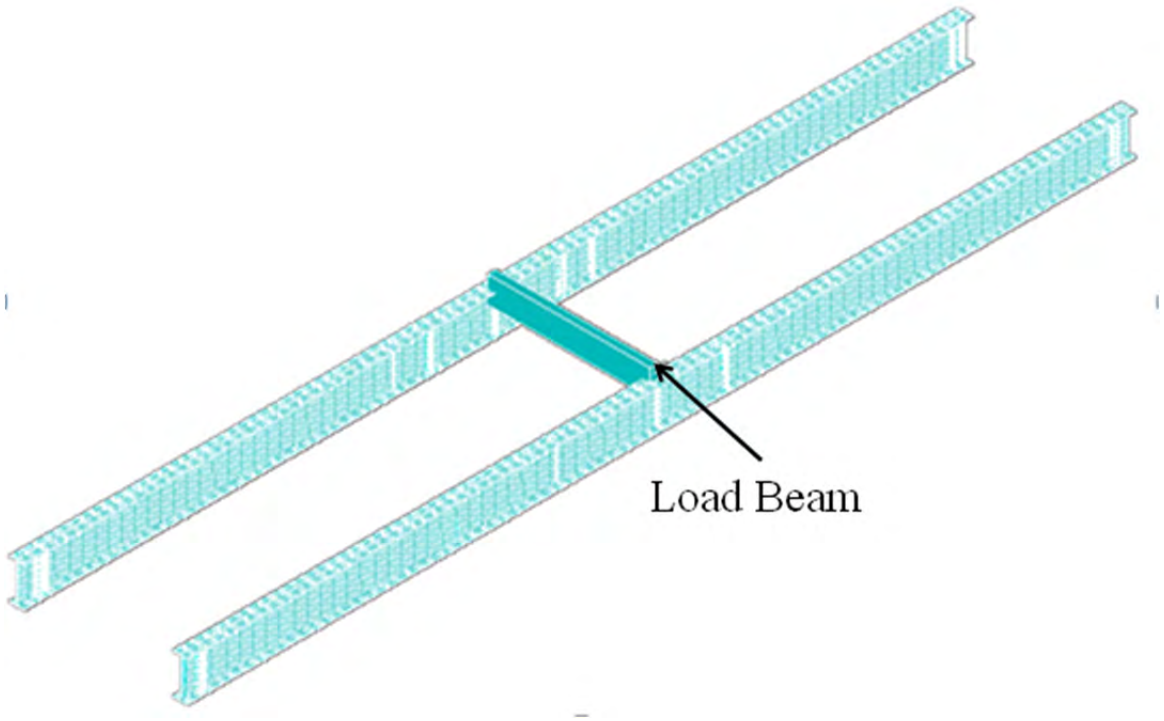

Figure 4.13: Twin girder model with load beam

4.4.5 Loading and Load Beam

The individual load beam reactions usually can be modeled as loads applied to the top flange of the girder. In the large scale, however, load beam not only provides vertical loads, but also causes horizontal friction at loading points, which effectively couples the girders in lateral movement. So in cases when intermediate cross-frames were not available, the coupling effect from load beams should be considered. When intermediate cross-frames were installed, the coupling of girders will be provided by intermediate cross-frame. Load beam was modeled as a zero mass beam element (BEAM4) with negligible flexural stiffness. This allowed a simple coincident node connection between the girders and load beam and acted to couple the translation of the girder top flanges. Although using a coupled node equation would typically work well in this situation, constraint equations and coupling cannot be simultaneously used on nodes. Because the load stiffeners were connected to the girder with constraint equations or multi-point constraint elements (see Section 4.4.2), at the same location as the load beam reaction, load coupling could not be used. Therefore the beam element was used to couple the girders. Because the beam element had no mass and negligible flexural stiffness, it did not act as a torsional brace between the girders or apply a torque to the girders.

4.4.6 Initial Imperfections

To model the laboratory girder specimens, their initial imperfections were measured as described in the previous chapter. These imperfections were included in the model by imposing displacements on the top and bottom flanges to capture the initial sweep and twist of the girder along the length. An analysis was performed to generate the initial imperfection geometry. Results from the analysis that generated the initial imperfection were used to define the geometry for the non-linear geometric buckling analysis using the UPGEOM command. The UPGEOM

command uses the deformed shape from a previous analysis to define the basic geometry of a model. The model showing the initial imperfections of GBP1 and GBP2 is in Figure 4.14.

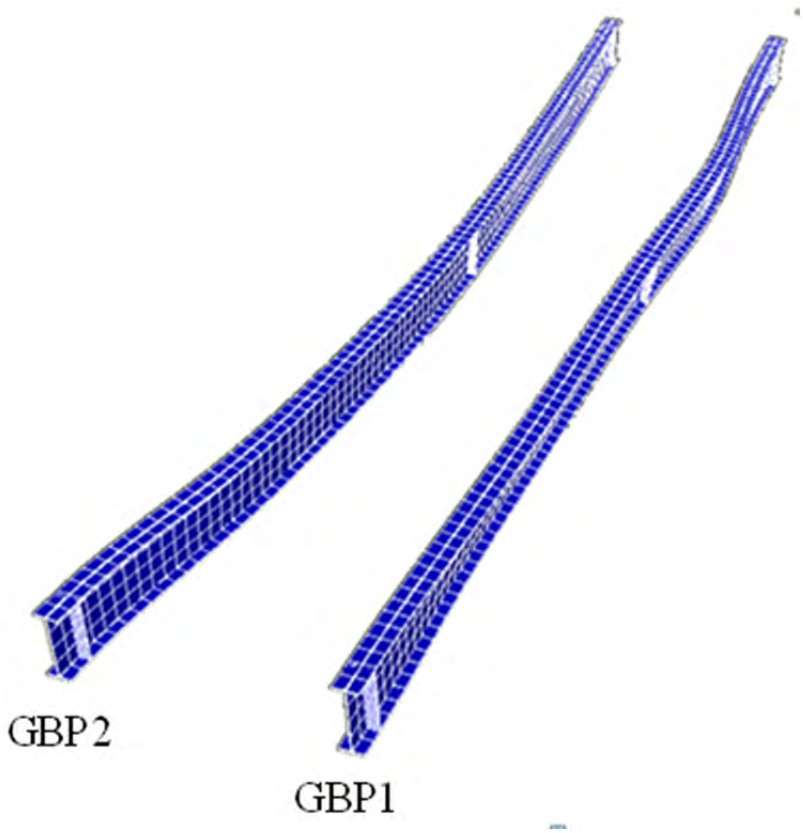

Figure 4.14: GBP1 and GBP2 initial imperfections (magnified 60x)

One issue that had to be considered was the impact the self-weight had on the initial imperfection. Because the specimen initial imperfection was measured with the girders installed in the test frame, the imperfection included the effects of the girder self-weight. In the nonlinear geometrical buckling analysis, gravity was not added to the model's initial imperfection until the first load step. If the imperfection measured in the laboratory was directly used in the model, at the conclusion of the first load step, the model initial imperfection would be larger than the actual specimen's initial imperfection.

This was accounted for by putting a reduction factor on the initial imperfection applied to the model. An iterative solution was used to determine the magnitude of the correction factor applied to the initial imperfection that was necessary so that once gravity was applied to the model would match the measured imperfection. Typical reduction factors were between 0.86 and 0.89.

4.4.7 Thrust Washer Bearings

The thrust washer bearing model was built from a series of compression-only line elements (LINK10). The compression-only elements allowed the girder to rotate up on the edge of the bearing in the same location as the specimen and therefore account for tipping effect. The elements of 4" diameter thrust washer have used steel material and were distributed around the outside diameter of the thrust washer. The top nodes of the line elements were connected to the

girder bottom flange via vertical constraint equations. The base of the line elements were fixed in the vertical direction and coupled in the horizontal direction to the top of the elements to prevent vertical movement at the bottom and differential lateral movement between the top and bottom of the bearing model. Finally one node at the center of the girder contact area was supported in the lateral and longitudinal direction (on the far end only the lateral direction was fixed) to prevent the girder from sliding off the bearing. With this modeling technique, the arrangement of the bearing elements did not depend on the bottom flange node locations.

4.4.8 Girder Model Validation

The validation of the girder model was done with both analytic solutions and single and twin girder laboratory data. The analytic solution used was the basic buckling strength covered in Chapter 2 (Background), with a coefficient (C_b) added to account for moment gradient and load height effects (SSRC 1998). The expression is repeated here for convenience.

$$M_{ocr} = \mathrm{C_b}\pi/L_b\sqrt{EI_yGJ + \pi^2E^2C_wI_y/L_b^2} \qquad (4.1)$$

where

$C_b = AB^{2y/h}$

A = 1.35 for mid-span point load or 1.12 for distributed load

$B = 1 - 0.180W^2+0.649W$ for mid-span point load or $1 - 0.154\mathrm{W}^2+.535\mathrm{W}$ for distributed load

$W = \frac{\pi}{L}\sqrt{\frac{EC_w}{GJ}}$

y = distance from mid-height to load (negative if above or positive if below)

h = distance between flange centroids

All other variables remain as defined in Chapter 2 (Background).

A W30x90 cross section was used to check the model against the analytic solution for top flange, bottom flange, and centroidal loading for cases of point loads, uniform distributed loads, as well as the uniform moment case. Unless otherwise noted, the fillets were not accounted for in the finite element model (FEM) or analytic solution. Simple supports were used in all cases and span to depth ratios considered ranged from 10 to 40.

The results for the uniform moment case are given in Table 4.2. From the table it can be seen that the model has good agreement (within 2%) with the analytic solution in all cases. Fillets were accounted for in the model as described in Section 4.4.1. The model was also checked against the analytic solution that used the AISC rolled shape quantities. These results are given in Table 4.3. These results show that accounting for the fillets with beam elements works well giving results within 1% of the analytic solution.

Table 4.2: Uniform moment FEA analytic validation

L/D	$M_{cr(analytic)}$	$M_{cr(FEM)}$	$M_{cr(FEM)}/M_{(analytic)}$
10	6400	6310	0.99
20	2150	2110	0.98
30	1260	1240	0.98
40	900	880	0.98

Table 4.3: Uniform moment FEA analytic validation—fillets included

L/D	$M_{cr(analytic)}$	$M_{cr(FEM)}$	$M_{cr(FEM)}/M_{cr(analytic)}$
10	6420	6410	0.99
20	2200	2180	0.99
30	1310	1290	0.99
40	935	925	0.99

Top flange loading for the mid-span point load and distributed load results are given in Table 4.4 and Table 4.5, respectively. Both load cases show that the finite element model has very good agreement with the analytic solution.

Table 4.4: Top flange mid-span point load validation—point load

L/D	$P_{cr(analytic)}$	$P_{cr(FEM)}$	$P_{cr(FEM)}/P_{cr(analytic)}$
10	73.6	70.6	0.96
20	13.8	13.5	0.98
30	5.9	5.7	0.98
40	3.3	3.2	0.98

Table 4.5: Top flange mid-span point load validation—distributed load

L/D	$W_{cr(analytic)}$	$W_{cr(FEM)}$	$W_{cr(FEM)}/W_{cr(analytic)}$
10	6420	6410	0.99
20	2200	2180	0.99
30	1310	1290	0.99
40	935	925	0.99

The split pipe stiffened girder model was validated using the previous analytic solutions developed by Ojalvo and Chambers (1977). The models used the same parameters as the original Ojalvo solutions that used simple supports and uniform moments with pipe diameters equal to the girder flange width and 1/4" wall thickness and a shear modulus of 12,000 ksi. The results for the W30x99 and W18x50 cross sections are given in Table 4.6 and Table 4.7, respectively.

The most likely reasons for the trend in the FEA model predicted buckling strength decreasing with respect to the Ojalvo solution as the span increases are the shear stiffness of the girder and warping restraint provided by the web. The FEA model accounts for these, while the Ojalvo solution does not. As the span increases these factors become less important allowing the Ojalvo solution to predict a stiffer response than the FEA at longer girder lengths.

Table 4.6: W30x99 Split pipe stiffened girder buckling comparison

L/D	$M_{cr(Ojalvo)}$	$M_{cr(FEM)}$	$M_{cr(FEM)}/M_{(Ojalvo)}$
10	12970	13090	1.01
15	6390	6350	0.99
20	3970	3890	0.98
25	2800	2720	0.97
30	2140	2060	0.96

Table 4.7: W18x50 Split pipe stiffened girder buckling comparison

L/D	$M_{cr(Ojalvo)}$	$M_{cr(FEM)}$	$M_{cr(FEM)}/M_{(Ojalvo)}$
10	6750	6800	1.01
15	3300	3300	0.99
20	2070	2030	0.98
25	1460	1420	0.97
30	1120	1080	0.96

Prior to proceeding to large scale laboratory testing, a mesh density study was conducted to ensure the appropriate density was used and that going to a denser mesh would neither improve nor degrade the analytic validation significantly. To do this the W30x99 split pipe stiffened cross section was selected so the split pipe and girder densities could be checked. As in the previous studies simple supports were used and the case of uniform moment was considered.

The density used to give the previous results was four elements per web area, two elements per flange area and four elements per pipe area, or 4-2-4. Therefore this density was increased to 6-3-6 and compared to the 4-2-4 density results. The results of this study provided in Table 4.8. From the table it can be seen that when the buckling moment is expressed to the nearest k-in, there is no difference in the results and the 4-2-4 density is sufficient.

Table 4.8: W30x99 Split pipe stiffened girder mesh density study

L/D	$M_{cr(4-2-4)}$	$M_{cr(6-3-6)}$	$M_{cr(6-3-6)}/M_{(4-2-4)}$
10	13090	13090	1.00
15	6350	6350	1.00
20	3890	3890	1.00
25	2720	2710	1.00
30	2060	2060	1.00

4.5 Cross-frame Modeling

After the connections and girder models were validated, bent plate and split pipe stiffener cross-frame models were developed using the validated connection models. These models were used to classify the impact of each connection on the cross-frame stiffness as well as compare the stiffness values of the cross-frames as discussed in Chapter 5 (Parametric Studies and Design Recommendations).

4.5.1 Bent Plate End Cross-frame Model

A picture of the bent plate cross-frame model is provided in Figure 4.15. The cross-frame in Figure 4.15 is designed to fit a pair of W30x90 girders (shown in the diagram for reference only—they were not part of this model) spaced 9' apart with a 53° skew angle. The cross-frame uses a single diagonal brace system that is capable of carrying tension and compression. The additional features of the bent plate cross-frame model are described below.

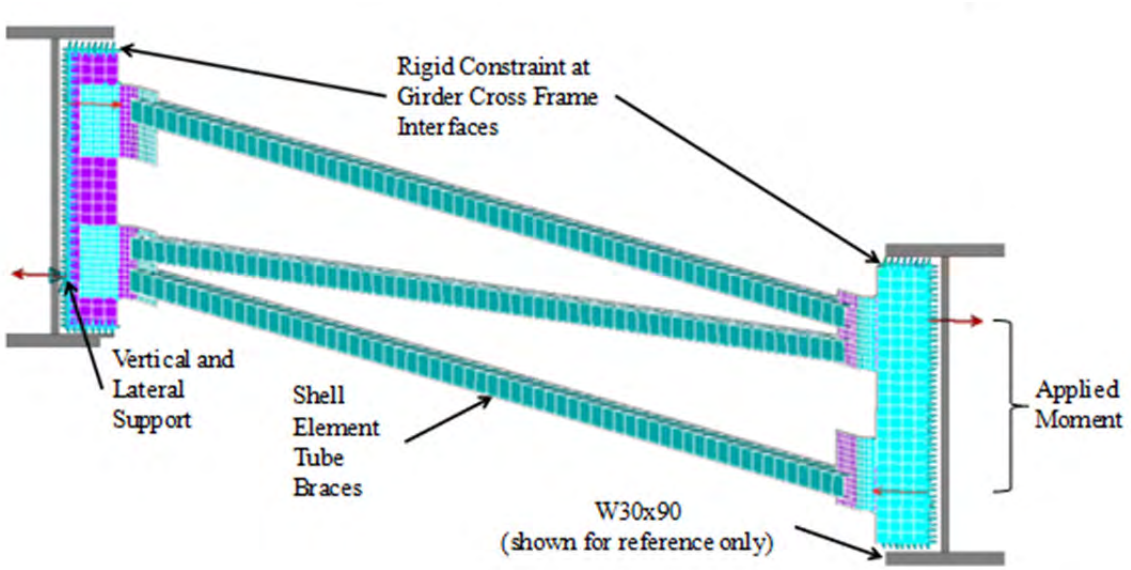

Figure 4.15: Bent plate cross-frame model (53° skew)

As shown in Figure 4.15, the boundary conditions for the cross-frame model consisted of a rigid constraint at the cross-frame-girder interface for rotation. This causes the edge of the connection plates to rotate as a rigid body about the longitudinal axis of the girder. Additionally, longitudinal restraint is applied at the same interface to prevent the cross-frame from moving along the length of the girder longitudinal axis. There is one node on the left connection plate that serves as the vertical and lateral support provided by the girder. There is a corresponding node on the right connection plate that provides vertical support.

To simulate the girder twist, a moment was applied to the end of each cross-frame in the plane of the girder's cross section as shown in Figure 4.15. Once an analysis was run, the rotation of the cross-frame was measured and then the cross-frame stiffness was calculated using Equation (2.27) (repeated below for convenience).

$$\beta_{braxial} = \frac{M}{\phi} \qquad (2.27)$$
(from Chapter 2)

The brace members were square hollow tubes composed of four shell elements (SHELL93). Therefore, because ANSYS does not directly provide forces for shell elements, the stresses were taken from the middle of the top and bottom brace shell elements and averaged to compensate for bending then multiplied by the brace area to recover the brace force. To retrieve the stresses at any cross section along the length of the brace, the ANSYS PATH command was used because it maps any structural response to a defined path. This allowed the stresses to be

measured at the ¼ and ¾ points along each brace's length (the same location as the strain gages on the test specimen) regardless of node placement.

4.5.2 Unskewed Cross-frame Model

An unskewed cross-frame model was constructed with shell elements to find the stiffness of the cross-frame brace members with rigid connections normal to the girder. This model was constructed such that all out of plane deformations were restricted and the connection plates and tabs connecting the braces to the connection plates were formed from a rigid material. A picture of this cross-frame is shown in Figure 4.16 with the standard cross-frame component nomenclature used in this report.

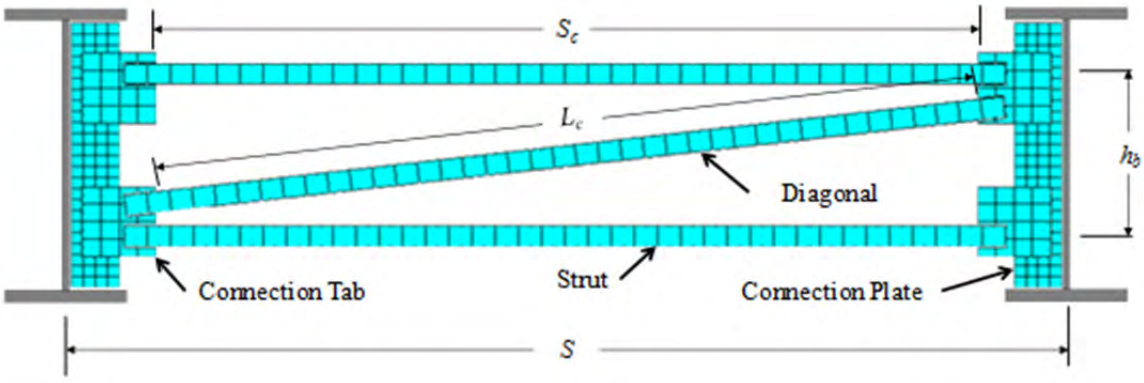

Figure 4.16: Unskewed cross-frame model

The unskewed cross-frame was used to calculate the axial and flexural cross-frame stiffness with a rigid connection condition. While this is the same quantity calculated in Chapter 2 using Equation (2.44), there are some differences between the FEA solution and the equation. The analytic solution only considers brace axial and flexural stiffness, while the shell elements used in the model account for other structural responses such as shear strength and axial force and moment interaction. Therefore, the cross-frame would likely be expected to be stiffer than the analytic solution for smaller girder spacings (S) and this difference should become smaller as S gets larger and the cross-frame deformation is dominated by bending with a relatively small axial force.

Table 4.1 shows the comparison of cross-frame stiffness as calculated by the FEA model and the analytic solution of Equation (2.44). A W30x90 girder cross section with HSS2.5x2.5x1/4 braces were used in the comparison. The comparison shows that the FEA solution is relatively conservative for smaller values of the girder spacing and closes to within 10% for a girder spacing of 15'. In general, for most common values of the girder spacing in Texas (8'-10'), the analytic solution of the cross-frame stiffness is approximately 20% conservative relative to the FEA model. The FEA model is used rather than the analytic solution in the next chapter to calculate the stiffness of the cross-frame braces to be consistent with the models used in the cross-frame connection stiffness calculations.

Table 4.9: FEA to analytic cross-frame stiffness comparison

Girder Spacing (ft)	$\beta_{Total(FEA)}/\beta_{Total(Analytic)}$
8	1.23
9	1.19
10	1.16
15	1.08

4.5.3 Split Pipe Cross-frame Model

The split pipe cross-frame model is shown in Figure 4.17. It was created using the previously mentioned techniques. The only difference was that the moment application was divided in half and distributed to each side of the split pipe. The next section describes the validation of the split pipe cross-frame model using large scale laboratory test data.

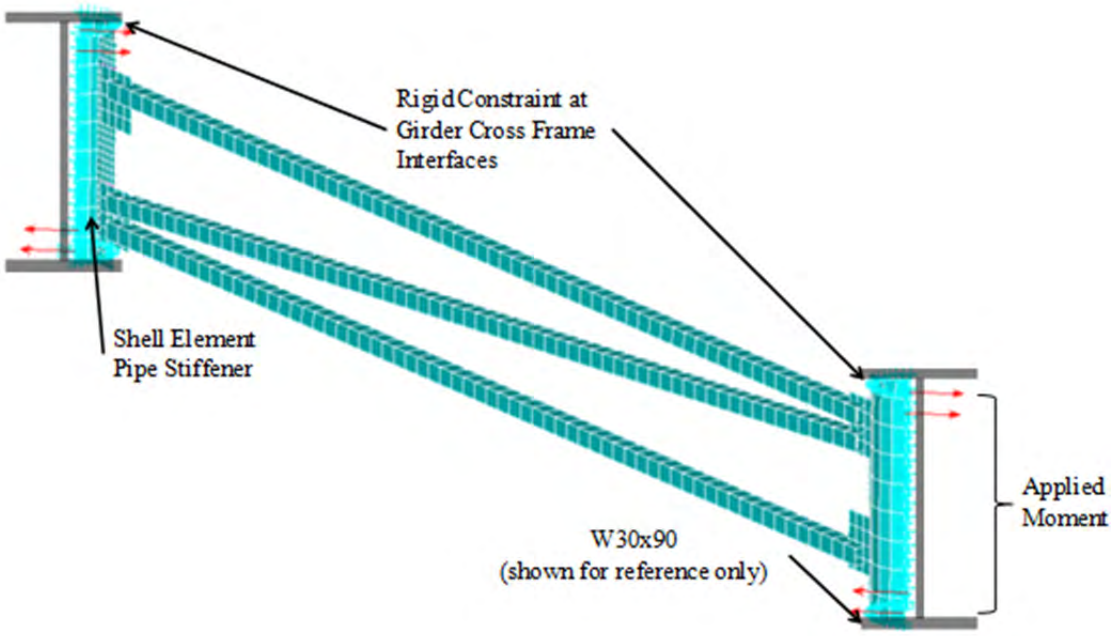

Figure 4.17: Split pipe cross-frame model (53° skew)

4.6 Single and Twin Girder Laboratory Test Validation

Once good agreement was achieved between the model and the analytic solutions, the model was then compared to the laboratory results from the single and twin girder lateral and buckling tests described in Chapter 3 (Experimental Program). This section provides a description of the results of this validation.

4.6.1 Single Girder Validation Results

The single girder model was run for lateral tests as described in Chapter 3 (Experimental Program). A picture of the finite element model with some of the key features called out is shown in Figure 4.18. Note that the 6-3-6 element density was used to correctly size the stiffener welds.

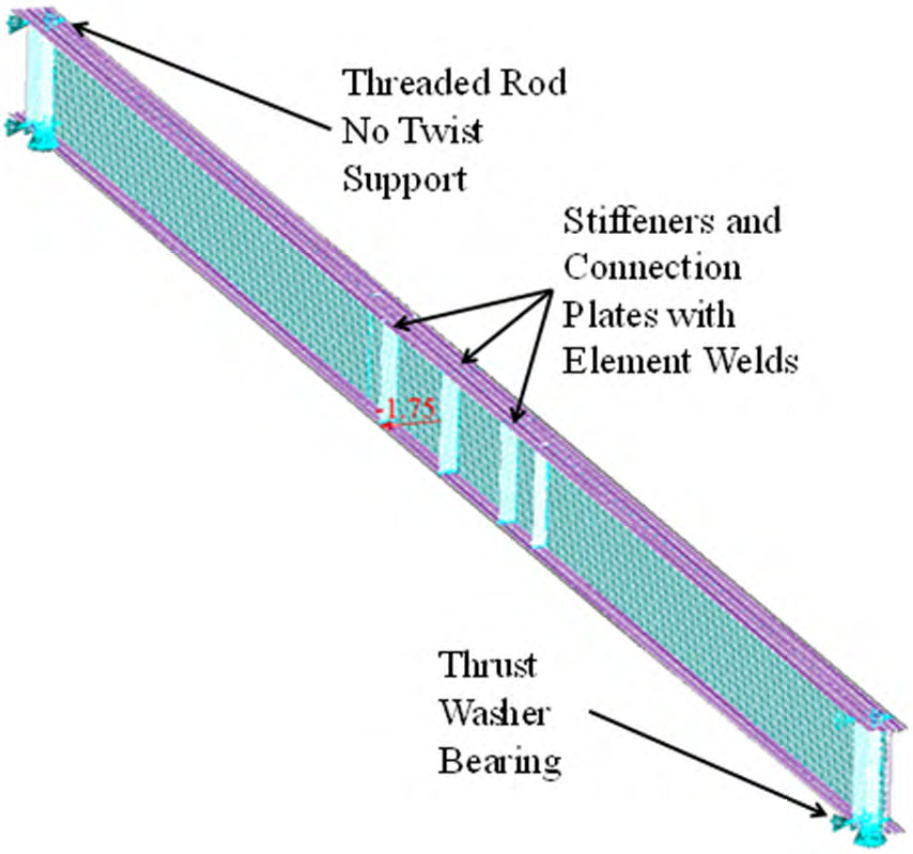

Figure 4.18: W30x90 single girder (GBP2) lateral deflection finite element model

The lateral load test validation results for both the plate (GBP2) and split pipe (GSP2) stiffened girders are shown in Figure 4.19 for the case of the lateral load applied at midheight. As would be expected, the results for both the plate and split pipe stiffened model show good agreement with the laboratory results. This shows that the bearing stiffener models behaved appropriately because the model correctly predicts that each simply undergoes a nearly rigid body twist while the girder mid-span deflects in a pure lateral mode.

The results do show that the split pipe stiffener model is slightly stiffer than the plate stiffened model. A similar trend was observed in the laboratory data. This is most likely due to a small deviation in the point of load application or deflection measurement point between the two specimens.

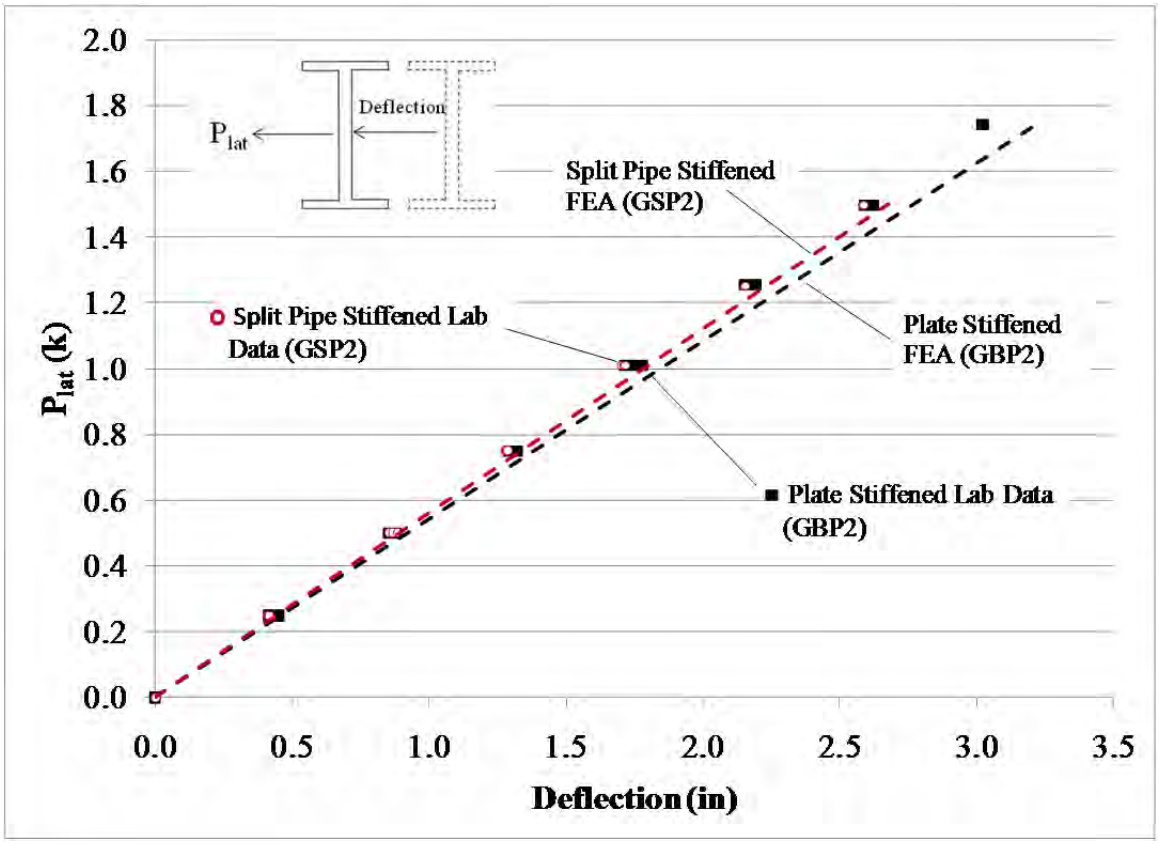

Figure 4.19: Single girder lateral load test results

Finally, it can be seen that the laboratory test specimens were slightly stiffer than the FEA models. Such a result is typically not the case in finite element modeling where the computational error usually results in the model being stiffer than the specimen. This counterintuitive result is most likely due to some friction between the threaded rods and the girder flanges on the side where the girder bears against the rods. In the model, the threaded rods are considered a friction free surface and the girder can slide freely against the support, while in the laboratory specimen friction between the girder flange and the rod results in a reaction that stiffens the system slightly. While this may be an issue in the lateral test where the girders were pulled directly against the threaded rods, during a buckling test, these reactions are relatively small and should have little effect on the results.

Next the single girder models were validated for a lateral load applied at the top flange. Because the lateral load is not applied at the shear center of the section, the loading results in both lateral deformation and twisting. The model was adjusted from the pure lateral test by moving the load to 25.75" above the bottom flange centroid and modeling a no slip condition along the top flange-threaded rod interface. Because the applied load was near the top of the cross section, the top threaded rods bore very tightly against the top flange and increased the friction. When these two adjustments were made to the models, good agreement was achieved between the FEA solutions and the laboratory data as shown in Figure 4.20.

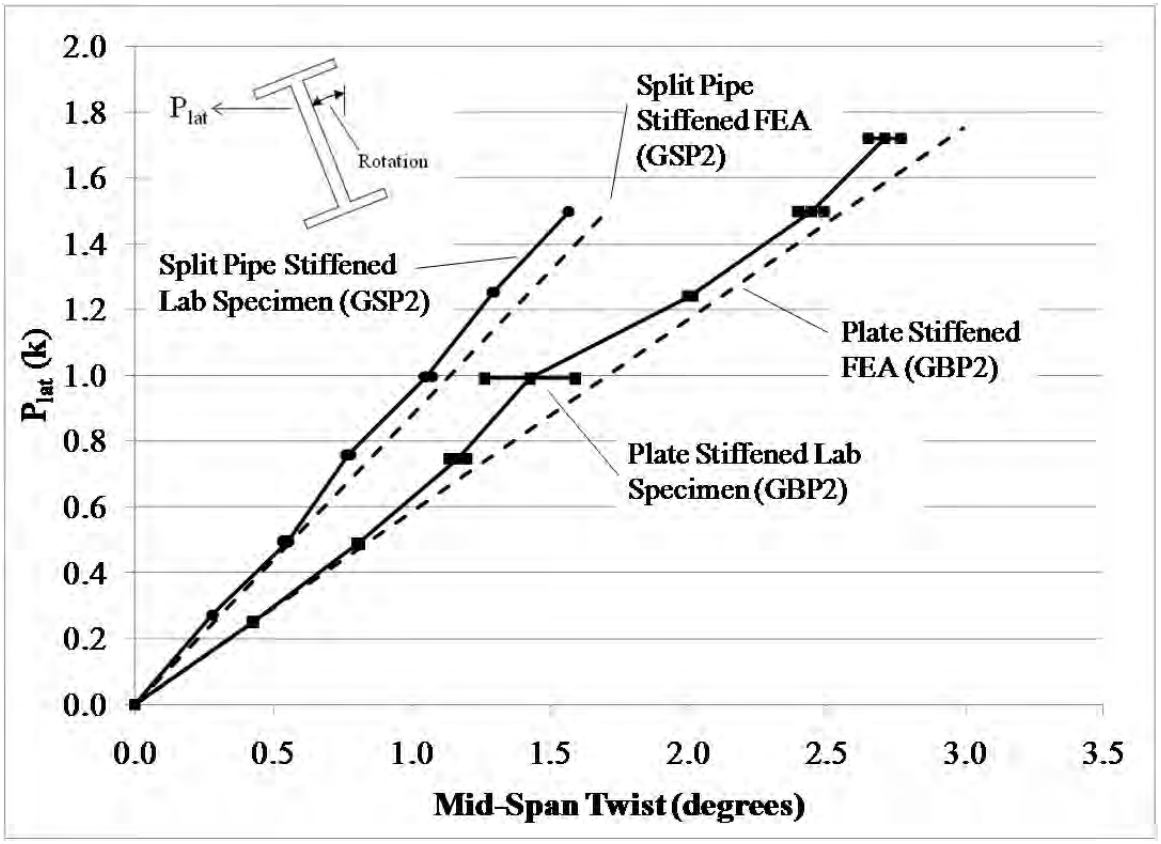

Figure 4.20: Single girder lateral deflection validation under top flange lateral load

4.6.2 Twin Girder Validation Results

Once good agreement was achieved between the FEA models and laboratory test results for the lateral load tests on the single girder, the series of twin girder buckling tests described in Chapter 3 (Experimental Program) were used to validate the finite element girder models. These comparisons provided insight into the accuracy of the modeling techniques for the load beam and gravity load simulators as well as ensured the girders were modeled appropriately. A picture of the model is shown in Figure 4.13. This section describes the results of these validations.

The plate stiffened girders (GBP1 and GBP2) were validated first and GBP2's vertical deflection results are shown in Figure 4.21. The results show that the FEA model has good agreement with the laboratory specimen. The FEA and specimen results become non-linear at the onset of buckling because the twist and translation of the cross section begin to counteract the vertical deflection. The validation data for GBP1 is similar and can be found in Appendix B (Finite Element Model Validation Data).

The mid-span top flange lateral deflection validation data for GBP2 is shown in Figure 4.22. The results show that there is good agreement between the model and the laboratory specimen. Based upon the maximum laboratory specimen loading, the model is 7% conservative. GBP1 had similar results for its top flange lateral deflection. It and all the other twin girder validation results are provided in Appendix B (Finite Element Model Validation Data).

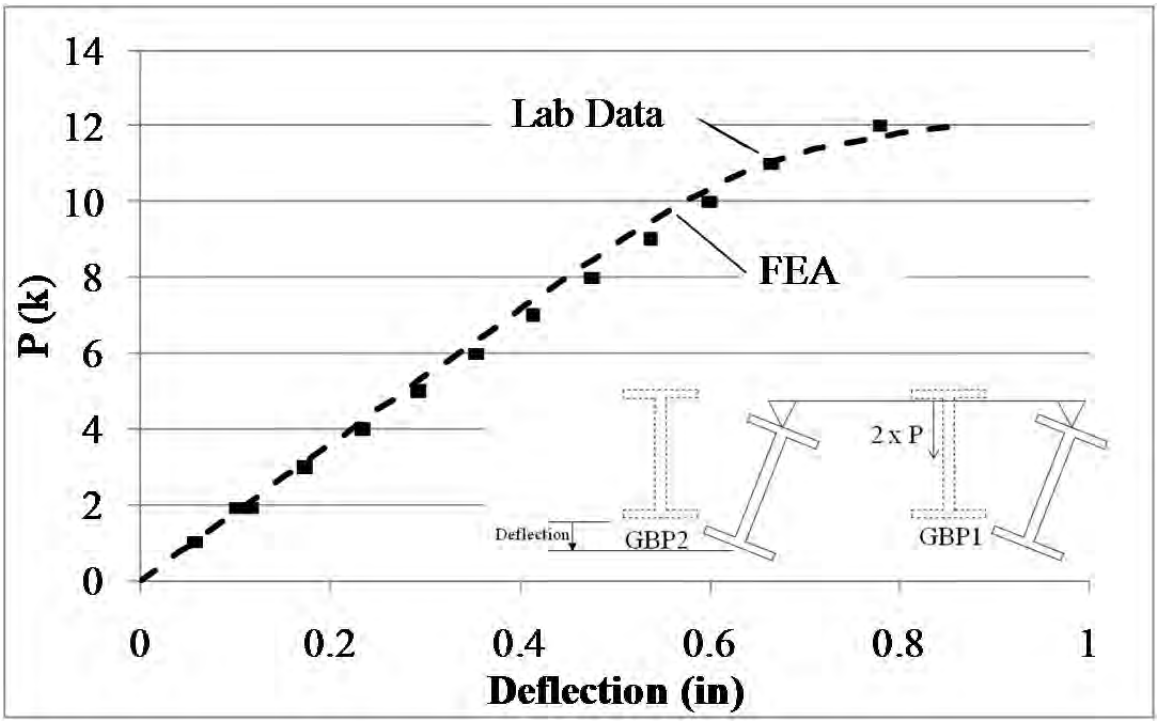

Figure 4.21: GBP2 mid-span vertical deflection validation

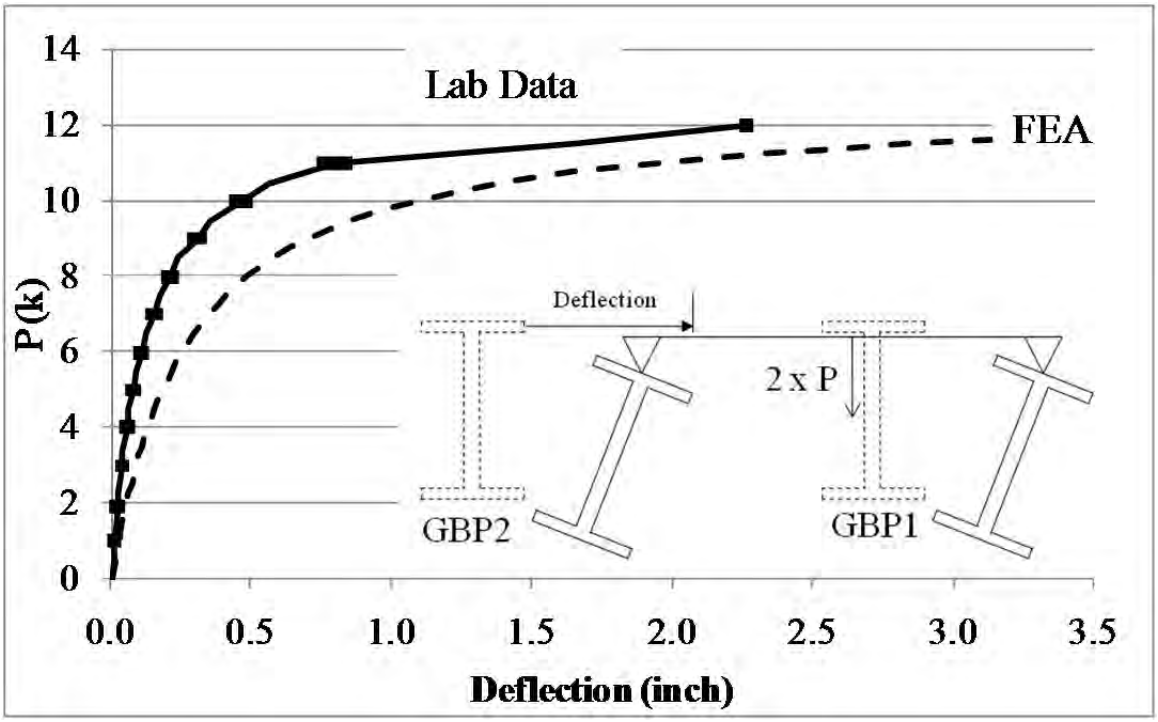

Figure 4.22: GBP2 mid-span top flange lateral deflection validation

4.7 Three Girder Laboratory Test Validation

The large scale laboratory tests on the three girder specimens, with split pipe or bent plate connection, described in Chapter 3 (Experimental Program) were used to validate the girder and cross-frame models. The three girder finite element model was built using the techniques covered in the previous sections of this chapter. The model geometry was based on the 53° skew, three girder laboratory specimen with either split-pipe or bent plate connected end frames as described in Chapter 3. The overall three-girder model provided an opportunity to put all the previous components together to ensure the model captured the full system behavior.

4.7.1 Model with End Cross-frames and Thrust Washer Bearings

The finite element model of the split pipe and bent plate girder specimens with end cross-frames is shown in Figure 4.23 and Figure 4.24 respectively. In the figures, areas instead of elements are shown and the load beams have been removed for clarity.

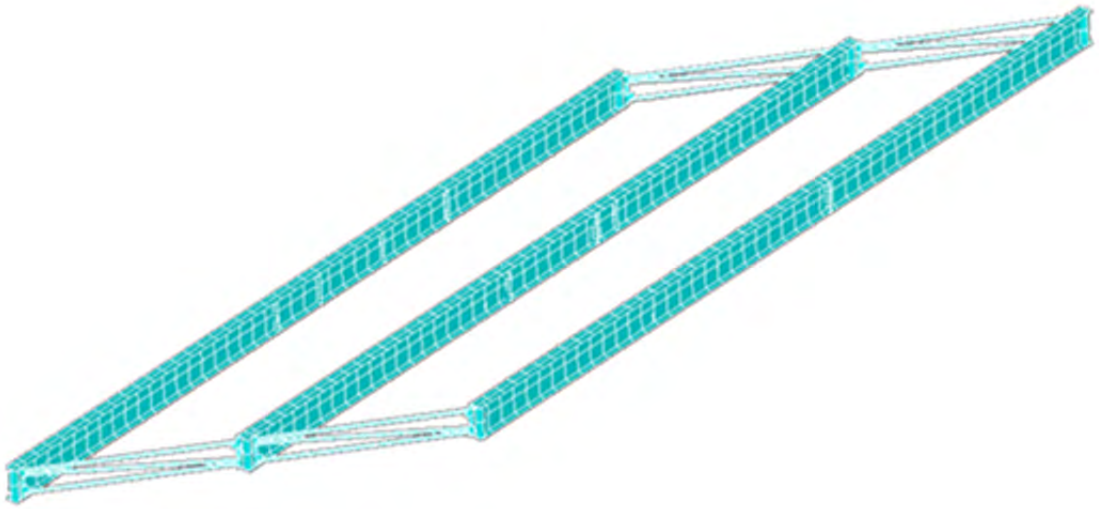

Figure 4.23: Three girder finite element model with split pipe-stiffener end cross-frames

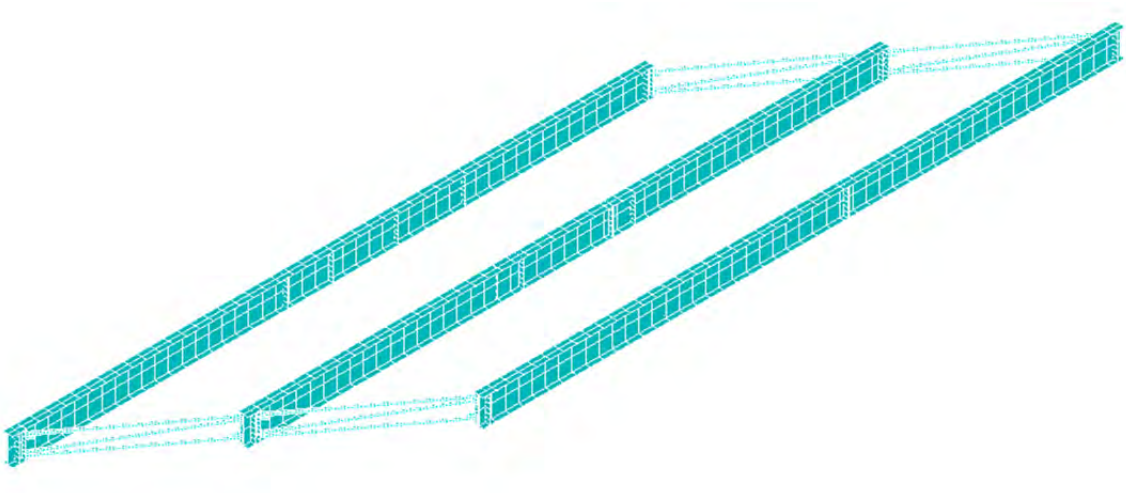

Figure 4.24: Three girder finite element model with bent plate end cross-frames

The mid-span vertical deflection validation results for GSP2 are shown in Figure 4.25. The model had good general agreement with the laboratory specimen. The FEA results show the same effect of the cross-frame resistance to the end twist of the girder as the laboratory data by plotting slightly stiffer than the analytic solution.

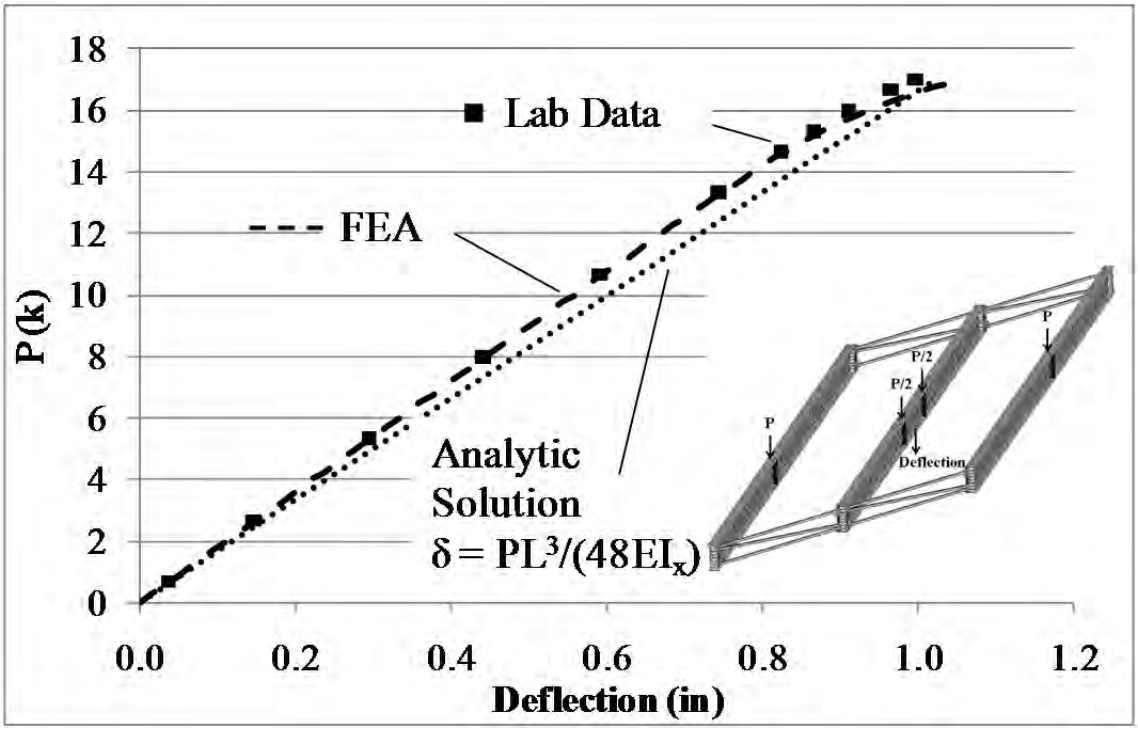

Figure 4.25: GSP2 Mid-span vertical deflection validation

A plot of GSP2's mid-span top flange lateral translation is shown in Figure 4.26. Again the model had good agreement with the laboratory test data. Similarly, the model had good agreement with the GSP2 end twist shown in Figure 4.27 and the northwest and southwest end cross-frame forces shown in Figure 4.28 and Figure 4.29, respectively. The slight differences in cross-frame forces appear to be due to the slightly conservative buckling load predicted by the model.

Similar agreement was found among all other measured structural responses in split pipe girder and bent plate girder models. Plots of all validation data are given in Appendix B (Finite Element Model Validation Results).

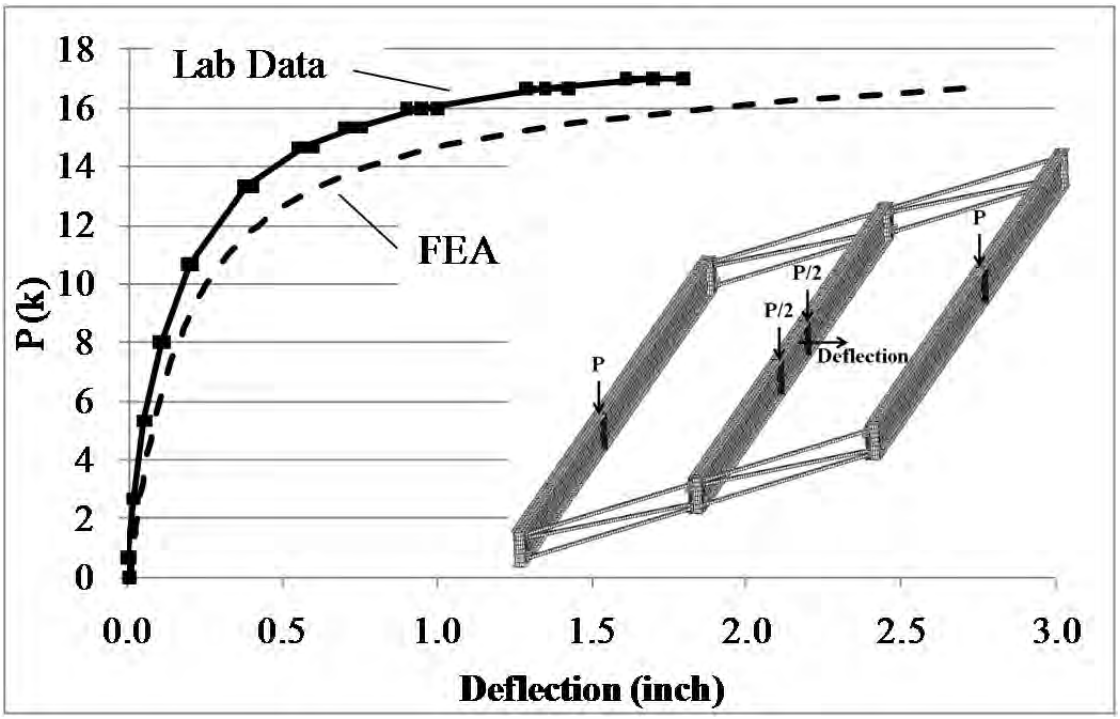

Figure 4.26: GSP2 top flange lateral deflection validation

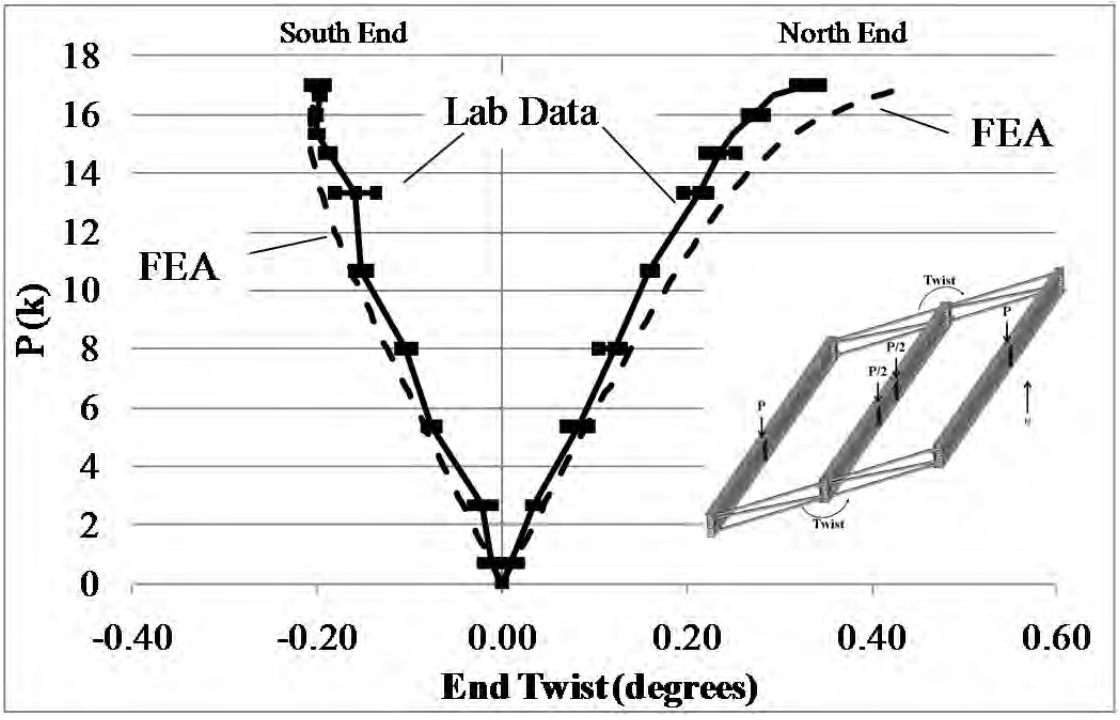

Figure 4.27: GSP2 end twist validation

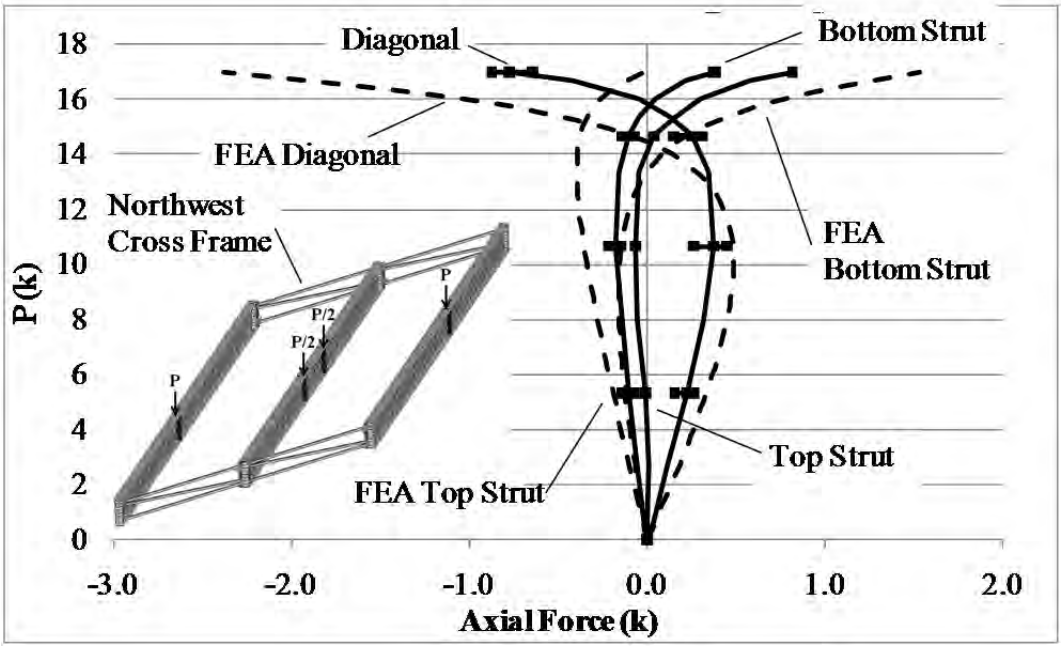

Figure 4.28: Northwest end cross-frame force validation

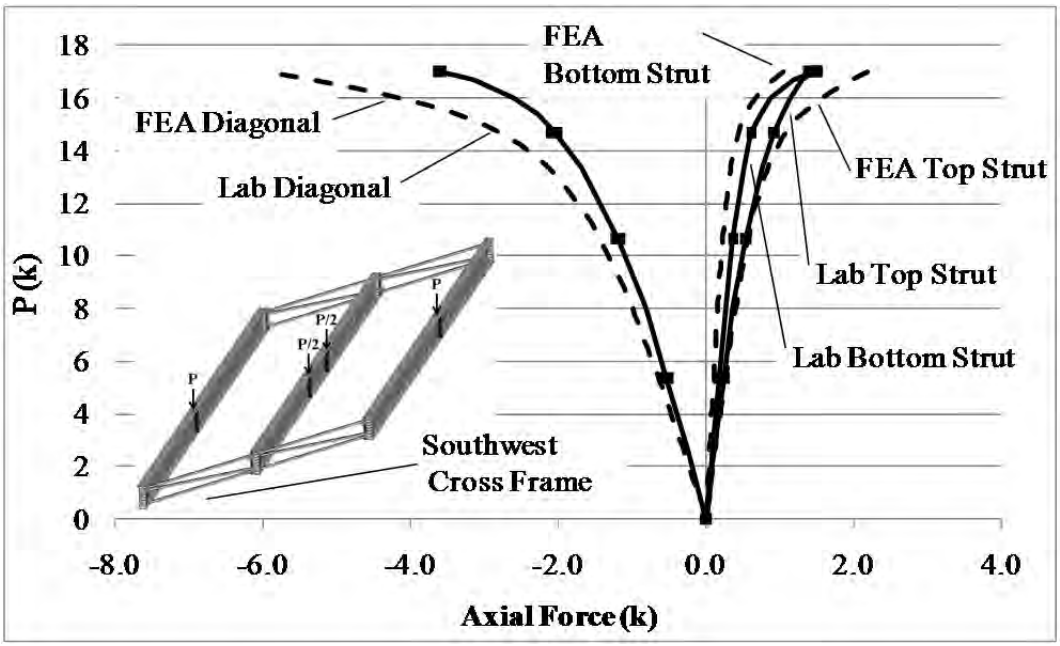

Figure 4.29: Southwest end cross-frame axial force validation

4.7.2 Model with End Cross-frames and Rubber Bearings

As mentioned in the previous chapter, instead of thrust washers two types of rubber bearings were used: pure rubber pads and rubber pads with shims. The bearing model used the same compression-only line elements (LINK10) used for thrust washer bearings as mentioned in Section 4.4.7. In the model, the square rubber bearing pads was simplified as nine elements lined up along the inner side of the bearing pads as shown in the Figure 4.30. As opposed to the nearly

infinite modulus of the thrust washer bearing model, modeling the rubber pads required inputting the modulus of the elements that correspond to the actual stiffness of the rubber pads used in the laboratory. Based on the axial stiffness obtained from laboratory results, the moduli of the link elements were calculated and are listed in Table 4.10. The area of the link elements was taken to be 1 in^2.

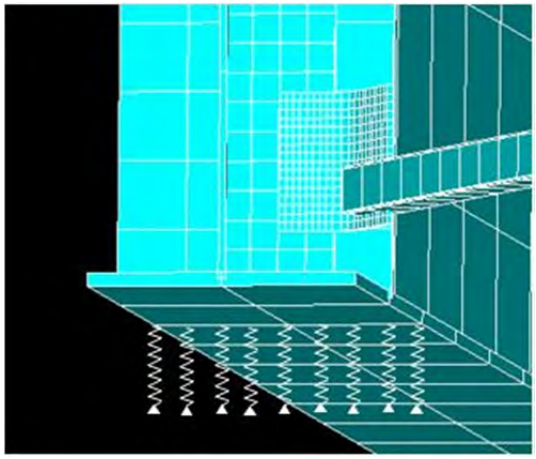

Figure 4.30: Model of rubber bearing pad

Table 4.10: Line element modulus

Bearing Type	Modulus (ksi)
Rubber Pad	8.9
Rubber Pad with Shims	71.9

The results of the large scale tests with the two types of bearing pads were compared with the FEA results. A few comparison results of end twists of girders are presented in Figure 4.31 to Figure 4.34. As seen in the results, the model can reasonably predict the girder twists, no matter which type of bearings or which type of cross-frame connection were used. All validation results such as girder end twists or brace forces are provided in Appendix B.

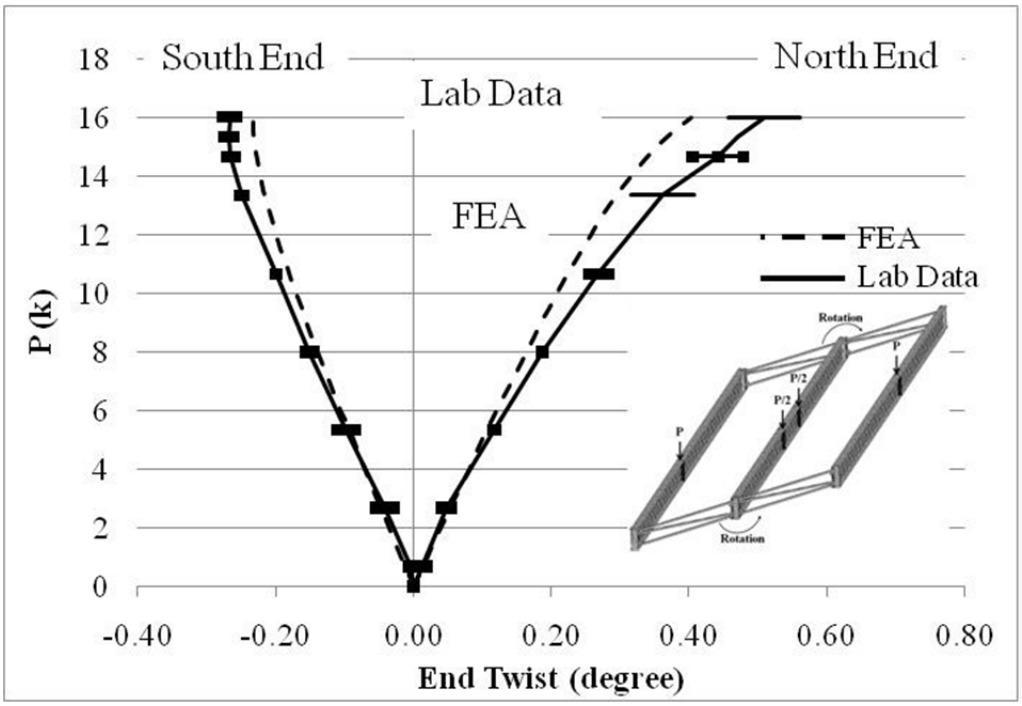

Figure 4.31: GSP2 end twist validation—rubber bearing

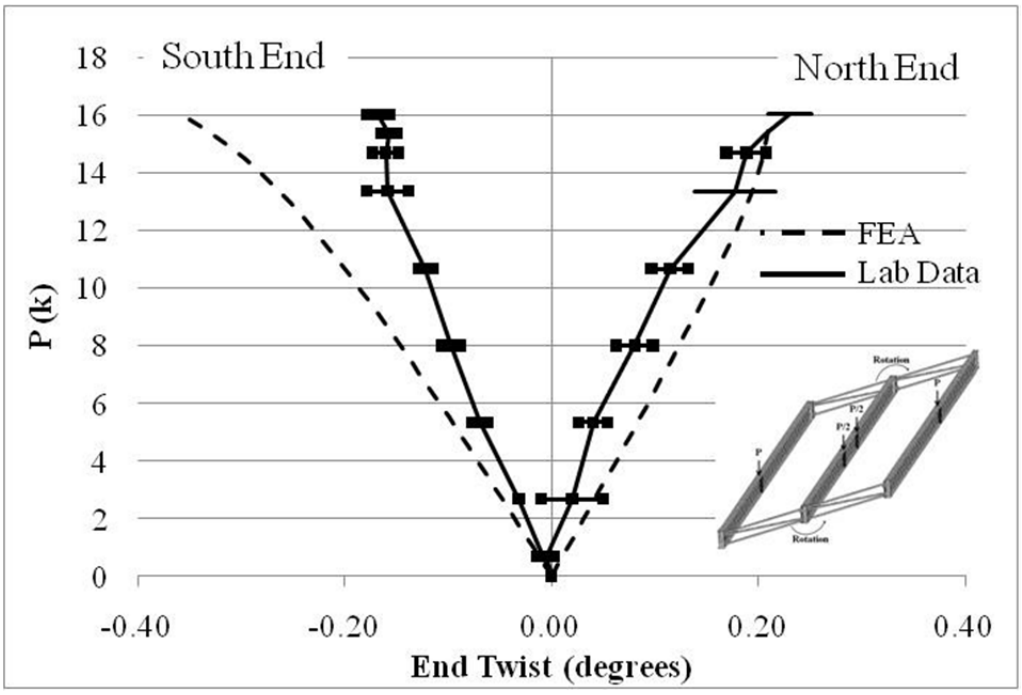

Figure 4.32: GSP2 end twist validation—rubber bearing with shims

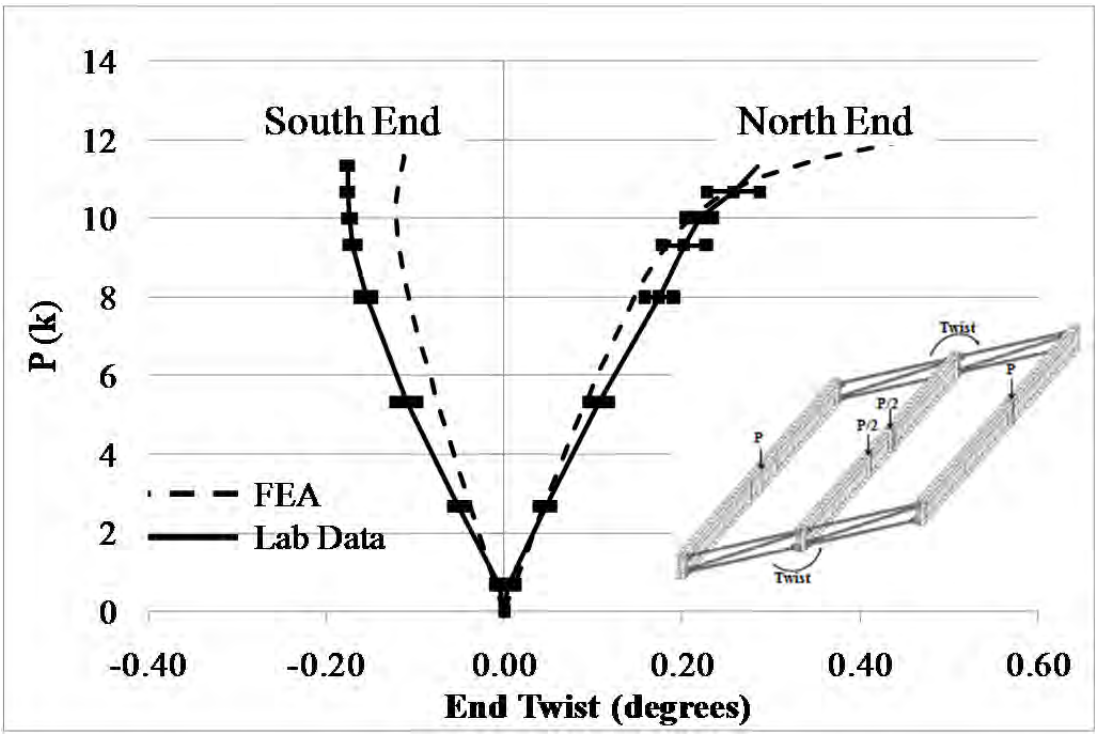

Figure 4.33: GBP2 end twist validation—rubber bearing

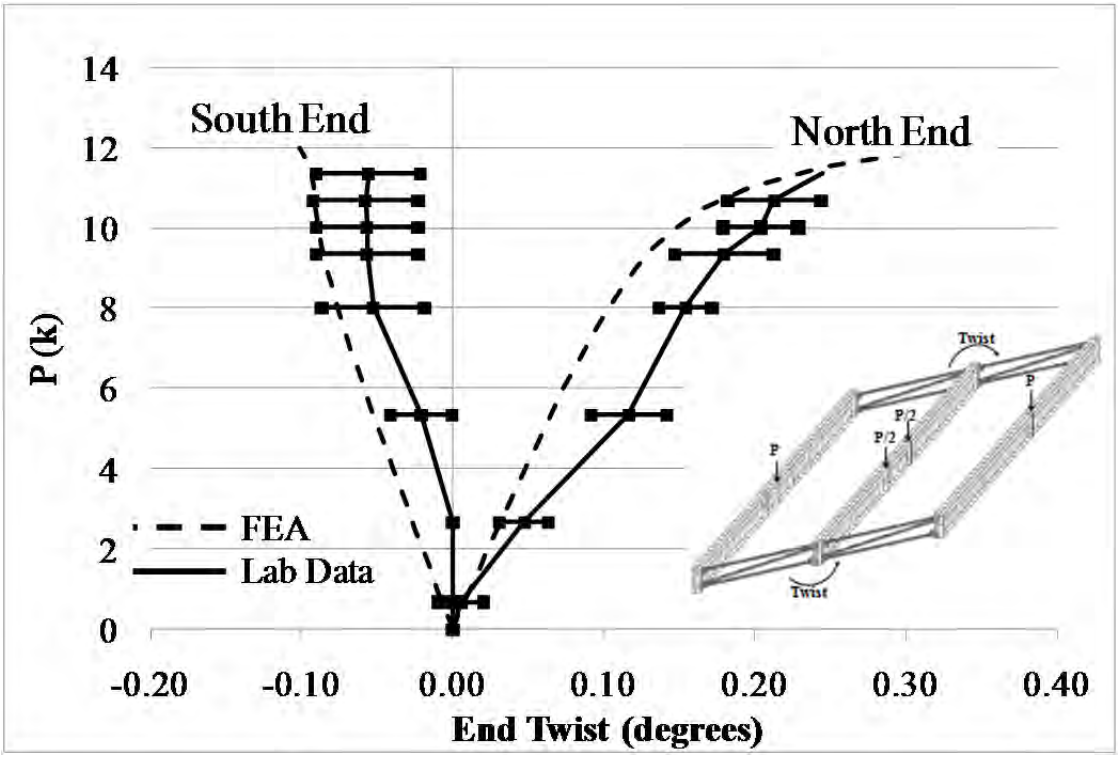

Figure 4.34: GBP2 end twist validation—rubber bearing with shims

4.7.3 Model with End and Intermediate Cross-frames and Thrust Washer Bearings

4.7.3.1 Intermediate Cross-frame Model

A simplified intermediate cross-frame model was constructed using truss elements (ANSYS LINK8) to investigate the impact of bracing patterns on girder behavior. This technique has been used successfully in previous research and has been found a very computationally efficient way to accurately match analytic results (Yura, Helwig, et al. 2008), (Wang and Helwig 2008).

A picture of a typical intermediate cross-frame is shown in Figure 4.35. The model uses a coincident node connection at the girder web-flange interface. A shell element full depth stiffener is incorporated into the model to prevent web distortion. This model differs from the actual cross-frame in two important ways. First the model assumes a rigid connection. This assumption is reasonable for a cross-frame perpendicular to the girder because connection plates have their strong axis aligned with the cross-frame forces. Second, the model assumes that the braces have no flexural stiffness. This is also a good assumption as long as the axial stiffness is large enough to significantly limit cross section twist. Finally, the model assumes the height of brace is the distance between flange centroids. In reality the height of the brace will be smaller. The impact of this assumption is that the axial brace forces may be smaller in the model because the distance between the axial forces that create the restraining couple is larger.

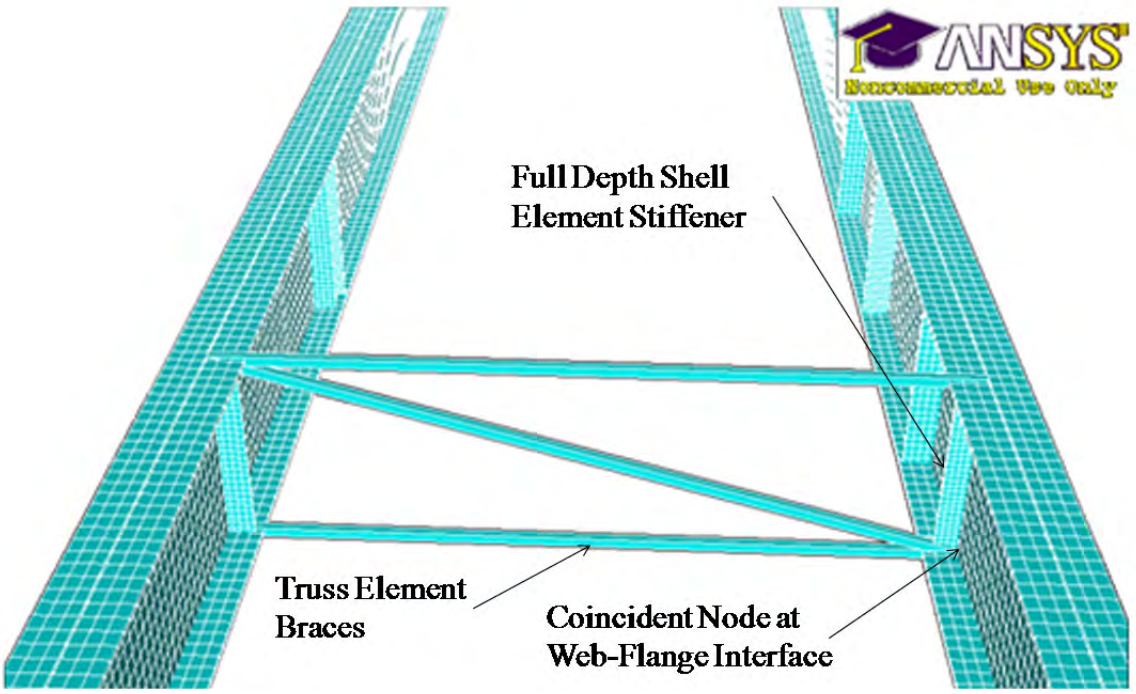

Figure 4.35: Truss element intermediate cross-frame model

The intermediate cross-frame model was validated using experimental results for specimens with staggered and continuous layouts for intermediate cross-frames described in Chapter 3. Because the girders were braced and had significantly smaller unbraced lengths than the no intermediate cross-frame case, buckling did not occur (the test was kept in the elastic

range so buckling was not allowed). Therefore, mid-span lateral deflections and twist were negligible (in the thousandths of an inch) and not compared. The key responses used for validation were the end and intermediate cross-frame forces as well as the twist at the girder ends. All validation results are presented in Appendix B and summaries and key findings are discussed below.

4.7.3.2 Staggered Intermediate Cross-frame Validation

An example of the axial force validation results for split pipe stiffened girders with staggered intermediate cross-frames is shown in Figure 4.36. The southwest intermediate cross-frame results showed that the model has a reasonable agreement with the top strut force, but some deviation between the bottom strut and diagonal. A similar pattern was found in the northeastern intermediate cross-frame (see Appendix B for these results). While the measured force levels are small in these members (no more than 200 lbs), there is a significant difference between the FEA and laboratory specimen. The difference between the model and FEA most likely has two primary sources.

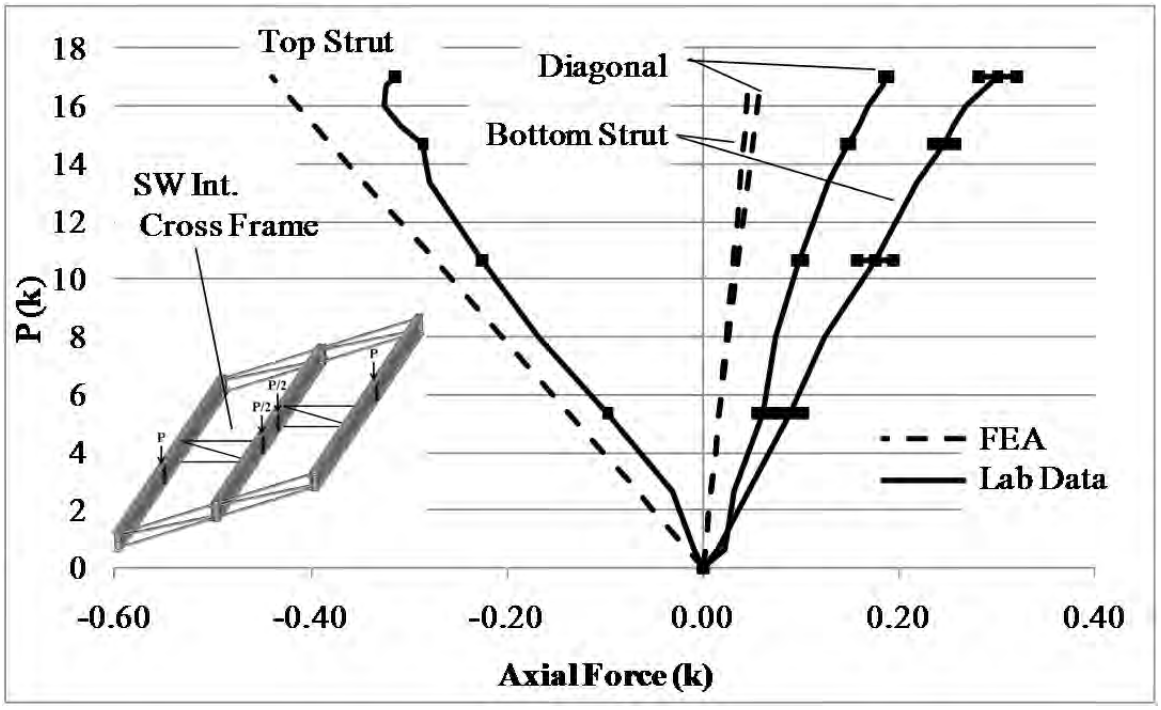

Figure 4.36: Intermediate cross-frame axial force validation (staggered layout)

The first source was the previously discussed difference between the finite element model and specimen. As mentioned, it is likely that the brace forces would be smaller in the model, and this is the case for the diagonal and bottom strut. Second, at the conclusion of testing it was noticed that the girders had shifted slightly (about 0.25" east) on their bearings. In the FEA model, however, considering the friction between the girder-bearing interfaces, bottom flanges of girders were fixed laterally on the bearings. This small discrepancy in the boundary conditions may have contributed to the difference between the FEA model and specimen.

Despite these anomalies, the measured and predicted end cross-frame forces had good agreement. The results for the southeastern end cross-frame are shown in Figure 4.37. Similar results were found for all the other end cross-frames and are provided in Appendix B (Finite Element Model Validation Results).

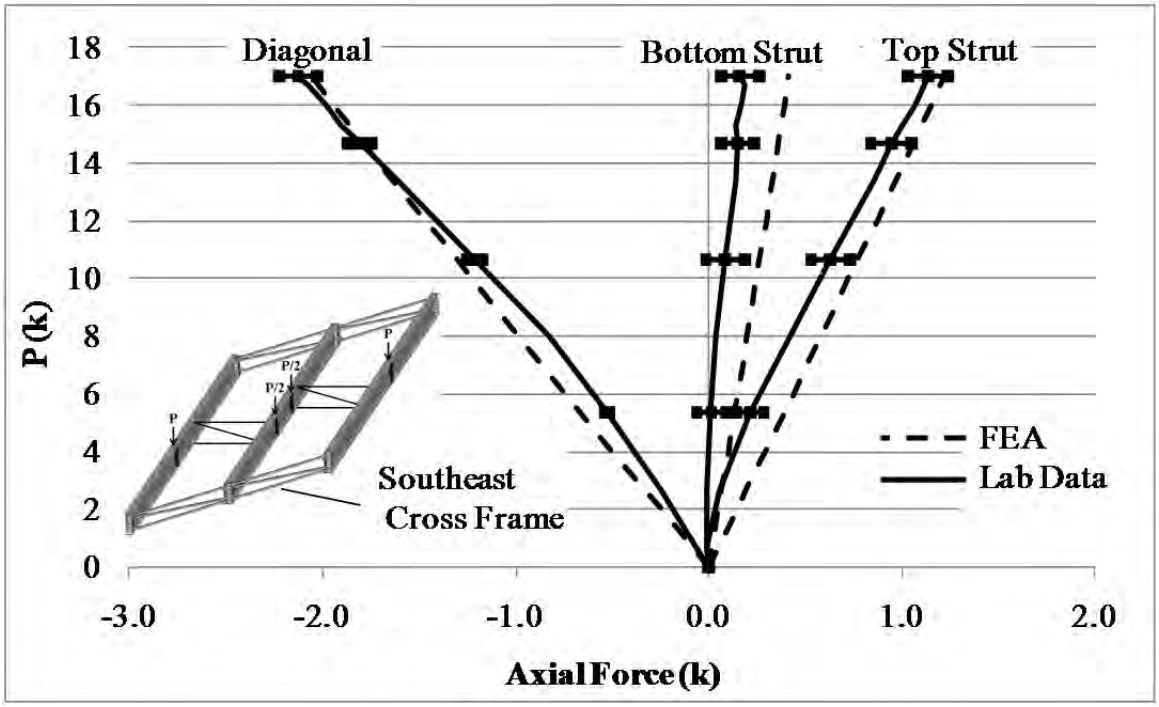

Figure 4.37: End cross-frame axial force validation (staggered layout)

Similar to the end cross-frame force results, the laboratory test and FEA results for the girder end twist had good agreement for the staggered intermediate cross-frame model. Results for GSP2 end twist are shown in Figure 4.38. Similar results were found for the other two girders and are provided in Appendix B (Finite Element Model Validation Results).

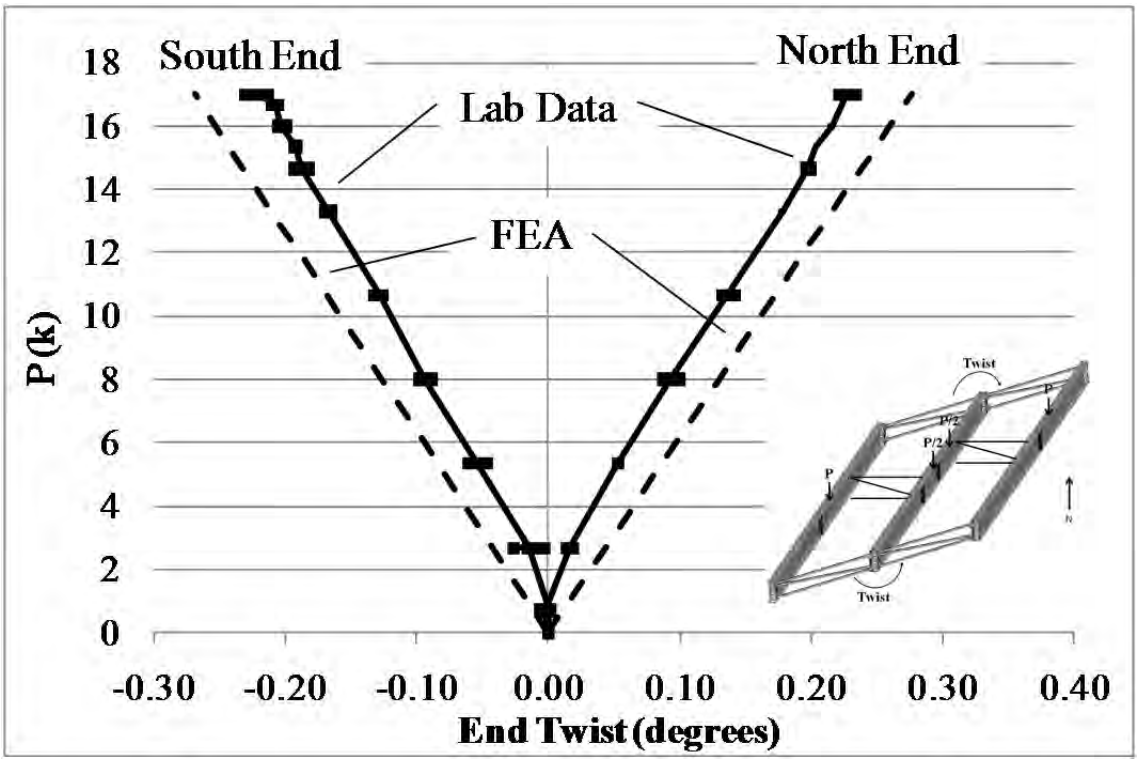

Figure 4.38: GSP2 end twist validation (staggered layout)

4.7.3.3 Continuous Intermediate Cross-frame Validation

An example of the axial force validation results for split pipe stiffened girders with the continuous intermediate cross-frames model is shown in Figure 4.39. The figure shows good agreement between the model and finite element results. Similar good agreement can be seen in the southeastern cross-frame axial forces as shown in Figure 4.40 and girder GSP2 end twist shown in Figure 4.41. All other validation results showed good agreement with the exception of two cross-frame members discussed below. All other validation results for the continuous cross-frame case are provided in Appendix B (Finite Element Model Results).

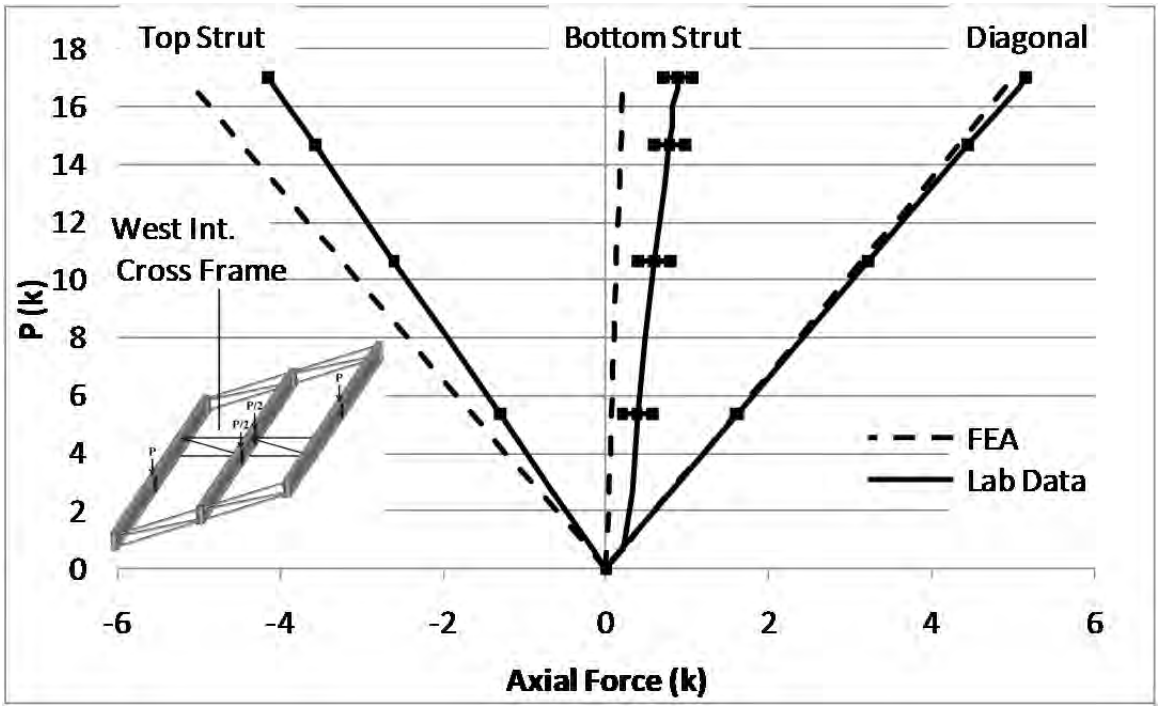

Figure 4.39: Intermediate cross-frame axial force validation (continuous layout)

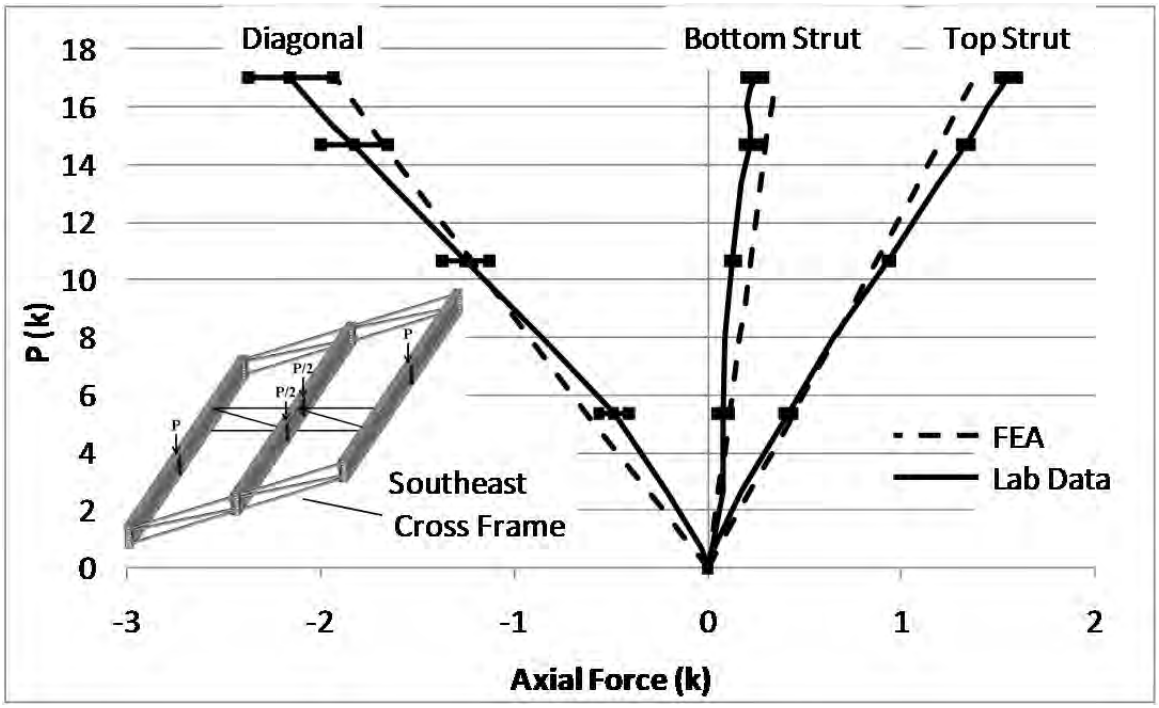

Figure 4.40: End cross-frame axial force validation (continuous layout)

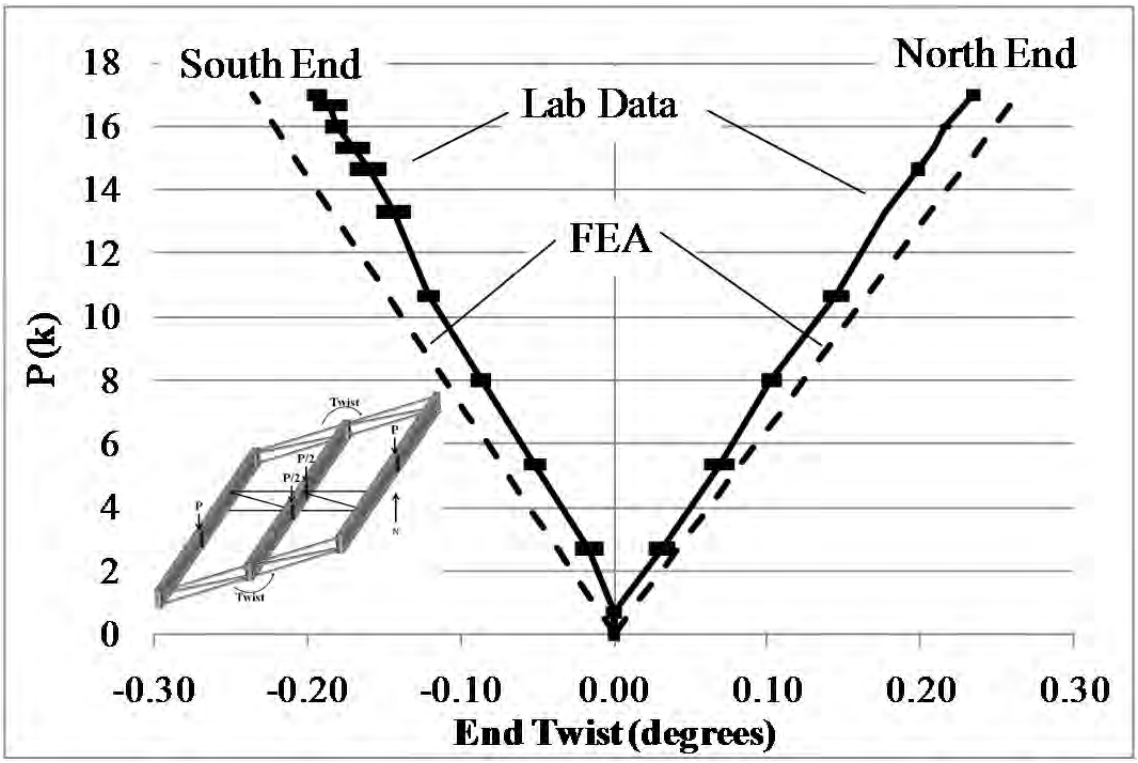

Figure 4.41: GSP2 end twist validation (continuous layout)

The only significant anomalies in the continuous cross-frame model validation data are seen in the bottom struts in the northern end cross-frames. The axial force validation data charts for the northeastern and northwestern cross-frames are given in Figure 4.42 and Figure 4.43, respectively. The northeastern bottom strut shows a sudden jump in force in the first load step and then the force remains constant, while the FEA shows a linear progression to the final load level. The reason for this may be the FEA bearing model. As mentioned in Section 4.4.7 the bottom flange at the FEA bearing is fixed against translation. This assumes that the specimen has enough friction between the flange and the bearing not to slide. If this is not the case, then the reaction is passed through the brace into the next bearing.

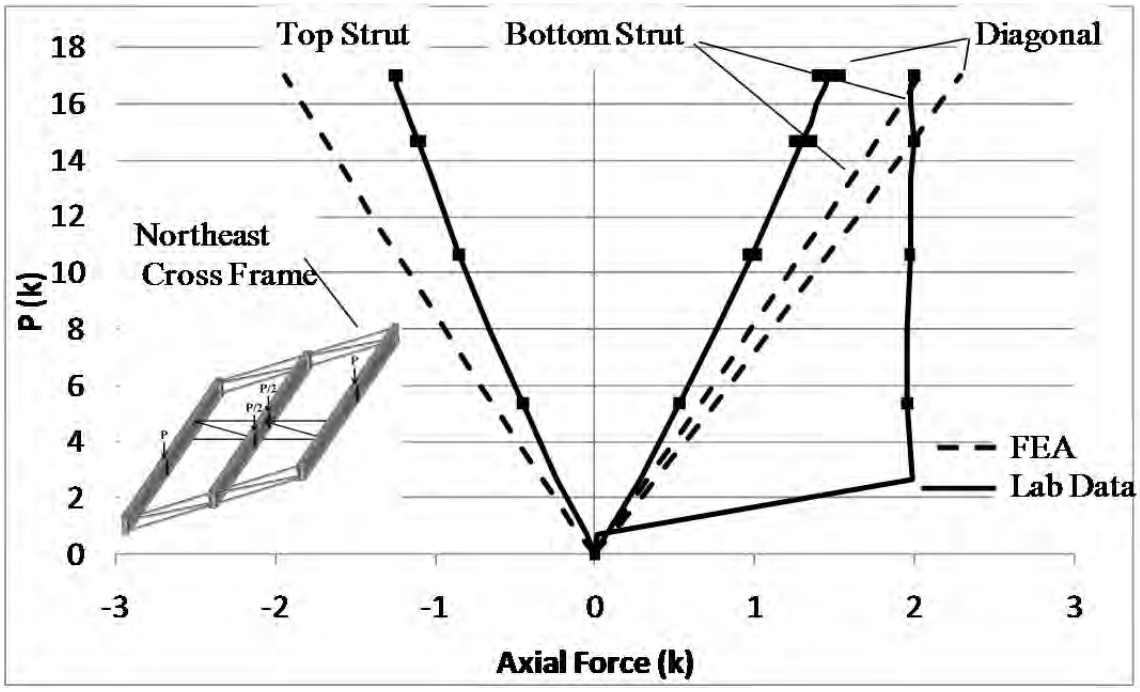

Figure 4.42: NE end cross-frame axial force validation (continuous layout)

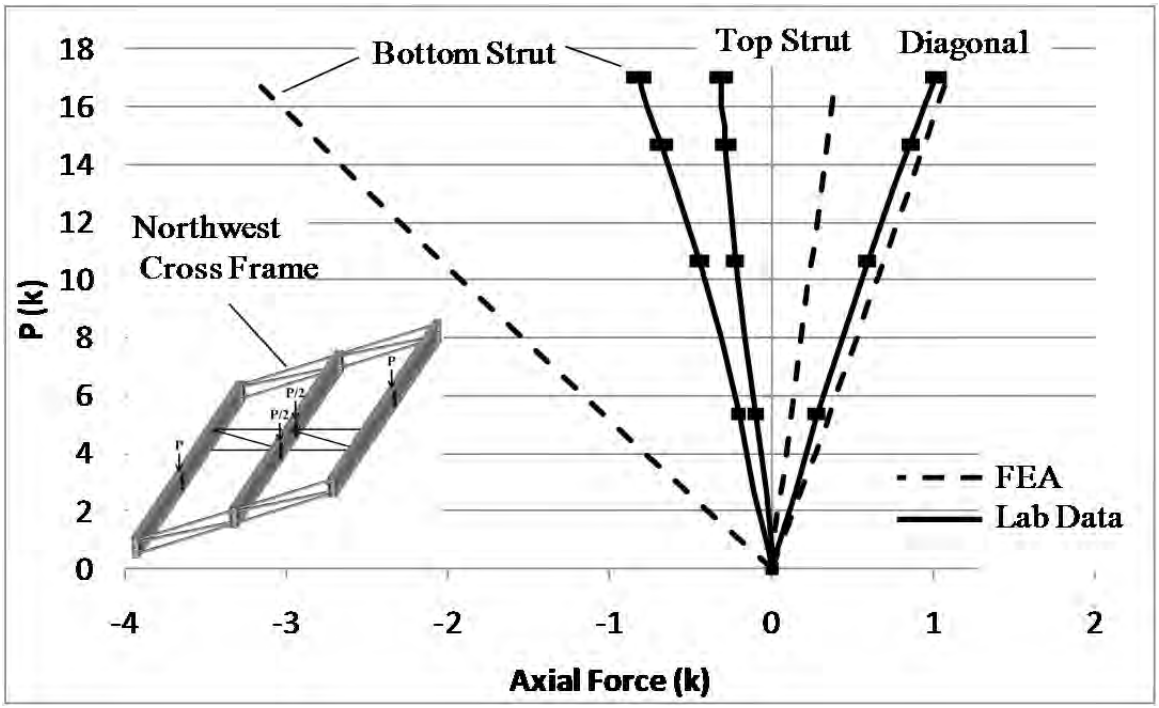

Figure 4.43: NE end cross-frame axial force validation (continuous layout)

In the case shown in Figure 4.42 and Figure 4.43, if the north end of GSP2 slides it will pull on the north east cross-frame bottom strut as shown in Figure 4.42. As the analysis progresses, the northeastern cross-frame's bottom strut counters the skew forces and therefore relieves the load on the northwestern cross-frame's bottom strut as shown in Figure 4.43.

While this explanation is plausible, it certainly may not be the only reason for the anomaly. However, the results from the staggered and continuous validation show that the overall model has good agreement with the laboratory specimen and the agreement between the two is very sensitive to the girders not sliding on the bearing.

4.7.3.4 Partial Loaded Specimen with Intermediate Cross-frame Validation

As discussed in Chapter 3, additional tests were conducted on the bent plate girder specimen to investigate the effect of the partial loading. These test results were also used to validate the FEA model. Intermediate cross-frame forces can be seen in Figure 4.44 through Figure 4.47. Similar to all previous validation results, the model also showed good agreement with those test results. A few sample validation results are shown here.

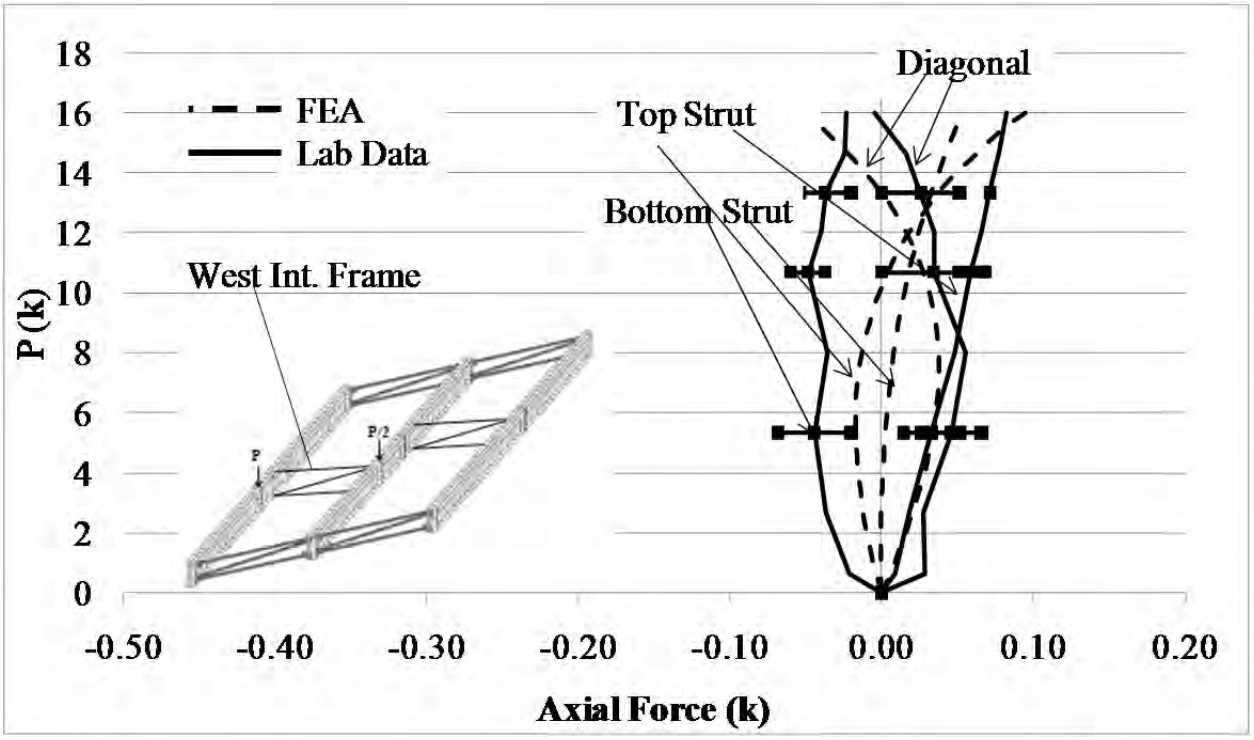

Figure 4.44: West intermediate cross-frame axial force validation (staggered layout)

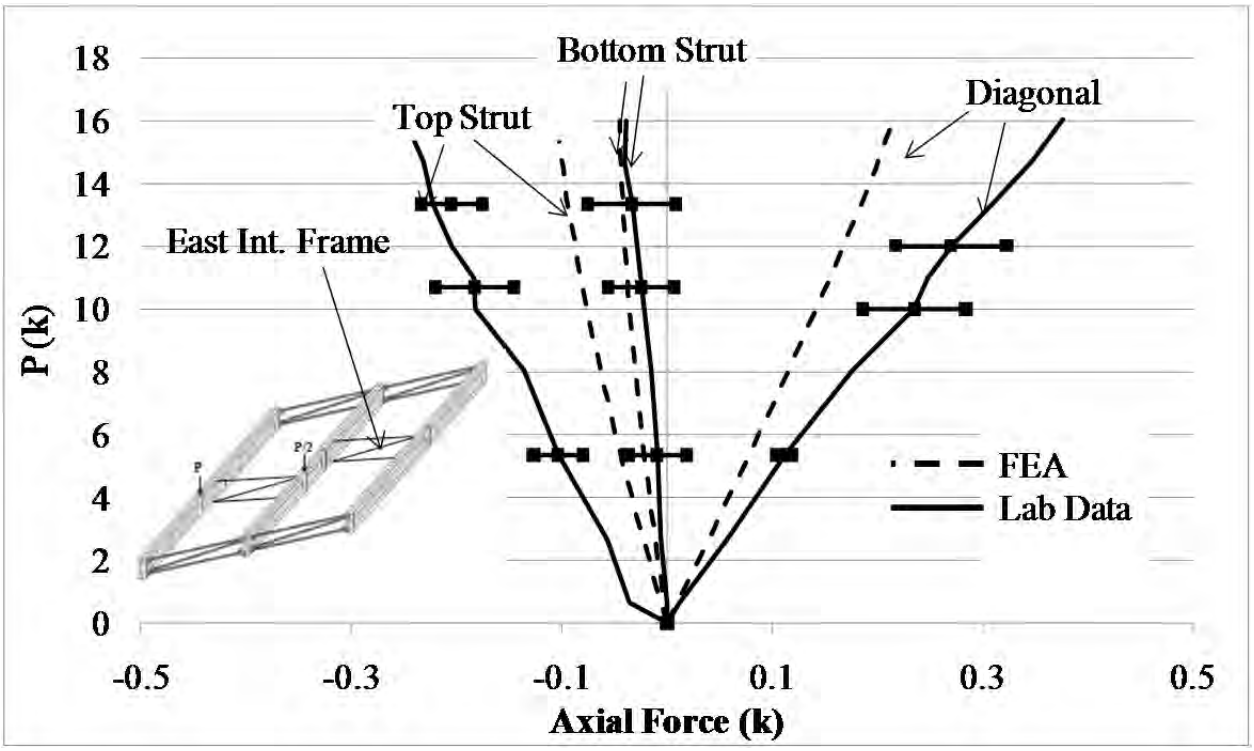

Figure 4.45: East intermediate cross-frame axial force validation (staggered layout)

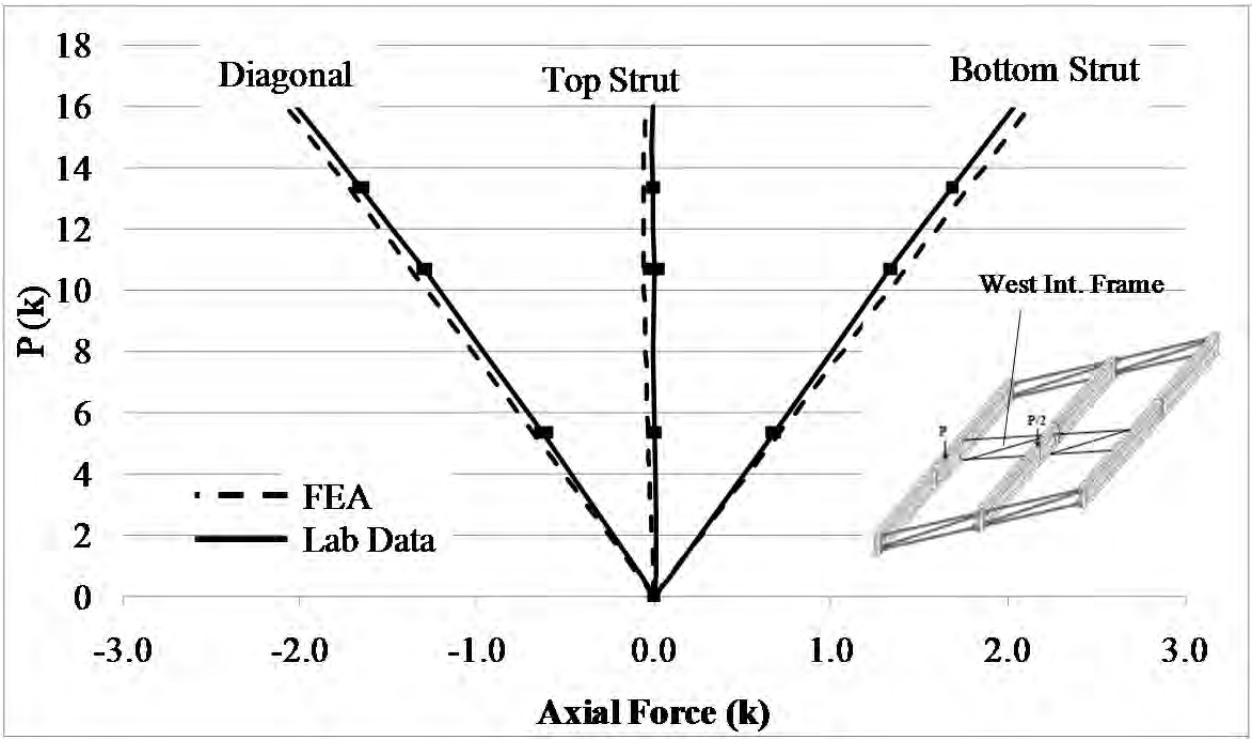

Figure 4.46: West intermediate cross-frame axial force validation (continuous layout)

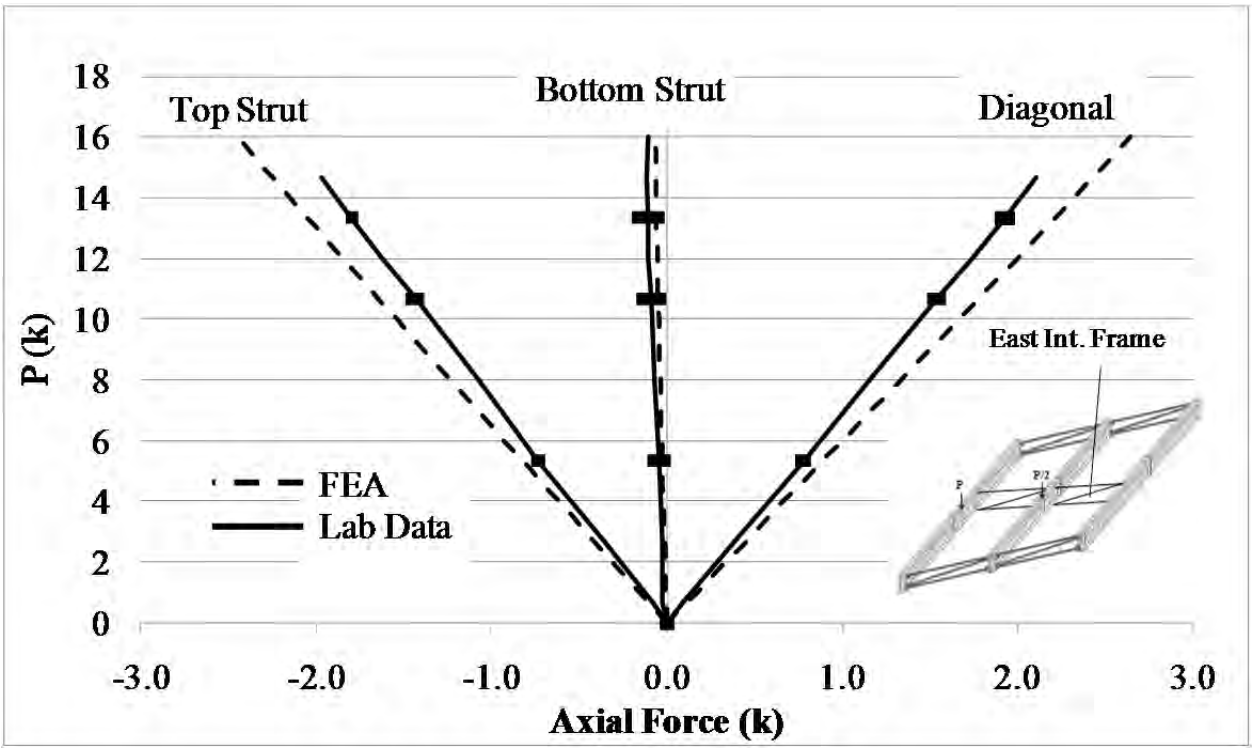

Figure 4.47: West intermediate cross-frame axial force validation (continuous layout)

4.8 Finite Element Modeling Summary

The results from the finite element model validation show that overall the modeling techniques used have a good agreement with the analytic equations and laboratory test results. Several important lessons were learned during the validation.

From the small scale tests it was learned that modeling the curved surfaces, like the bent plate, in ANSYS with shell elements requires a bend to element thickness ratio greater than three. A ratio below three resulted in poor agreement with laboratory results. The connection testing validation also showed that modeling welds can be important. The weld between the bent plate and connection plate adds significantly to the bent plate stiffness and when modeled gave good agreement between the FEA and laboratory data.

A similar lesson about welds was learned from the large scale buckling tests. During the girder validation, it was learned that fastening the stiffeners to the connection plates via constraint equations did not engage the warping restraint the plate stiffeners provide to the girders. Although this restraint is relatively small, it can significantly affect the girder buckling strength. When these welds were modeled using multi-point constraint elements, the FEA solutions had good agreement with the laboratory results.

However, there is a place for using constraint equations to connect the stiffeners and girders. During the analytic solution validation, it was learned that the constraint equations do prevent alternate modes of failure not accounted for in the analytic solutions used (such as local buckling) but do not affect the warping restraint provided by the stiffeners. Because the warping restraining provided by the stiffeners are generally not reflected in the analytic solution, when comparing with these solutions it may be desirable to have a model that does not engage the

warping stiffness provided by the stiffeners.. Modeling the stiffeners in this way for the analytic validations gave good agreement between the model and analytic results.

Finally, it was shown that modeling intermediate cross-frames perpendicular to the girders with truss elements gives good results compared to the laboratory data. This is especially important for modeling larger bridges with numerous intermediate cross-frames. Using truss elements is very computationally efficient in these cases where creating the intermediate cross-frames from shell elements could make the computational effort prohibitive in many cases.

Using the above lessons learned, the overall model performed well during validation. These models and techniques were then used to perform parametric studies to understand skewed steel girder buckling behavior and draw conclusions that can be applied to design guidance. These studies and guidance are covered in Chapter 5 (Parametric Studies and Design Recommendations).

Chapter 5. Parametric Studies

5.1 Introduction

The validated finite element model that was outlined in Chapter 4 (Finite Element Modeling) was used to perform several parametric studies to establish guidelines for the design of skewed end cross-frame connections. This chapter provides an overview of those studies and the proposed design guidelines. Some of the key factors that were considered and summarized in this chapter include the impact the cross-frame connection on the overall brace stiffness, the skew angle at which the connection stiffness becomes the limiting component for the cross-frame stiffness, the effect of girder end twist on buckling strength, and an investigation on the increase in buckling strength due to warping restraint provided by the split pipe stiffener.

5.2 General Parametric Study Method

The parametric studies summarized in this chapter were based on the five representative cross sections shown in Figure 5.1. These cross sections were created considering current TxDOT guidelines (Texas Steel Quality Council 2007), previous research (Zhou 2006), and a survey of bridge plans provided by TxDOT. In each section of the chapter, a brief description is provided of the FEA model that was used, along with the constant and variable parameters investigated. Results of the study are presented along with proposed guidelines for current design and construction practices. Results that are not shown in this chapter are provided in Appendix C (Parametric Study Results).

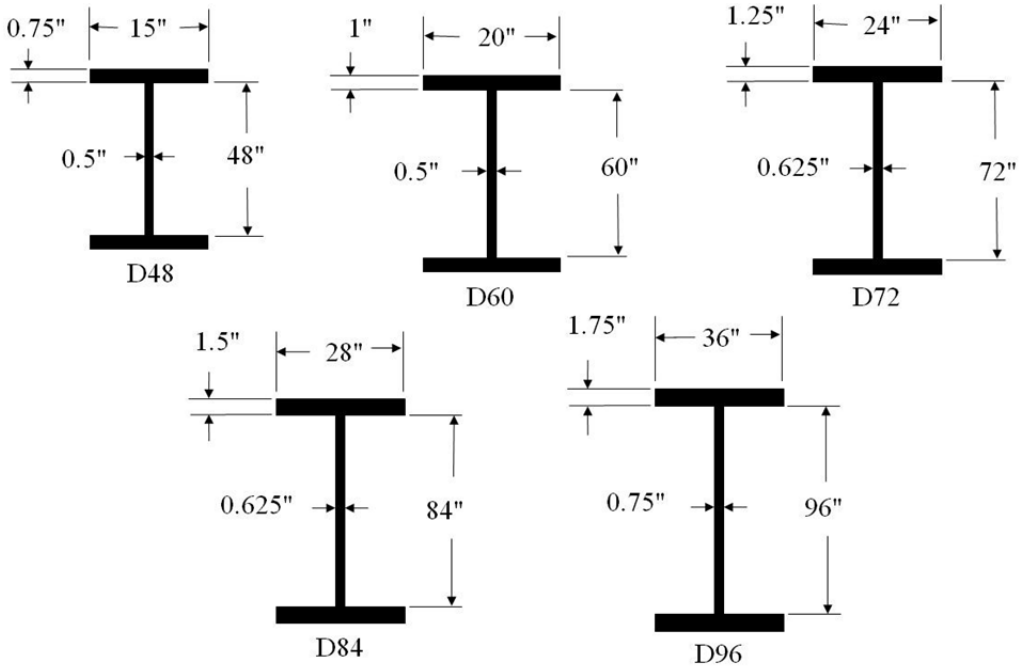

Figure 5.1: Parametric study cross sections

5.3 Cross-frame Stiffness Parametric Study

The purpose of the cross-frame stiffness parametric study is twofold. First, it was used to determine at what skew angle the bent plate begins to limit the cross-frame stiffness so that an equation to describe the bent plate stiffness could be developed. This quantity was used in Equation (2.49) to calculate the impact of the bent plate connection on the overall cross-frame stiffness. Second, the parametric study was used to compare the stiffness of a cross-frame using the bent plate connection against one using the split pipe stiffener connection.

5.3.1 Bent Plate Stiffness

The bent plate stiffness was determined for a ½" thick bent plate and ½" thick connection plate because this is the smallest bent plate and connection plate that meet current TxDOT guidelines (Texas Steel Quality Council 2007). A 2.5" bend radius was used in the study. The impact of varying these parameters on cross-frame stiffness was also considered.

The impact of the stiffness of various components of the bracing system on the overall cross-frame stiffness (β_T) was presented in Equation (2.18). Chapter 2 also contains the derivation of the connection stiffness ($\beta_{conn\text{-}tors}$) contribution to the overall cross-frame stiffness and the adjustment to the brace axial stiffness for skew (β_{brskew}). Adding the connection stiffness to the other system components results in the expression provided in Equation (5.1).

$$\frac{1}{\beta_T} = \frac{1}{\beta_{brskew}} + \frac{1}{\beta_{sec}} + \frac{1}{\beta_g} + \frac{1}{\beta_{conn-tors}} \tag{5.1}$$

A typical bent plate cross-frame has four bent plates and two connection plates whose combined axial stiffnesses together affect the cross-frame torsional stiffness ($\beta_{conn\text{-}tors}$) as shown in Figure 5.2. Quantifying $\beta_{conn\text{-}tors}$ in Equation (5.1) requires an assessment of the axial stiffness of the four individual bent plate connections perpendicular to the girder. The axial stiffness of the individual bent plate to connection plate connection is referred to as β_{conn}. Once β_{conn} is known, it is used in Equation (2.49) (see Chapter 2) to calculate the connection torsional stiffness of ($\beta_{conn\text{-}tors}$). The connection torsional stiffness is then used in Equation (5.1) to calculate the overall cross-frame stiffness. The challenge in this process is to accurately calculate β_{conn}. Therefore, the parametric study was used to first assess $\beta_{conn\text{-}tors}$ and then use it to calculate β_{conn} to see if the process would give similar values of the bent plate connection stiffness for different cross-frame geometries. This serves as a check on the accuracy of the method. This process is described below.

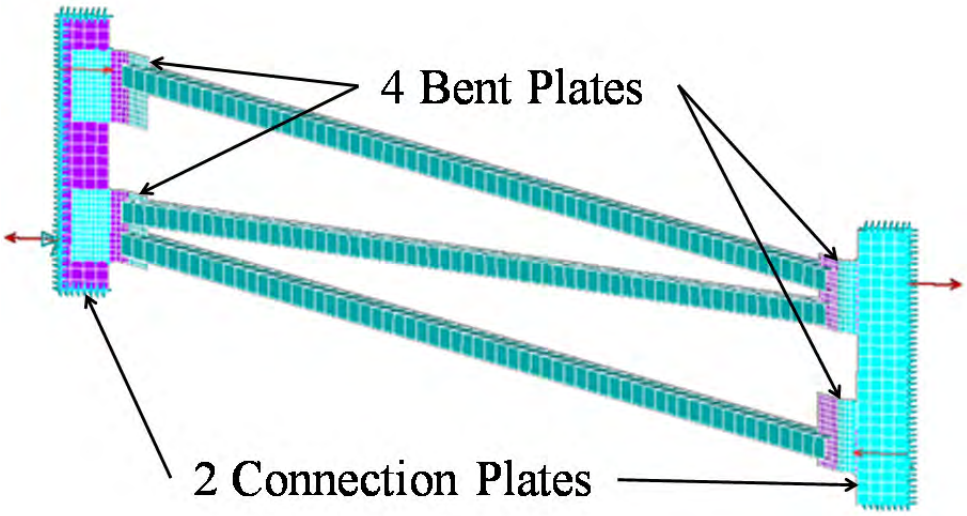

Figure 5.2: Components comprising the cross-frame connection stiffness ($\beta_{conn\text{-}tors}$)

Estimating the bent plate connection stiffness begins with Equation (2.49), which defines the connection contribution to the cross-frame connection torsional stiffness ($\beta_{conn\text{-}tors}$) in terms of the values of the individual connection stiffness (β_{conn}) and cross-frame geometry. This equation is repeated below for convenience.

$$\beta_{conn-tors} = \frac{\beta_{conn}\, h_b^2}{\frac{2L_c^2}{S^2} + 1} \qquad (2.49)$$

(from Chapter 2)

By rearranging the equation, the individual connection stiffness can be isolated as shown in Equation (5.2).

$$\beta_{conn} = \frac{\left(\frac{2L_c^2}{S^2} + 1\right)\beta_{conn-tors}}{h_b^2} \qquad (5.2)$$

Using the bent plate cross-frame model and the unskewed cross-frame finite element model described in Chapter 4, βconn-tors can be found using Equation (5.1) once the total brace stiffness is found from a finite element analysis. In the bent plate cross-frame models, the girder cross section stiffness (βsec) and girder in-plane stiffness (βg) are infinite and can be dropped from Equation (5.1). This matches the case of an end cross-frame, because the girder does not deflect vertically at the abutment, and a full depth cross-frame is typically used to connect the cross-frame to the girder. The skewed brace stiffness (βbrskew) can be found by using the unskewed cross-frame model described in Section 4.5.1.2 and then multiplying the finite element brace stiffness given from this model by the cosine squared of the skew angle as described in Equation (2.43). The total cross-frame stiffness (βT) can then be found by using the bent plate cross-frame model described in Section 4.5.1.1. Once these values are known, Equation (5.1) can

be used to solve for βconn-tors and then substituted into Equation (5.2) to solve for the bent plate connection stiffness (βconn).

It is important to note that the final result from this procedure is not the actual stiffness value of the individual bent plates, but is instead the combined effect of all four bent plates and the two connection plates on the cross-frame stiffness. Calculating the actual stiffness of each of the four bent plates in the cross-frame would require knowledge of the forces and deformations of each plate. Because each plate may have tension and compression members connected to it at various angles, the state of force and deformation in each plate is unique, non-linear, and complicated. Rather, the proposed method relies on small deflection assumption to assume linearity and considers the overall impact of all the plates as a whole on the cross-frame stiffness. This approach is a reasonable assumption based upon the small scale testing that showed if the forces in the braces remain relatively low (below 5 kips for the 5/16" thick plates in the small scale testing) then the deformation response of the plate is nearly linear.

If the finite element analysis is run for various cross-frame geometries for the same bent plate, the bent plate stiffness should vary only slightly due to the differing brace height, diagonal orientation and other geometric differences that affect the size and the forces entering the plate. To check this condition a parametric study was performed using the five cross sections shown in Figure 5.1 for skew angles ranging from 15° to 60° in 15° increments. The girder spacings used were 10', 8', and 6' because 10' is the maximum recommended plate girder spacing in Texas (Texas Steel Quality Council 2007). The cross-frames were made up of HSS3.5x3.5x3/8 members, which is a similar brace area used in the Texas standard plans (Texas Department of Transportation 2006). All connection plates were half as wide as the flange width. A check of the individual bent plate connection stiffness is shown in Figure 5.3 for an 8' girder spacing.

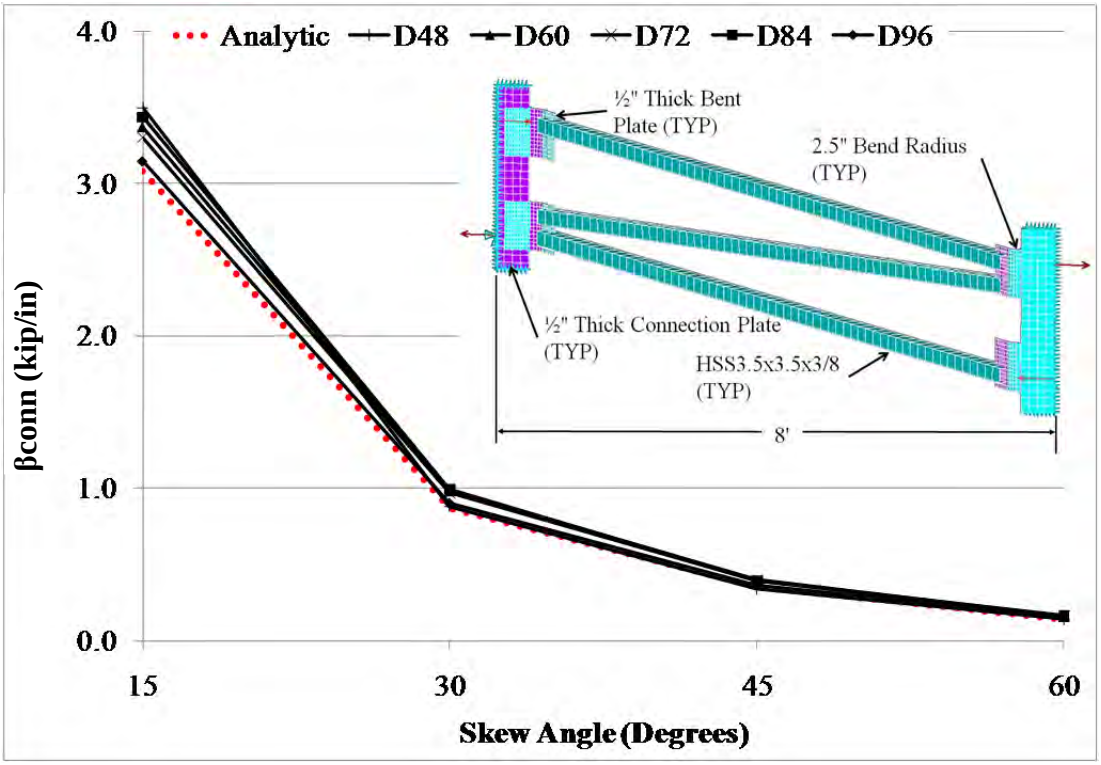

Figure 5.3: Bent plate connection stiffness parametric study result (S=8')

From the results in Figure 5.3 it can be seen that, the bent plate connection stiffness from Equation (5.2) only varies a small amount between the different girder geometries. This shows the plate stiffness is not very sensitive to the girder geometry at an 8' girder spacing, which was expected and shows that Equation (5.2) does a reasonable job of predicting the bent plate stiffness at the 8' girder spacing. To develop an equation describing the bent plate stiffness, an exponential curve fit was used for the minimum bent plate stiffness values at each skew angle from 15° to 60°. The analytic equation is plotted with the FEA results in Figure 5.3 and is given as Equation (5.3).

$$\beta_{conn} = (70\alpha + 5000)e^{-q\alpha} \tag{5.3}$$

where

$q = 0.045 + (\alpha - 15)/100 \leq 0.07$

α = skew angle in degrees ($15° \leq \alpha \leq 60°$)

The limits on α above do not necessarily mean that the expressions will not work for skew angles outside this range, but instead reflect the range of angles considered in the study. With the individual connection stiffness defined, the total cross-frame stiffness for each cross section was calculated using Equations (5.3), (2.49), and (5.1), normalized with respect to the zero skew case and plotted against the skew angle. This stiffness was compared to the cross-frame stiffness results from the FEA models. Results for the D48 and D72 cross sections shown in Figure 5.1 are given in Figure 5.4 and Figure 5.5, respectively.

From the figures it can be seen that Equation (5.3) has good agreement with the finite element model results. The results for the 8' girder spacing for all cross sections tested (D60, D84, and D96 shown in Figure 5.1) can be found in Appendix C (Parametric Study Results). All other cross sections had the same good agreement between the FEA and analytic solutions.

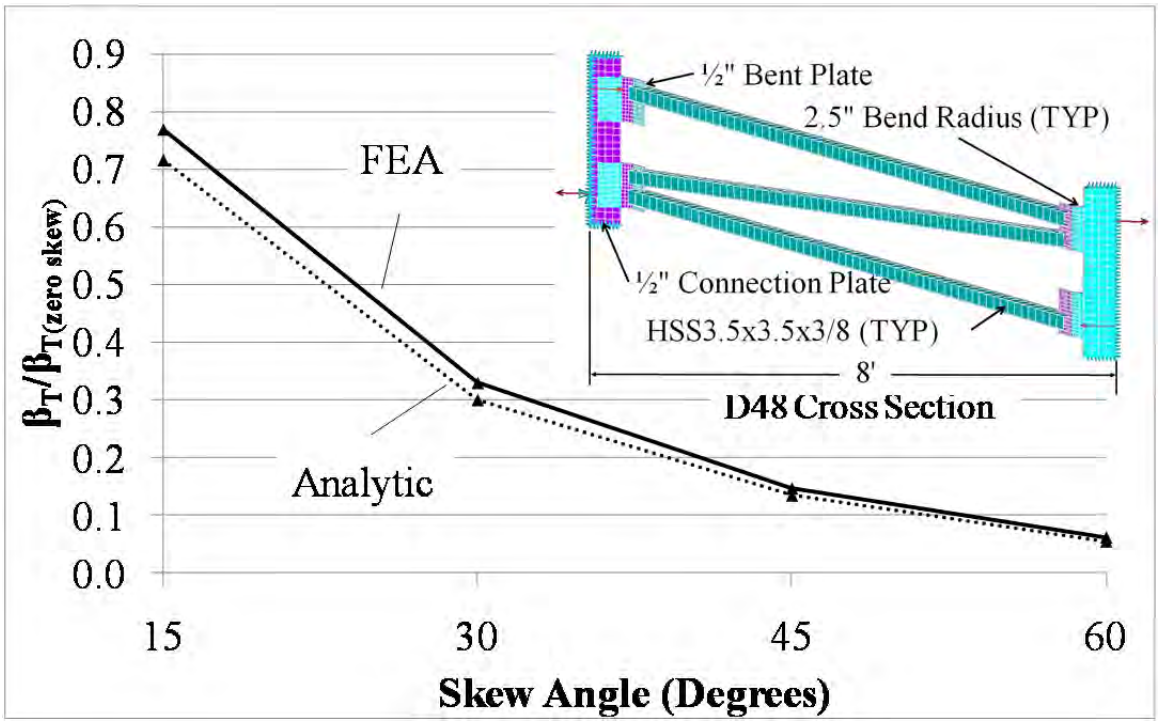

Figure 5.4: Analytic to FEA cross-frame stiffness comparison (cross section D48)

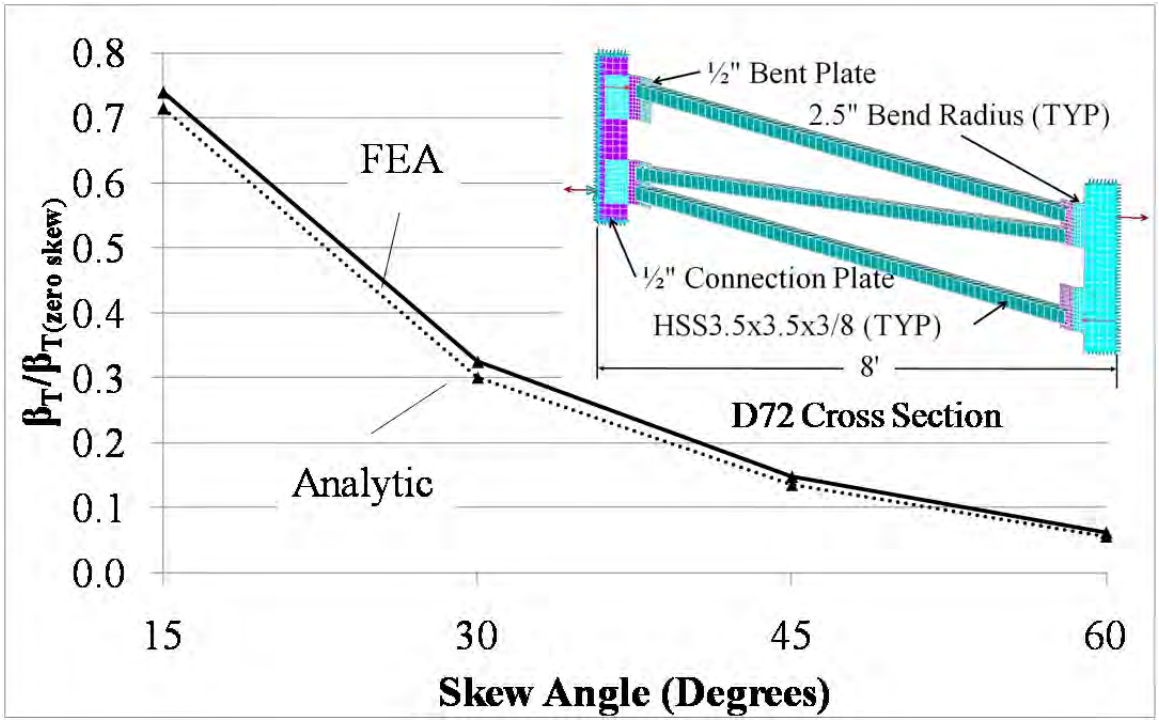

Figure 5.5: Analytic to FEA cross-frame stiffness comparison (cross section D72)

In addition to the 8' girder spacing, an additional study was run using a 10' girder spacing. The results for the D96 cross sections are shown in Figure 5.6. The figure shows that the analytic equation over-estimates the cross-frame stiffness by about 20% at a 15° skew and about 100% at

a 60° skew when a 10' spacing is used. Similar poor agreement was found in the shallower cross sections as well.

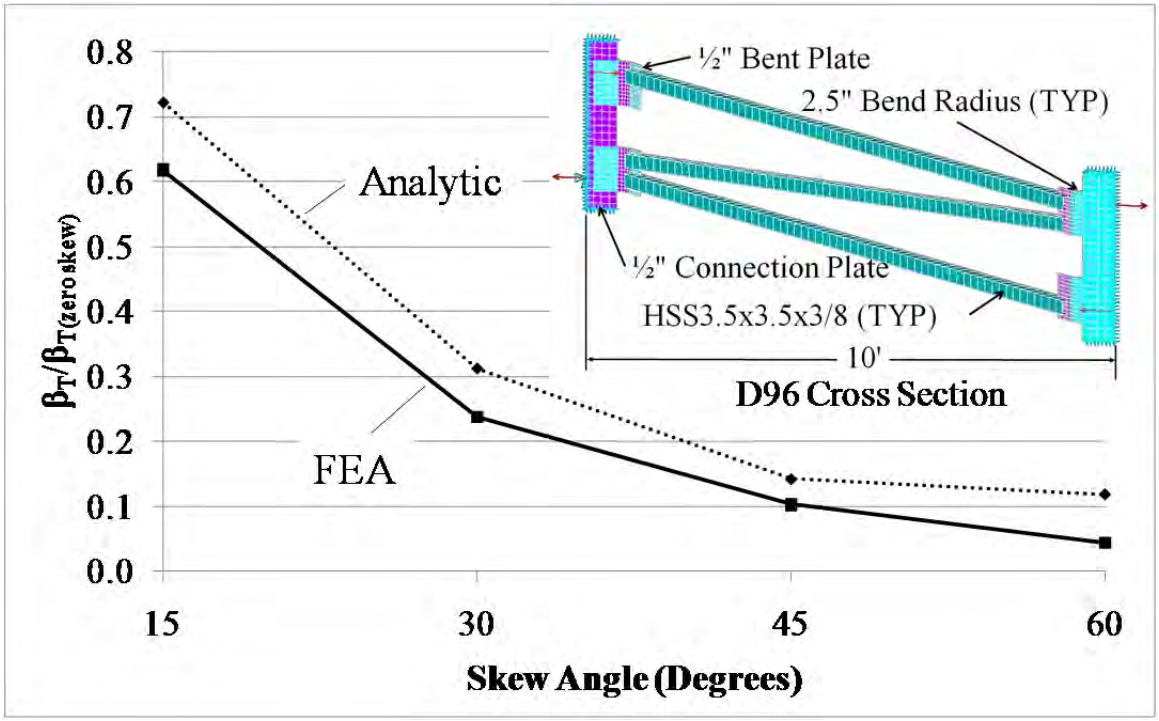

Figure 5.6: Analytic to FEA cross-frame stiffness comparison (cross section D96)

To more accurately extend Equation (5.3) to girder spacings other than 8', the equation is multiplied by the ratio of the 8' spacing for which it was derived to the desired girder spacing. The resulting equation is shown in Equation (5.4).

$$\beta_{conn} = \frac{8}{S}(70\alpha + 5000)e^{-q\alpha} \tag{5.4}$$

where

S = girder spacing in feet

All variables remain as previously defined.

The cross-frame stiffness using Equation (5.4) for the connection stiffness compared to the FEA solution for the D48 and D96 cross section are plotted in Figure 5.7 and Figure 5.8, respectively. The analytic solution now shows good agreement with the FEA solution. All other cross sections show agreement and can be found in Appendix C (Parametric Study Results).

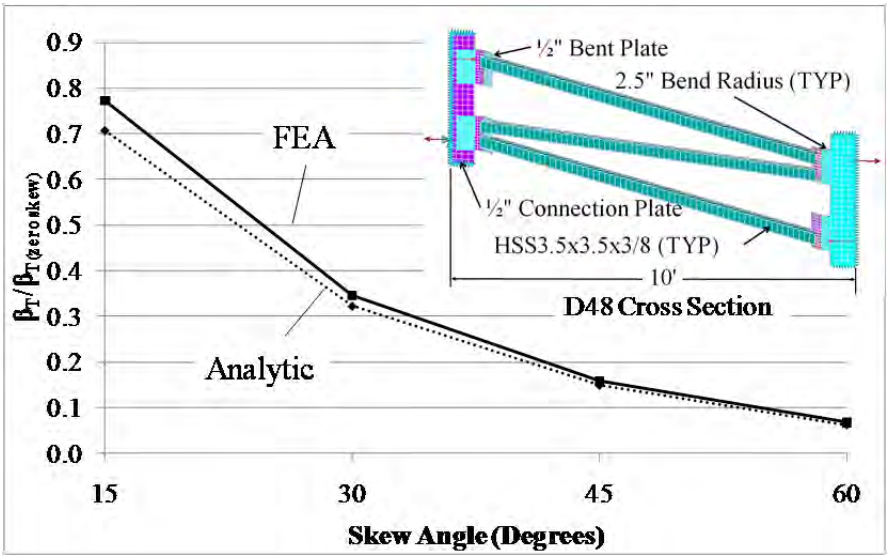

Figure 5.7: Analytic to FEA cross-frame stiffness comparison (cross section D48)

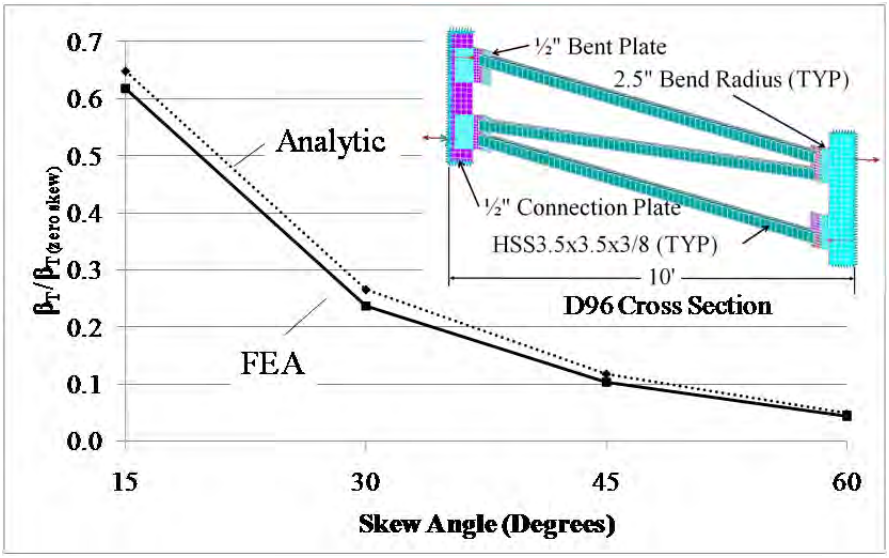

Figure 5.8: Analytic to FEA cross-frame stiffness comparison (cross section D96)

Finally, the case where the girder spacing is smaller than 8' was checked. The analysis was run again for the D48 and D60 cross section at a 6' spacing and compared to the analytical solution using Equation (5.4) to calculate the connection stiffness. The results are shown in Figure 5.9 and Figure 5.10. Again, the analytic results show good agreement with the FEA results.

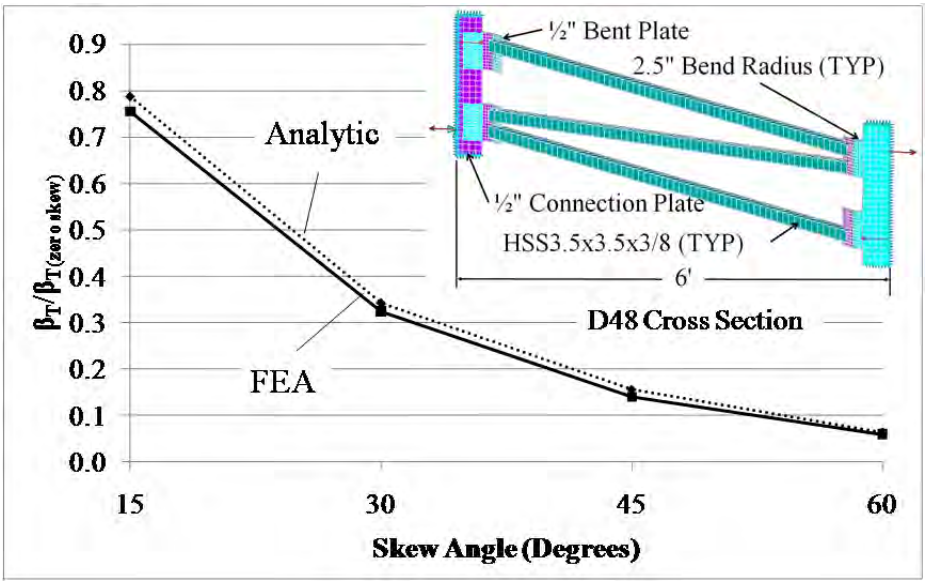

Figure 5.9: Analytic to FEA cross-frame stiffness comparison (cross section D48)

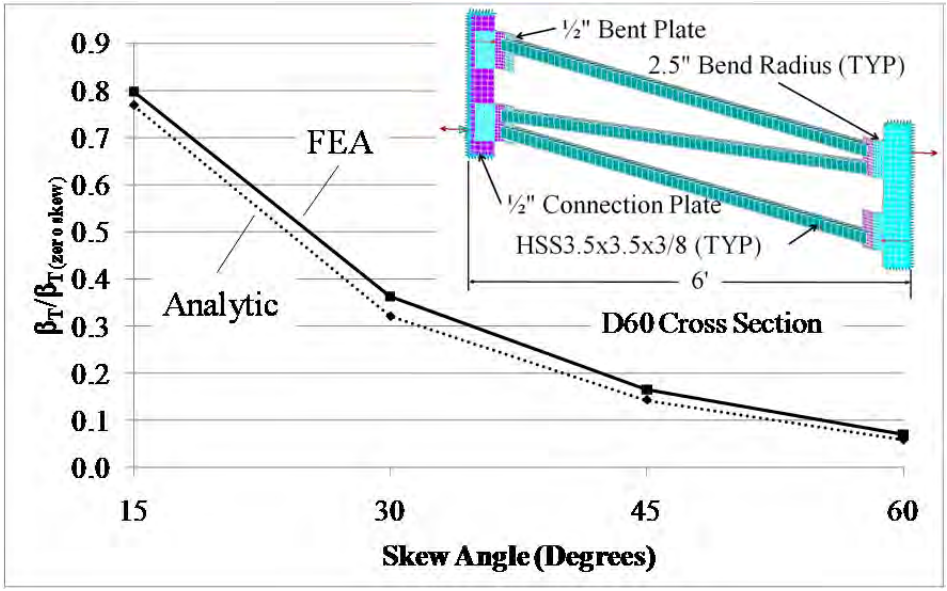

Figure 5.10: Analytic to FEA cross-frame stiffness comparison (cross section D60)

5.3.2 Critical Bent Plate Connection Stiffness Skew Angle

While the previous cross-frame connection stiffness equations are useful in quantifying cross-frame stiffness, an important aspect of the connection stiffness is to determine what angle the connection stiffness begins to limit the cross-frame stiffness. Identifying the limiting angle provides designers the ability to determine the most efficient action to stiffen a cross-frame. If the connection governs, then strengthening the connection is the most efficient alternative. Similarly if the brace stiffness is the limiting component, then strengthening the brace has the most impact. For girders with full depth stiffeners and end cross-frame values of the in-plane and cross sectional girder stiffness are near infinity; therefore, the lower of remaining terms of Equation (5.1) (the brace and connection stiffnesses) becomes the limiting component for the

total cross-frame stiffness. By forming the ratio of the connection stiffness ($\beta_{conn\text{-}tors}$) to brace stiffness (β_{brskew}) and plotting this ratio against the skew angle for each of the parametric cross sections, the range of skew angles where the connection stiffness limiting the cross-frame stiffness can be identified by tracing the horizontal line where the ratio equals one.

An example of such a plot is given in Figure 5.11. Where the plots are above the red horizontal line, the HSS3.5x3.5x3/8 brace limits the cross-frame stiffness and below the line the connection limits the stiffness. The range of skew angles where the connection begins to limit the cross-frame stiffness is centered around 20°. Of course the plot shown is specific to the brace size, bent plate, and girder spacing shown in the figure.

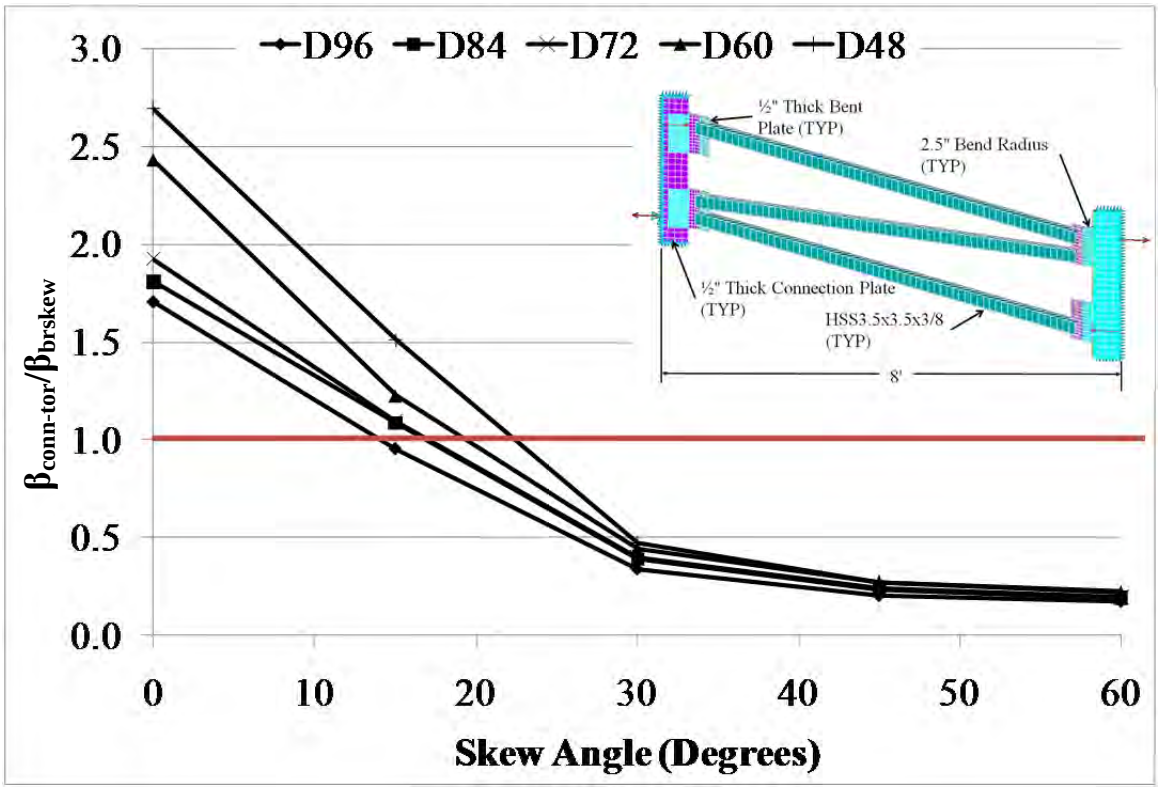

Figure 5.11: Bent Plate cross-frame connection-brace stiffness ratio

5.3.3 Plate Thickness and Bend Radius Impact on Cross-frame Stiffness

Because much of the previous analysis in this chapter has been specific to a ½" thick bent plate and ½" connection plate, varying these parameters was also checked to ensure that increasing the plate thickness can stiffen the connection sufficiently to improve the behavior. Primarily designers will be most interested in which portion of the connection (the bent plate or connection plate) has the greatest impact on the connection's overall stiffness. Therefore, beside the basic case of ½" thick bent plate and connection plate the cases of ¾" bent plates and connection plates were checked.

The results of varying the bent plate and connection plate thickness from ½" to ¾" are shown in Figure 5.12 for the D72 cross section. The results are normalized by the ½" thick bent plate and connection plate standard case ($\beta_{T(standard)}$) used in the previous analysis. As can be seen from the figure, strengthening one or both of the plates does stiffen the connection, so the

previous equations developed are conservative if used for these additional cases. Also, strengthening the connection plate is generally more effective than just stiffening the bent plate. Increasing the thickness from 0.5 in. to 0.75 in. as much as doubled the stiffness of the overall connection depending on the skew angle. Results for the other parametric cross study sections are provided in Appendix C (Parametric Study Results).

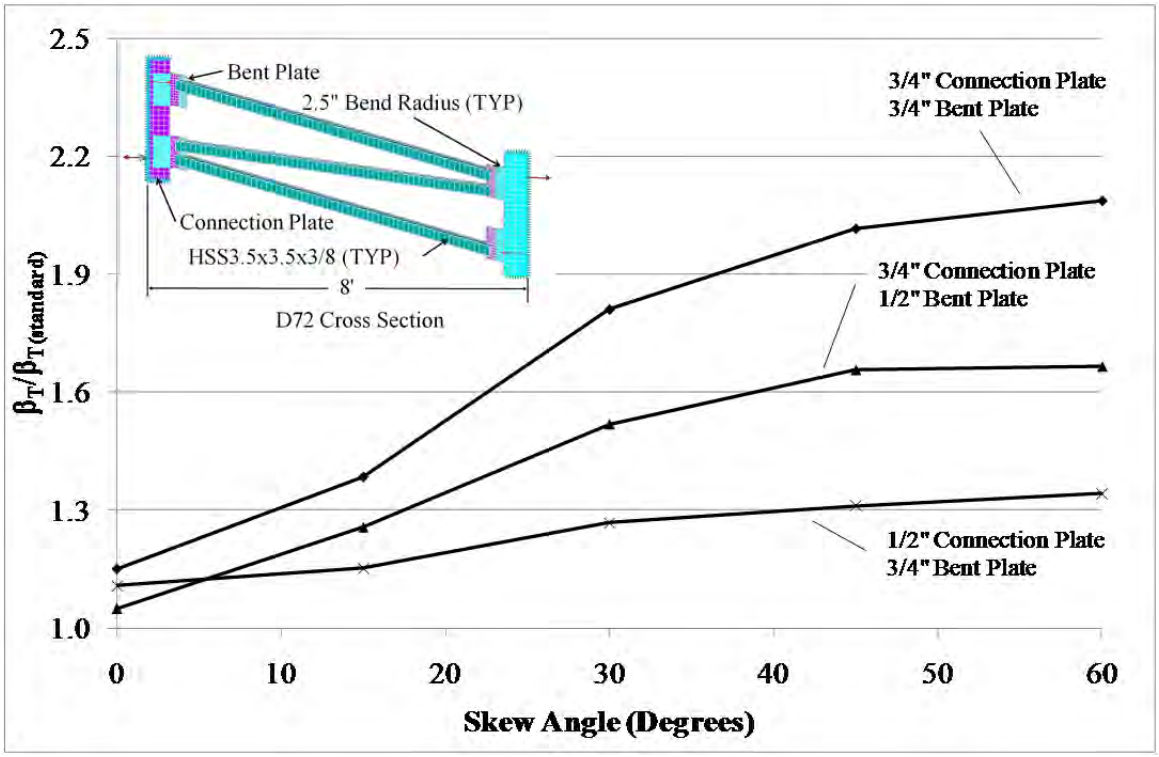

Figure 5.12: Plate thickness impact on bent plate connection (2.5" bend radius)

Another parameter that may impact the bent plate stiffness is the bend radius. The connection tests outlined in Chapter 3 showed that the bend radius of the bent plate did impact the connection stiffness. Therefore, another set of cases were run with a bend radius of 3.5" to compare to the 2.5" bend radius cases. The results of the analysis are shown in Figure 5.13 with the percent change in cross-frame stiffness due to increasing the bend radius from 2.5" to 3.5" plotted against skew angle. From the figure it can be seen that increasing the bend radius from 2.5" to 3.5" can decrease the cross-frame stiffness nearly 10% at the larger skew angles. At skew angles less than 30°, the cross-frame stiffness actually increases slightly because increasing the bend radius shortens the brace length a small amount. The plots for the other cross sections considered in this analysis are given in Appendix C (Parametric Study Results).

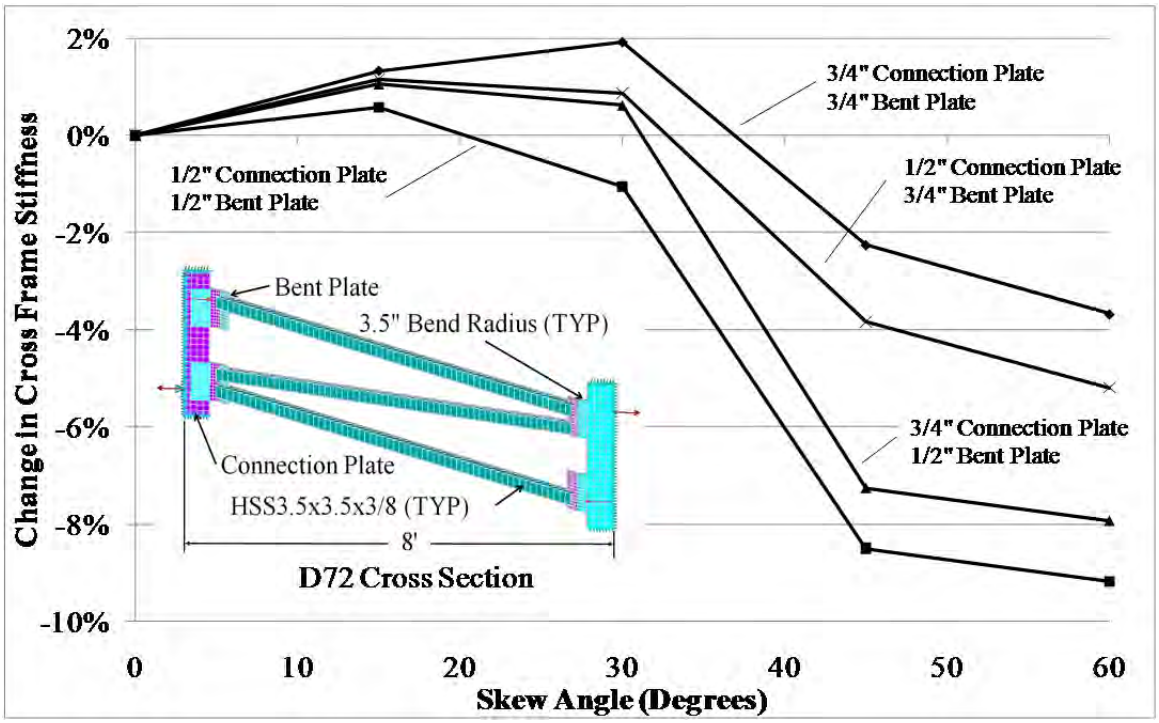

Figure 5.13: Change in cross-frame stiffness for 2.5" and 3.5" bend radii

5.3.4 Cross-frame Connection Comparison

To compare the bent plate and split pipe stiffener cross-frame connections, a similar analysis used in the previous section was run using the split pipe cross-frame model described in Chapter 4. The parameters for the split pipe stiffener cross-frame were the same as for the bent plate cross-frame. In both cases the connection plate was ½" thick, and the bent plate and split pipe connection tabs were also ½" thick. The height of brace (h_b) was also held constant for both connections. A ½" thick pipe was considered, and like the bent plate cases, the brace members were HSS3.5x3.5x3/8. The only parameter common to the two cross-frame types that changed was the length of the braces. Because the split pipe connection requires a longer connection length, the split pipe connection brace members were about 6" shorter than the bent plate brace members. In the comparisons below, the standard bent plate case with the 2.5" bend radius was considered.

The results of the analysis for all five parametric study cross sections with pipe diameters 2 inches less than the flange width (BFL) are shown in Figure 5.14. The split pipe cross-frame stiffness values have been normalized by the bent plate cross-frame stiffness values. Therefore the data on the vertical axis represents the increase in stiffness of the split pipe cross-frame compared to the bent plate cross-frame stiffness.

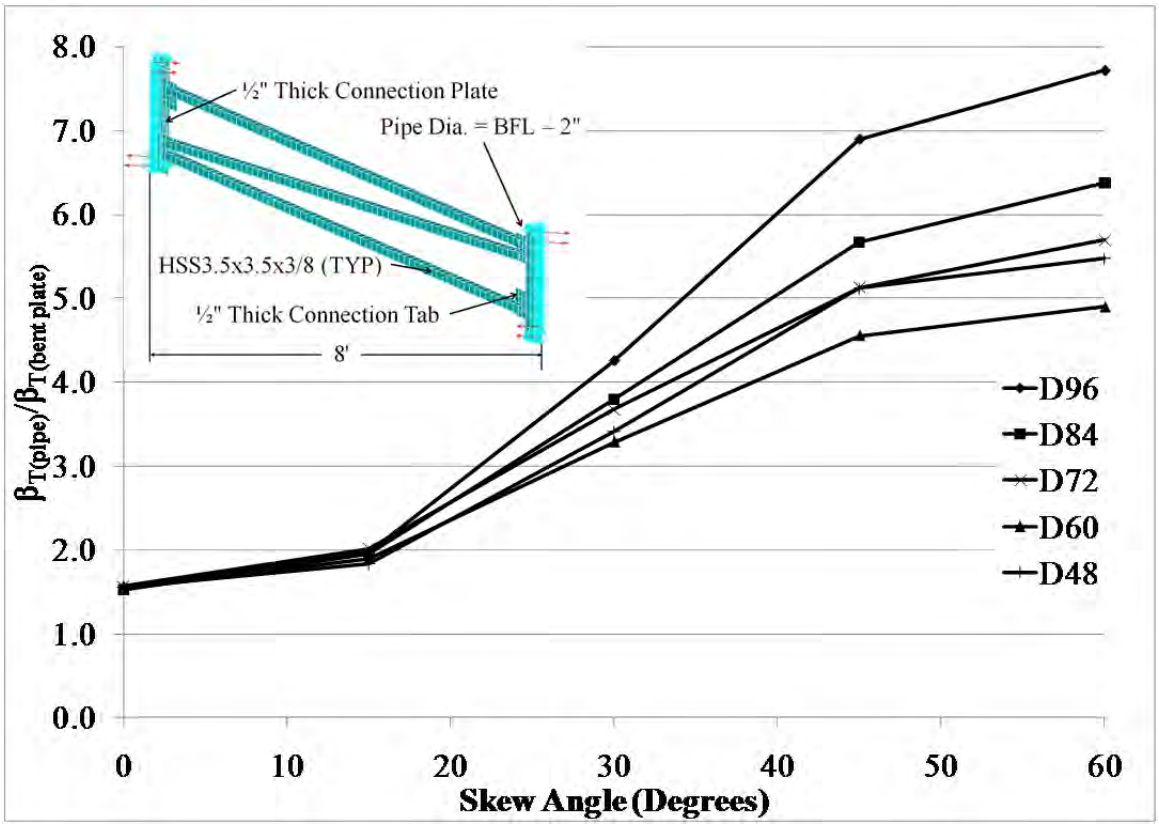

Figure 5.14: Split pipe to bent plate connection cross-frame stiffness (BFL-2)

From the figure it can be seen that the split pipe detail is much stiffer than the bent plate detail. At the larger skew angles the split pipe stiffener cross-frame reaches from 5 to 8 times as stiff depending on the depth of the girder cross section.

In the previous study the pipe diameter was as large as physically possible to fit the girder (2 inches less than the flange width). To check a lower bound on the split pipe cross-frame stiffness, the pipe diameter was reduced to half the flange width. These results are plotted in Figure 5.15. The figure shows a moderate reduction in the stiffness of the split pipe connection relative to the bent plate connection, which is expected because the braces must get longer as the pipe diameter decreases. However, even with this stiffness reduction, the split pipe stiffener shows a significant increase in stiffness over the bent plate detail.

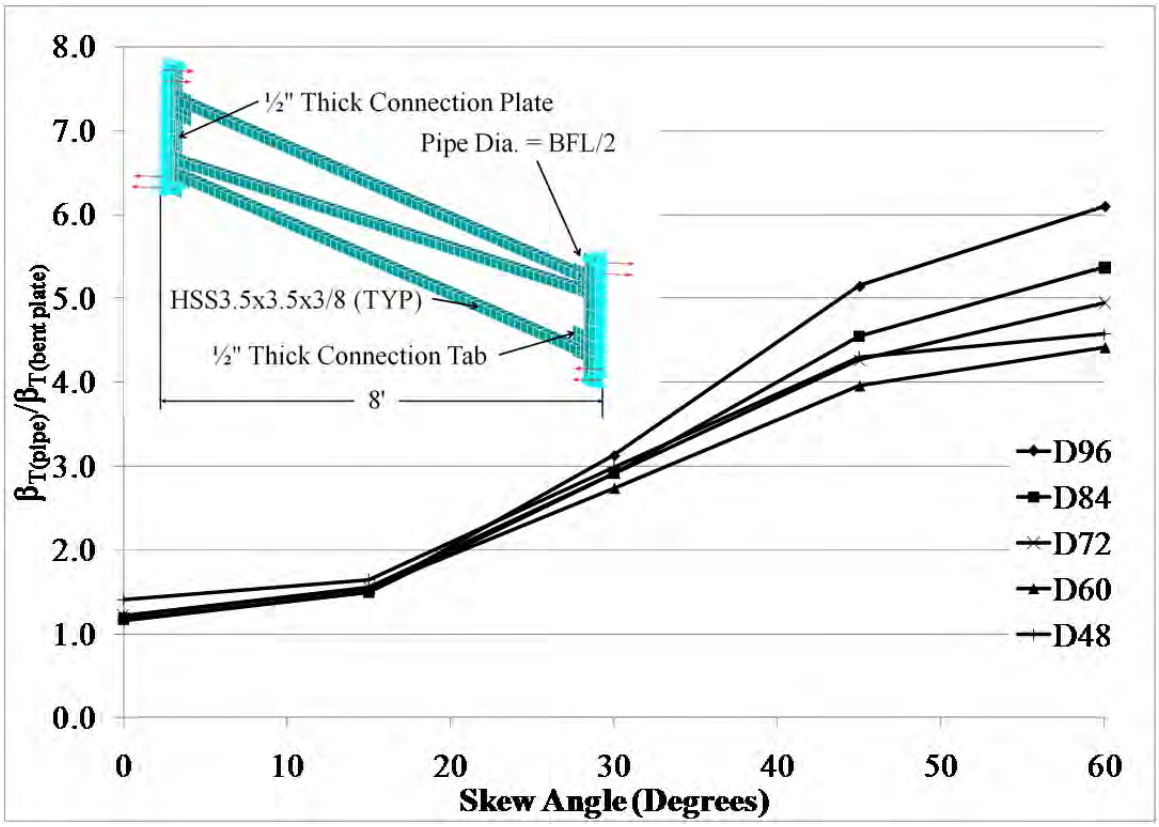

Figure 5.15: Split pipe to bent plate connection cross-frame stiffness (BFL/2)

5.3.5 Critical Split Pipe Connection Skew Angle

The next analysis performed was to determine at what skew angle the split pipe stiffener would be the limiting stiffness component. A plot similar to that used in the previous section for the bent plate analysis was created. The analysis results are given in Figure 5.16 and show that for the cross sections and braces considered, the split pipe connection is not the limiting component stiffness in any case.

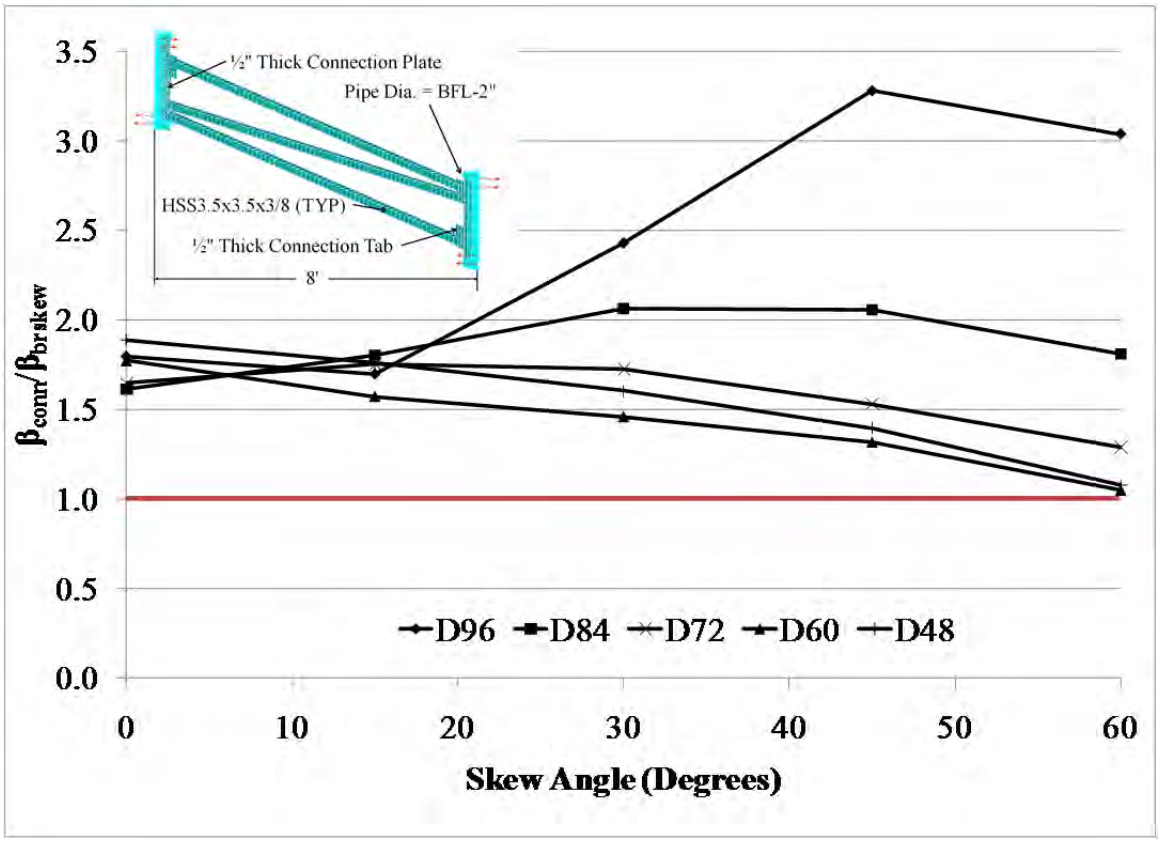

Figure 5.16: Split pipe cross-frame connection-brace stiffness ratio

However, even though the split pipe connection may not be the limiting component stiffness, it does still have a finite stiffness that does result in a decrease of the total cross-frame stiffness. To determine the impact of the split pipe connection on the cross-frame stiffness, the total cross-frame stiffness (including the split pipe cross-frame connection stiffness) was normalized by the cross-frame with an infinite connection stiffness and plotted against the skew angle. The results are shown in Figure 5.17.

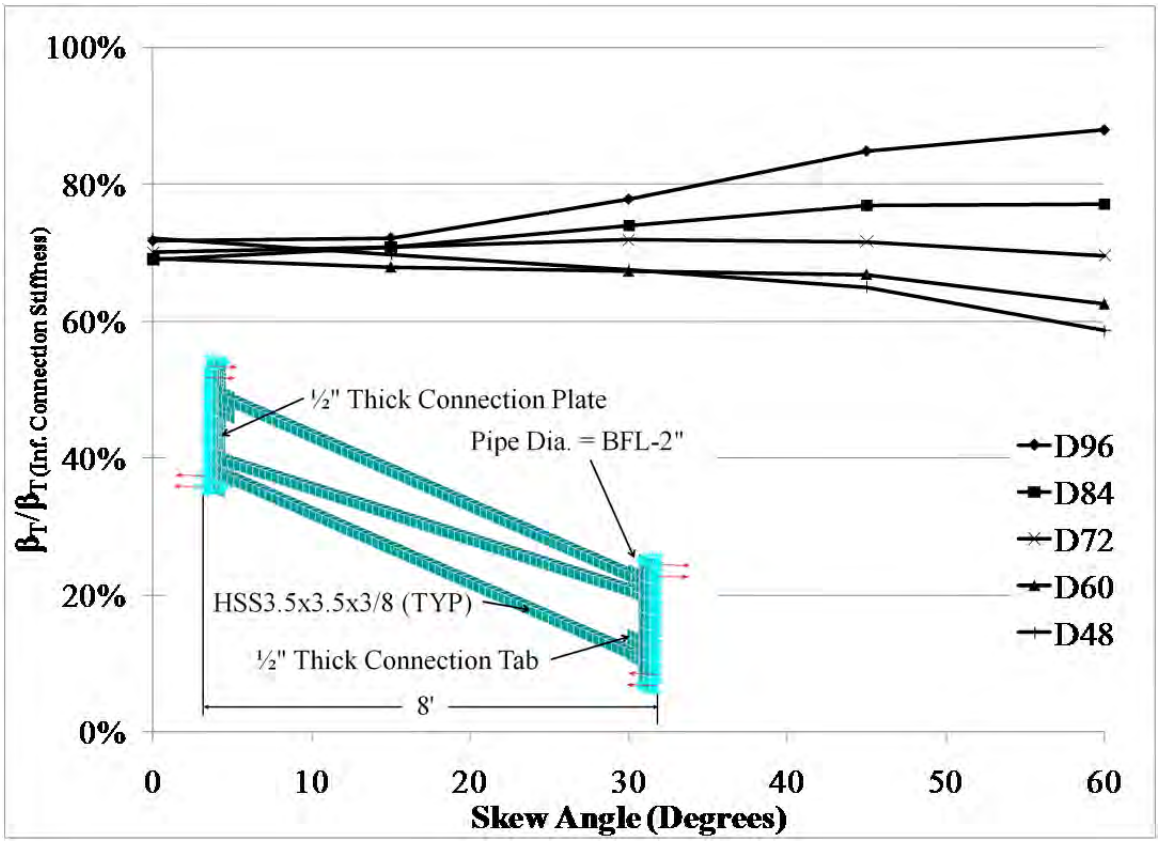

Figure 5.17: Split pipe connection impact on cross-frame stiffness (BFL-2)

The results show that the impact of the split pipe connection on the cross-frame stiffness is fairly uniform until the 30° skew is reached. For skews larger than 30°, the cross section depth becomes an important factor. A reasonable estimate of the reduction in cross-frame stiffness due to the split pipe connection flexibility for cross sections at least 72" deep is 30%. For cross sections less than 72" the reduction can be taken as 30% for skews up to 30° and 40% for skews between 30° and 60°. These recommendations are based upon the assumption of standard conditions of an end cross-frame, namely that the girder in-plane and cross-sectional stiffness are large and therefore not included in the total cross-frame stiffness calculation.

5.3.6 Connection Stiffness Summary

The preceding analysis demonstrated that the split pipe stiffener connection is much stiffer than the bent plate connection, especially at larger skew angles. Therefore, the split pipe connection provides better control of twist at the end of skewed steel girder bridges. While the stiffer connection will certainly help mitigate construction issues such as cross-frame to girder fit-up, there is still some question as to whether limiting twist will improve the girder's elastic buckling strength. In Chapter 2 the impact of girder twist was discussed in terms of previous research efforts, which found that the buckling strength is not greatly affected by moderate twist at the end of the girders. The next section presents results demonstrating the effect of end twist as a function of the cross-frame stiffness.

5.4 Girder End Twist Parametric Study

The purpose of this portion of the parametric study was to determine if Equation (2.51) (repeated below for convenience) is accurate in terms of predicting the decrease in buckling strength due to girder end twist allowed by skewed cross-frames. Because this equation was formulated from an equation for support twist rather than twist allowed by cross-frames, it must be validated to determine its accuracy.

$$n = 1 - \frac{4}{3}\left(\frac{GJ}{L}\right)_{girder}\left(\frac{1}{\beta_T}\right) \qquad (2.51)$$

(from Chapter 2)

where

n = ratio of buckling strengths with and without end twist M_{cr}/M_o (M_{cr} = strength with end twist, M_o is strength without end twist).

To validate the equation accuracy, a parametric study was conducted using a twin girder finite element model with the same end cross-frames from the cross-frame stiffness parametric study. A picture of the bent plate and split pipe cross-frame models are given in Figure 5.18 and Figure 5.19.

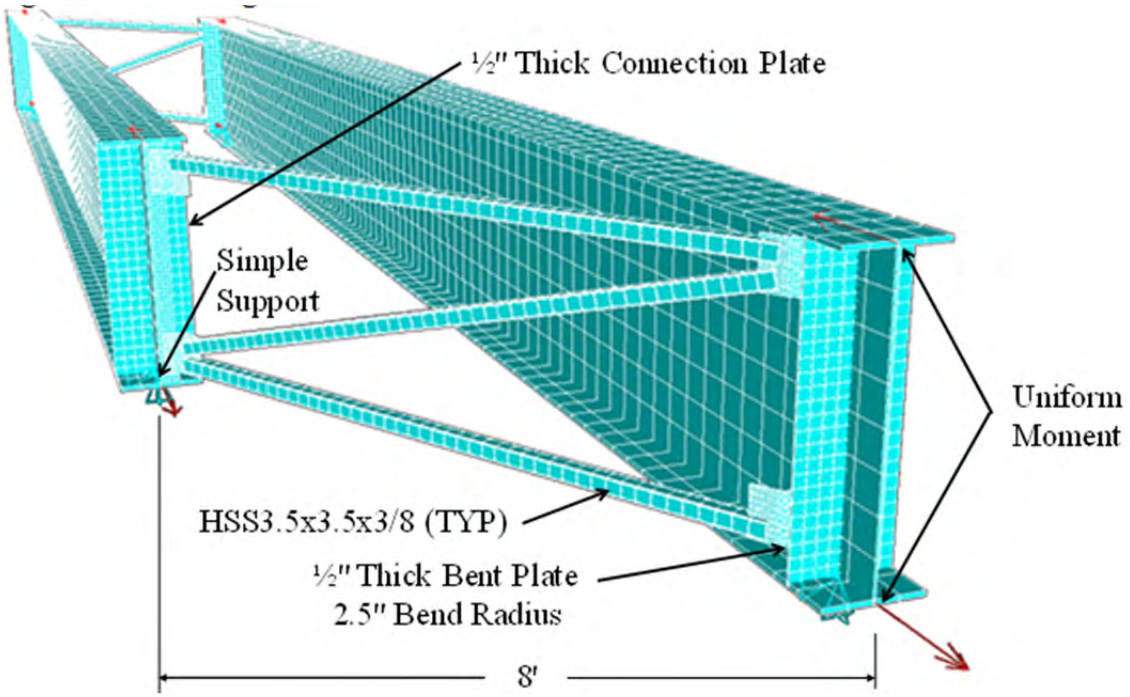

Figure 5.18: Bent plate cross-frame twin girder model

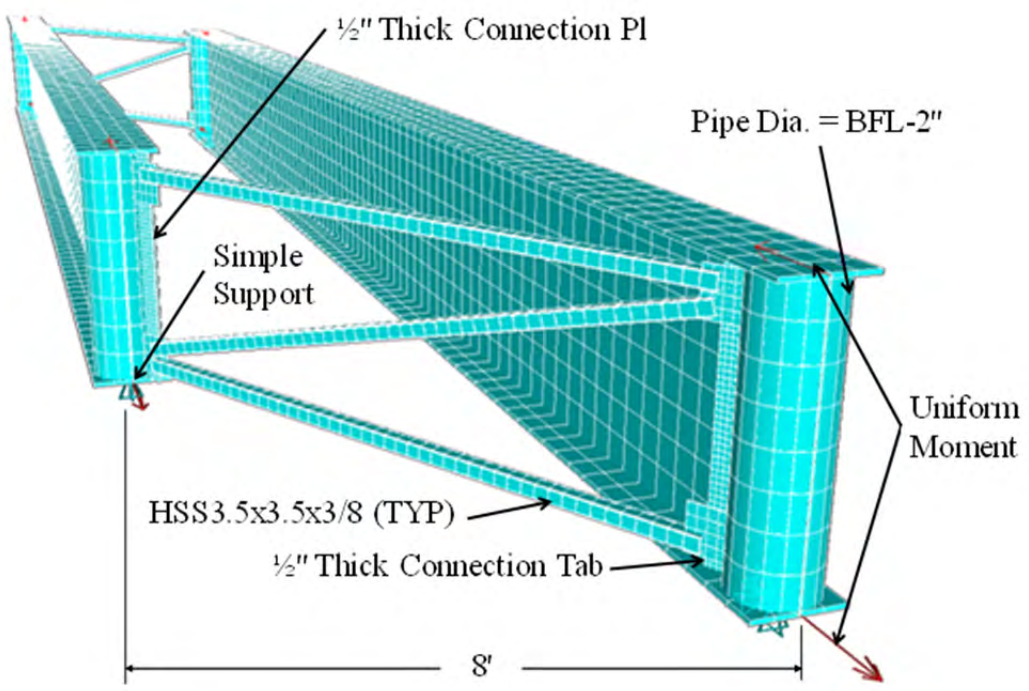

Figure 5.19: Split pipe cross-frame twin girder model

The parameters in this study remained the same as in the base cases from the cross-frame stiffness study with the bent plate and its connection plates as well as the split pipe and its connection plate and tabs all being ½" thick. The brace members were HSS3.5x3.5x3/8 and the split pipe diameters were taken as 2" less than the flange width. The twin girder model was subjected to a uniform moment, and an eigenvalue buckling analysis was conducted to determine the critical buckling moment for span-to-depth ratios ranging from 10–40 and skew angles of 15°, 30°, 45°, and 60°. The data shown below are normalized with respect to the no twist case (M_o) for each model.

Figure 5.20 and Figure 5.21 show the results for the D60 and D72 cross sections with bent plate cross-frames. From the figures it can be seen that as the skew and associated end twist increase, the buckling capacity decreases. This effect is the most significant at the shorter span-to-depth ratios, but the decrease in buckling capacity is minimal. The D60 cross section at the span-to-depth ratio of 10 and 60° skew is the largest decrease in buckling capacity at just over 6%. At a span-to-depth ratio of 10, the beam is likely to experience significant yielding prior to buckling. All other cases were typically less than 4%. Results for other cross sections with the bent plate cross-frame connection are provided in Appendix C (Parametric Study Results).

With the decrease in buckling capacity due to end twist being small when the bent plate connection is used, the current practice of simply ignoring reductions in buckling capacity due to end twist appears to be justified. When Equation (2.51) is applied to predict the buckling capacity reduction, it underestimates the reduction significantly, seldom resulting in a reduction greater than 1%. While better results can be achieved by changing the 4/3 constant in the equation to a value close to 30, the results are still not consistent. In some cases the equation with a constant of 30 over-predicts the reduction by 3% and in others it under-predicts it by 5%. With such small actual reductions, such variability makes such an equation unnecessary. As in current practice, ignoring the end twist effect on the girder buckling strength is acceptable, especially

because tipping restraint provided by the bearing was conservatively ignored in the analysis and will generally more than compensate for the loss of buckling strength due to end twist.

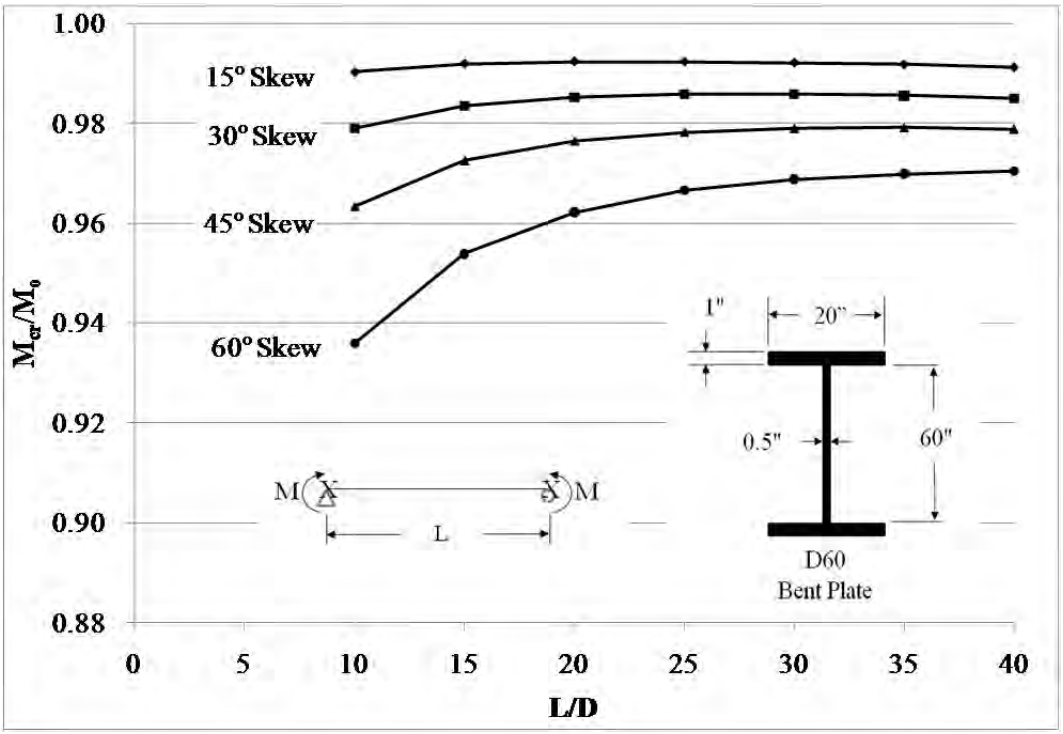

Figure 5.20: D60 cross section buckling strength with end twist

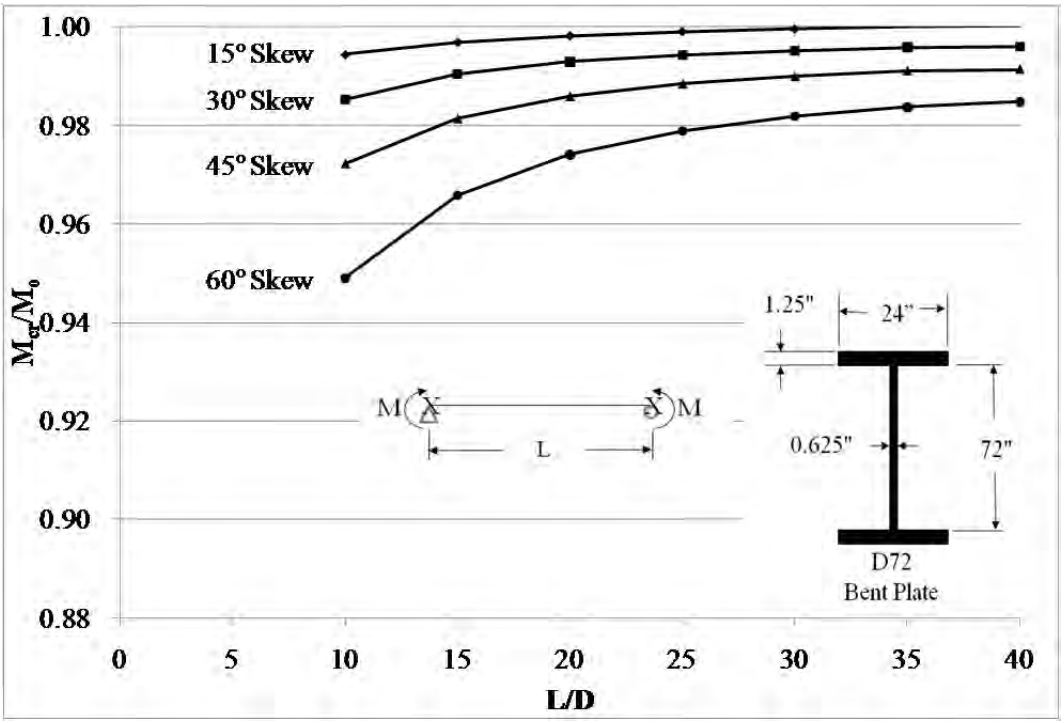

Figure 5.21: D72 cross section buckling strength with end twist

In addition to the bent plate details, the same cases for the split pipe stiffener were investigated using the finite element model shown in Figure 5.19. The results for the D84 cross section are shown in Figure 5.22. As shown in the previous section of this report, the split pipe connection is significantly stiffer than the bent plate connection and should limit twist better than the bent plate connection. The results of the larger stiffness are demonstrated with the very small buckling strength reductions shown in Figure 5.22. In no case did the buckling of a split pipe stiffened section drop below 98% of the no twist case. In some cases (such as the 15° skew case below) the cross-frame provides some warping restraint and the buckling capacity is greater than the no twist case. The results from the other cross sections considered are provided in Appendix C (Parametric Study Results).

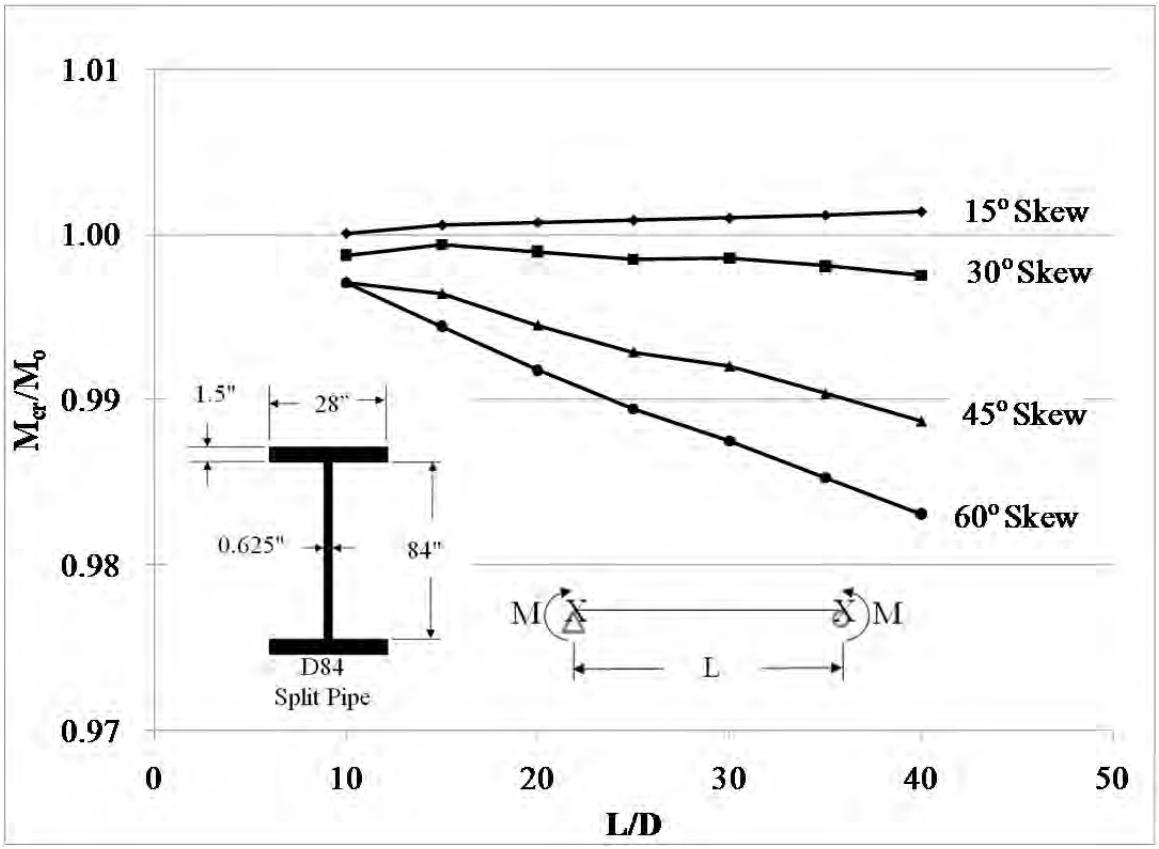

Figure 5.22: D84 cross section buckling strength with end twist

To directly assess the impact of the connection type on end twist and girder strength, a non-linear geometric analysis was conducted to check the end twist and cross-frame forces to the D60 cross section at an L/D of 30 (150' length). The same models pictured in Figure 5.18 and Figure 5.19 were used to compare the responses between the bent plate and split pipe stiffener connections.

The results for the end twist comparison are provided in Figure 5.23. The data in the figure demonstrate that the split pipe stiffener connection is slightly better at limiting girder twist prior to the onset of buckling. As the girder with the bent plate connection buckles, the end twist rapidly increase as would be expected during buckling. A corresponding response can be seen in the end cross-frame diagonal forces as shown in Figure 5.24.

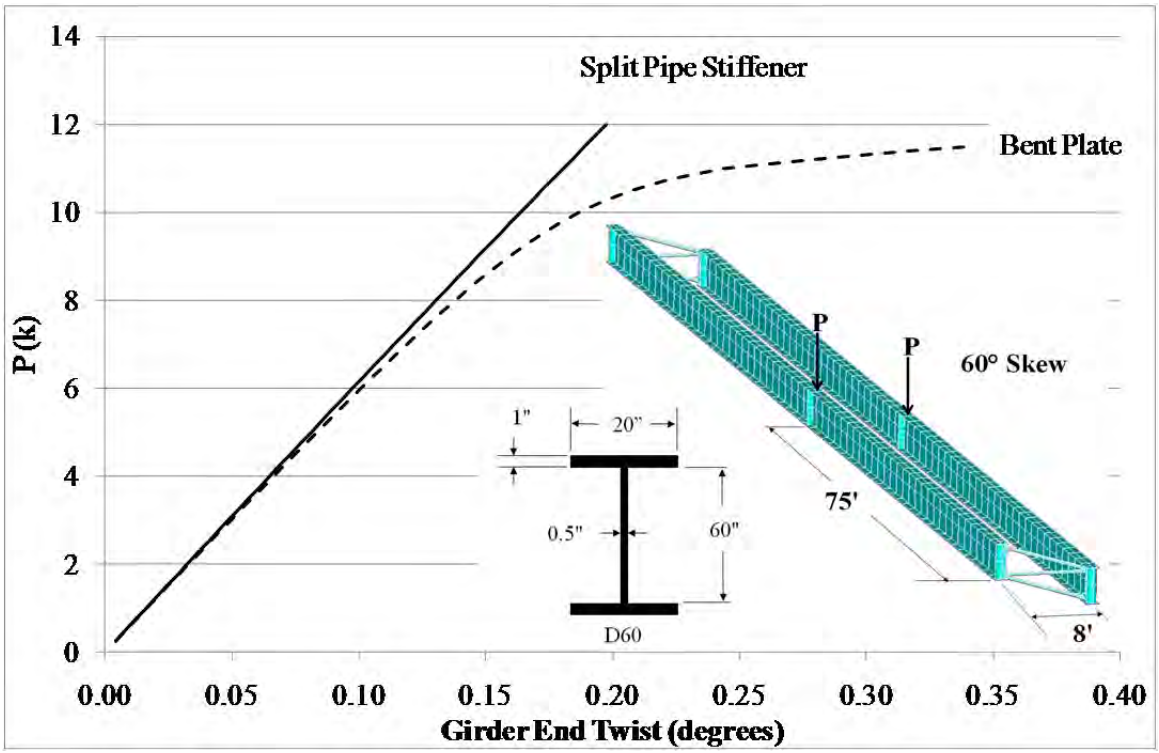

Figure 5.23: Girder end twist comparison

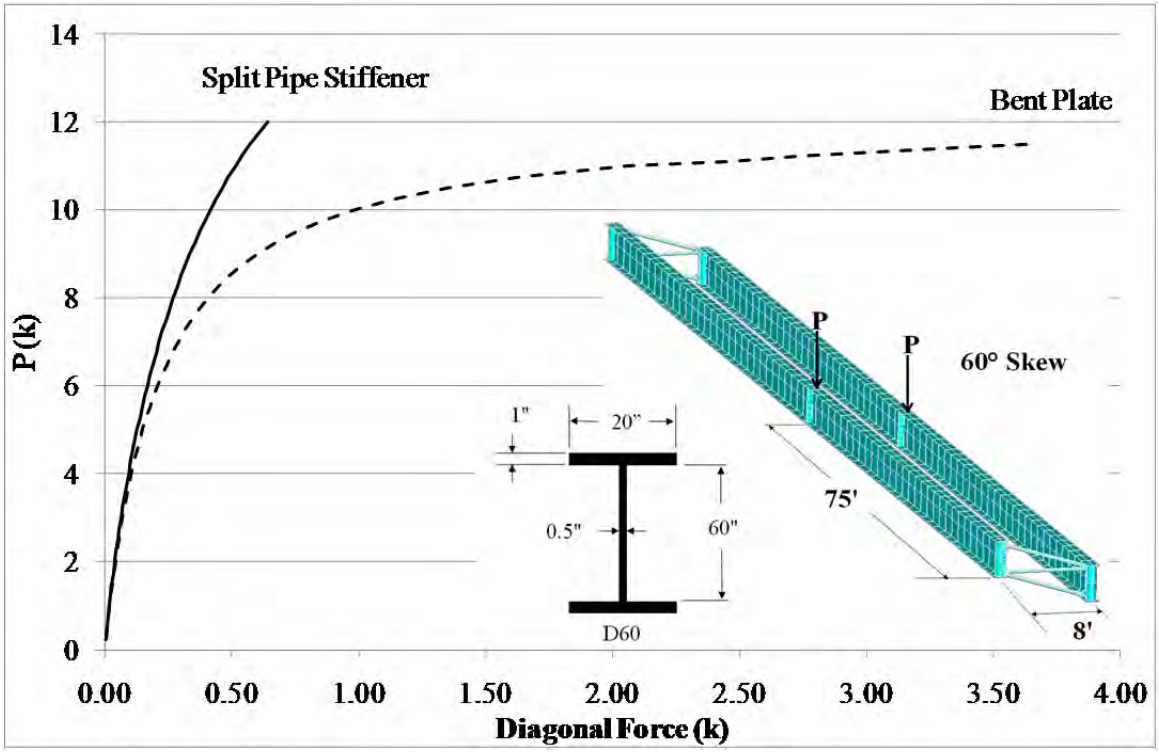

Figure 5.24: Cross-frame diagonal force comparison

The two preceding figures show that the split pipe stiffener connection does reduce the girder end twist and the corresponding brace forces compared to the bent plate connection. While this is in part due to the higher connection stiffness, the majority of the reduction is due to the increase in buckling strength as a result of the warping restraint provided by the split pipe stiffener.

5.4.1 End Twist Summary

The end twist parametric study demonstrated that end twist does result in a slight decrease in the elastic buckling capacity of the girder. For the common bent plate connection, the reduction is small and can be neglected as has been done in the past. The slight reduction in capacity is typically offset by the tipping restraint provided by the bearings. The reduction in buckling capacity for the split pipe stiffener is even smaller than the bent plate and typically does not exceed 2%, which can generally be disregarded.

The split pipe stiffener has been shown to be a much stiffer connection than the bent plate and will therefore better control girder end twist. While this may not significantly enhance the girder buckling strength, it will help mitigate construction fit-up issues and aid in keeping the girder web plumb during the concrete deck placement. Finally, while the stiffness of the split pipe connection does help stabilize the girder end, the majority of its benefit seems to be the warping restraint the detail provides. This impact is discussed in the next section.

5.5 Split Pipe Stiffener Warping Restraint Parametric Study

The results of the twin girder buckling tests described in Chapter 3 (Experimental Program) showed that the split pipe stiffener significantly increased the buckling capacity of the girders in the laboratory. To extend these results to other cross sections and pipe sizes and find an analytic equation to calculate the increased girder buckling capacity due to the warping restraint provided by a split pipe stiffener, a parametric study was conducted using the cross section, pipe diameter and span-to-depth ratio as the primary variables.

In Chapter 2 (Background) a method to predict the buckling capacity of a split pipe stiffened girder was proposed. This method used a torsional effective length factor (K_z) in the non-uniform torsional resistance portion of the basic buckling strength equation as shown in Equation (2.55) (repeated below for convenience).

$$M_{cr} = \mathrm{C_b}\pi/L_b\sqrt{EI_yGJ + \pi^2E^2C_wI_y/(K_zL_b)^2} \qquad (2.55)$$
(from Chapter 2)

To determine K_z the use of the non-sway alignment chart from the AISC Manual of Steel Construction was proposed with G_z values as given in Equation (2.56) (repeated below). However, to properly calculate G_z, the split pipe boundary conditions must be known. Therefore a multiplier (m) was proposed to account for the changes in the relative flexural stiffness of the girder flange to pipe torsional stiffness. The purpose of this parametric study was to find suitable values for m that give good agreement between the finite element model and Equation (2.55) and to determine if the increase in buckling capacity due to the split pipe warping restraint was significant when the girder and pipe geometries were varied.

$$G_z = \left(\frac{EI}{L_b}\right)_{flange} \Big/ m\left(\frac{GJ}{L}\right)_{pipe} \qquad (2.56)$$
(from Chapter 2)

The parametric study focused on a single girder with simple supports and no twist at the end. The cross section, loading condition, pipe diameter, and span lengths were all varied during the study. The girder cross sections used were those pictured in Figure 5.1. A variety of loads was considered including, uniform moment, a point load at mid-span, and distributed loads. The point loads and gravity loads were applied at midheight of the cross section. Pipes ranged in diameter from half the flange width to two inches less than the flange width and were ½" thick. Span-to-depth ratios that were considered ranged from 10 through 40.

After running all the cases, a trial and error analysis was employed to find values of *m* for ranges of the ratio of the pipe torsional stiffness to the flange flexural stiffness. The results of this analysis are summarized in Table 5.1. Results for three cross sections and three different loading conditions are given in Figure 5.25, Figure 5.26, and Figure 5.27 for the largest and smallest pipe diameters considered. The results are normalized by the non-stiffened buckling capacity of the cross section at the span-to-depth ratios plotted. Results for the other cross sections and load cases that were considered are provided in Appendix C (Parametric Study Results).

Table 5.1: m-values

$\boldsymbol{m}$	$\dfrac{\left(\frac{GJ}{L}\right)_{pipe}}{\left(\frac{EI}{L}\right)_{flange}}$
1.0	< 4
1.5	≥4 and <6
3.0	≥ 6

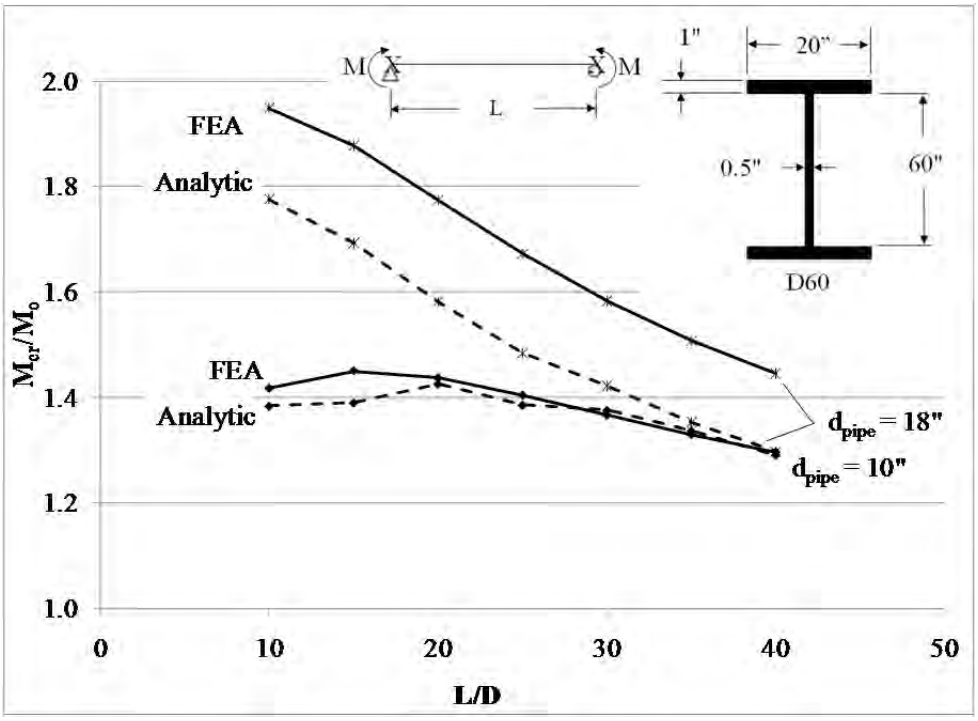

Figure 5.25: D60 split pipe stiffened buckling capacity (uniform moment)

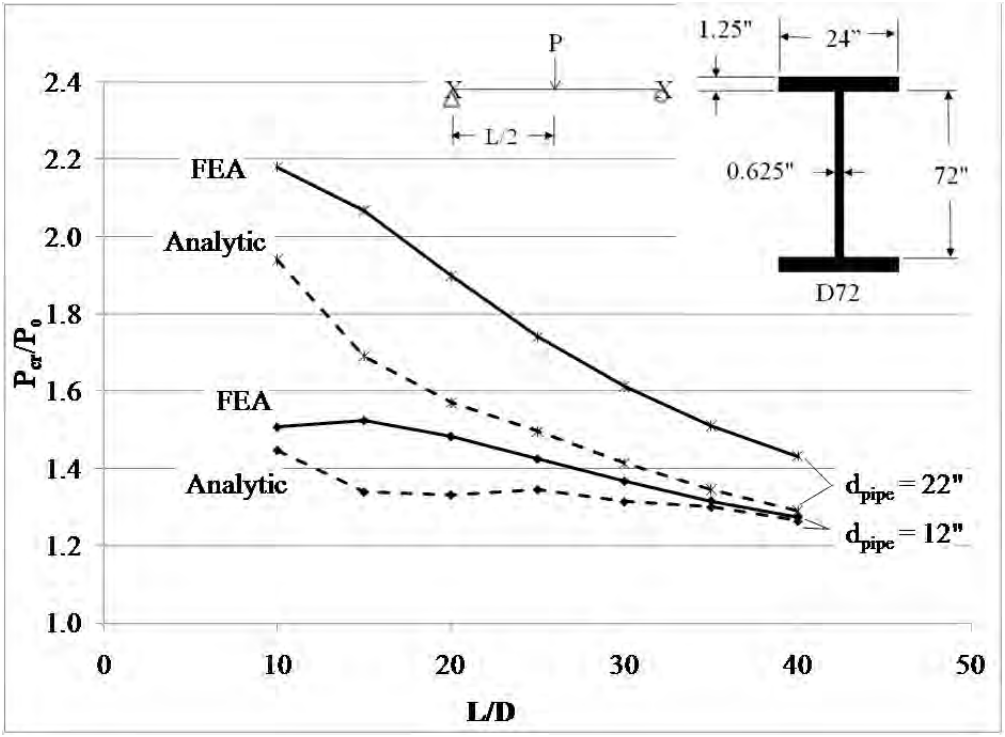

Figure 5.26: D72 split pipe stiffened buckling capacity (mid-span point load)

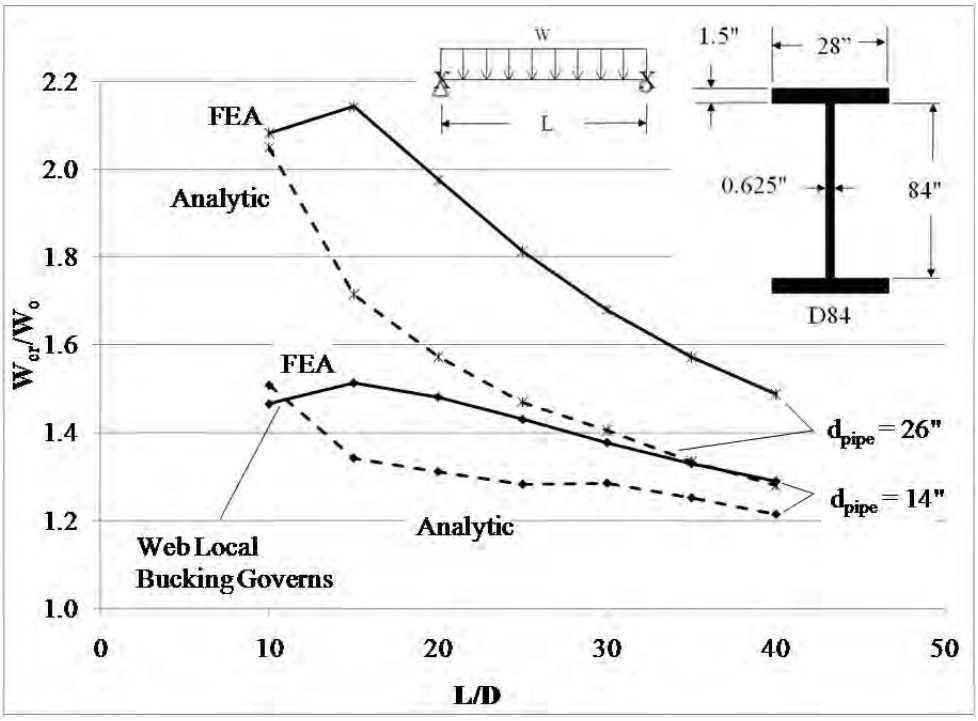

Figure 5.27: D84 split pipe stiffened buckling capacity (distributed load)

The results in the preceding three charts show good agreement between the FEA model and the analytic solution. All other cases, including the pipe diameter values between the ones displayed, show similar good agreement. From the graphs it can be seen that, as in the twin girder laboratory buckling results, the warping restraint provided by the split pipe significantly strengthens the elastic buckling capacity of the girders from 40% to 80% in the 20–30 span-to-depth ratio range. Also, the analytic solution is moderately conservative when larger pipe sizes are used and less so when smaller pipe sizes are used. The reasons for these deviations can be explained based on the underlying assumptions made in formulating the analytic solution.

Equation (2.55) is based upon the assumption that the split pipe stiffener will only impact the warping resistance of the cross section. However by adding the split pipe stiffener to the girder cross section, the torsional constant at the ends of the girder is changed from that of an open I-shaped section to a closed shape and the rate of change of the twist in the cross section is reduced at the end regions. Therefore the uniform torsional resistance of the cross section increases significantly at the girder ends (Heins and Potocko 1979). This increase is reflected in the near uniform difference of about 20% between the analytic solution, which does not account for this increase, and the FEA solution. As the pipe diameter decreases, so does the increase in the girder's uniform torsional resistance. This is reflected in the much smaller difference between the analytic solution and the FEA results at the smaller pipe diameters.

Another source of deviation between Equation (2.55) and the FEA solution is the discrete *m*-values selected to determine G_z. The *m*-value will actually vary between the discrete ratio limits shown in Table 5.1. As the values of $(GJ/L)_{pipe}/(EI/L)_{girder}$ are closer to the limits given in Table 5.1, the accuracy of the analytic solution improves. This can be seen from the values shown on the graphs in Figure 5.28 and Figure 5.29. Where the relative stiffness ratio (value shown on the upper horizontal axis) is close to the limits of 4 and 6, the solution is very accurate.

As the relative stiffness ratios get farther from the Table 5.1 values, the analytic solution becomes more conservative.

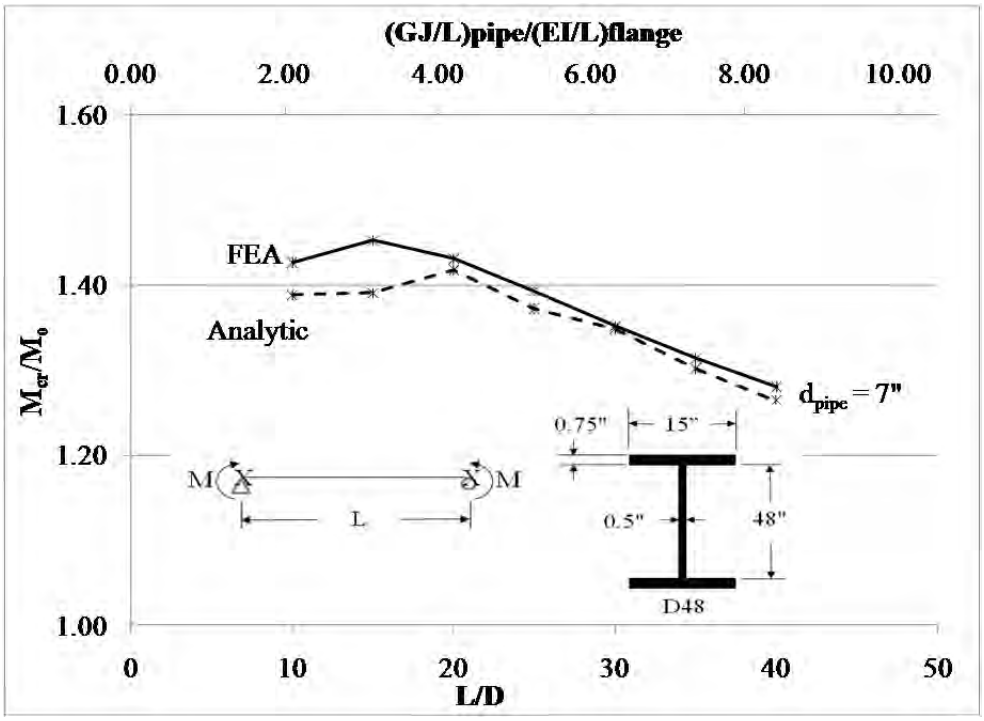

Figure 5.28: D48 split pipe stiffened buckling capacity (uniform moment)

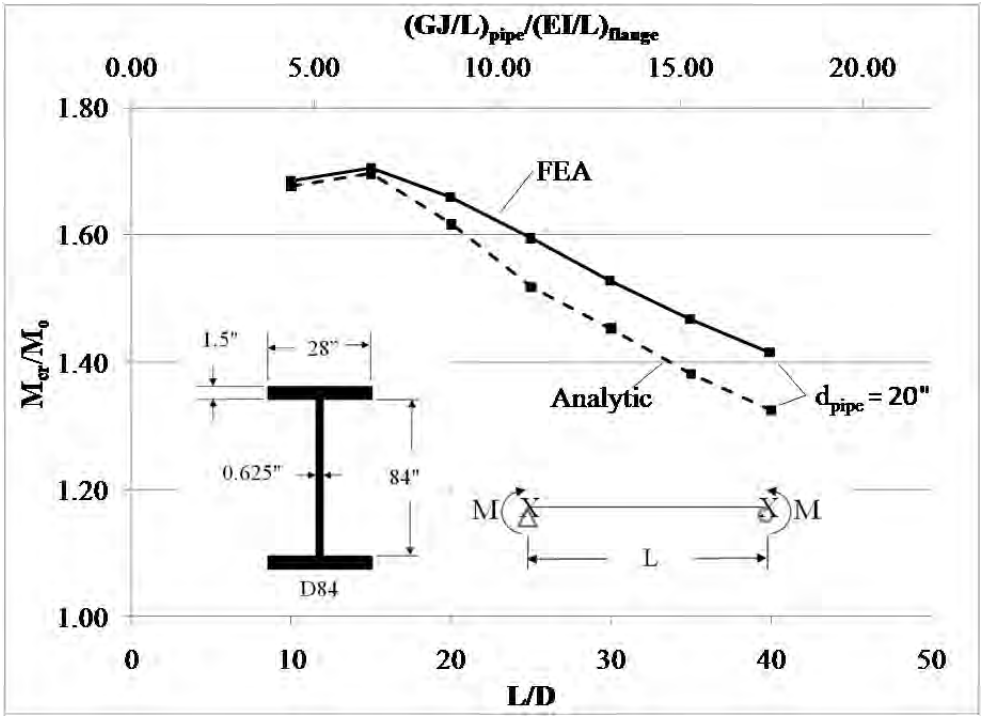

Figure 5.29: D84 split pipe stiffened buckling capacity (uniform moment)

5.5.1 Warping Restraint Summary

As was demonstrated with the laboratory testing results discussed in Chapter 3 (Experimental Program), warping restraint applied at the ends of the section can provide a significant increase in a girder's elastic buckling capacity in the wide range of girder and pipe geometries investigated. The use of Equation (2.55) with the *m*-values given in Table 5.1 had good agreement with the finite element results and can be used to calculate the increase in buckling capacity due to a split pipe stiffener at the girder end. The results summarized in this chapter have focused on the elastic buckling behavior. The recommendations should be applicable up to the elastic limit of the material.

5.6 Intermediate Cross-frame Layout Parametric Study

The laboratory tests with two different cross-frame layouts, the staggered and the continuous, have been described in Chapter 3. The comparison of those test results leads to a conclusion that the intermediate cross-frame members in the staggered layout experience significantly lower axial force than those in the continuous layout. The same finding can be also seen in the FEA model discussed in Chapter 4. But because only a one line of braces were used in the test setup, more general cases should be examined to verify the conclusion.

A parametric study was conducted on two sets of models: one set of 3-girder models and another set of 4-girder models. Each set included a staggered layout model and a continuous layout model. Three lines of cross-frames were put in each bay with the two different layouts. Pictures of those models are presented in Figure 5.30 and Figure 5.31. All models are composed of 120-foot long D60x20 girders with 56.3°skewed supports. The end frames were connected to girders by using bent plates and intermediate cross-frames were modeled using line elements. The spacing of cross-frame is generally 30 feet except that the braces attached to the ends of the girders were moved 2 feet away from the supports to avoid the effects of large differential deflection discussed in Chapter 1. Two girders were loaded near mid-span by 36-kips downward point loads to simulate a simplified HS20 truck loaded on one lane.

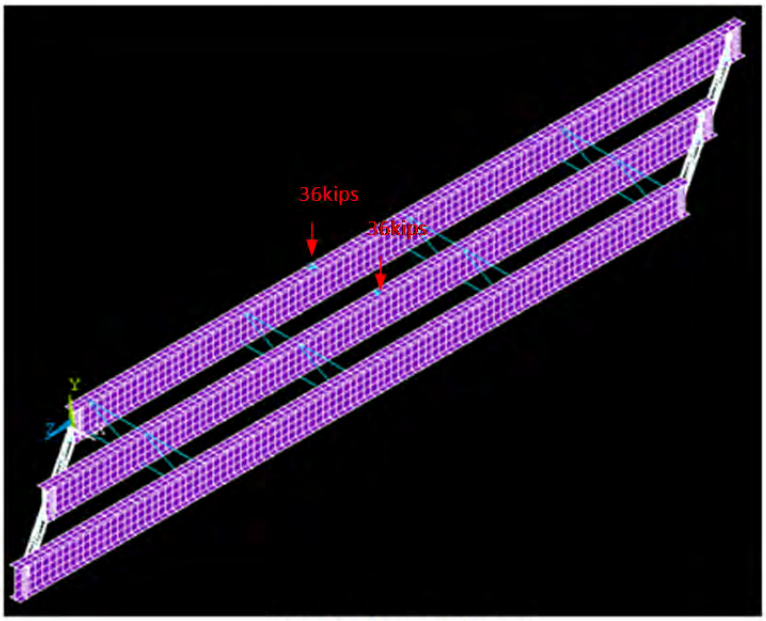

(a) Continuous layout

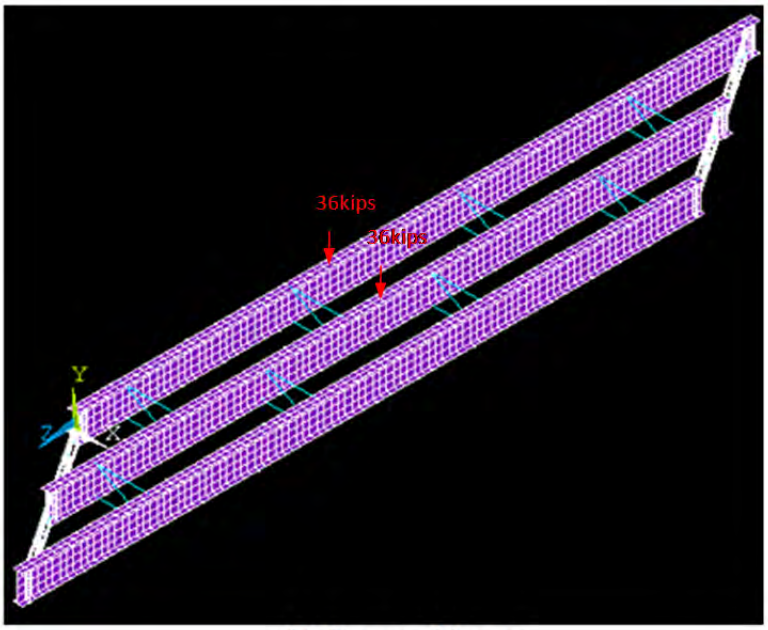

(b) Staggered layout

Figure 5.30: Three D60x20 girders model with intermediate cross-frames

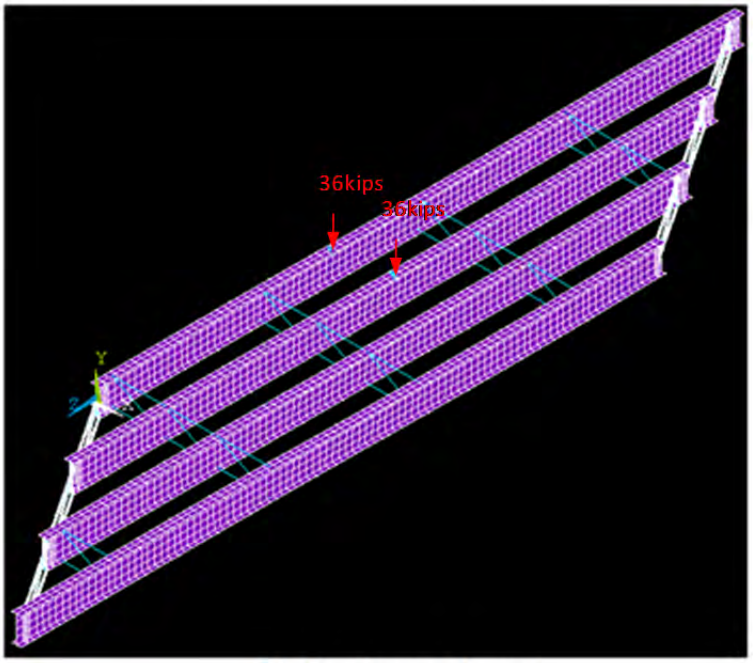

(a) Continuous layout

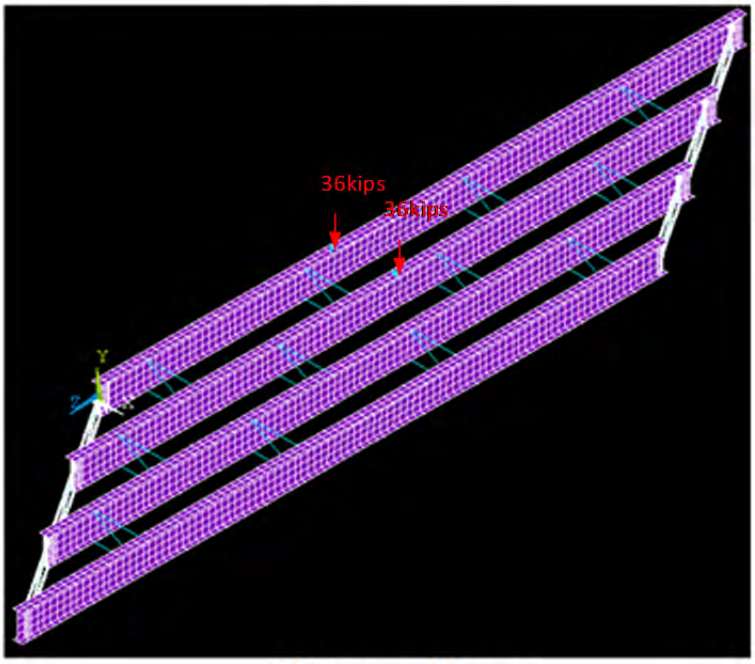

(b) Staggered layout

Figure 5.31: Four D60x20 girders model with intermediate cross-frames

Large displacement analyses were performed on the models. The axial forces of the cross-frame members were obtained to study the effect of the brace layout on the axial forces in intermediate cross-frame. Because the highest induced force in a cross-frame usually occurs in diagonal members, and also because cross-frames are usually designed in uniform sizes to reduce the cost, the controlling value in the design of the cross-frames is the maximum force in the

diagonals. Figure 5.32 and Figure 5.33 show the bridge models along with their diagonal forces near the associated cross-frames.

In the three girder models with the continuous cross-frame layout, the maximum brace force value is 19 kips, compared to 8 kips in the staggered layout. In the four girder models, the maximum brace force value for the continuous layout is 27 kips and that for the staggered layout is 9 kips. It can be observed from this study that, by staggering the cross-frames, the live load induced forces in the cross-frame members are generally significantly reduced.

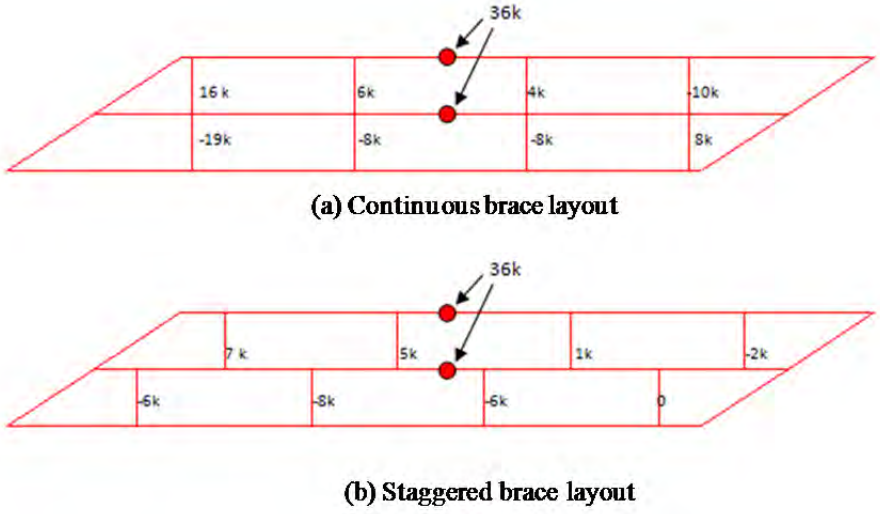

Figure 5.32: Three girder model diagonal axial forces

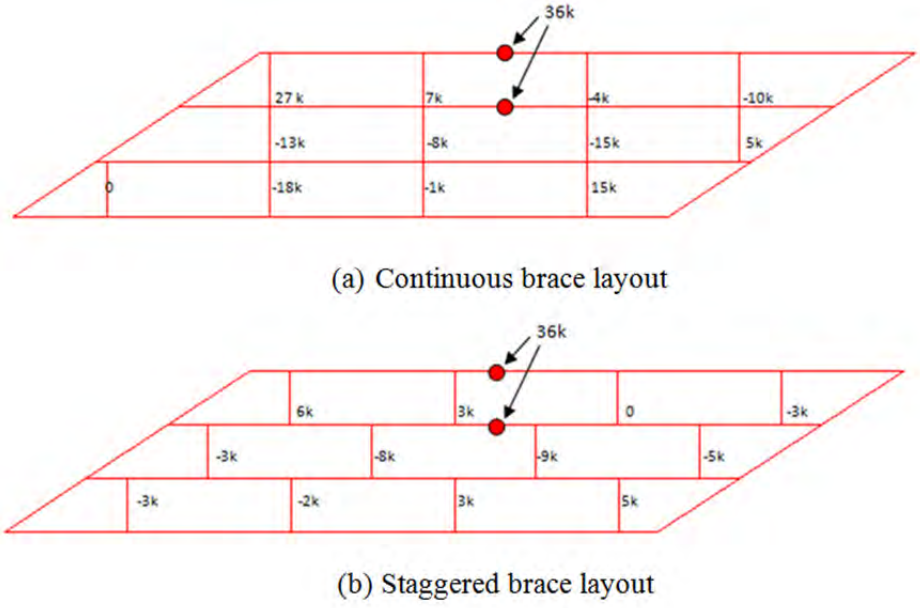

Figure 5.33: Four girder model diagonal axial forces

5.7 Parametric Study Results Conclusions

Several conclusions can be drawn from the results of the parametric studies. Most importantly, the skewed cross-frame connection stiffness is not infinite as currently assumed. Whether a split pipe or bent plates are used, the connection stiffness is finite and in the cases studied can decrease the cross-frame stiffness by 20% or more.

Designers have several options possible to increase the stiffness of connections in skewed end cross-frames. First, if a bent plate is used, the bent plate and connection plate thickness can be increased. Increasing the thickness of the connection plate is generally more efficient than just increasing the bent plate thickness. The most effective result was increasing the thickness of both the bent plate and the connection plate. Second, the designer may choose to use a split pipe stiffener connection rather than the bent plate.

The split pipe stiffener connection was shown to significantly increase the connection stiffness and reduce twist at the girder ends. While end twist was not a significant factor in decreasing the girder buckling strength, reducing girder end twist will help ease cross-frame fit-up issues during erection and help achieve a vertical web at the girder ends when the concrete slab is placed. However, the largest source of stability for the split pipe stiffener comes from the warping restraint provide to the girder end.

The impact of warping restraint was shown to be significant in all the cases investigated. By increasing the elastic buckling strength in the end spans, the first row of intermediate cross-frames may be moved farther from the abutment and therefore reduce the differential deflections along the first row of intermediate cross-frames. This in turn will mitigate the fatigue issues in connecting the intermediate cross-frames to the girder tension flange.

The brace layout proved to have significant impact on cross-frame forces. By staggering the cross-frames in the direction parallel to the skew angle of the bridge, the maximum live load induced forces in the cross-frame member decreases significantly.

Chapter 6. Fatigue Study

6.1 Fatigue Concerns for Split Pipe Stiffener

In evaluating the feasibility of the split pipe connection detail, an issue of concern is the fatigue performance of this detail. Of particular interest is the question of whether the proposed split pipe detail would be worse than the currently used plate stiffener in fatigue loading. Thus an investigation was needed to ensure that replacing the plate stiffener with the pipe stiffener will not lead to fatigue failures.

Bridges are subject to continual loading cycles throughout their functional life. This type of loading can cause fatigue failures that result not from yielding the material, but from crack growth in the material itself at below-yield stress levels. A connection may be able to handle high stresses well under a single load application in laboratory testing, but cause fatigue failure either in the connection itself or in the bridge element to which it's connecting, over the course of millions of repeated loads.

Fatigue results from crack-growth due to these repeated cycles. All steel begins with some level of cracking already present into it. Handling and, in particular, welding lead to the formation of larger cracks and imperfections in the steel. As loads cycles on and off of the steel, the cracks slowly grow until a fracture occurs. The growths of the cracks occur not as a function of the maximum stress seen but rather the change in stresses the steel experiences. Thus a large, constant load is not likely to cause fatigue issues, but a small, varying load is. It also means that the variable of interest when performing fatigue studies is not the absolute stress seen by an object but the range of stresses and total number of cycles undergone at that stress range.

Both the pipe stiffener and conventional plate stiffeners are welded to the girder flanges and web. The potential difference in fatigue life results from the dissimilar geometries of the connections. An issue of interest is whether the pipe stiffener introduces more severe stress concentrations than conventional plate stiffeners. Points of stress concentration can be sites for crack formation and growth which lead to eventual fatigue failure (Unsworth 2003).

AASHTO has several general details which it rates for fatigue. It gives category A through E ratings (with the addition of B', C', and E' categories) that represent how that detail is expected to behave under repeated loading. This can be seen in Figure 6.1 (AASHTO 2010).

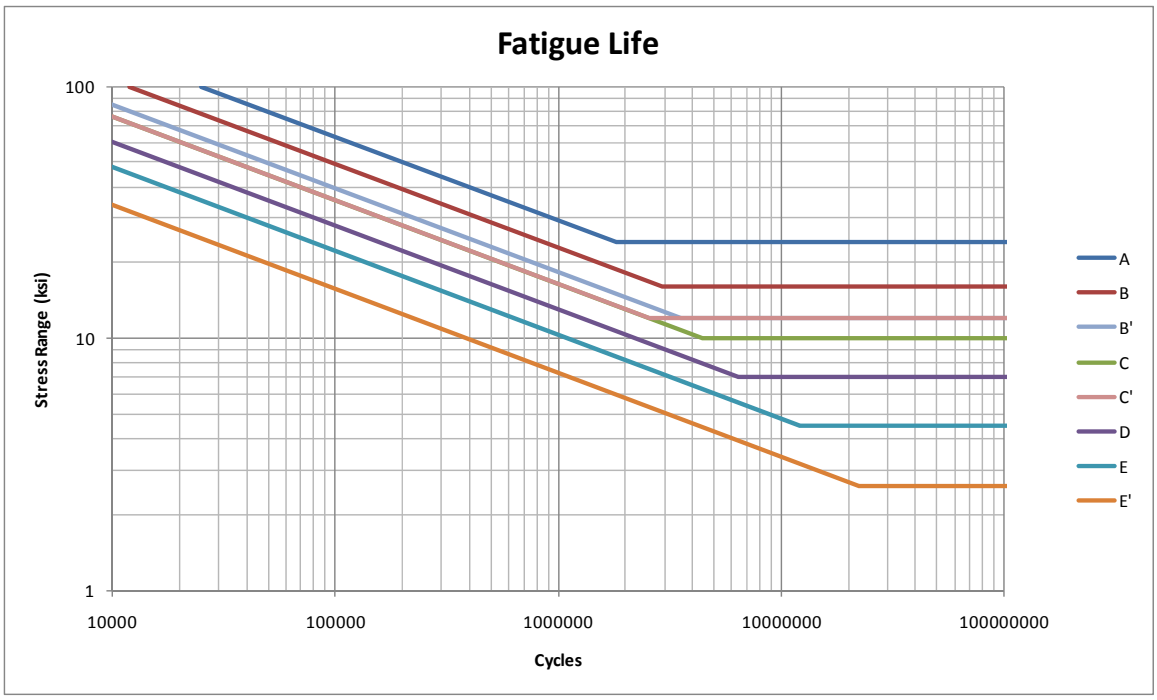

Figure 6.1: AASHTO fatigue categories

The fatigue categories represent how many cycles a particular detail should be able to undergo given a specific stress range before failure. The details AASHTO has compiled have already been tested to ensure compliance with their rating. The plate stiffener currently has a category C rating as designated by AASHTO. Consequently it would be desirable for the pipe stiffener at achieve a category C rating or better to ensure that its fatigue performance is not worse than the conventional plate stiffener.

6.2 Previous Research on Fatigue

A review of the literature revealed no previous research on the fatigue performance of pipe stiffeners. Although previous research has been conducted on the warping restraint provided by pipe stiffeners, this work was related to building applications and thus fatigue was not a significant concern (Ojalvo and Chambers, Effects of Warping Restraints on I-Beam Buckling 1977). Previous research on plate stiffeners had already resulted in a category C rating (Roy et al. 2003). A goal of this project was not to investigate fatigue performance of plate stiffeners directly, but instead to provide a comparison between plate stiffeners and pipe stiffeners.

Research had been done on built-up girders with corrugated webs (Anamia et al. 2005). The geometry and construction is somewhat similar to the welded, circular geometry in the pipe stiffener. Although the two are not identical, fatigue research for corrugated webs may be able to provide insights into the fatigue behavior of the pipe stiffener.

The general findings of interest from the research on girders with corrugated welds were their fatigue category and the point of interest for hot spot stresses. It was found that at Category B' rating would best fit the research results (Anamia and Sauseb 2005), which would be sufficient so as to match the plate stiffener if these results carried over to the pipe stiffener. It was found that the point most susceptible to cracking in the corrugated web girders was along the

bend at a 45^o angle, which serves as a point of comparison for the results from the tests on the pipe stiffener (Sause et al. 2003).

6.3 Layout of Fatigue Research Program

In order to determine the fatigue properties of the pipe stiffener, a two-part research program was undertaken. The first was to perform physical testing on the split pipe and the second was to do computational analysis using a finite element model to further investigate the connection.

The physical testing was designed to compare the pipe stiffener directly to the plate stiffener by testing both connections simultaneously in the same girder. Due to the time and cost involved in fatigue testing, only a limited number of tests were conducted. Similar to previous tests on corrugated web girders, the girders with plate and pipe stiffeners were tested using a four-point loading arrangement that provided for constant moment in the region of the girder with the stiffeners.

Once the laboratory testing was complete, finite element models were developed of the connections. These models were used to closely examine the stress-fields generated in the girder at the stiffener locations. The models were also used to examine variables that were not included in the test program, such as variations in pipe diameter and wall thickness, weld size, girder dimensions, and other parameters.

The experiments and analysis described above focused on the impact the pipe stiffener would have on the potential for fatigue failure of the girder. As a last stage of this research project, a brief investigation was conducted to evaluate the potential for fatigue problems within the pipe stiffener itself, due to localized distortions arising from the connection of the cross-frame to the pipe stiffener. This portion of the study was conducted exclusively with finite element analysis.

6.4 Laboratory Testing

A program was designed and implemented to test both the proposed pipe stiffener connection along with the plate stiffener connection that it would replace, for fatigue performance. This program was intended to evaluate the proportional fatigue behavior of the pipe stiffener as compared with the original solution. The data would then also be used to validate a finite element model which could be used to investigate the fatigue effects of various parameters of the pipe stiffener design, such as the pipe thickness and diameter.

6.4.1 Test Specimens

The items to be tested, referred to here as the ‘specimens,’ are four different girders. Six girders were fabricated in this process, but only four were tested and only those will be described in this report. Each girder was a W21x101 rolled wide flange beam of ASTM A992 steel. Each girder was then fitted with six different connections: two split pipes, two plate stiffeners with no skew, and two plate stiffeners with either a 30^o or 60^o skew. Figure 6.2 shows the girder details.

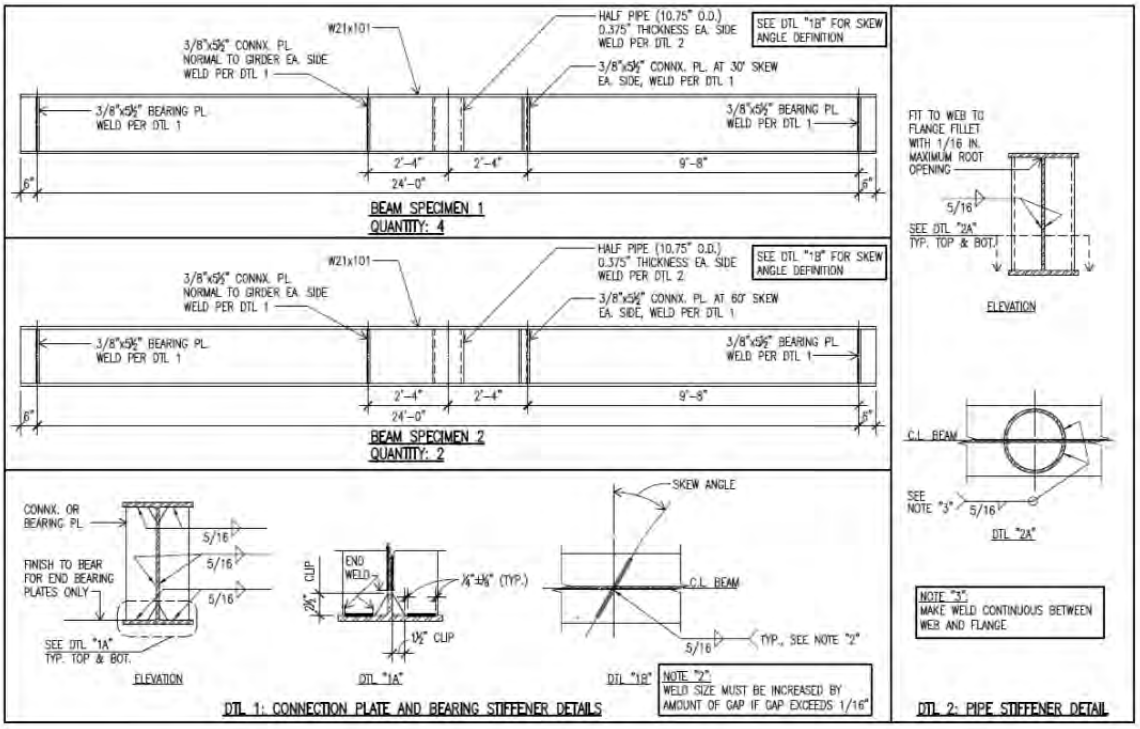

Figure 6.2: Design of specimens

6.4.2 Testing Procedure

A cyclic load was applied to a spreader beam that rested on the girder being tested. This girder was supported with two simple supports at either end. This four-point loading provided a length of constant moment at the center of the section underneath the spreader beam where the six connections were located. A photo of the testing apparatus can be seen in Figure 6.3.

Figure 6.3: Arrangement of the tests

The load induced a stress range of predetermined magnitude into the girder. The number of load cycles applied to the beam was recorded along with that stress range until a fatigue crack appeared at one of the connections. These data points served as the results to the physical testing, and could be used to compare against the AASHTO fatigue categories to determine what rating the split pipe should be given as well as a direct comparison to the performance of the plate stiffeners that were tested with the pipe stiffeners.

6.4.3 Inspection for Cracks

During the loading of the specimens and after completion of testing, each beam was examined using non-destructive and destructive testing for the presence of cracks. Non-destructive testing consisted of both visual inspection as well as magnetic particle inspection. Inspection for cracks was done both during testing and after failure. In general, most cracks were discovered while loading was taking place as the crack would open and close as a result of the loading cycles and these changes made the cracks more apparent.

Destructive testing was used to find cracks that had initiated below the surface of the beam, or had not become large enough to be able to see either through general visual inspection or magnetic particle inspection. The section of the beam which was removed was then cut into small slices, typically about three quarters to one inch wide, using a band. These specimens were then bent manually. If there was a crack present, the bending of the piece would tend to open the crack, making it visible. An example of a crack discovered through destructive testing is shown in Figure 6.4.

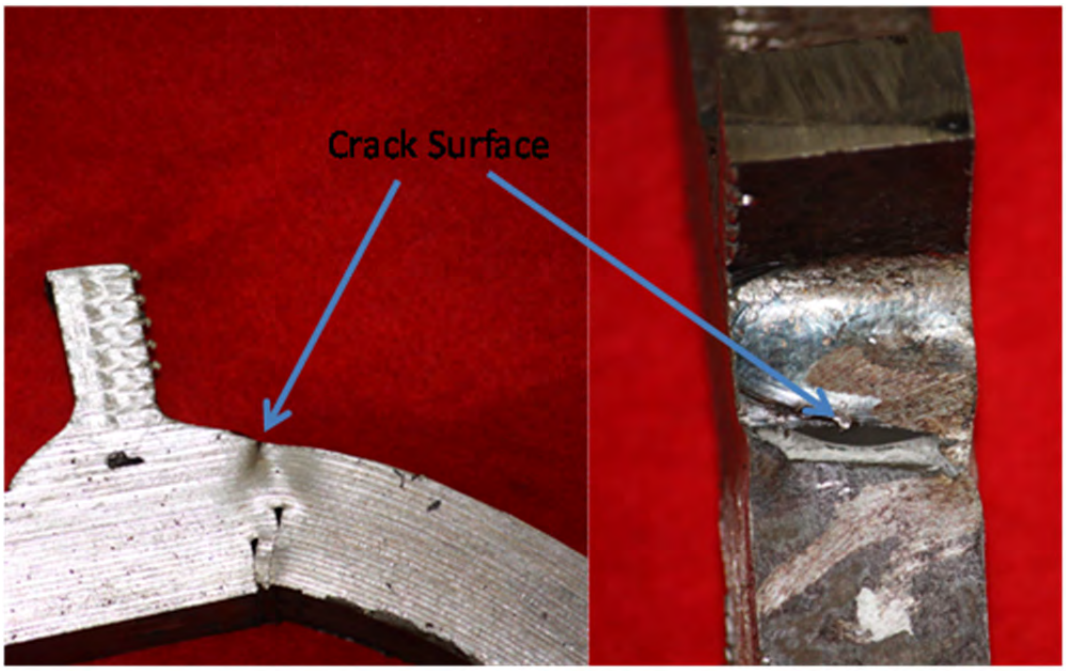

Figure 6.4: Destructive testing revealing a crack

6.5 Results of Laboratory Testing

Each beam tested represented six individual connections between stiffeners and the girder tension flange. These six connections included two perpendicular stiffeners, two skewed stiffeners which were placed at either a 30° or 60° angle, and two pipe stiffeners.

6.5.1 Skewed Plate Stiffeners

There were eight different plate stiffeners tested at an angle or skew, four at 30° and four at 60° (Table 6.1). Of those eight, three failed during testing. Because of the method employed to stop crack propagation: the addition of a plate over the crack, the equivalent skewed plate stiffener that was on the reverse side of the beam was not tested after the cracking of its partner and so can only be said to be better than the fatigue life achieved by the first one to fail.

Table 6.1: Performance of skewed stiffeners

Beam	***Stiffener on Specimen (deg)***	***Stress Range (ksi)***	***Total Cycles (cycles)***	***Failure / Run-Out***
30A	30	15.2	2,059,727	Failure
30B	30	15.4	3,250,000	Run-Out
60A	60	15.6	1,451,654	Failure
60B	60	21.7	501,593	Failure

Table 6.1 shows a summary of each of the skewed or angled stiffeners. In none of the four beams tested did the skewed stiffeners outperform either of the other two connection types (the pipe stiffener and perpendicular plate stiffener). Both failures of a 60° skewed plate stiffener occurred after they had passed the category C threshold but before they reached the B' category. The failure of the 30° skewed stiffener occurred past the B' category, and two 30° stiffeners (those on Beam 30B) ran-out past the B' category (but at a stress range that did not allow passing the B category line).

6.5.2 Perpendicular Plate Stiffeners

Every one of the four beams tested had two perpendicular stiffeners welded to them. Thus a total of eight perpendicular stiffeners were tested, out of which one failed due to fatigue cracking. Two of them, when taken apart following testing, showed evidence that fatigue cracks had developed, but had not been detectable before dissection. The remaining five did not crack and showed no incipient cracks upon dissection. Their performance is shown in Table 6.2.

Table 6.2: Performance of perpendicular stiffeners

Beam	***Stress Range (ksi)***	***Total Cycles (cycles)***	***Failure / Run-Out***
30A	15.2	2,870,288	Run-Out
30B	15.4	3,250,000	Run-Out
60A	15.6	3,017,629	Run-Out
60B	21.7	1,101,038	Failure

6.5.3 Split Pipe Stiffeners

There were two pipe stiffeners on each of the four beams tested, none of which failed or showed developing cracks after dissection. In every testing case some other method of failure forced termination of testing before any cracks could be detected at the pipe stiffeners. Each data point collected for the pipe stiffeners exceeded the AASHTO category B' limit, but did not reach category B. The pipe stiffener connections in this test can be said to be better than the category B' as specified in AASHTO.

6.5.4 Summary of Results

The primary purpose of the laboratory testing was to evaluate the pipe stiffener's fatigue performance in relationship to that of more conventional stiffeners. The tests were also intended to provide data for validation of finite element models that can be used for further in depth studies.

6.5.5 Evaluation of the Split Pipe

Table 6.3 shows the full results for each beam tested. The first three tests (30A, 60A, and 30B) all had a stress range of approximately 15 ksi, and reached about three million cycles. In none of these cases did anything but the skewed stiffener fail. The fourth beam was tested at a

stress range of approximately 22 ksi for about one million cycles. Here both the skewed stiffener and the perpendicular stiffener failed.

Table 6.3: Summary of results

Beam	***Angle of Skewed Stiffener (deg)***	***Stress Range (ksi)***	***Failure of Skewed Stiffener (cycles)***	***Second Failure (cycles)***	***Type of Failure***
30A	30	15.2	2,059,727	2,870,288	Flange Crack
60A	60	15.6	1,451,654	3,017,629	Friction Crack
30B	30	15.4	N/A	3,250,000	Run-Out
60B	60	21.7	501,593	1,101,038	Crack at Perpendicular Stiffener

Figure 6.5 shows the final results of the laboratory testing. Each of the 24 connections tested performed above the AASHTO category C line, and all but the 60° skewed stiffeners out-performed the category B' line. However, it should be noted that the reference AASHTO lines are drawn for design, and are two standard deviations below the mean. The testing concluded for this project had an insufficient number of data points to obtain a reliable standard deviation. However, passing the design C category line by such a small margin, it is unclear that the 60° stiffeners would actually achieve a C category rating after more exhaustive testing.

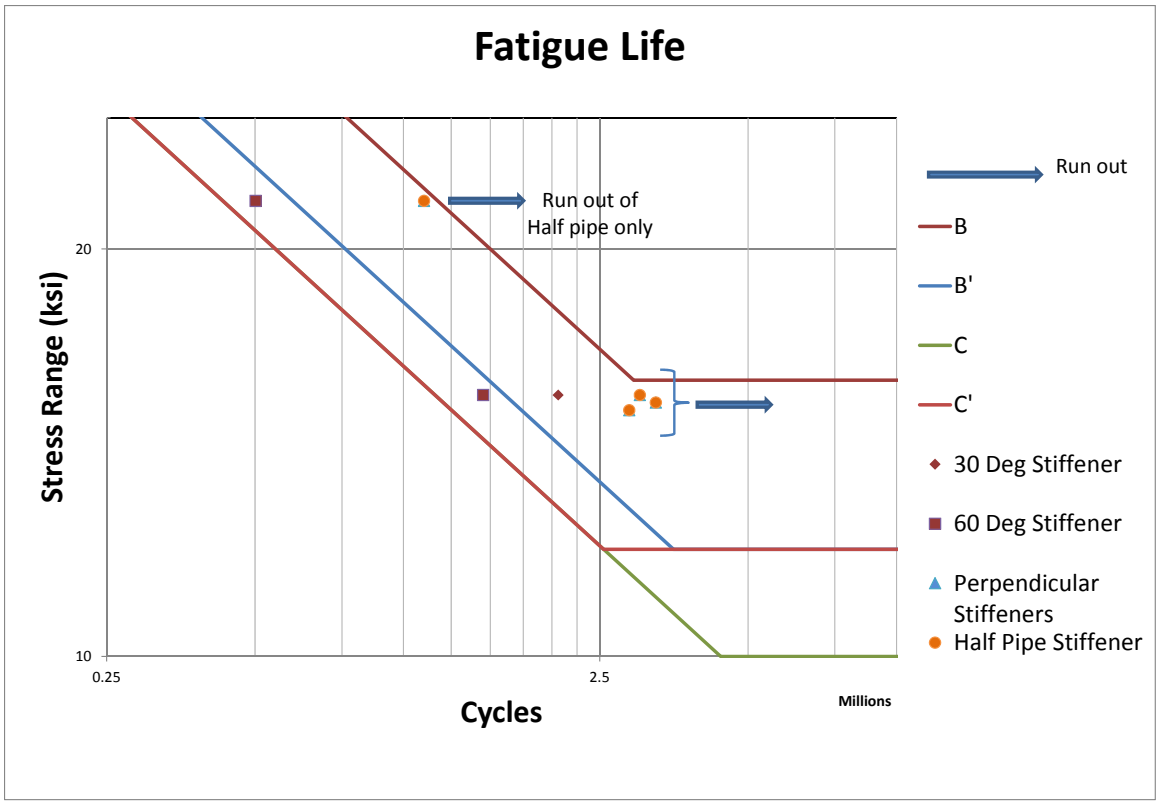

Figure 6.5: An S-N plot of each of the beams tested

6.6 Finite Element Model

After the laboratory testing was completed, a finite element model was generated to investigate different designs for the split pipe connection. The results would be used to ensure that the laboratory testing was applicable over a wide range of designs and not just the one connection detail tested. Both a plate stiffener model and a pipe stiffener model were created and tested so as to validate the results against the physical experimentation. The pipe stiffener model was used for a parametric study of multiple design details. An example of this model can be seen in Figure 6.6.

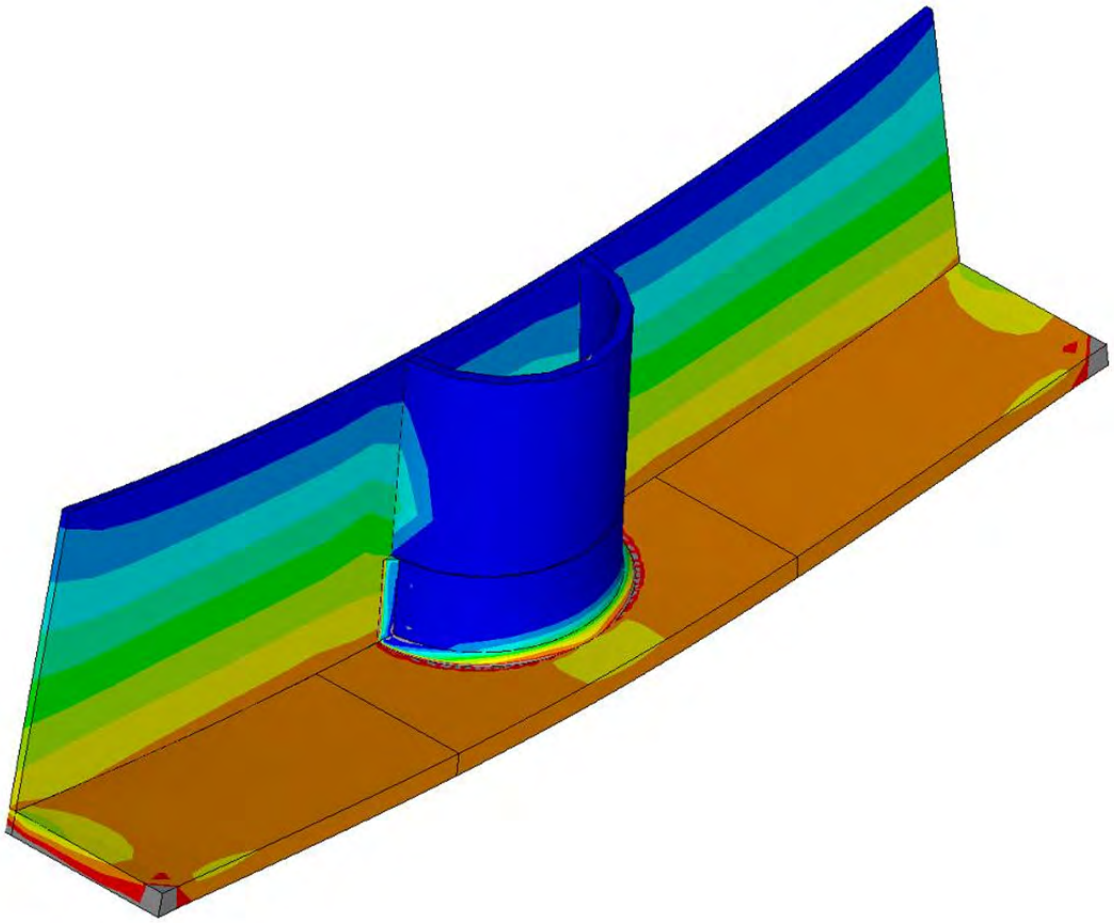

Figure 6.6: Model of split pipe

6.6.1 DNV Stress Factor

DNV, which stands for Det Norske Veritas, is a Norwegian organization that provides codes and guidelines for fatigue analysis and design. DNV has provided a method to consistently calculate the stress concentration factor in a finite element model. The DNV method was used to find all stress values through-out the computational experimentation (DNV 2010).

6.6.2 Critical Hot Spot

Three hot spots, or points of high stress concentration, were identified and examined for every split pipe modeled. These hot spots can be seen in Figure 6.7, with the hot spots located at the web, 45^{o} along the split pipe, and by the flange's edge. The paths shown there represent the location of the stresses measured as described by the DNV method (DNV 2010). After analysis of all completed testing, it was found that the greatest stress concentration occurred 45° along the weld of the pipe stiffener in every design tested. In no case did either of the other two hot spots produce stresses that exceeded the 45° spot for that model. All data presented, unless otherwise noted, will be for the stress concentration factor at the 45° hot spot.

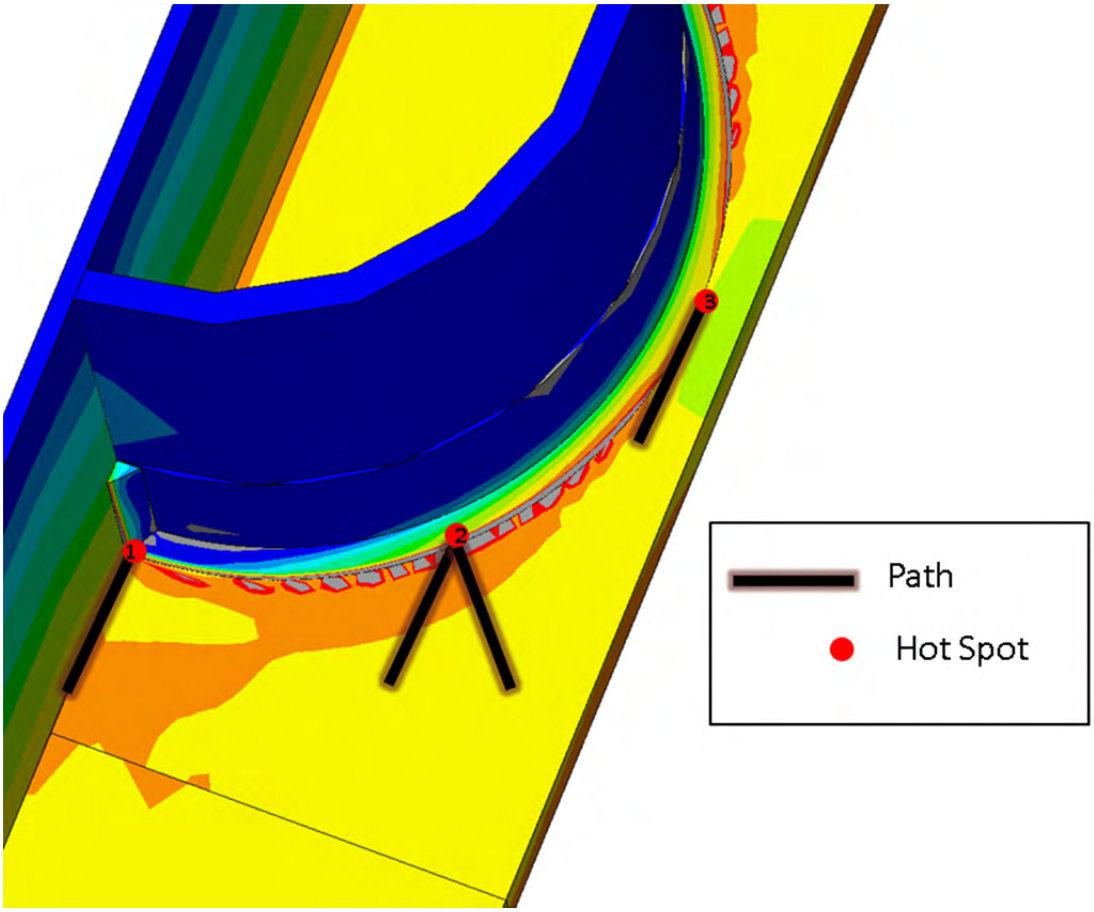

Figure 6.7: Location of hot spots

6.6.3 Parameters of Interest

Once the model was created, verified, and the method of data extraction determined, the next step was to determine which design parameters to investigate using the model. To do this, the important parameters that define the girder, the split pipe and the weld were altered both separately and together to determine their impact on the fatigue life of the connection. The first step of this process was to determine which of the parameters had an influence on the stress concentration factor, and which were not critical. The parameters that described the model are shown in Table 6.4.

Table 6.4: Parameters of interest

Parameter Symbols	*Descriptions*
d_G	Girder Depth: total depth including flanges thickness
t_F	Flange Thickness: constant through the model
t_W	Web Thickness: constant throughout the model
b_F	Flange Width
t_S	Split Pipe Wall Thickness
b_S	Split Pipe Outside Radius
a_W	Weld Size: length of the legs of weld

6.7 Analysis of Data

The first set of data collection involved altering only one parameter at a time. The main purpose of these experiments was to determine if the parameter in question had a significant impact on the results. This was accomplished purely through visual analysis by creating a graph of the results and looking for a pattern.

Once the critical parameters had been chosen and the testing completed several hundred data points had been generated. It became impractical to determine the relationship between the varying parameters and the stress concentration factor by simple, visual inspection. Some more complete method had to be developed so as to examine all possible factors and do so without requiring human judgment for every analysis as the time taken for such an approach would be prohibitive.

6.7.1 Goals of Analysis

The major goal of the computational analysis was to determine if the results of laboratory testing could be applied across a wide spectrum of designs. However, it was also hoped that the modeling would lead to a determination of what factors most influenced the fatigue life, how potential problems could be avoided, and as a guide to possible further research.

6.7.2 Plate Stiffener Results

The wide range of stress concentration factors found from this study showed a significant impact of the skew angle on the stress concentration for plate stiffeners. As the angle of the skew increased so did the stress concentration factor in a nearly linear relationship.

Figure 6.8 shows the results of the 36 different models tested. The clear, linear relationship can be seen as the stress concentration factors increases up to a value of approximately 1.35 at a skew of 70^o. These values clearly show the increase of the stress concentration factor with the skew angle.

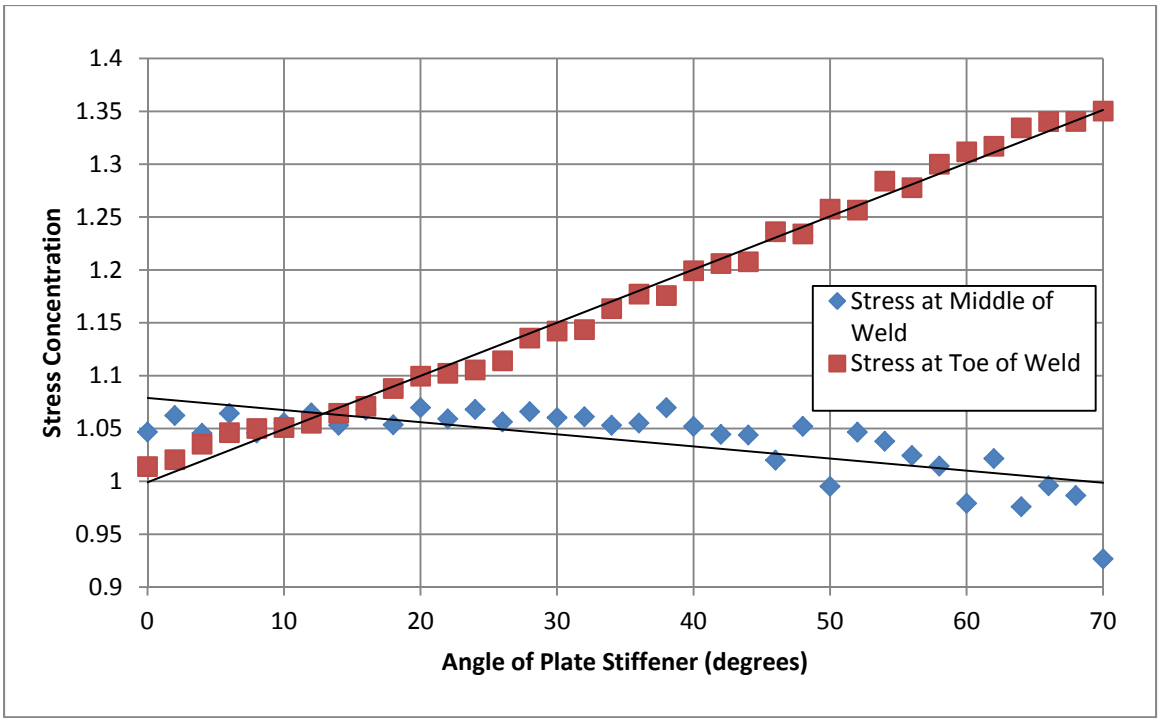

Figure 6.8: Stress concentration factor for plate stiffeners at varying skew angles

6.7.3 Split Pipe Stiffener Results

Approximately 450 different finite element models were analyzed for this pipe stiffener. In order to determine the relationship between the parameters that defined the model and the stress concentration factor an equation was generated that conformed to Equation 6.1.

$$f(d_G, t_F, b_F, t_S, b_S, a_W) = SCF \tag{6.1}$$

A complex, genetic algorithm was created that searched through a large number of variations of possible functions in order to determine the one that best fit the data produced by the finite element models. This equation revealed the relationship between the parametric input and the stress concentration factor and was able to predict what the stress concentration factor would be for untested combinations of parametric inputs. The final solution is Equation 6.2, which had a correlation coefficient of 0.93.

$$SCF = \frac{t_S}{t_F}\sqrt{\frac{2 \times a_W}{5 \times b_S}} + 1.0 \tag{6.2}$$

The most important factor shown in Equation 6.2 is the ratio of the pipe stiffener's thickness to the flange thickness. However, the ration of the weld size to the pipe radius also

plays a role in determining the stress concentration factor. The smaller both of these ratios are, the smaller the stress concentration factor is.

Figure 6.9 shows the stress concentration factors generated from all 405 models run. The histogram demonstrates an average stress concentration factor of 1.07 with which was also the median value. If the stress concentration can be considered normally distributed, then the standard deviation of the results is 0.023. This gives a range of 1.02 to 1.12 for two standard deviations from the mean (representing a 95% confidence interval for normally distributed data).

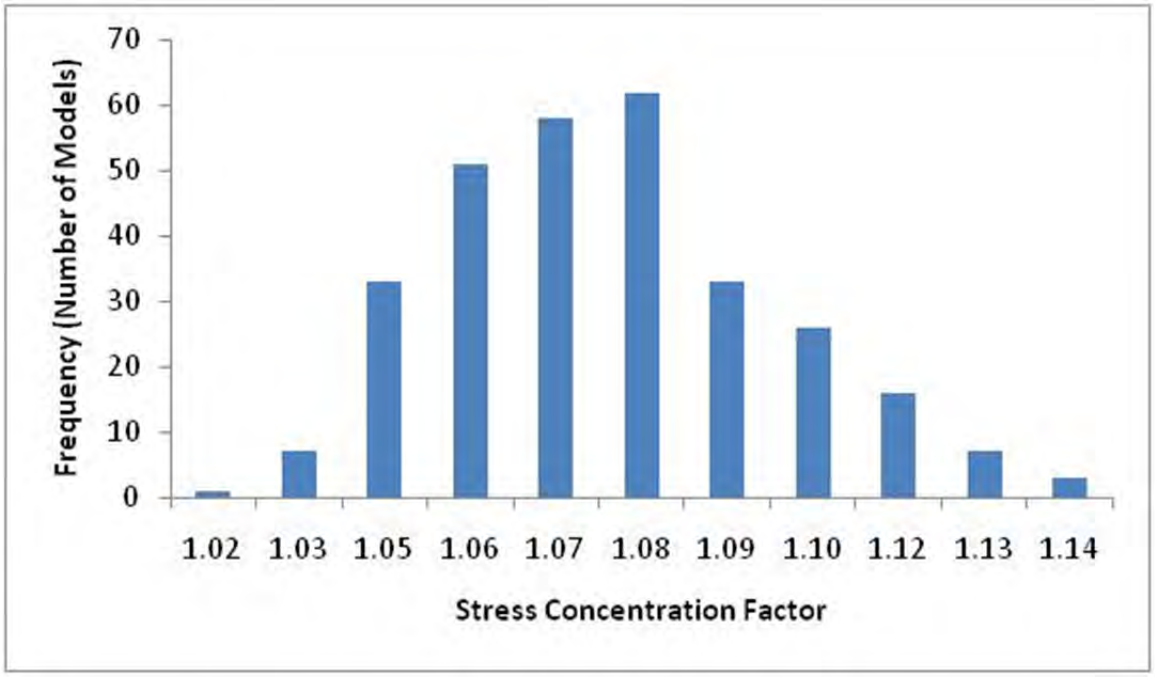

Figure 6.9: Summary of Results from Initial Parametric Testing

6.7.4 Comparison of Split Pipe Stiffener with Plate Stiffener

When comparing the two specimens tested in the laboratory, the computational model showed a stress concentration factor of 1.08 for both the pipe stiffener and the perpendicular plate stiffener based on a line of best fit from the data. As the skew angle increased the plate stiffener's stress concentration factor increased with it up to a value of 1.35 for a 70^{o} skew.

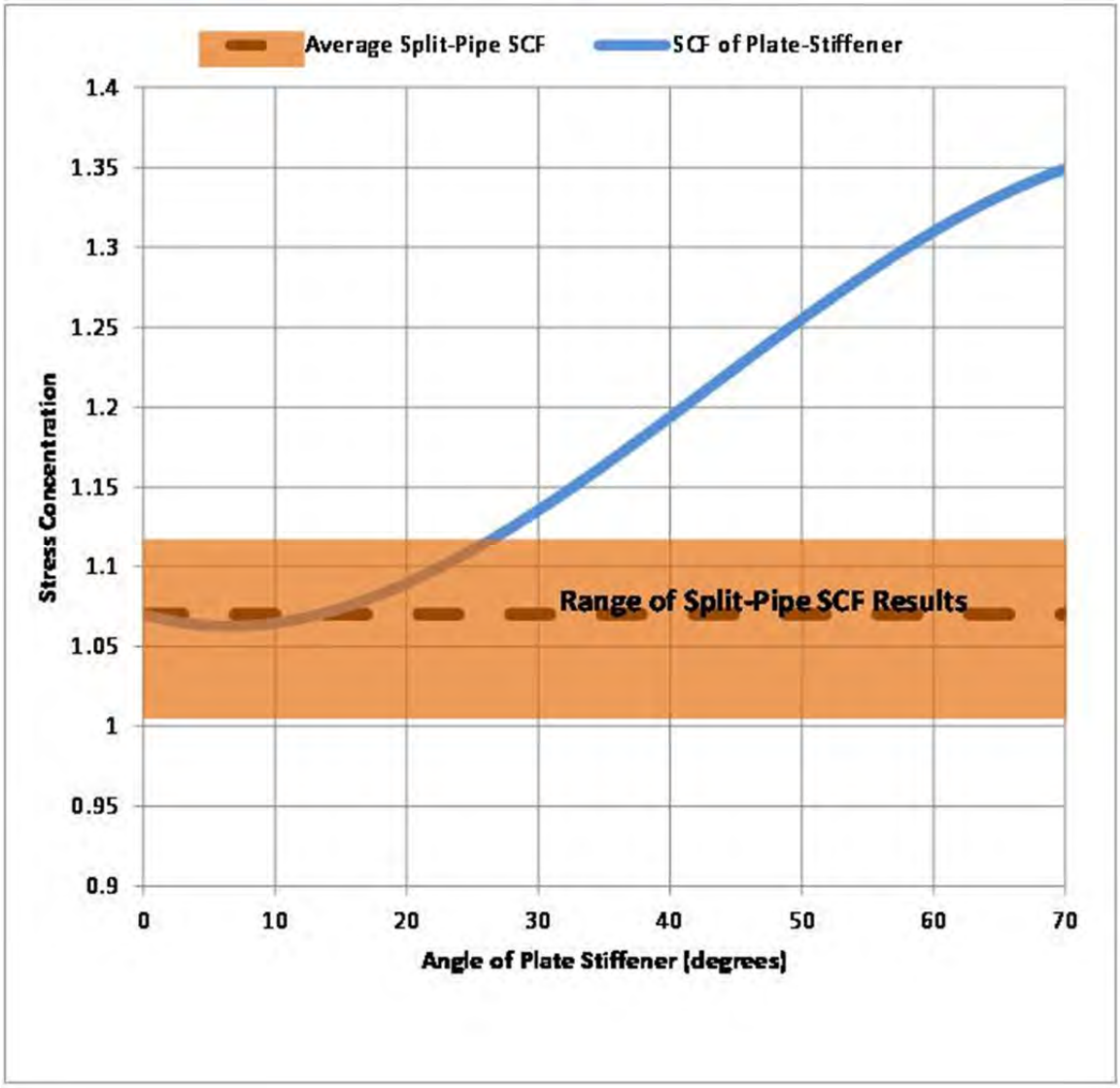

Figure 6.10: Stress concentration factor comparison between plate stiffeners and pipe stiffeners

A direct comparison of the plate stiffener to the pipe stiffener is provided in Figure 6.10. This figure shows the results for the plate stiffeners at various skew angles (with the same geometry as the specimen tested in the laboratory) as compared to the general results from the pipe stiffener. The shaded box represents the range of SCFs that were found for the pipe stiffener, and the dashed line is the average value.

These results are more telling for the plate stiffener than the pipe stiffener. The plate stiffener at low skew angles appears to perform at about the same level as the split pipe. At 30^{o} skews and less it is within two standard deviations of the split pipe's average stress concentration factor level. As the skew angle increases, the SCF quickly jumps out of range of the pipe stiffener.

6.8 Distortional Fatigue Concerns for Split Pipe Stiffener

The issue of distortional fatigue in the pipe stiffener was not studied in the laboratory, but an initial investigation was performed through finite element analysis. Distortional fatigue in the pipe stiffener would result when the cross-frame, connected to the pipe stiffener, forced the stiffener to distort between the cross-frame connection and the girder's flange. Because the pipe stiffener is only expected to be used at support locations, distortional effects that would result from relative rotation or displacement between the girders should be minimal.

6.8.1 Basic Models

There were two main model types created: a plate stiffener connection and a split pipe connection. Though the plate stiffener is not subject to distortional fatigue effects it represents a cross-frame connection which has no known fatigue issues. Thus if the pipe stiffener can be shown to have similar or decreases stresses as a result of cross-frame forces it would suggest that the connection is a safe one for fatigue. An identical loading of 10 kips was applied to each model and the maximum stress was found using the DNV method.

6.8.2 Plate Stiffener Model

The plate stiffener had a connection-plate connected to it that was bent at a given angle of skew. The plate stiffener itself remained perpendicular to the web through all the tests, only the bend of the connection plate changed, based on the skew. This bent plate was then connected to the cross-frame itself which was represented by a given, axial loading. An example can be seen in Figure 6.11.

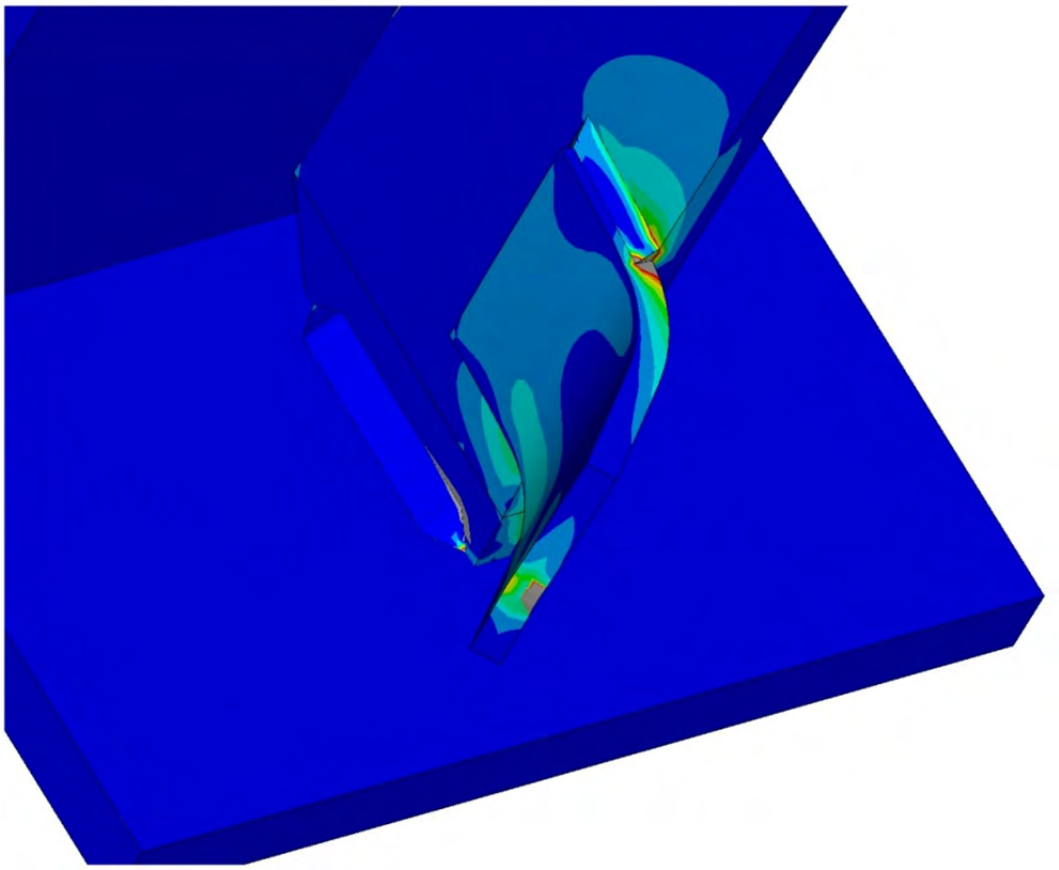

Figure 6.11: Plate stiffener model (principle stresses shown)

6.8.3 Split Pipe Stiffener Model

The split pipe model was created using the same code that was used for the flexural fatigue investigation. A connection to the cross-frame was also added to the original model and a load applied in the same manner as was done for the plate stiffener's distortional fatigue model. Two models were examined, one with an intermediate connection plate (Figure 6.12) and one without (Figure 6.13).

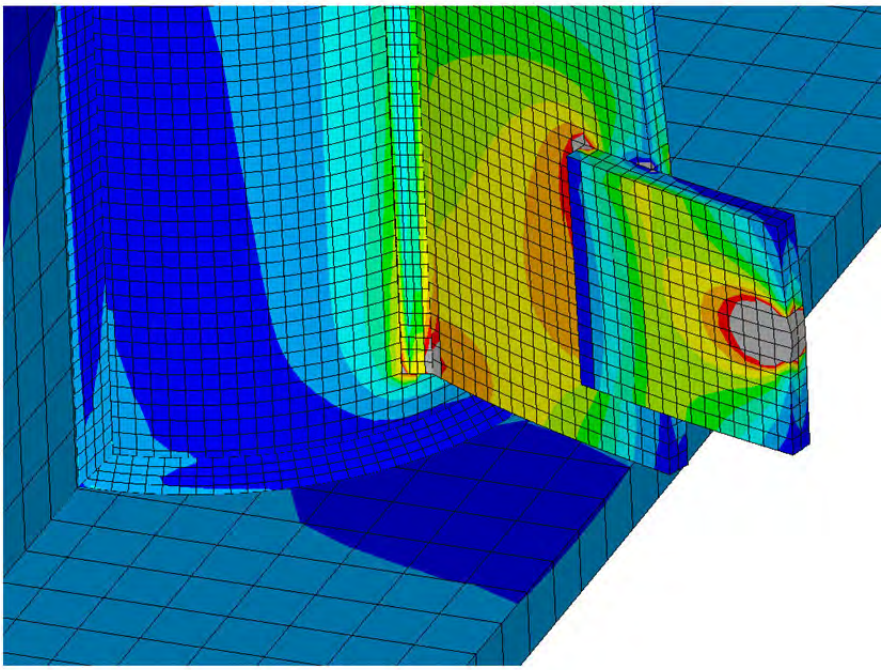

Figure 6.12: Pipe stiffener with intermediate connection plate

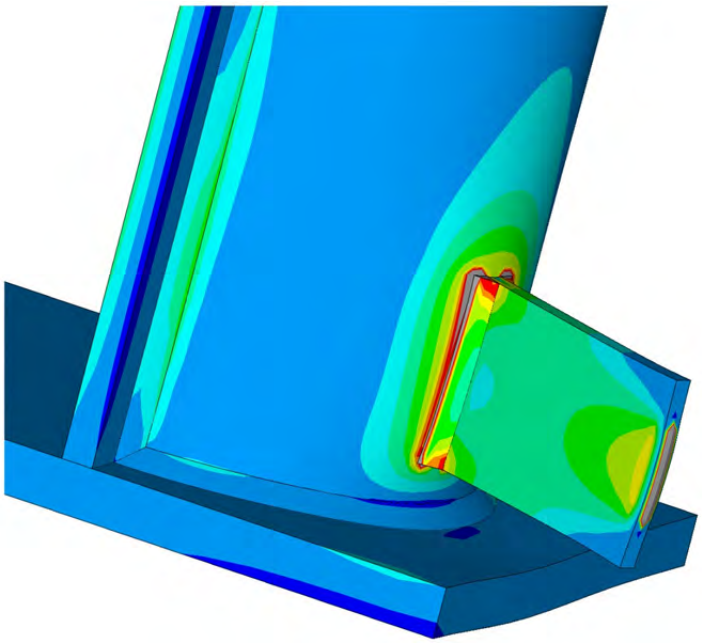

Figure 6.13: Pipe stiffener with direct connection

6.8.4 Finite Element Results

Approximately 1,750 models were generated, completing a parametric analysis of both the plate stiffener and the pipe stiffener. Both connection types appeared to have predictable (non-random) results, with the plate stiffener stresses controlled by the thickness of the plate and

the angle of skew. The results clearly showed that the larger the skew the larger the stress. The pipe stiffener showed a smaller variation in stresses, and a lower average and median stress.

The stresses from this study did not display a Gaussian distribution, as can be seen from the two histograms representing the variation of stresses in the plate stiffener and pipe stiffener (Figure 6.14 and Figure 6.15 respectively). The horizontal scale for the pipe stiffener results is one fifth the plate stiffener scale in response to the lower value of the stresses found in the pipe stiffener.

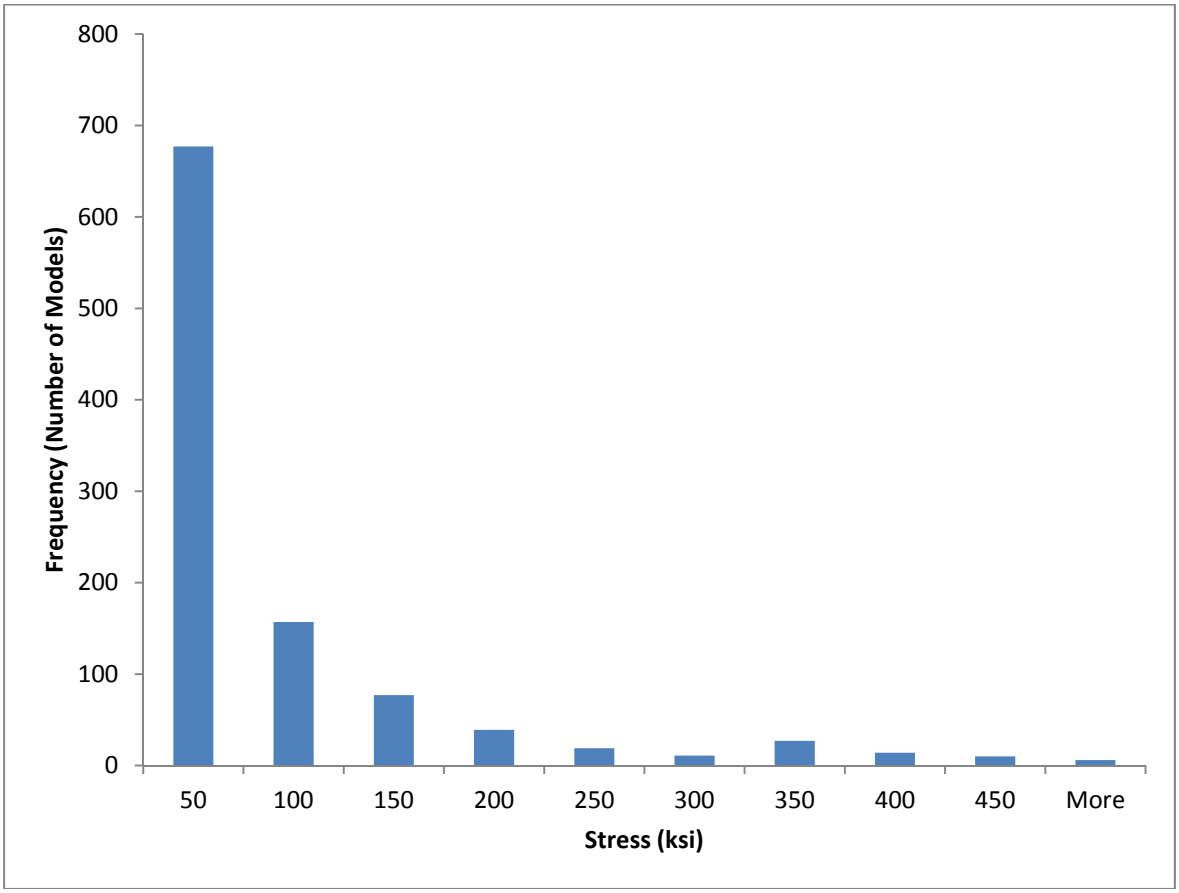

Figure 6.14: Histogram of plate stiffener stresses

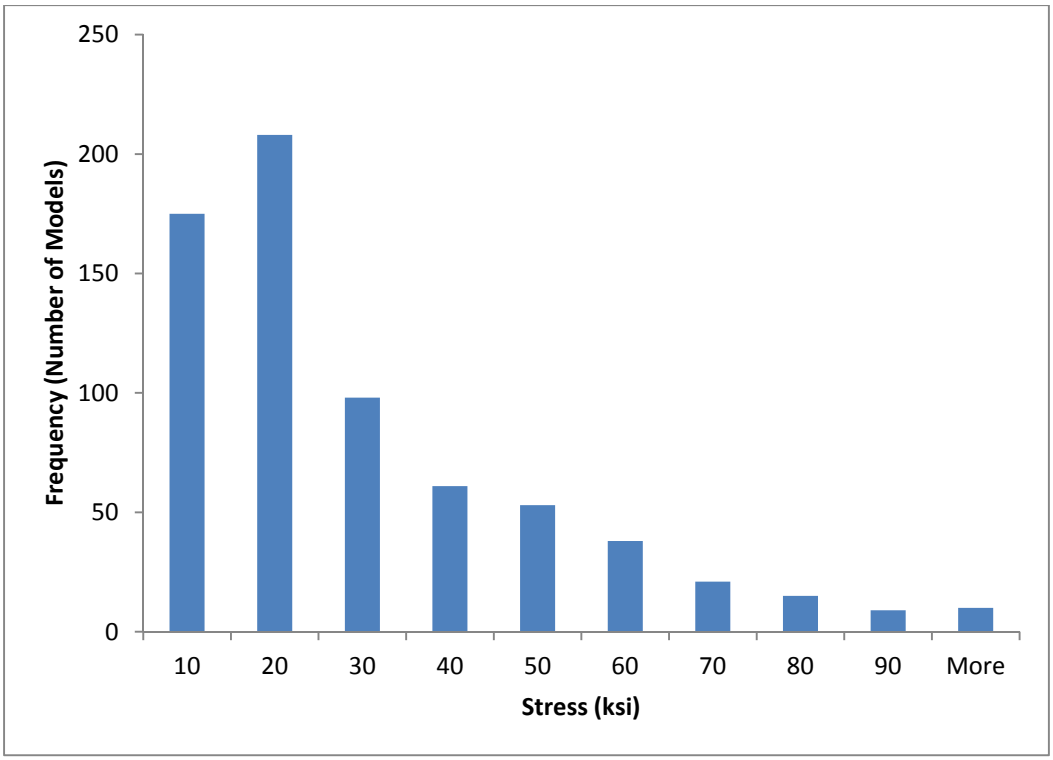

Figure 6.15: Histogram of pipe stiffener stresses

The average stress value found for the plate stiffener was 67 ksi and the average for the pipe stiffener was 25 ksi, 40% less than for the plate stiffener. The median values followed that same pattern, being 25 ksi and 17 ksi respectively. The range of results also favored the pipe stiffener. The plate stiffener produced stresses of which more than 25% exceeded 100 ksi. The pipe stiffener had only one result that exceeded 100 ksi. The wide variability demonstrated by the plate stiffener indicated that designs within the scope of typical detailing could result in large stress concentrations.

Because there is no history of fatigue problems with the bent plate connection, this result suggests that cross-frame connections to the split pipe are not expected to cause distortion-induced fatigue problems. However, it should be recalled that this study was largely qualitative in nature, and there was no laboratory test data available to validate the model. Laboratory testing of the cross-frame to split pipe connection would be desirable in the future to provide additional insights into the potential for distortional fatigue problems in the pipe stiffener and to provide data for validation of computational models.

6.9 Conclusions of Fatigue Investigation

Based on the physical and computational results, it is recommended that the split pipe be given a category C rating and be used in place of the plate stiffener where applicable. There was no indication by any of the results found here that the pipe stiffener would perform worse than the plate stiffener, and thus no reason to give it a worse rating. Though there was some justification found for improving the rating, it was not sufficient so as to recommend a higher AASHTO fatigue category rating.

Chapter 7. Conclusions and Design Recommendations

7.1 General Conclusions

The results of this research demonstrated that the split pipe stiffener cross-frame connection is much stiffer than the bent plate connection detail. In general, using the stiffer split pipe connection will help limit girder end twists compared to the traditional bent plate connection detail. In addition to a stiffer connection, the split pipe stiffener offers warping restraint to the end of the girder which significantly increases the girder torsional stiffness and therefore significantly increases the girder elastic buckling strength. This increased buckling strength permits the safe use of larger unbraced lengths. Therefore, using the split pipe stiffener to increase the girder buckling capacity near the supports will likely allow the nearest row of intermediate cross-frames to be moved farther away from the supports. Doing so will move the intermediate cross-frames into a region of smaller differential girder deflections and therefore reduce the live load forces induced in the cross-frames and mitigate the potential for associated fatigue cracking. The higher buckling strength of girders with split pipe stiffeners may also allow a reduction in the total number of cross-frames needed in a bridge. Overall, the increase in girder torsional stiffness and buckling capacity that results from the use of the split pipe stiffener will enhance the safety of the girder at all stages of construction: during transportation, lifting, erection, and placement of the concrete deck.

This research also found out that cross-frame layout has a large impact on live load induced forces in the cross-frame members. The staggered layout results in significantly lower force levels in cross-frame members, compared to the more conventional continuous layouts. Therefore, the staggered layout is generally recommended in skewed bridge when the fabrication and installation costs are justified.

In arriving at the above conclusion, many lessons were learned and several recommendations can be made. These lessons and recommendations are divided among the finite element modeling and design of the bent plate and split pipe stiffener connections and summarized below.

7.2 Computational Modeling Lessons and Recommendations

Several lessons were learned while modeling the girders and cross-frames for this research. First, the ANSYS SHELL93 element proved to be a computationally efficient way to model I-shaped girder buckling. In addition to modeling the flat plates that make up the cross section, the shell element was very accurate in modeling the curved surfaces of the bent plate and split pipe stiffener as long as the bend radius to element thickness ratio was three or greater.

However, using shell elements presents a challenge in appropriately modeling the interface between the elements when the structural components do not intersect at their midsections or have differing mesh densities. It is recommended that if shell elements intersect at their mid-thicknesses with differing mesh densities and little deformation is expected between the elements, constraint equations be used to connect the elements. If the elements do not intersect at their mid-thicknesses or large deformations are expected, then rigid beam elements (ANSYS MPC 184) should be used to make the connection.

Another lesson learned in modeling the connections was the importance of considering the effect of weld geometry on the plate connection stiffness. Two examples where the weld

geometry was important in this research were at the bend in the bent plate to connection plate overlap and the plate stiffener to girder welds. It is recommended that weld models using rigid beam elements should be used if there is the possibility that a weld will significantly stiffen a connection. Additionally, when modeling a laboratory specimen with plate stiffeners, the welds should be modeled. In this research, the stiffener to flange welds were found to more accurately engage the warping restraint provided by the stiffeners if the actual weld geometry was included in the model. And finally, if trying to match an analytic solution with a finite element model containing web stiffeners, then constraint equations should be used at the girder to stiffener interface so the finite element model does not contain warping restraint not predicted by the analytic solution.

Modeling the end cross-frames with a very detailed shell element model was required in this study to accurately capture the connection stiffness of the skewed cross-frames. However, simply modeling the non-skewed intermediate cross-frames with truss elements connected at the girder web to flange interface were sufficiently accurate for predicting the laboratory specimen brace forces and girder rotations. Therefore it is recommended that truss elements be used for unskewed cross-frame members rather than shell elements as the truss members provide an accurate and computationally efficient solution.

Finally, the modeling of bearing pads can have significant impact on the accuracy of results of end twists of girders. Most bridge design programs usually assume a pin at the girder support. However, if the girder tipping restraint provided by bearing pads is considered, the real end twists of girders could be smaller than what would otherwise be calculated. Therefore, if a more accurate end twist of girder is expected, a more accurate bearing model is needed. The laboratory and FEA results demonstrate that the bearing pads model with linear springs can give reasonably results to the tilt effect.

7.3 Design Recommendations for the Bent Plate Connection

The results of this research demonstrated that the connection stiffness has a significant impact on the end cross-frame stiffness and can be the limiting component stiffness at skew angles of 20° or greater. Therefore it is recommended that the connection stiffness be considered in calculating the stiffness of the skewed cross-frames for skew angles of 20° or larger using Equation (5.1) below.

$$\frac{1}{\beta_T} = \frac{1}{\beta_{brskew}} + \frac{1}{\beta_{sec}} + \frac{1}{\beta_g} + \frac{1}{\beta_{conn-tors}} \qquad (5.1)$$
(from Chapter 5)

The torsional stiffness of the bent plates is given in Equation (2.49) and (5.4). All other variables remain as defined in Chapters 2 and 5.

$$\beta_{conn-tors} = \frac{\beta_{conn}\, h_b^2}{\frac{2L_c^2}{S^2} + 1} \qquad (2.49)$$
(from Chapter 2)

$$\beta_{conn} = \frac{8}{S}(70\alpha + 5000)e^{-q\alpha} \quad (5.4)$$
(from Chapter 5)

If it is found that the stiffness of the bent plate connection needs to be increased to satisfy the stiffness requirement of braces, it is recommended that the thickness of both the connection plate and bent plate be increased from the standard 1/2" thickness to 3/4" thickness, or that a split pipe stiffener connection be considered as an alternative.

Results of this research showed that the flexibility of the bent plate connection in end cross-frames will not, in general, significantly reduce the girder lateral buckling capacity. Further, girder tipping restraint provided by the bearings enhances girder stability and helps offset the impact of the bent plate connection flexibility in end cross-frames. Consequently, the current design practice of using the bent plate connection in end cross-frames in skewed bridges is still acceptable. However, because the split pipe stiffener offers several advantages over the bent plate stiffener, it makes a better option in skewed cross-frame connections. Note also that although the bent plate connection is acceptable in skewed end cross-frames, the bent plate connection should not be used with skewed intermediate cross-frames for skew angles greater than 20°.

7.4 Split Pipe Stiffener Design Recommendations

7.4.1 Advantages of Using Split Pipe Stiffener

The use of the split pipe stiffener for connecting skewed cross-frames to girders offers several advantages First of all, the split pipe stiffener offer advantages in fabrication and construction. The split pipe stiffener allows a perpendicular connection between the split pipe and the cross-frame connection tab for any skew angle. The detail has the potential to standardize the cross-frame connection across a wide variety of bridge applications. Such standardization removes the bent plate variables such as bend radius and plate size that were shown to affect connection stiffness. The split pipe stiffener can also serve as a bearing stiffener, and essentially requires a similar total length of welding compared to the current connection details employed in Texas that consist of two bearing plate stiffeners and two cross-frame connection plates.

From a structural performance point of view, the most important advantage of the split pipe stiffener is the increased torsional warping restraint that the stiffener provides for the girder. As a result, girders with split pipe stiffeners have significantly higher buckling capacities than girders with conventional plate stiffeners. This increased buckling capacity permits larger unbraced lengths for the girder, which allows the first line of intermediate cross-frames to be moved farther from the skewed end frames. This can alleviate congestion of cross-frames near the ends of skewed bridges and also alleviates the large live load induced forces that can occur in intermediate cross-frames that are placed close to the skewed end of a bridge. The increased buckling capacity of girders with split pipe stiffeners may also allow a reduction in the total number of cross-frames needed in a bridge. In addition, the increased buckling capacity provided by the split pipe will enhance girder safety during transportation and lifting. Finally, the split pipe stiffener provides a much stiffer connection between the cross-frame and the girder as compared to the conventional bent plate connection. This increased connection stiffness makes the end cross-frames more effective in controlling girder end twist and therefore helps maintain girders in a plumb condition.

The fatigue performance of the split pipe stiffener was found to be at least as good as the current plate stiffener detail. Consequently, use of the split pipe stiffener is not expected to introduce fatigue problems. The fatigue testing showed that conventional plate stiffeners welded to a girder at a skew angle resulted in earlier fatigue failure of the girder than a plate stiffener welded perpendicular. Based on these results, when using a split pipe stiffener, it is recommended that the cross-frame connection plate be welded to the pipe only and not the girder flanges. This will avoid a skewed weld to the tension flange. This is particularly important at interior supports for continuous girders where high stress levels are expected in the girder flanges.

7.4.2 Recommended Split Pipe Sizes

Based on a survey on typical steel bridges constructed in Texas, flanges of girders are usually in the range of 12″ to 24″ wide. Therefore, the two recommended pipe sizes, as listed in Table 7.1, can be used for the majority of steel bridge construction in Texas. These sizes should be considered as a starting point in designing the split pipe stiffener. The final size of the pipe should be selected to provide the required warping restraint for the girder based on the required buckling strength of the girder, as discussed below. Because the split pipe will also normally serve as a bearing stiffener, the pipe size should also be checked for adequacy as a bearing stiffener.

Table 7.1: Recommended pipe sizes

Type	***Size of pipe***
Pipe1	10″× 1/2″
Pipe2	18″× 3/4″

7.4.3 Girder Flexural Design with Split Pipe Stiffeners

When warping restraint is to be considered in the calculation of the lateral torsional buckling strength of a girder, Equation (2.55) can be used. This is the regular lateral torsional buckling strength equation modified by torsional effective length factor K_z.

$$M_{cr} = C_b \pi / L_b \sqrt{EI_y GJ + \pi^2 E^2 C_w I_y / (K_z L_b)^2} \qquad (2.55)$$
(from Chapter 2)

A normalized method was designed to simply use of the AISC non-sway alignment chart to determine K_z. In using the alignment chart, G-values at the ends of the beam are defined by Equation (2.56) and the m-values are listed in Table 5.1 of this report.

$$G_z = \left(\frac{EI}{L_b}\right)_{flange} \Big/ m\left(\frac{GJ}{L}\right)_{pipe} \qquad (2.56)$$
(from Chapter 2)

Being able to evaluate warping restraint makes it possible to calculate the required L_b when the split pipe stiffeners are used at the end of a girder. A design example is provided in

Appendix D to illustrate this method. In this example, a bracing system for a skewed bridge is laid out to stabilize girders during the deck cast for both the plate-stiffened girders and the split pipe stiffened girders. Comparison of the results also shows the advantages of using the split pipe stiffener.

7.4.4 UT Bridge

Alternatively, UT Bridge, a PC-based user-friendly 3-D finite element analysis program, can be used to analyze the bracing system when the split pipe stiffener is used. The program is designed to analyze straight or curved I-girder bridges during girder erection and concrete deck placement. The program provides built-in options for modeling both regular plate-stiffener and the split pipe-stiffener for the bridge. Eigenvalues of the model can be calculated for the input model under specified construction steps and conditions. For more information about the program, go to Ferguson Structural Engineering Laboratory website and the link of the program is at http://fsel.engr.utexas.edu/software/index.cfm.

References

AASHTO/NSBA Steel Bridge Collaboration. *Guidelines for Design for Constructibility.* AASHTO, 2003.

American Association of State Highway and Transportation Officials. *AASHTO LRFD Bridge Construction Specifications.* Washington, DC: AASHTO, 2010.

American Association of State Highway and Transportation Officials. *AASHTO LRFD Bridge Design Specifications.* Washington, DC: AASHTO, 2010.

American Institute of Steel Construction. *Manual of Steel Construction.* Chicago: American Institute of Steel Constrution, 2005.

Anamia, K., Sauseb R., and Abbas, H. H. "Fatigue of web-flange weld of corrugated web girders: 1. Influence of web corrugation geometry and flange geometry on web-flange weld toe stresses." *International Journal of Fatigue*, Elsevier Ltd., 27(4), 373-381, 2005.

Anamia, K., and Sauseb, R. "Fatigue of web-flange weld of corrugated web girders: 2. Analytical evaluation of fatigue strength of corrugated web-flange weld." *International Journal of Fatigue*, Elsevier Ltd., 27(4), 383-393, 2005.

ANSYS Inc. "Elements Reference." *Release 11.0 Documentation for ANSYS.* 2010.

Battistini, Anthony. "Skewed Cross-frame Connection Stiffness." *Dissertation presented to The University of Texas.* Austin, TX, December 2009.

Bose, B. "The Influence of Torsional Restraint Stiffness at Supports on the Buckling Strength of Beams." *The Structural Engineer*, December 1982: 69-75.

DNV "Fatigue Design of Offshore Structures," Det Norske Veritas, Høvik, Norway, 2010.

Fischer, M. "Das Stabilitätsproblem des in Höhe des oberen Flansches wirklichkeitsnah belasteten I-Trägers". Der Stahlbau, 1970, 39, H.9, S. 267-275 und 42, H.5, S. 129-138

Flint, A.R. "The Influence of Restraints on the Stability of Beams." *The Structural Engineer*, 1951: 235-246.

Heins, Conrad P., and Robert A. Potocko. "Torsional Stiffeneing of I-Girder Webs." *ASCE Journal of the Structural Division* (ASCE), August 1979: 1689-1698.

Helwig, Todd A. "Lateral Bracing of Bridge Girders by Metal Deck Forms." *PhD. Dissertation Submitted to University of Texas.* Austin, TX, August 1994.

Helwig, Todd A, Joseph A Yura, and Karl H. Frank. "Bracing Forces in Daphragms and Cross-frames." *Proceedings Structural Stalbility Research Council Conference.* Milwaukee: Structural Steel Sability Research Council, 1993. 129-140.

Herman, Reagan S, Todd A Helwig, and Zhou Chong. "Use of Lean-On Cross-Frame Bracing in Steel Girder Bridges." *Structures Congress: New Horizons and Better Practices.* Long Beach: ASCE, 2007. 79.

Hunt, Fred A. "The Suppression of Warping in Thin-Walled Beams." *M.S. Thesis Submitted to The Ohio State University.* 1973.

Linder, J., Schmidt, J.S. "Biegedrillknicken von I-Trägem unter Berücksichtigung wirklichkeitsnaher Lasteinleitung," *Der Stahlbau*, 1982, 51, H.9, S. 257-263.

Meck, Harold R. "Experimental Evaluation of Lateral Buckling Loads." *Journal of The Engineering Mechanics Division*, April 1977: 331-337.

Ojalvo, M., and R.S. Chambers. "Effects of Warping Restraints on I-Beam Buckling." *ASCE Journal of the Structural Division* 103, no. ST12 (1977): 2351-2360.

Roy, S., Fisher, J. W., and Yen, B. T. "Fatigue resistance of welded details enhanced by ultrasonic impact treatment (UIT)." *International Journal of Fatigue*, Elsevier Ltd., 25(9-11), 1239-1247, 2003.

Sause, R., Abbas, H. H., Driver, R. G., Anami, K., and Fisher, J. W. (2003). "Fatigue Resistance of Corrugated Web Girders." *ATLSS Report No. 03-20*, PennDOT, Bethlehem, PA, 2003.

Schmidt, Lewis C. "Restraints Against Elastic Lateral Buckling." *Journal of the Engineering Mechanics Diviaion*, December 1965: 1-10.

Southwell, R.V. "On the Analysis of Experimental Observations in Problems of Elastic Stability." *Proceedings of the Royal Society of London.* (The Royal Society) 135, no. 828 (April 1932): 601-616.

Structural Stability Research Council. *Guide to Stability Design Criteria for Metal Structrues.* Edited by T.V. Galambos. New York: John Wiley & Sons, 1988.

Texas Department of Transportation. "LRFD Design Manual." *Texas Departmant of Transportation.* April 2007. http://onlinemanuals.txdot.gov/txdotmanuals/lrf/lrf.pdf (accessed May 9, 2008).

Texas Department of Transportation "Miscellaneous Details Steel Girders and Beams." *Texas Department of Transportation.* April 2006. ftp://ftp.dot.state.tx.us/pub/txdot-info/cmd/cserve/standard/bridge/spgdste1.pdf (accessed February 2, 2008).

Texas Steel Quality Council. "Preferred Practices for Steel Bridge Design, Fabrication, and Erections." *Texas Depratment of Transportation.* April 1, 2007. http://www.dot.state.tx.us/publications/bridge/steel_bridge.pdf (accessed May 9, 2008).

Timoshenko, Stephen P., and James M. Gere. *Theory of Elastic Stability.* New York: McGraw-Hill, 1961.

Ude, Todd. "Field Study of Skewed I-Girders During Construction." *Proceedings of the World Steel Bridge Symposium.* San Antonio: National Steel Bridge Alliance, 2009.

Unsworth, J. F. "Heavy Axle Load Effects on Fatigue Life of Steel Bridges." *Transportation Research Record*, National Research Council, (1825), 38-47, 2003

Wahr, Andrew. "The Fatigue Performance of Cross-frame Connections." *Master's Thesis To Be Submitted to The University of Texas.* Austin, TX, 2010.

Wang, Liqun. "Cross-Frame and Diaphragm Behaviour for Steel Bridges with Skewed Supports." *Ph.D. Dissertation Submitted to the University of Houston.* Houston, TX, August 2002.

Wang, Liqun, and Todd A. Helwig. "Stability Bracing Requirements for Steel Bridge Girders with Skewed Supports." *Journal of Bridge Engineering* 13, no. 2 (March/April 2008): 149-157.

Whisenhunt, Todd Walter. "Measurement and Finite Element Modeling of the Non-Composite Deflections of Steel Plate Girder Bridges." *M.S. Thesis Submitted to North Carolina State University.* Raleigh, NC, 2004.

Winterling, Jason. "Monitoring Dead Load and Construction Stresses of a Heavily Skewed HPS Bridge." *M.S. Thesis Submitted to the University of Delaware.* Newark, DE, 2007.

Yarimici, Erol, Joseph A Yura, and Le-Wu Lu. *Techniques for Testing Structures Permitted to Sway.* Bethlehem: Lehigh University, 1966.

Yura, Joseph, Brett Phillips, Swarna Raju, and Stuart Webb. *Bracing of Steel Beams in Bridges.* Austin: Center for Transportation Research, 1992.

Yura, Joseph, Todd Helwig, Herman Reagan, and Chong Zhou. "Global Lateral Buckling of I-Shaped Girder Systems." *Journal of Structural Engineering* 134, no. 9 (2008): 1-8.

Zhou, Chong. "Utilizing Lean-On Cross-Frame Bracing for Steel Bridges." *Ph.D. Dissertation Submitted to the University of Houston.* Houston, TX, December 2006.

APPENDIX A: Large Scale Experimental Results

A.1 GIRDER INITIAL IMPERFECTIONS

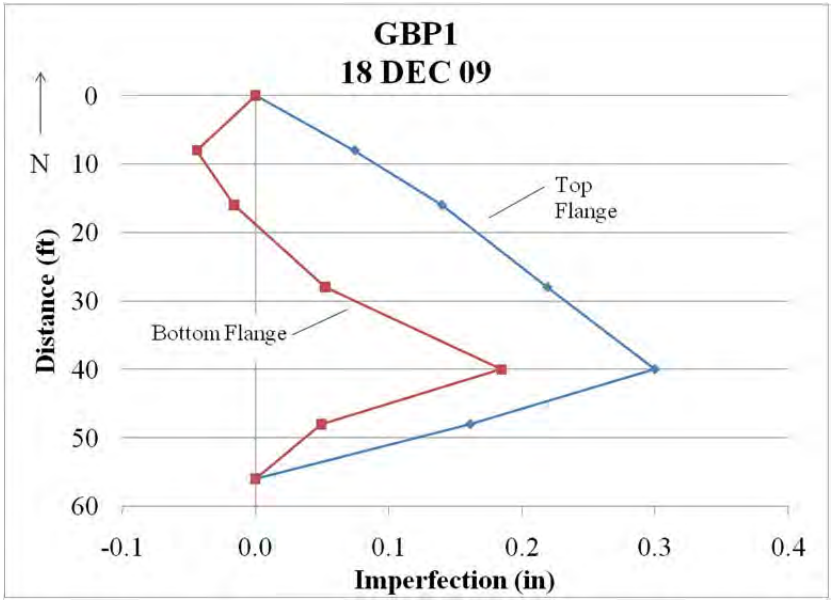

Figure A.1: Girder GBP1 Initial Imperfection as of 18 DEC 09

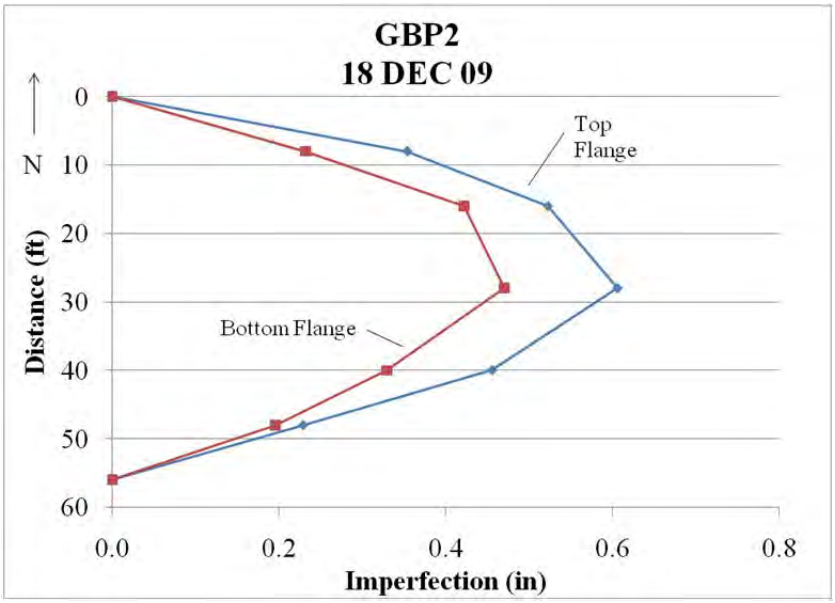

Figure A.2: Girder GBP2 Initial Imperfection as of 18 DEC 09

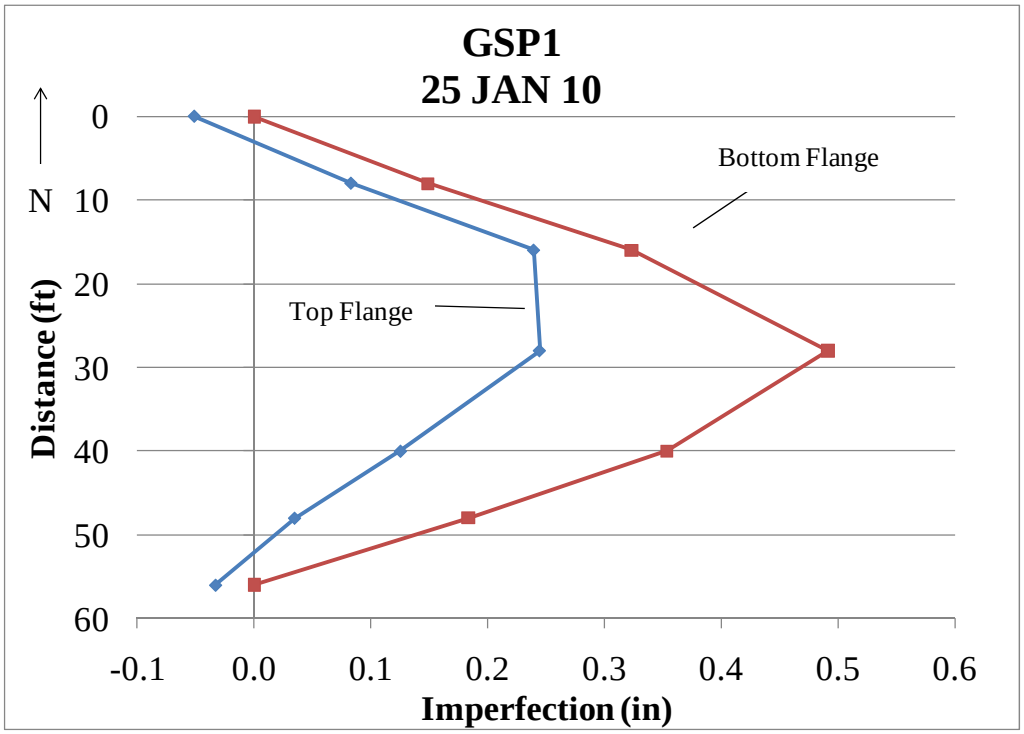

Figure A.3: Girder GSP1 Imperfection as of 25 JAN 10

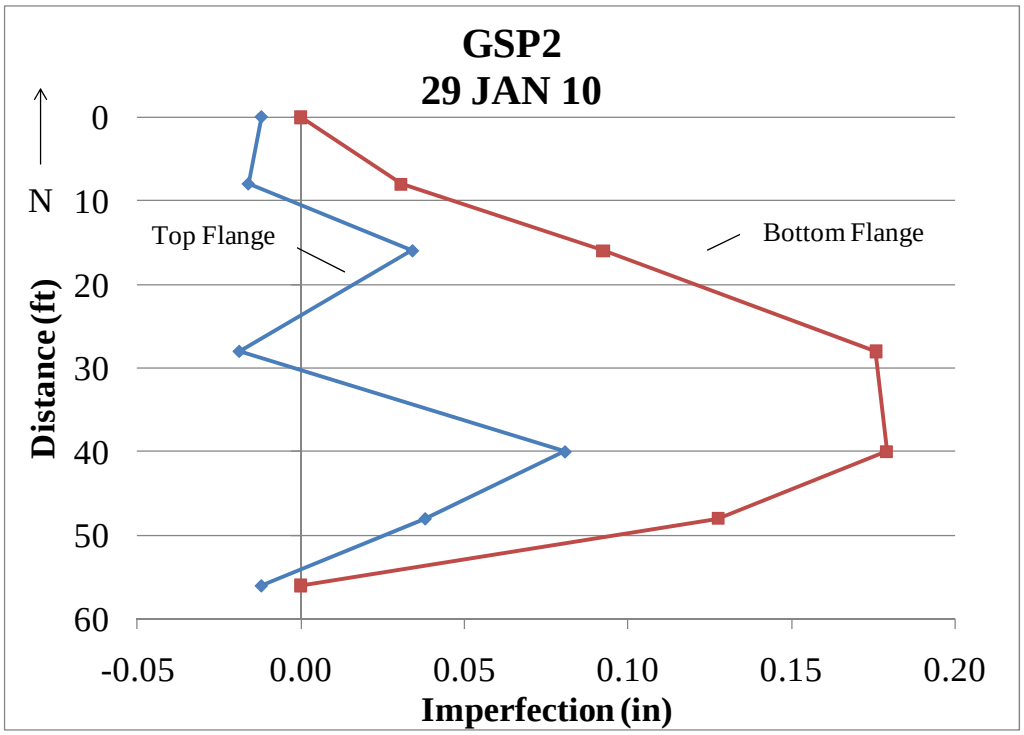

Figure A.4: Girder GSP2 Imperfection as of 25 JAN 10

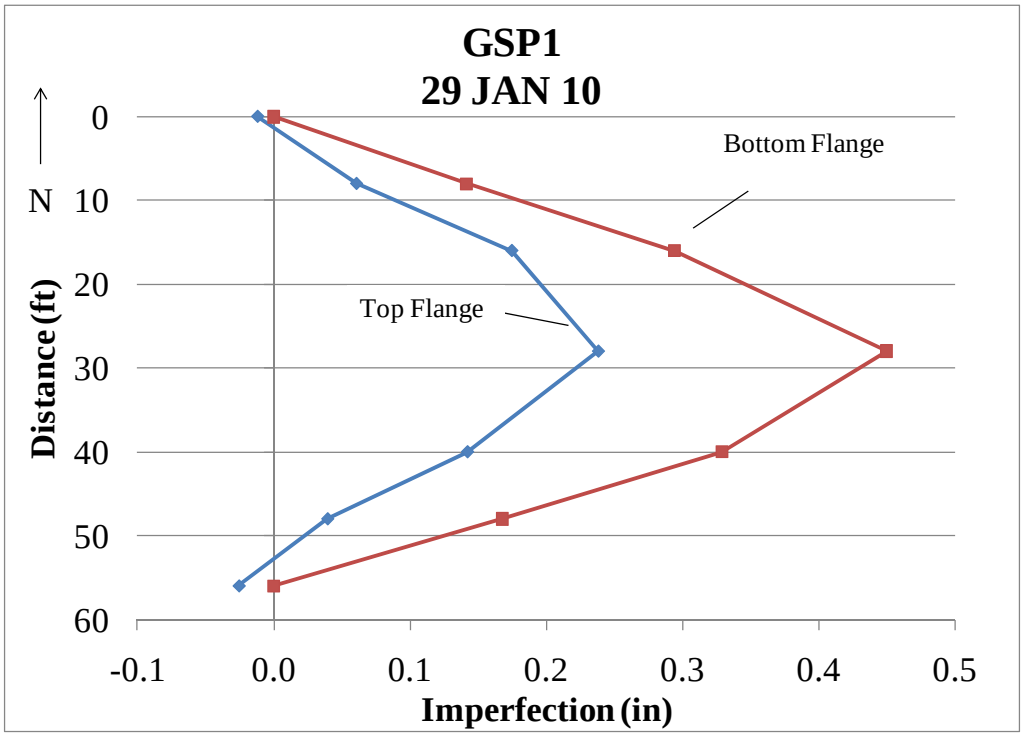

Figure A.5: Girder GSP1 Imperfection as of 29 JAN 10

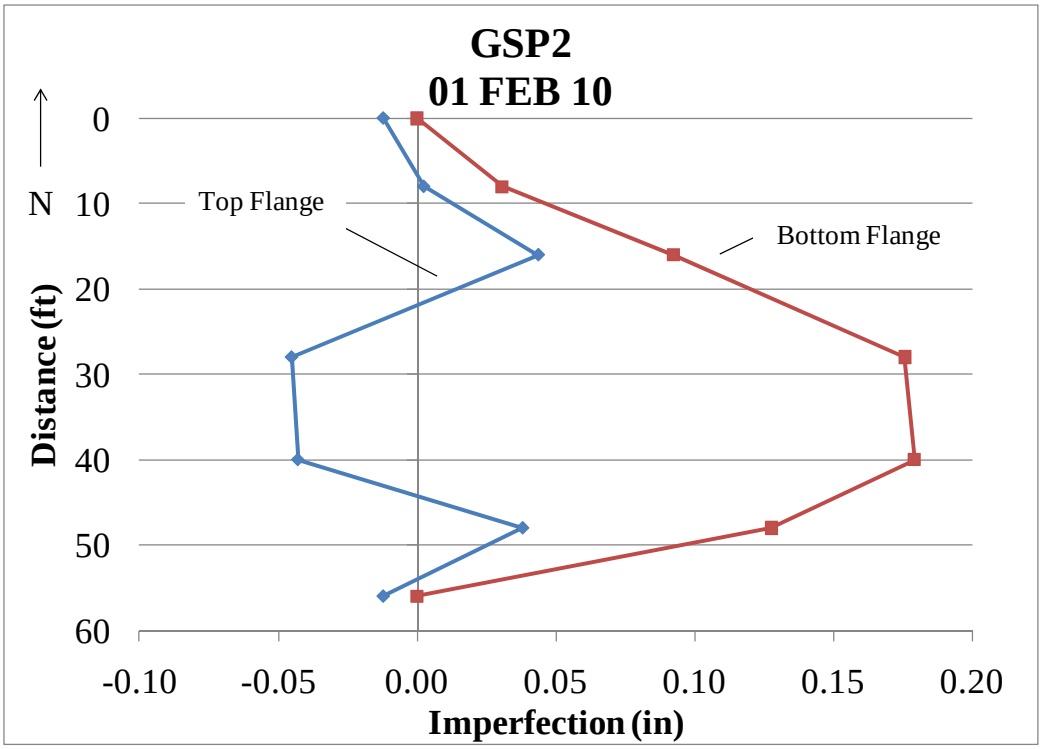

Figure A.6: Girder GSP2 Imperfection as of 1 FEB 10

A.2 TWIN GIRDER BUCKLING TEST RESULTS

A.2.1 Plate Stiffened Specimens (GBP1 and GBP2)

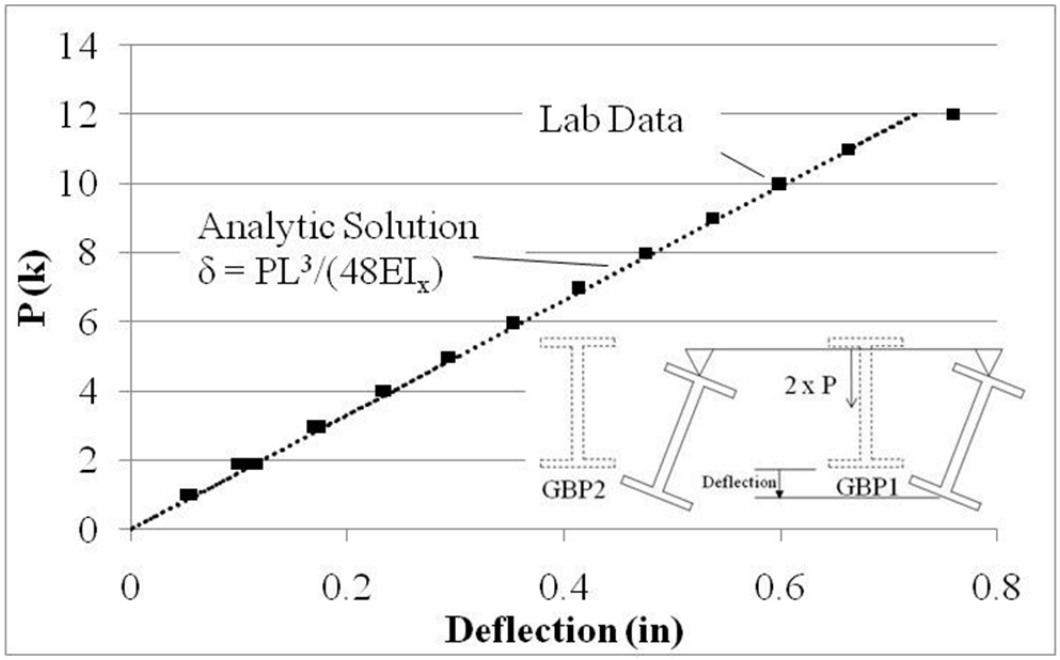

Figure A.7: GBP1 mid-span vertical deflection (down is positive)

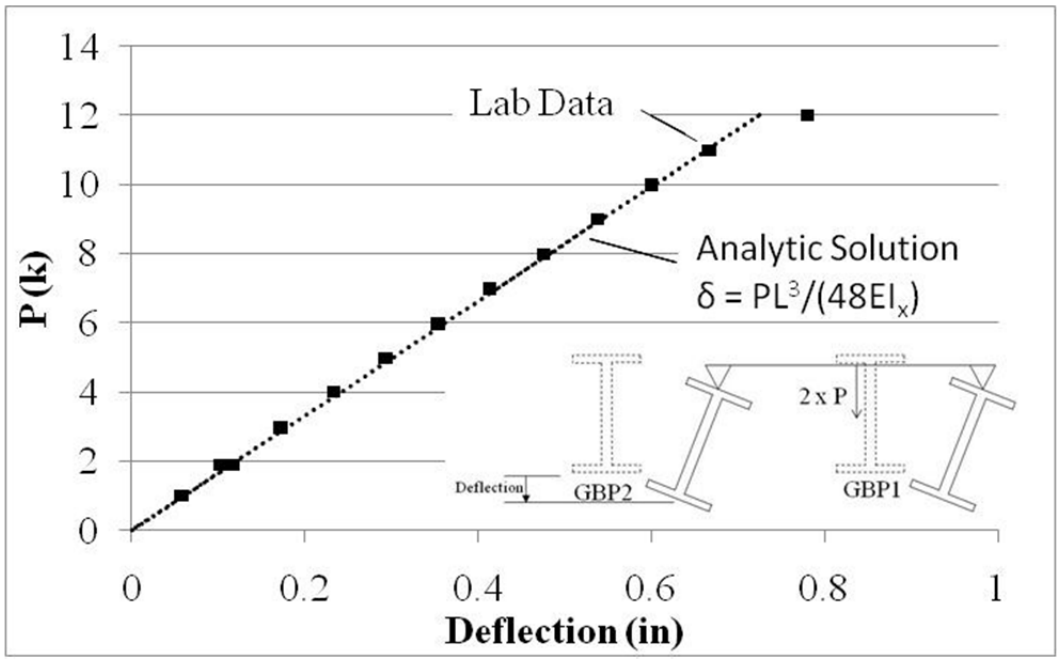

Figure A.8: GBP2 mid-span vertical deflection (down is positive)

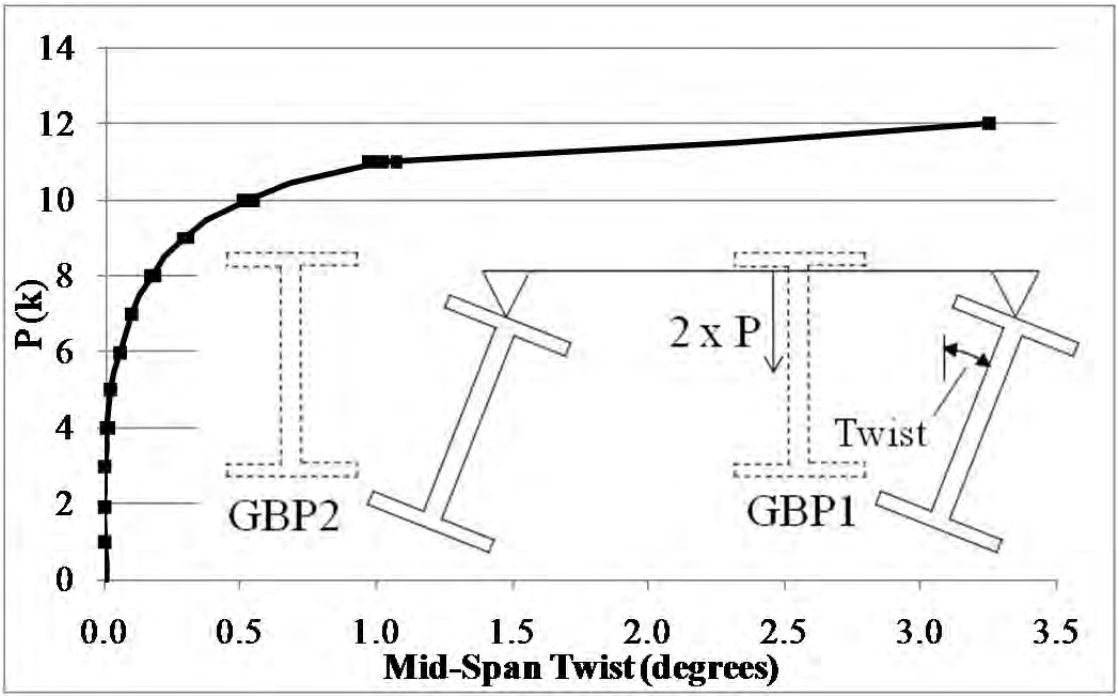

Figure A.9: GBP1 mid-span twist (CW looking north is positive)

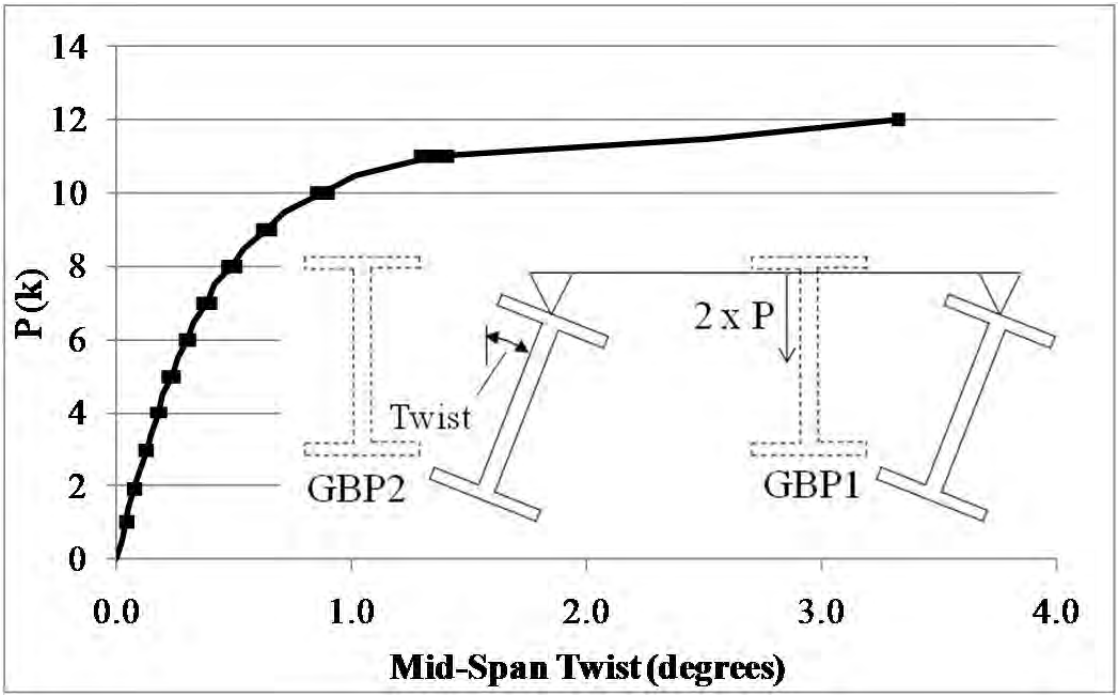

Figure A.10: GBP2 mid-span twist (CW looking north is positive)

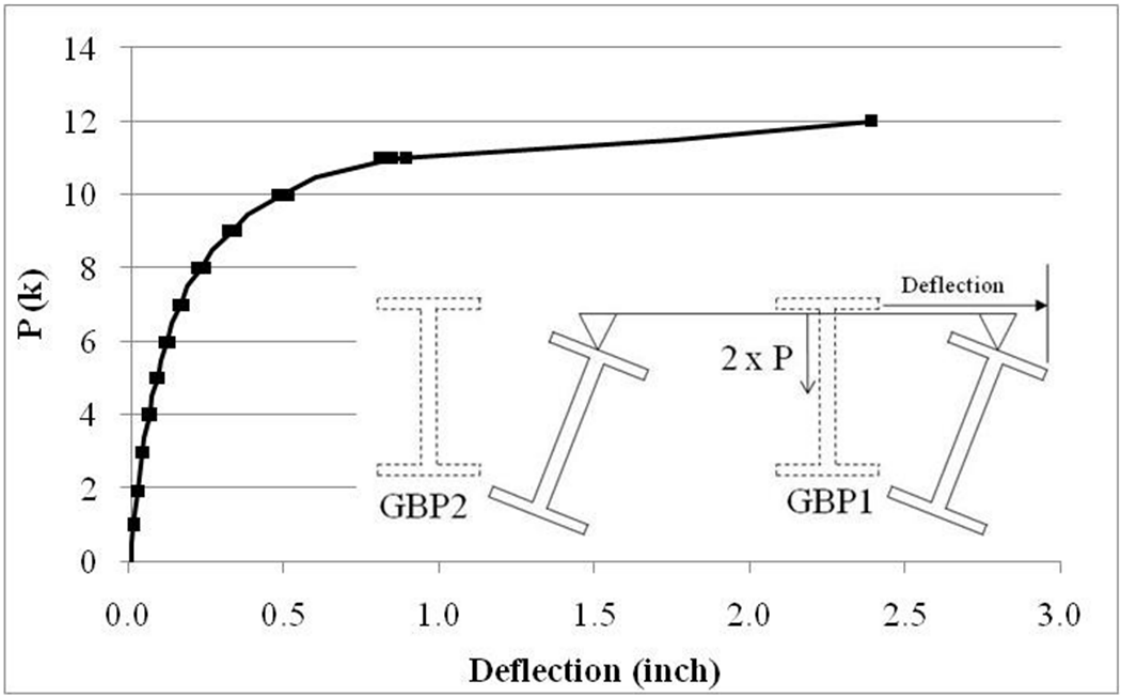

Figure A.11: GBP1 mid-span top flange lateral deflection (east is positive)

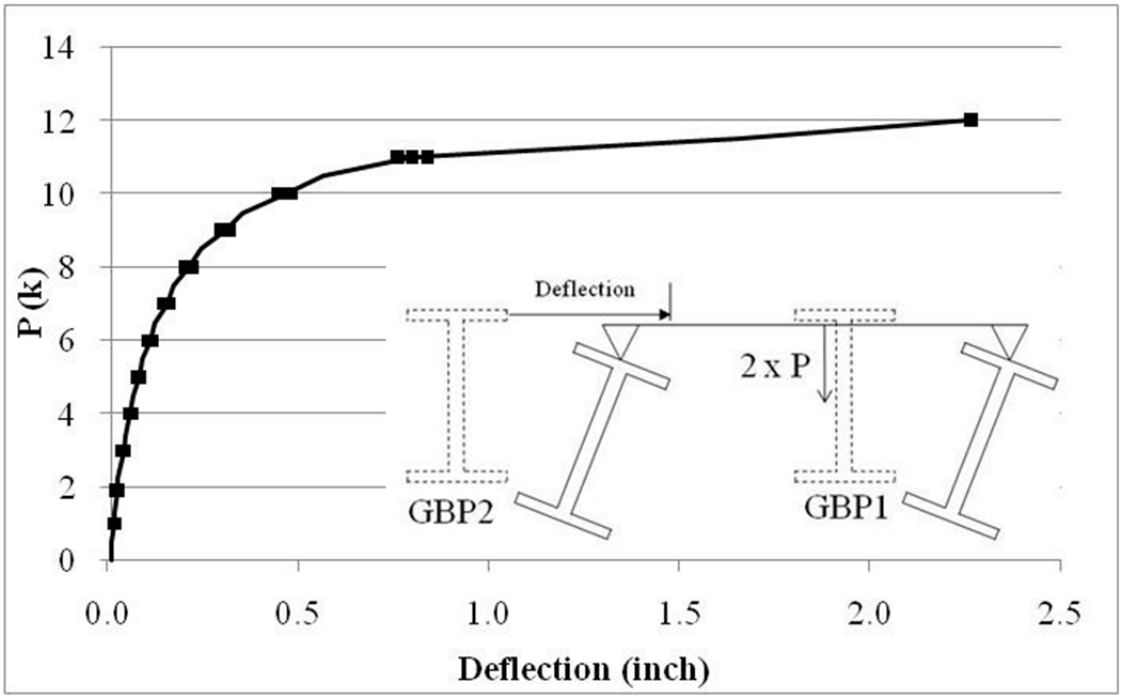

Figure A.12: GBP2 mid-span top flange lateral deflection (east is positive)

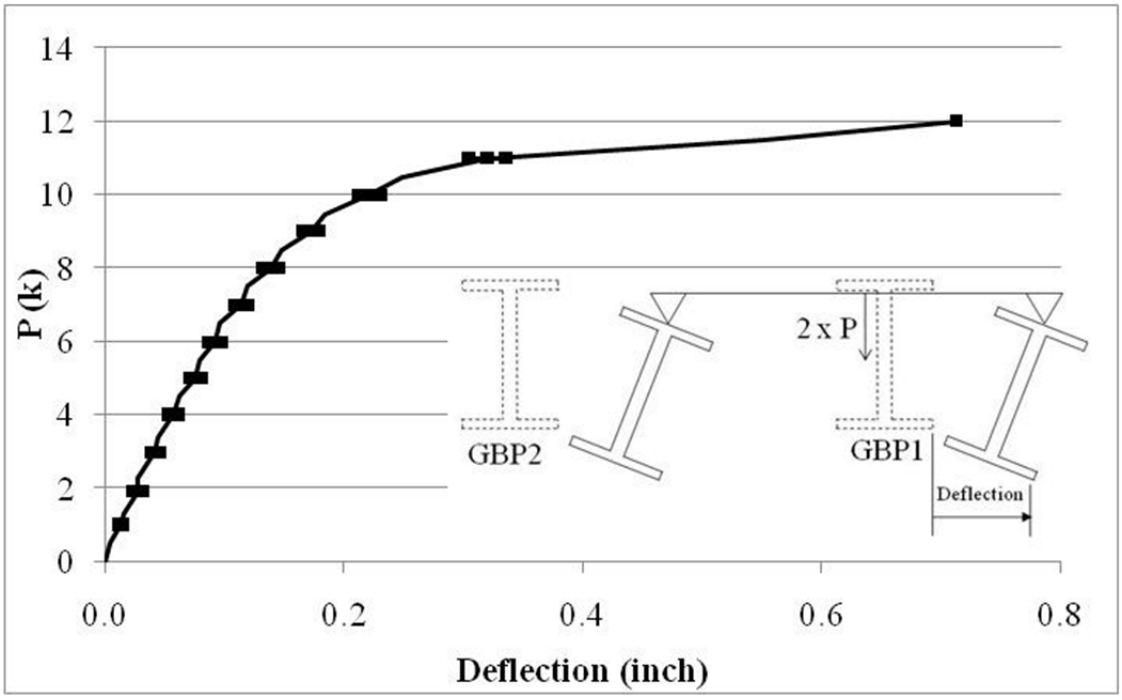

Figure A.13: GBP1 mid-span bottom flange lateral deflection (east is positive)

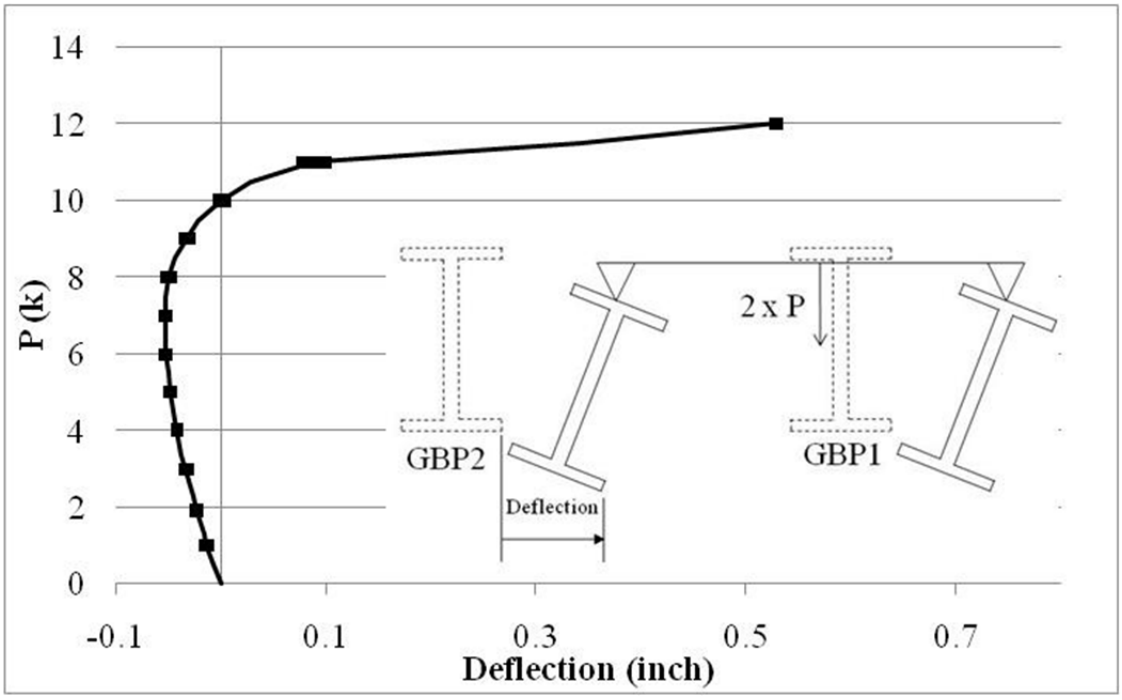

Figure A.14: GBP2 bottom flange mid-span lateral deflection (east is positive)

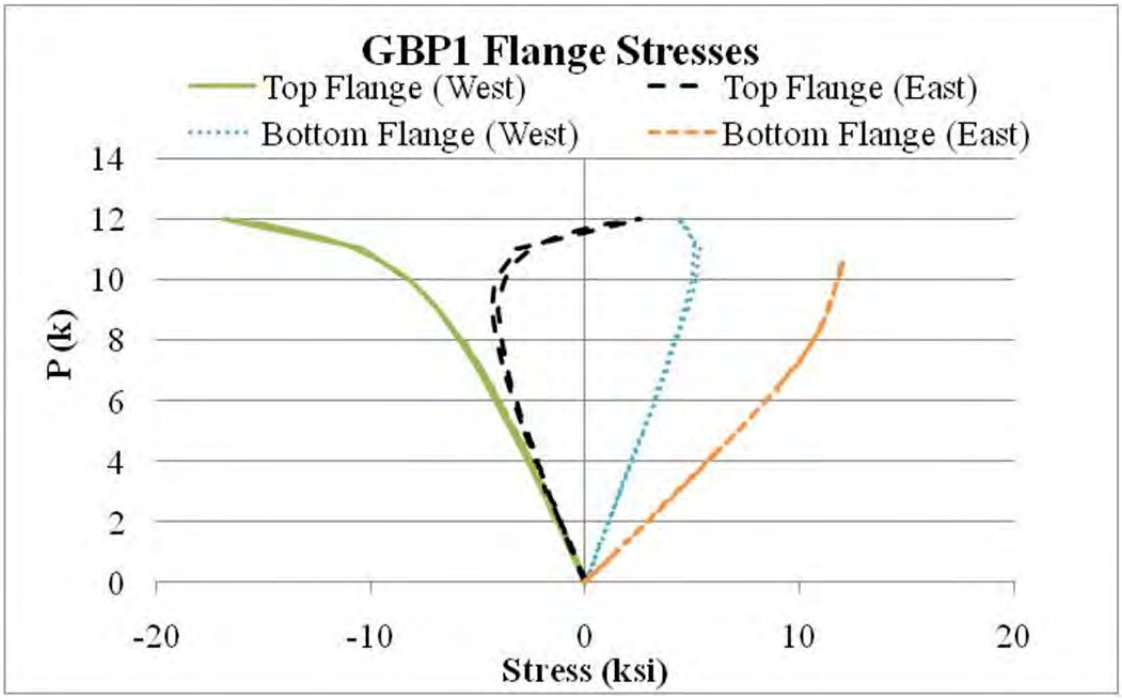

Figure A.15: GBP1 mid-span flange stresses (tension is positive)

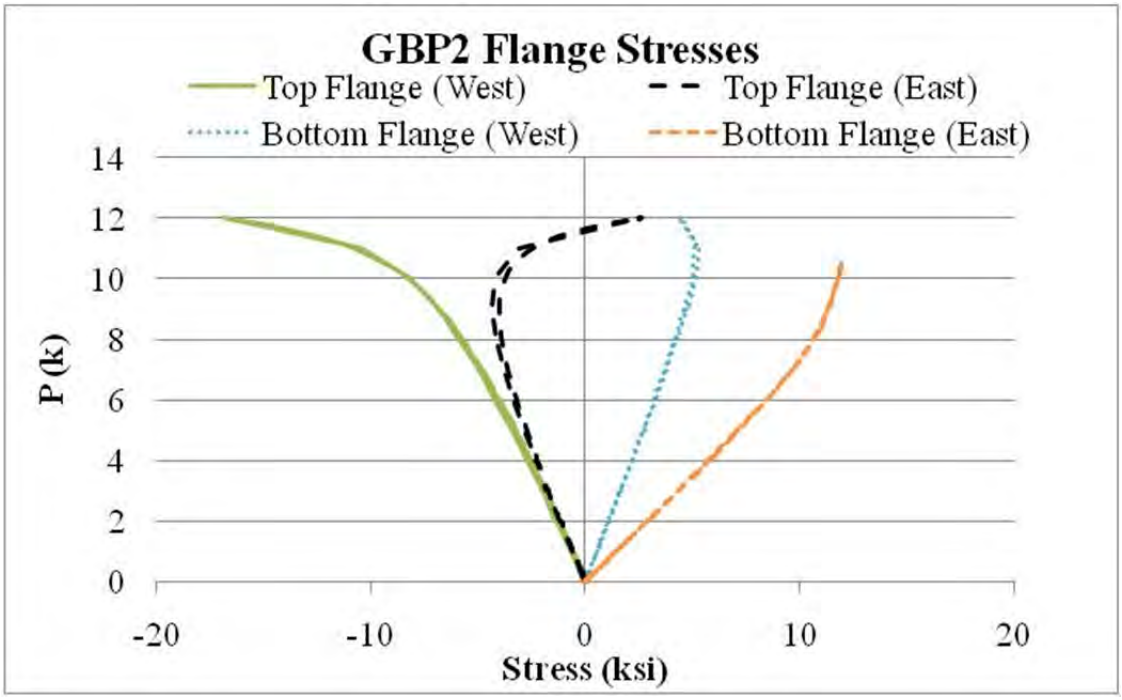

Figure A.16: GBP2 mid-span flange stresses (tension is positive)

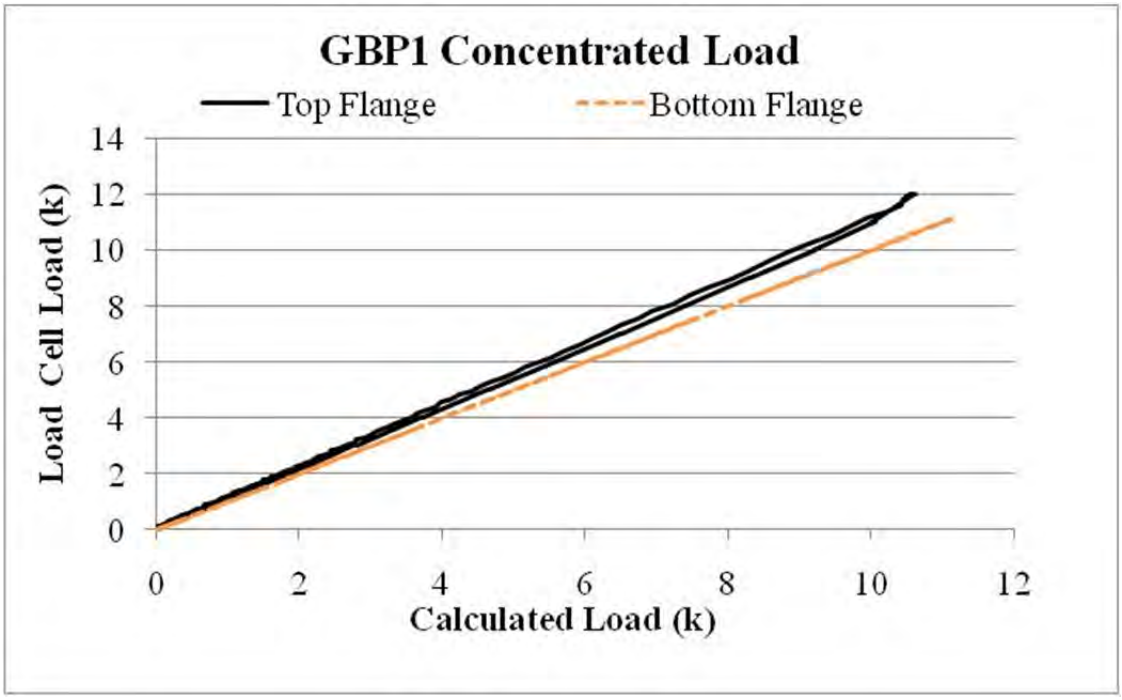

Figure A.17: GBP1 calculated applied load from mid-span flange stresses

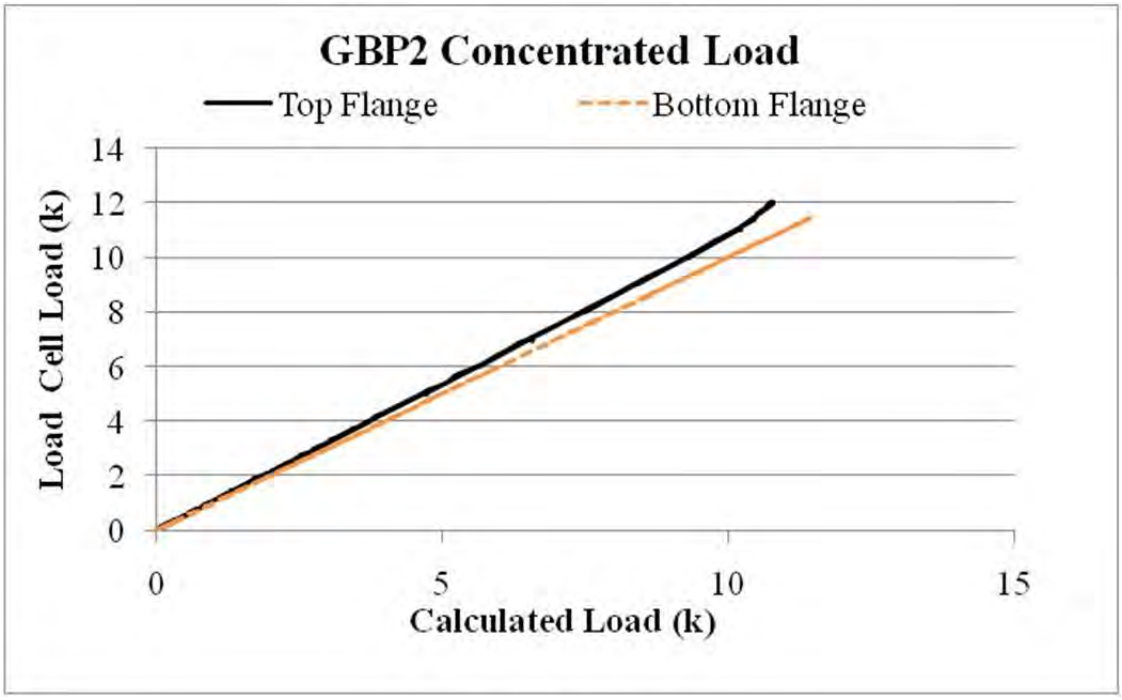

Figure A.18: GBP2 calculated applied load from mid-span flange stresses

A.2.2 Pipe Stiffened Specimens (GSP1 and GSP2)

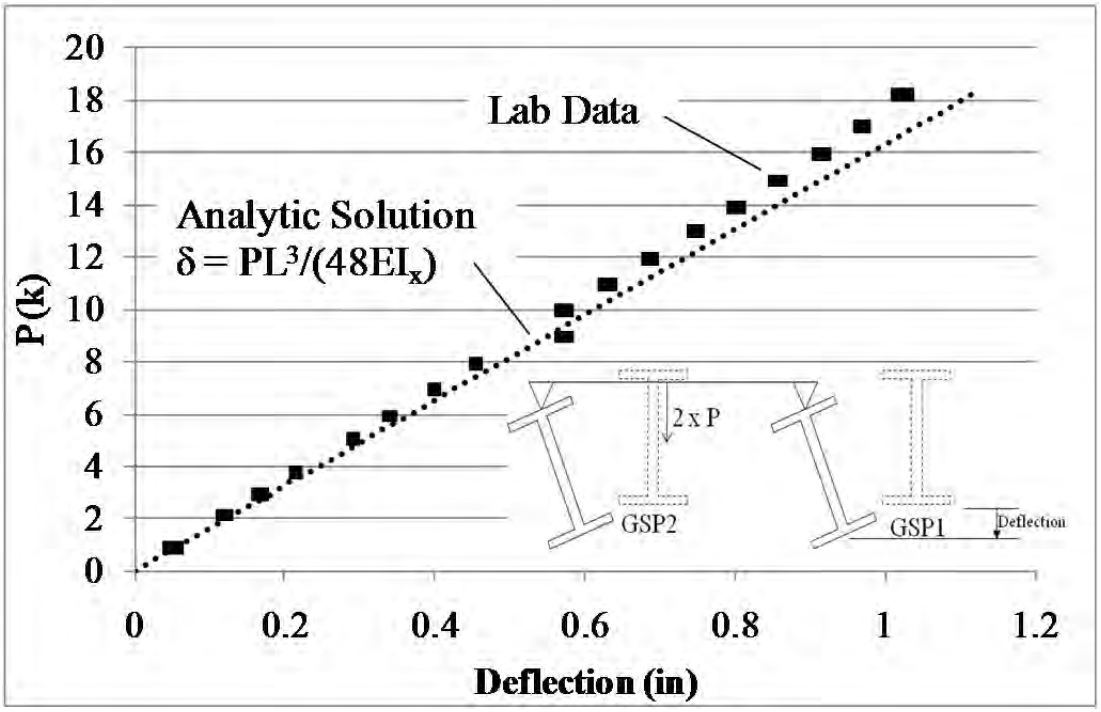

Figure A.19: GSP1 mid-span vertical deflection (down is positive)

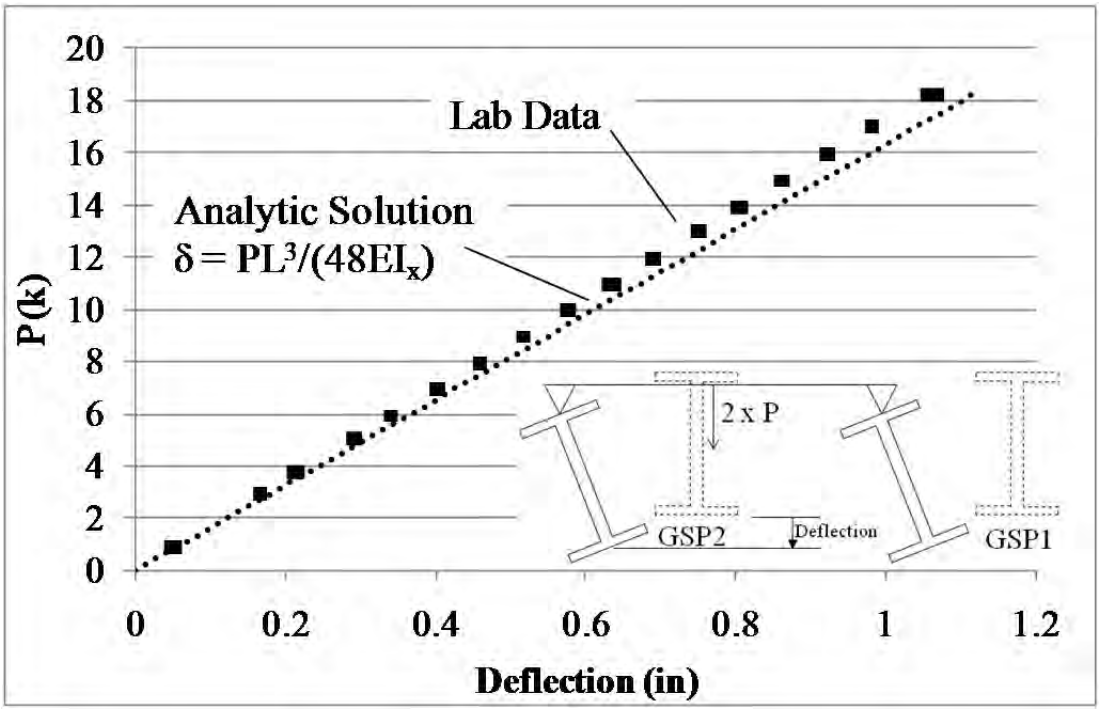

Figure A.20: GSP2 mid-span vertical deflection (down is positive)

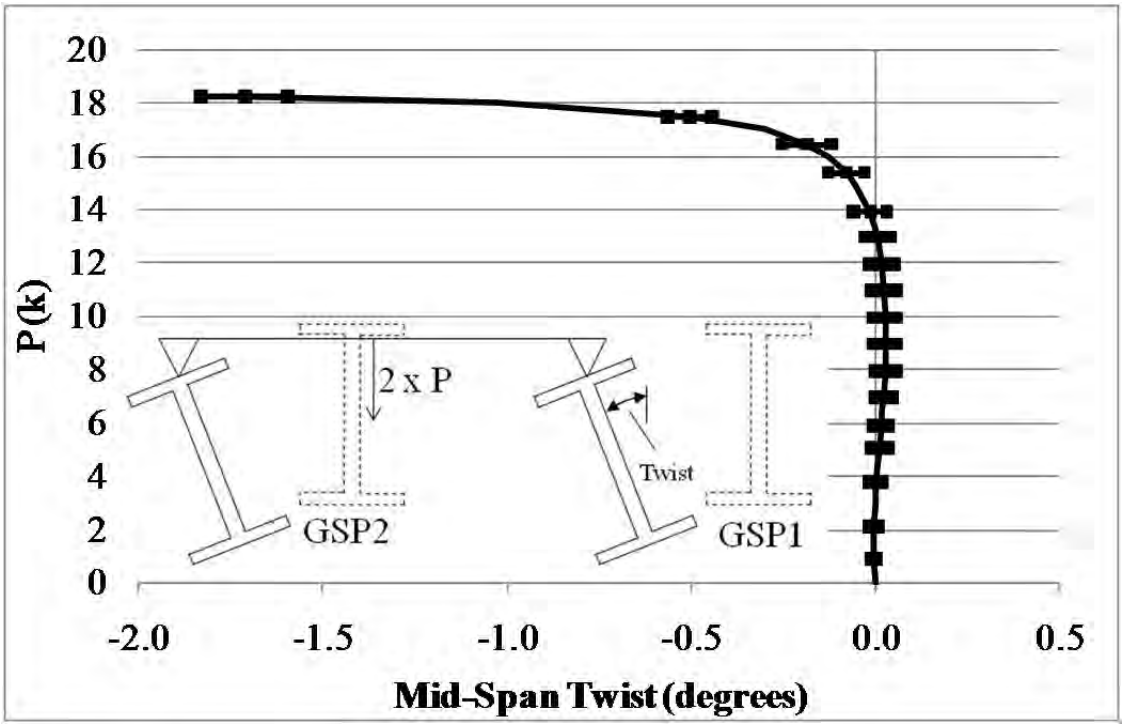

Figure A.21: GSP1 mid-span twist (CW looking north is positive)

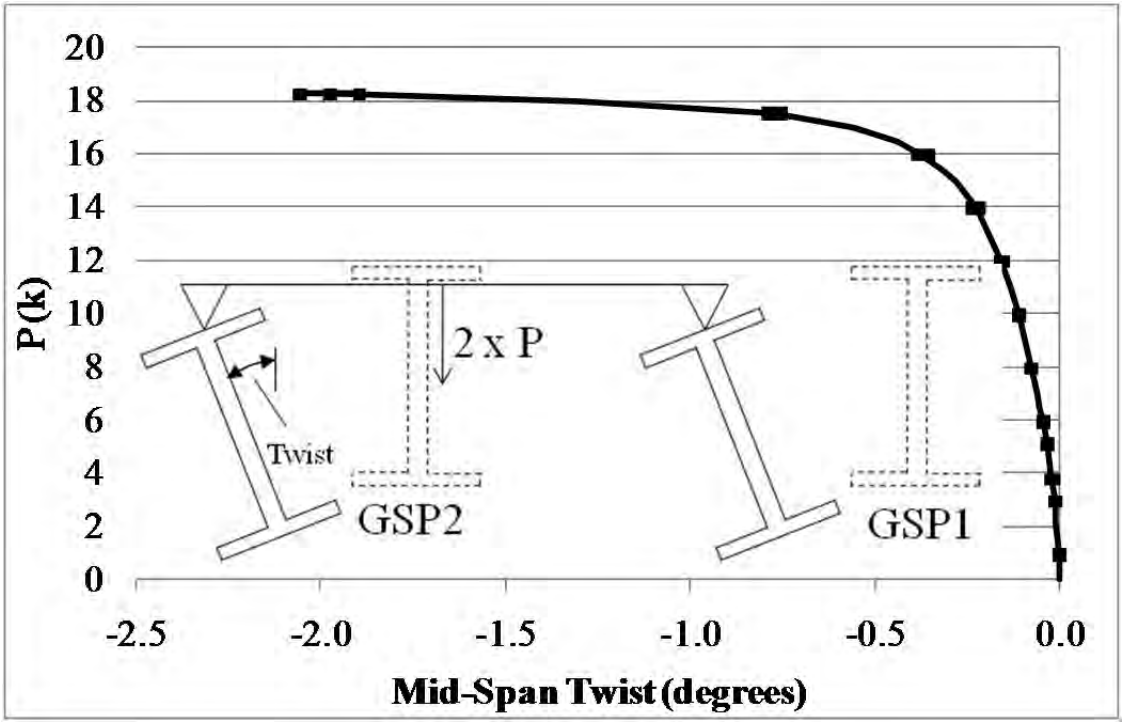

Figure A.22: GSP2 mid-span twist (CW looking north is positive)

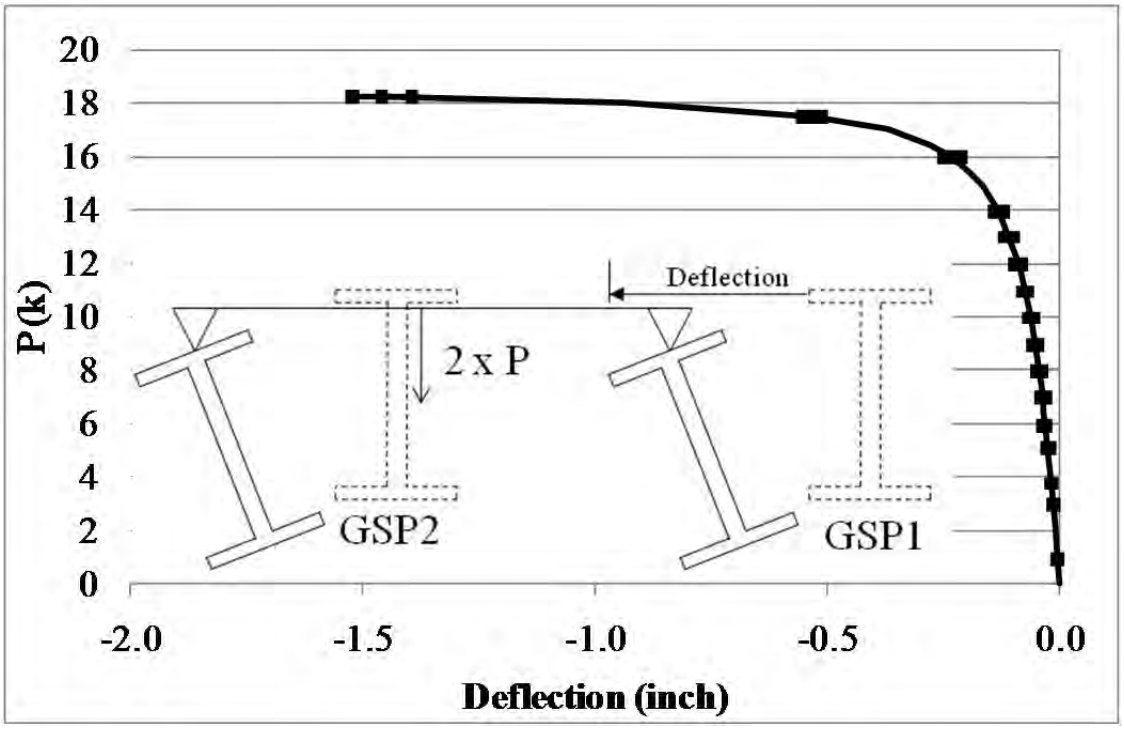

Figure A.23: GSP1 mid-span top flange lateral deflection (east is positive)

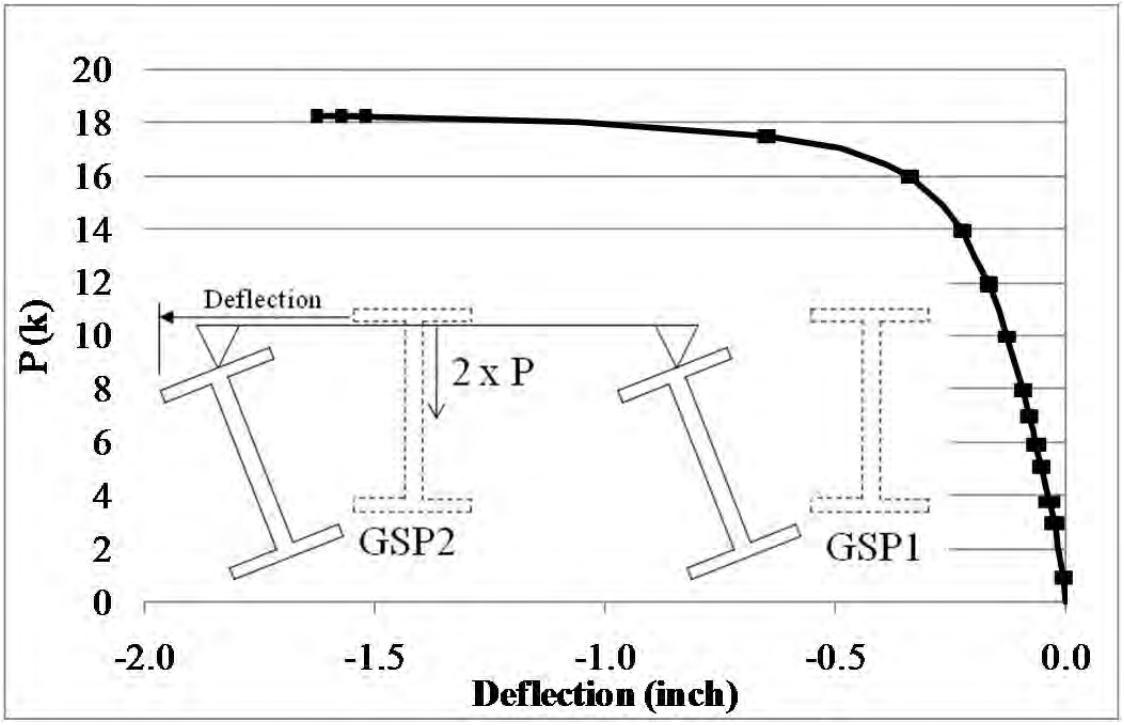

Figure A.24: GSP2 mid-span top flange lateral deflection (east is positive)

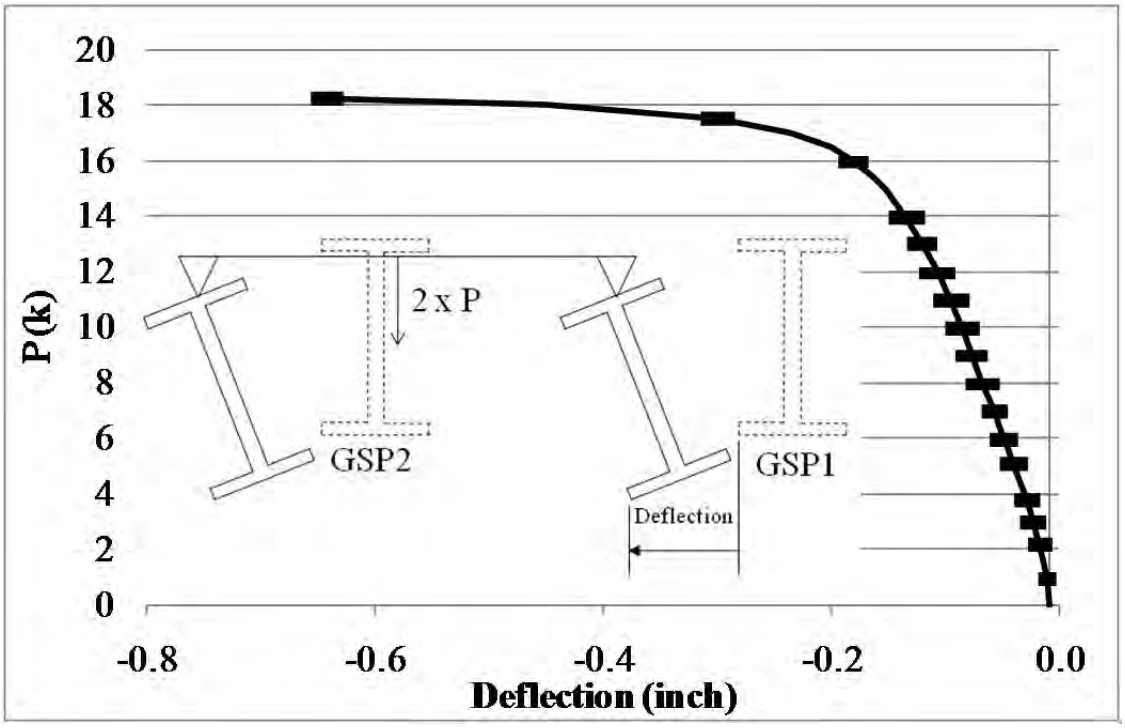

Figure A.25: GSP1 mid-span bottom flange lateral deflection (east is positive)

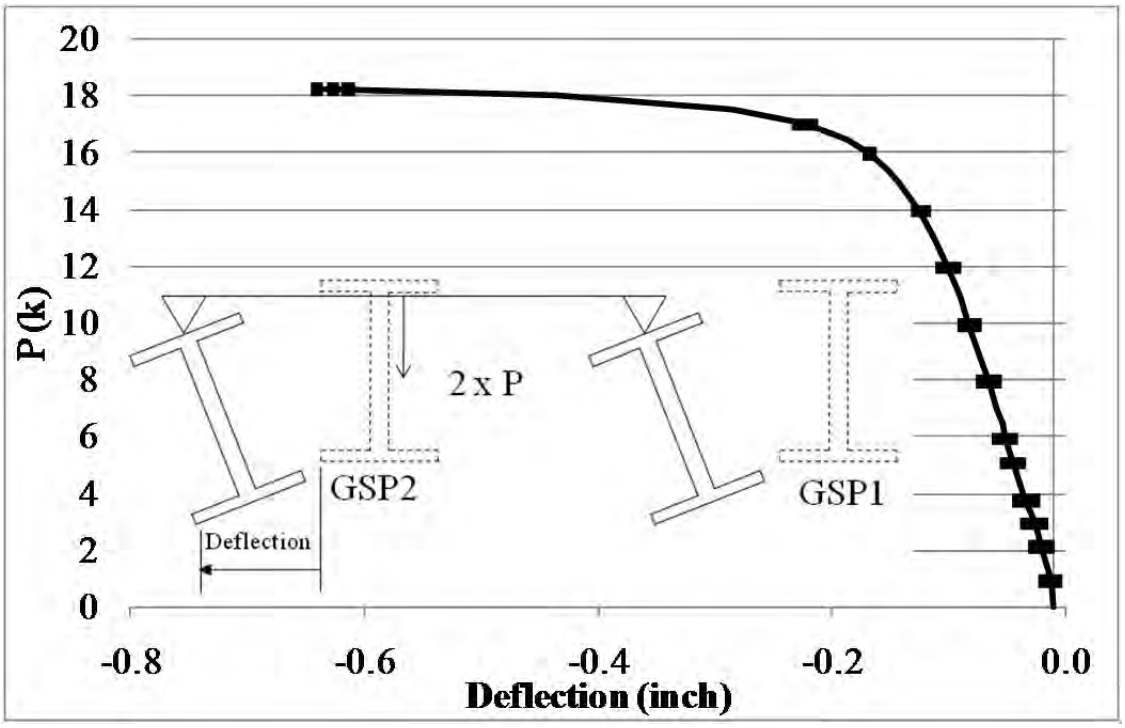

Figure A.26: GSP2 bottom flange mid-span lateral deflection (east is positive)

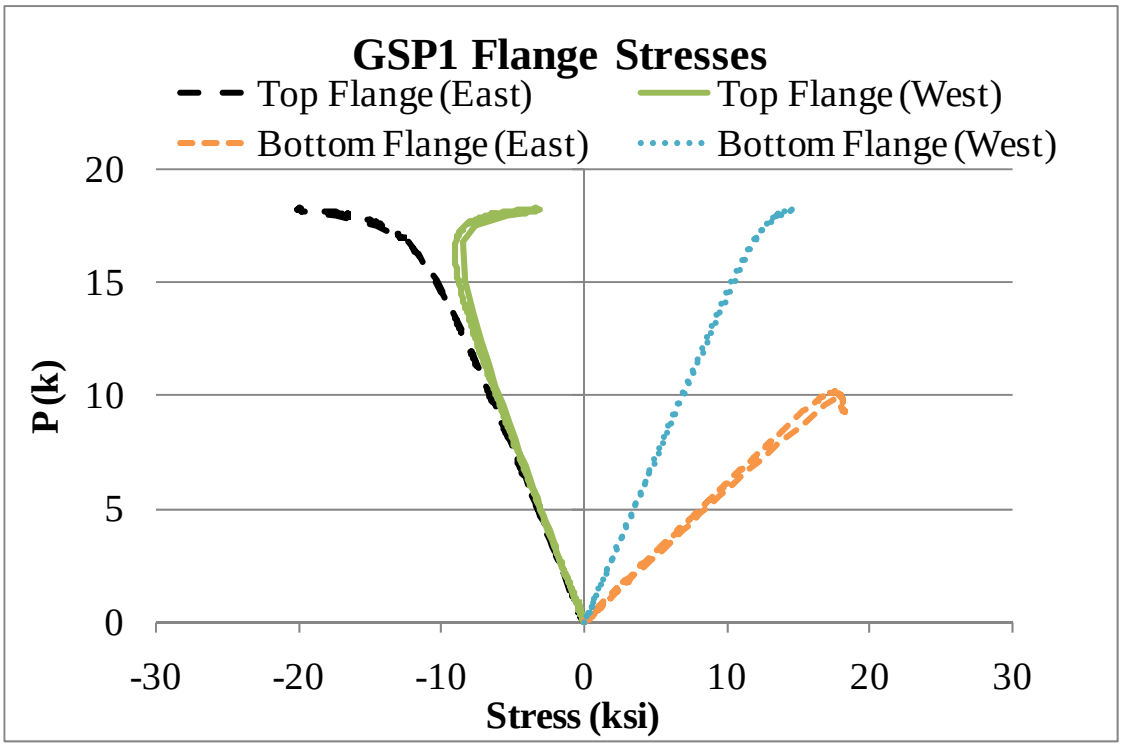

Figure A.27: GSP1 mid-span flange stresses (tension is positive)

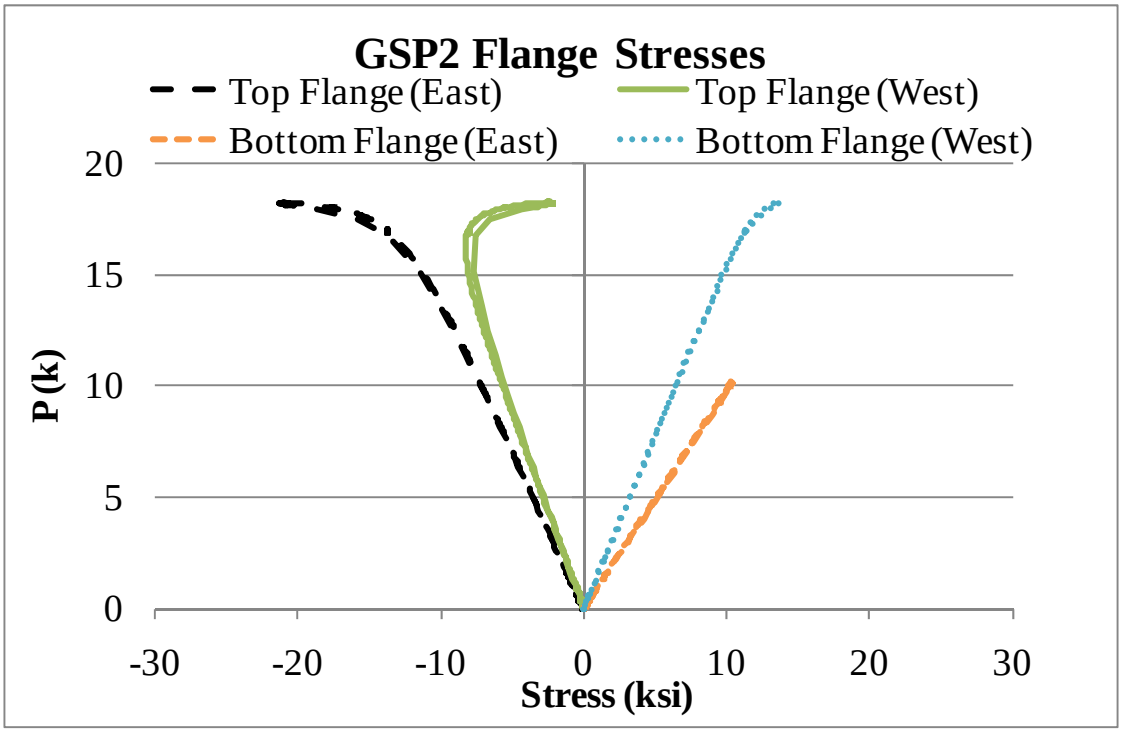

Figure A.28: GSP2 mid-span flange stresses (tension is positive)

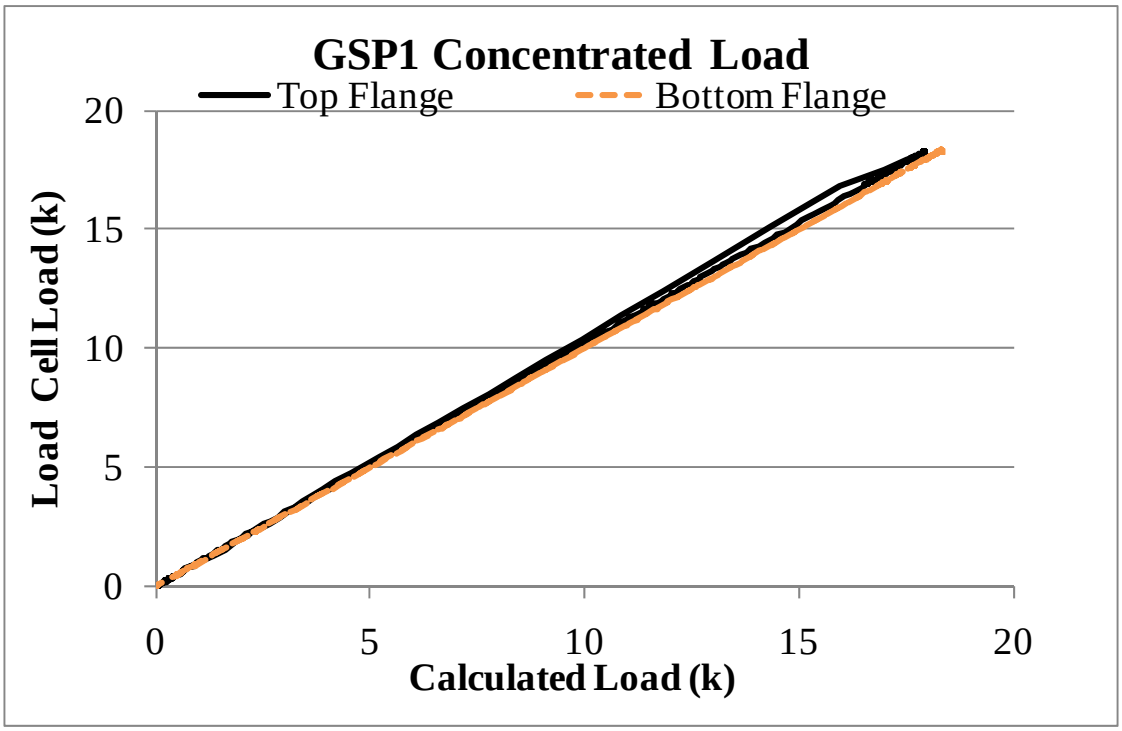

Figure A.29: GSP1 calculated applied load from mid-span flange stresses

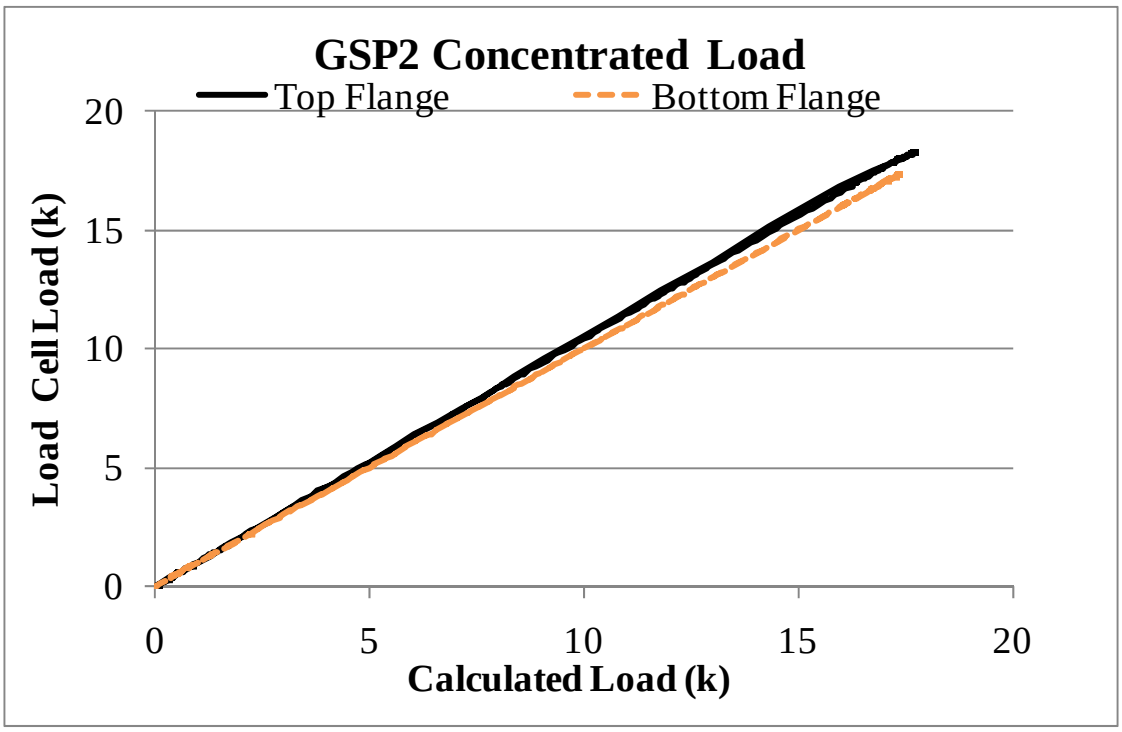

Figure A.30: GSP2 calculated applied load from mid-span flange stresses

A.3 THREE GIRDER SPLIT-PIPE END FRAME TEST RESULTS

A.3.1 Thrust Washer Bearing with No Intermediate Cross Frames

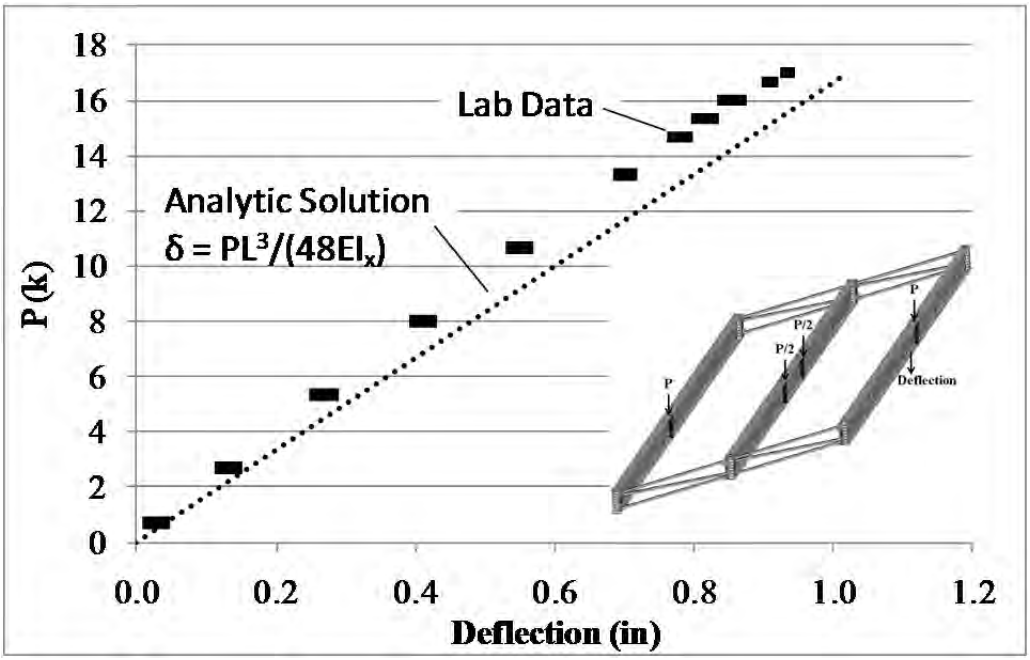

Figure A.31: GSP1 mid-span vertical deflection

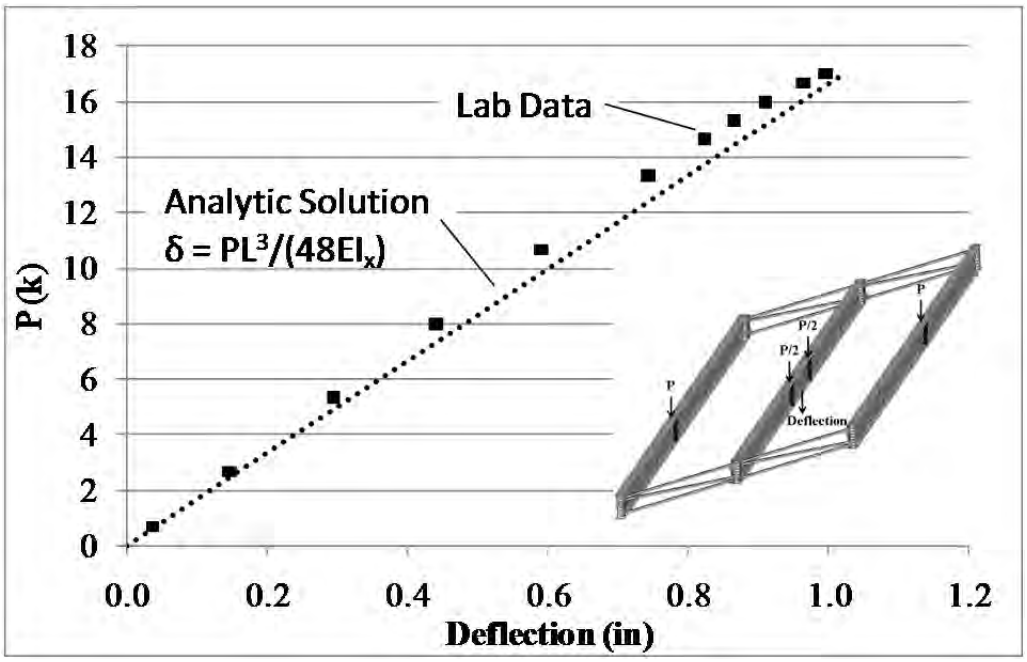

Figure A.32: GSP2 mid-span vertical deflection

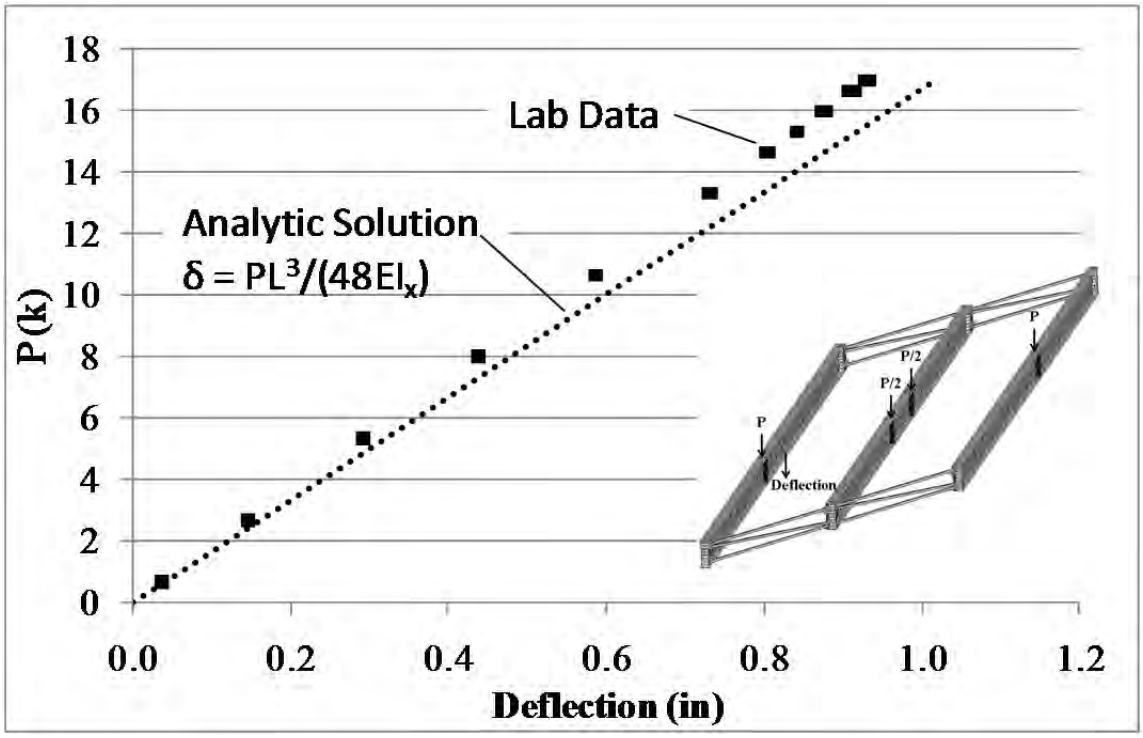

Figure A.33: GSP3 mid-span vertical deflection

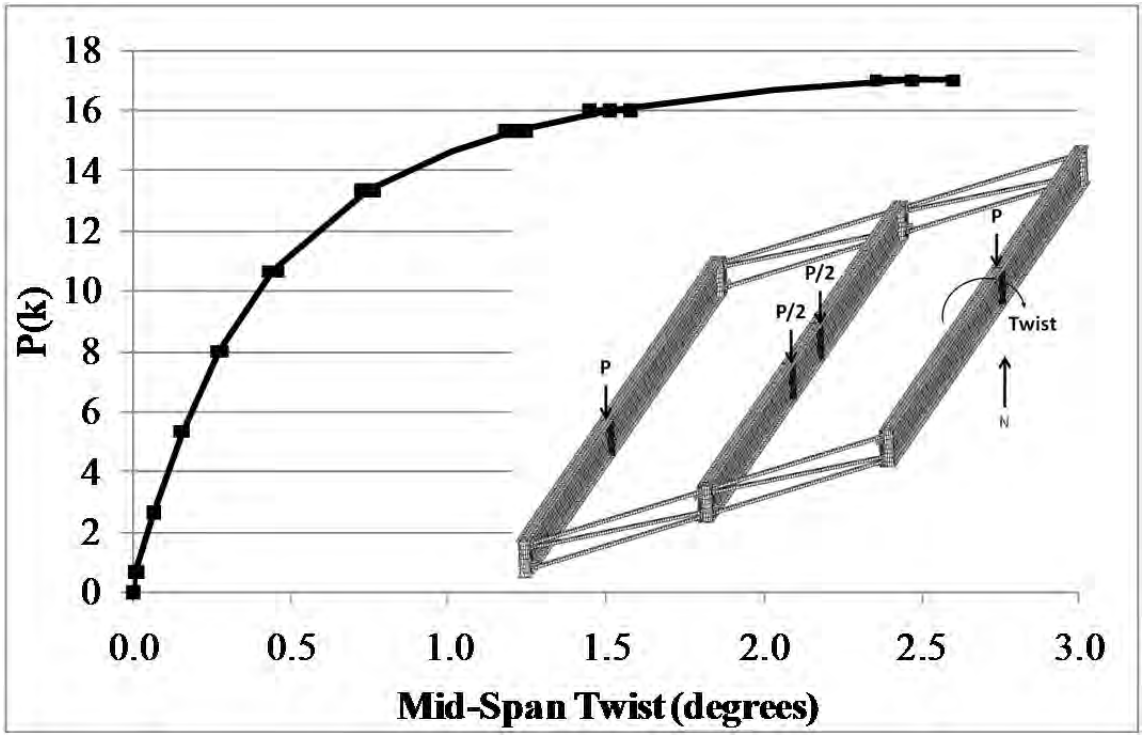

Figure A.34: GSP1 mid-span twist

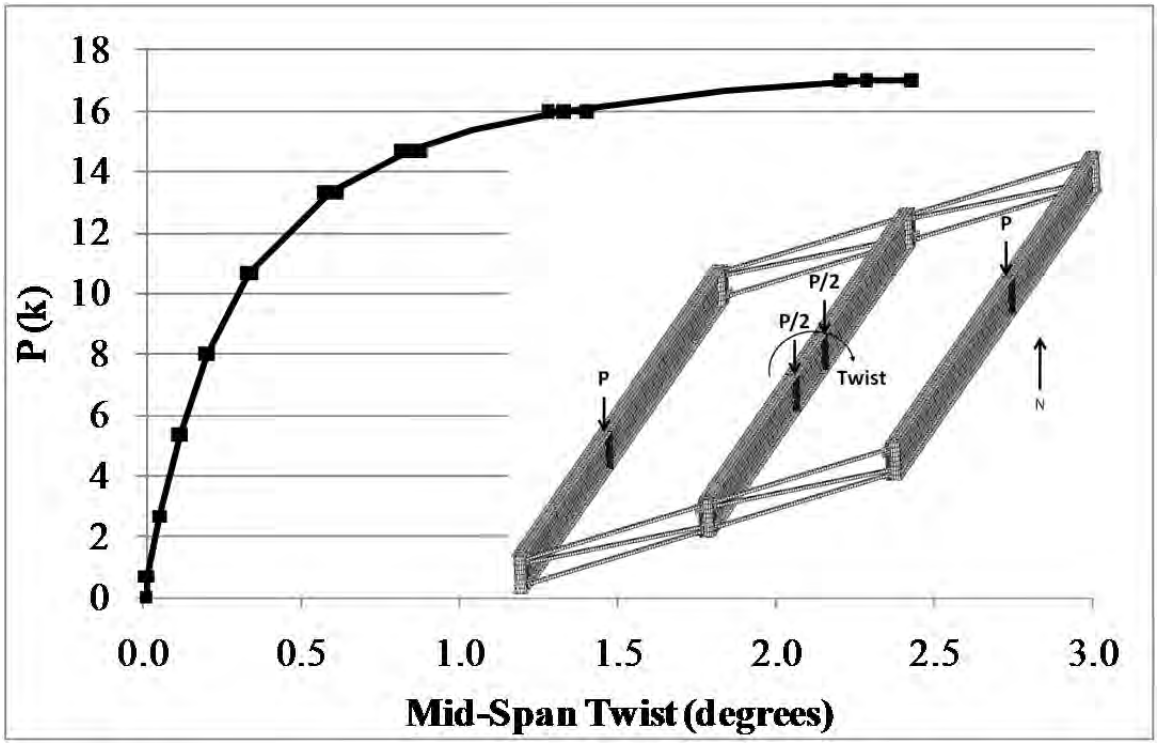

Figure A.35: GSP2 mid-span twist

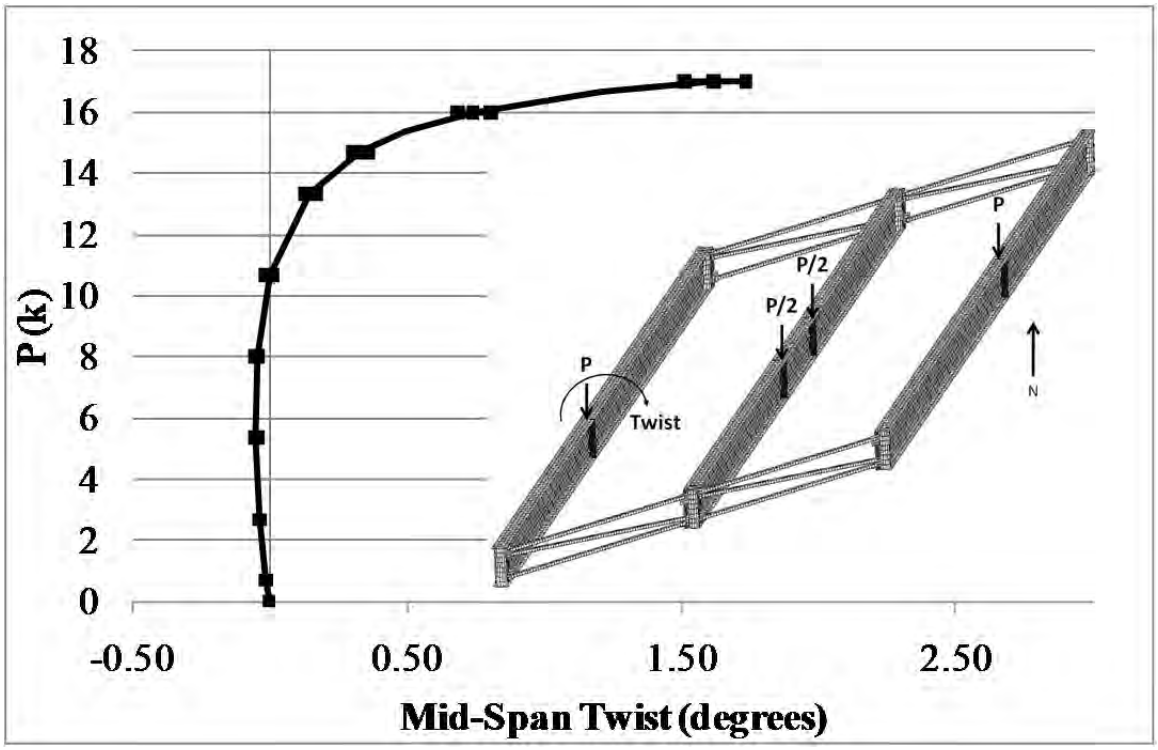

Figure A.36: GSP3 mid-span twist

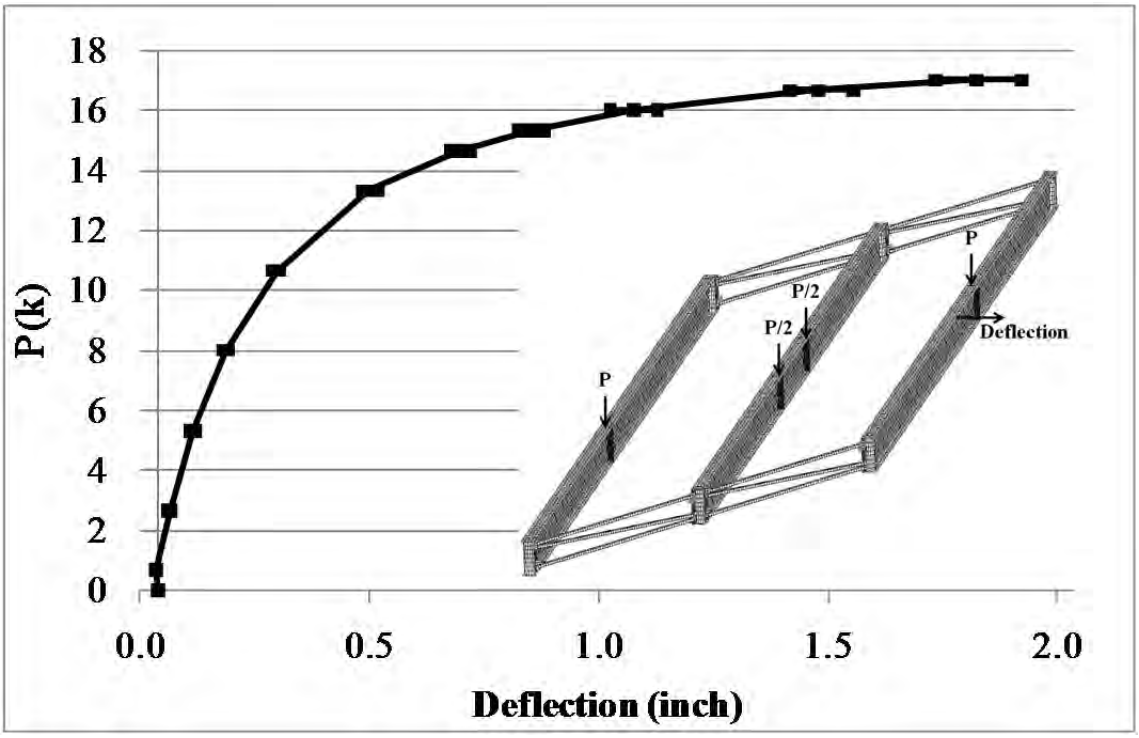

Figure A.37: GSP1 mid-span top flange lateral deflection

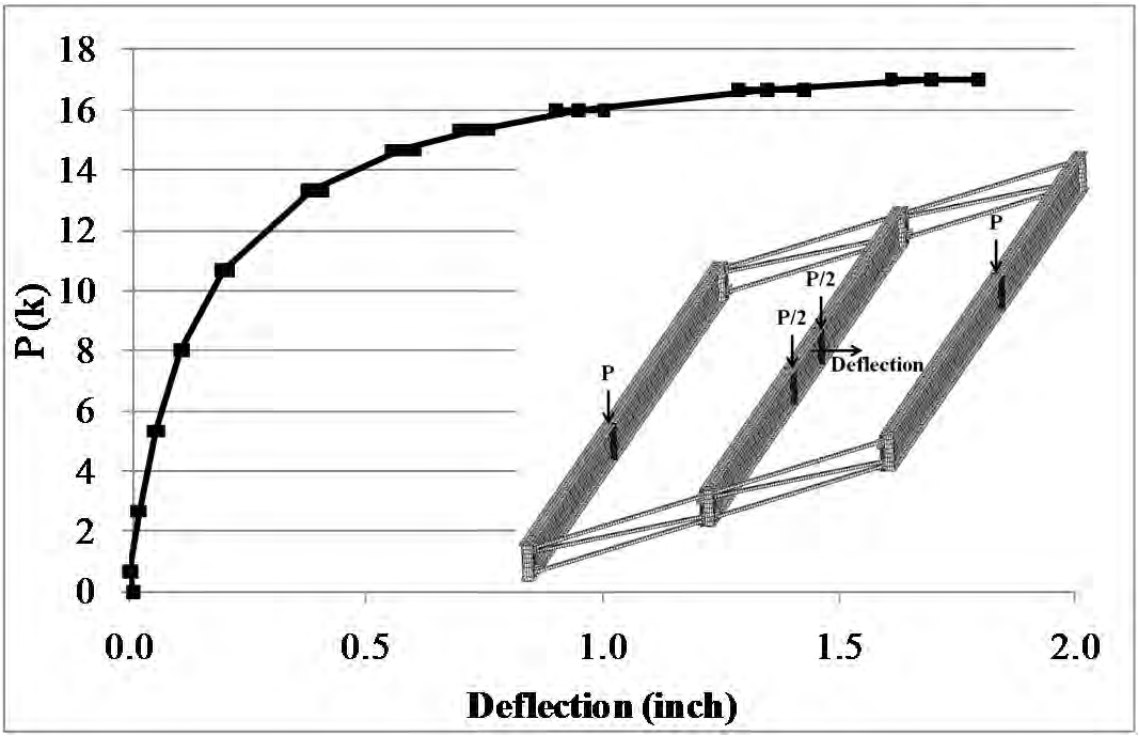

Figure A.38: GSP2 mid-span top flange lateral deflection

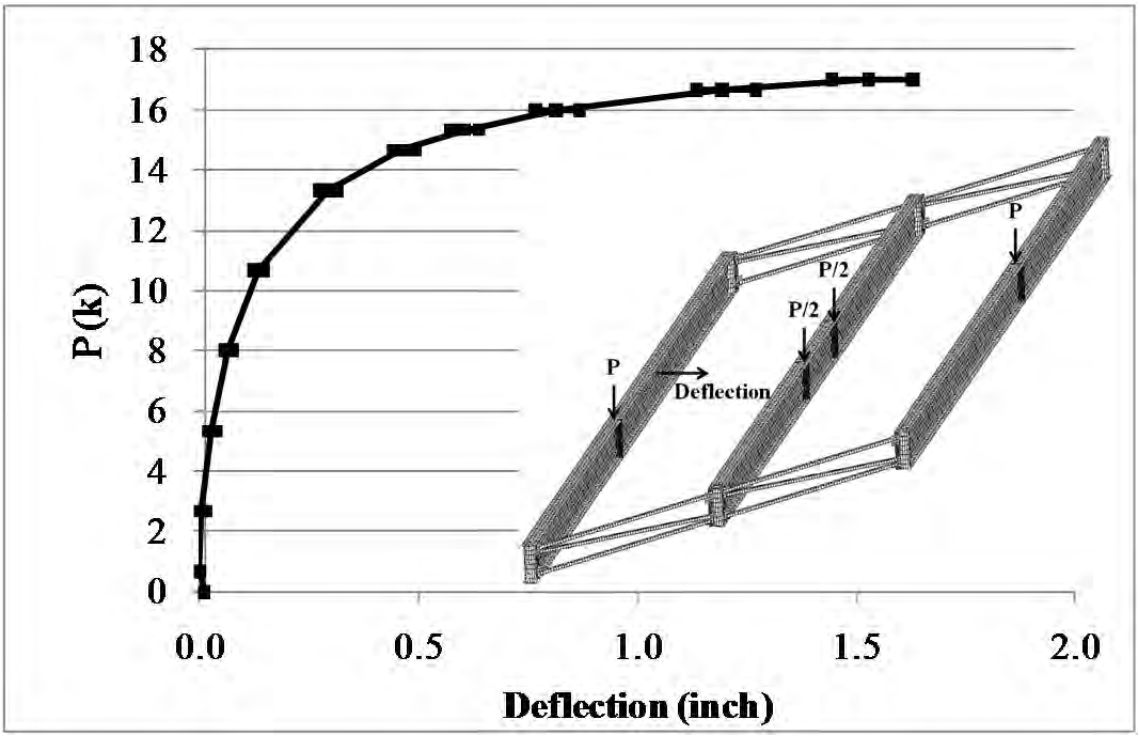

Figure A.39: GSP3 mid-span top flange lateral deflection

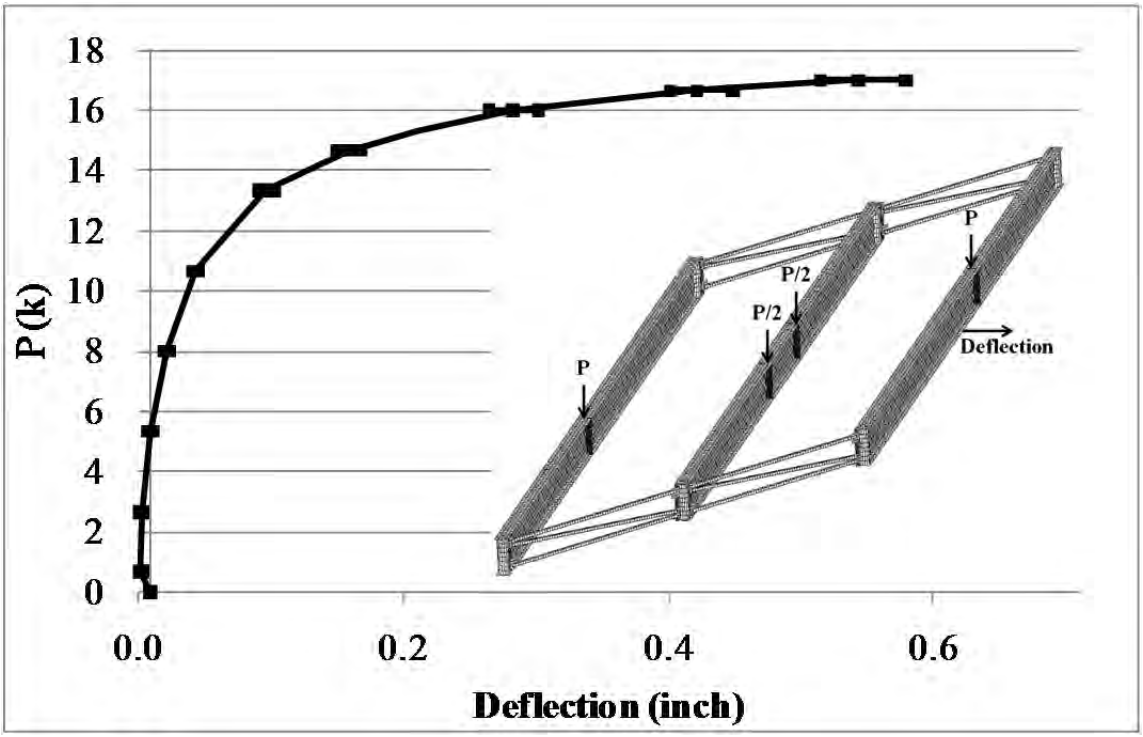

Figure A.40: GSP1 mid-span bottom flange lateral deflection

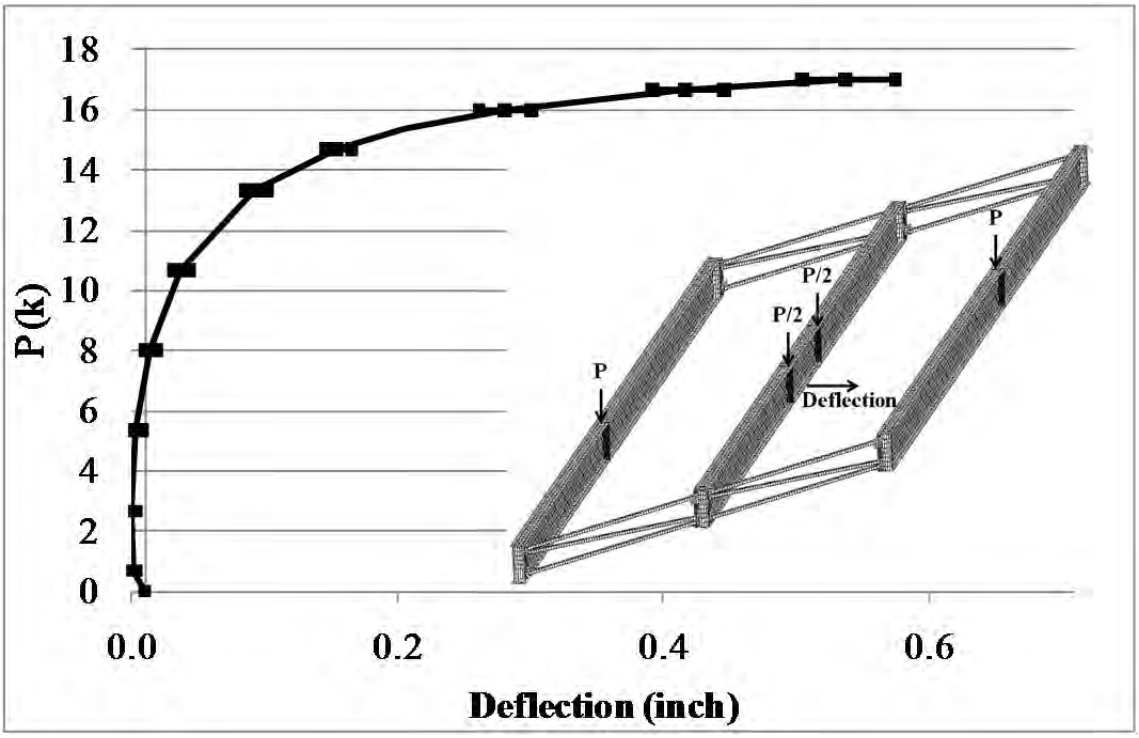

Figure A.41: GSP2 mid-span bottom flange lateral deflection

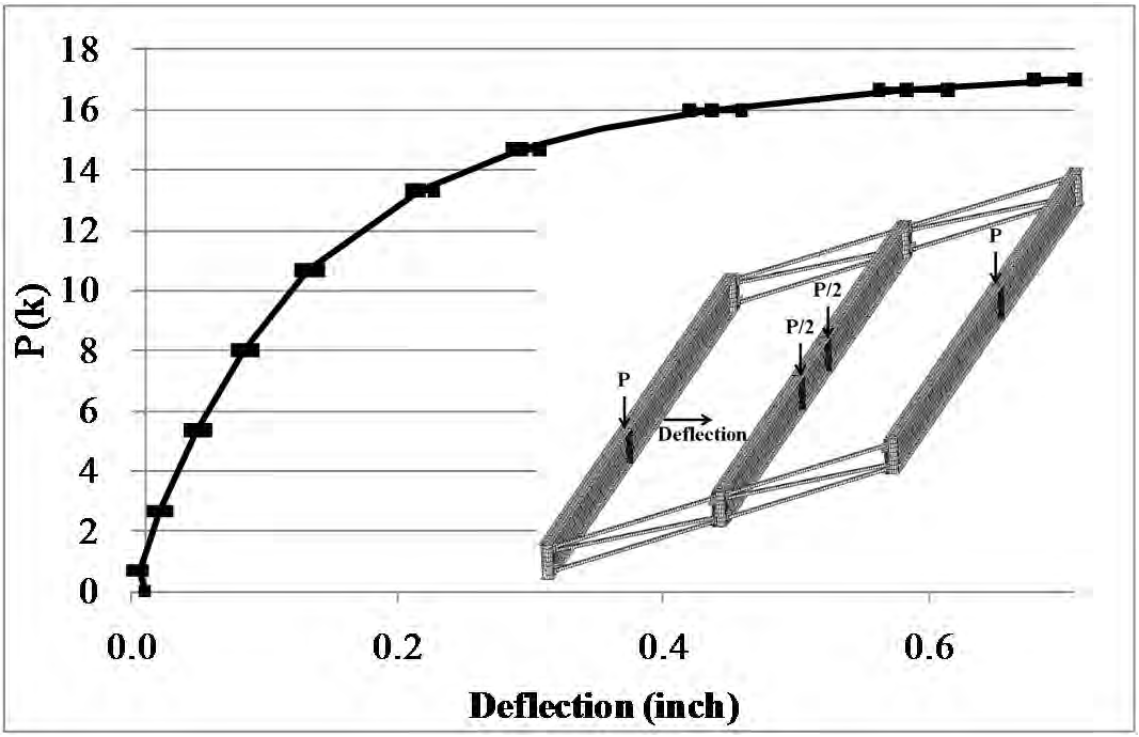

Figure A.42: GSP3 mid-span bottom flange lateral deflection

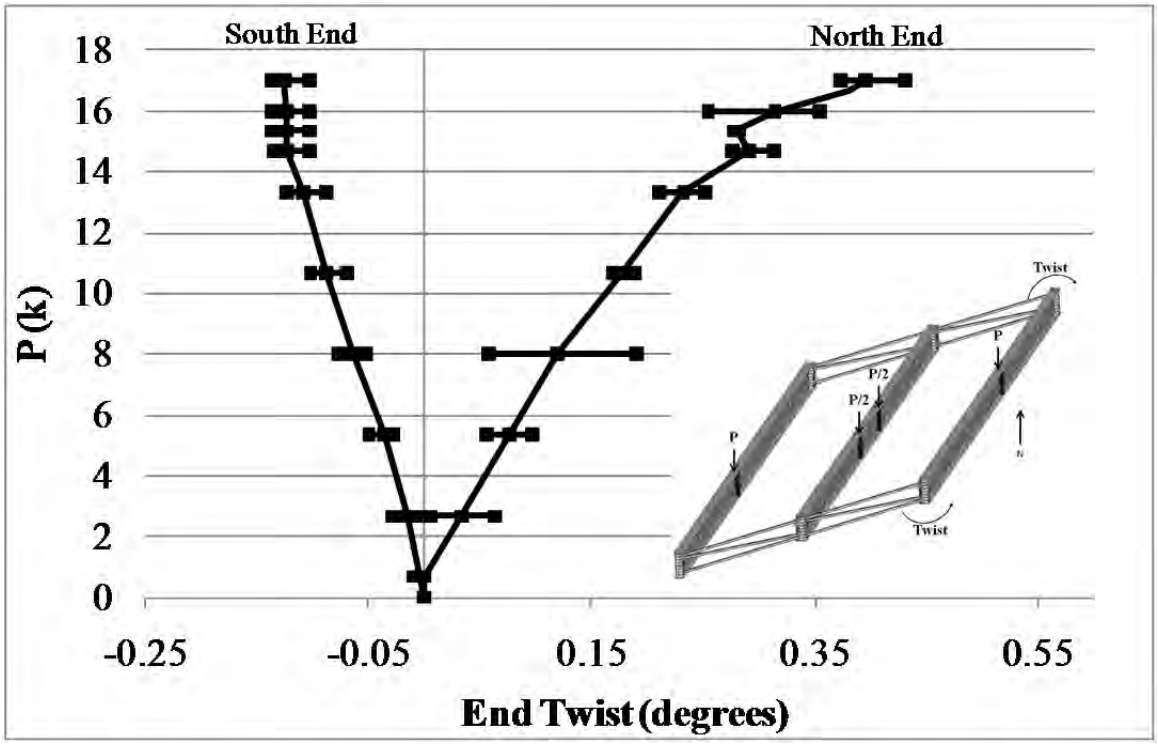

Figure A.43: GSP1 end twists

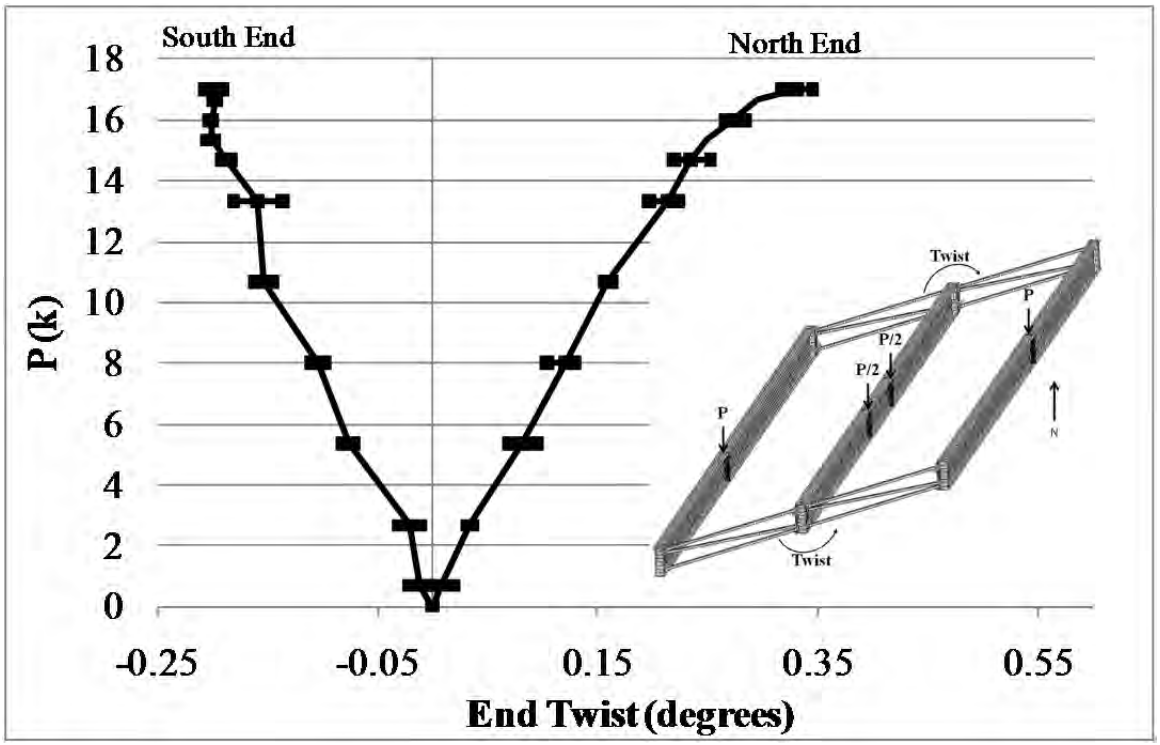

Figure A.44: GSP2 end twists

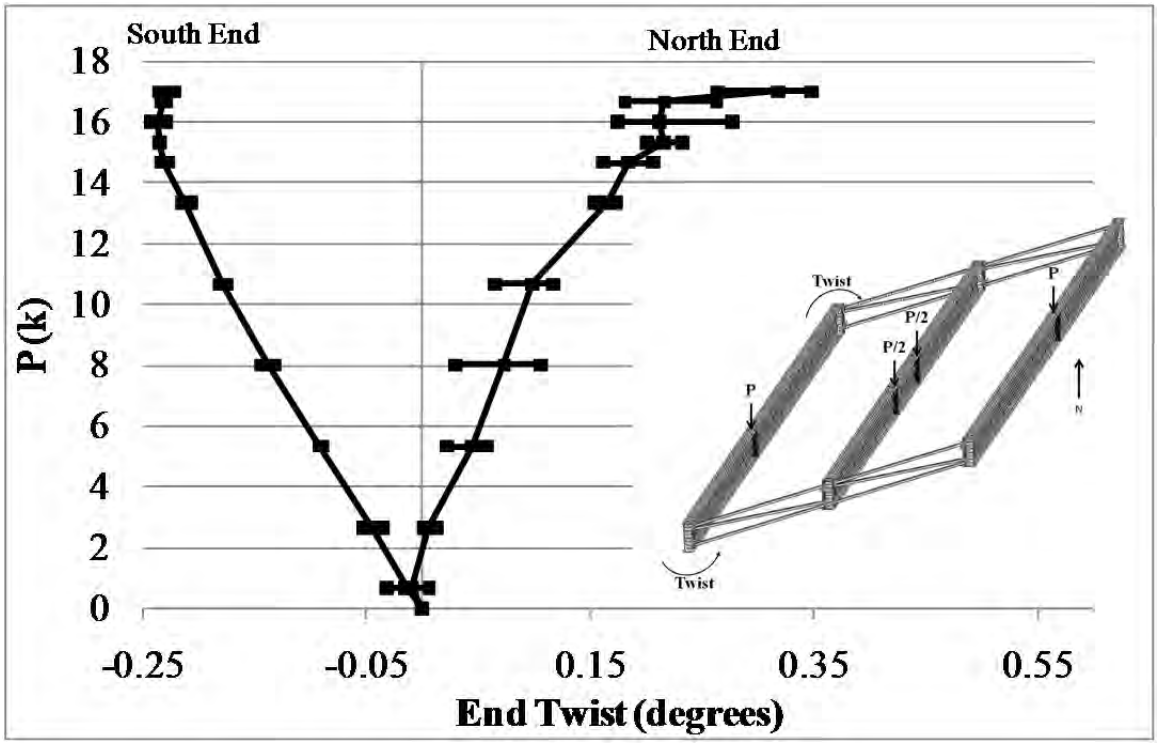

Figure A.45: GSP3 end twists

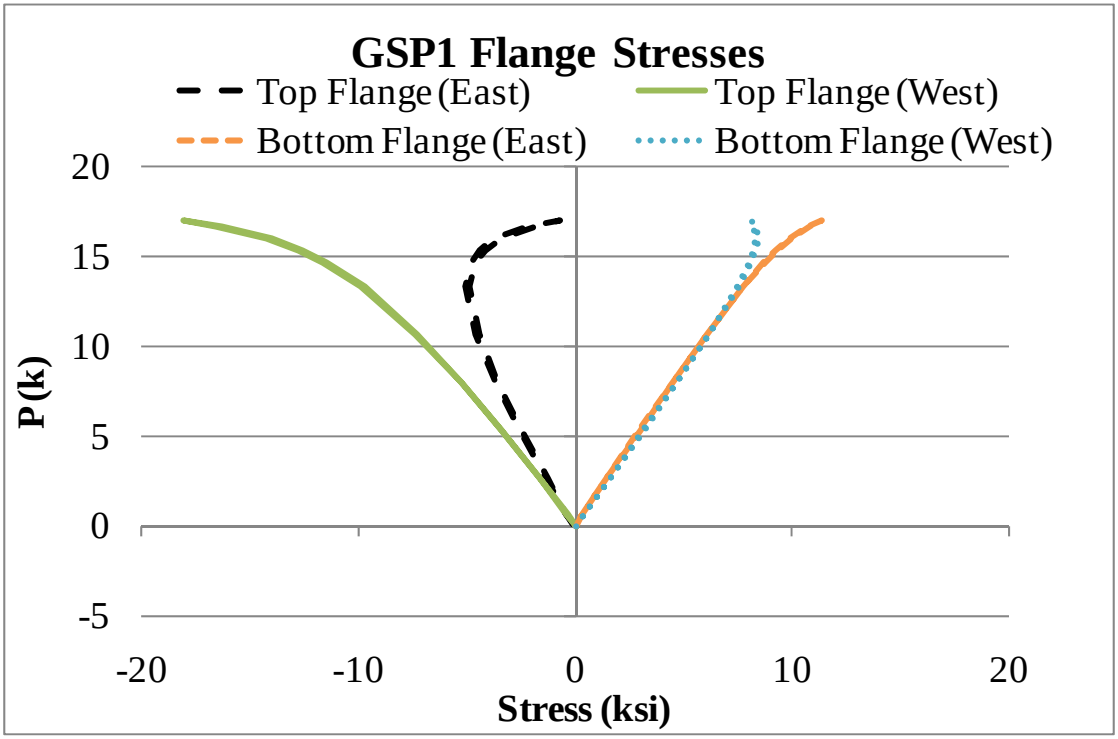

Figure A.46: GSP1mid-span flange stresses

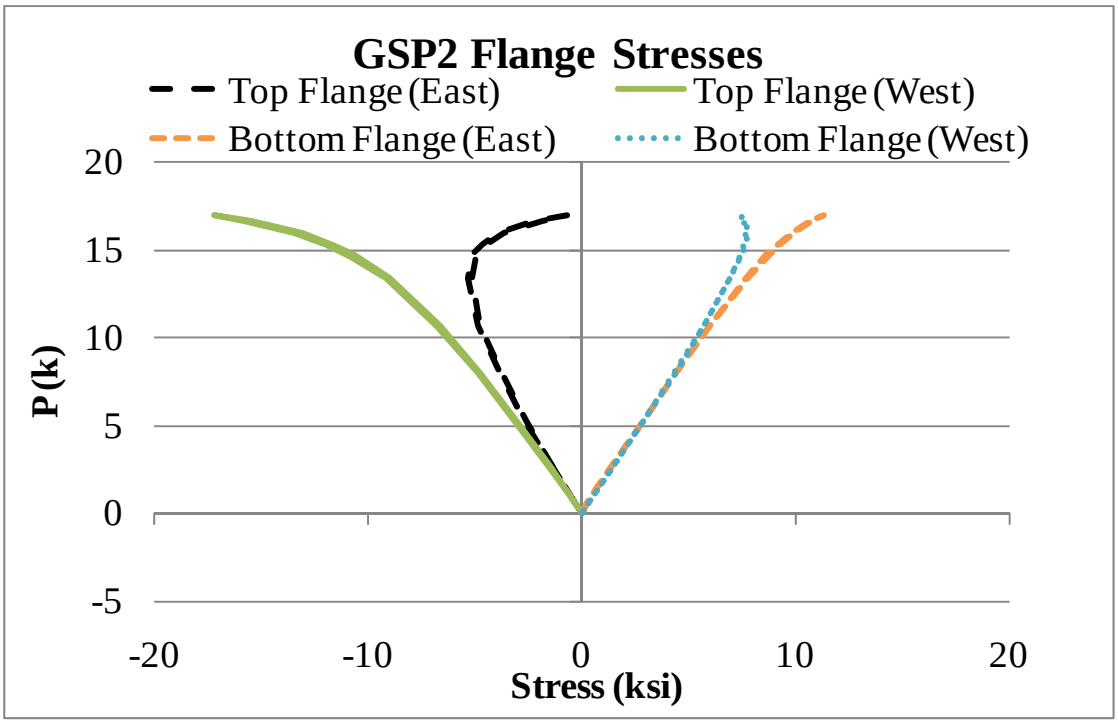

Figure A.47: GSP2 mid-span flange stresses

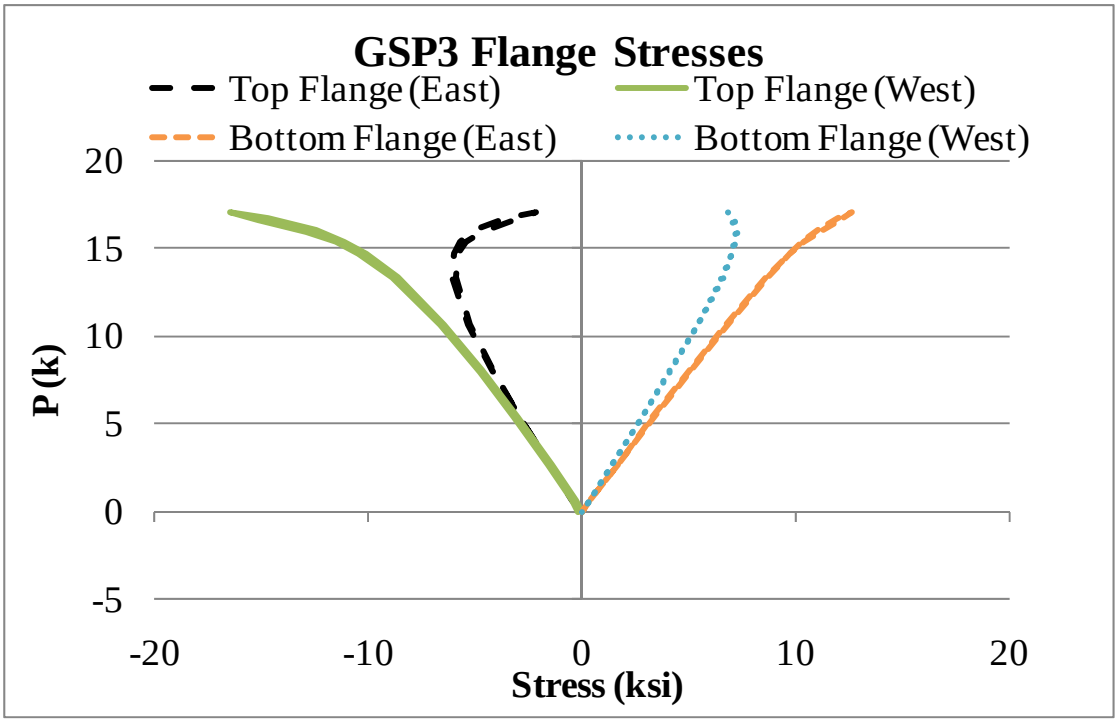

Figure A.48: GSP3 mid-span flange stresses

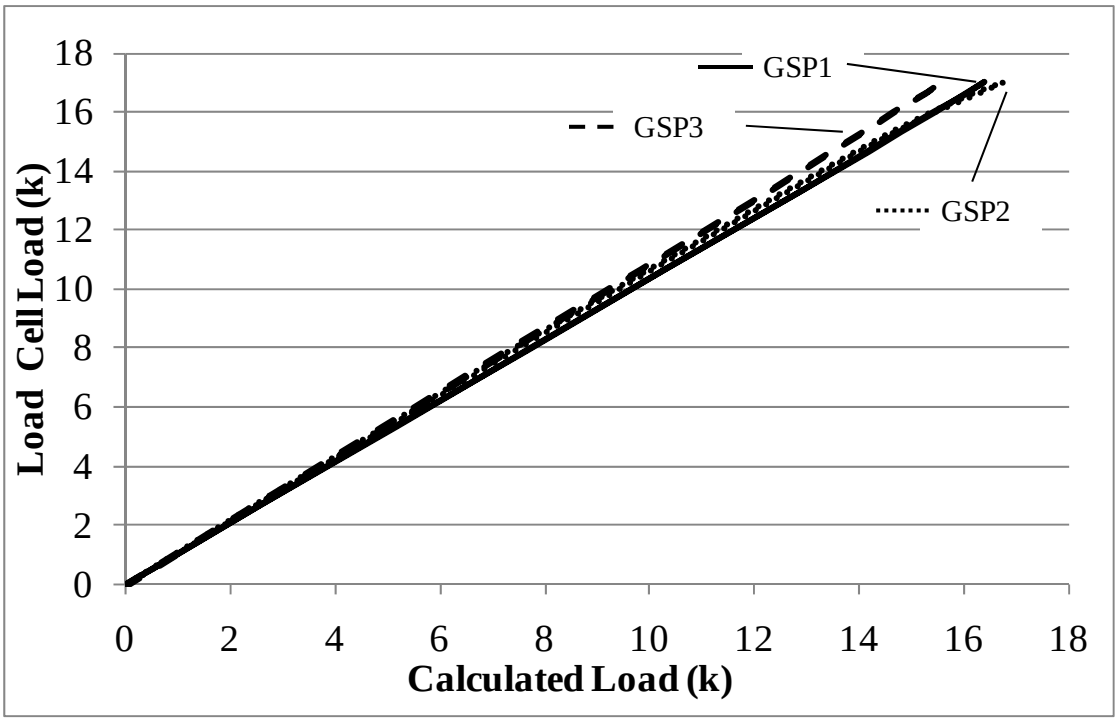

Figure A.49: Calculated girder loads from flange stresses

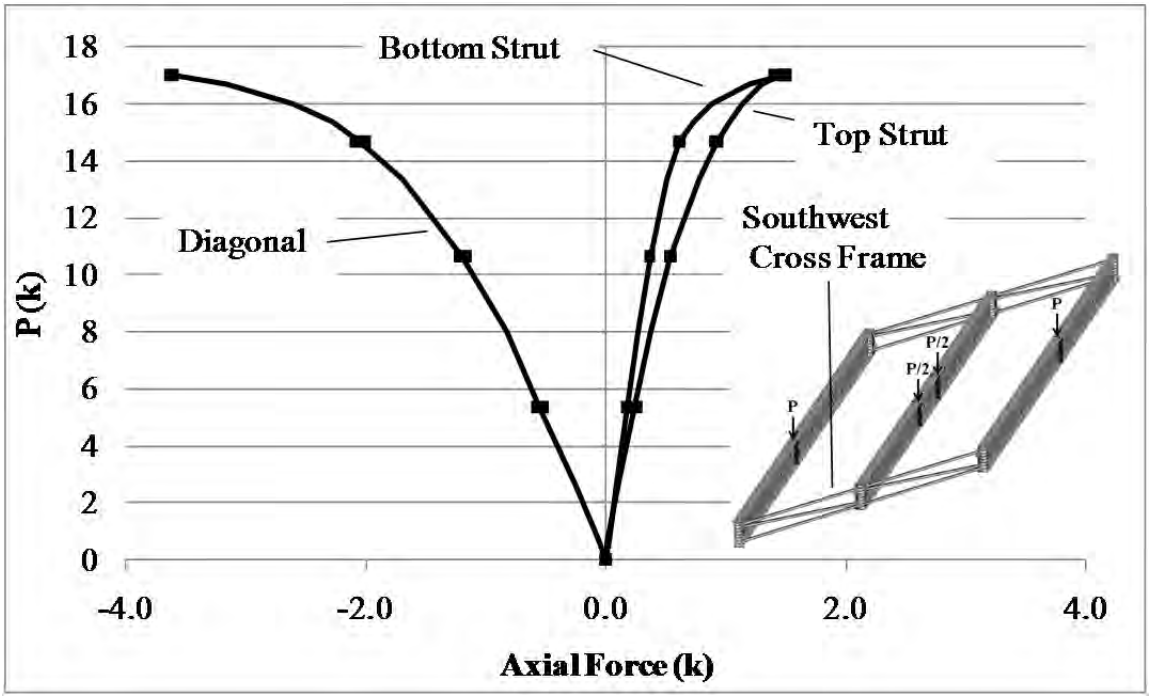

Figure A.50: Southwest cross frame axial brace forces

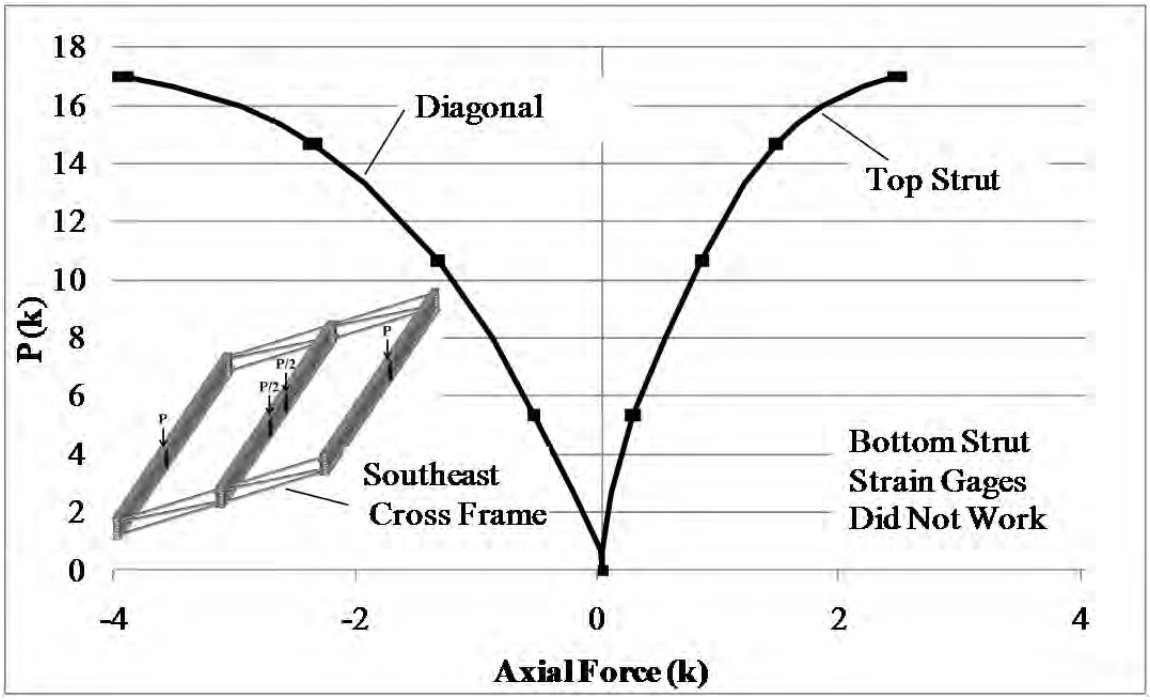

Figure A.51: Southeast cross frame axial brace forces

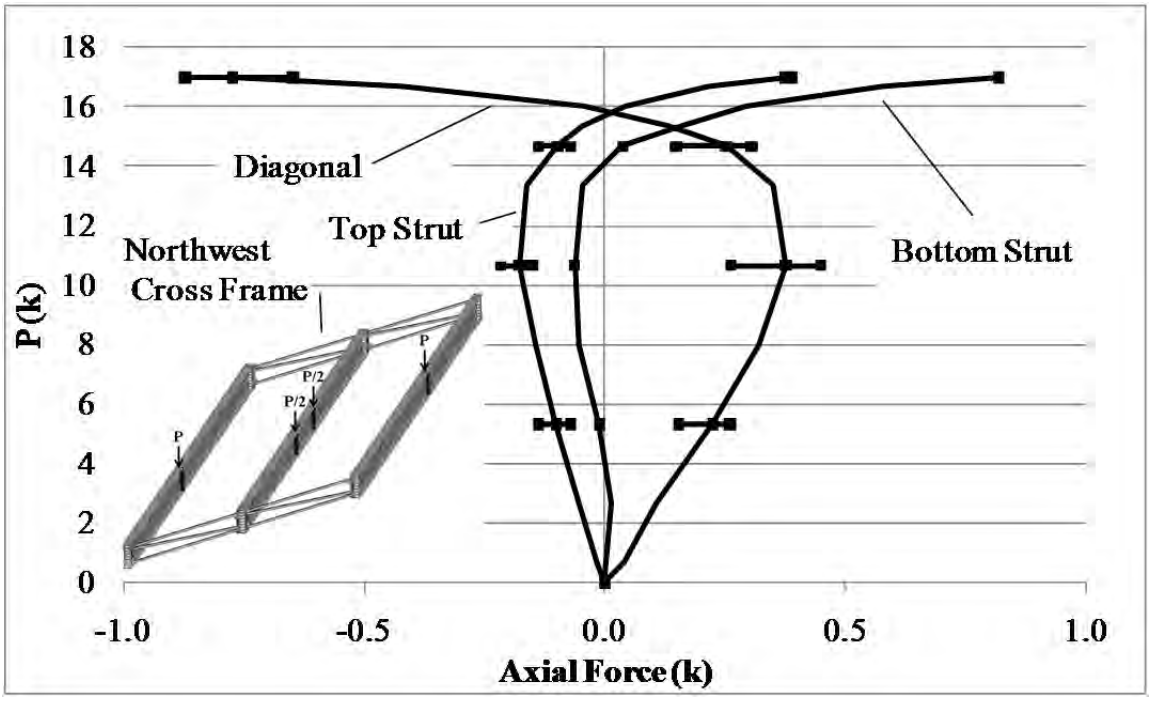

Figure A.52: Northwest cross frame axial brace forces

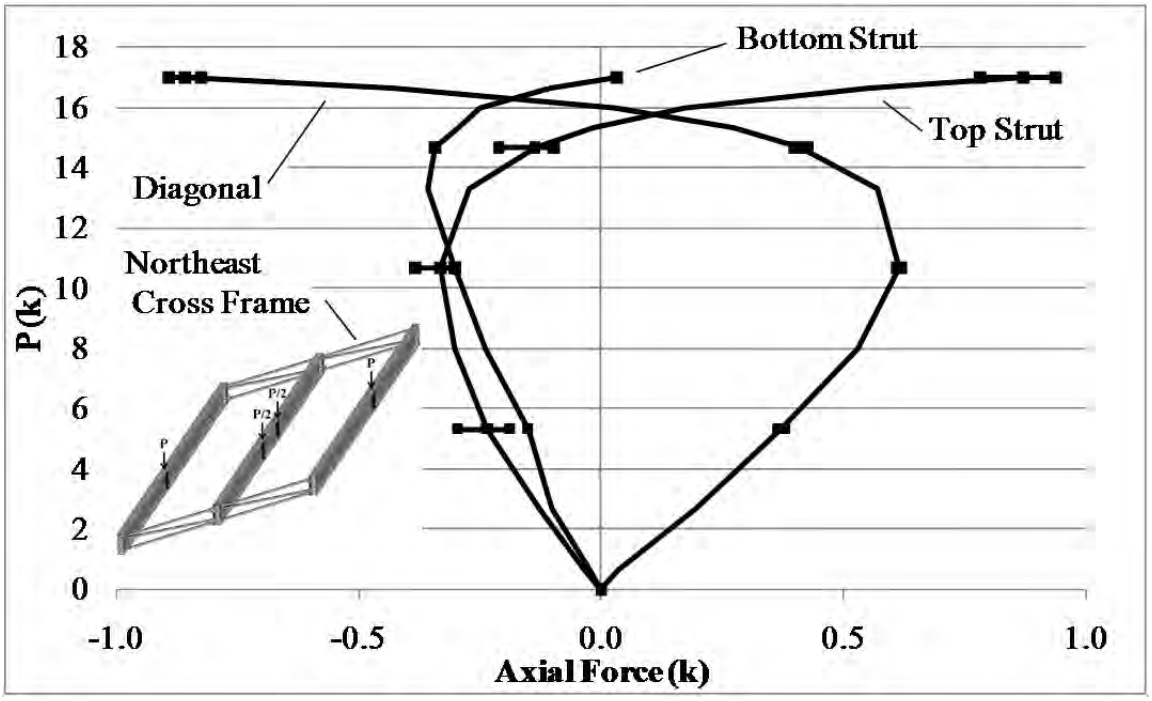

Figure A.53: Northeast cross frame axial brace forces

A.3.2 Thrust Washer Bearing with Staggered Intermediate Cross Frames

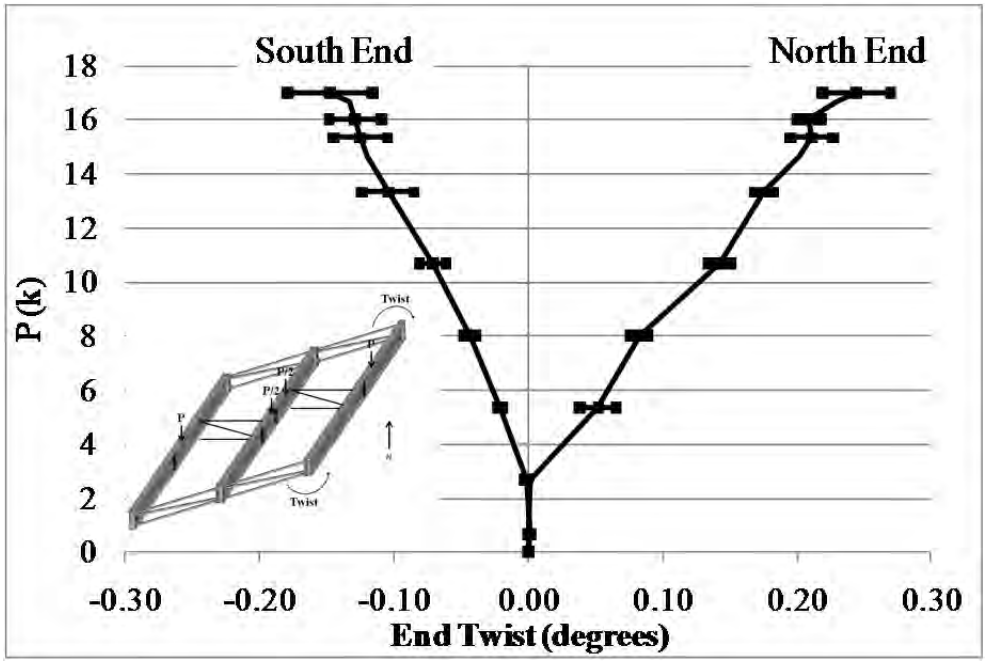

Figure A.54: GSP1 end twist

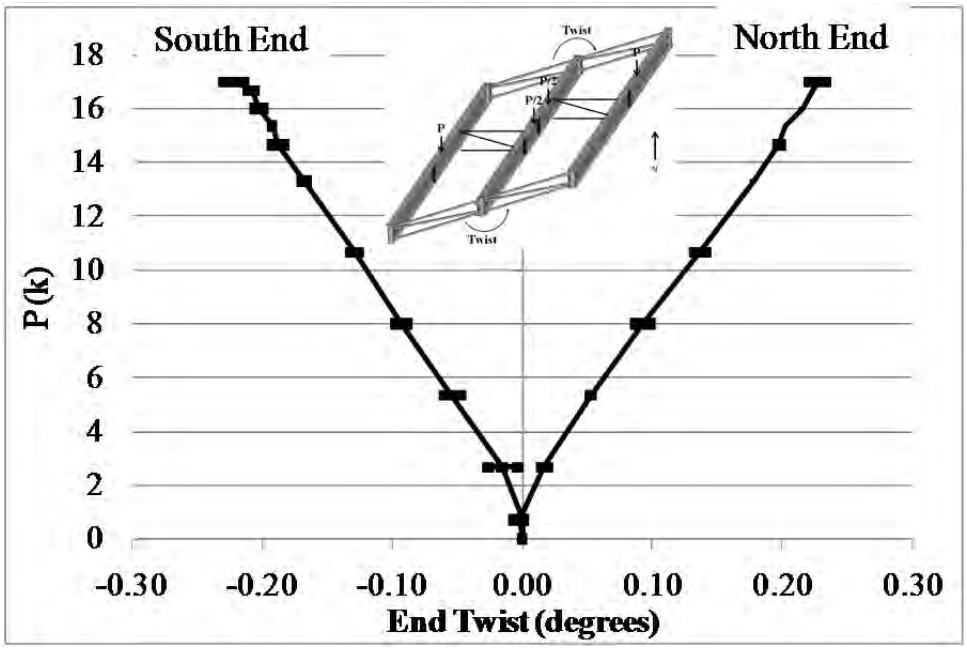

Figure A.55: GSP2 end twist

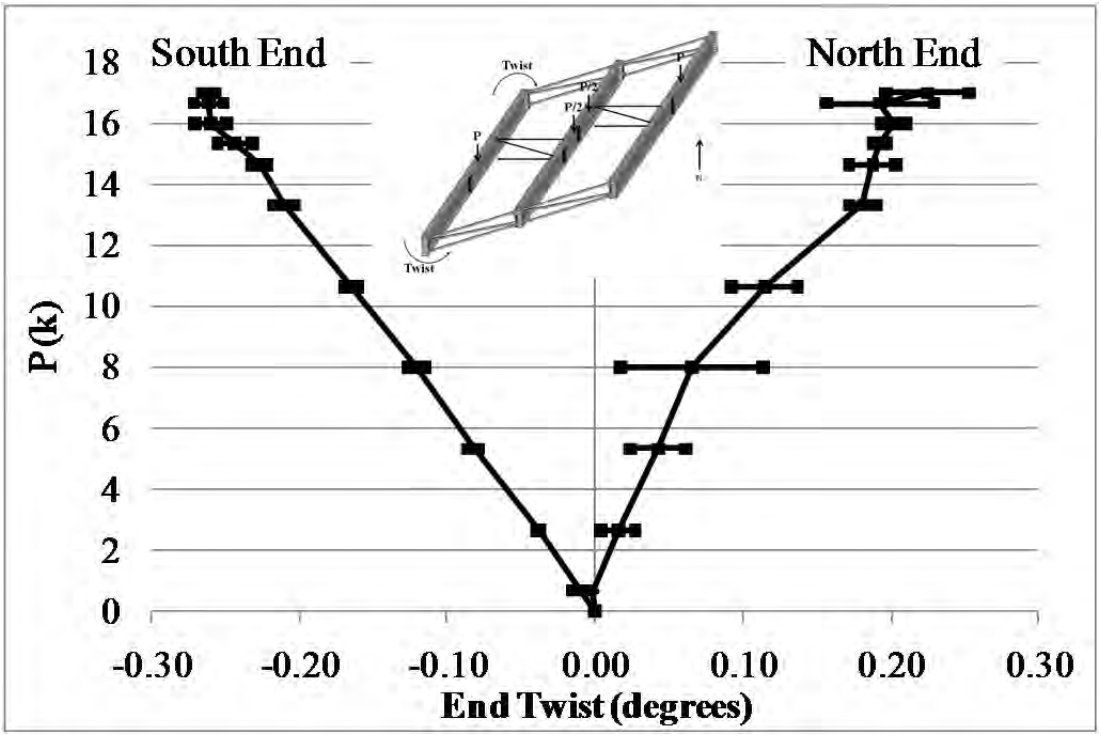

Figure A.56: GSP3 end twist

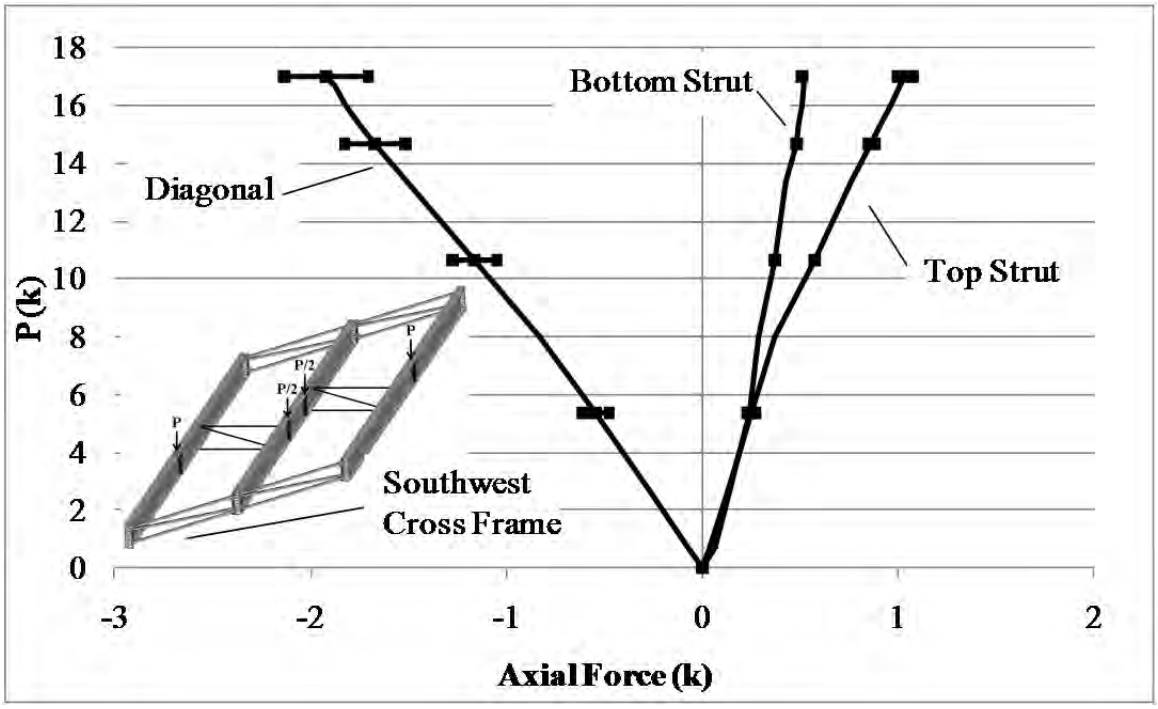

Figure A.57:SW end cross frame axial forces

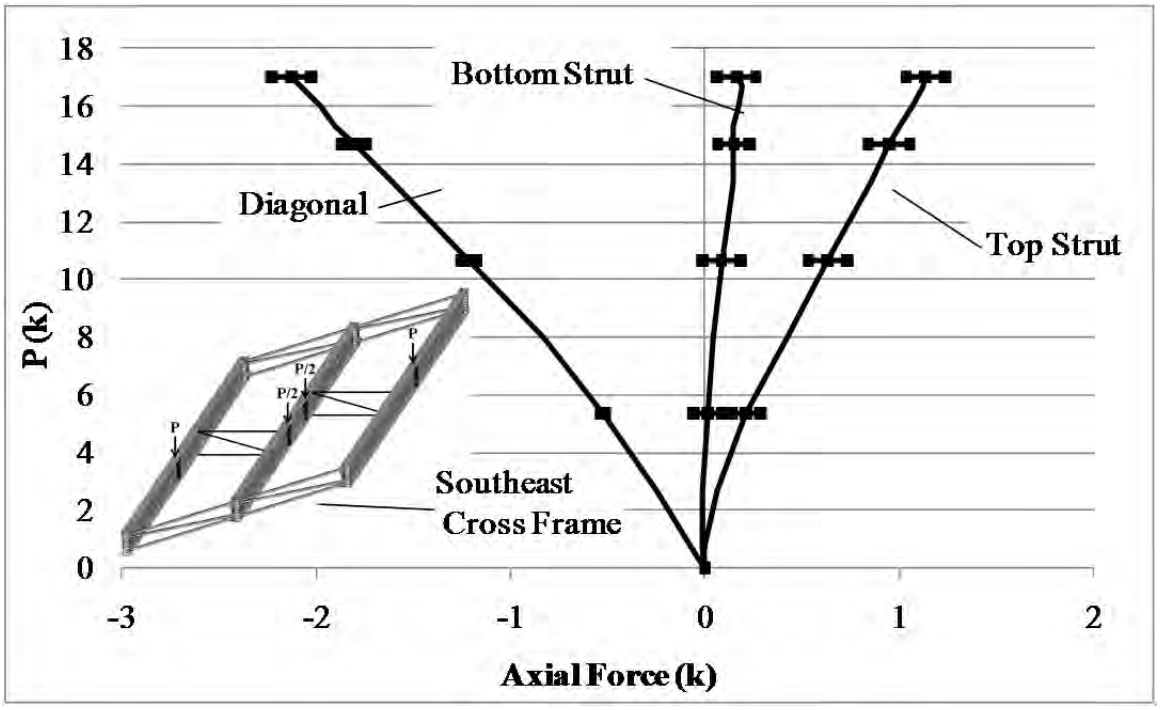

Figure A.58: SE end cross frame axial forces

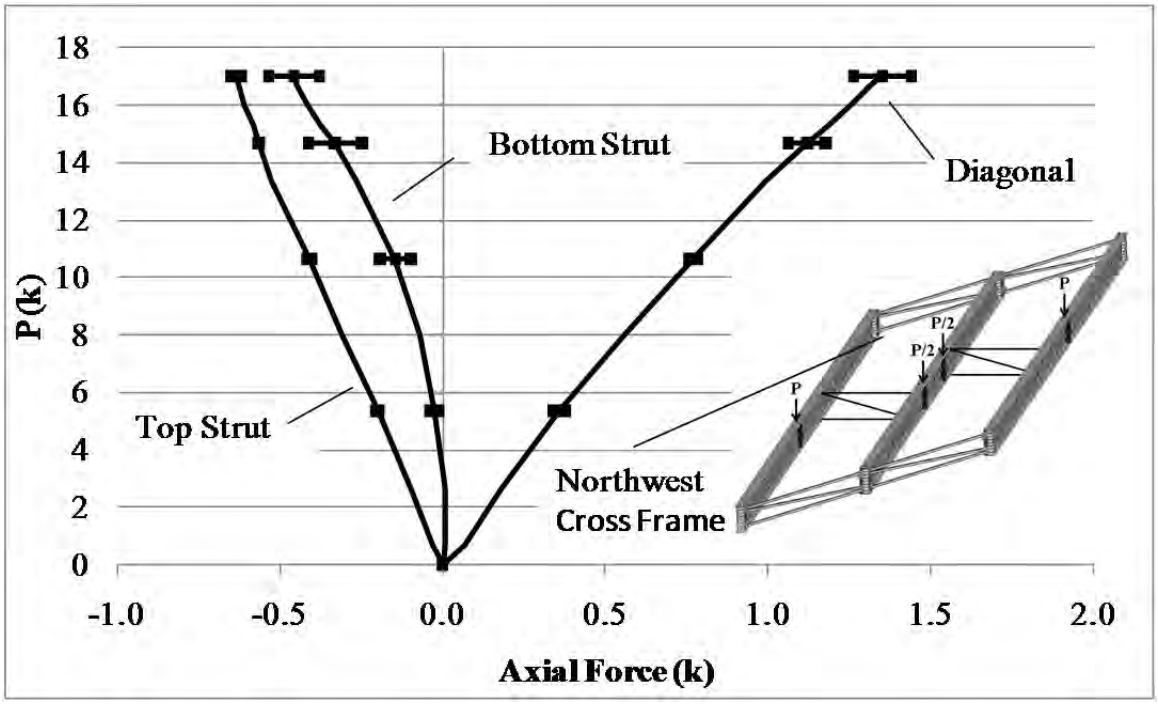

Figure A.59: NW end cross frame axial forces

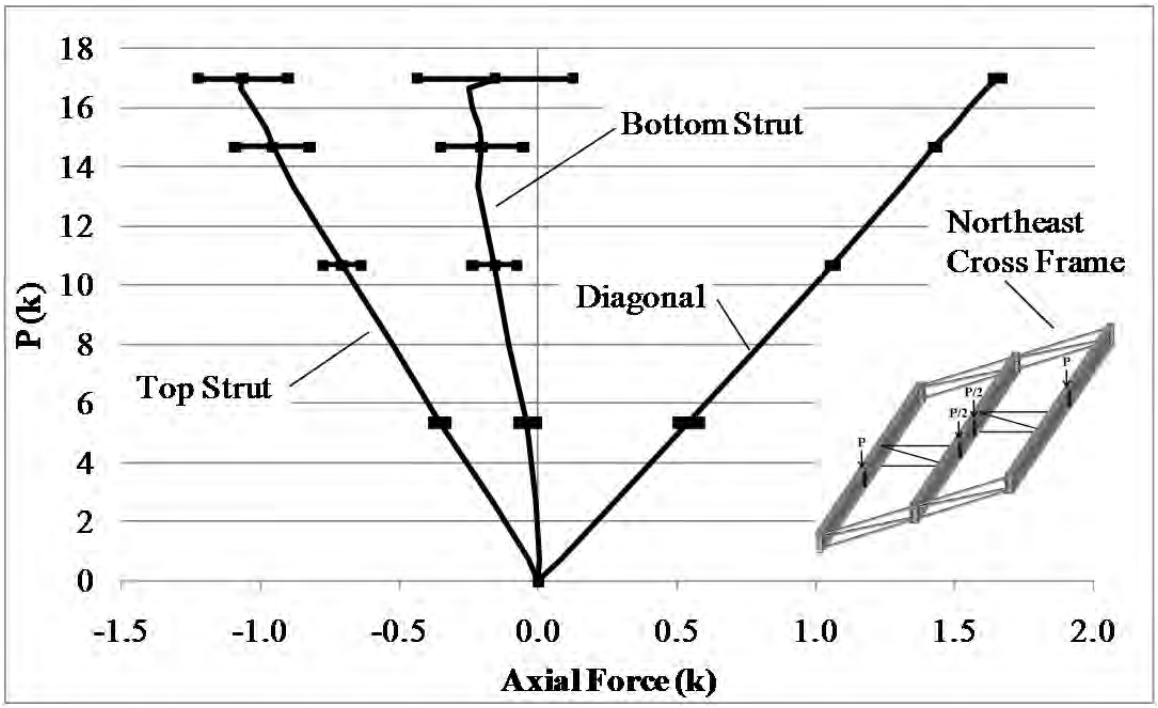

Figure A.60: NE end cross frame axial forces

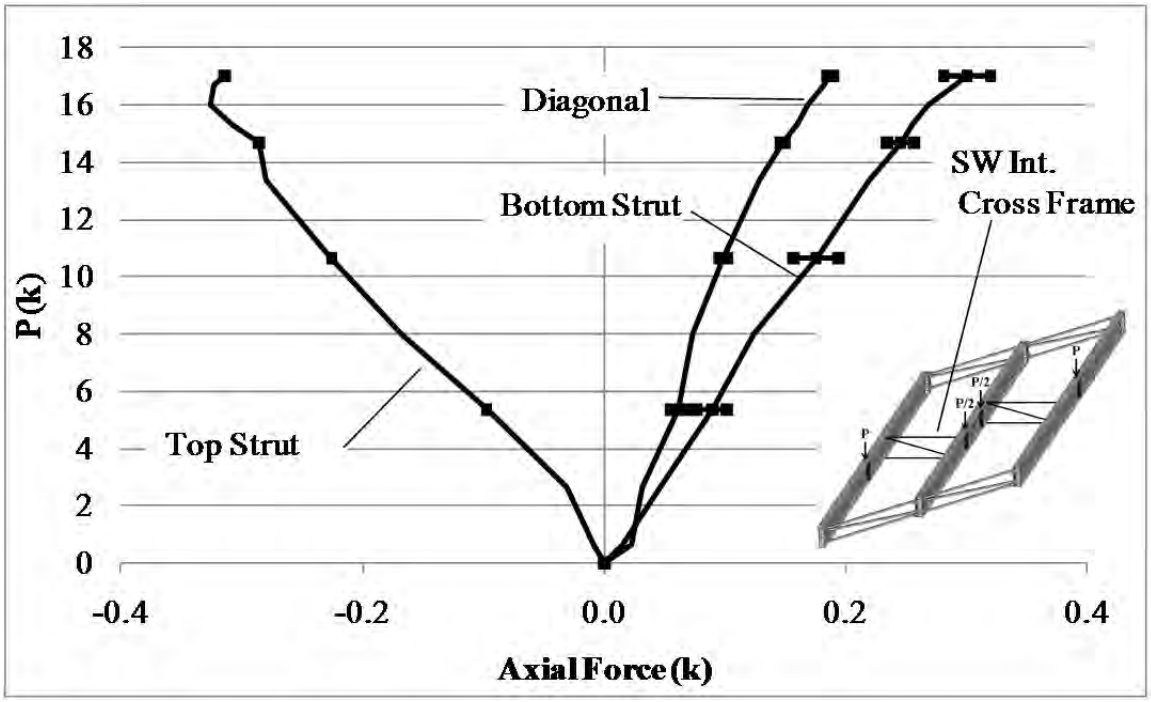

Figure A.61: SW intermediate staggered cross frame axial forces

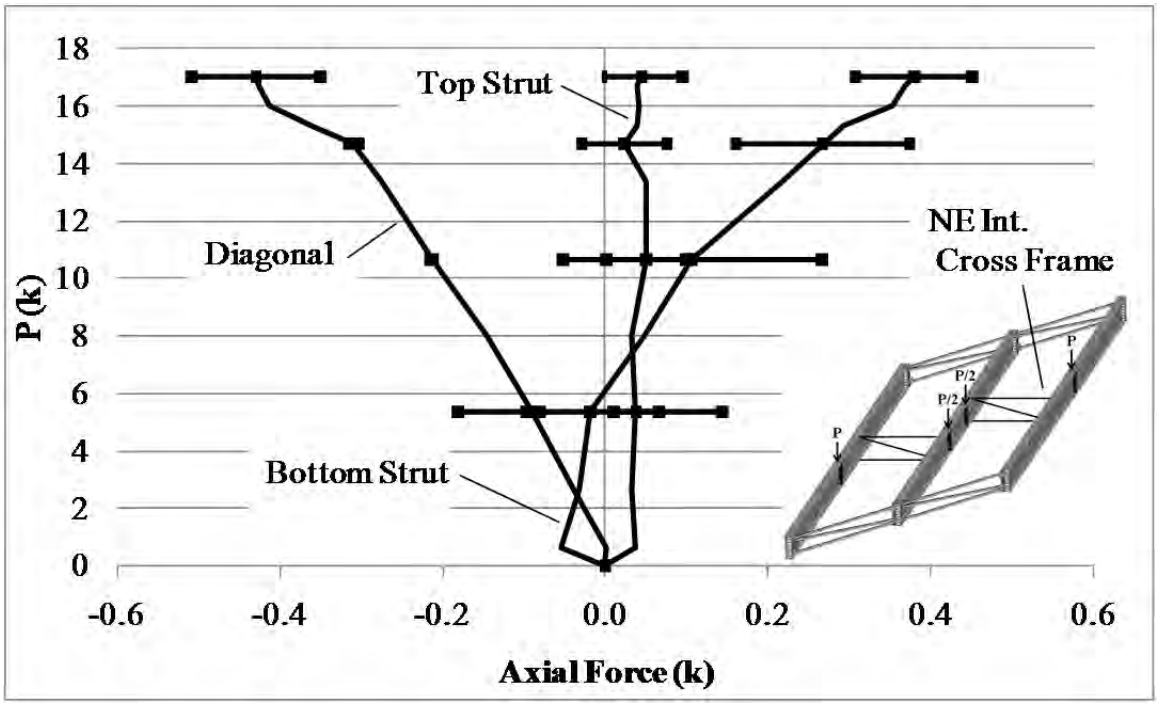

Figure A.62: NE intermediate staggered cross frame axial forces

A.3.3 Thrust Washer Bearing with Continuous Intermediate Cross Frames

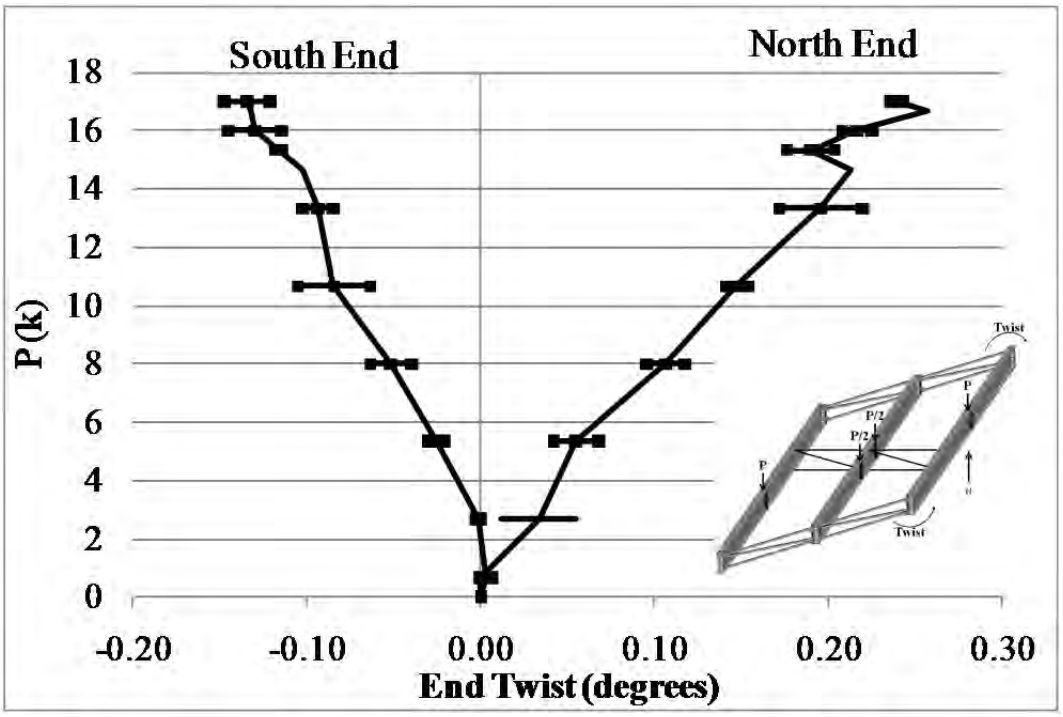

Figure A.63: GSP1 end twist

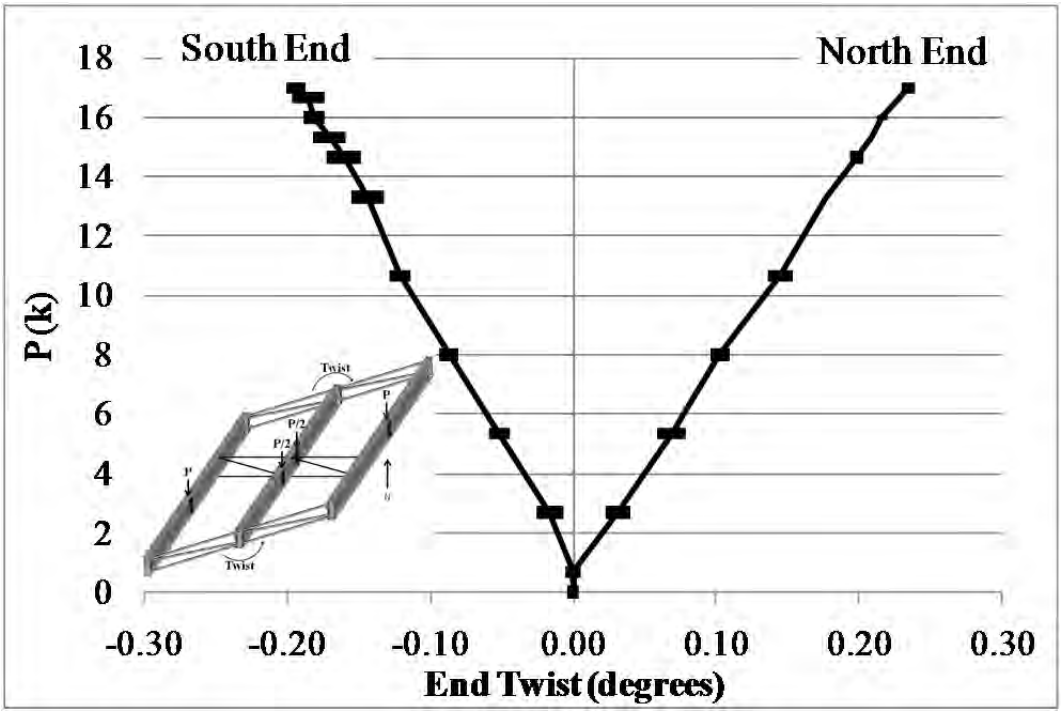

Figure A.64: GSP2 end twist

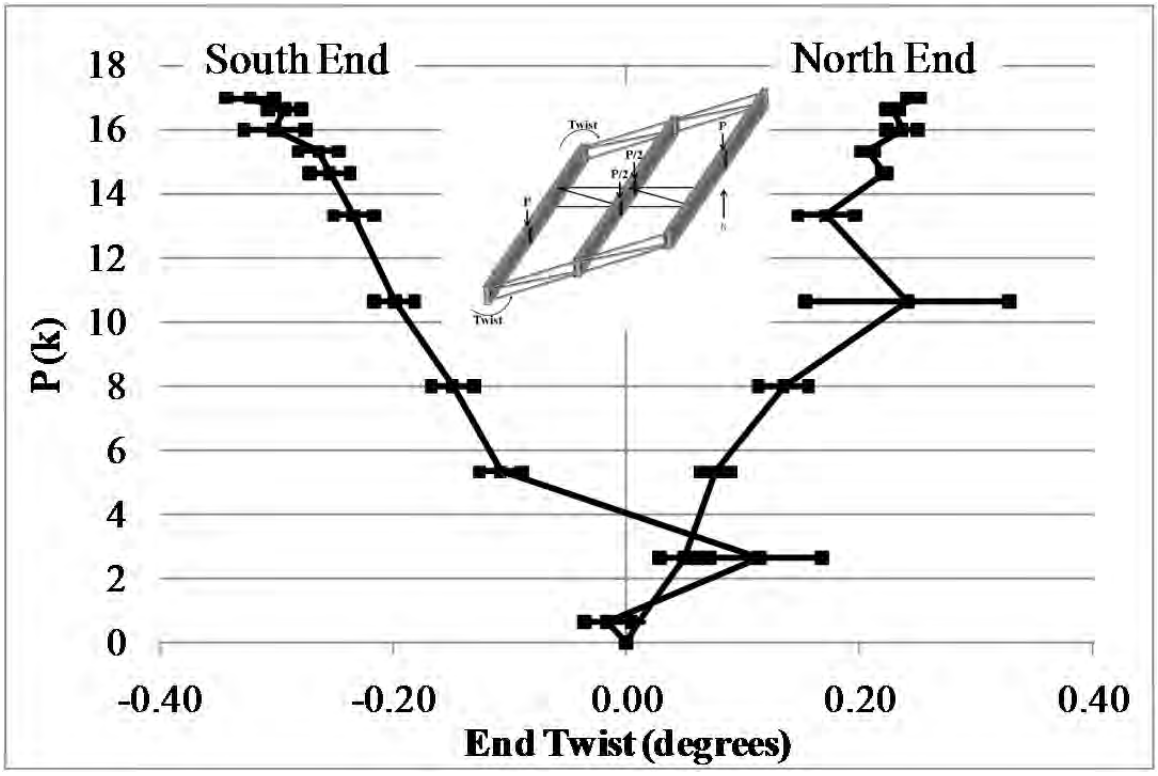

Figure A.65: GSP3 end twist

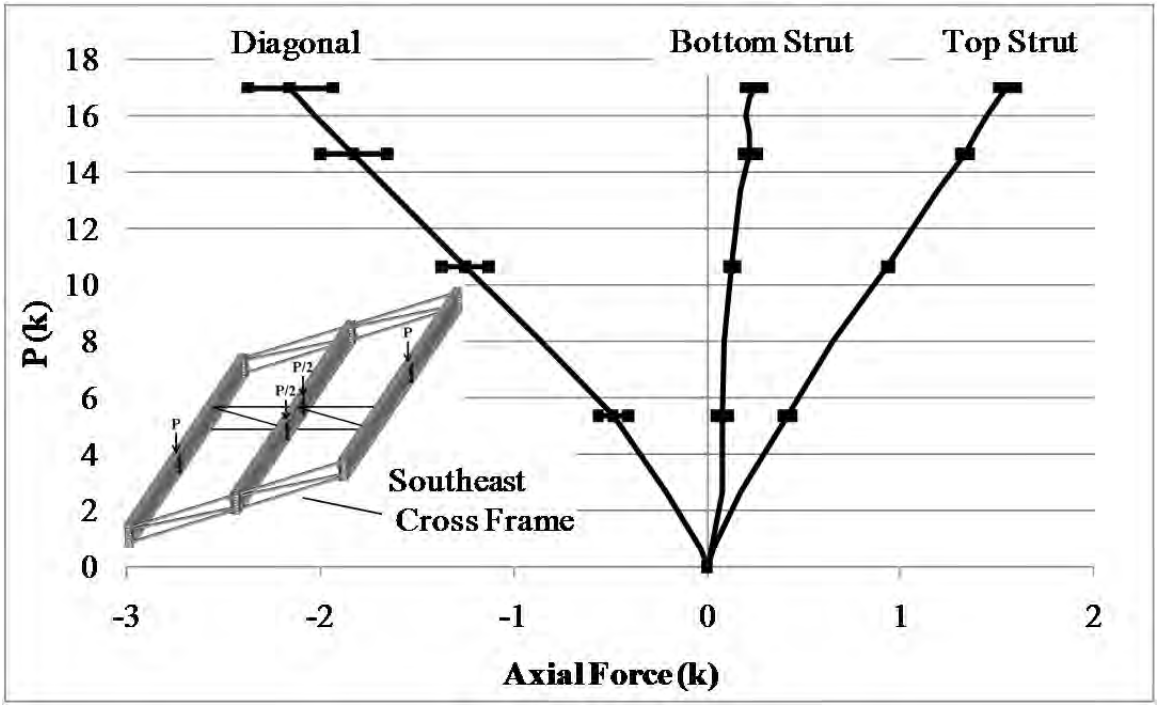

Figure A.66: SE end cross frame axial forces

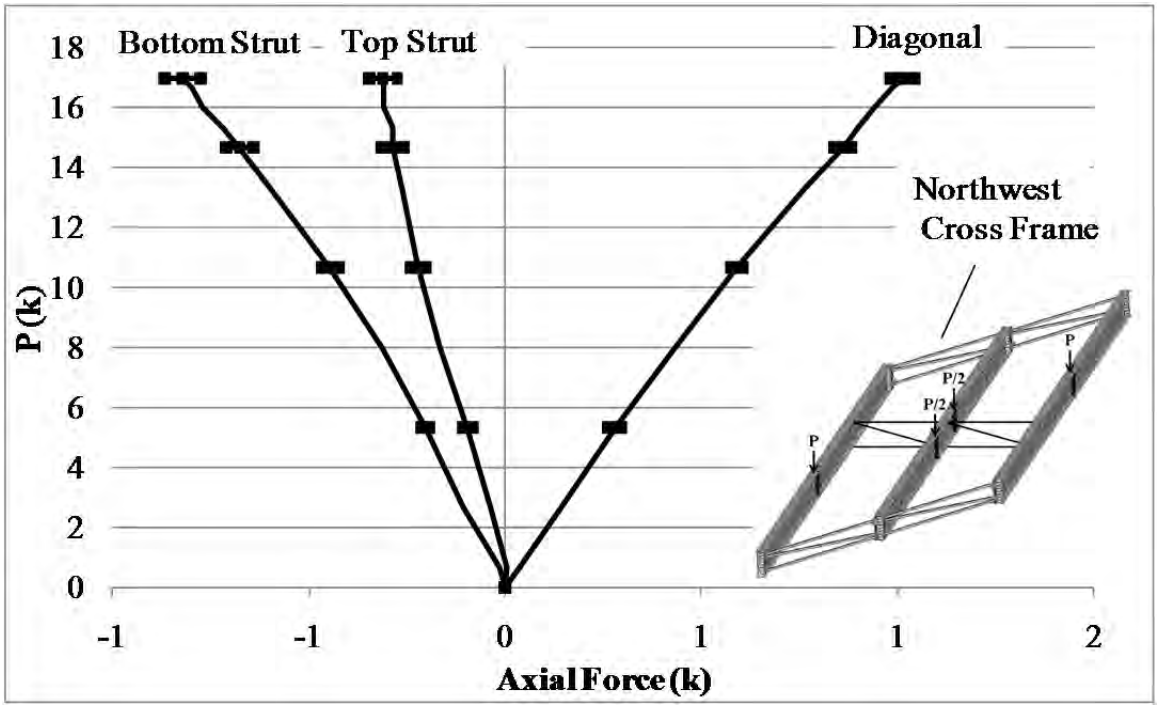

Figure A.67: NW end cross frame axial forces

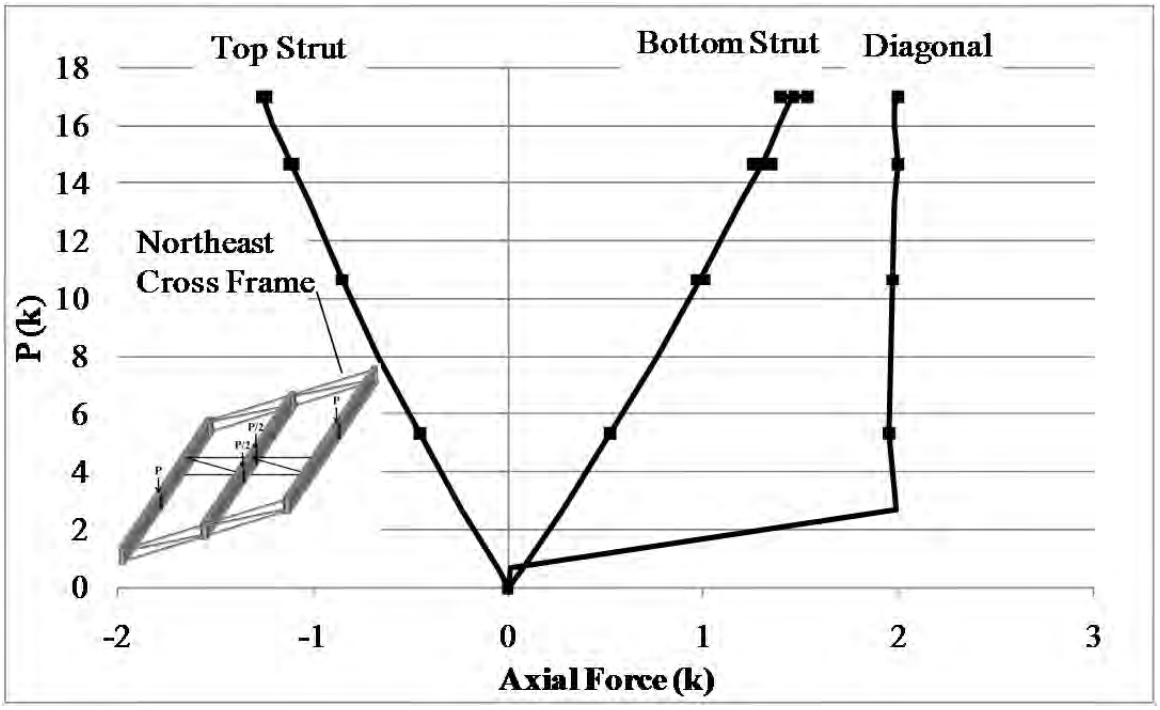

Figure A.68: NE end cross frame axial forces

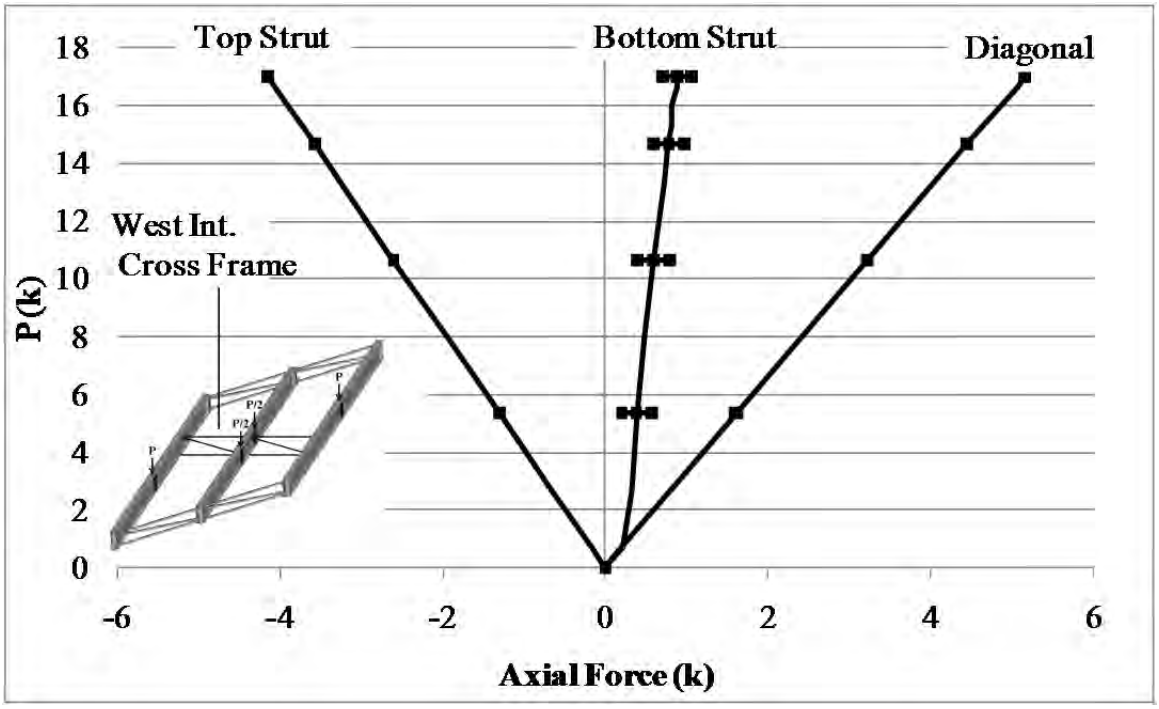

Figure A.69: West intermediate cross frame axial forces

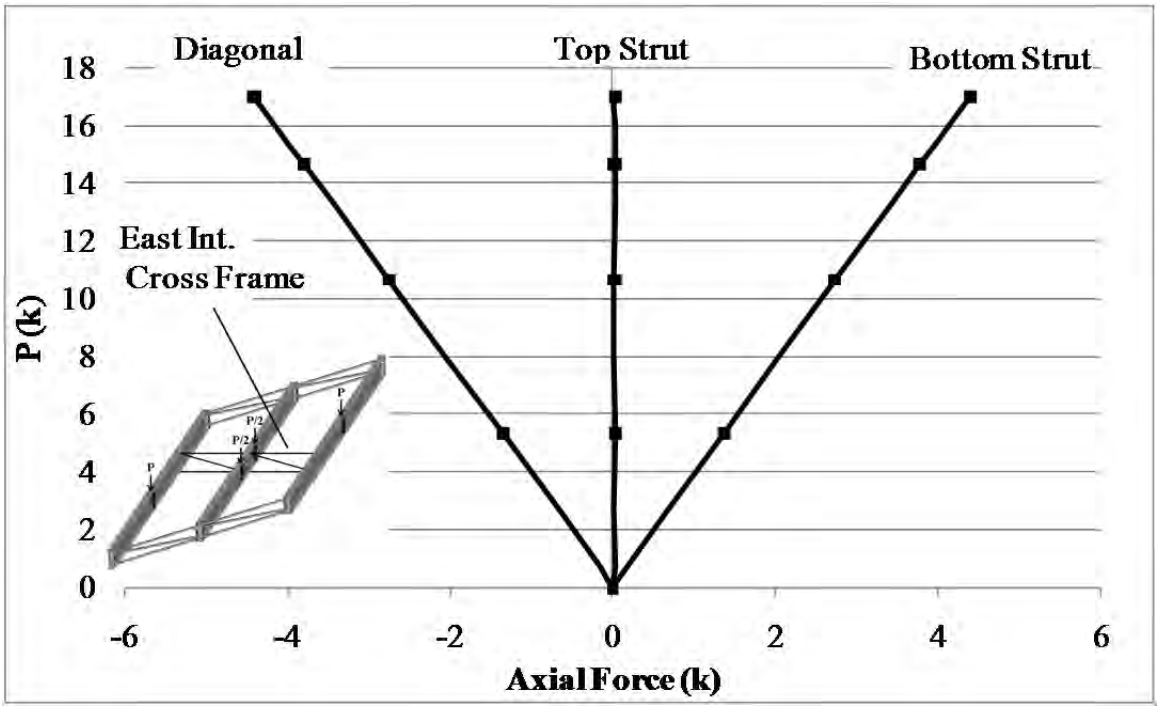

Figure A.70: East intermediate cross frame axial forces

A.3.4 Rubber Bearing with No Intermediate Cross Frames

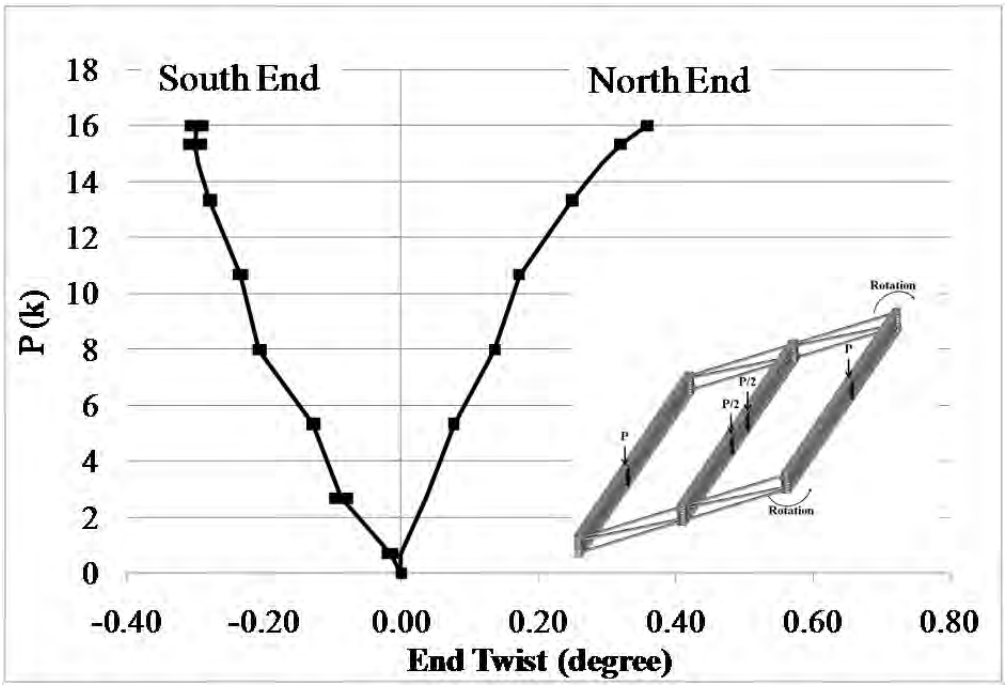

Figure A.71: GBP1 end twists

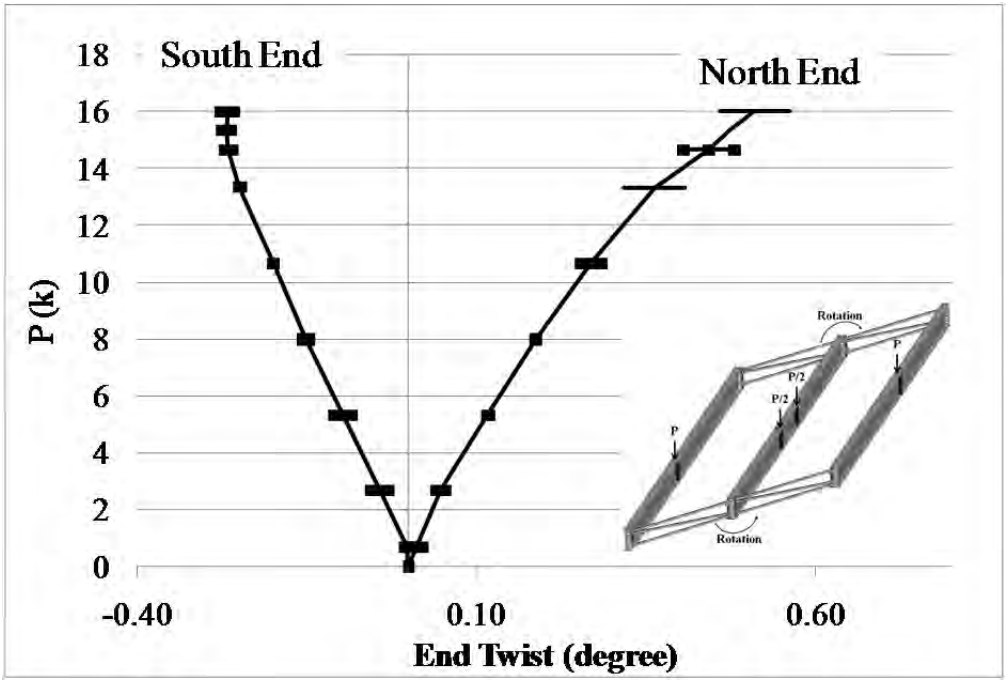

Figure A.72: GBP2 end twists

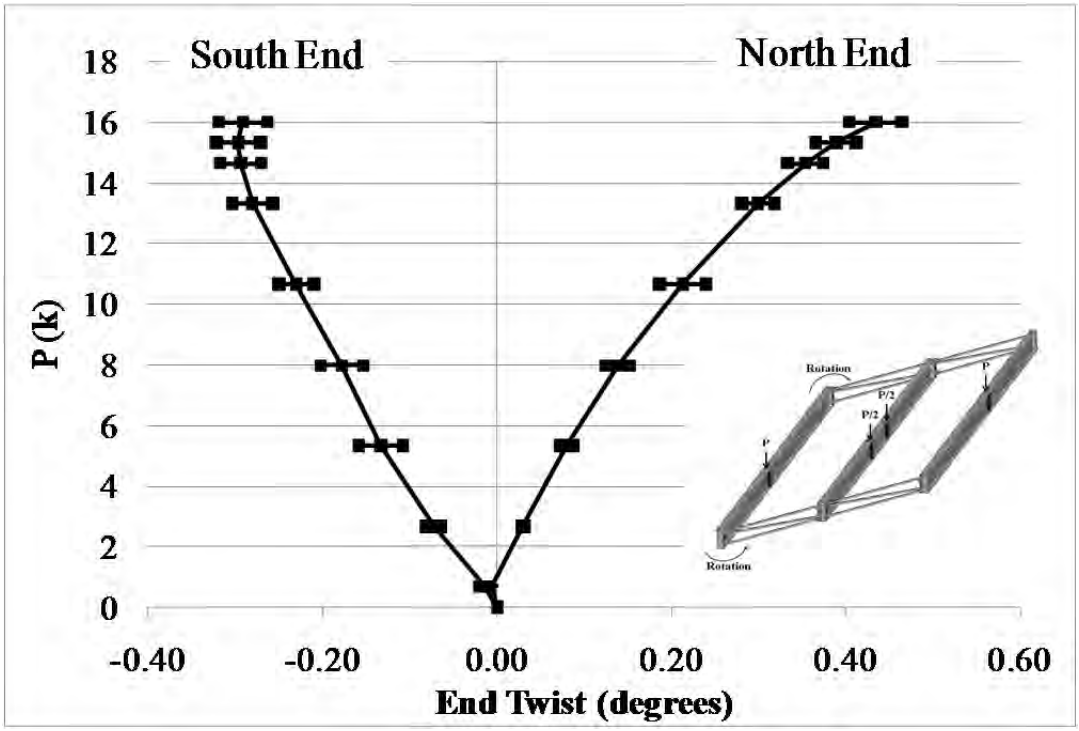

Figure A.73: GBP3 end twists

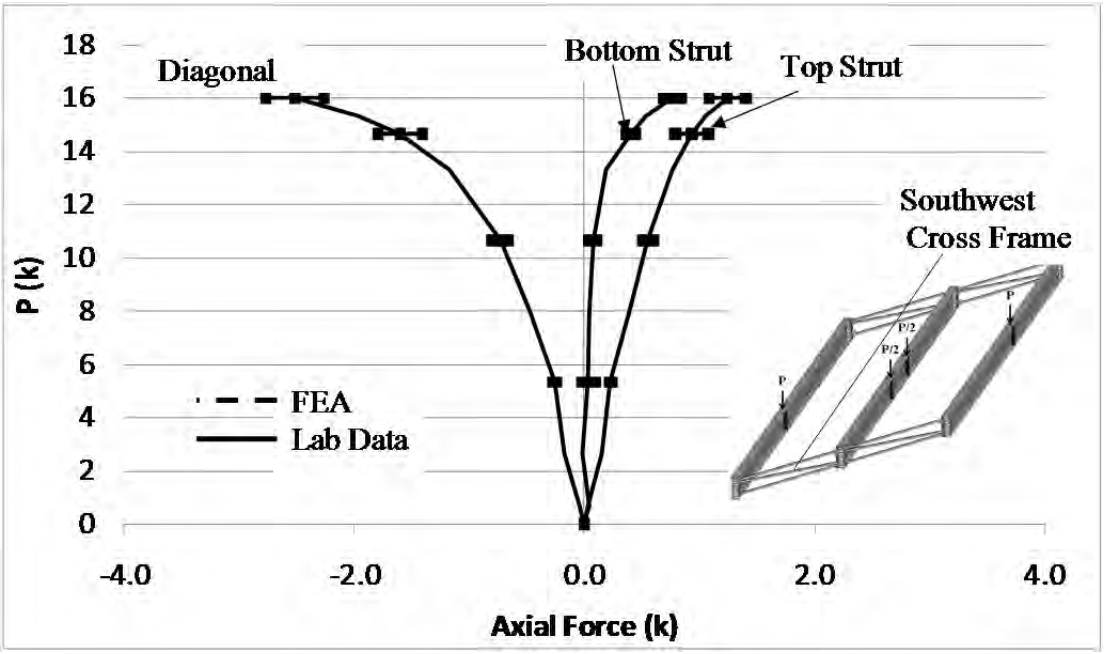

Figure A.74: SW end cross frame axial forces

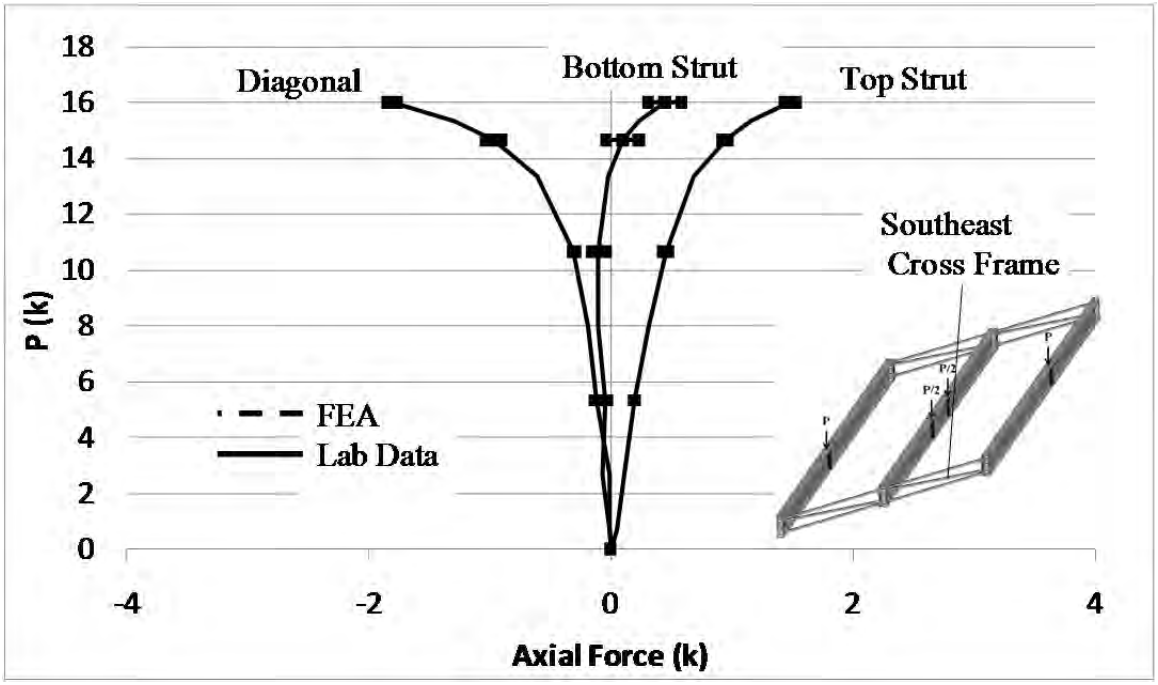

Figure A.75: SE end cross frame axial forces

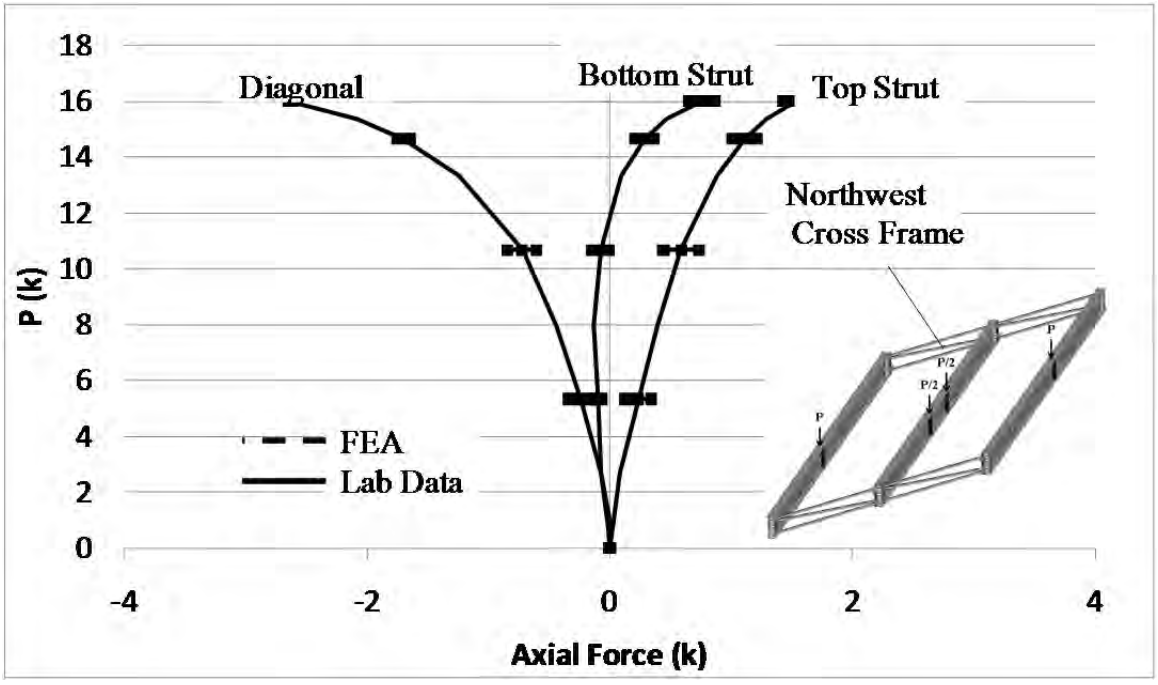

Figure A.76: NW end cross frame axial forces

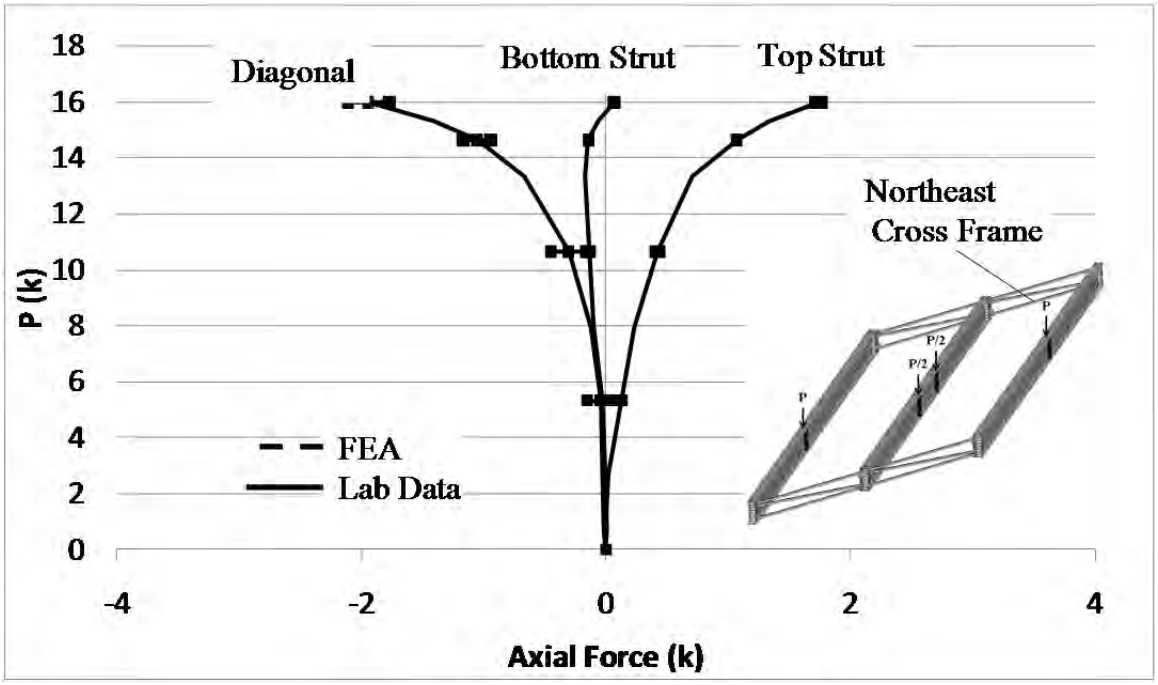

Figure A.77: NE end cross frame axial forces

A.3.5 Rubber Bearing with Shim with No Intermediate Cross Frames

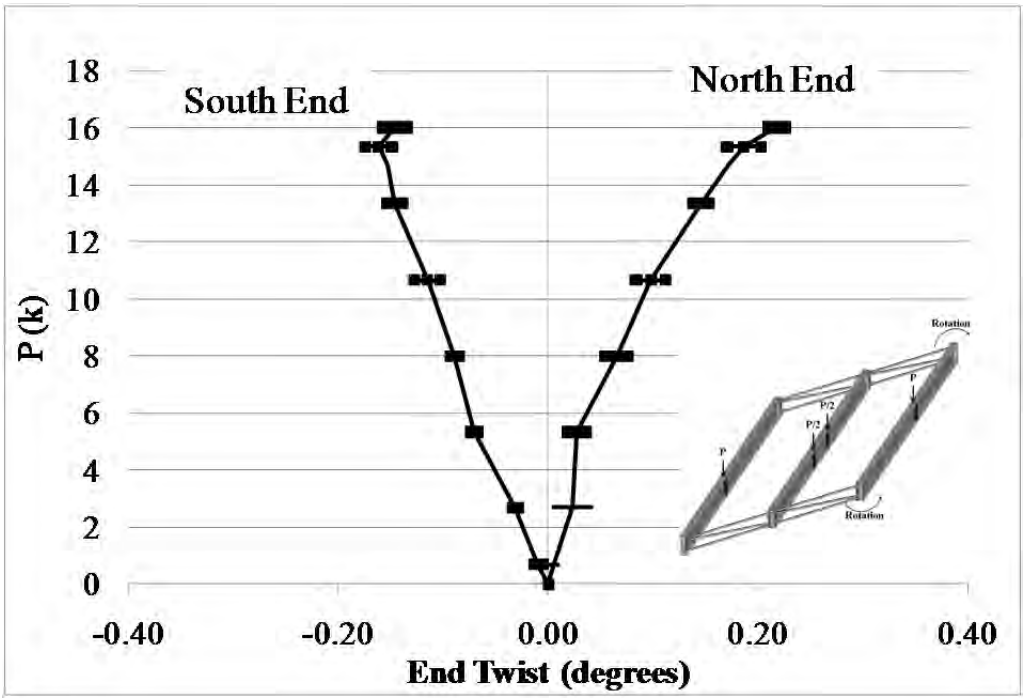

Figure A.78: GBP1 end twists

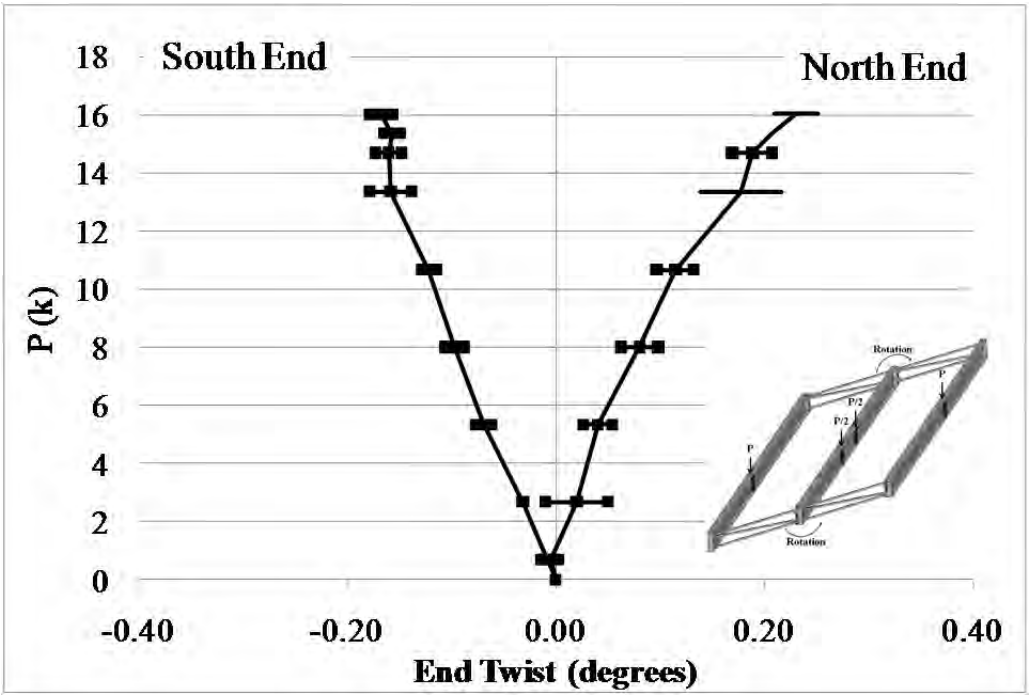

Figure A.79: GBP2 end twists

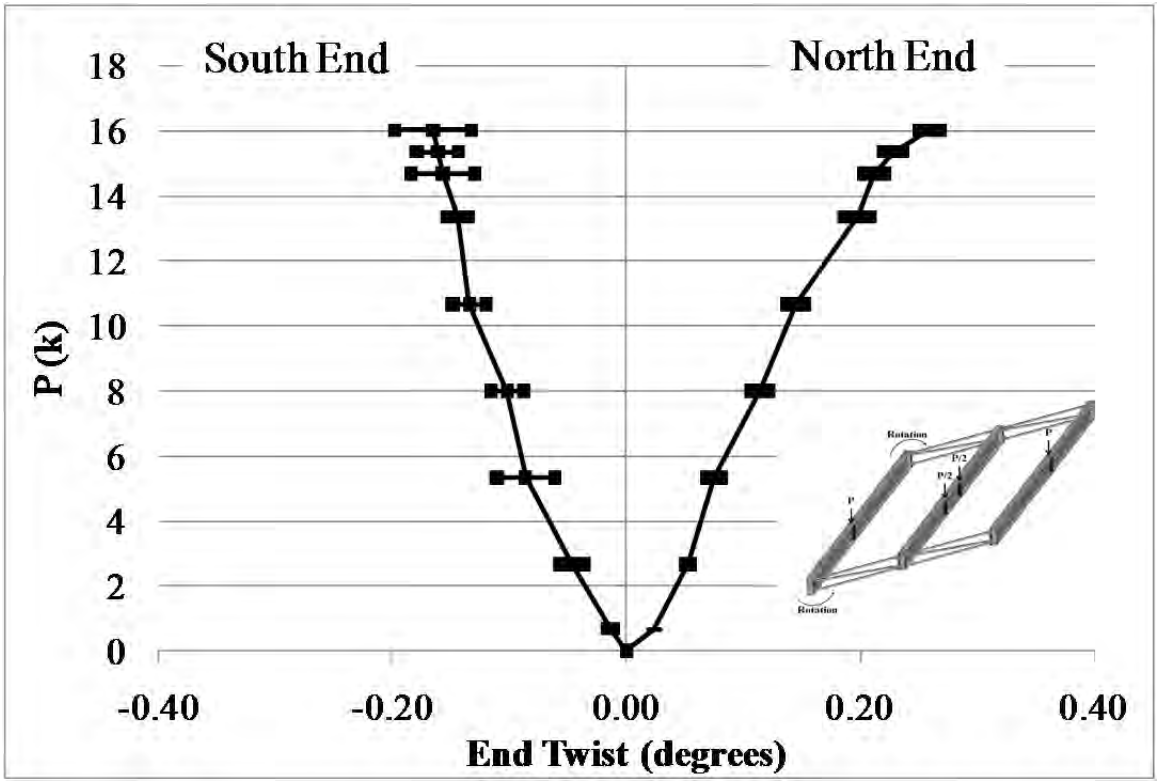

Figure A.80: GBP3 end twists

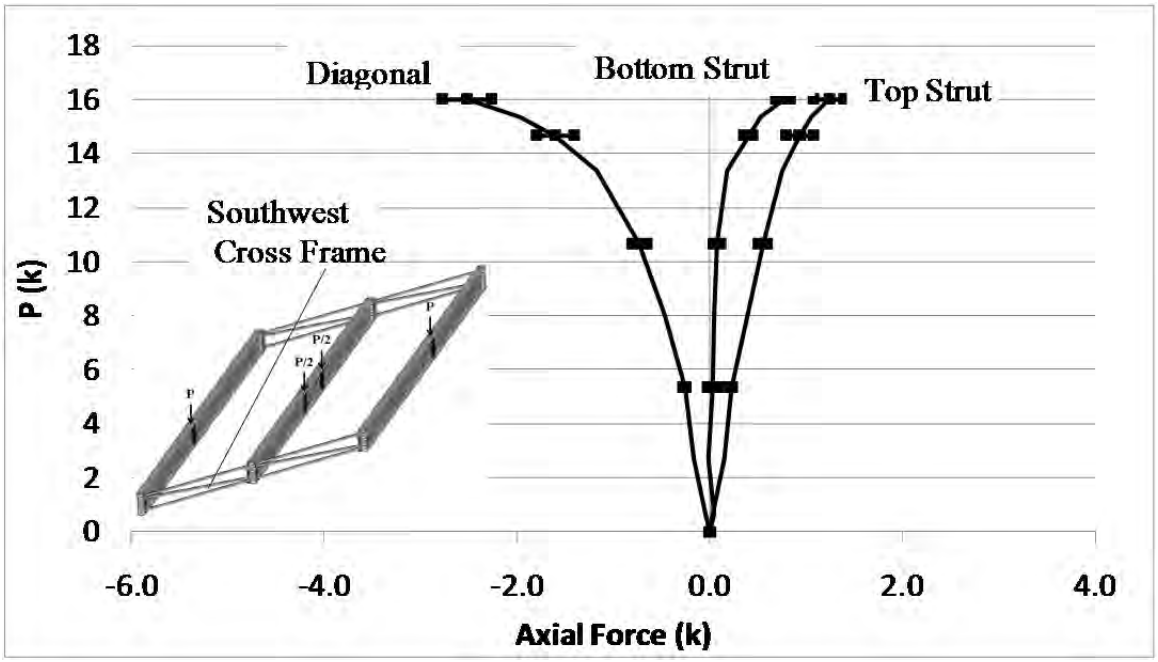

Figure A.81: SW end cross frame axial forces

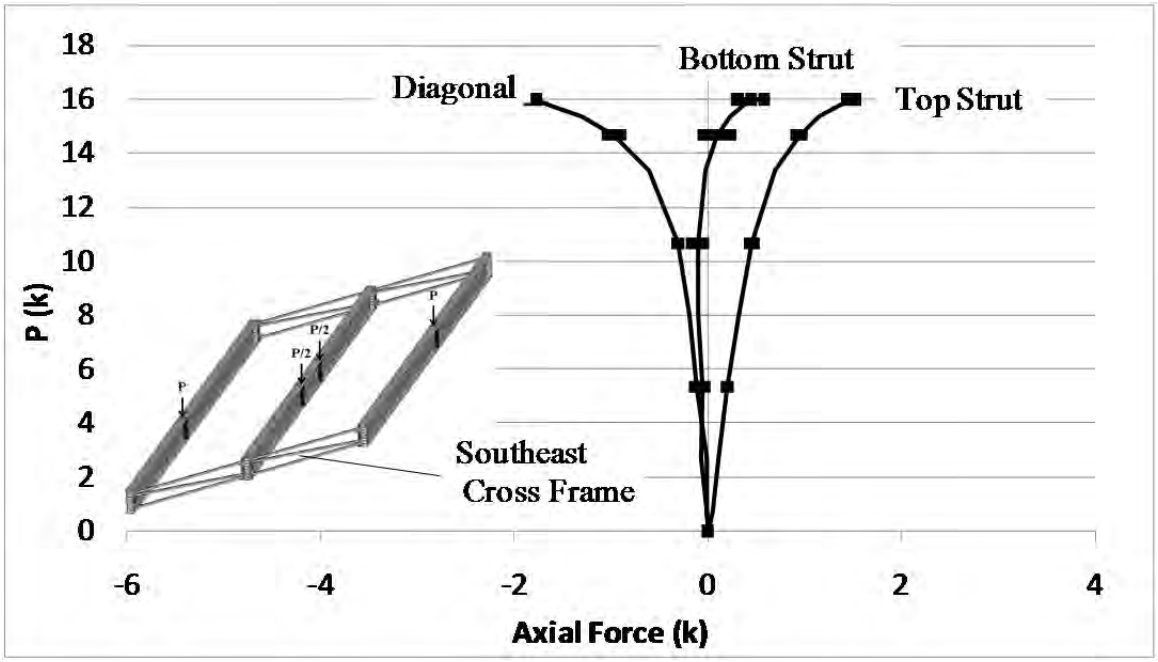

Figure A.82: SE end cross frame axial forces

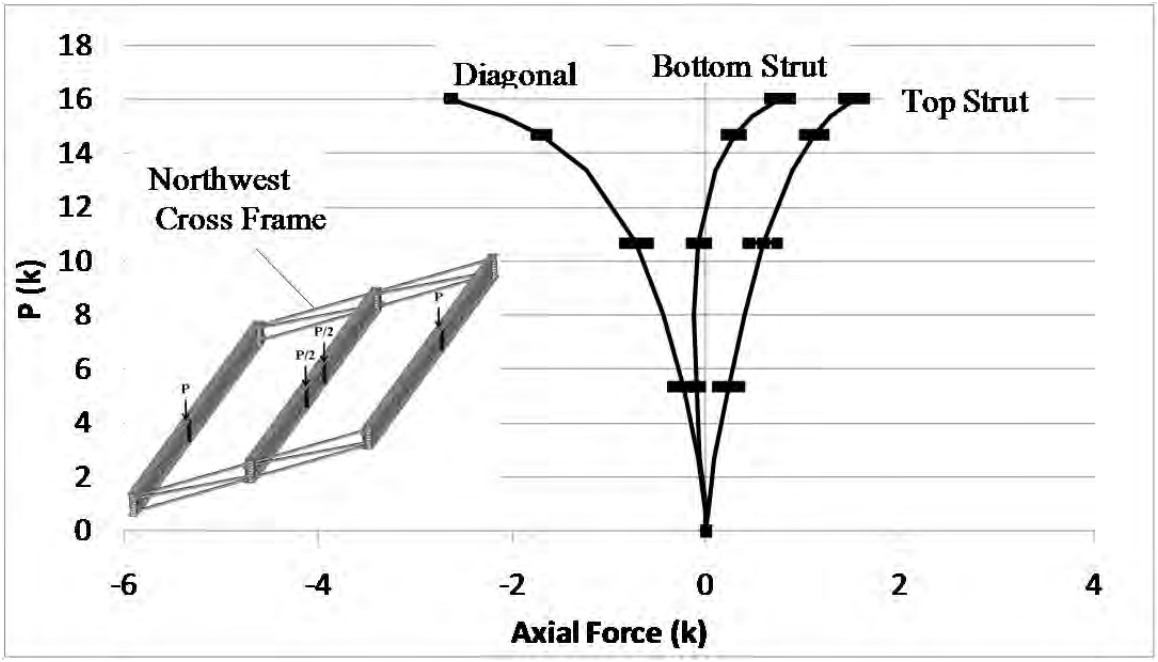

Figure A.83: NW end cross frame axial forces

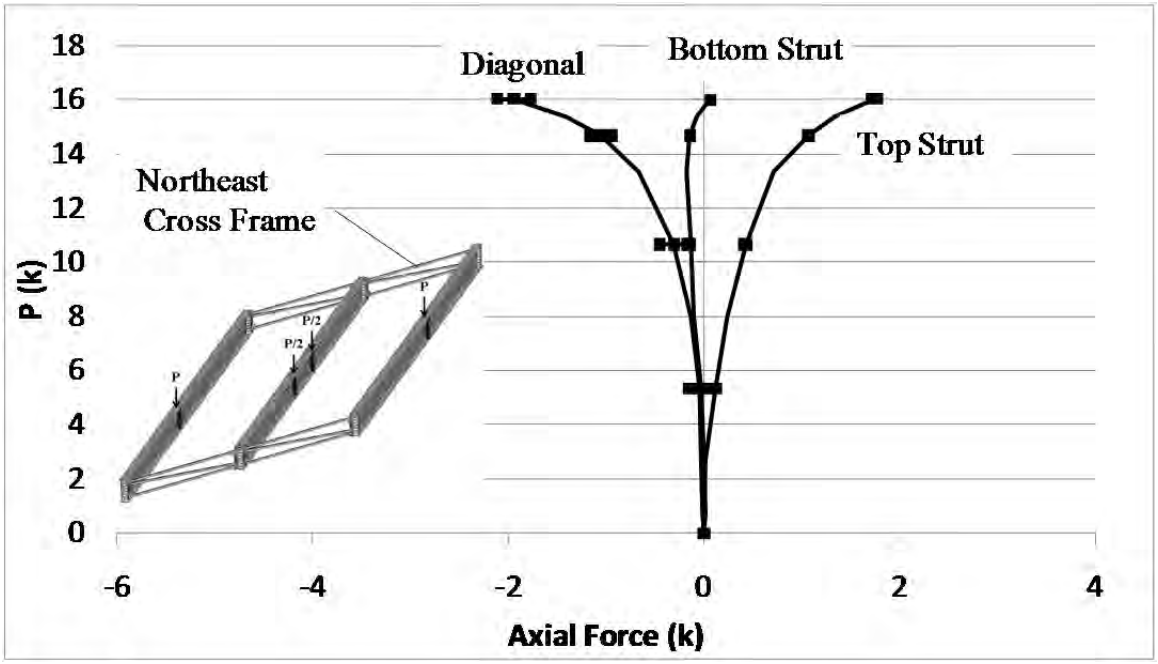

Figure A.84: NE end cross frame axial forces

A.4 THREE GIRDER BEND PLATE END FRAME TEST RESULTS

A.4.1 Thrust Washer Bearing with No Intermediate Cross Frames

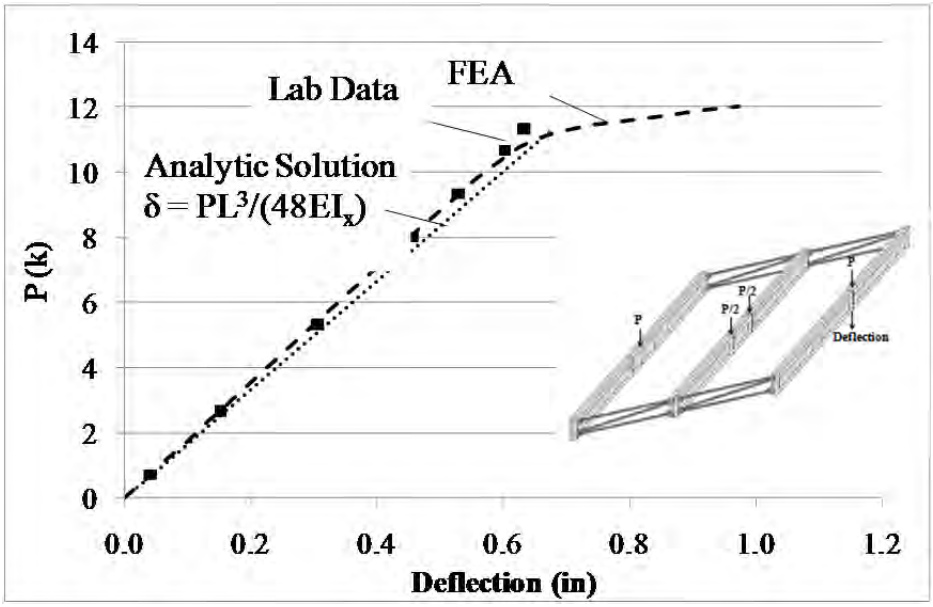

Figure A.85: GBP1 mid-span vertical deflection

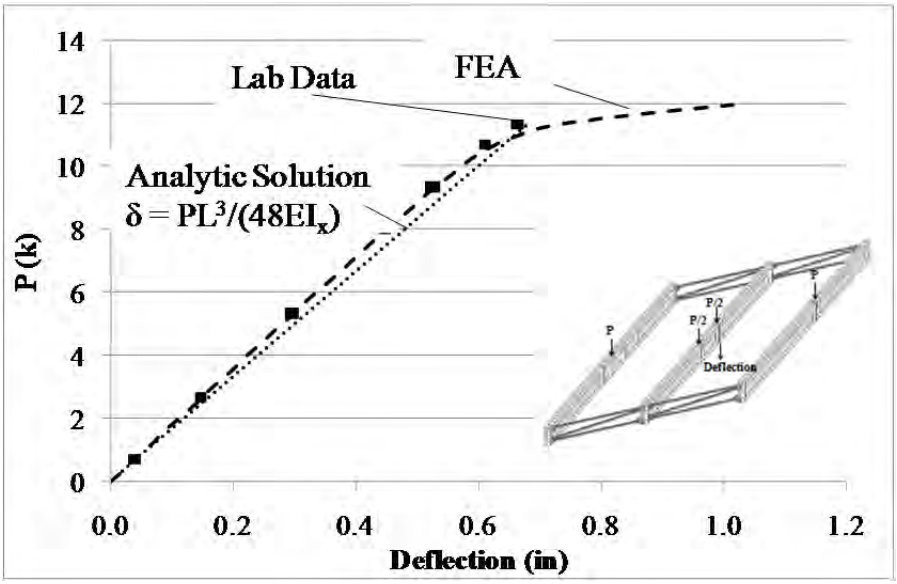

Figure A.86: GBP2 mid-span vertical deflection

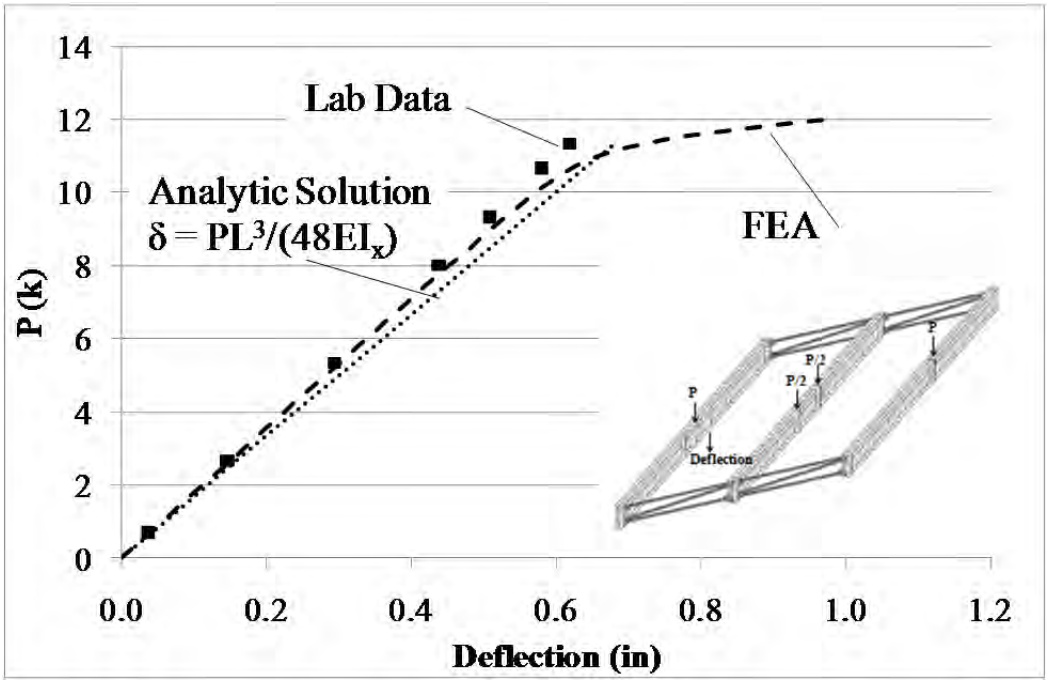

Figure A.87: GBP3 mid-span vertical deflection

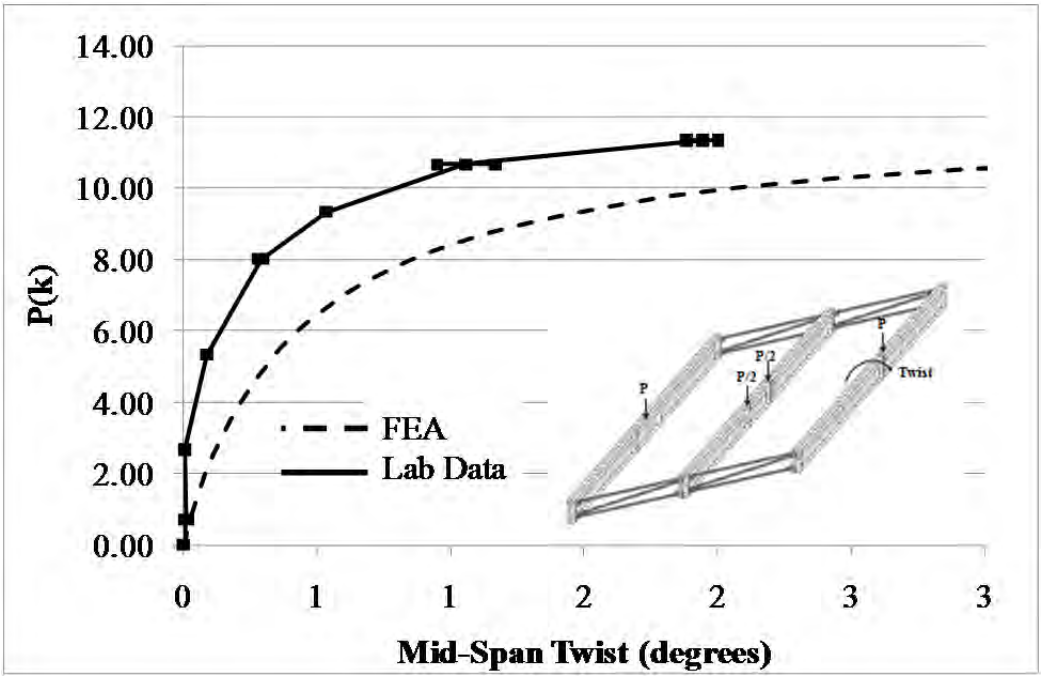

Figure A.88: GBP1 mid-span twist

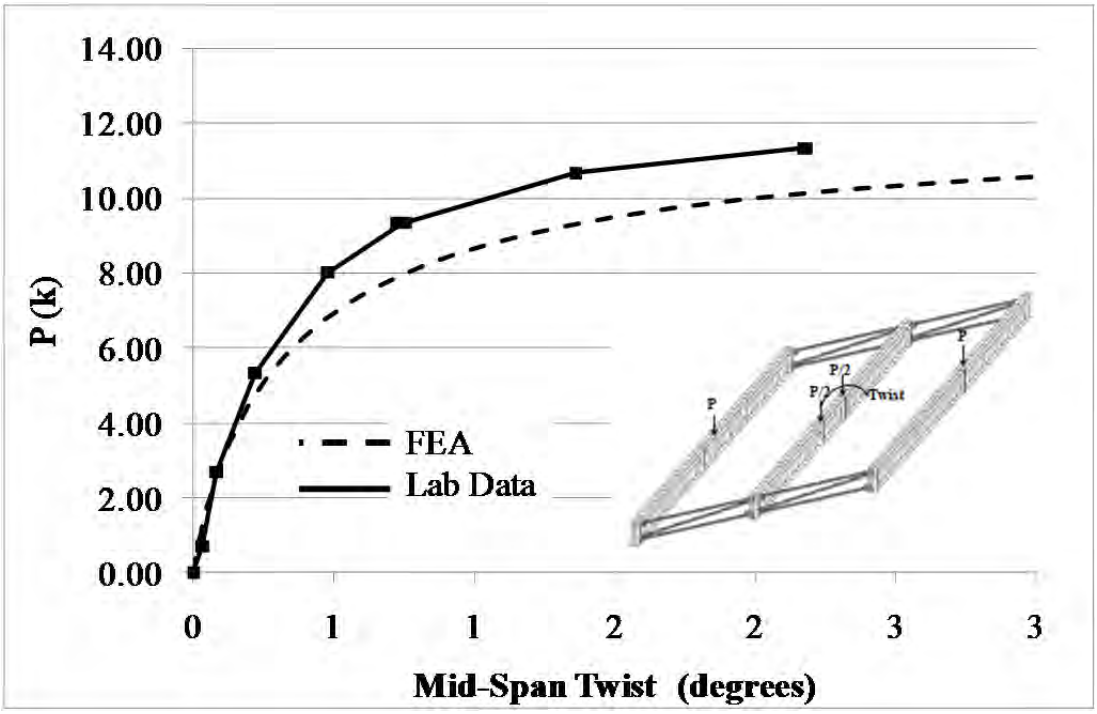

Figure A.89: GBP2 mid-span twist

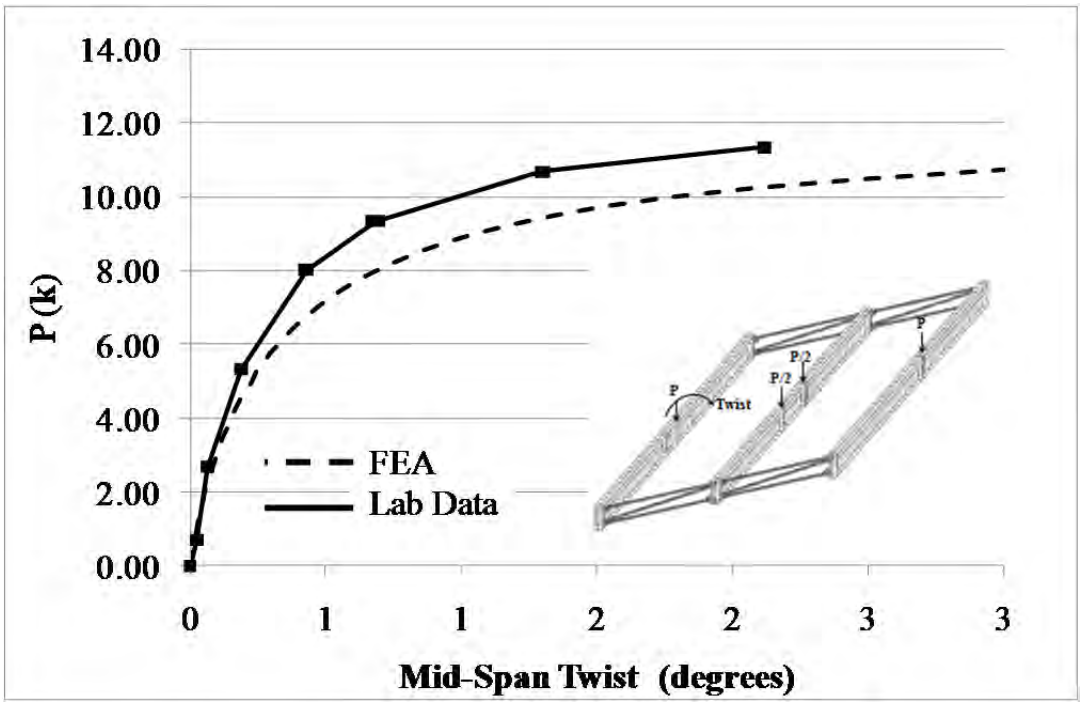

Figure A.90: GBP3 mid-span twist

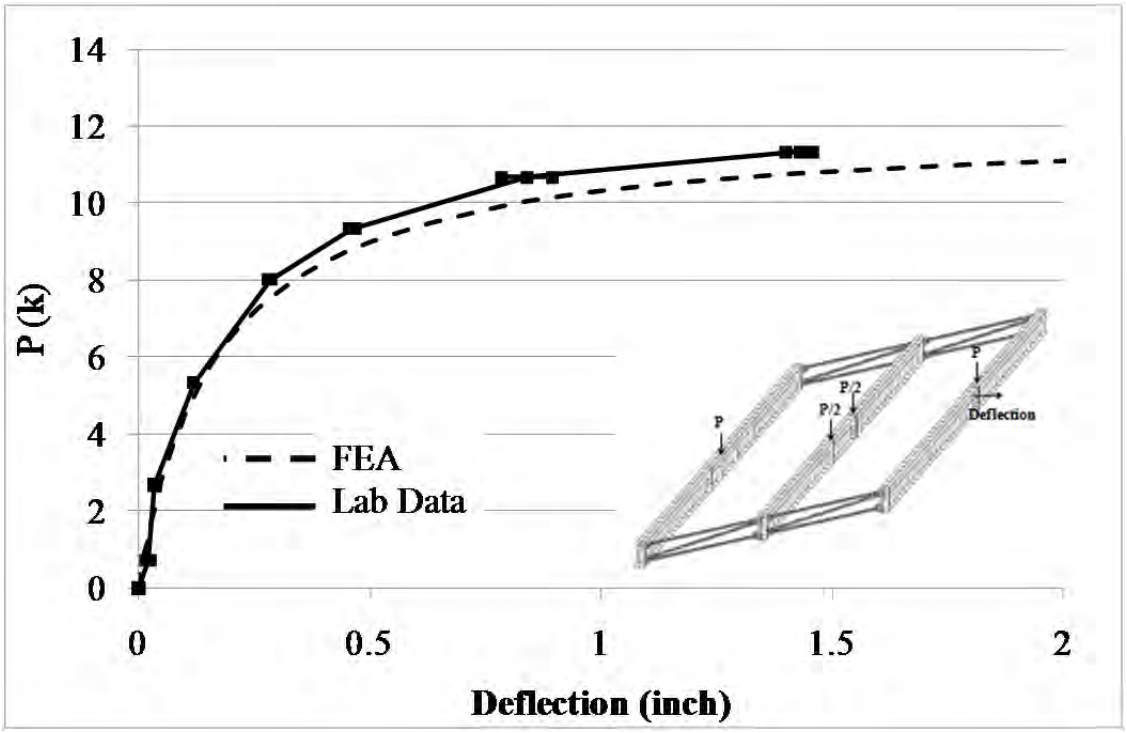

Figure A.91: GBP1 top flange deflection

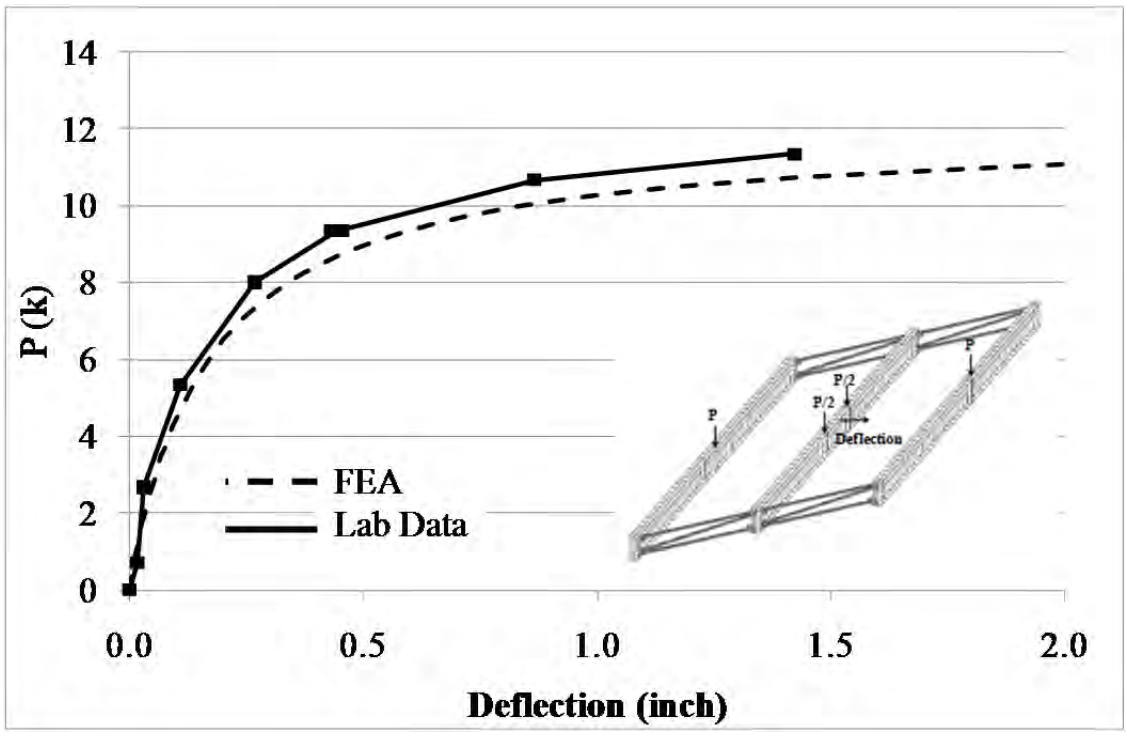

Figure A.92: GBP2 top flange deflection

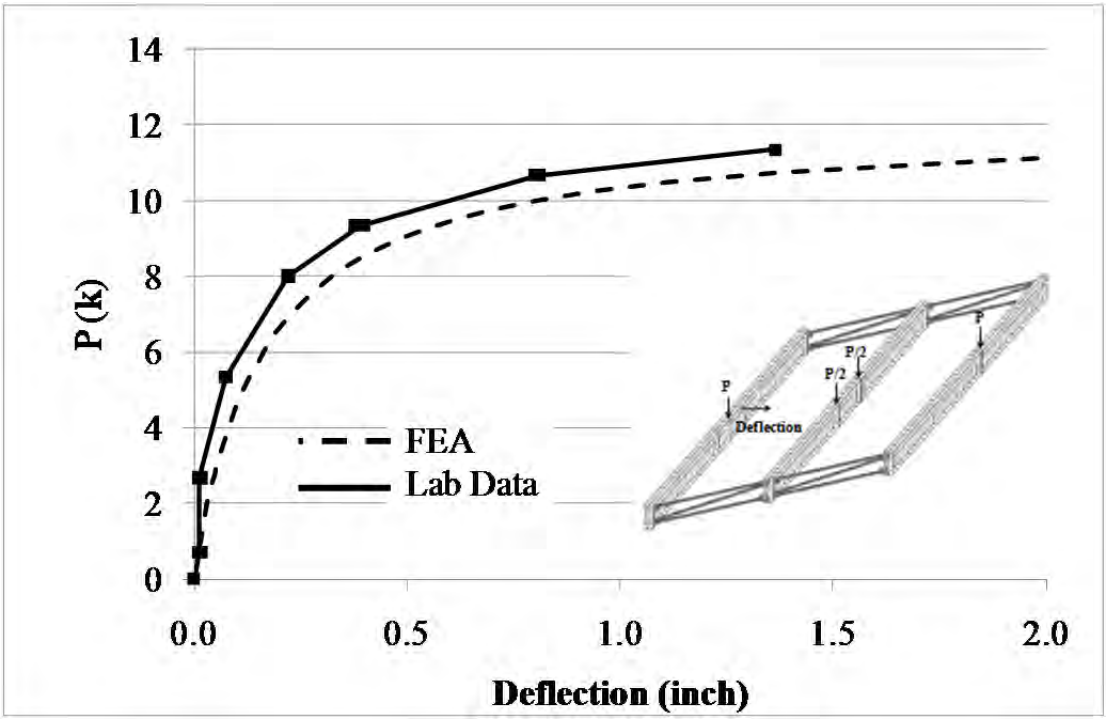

Figure A.93: GBP3 top flange deflection

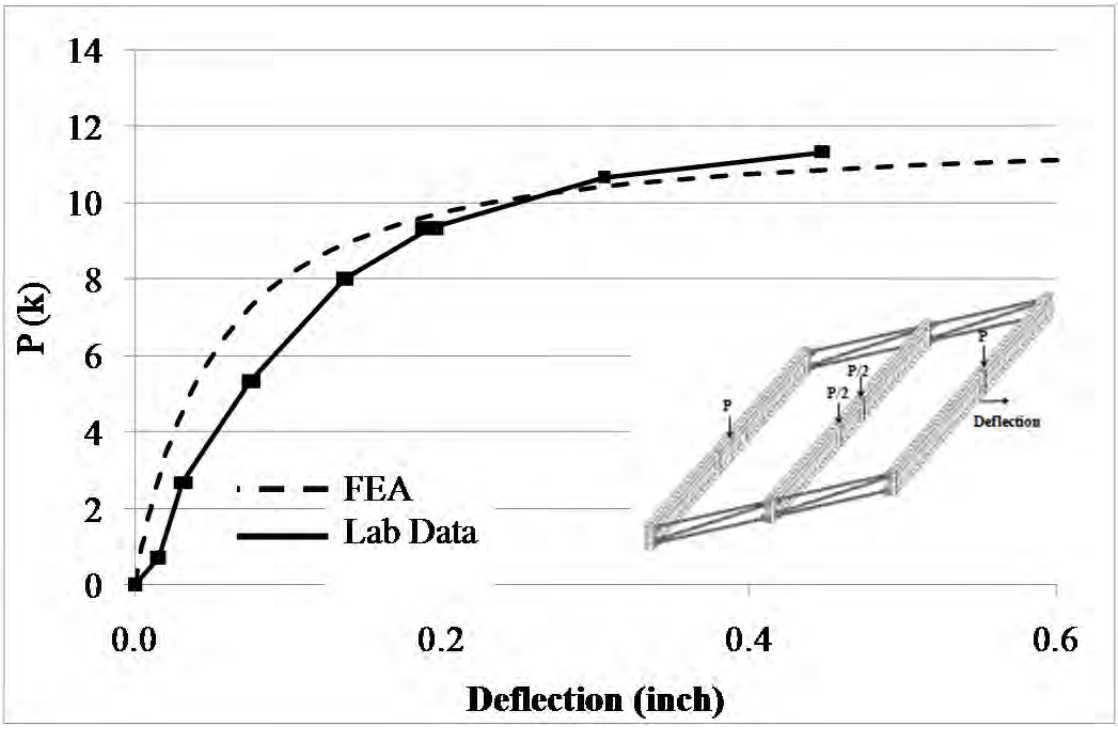

Figure A.94: GBP1 bottom flange deflection

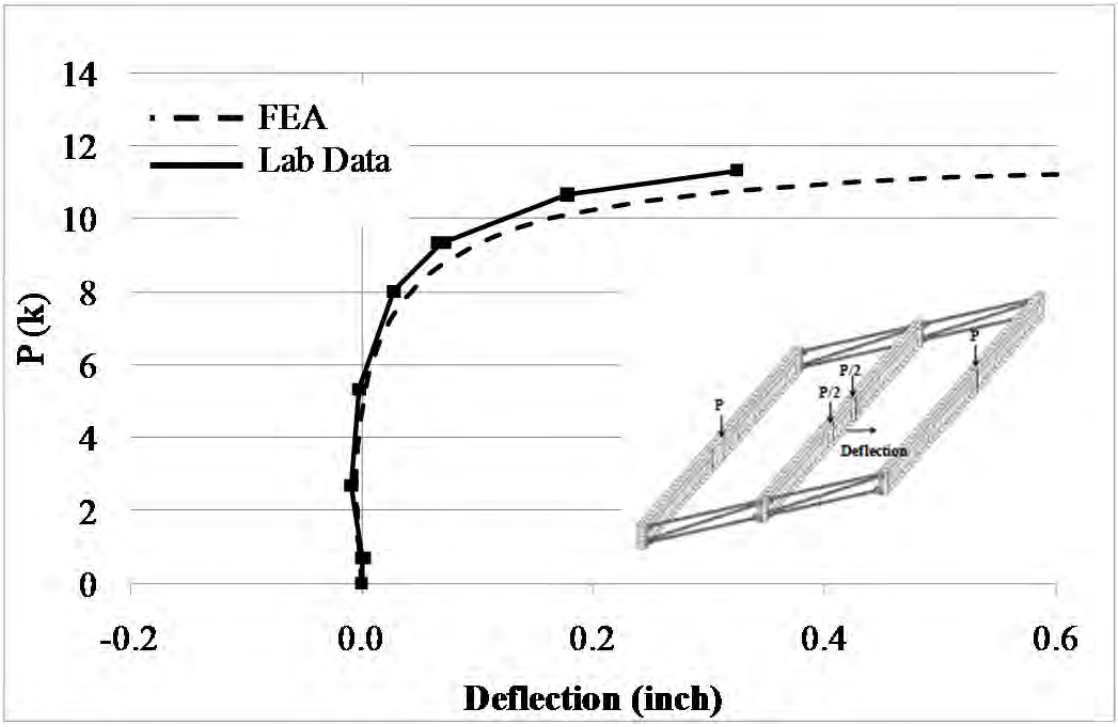

Figure A.95: GBP2 bottom flange deflection

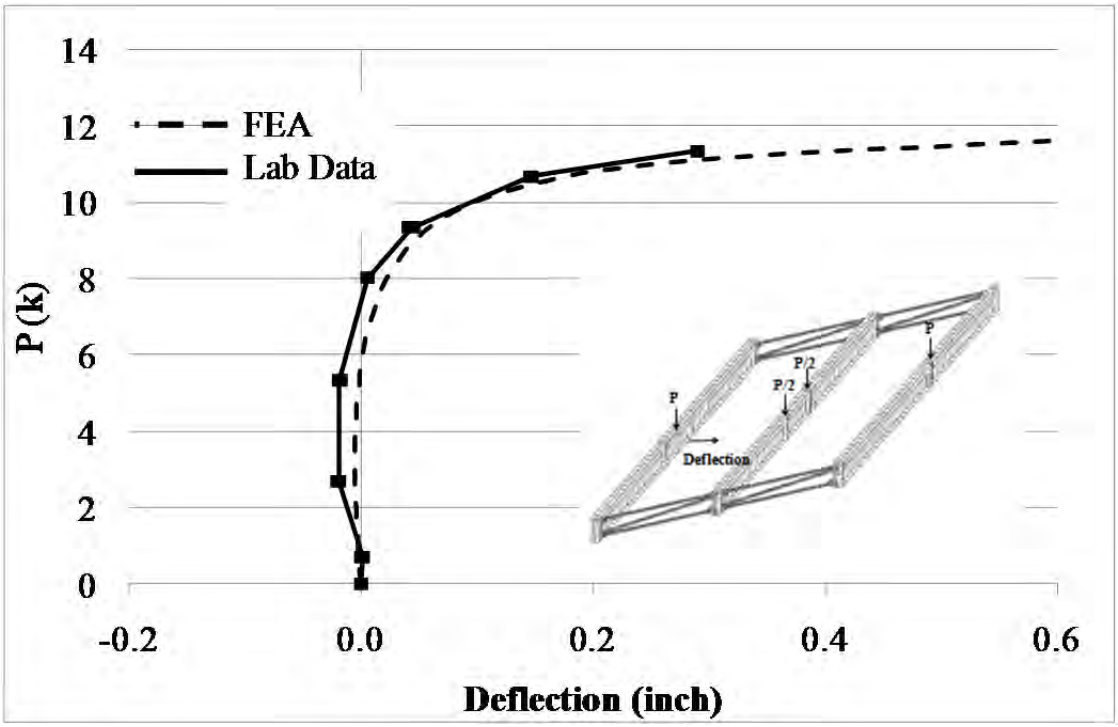

Figure A.96: GBP3 bottom flange deflection

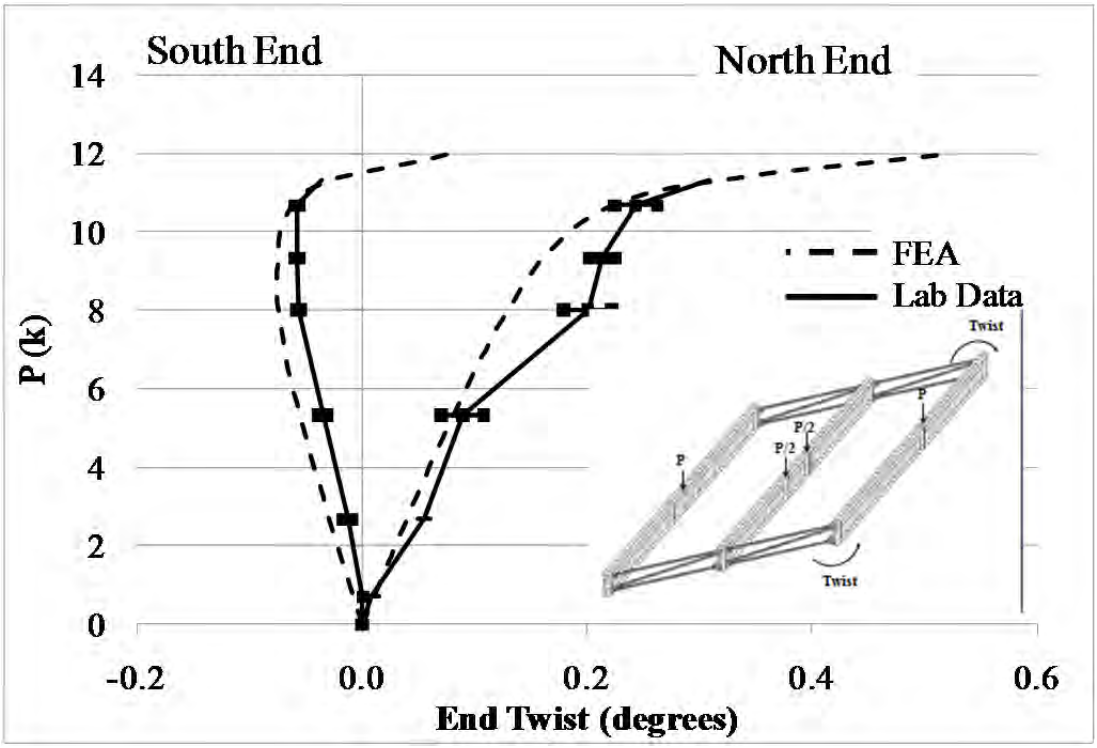

Figure A.97: GBP1 end twist

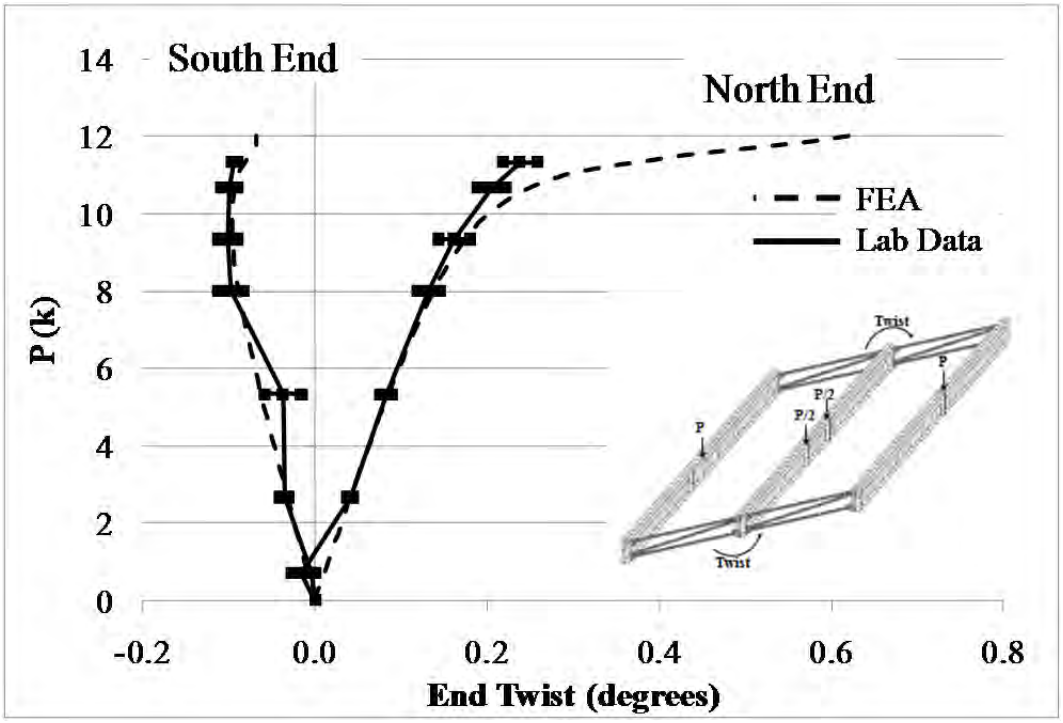

Figure A.98: GBP2 end twist

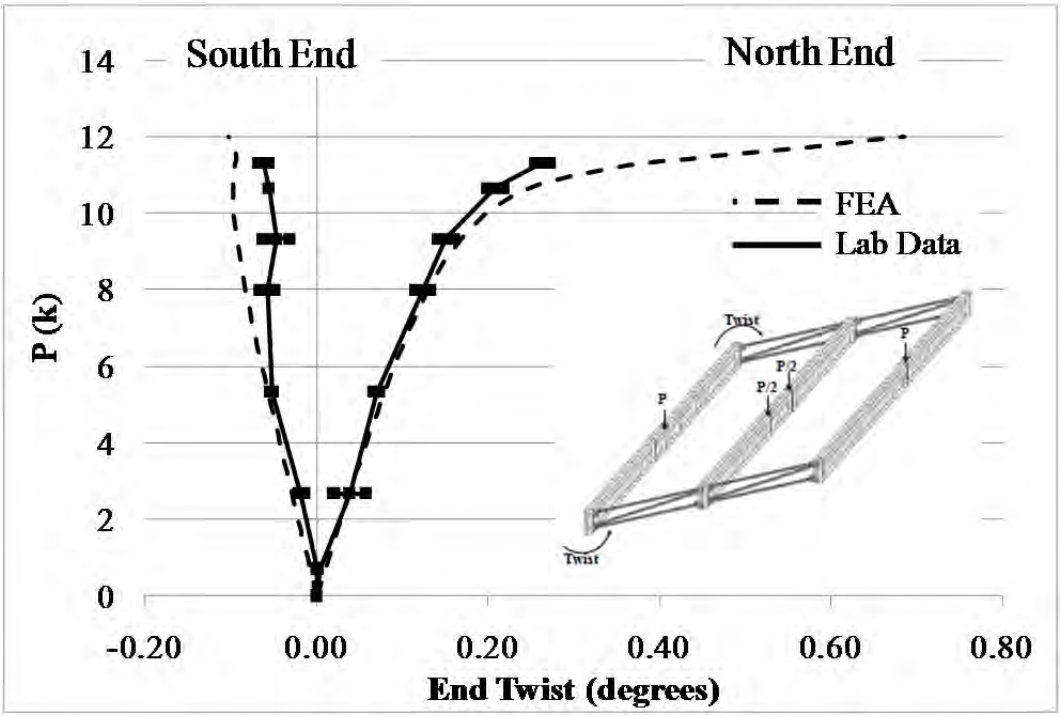

Figure A.99: GBP3 end twist

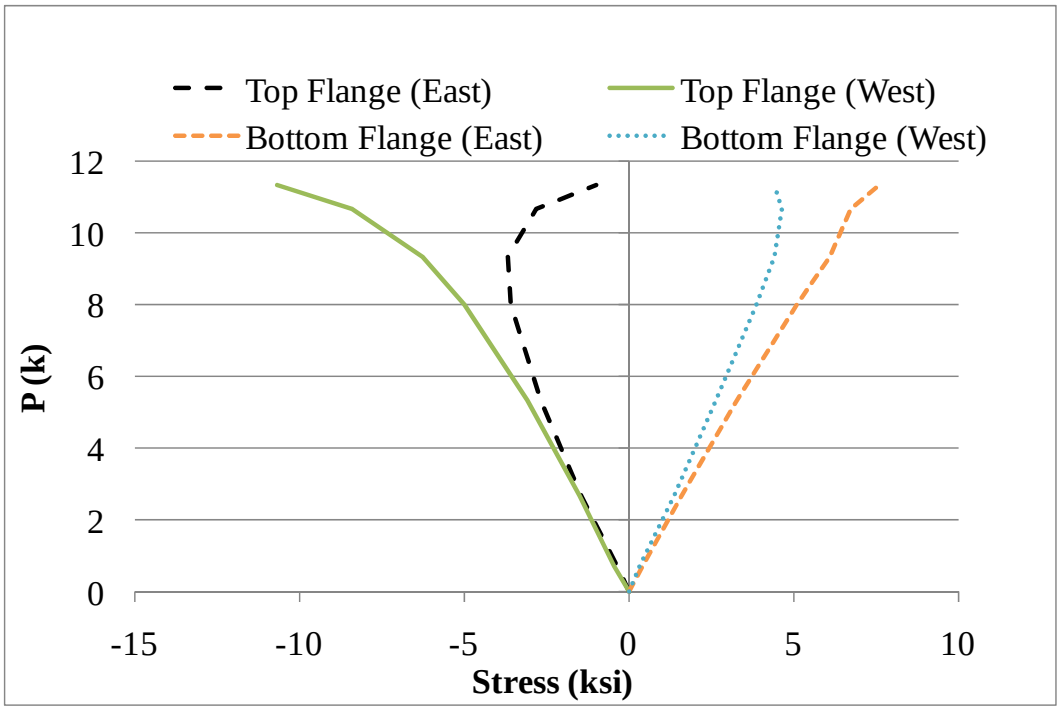

Figure A.100: GBP1 flange stresses

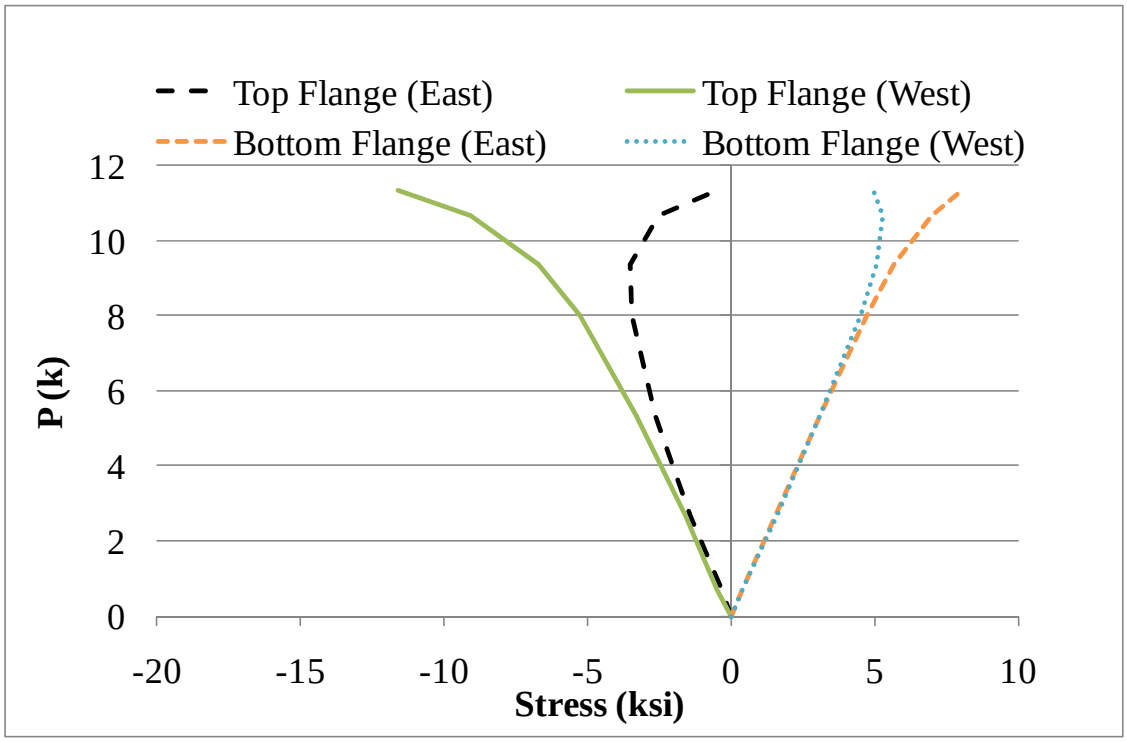

Figure A.101: G BP2 flange stresses

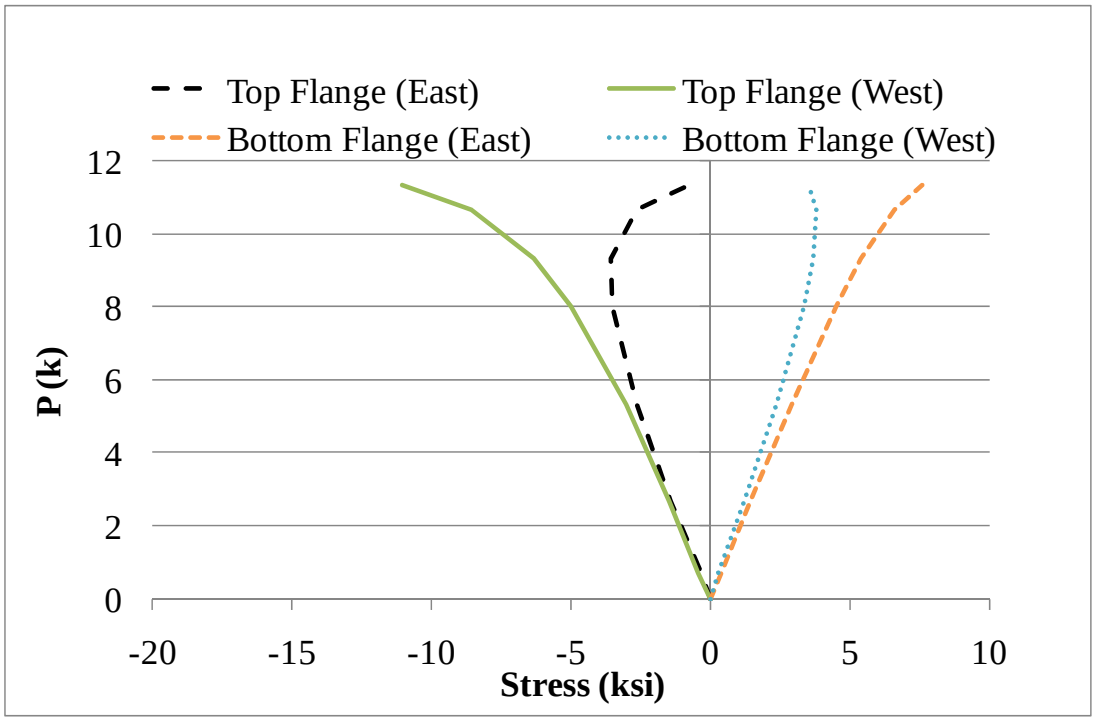

Figure A.102: GBP3 flange stresses

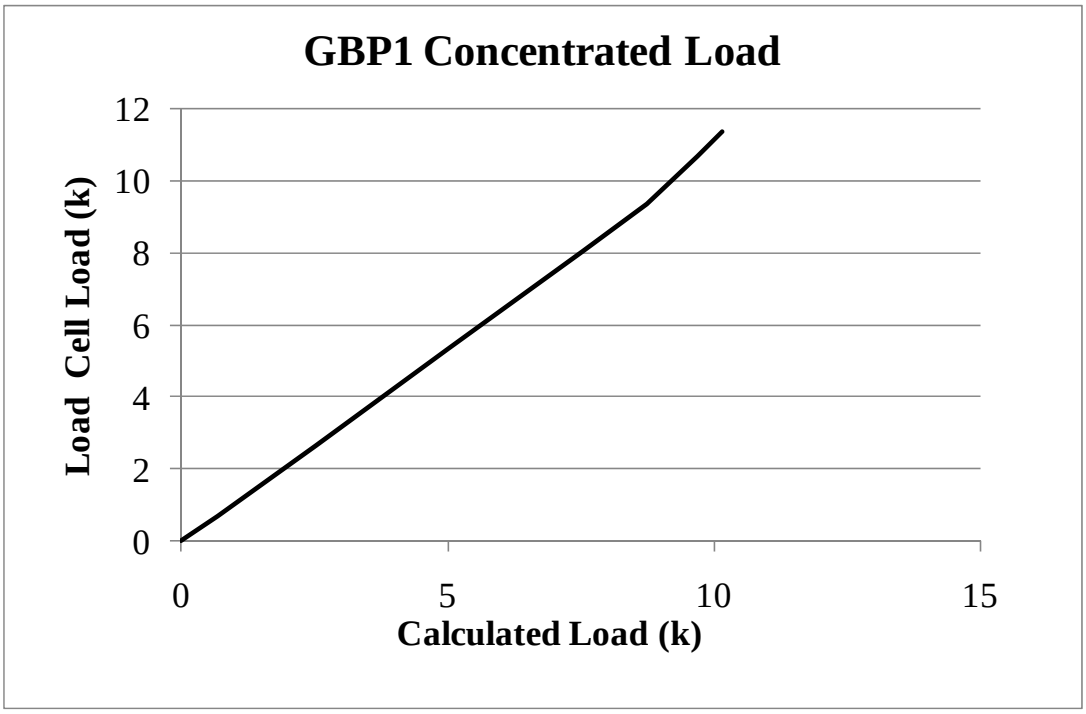

Figure A.103: GBP1 calculated girder loads from flange stresses

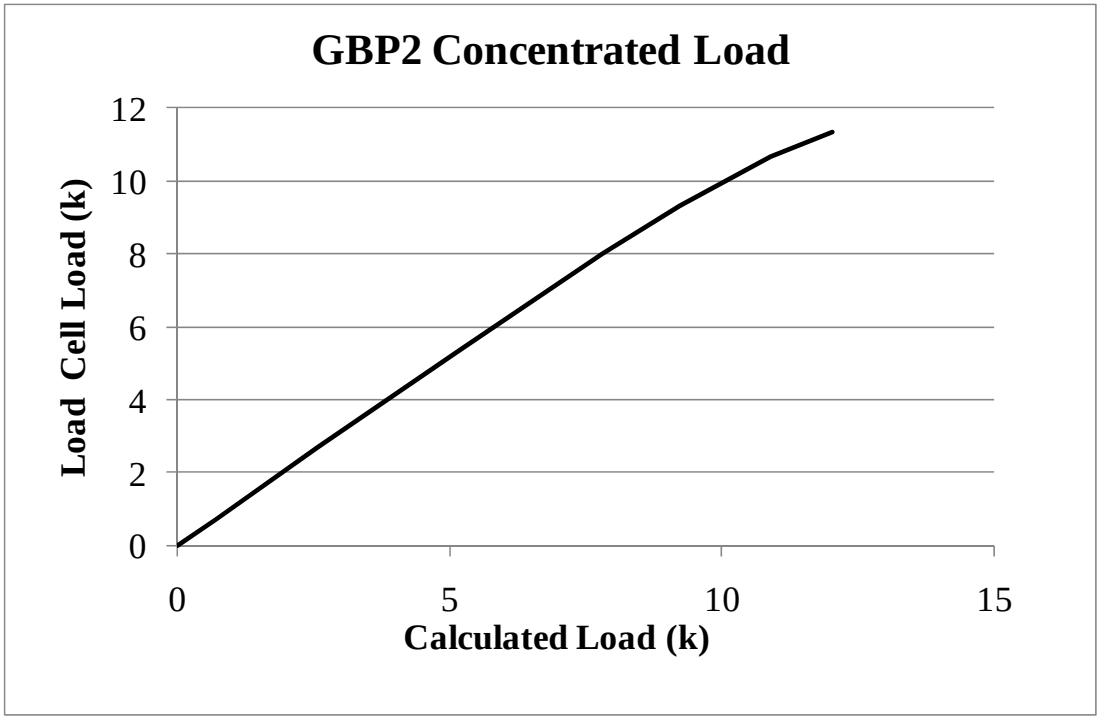

Figure A.104: GBP2 calculated girder loads from flange stresses

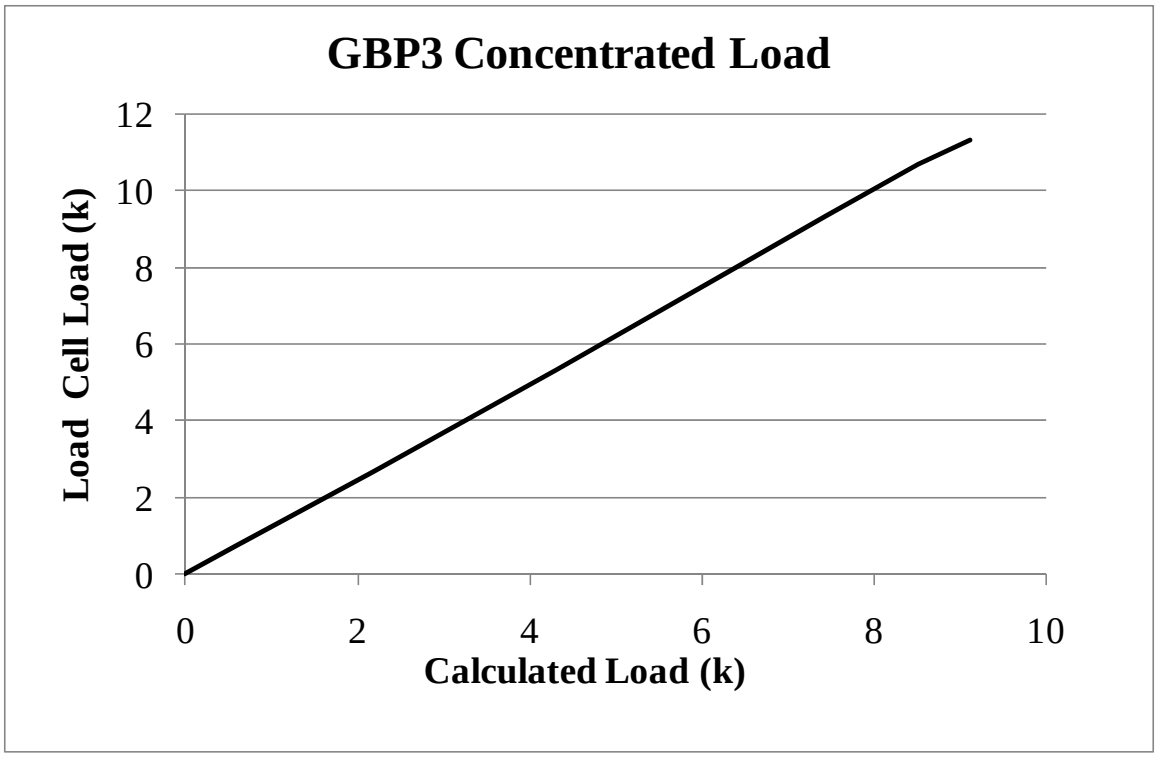

Figure A.105: GBP3 calculated girder loads from flange stresses

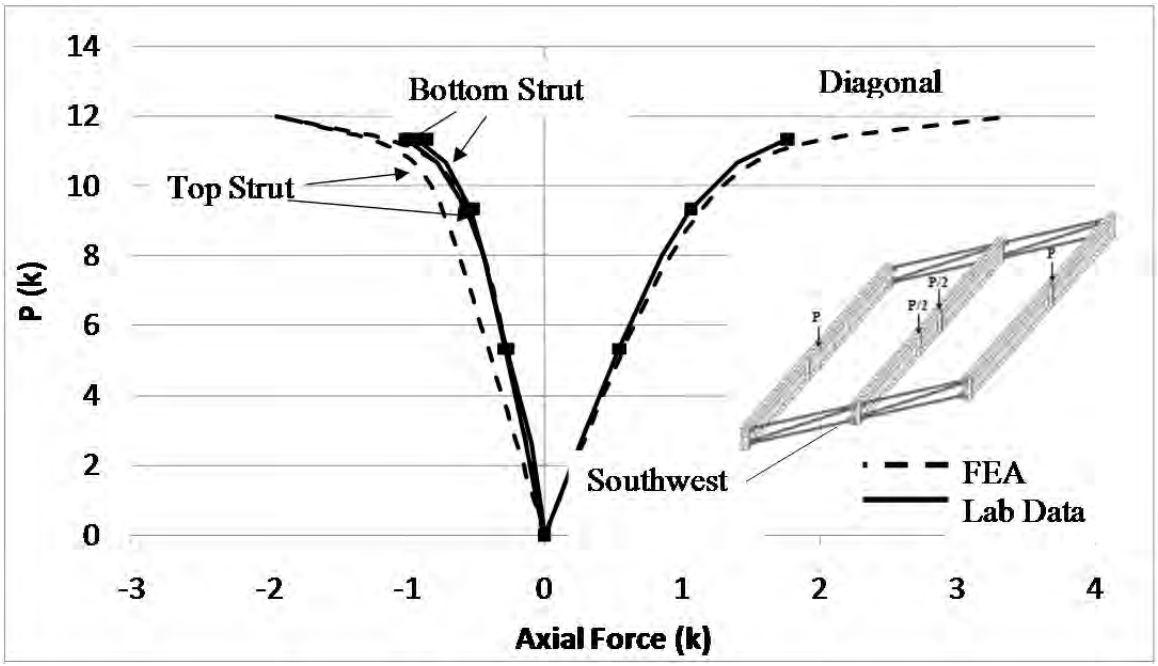

Figure A.106: SW end frame axial forces

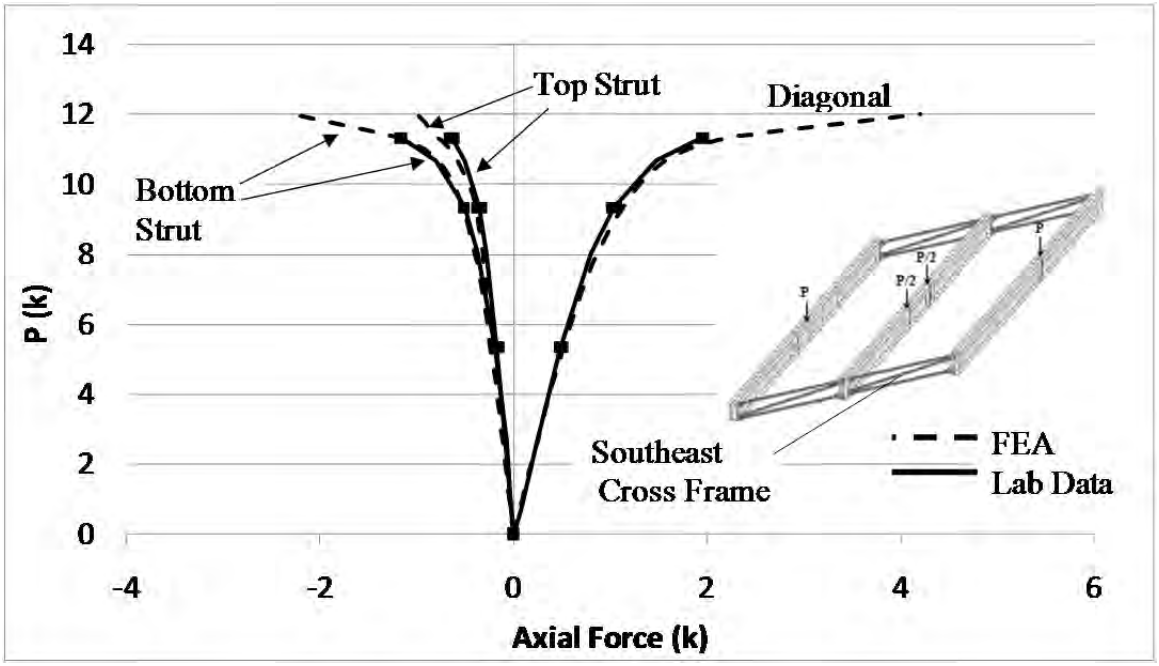

Figure A.107: SE end frame axial forces

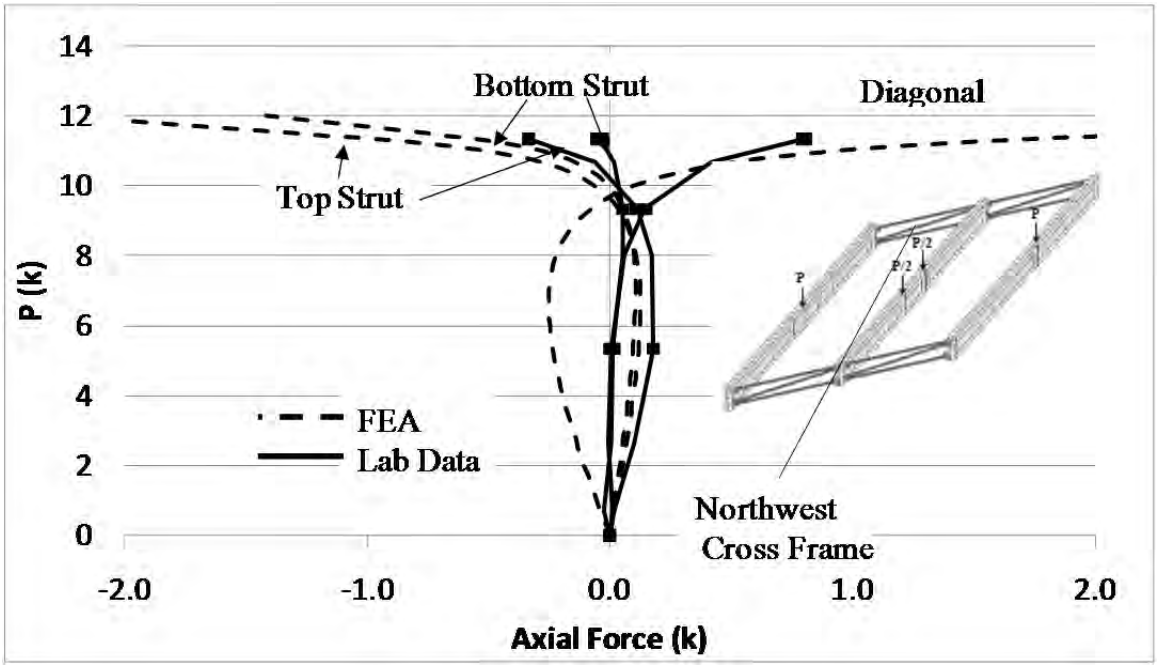

Figure A.108: NW end frame axial forces

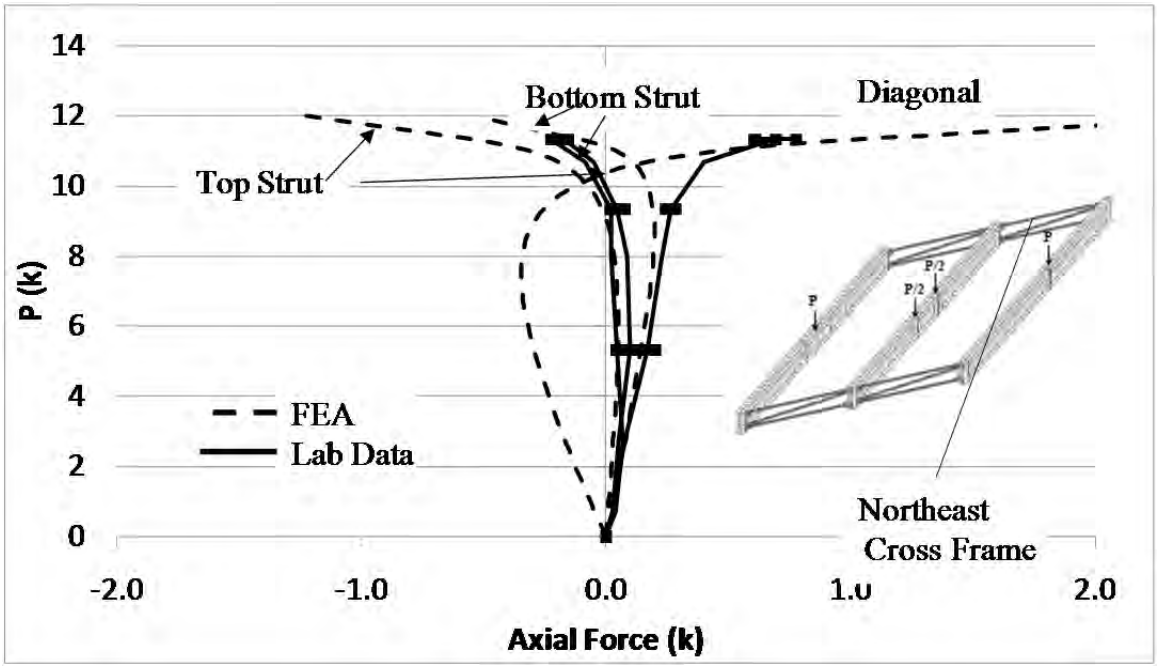

Figure A.109: NE end frame axial forces

A.4.2 Thrust Washer Bearing with Staggered Intermediate Cross Frames

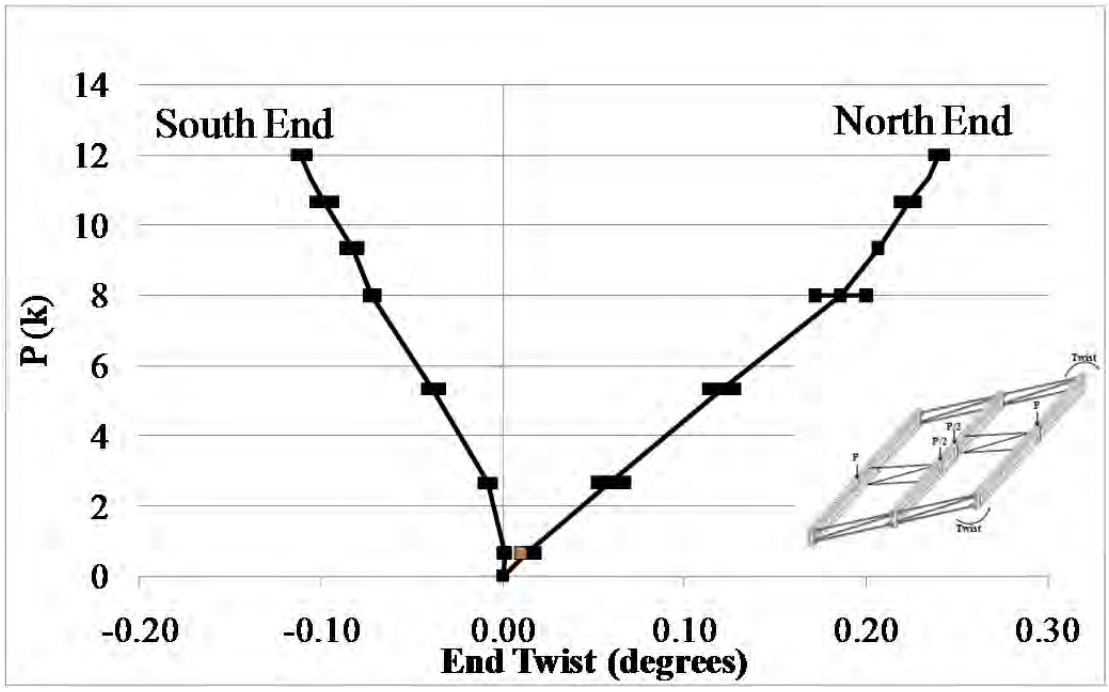

Figure A.110: GBP1 end twists

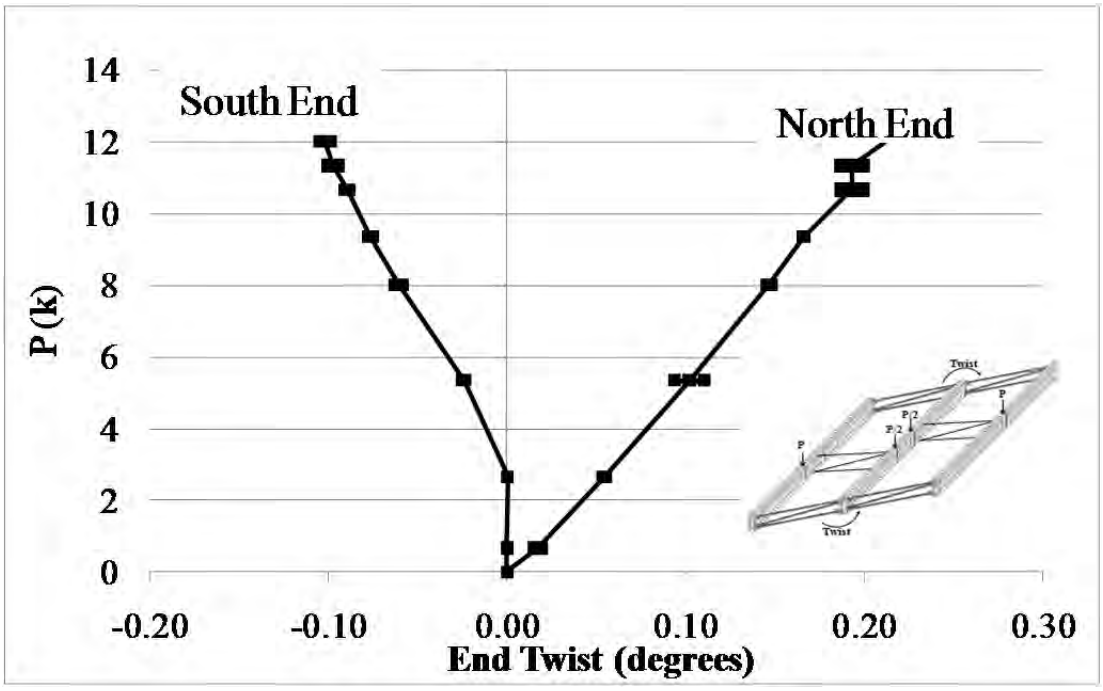

Figure A.111: GBP2 end twists

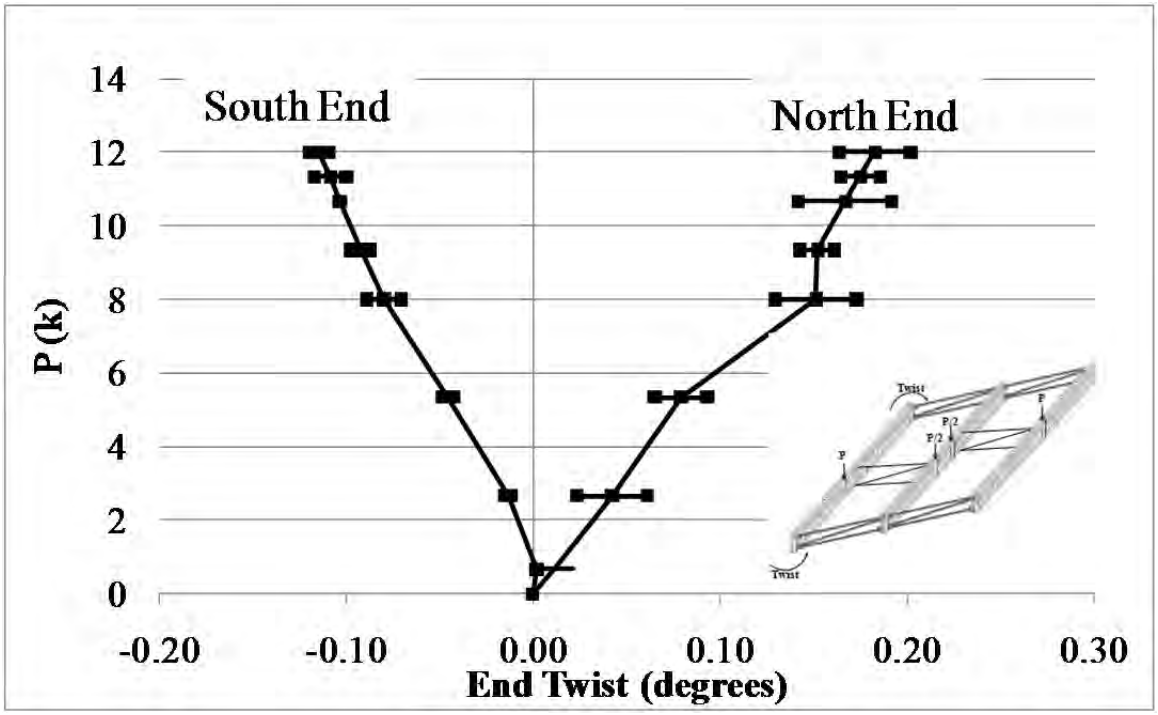

Figure A.112: GBP3 end twists

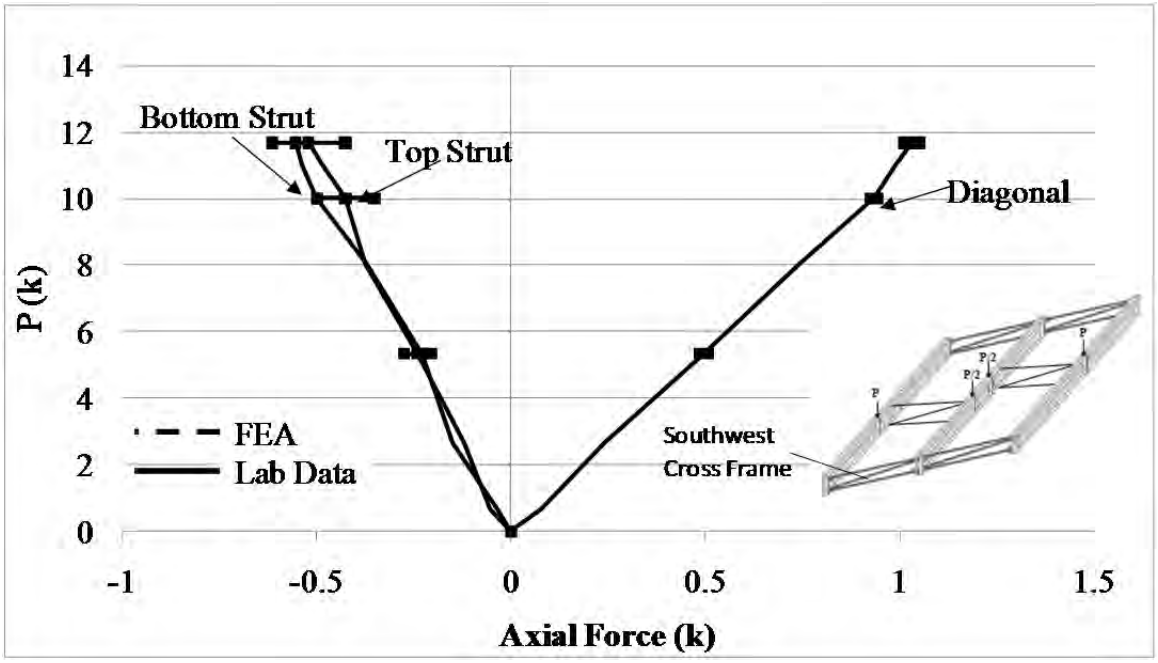

Figure A.113: SW end frame axial forces

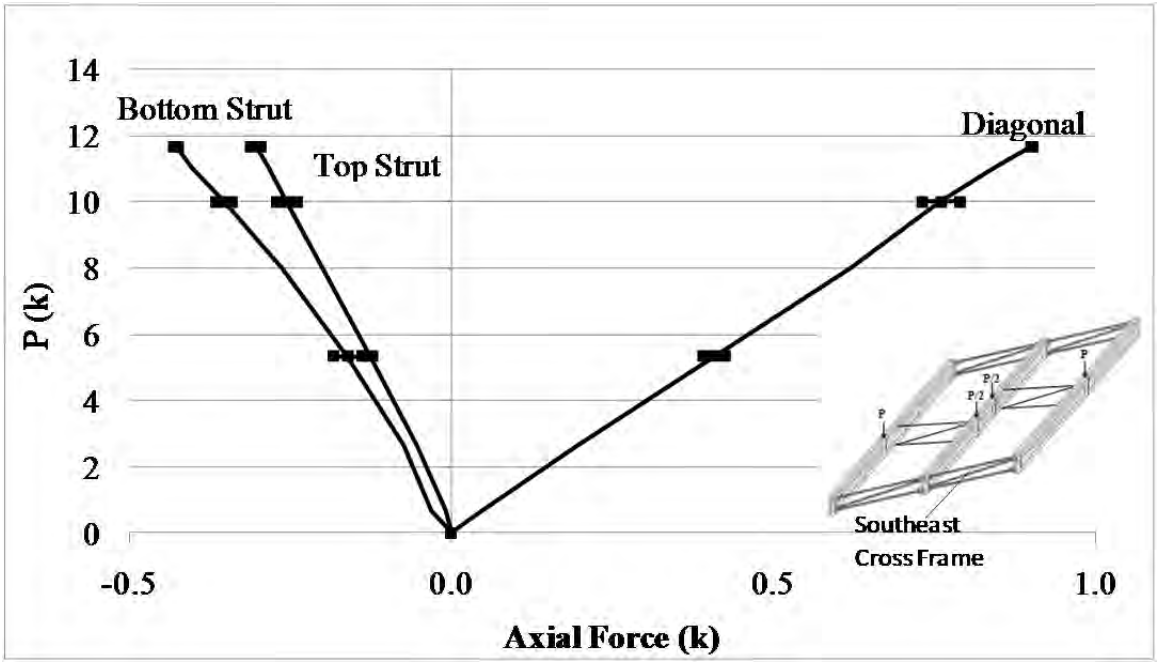

Figure A.114: SE end frame axial forces

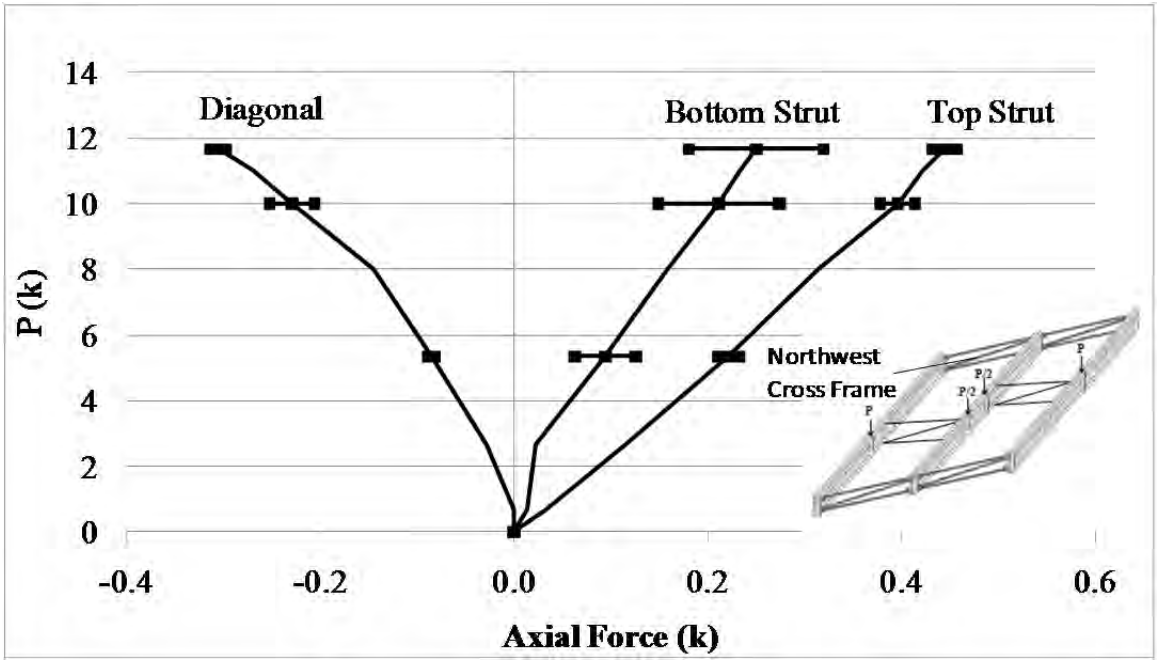

Figure A.115: NW end frame axial forces

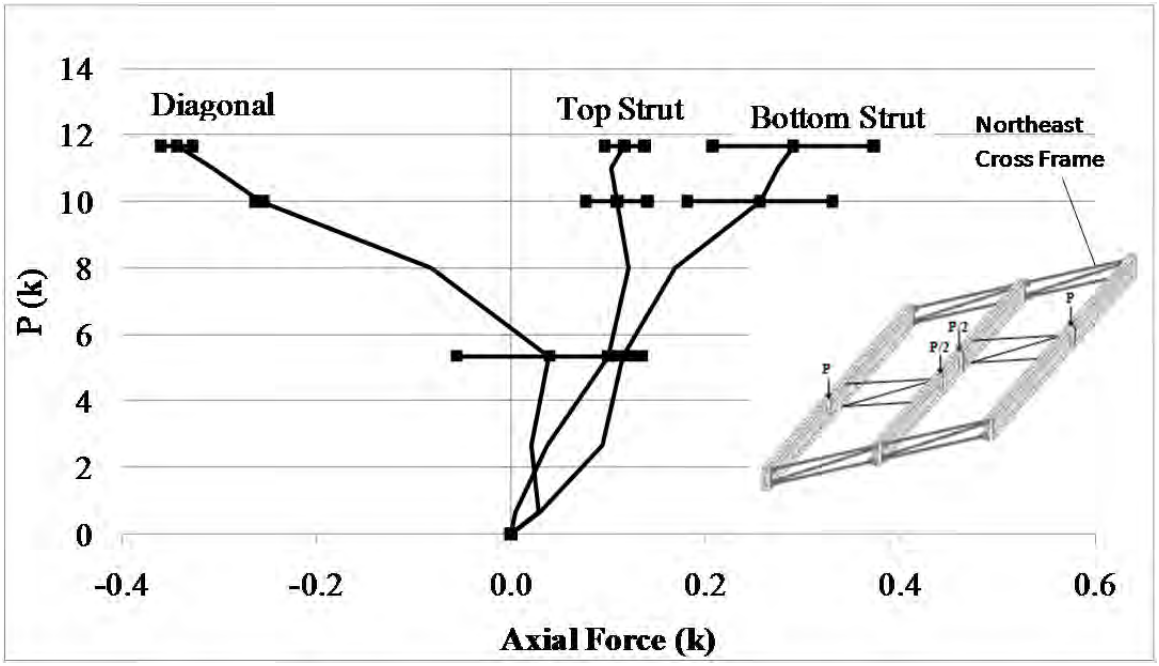

Figure A.116: NW end frame axial forces

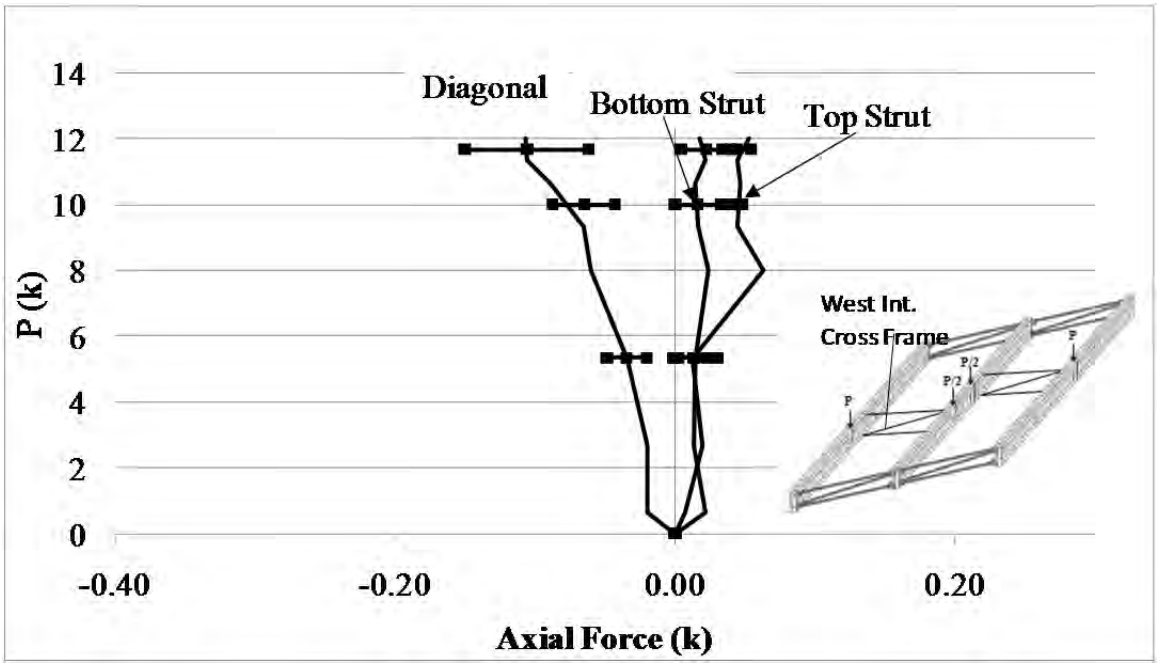

Figure A.117: West intermediate cross frame axial forces

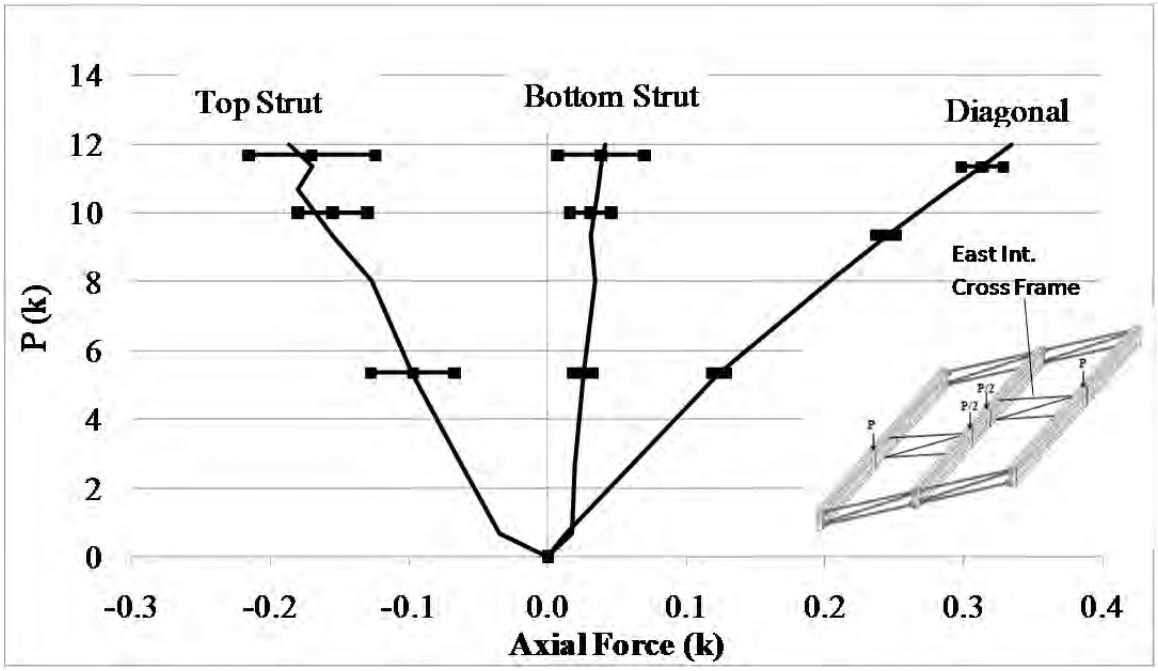

Figure A.118: East intermediate cross frame axial forces

A.4.3 Thrust Washer Bearing with Staggered Intermediate Cross Frames – Partial Loading

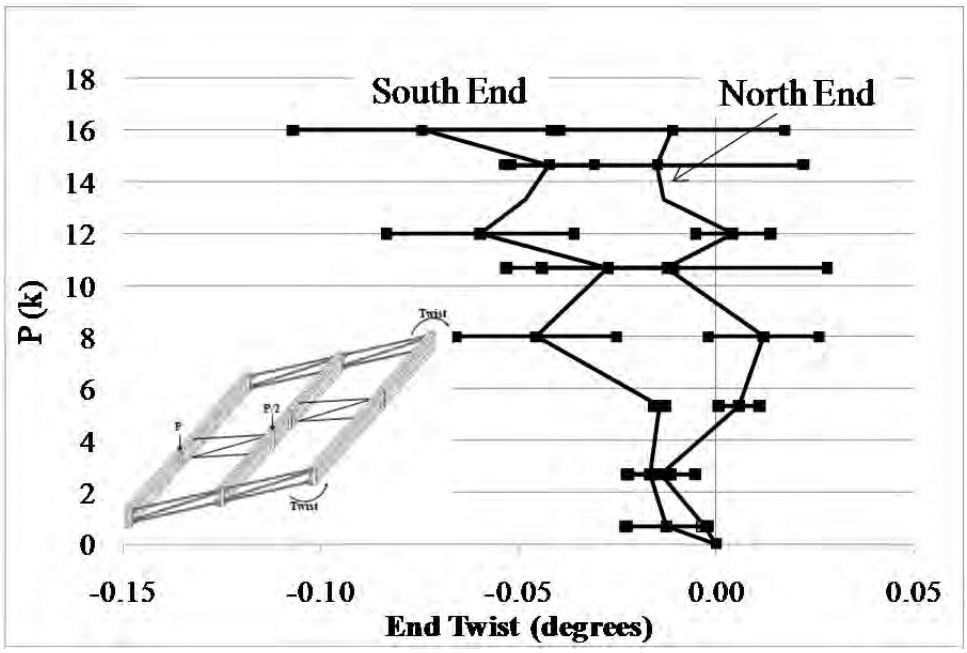

Figure A.119: GBP1 end twists

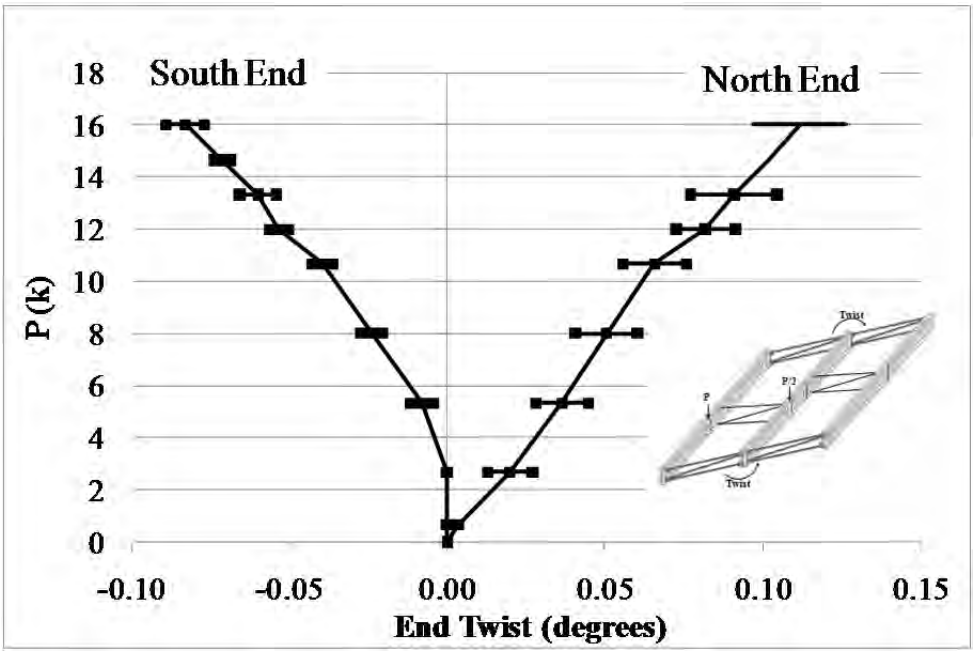

Figure A.120: GBP2 end twists

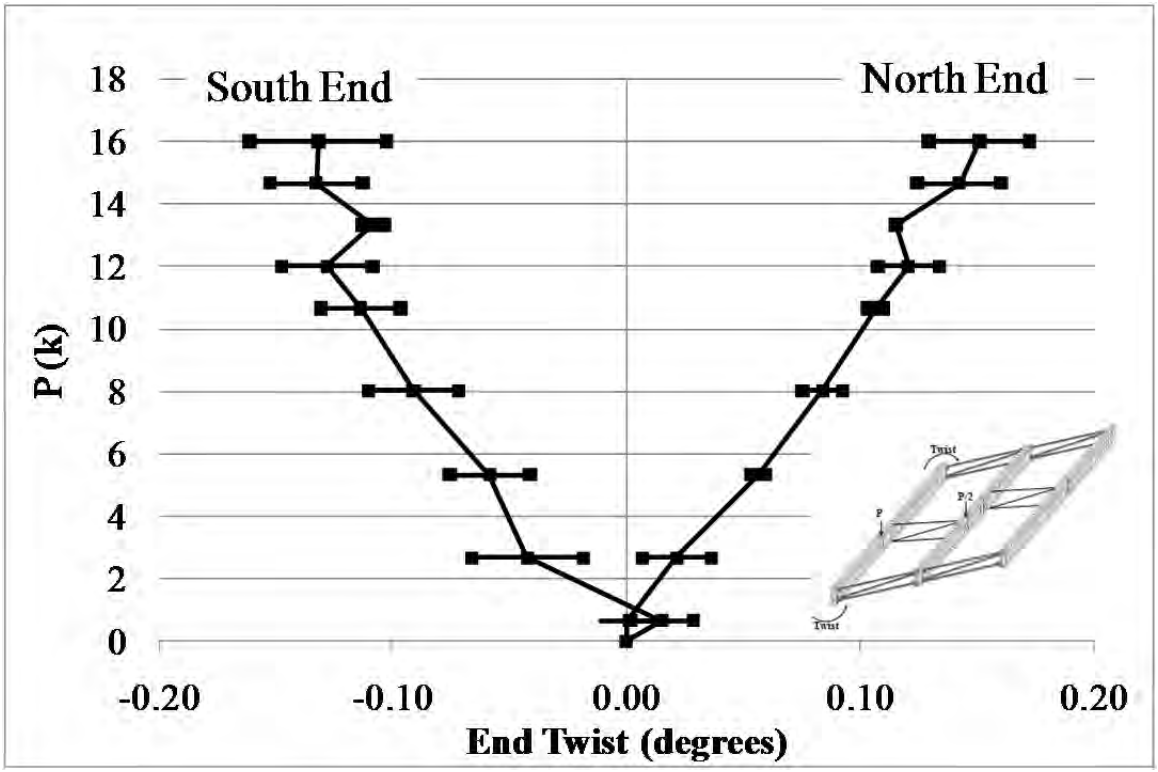

Figure A.121: GBP3 end twists

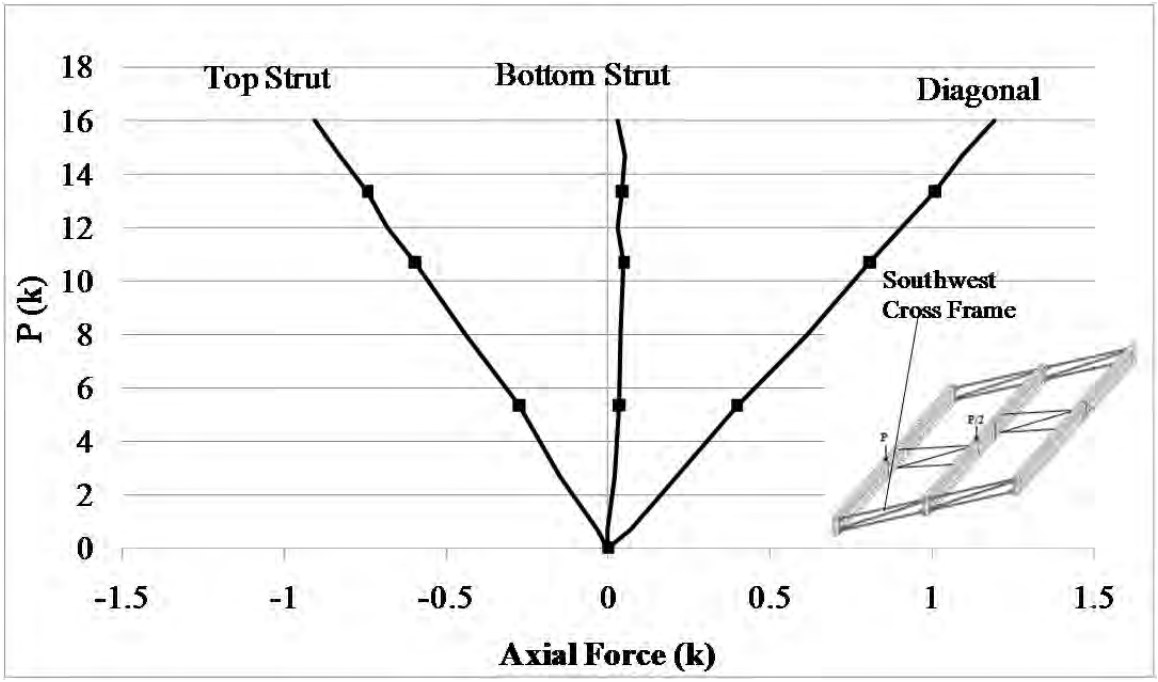

Figure A.122: SW cross frame axial forces

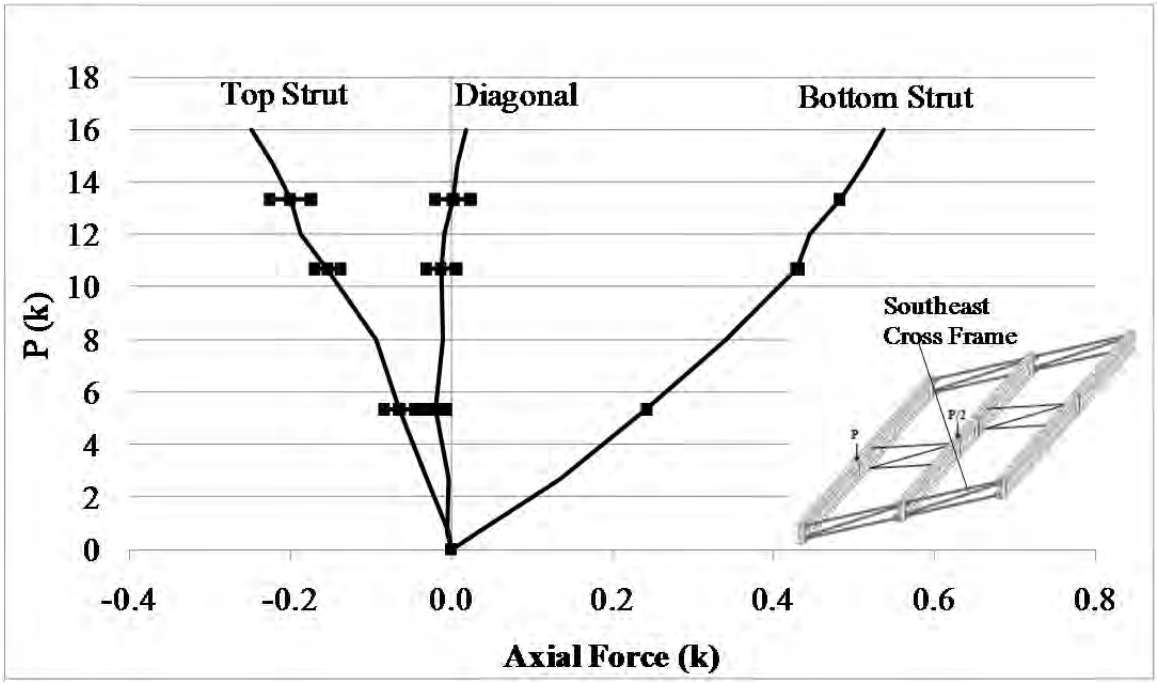

Figure A.123: SE cross frame axial forces

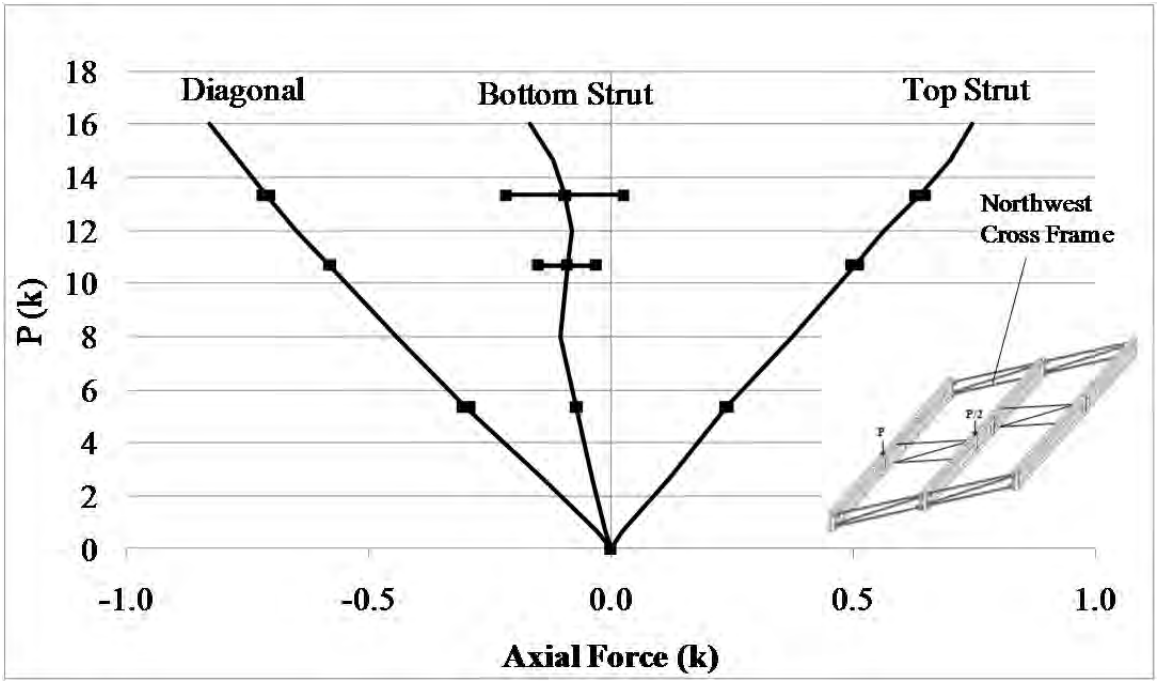

Figure A.124: NW cross frame axial forces

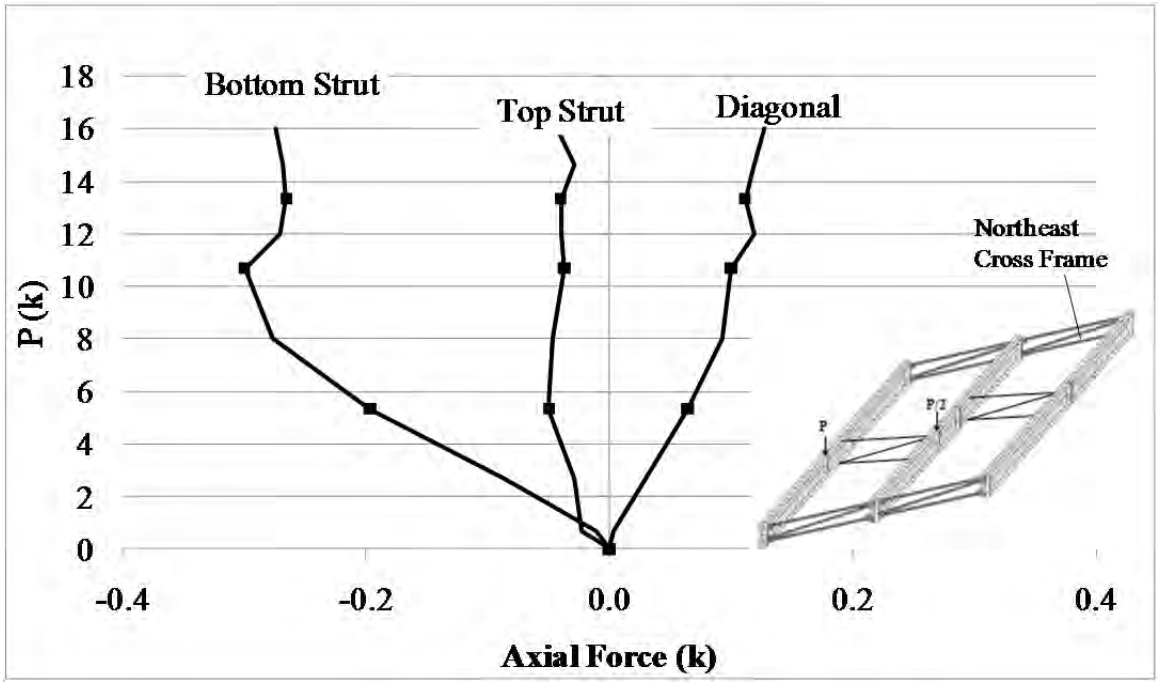

Figure A.125: NE cross frame axial forces

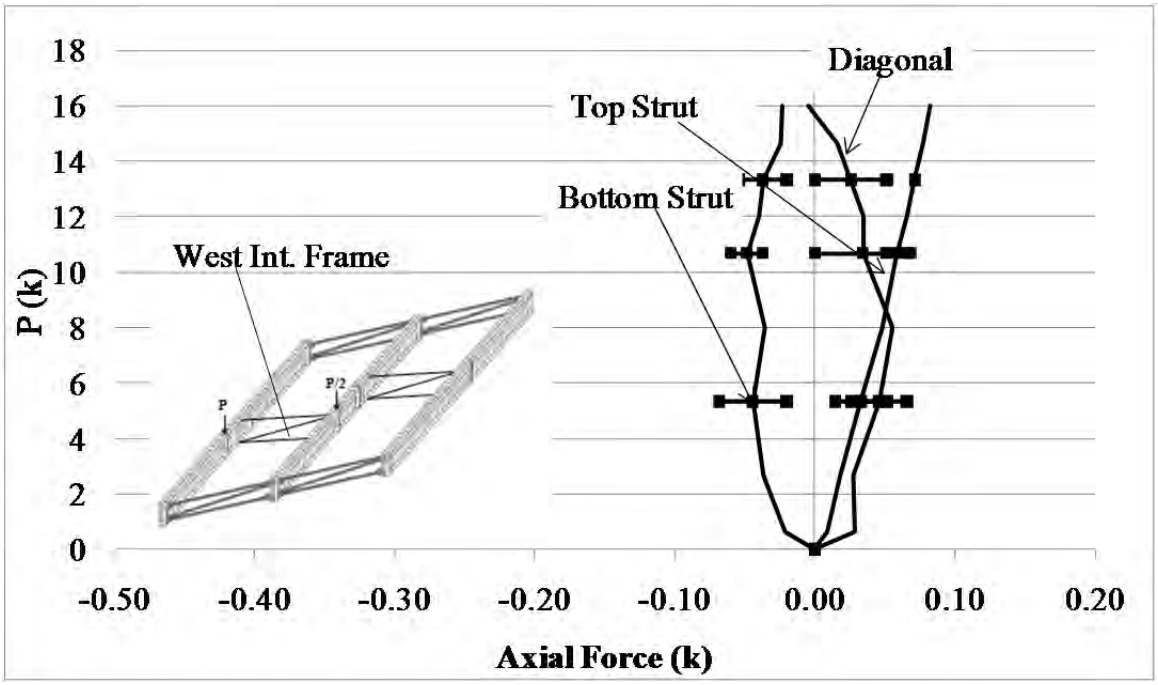

Figure A.126: West intermediate cross frame axial forces

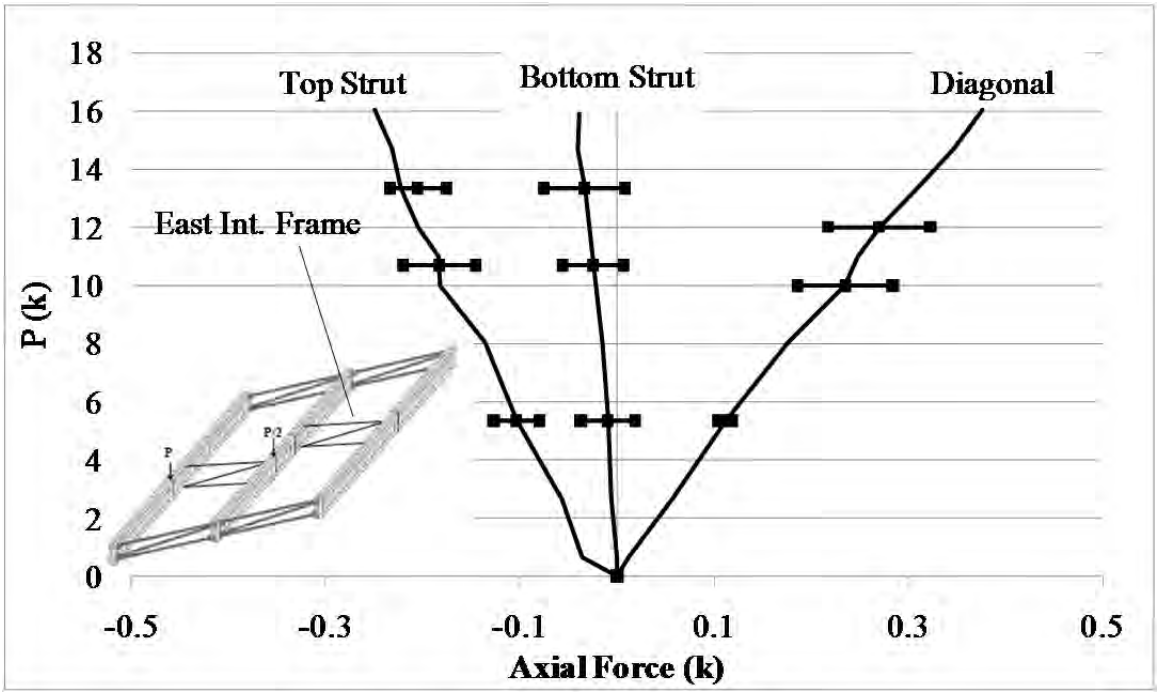

Figure A.127: East intermediate cross frame axial forces

A.4.4 Thrust Washer Bearing with Continuous Intermediate Cross Frames

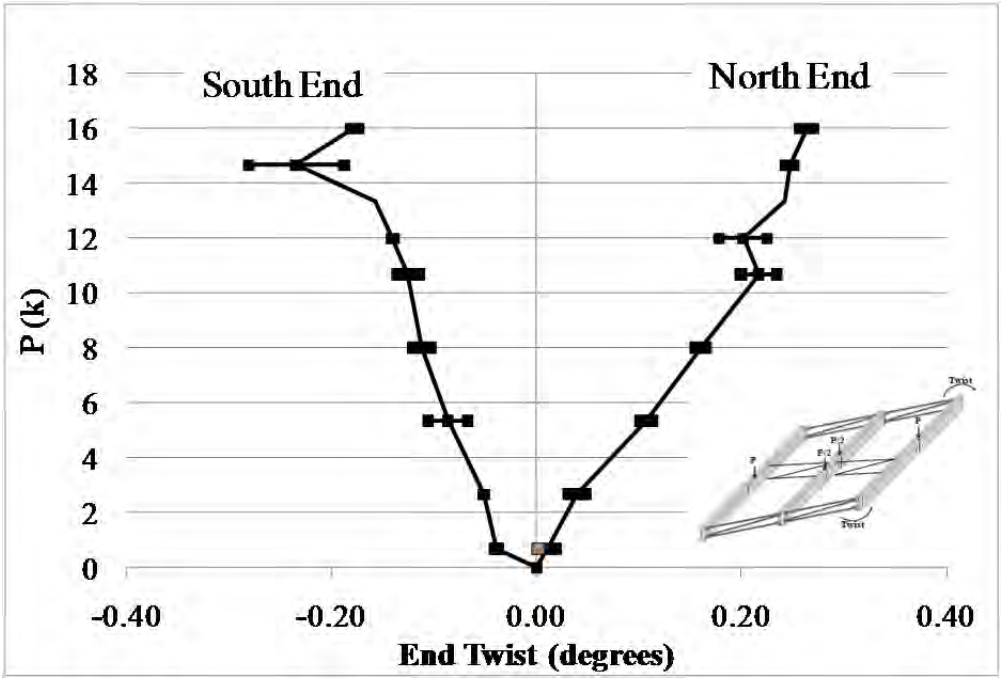

Figure A.128: GBP1 end twists

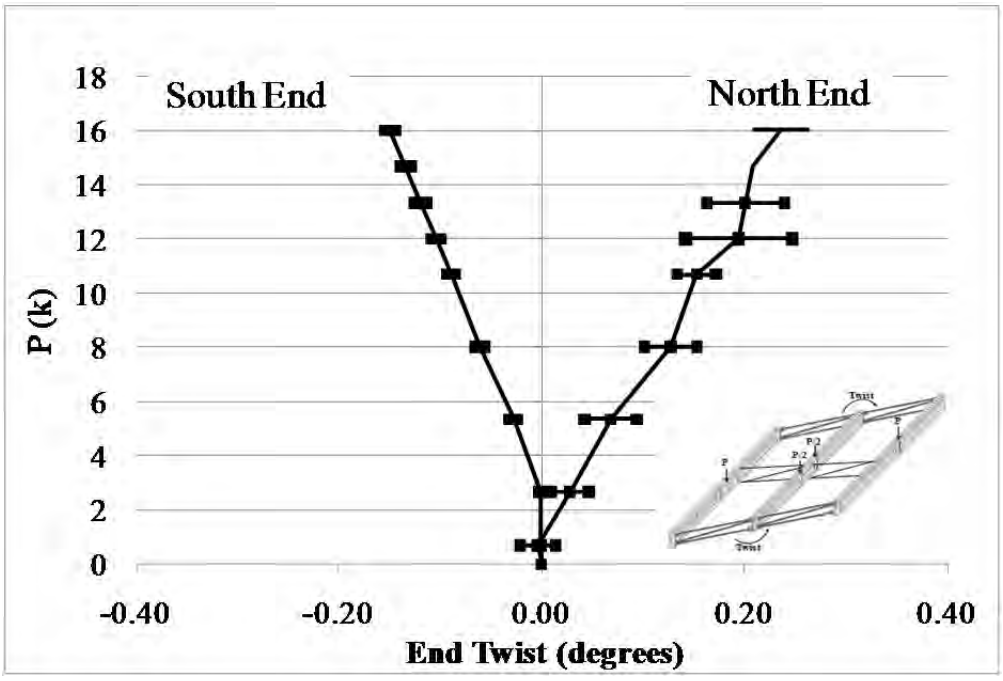

Figure A.129: GBP2 end twists

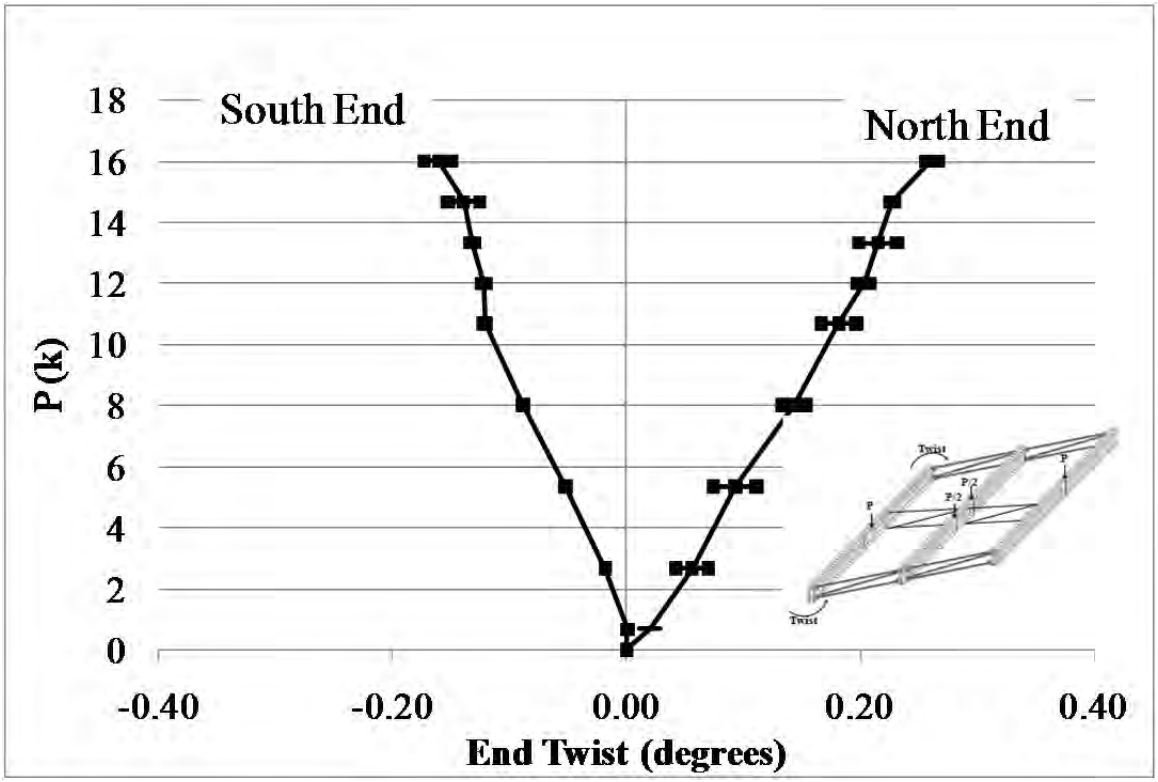

Figure A.130: GBP3 end twists

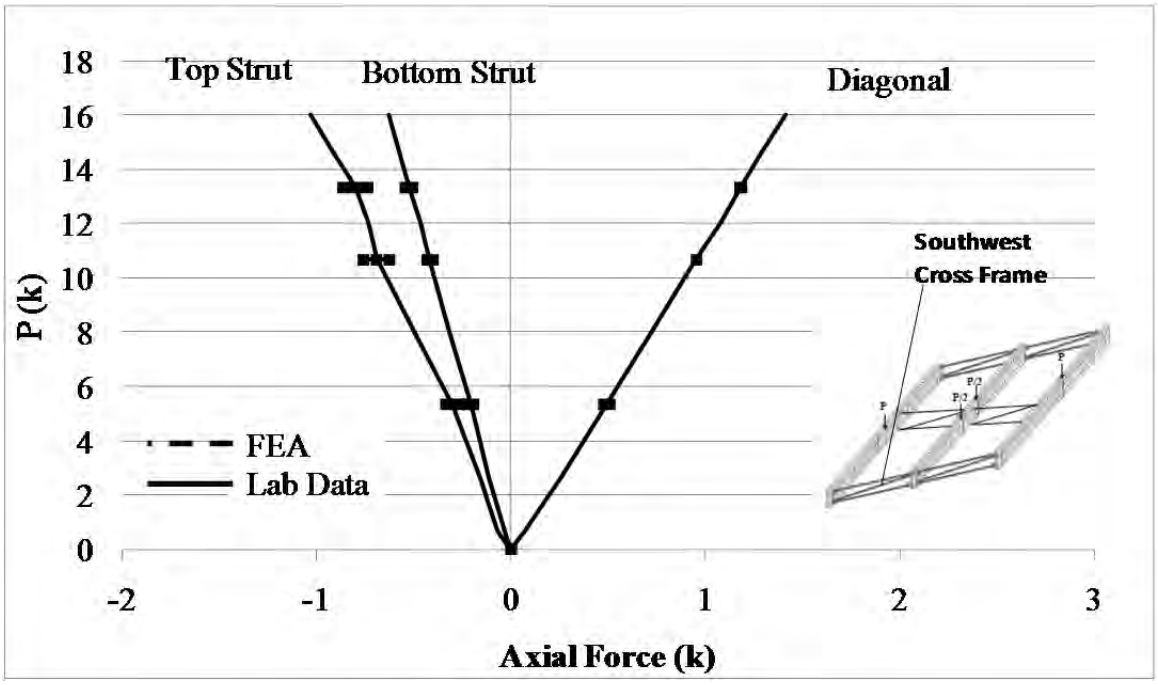

Figure A.131: SW end cross frame axial forces

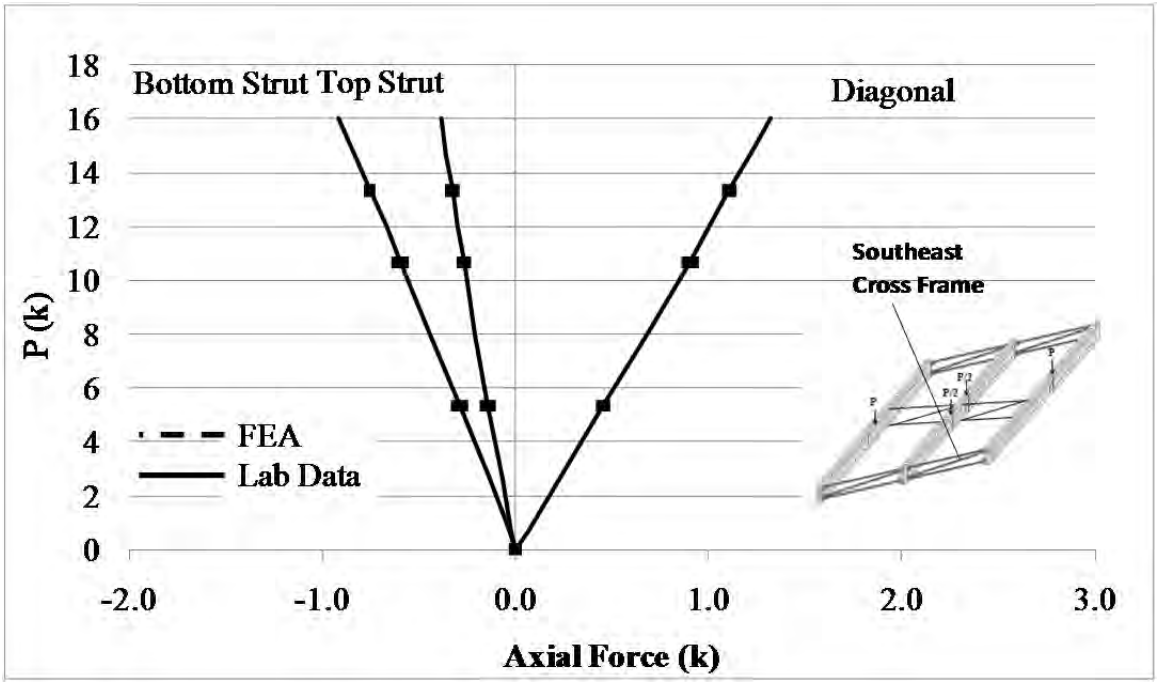

Figure A.132: SE end cross frame axial forces

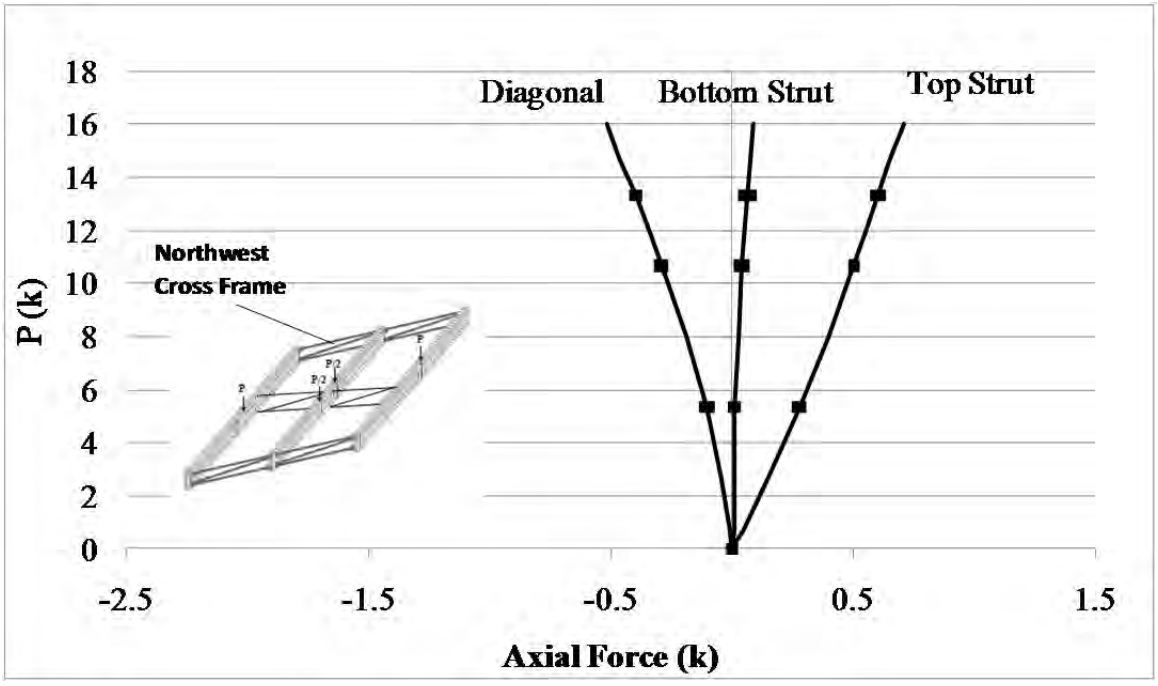

Figure A.133: NW end cross frame axial forces

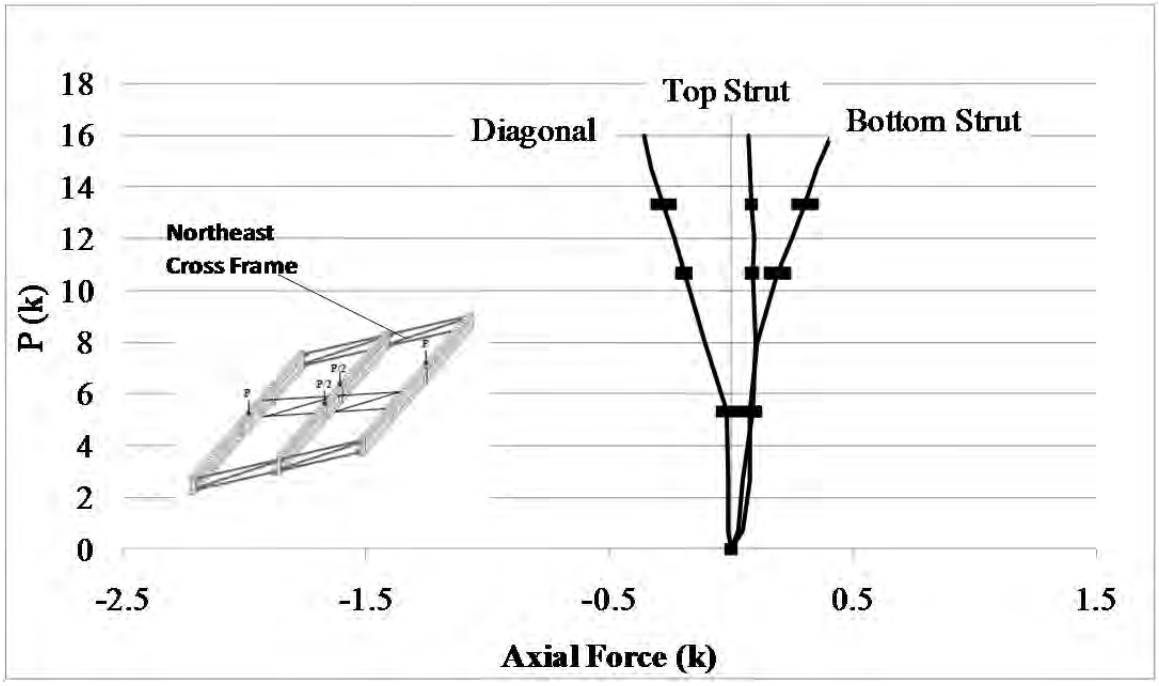

Figure A.134: NE end cross frame axial forces

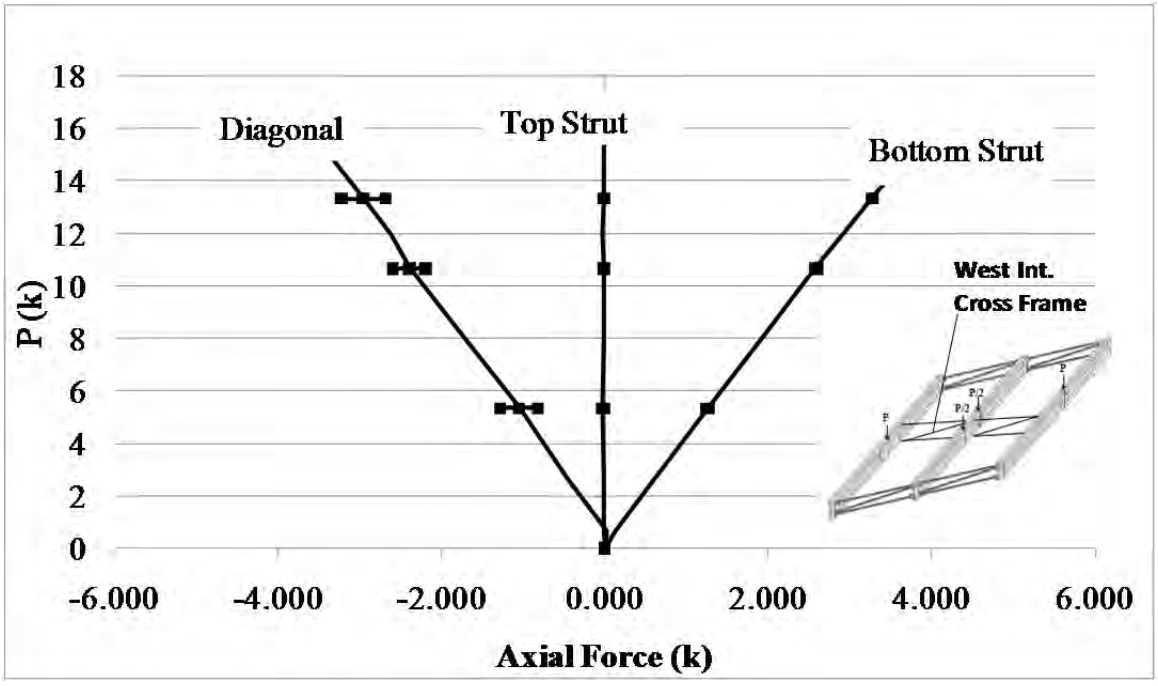

Figure A.135: West intermediate cross frame axial forces

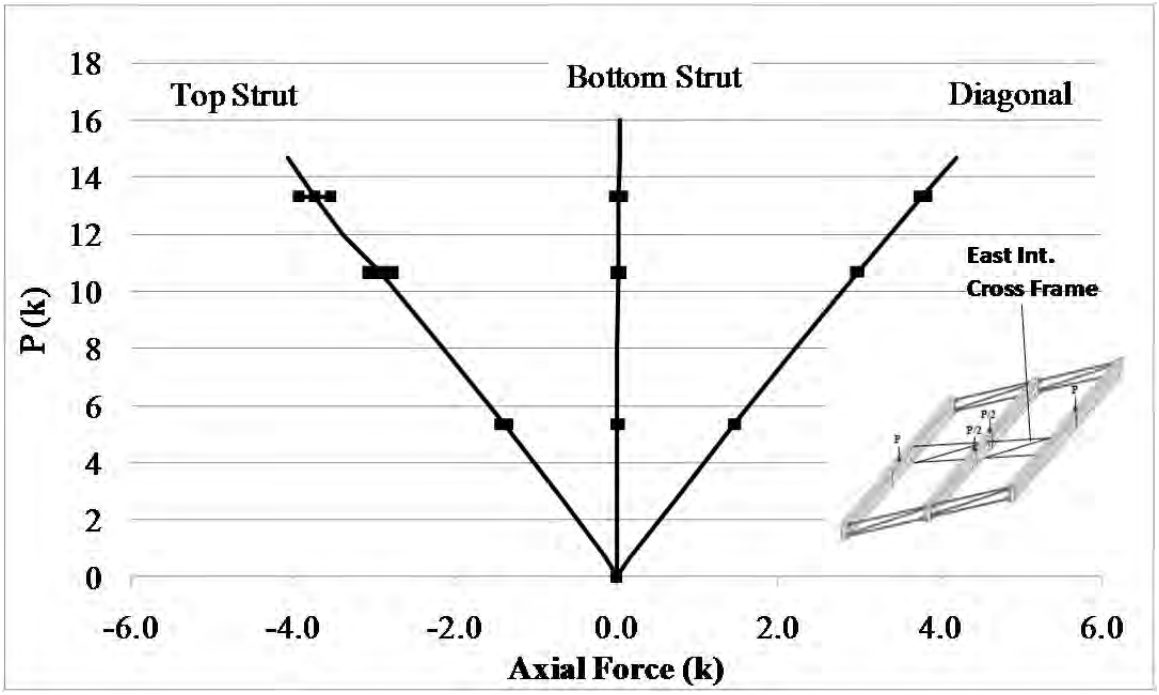

Figure A.136: East intermediate cross frame axial forces

A.4.5 Thrust Washer Bearing with Continuous Intermediate Cross Frames – Partial Loading

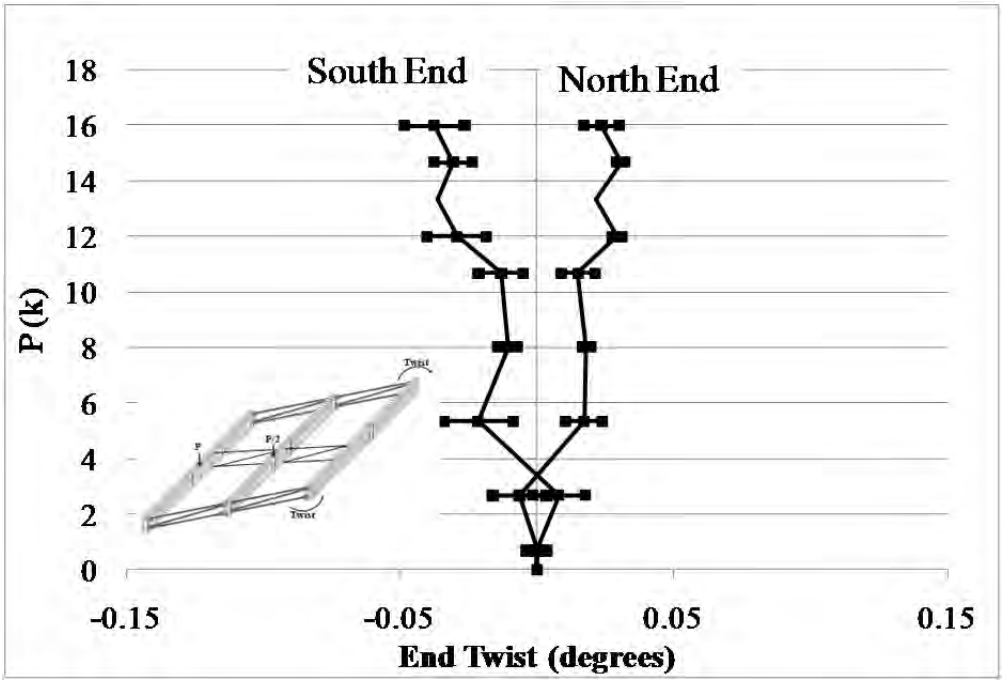

Figure A.137: GBP1 end twists

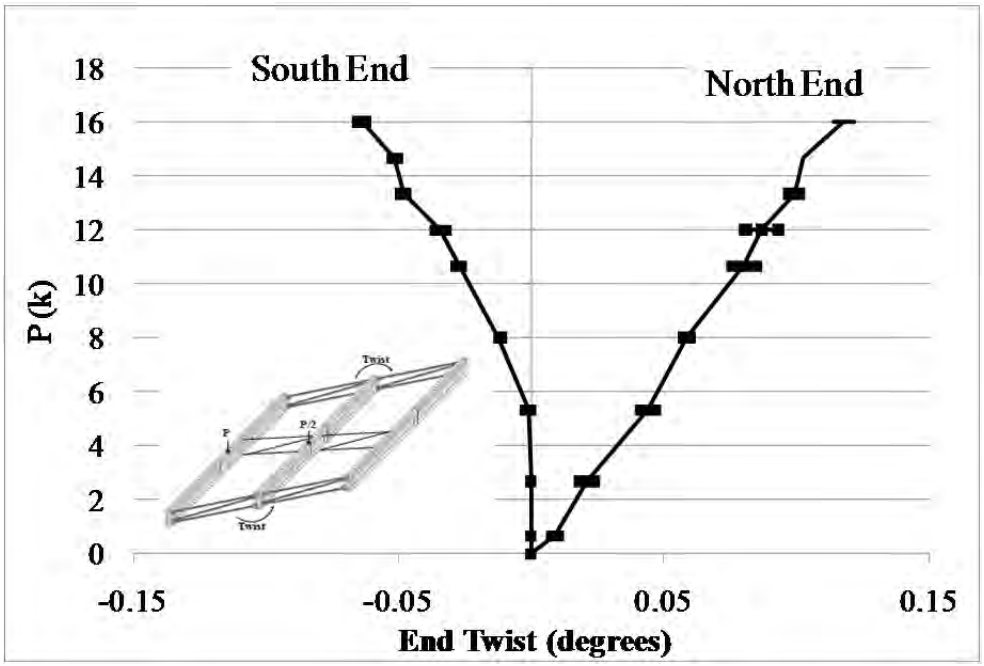

Figure A.138: GBP2 end twists

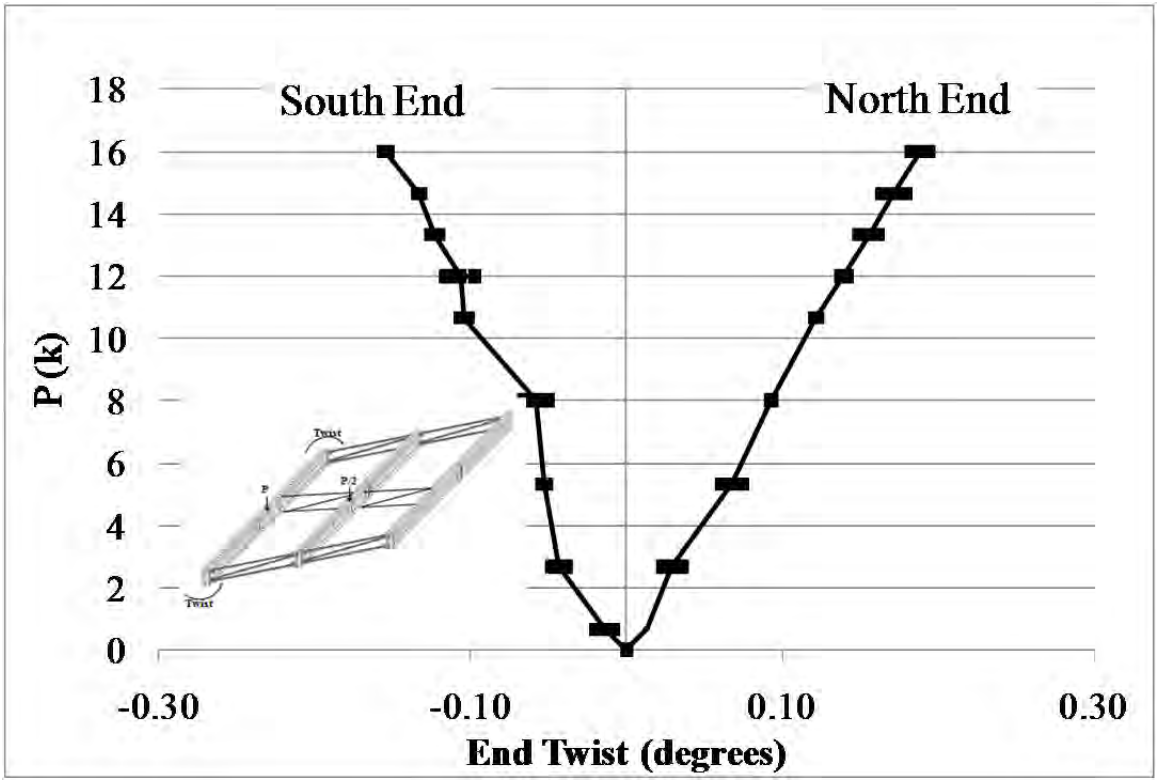

Figure A.139: GBP3 end twists

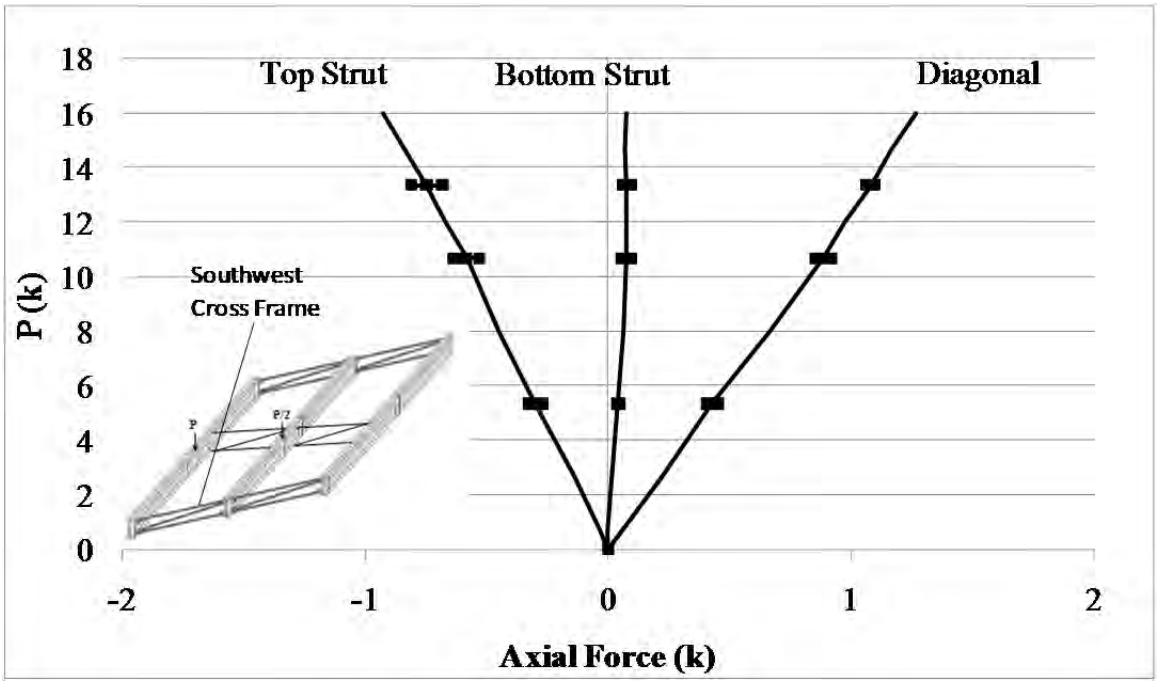

Figure A.140: SW end cross frame axial forces

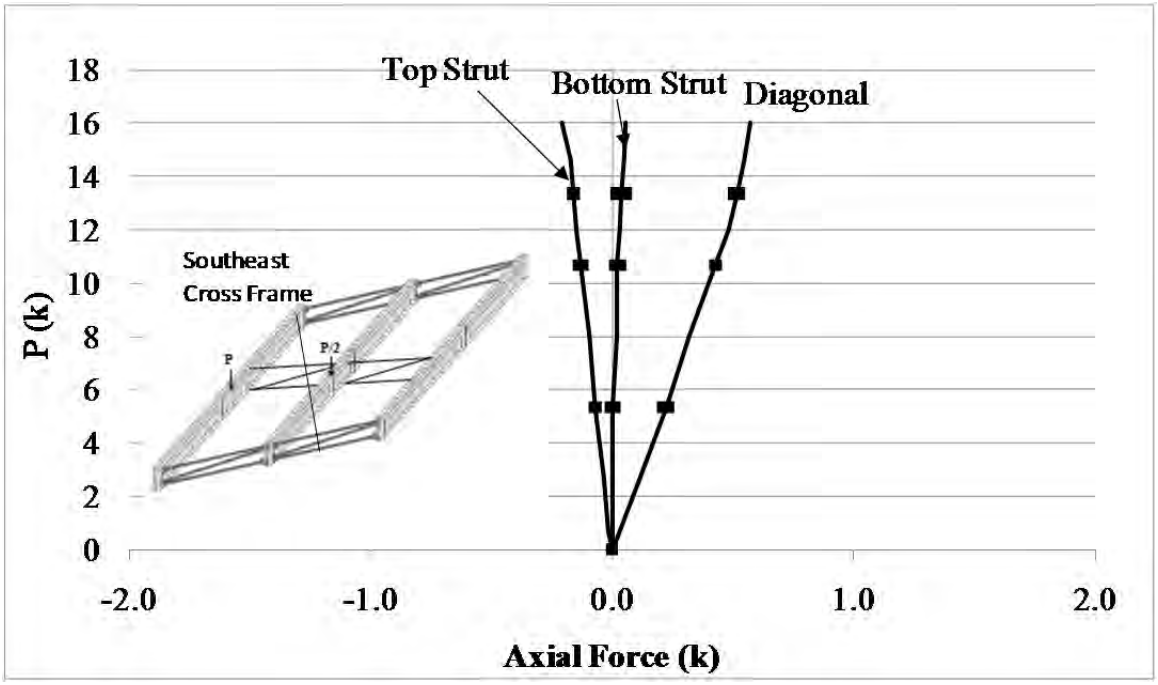

Figure A.141: SE end cross frame axial forces

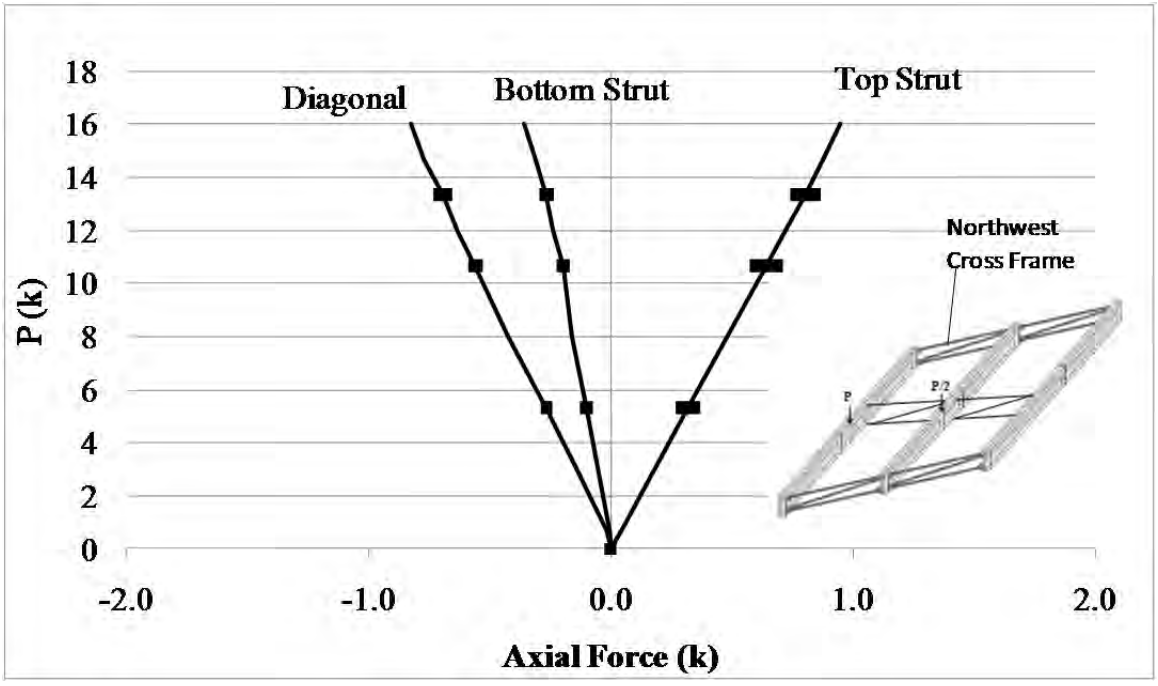

Figure A.142: NW end cross frame axial forces

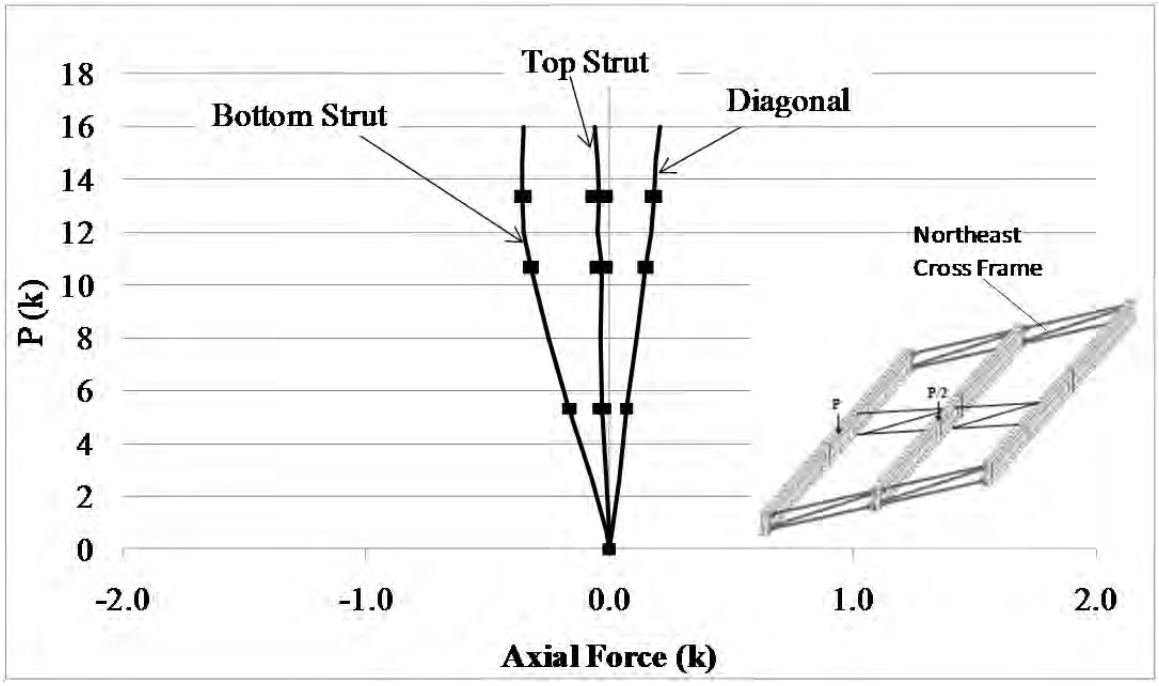

Figure A.143: NE end cross frame axial forces

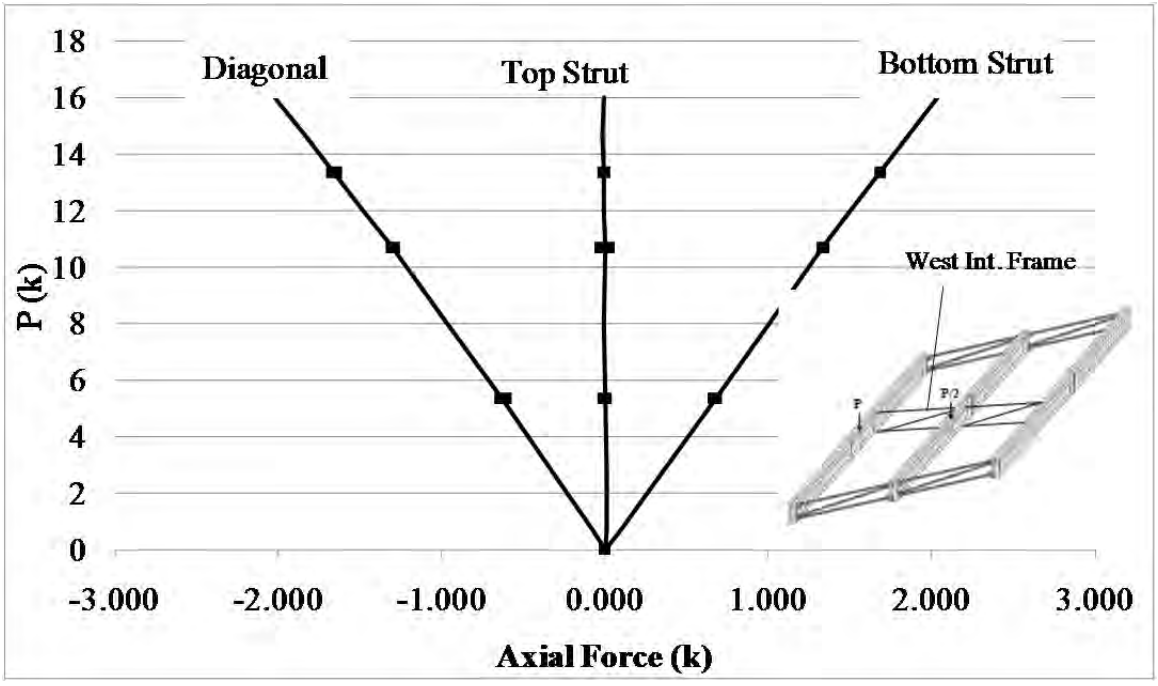

Figure A.144: West intermediate cross frame axial forces

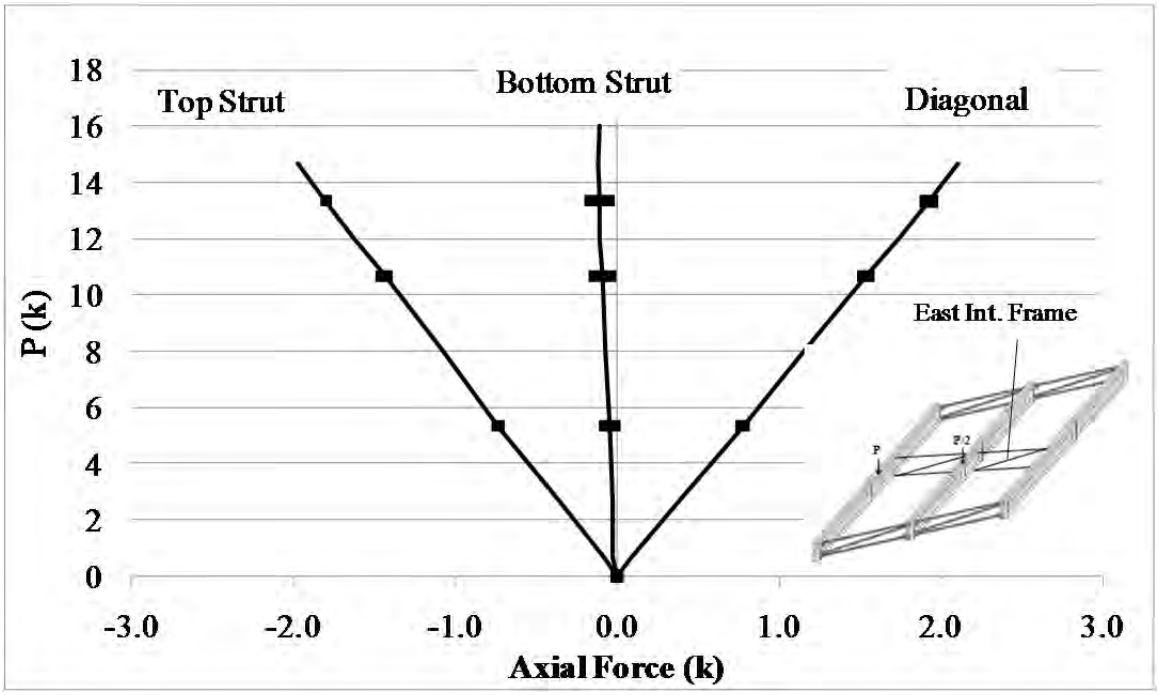

Figure A.145: East intermediate cross frame axial forces

A.4.6 Rubber Bearing with No Intermediate Cross Frames

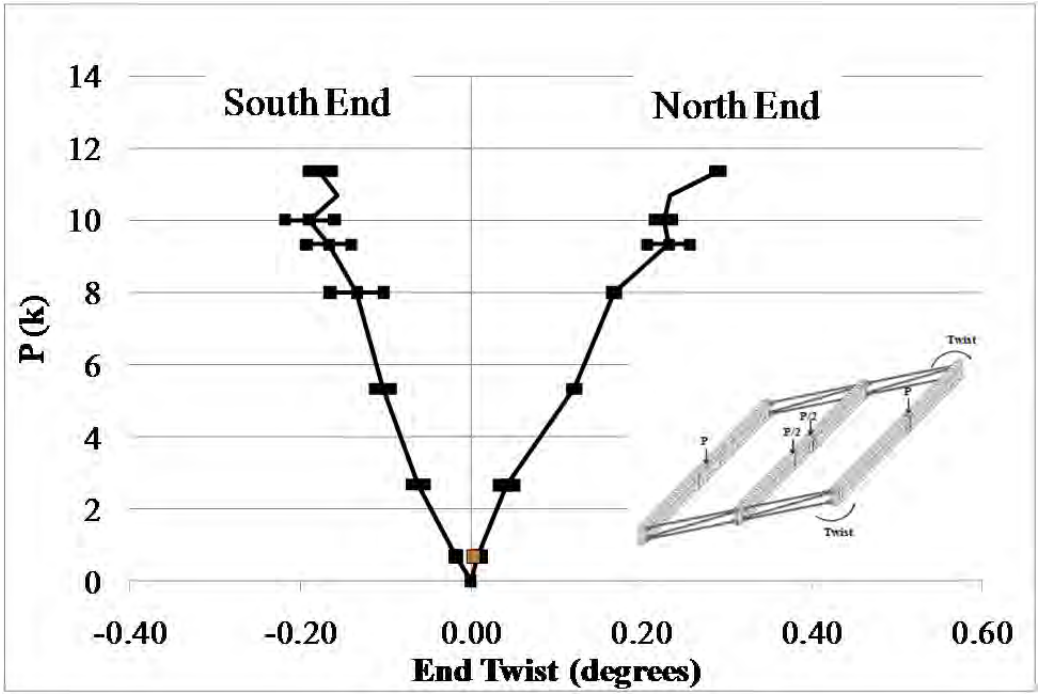

Figure A.146: GBP1 end twists

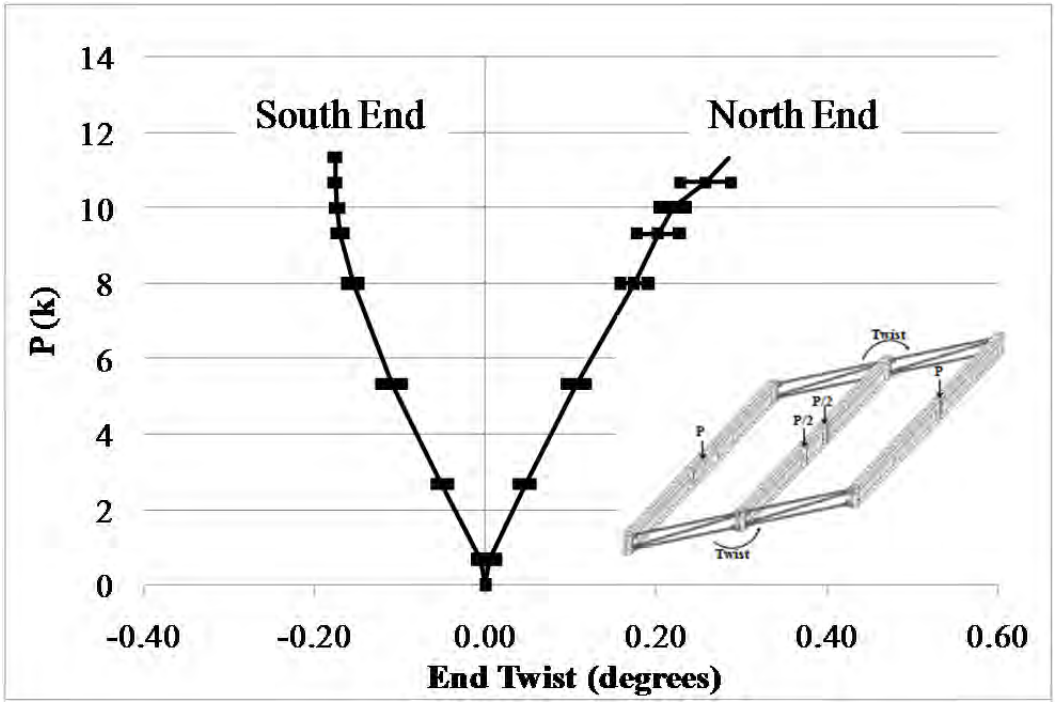

Figure A.147: GBP2 end twists

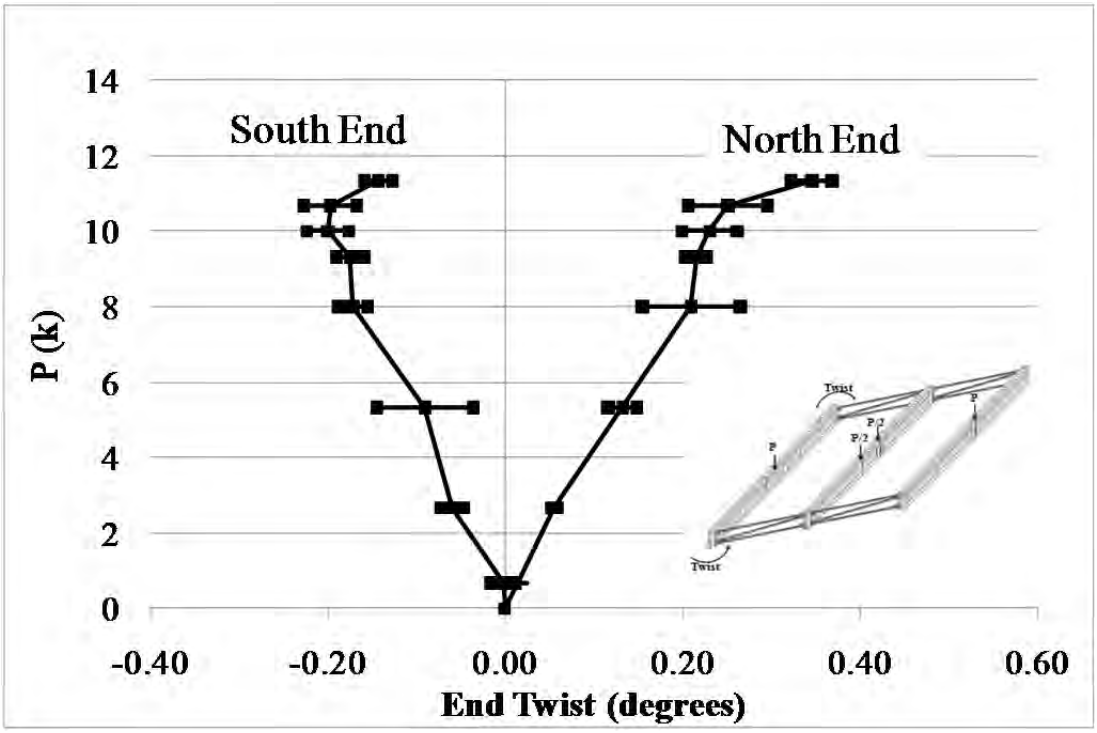

Figure A.148: GBP3 end twists

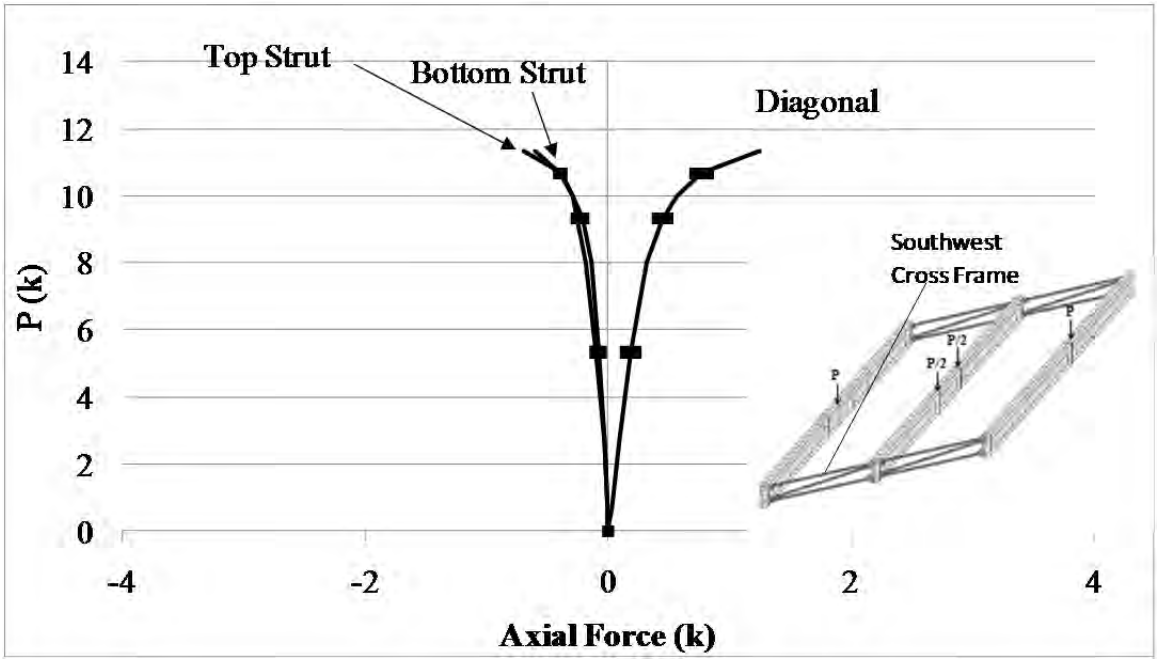

Figure A.149: SW end cross frame axial forces

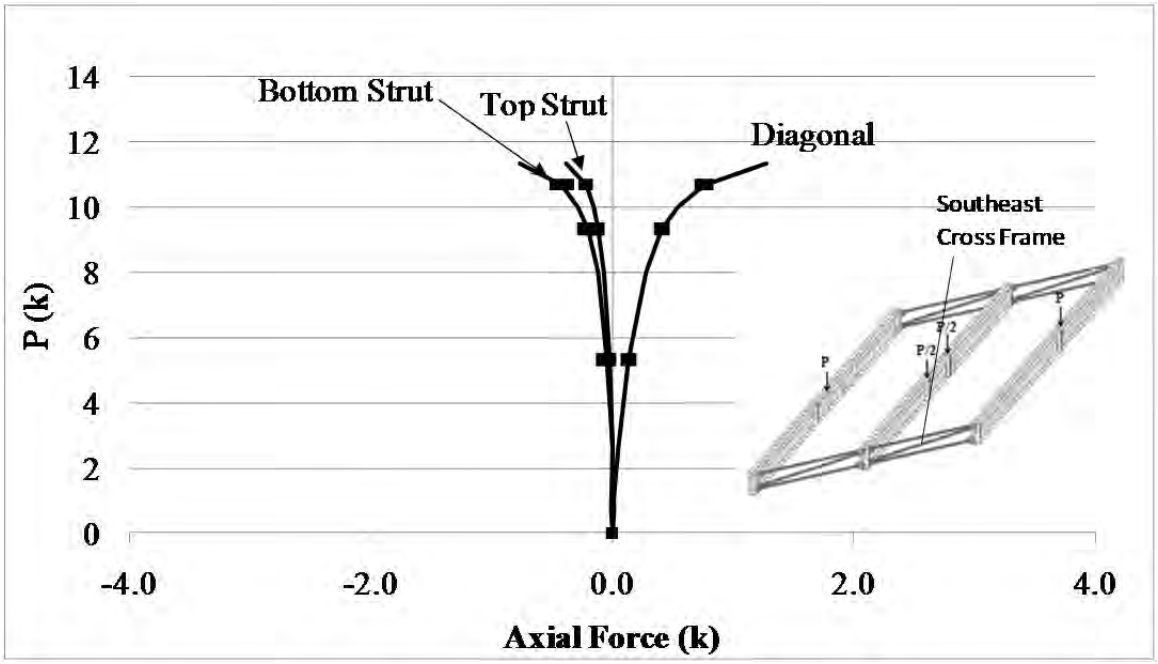

Figure A.150: SE end cross frame axial forces

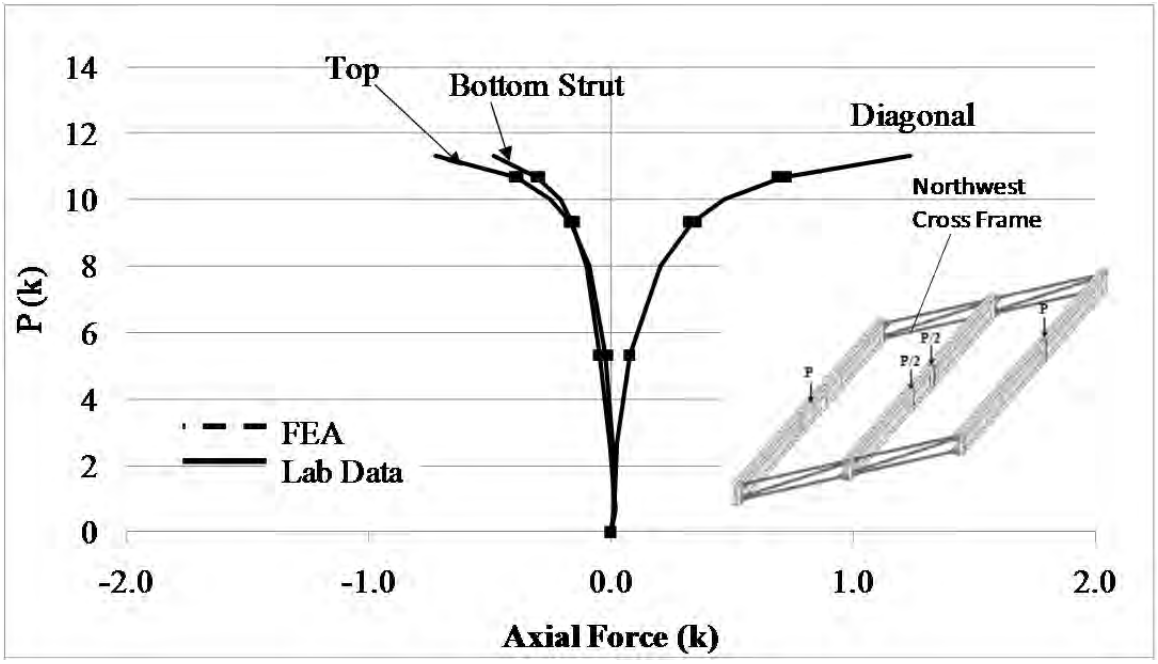

Figure A.151: NW end cross frame axial forces

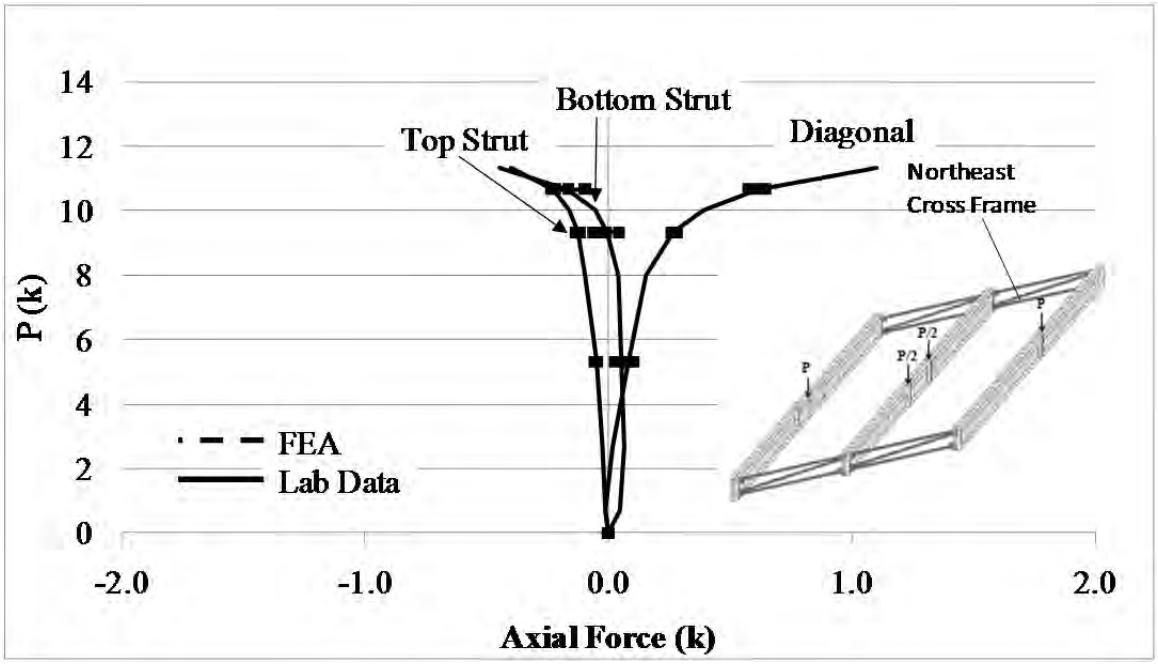

Figure A.152: NE end cross frame axial forces

A.4.7 Rubber Bearing with Shim with No Intermediate Cross Frames

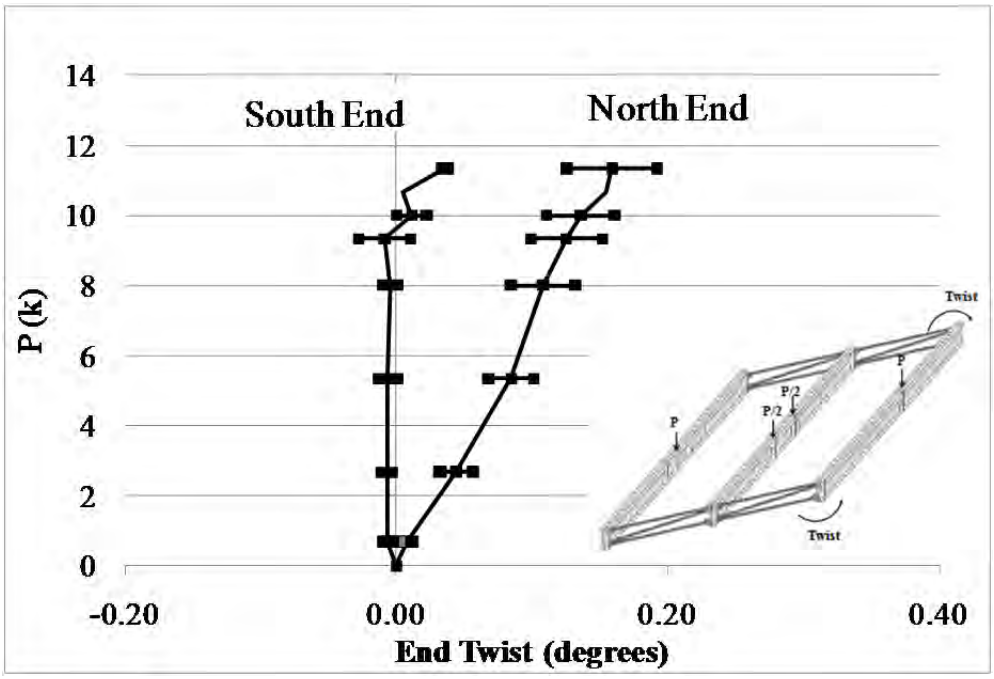

Figure A.153: GBP1 end twists

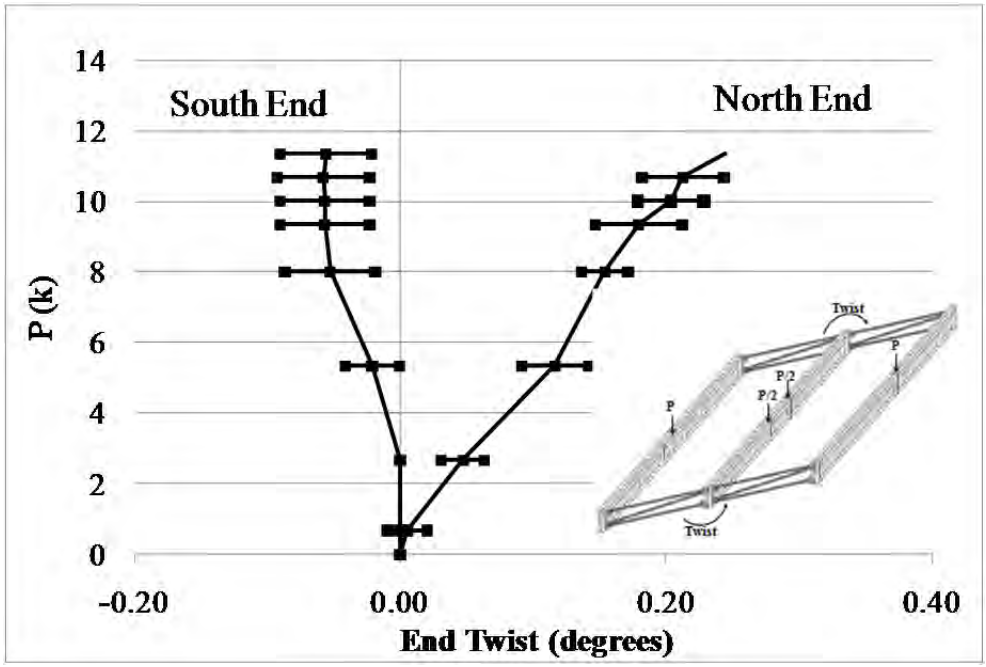

Figure A.154: GBP2 end twists

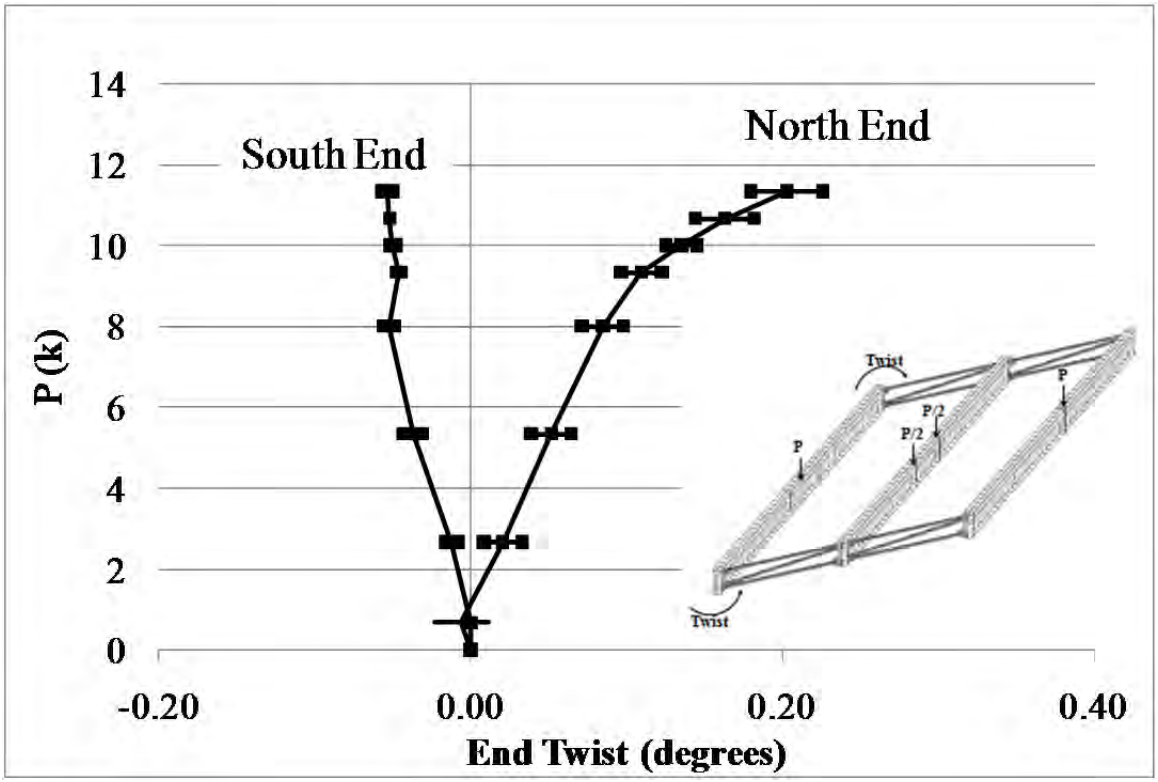

Figure A.155: GBP3 end twists

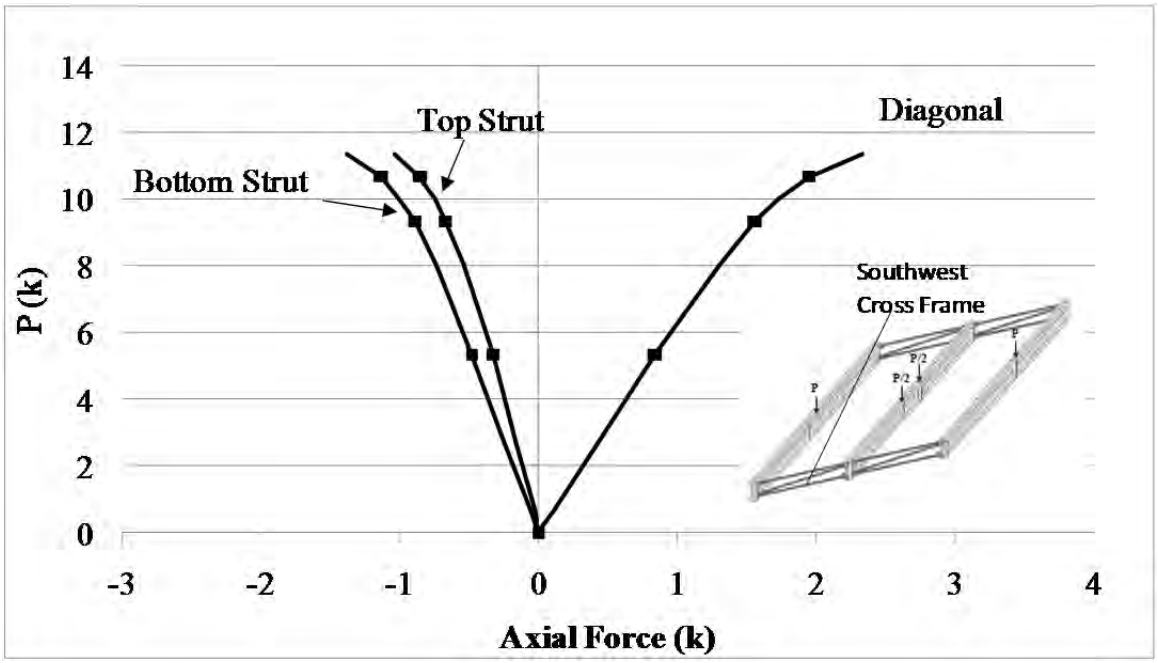

Figure A.156: SW end cross frame axial forces

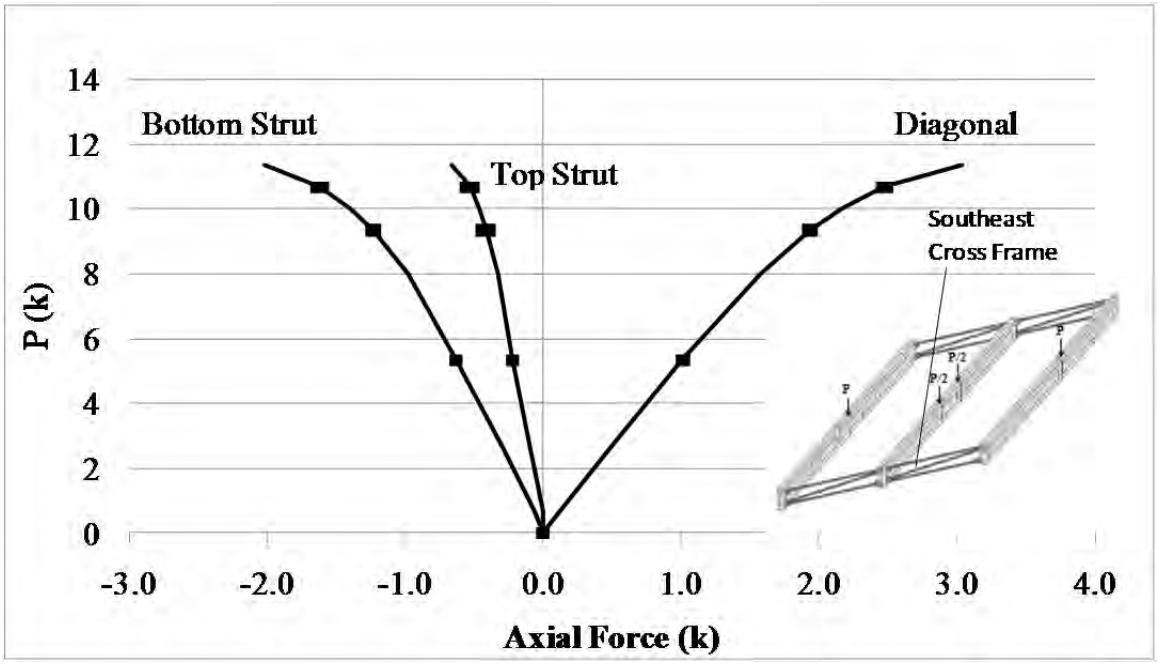

Figure A.157: SE end cross frame axial forces

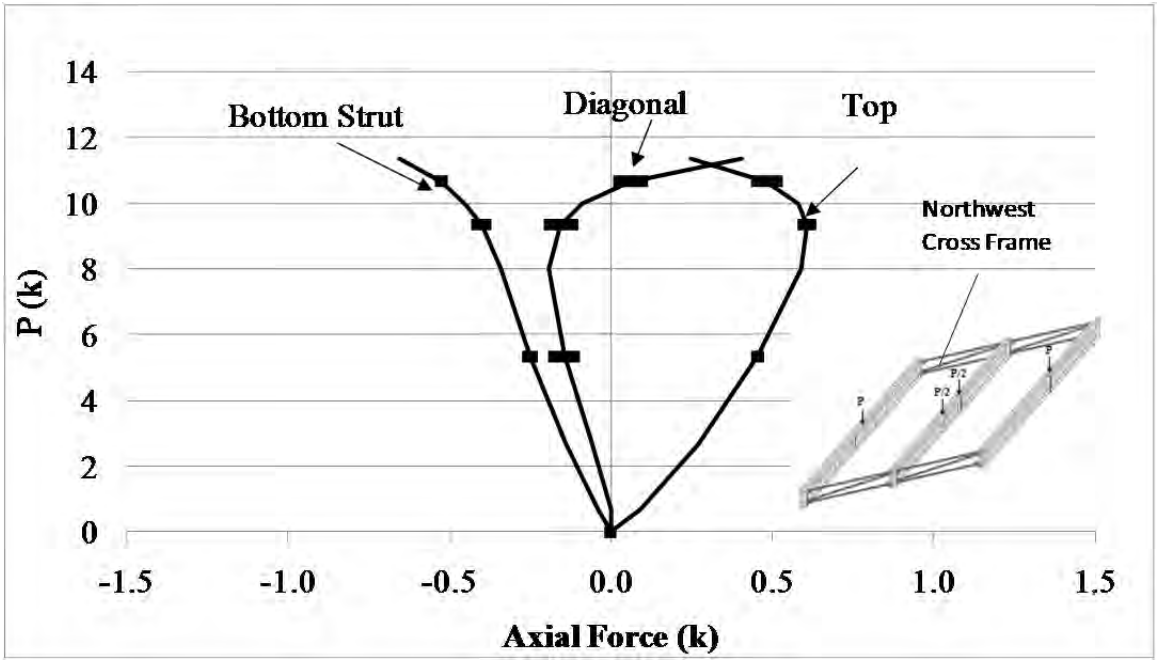

Figure A.158: NW end cross frame axial forces

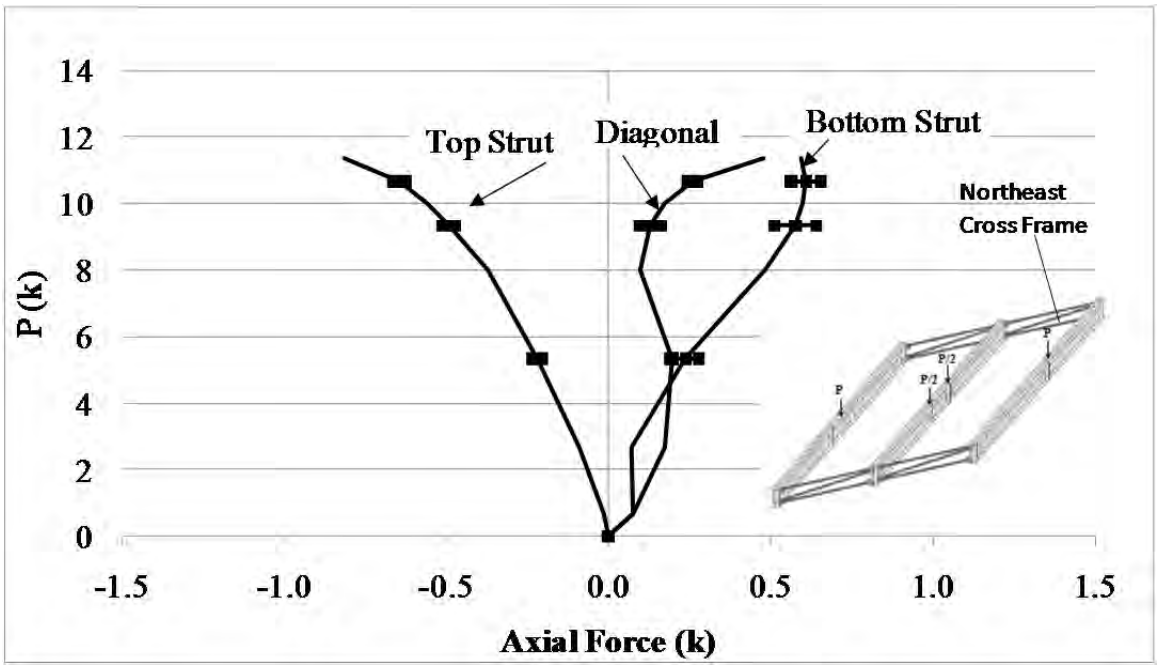

Figure A.159: NE end cross frame axial forces

APPENDIX B: Finite Element Model Validation Results

B.1 CONNECTION MODEL VALIDATION

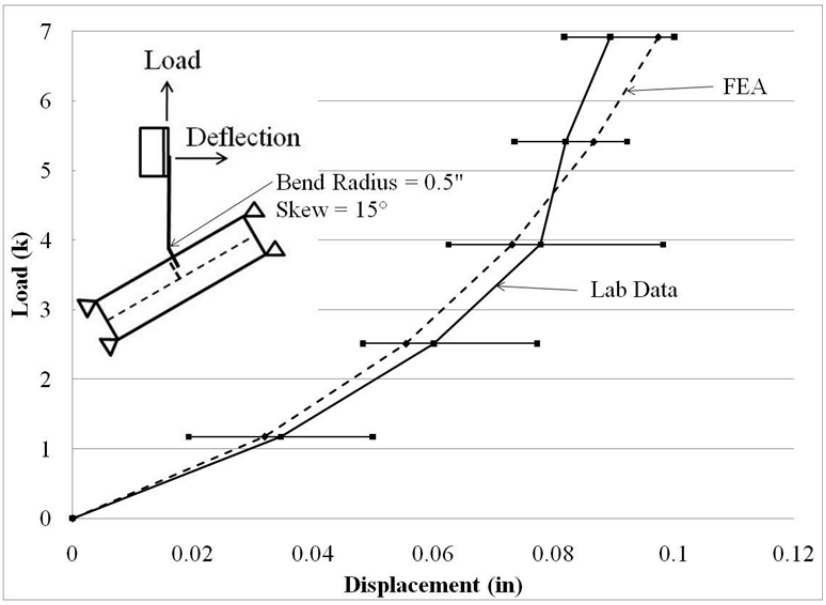

Figure B.1: 15° skew specimen and FEA lateral deflection results

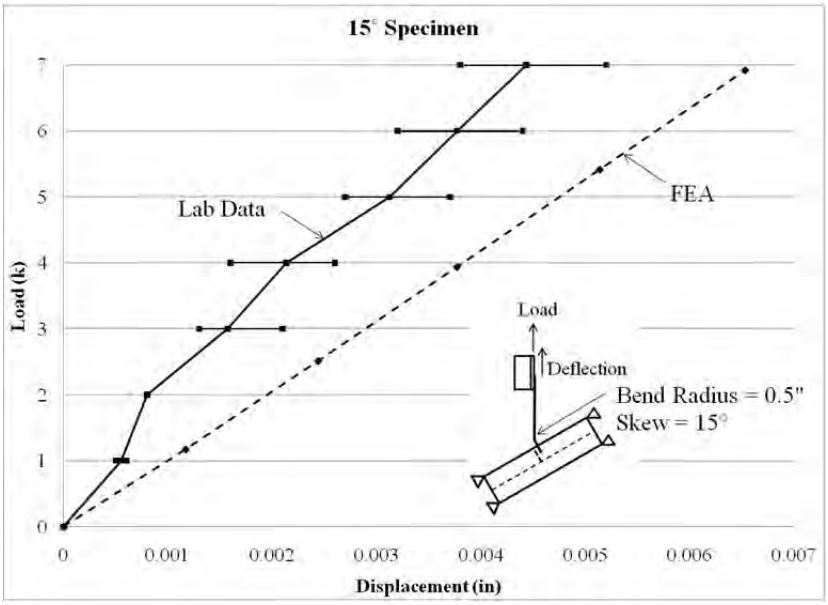

Figure B.2: 15° skew specimen and FEA lateral deflection results

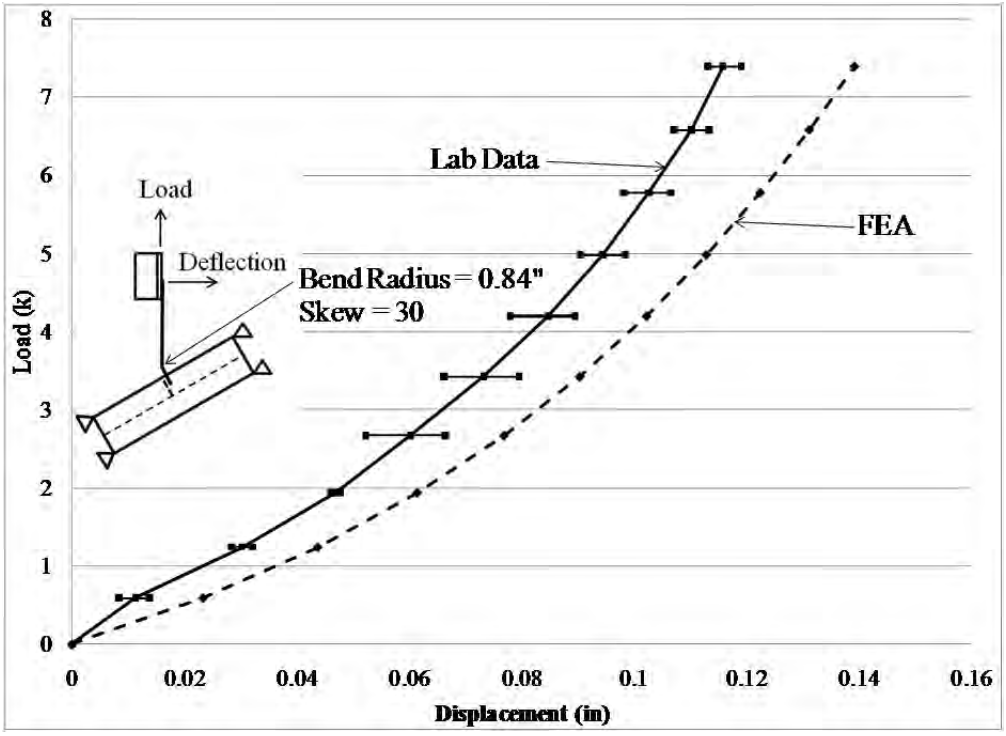

Figure B.3: 30° skew specimen and FEA lateral deflection results

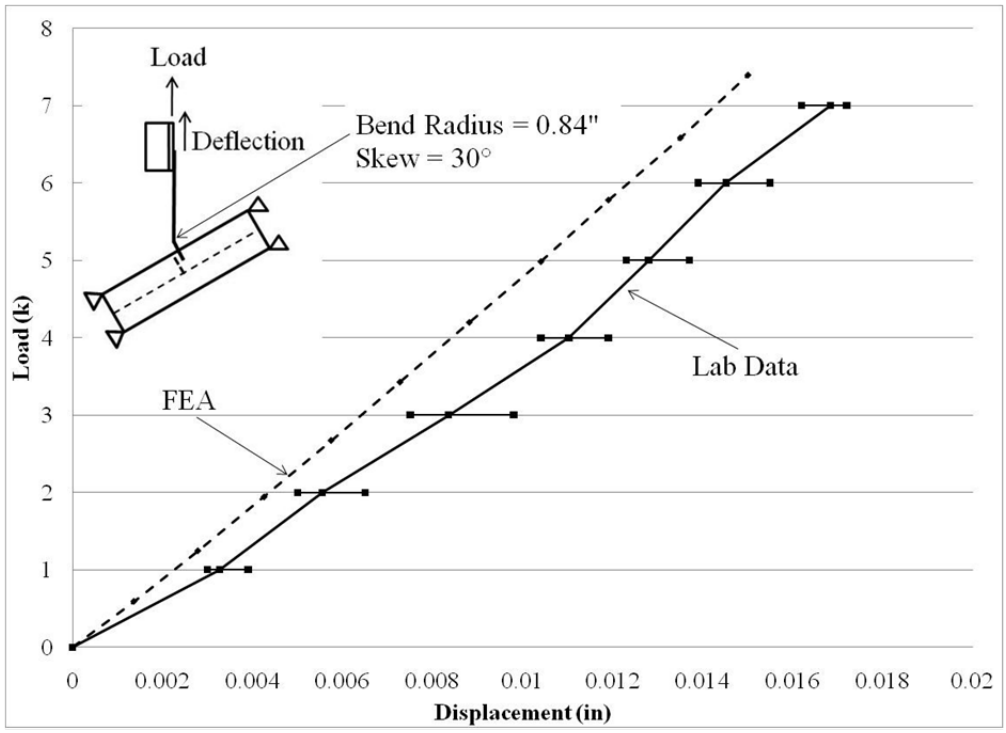

Figure B.4: 30° skew specimen and FEA vertical deflection results

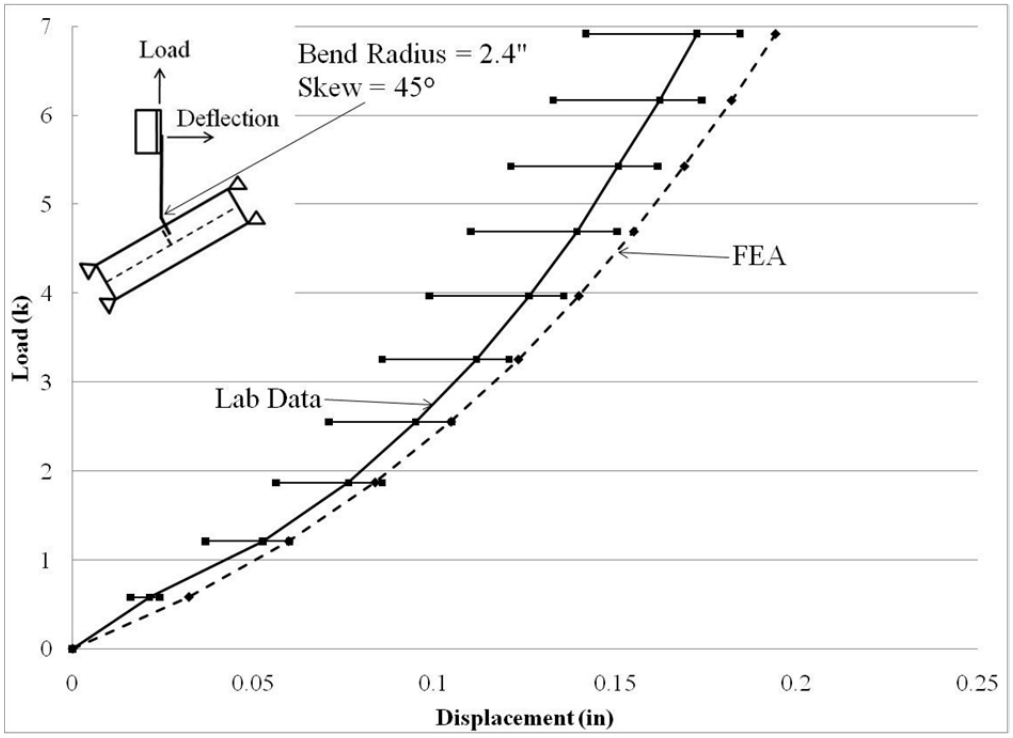

Figure B.5: 45° skew specimen and FEA lateral deflection results

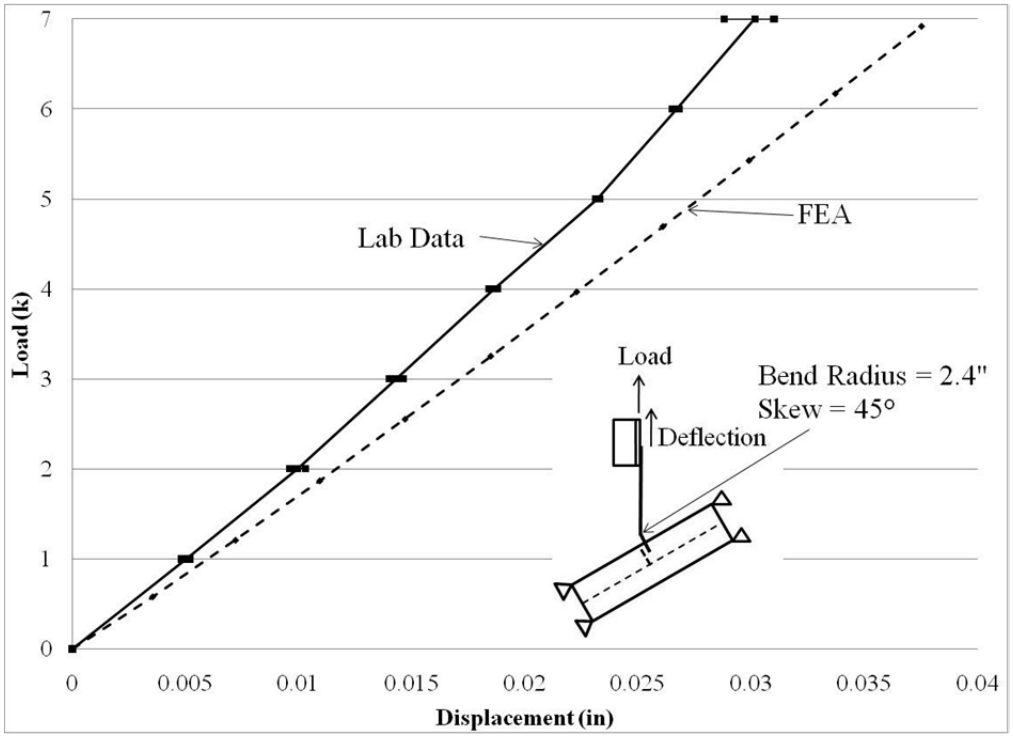

Figure B.6: 45° skew specimen and FEA vertical deflection results

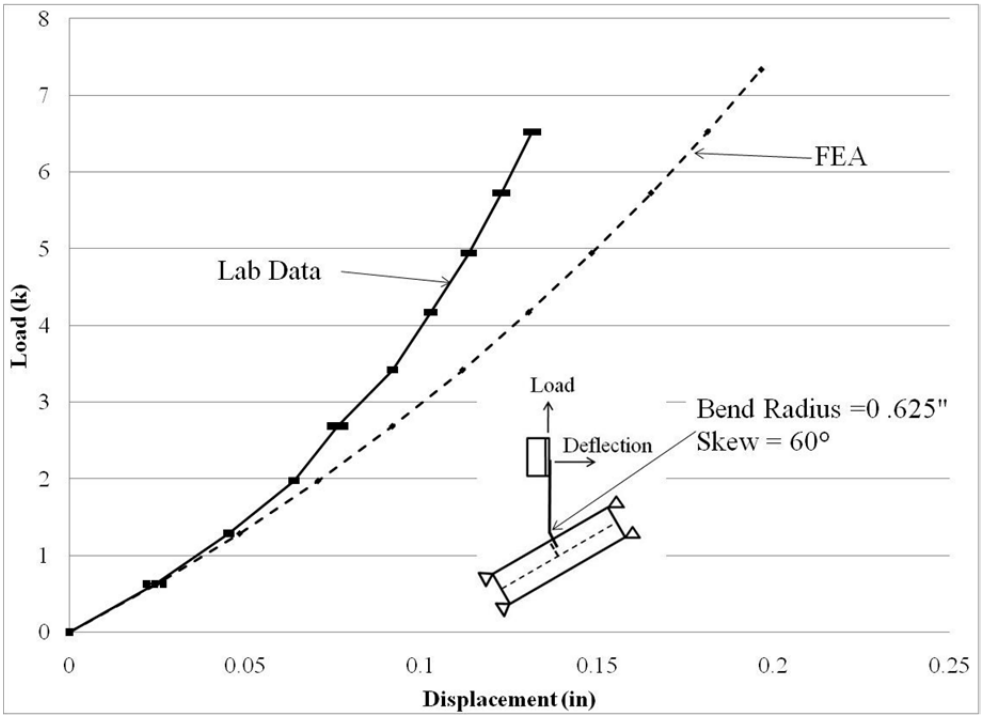

Figure B.7: 60° skew specimen and FEA lateral deflection results

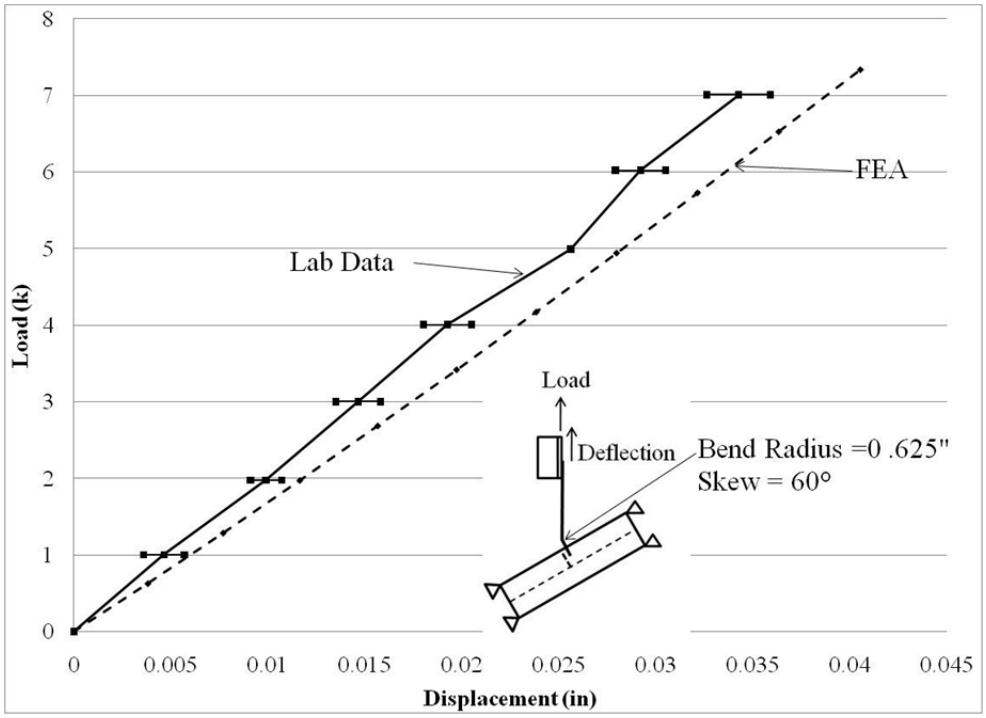

Figure B.8: 60° skew specimen and FEA vertical deflection results

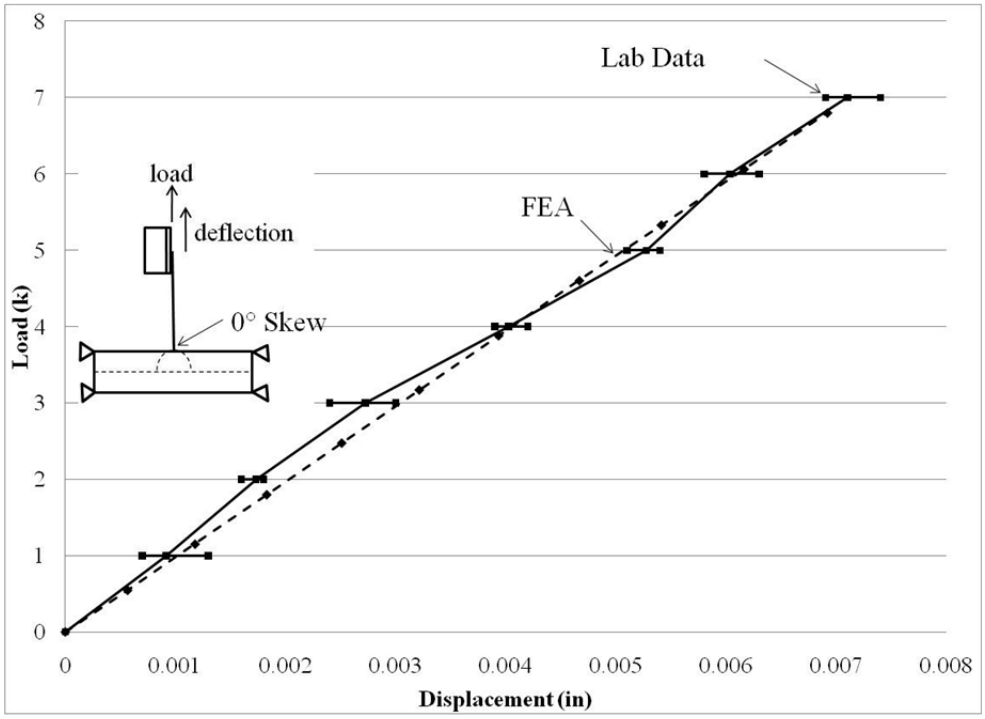

Figure B.9: 0° skew pipe specimen and FEA vertical deflection results

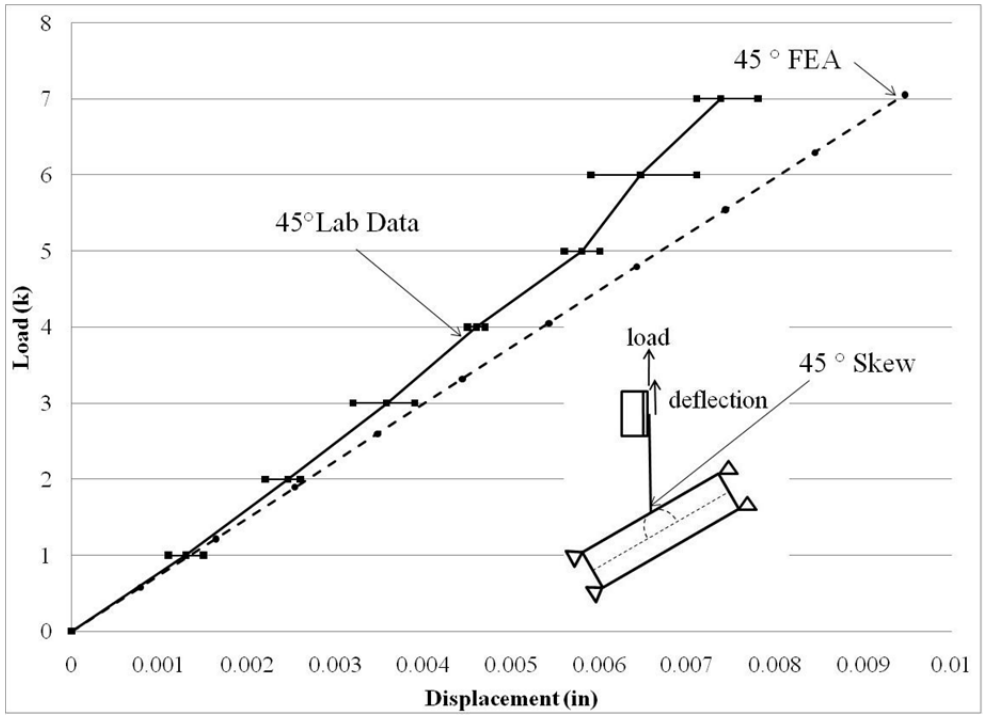

Figure B.10: 45° skew pipe specimen and FEA vertical deflection results

B.2 TWIN GIRDER VALIDATION RESULTS

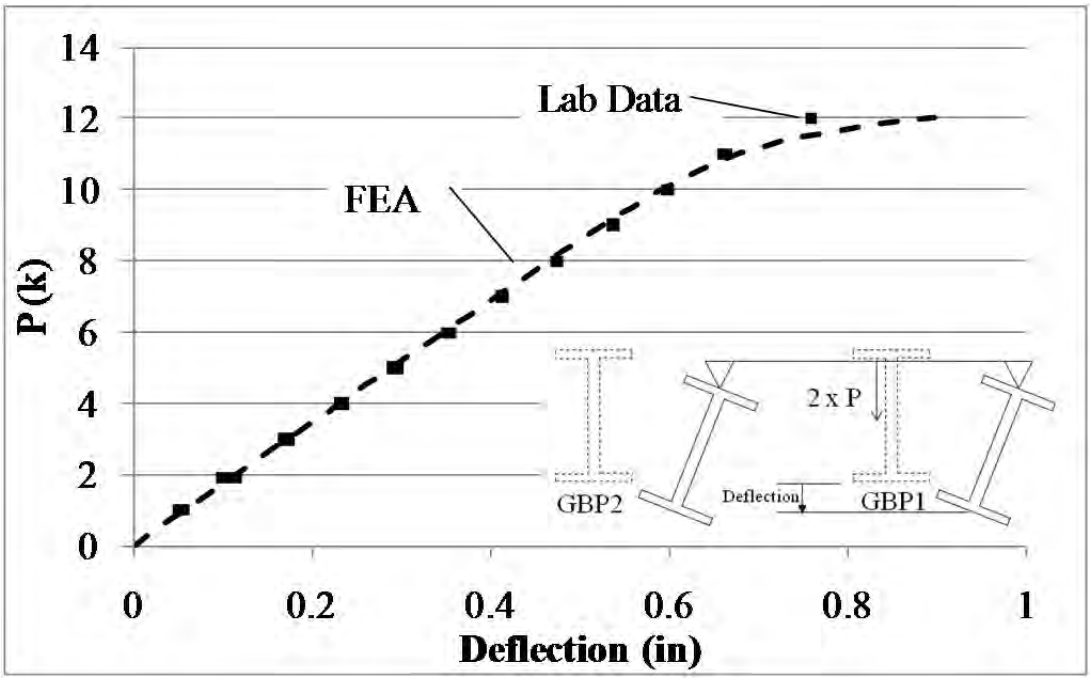

Figure B.11: GBP1 vertical deflection validation results

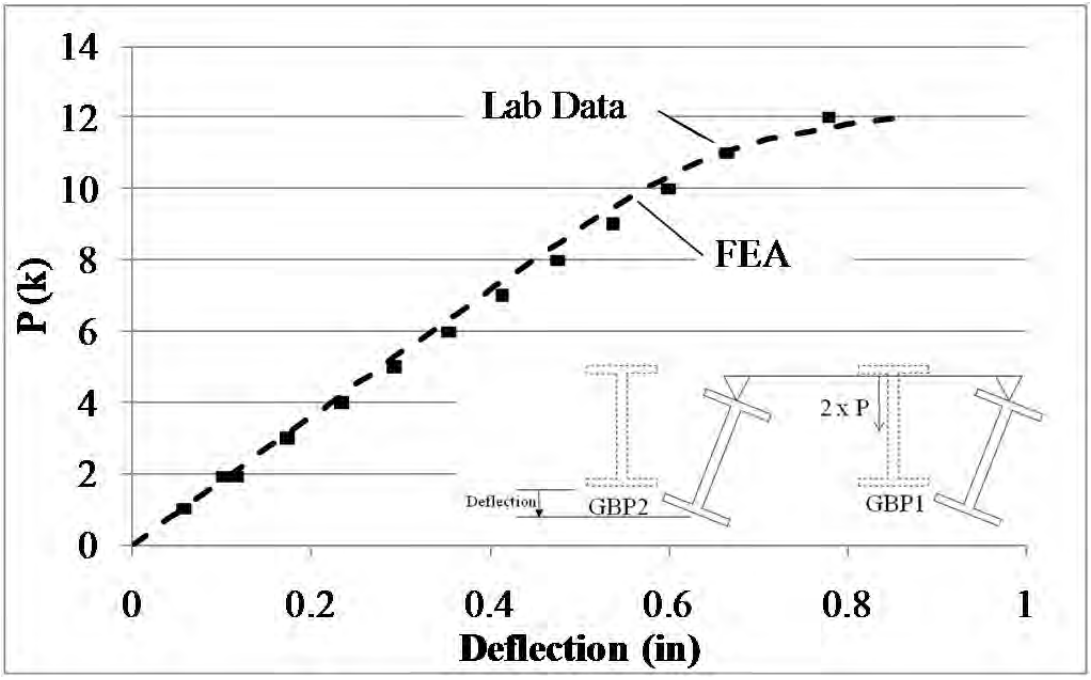

Figure B.12: GBP2 vertical deflection validation results

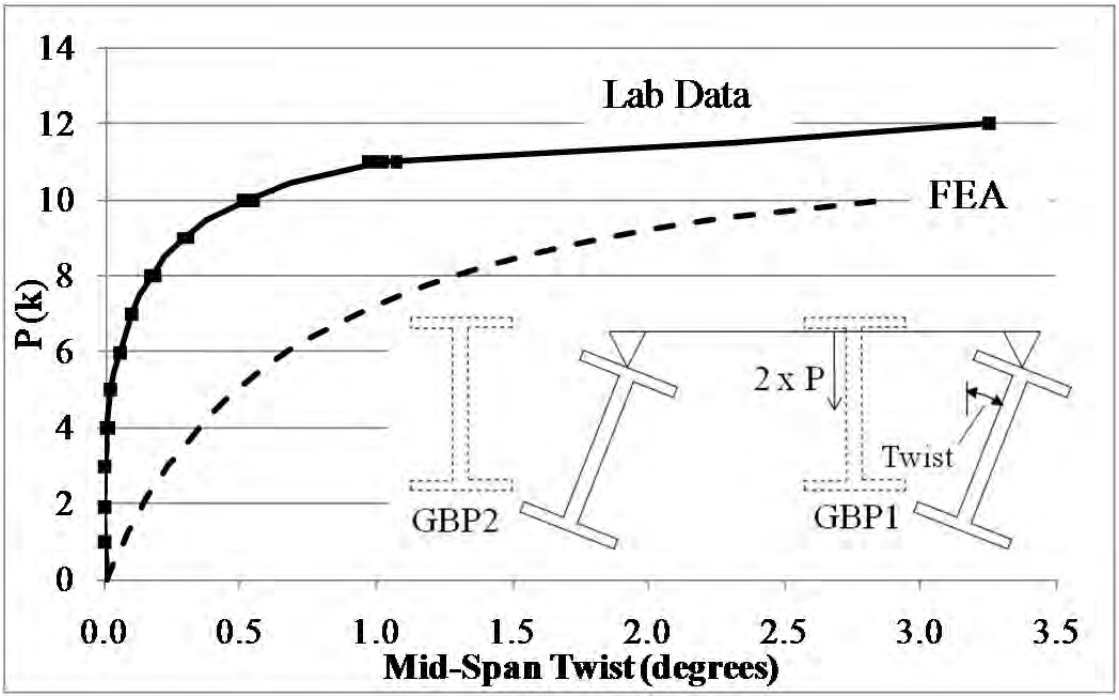

Figure B.13: GBP1 mid-span twist validation results

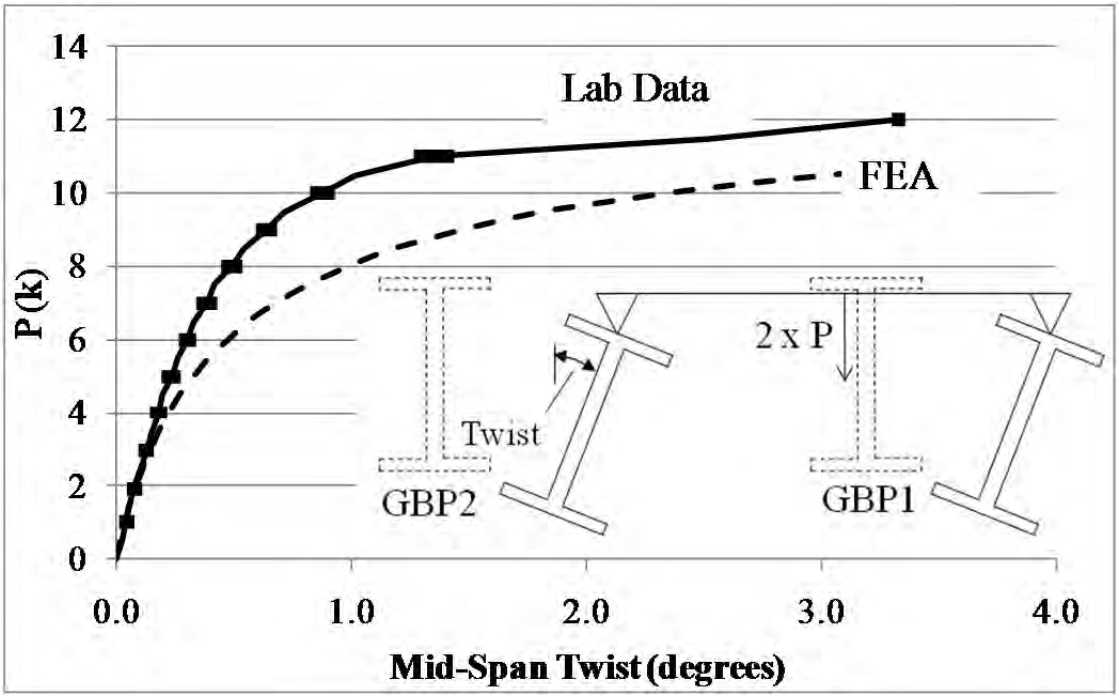

Figure B.14: GBP2 mid-span twist validation results

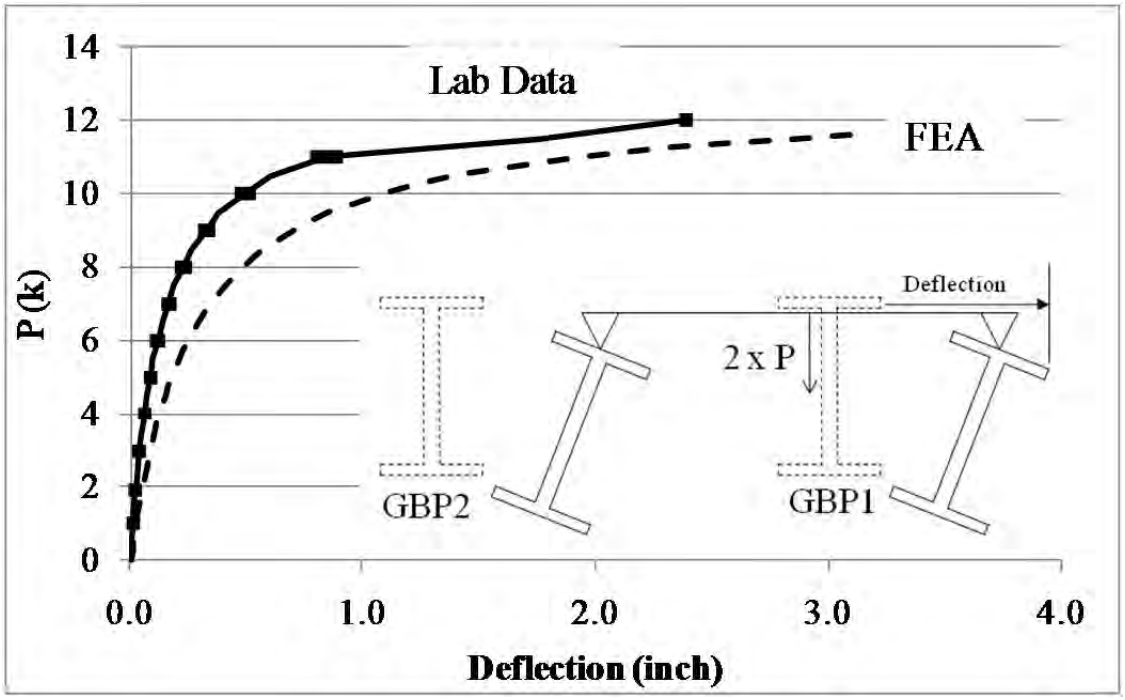

Figure B.15: GBP1 mid-span top flange lateral deflection validation results

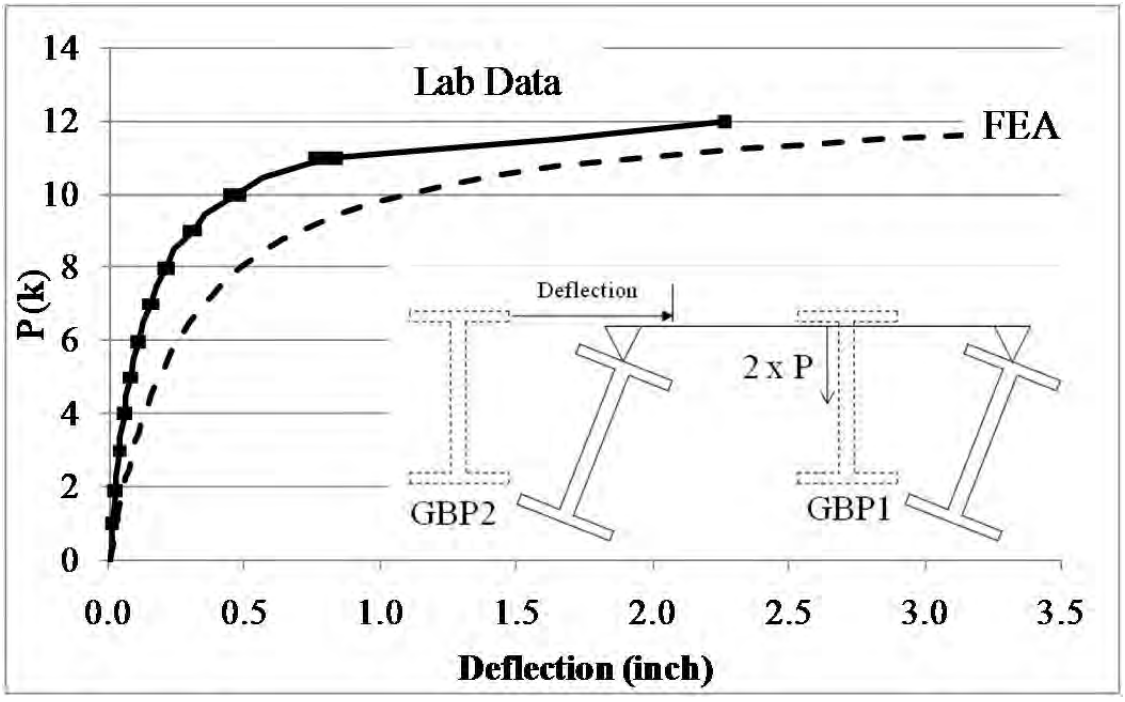

Figure B.16: GBP2 mid-span top flange lateral deflection validation results

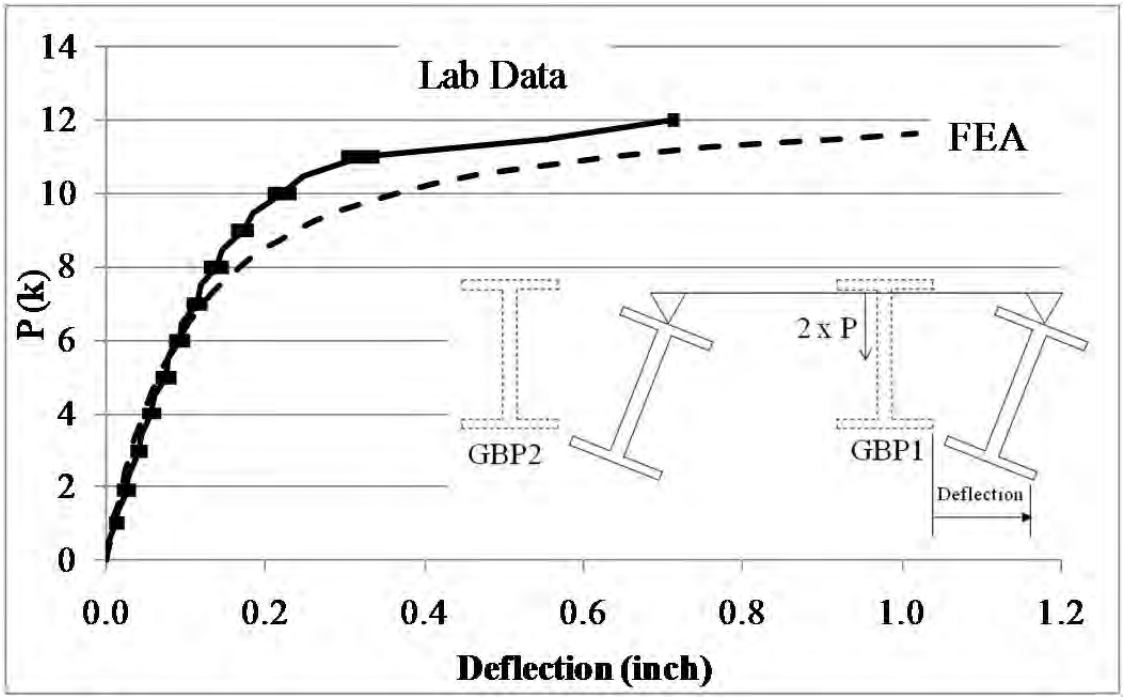

Figure B.17: GBP1 mid-span bottom flange lateral deflection validation results

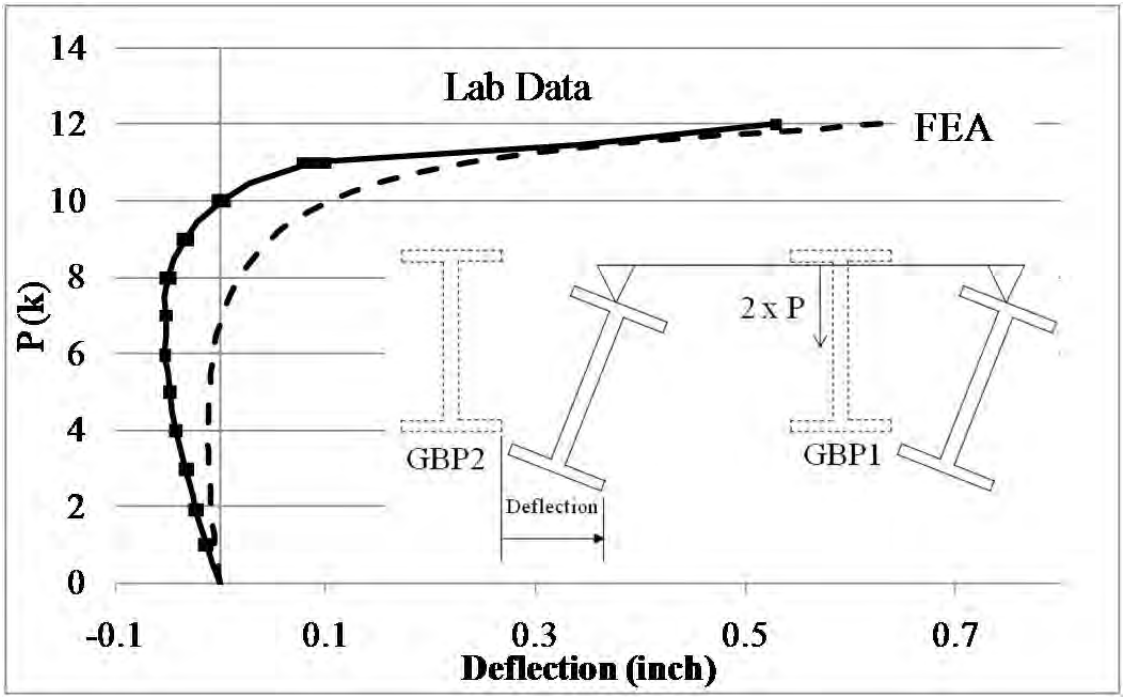

Figure B.18: GBP2 mid-span bottom flange lateral deflection validation results

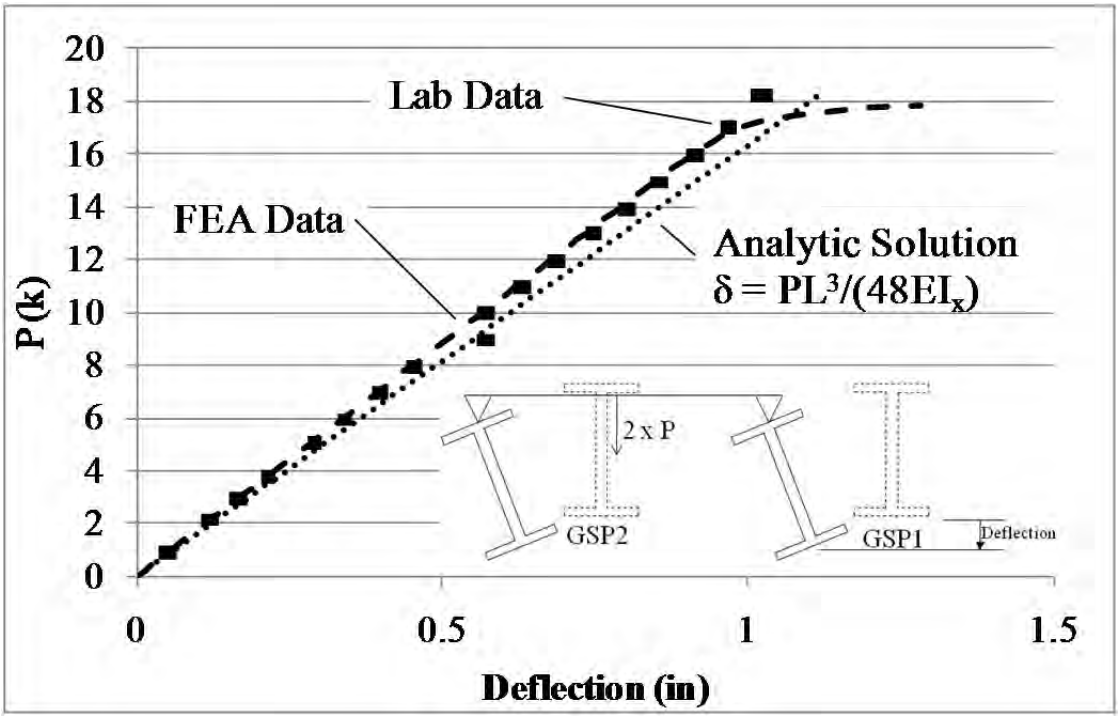

Figure B.19: GSP1 vertical deflection validation results

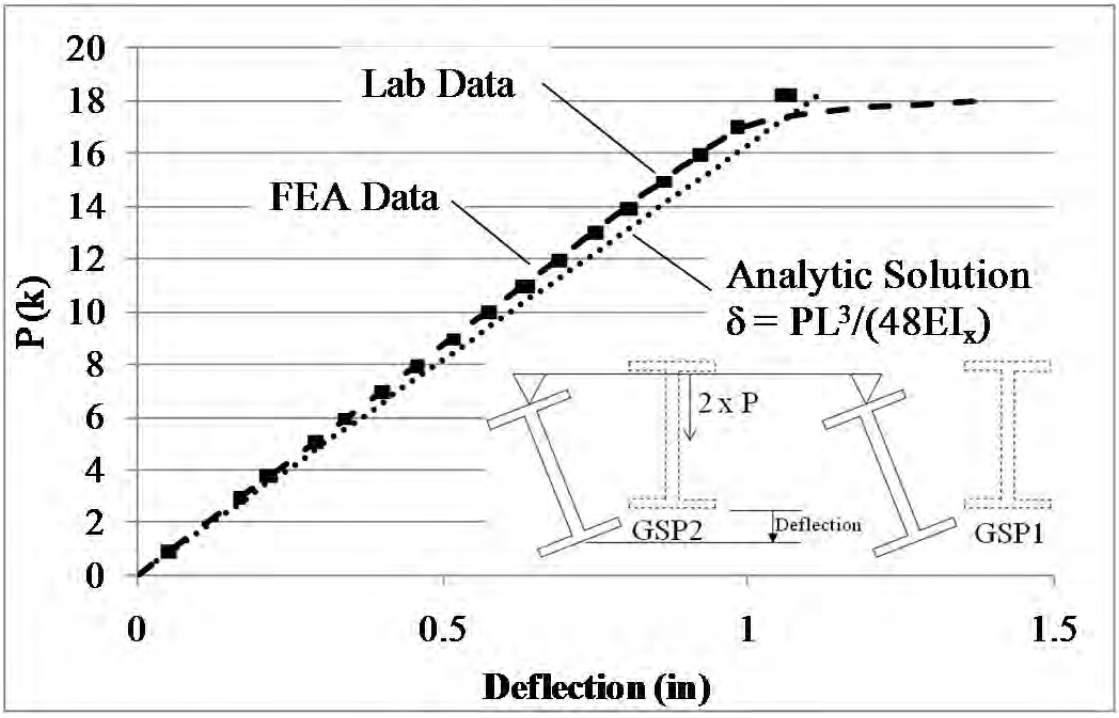

Figure B.20: GSP2 vertical deflection validation results

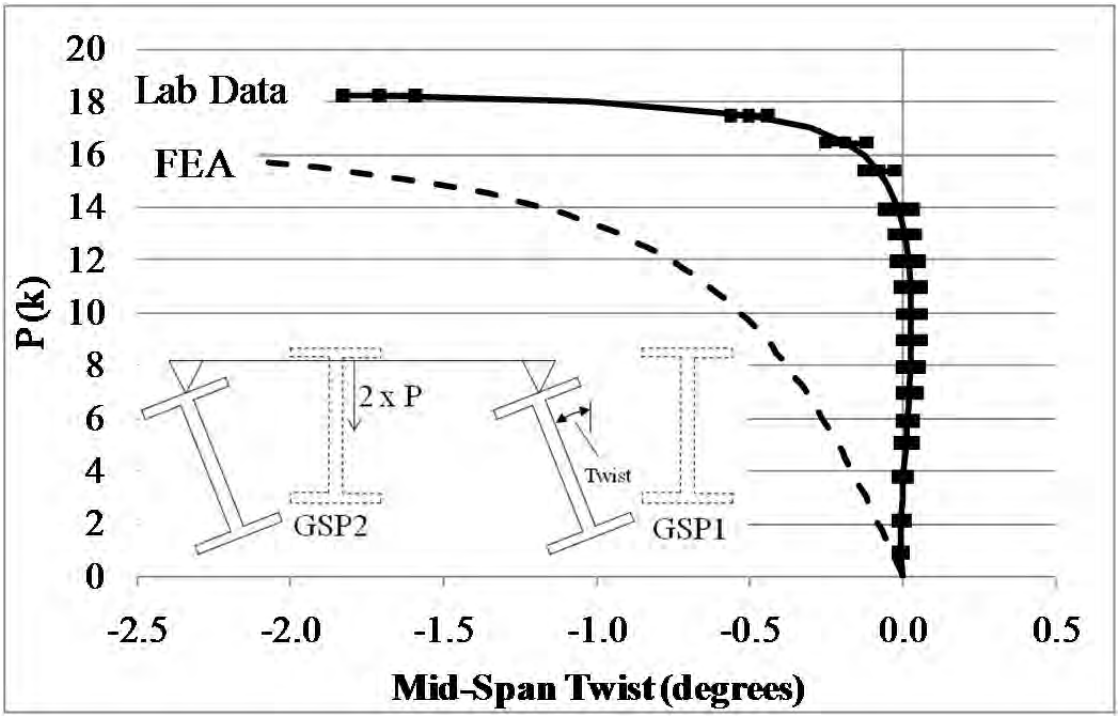

Figure B.21: GSP1 mid-span twist validation results

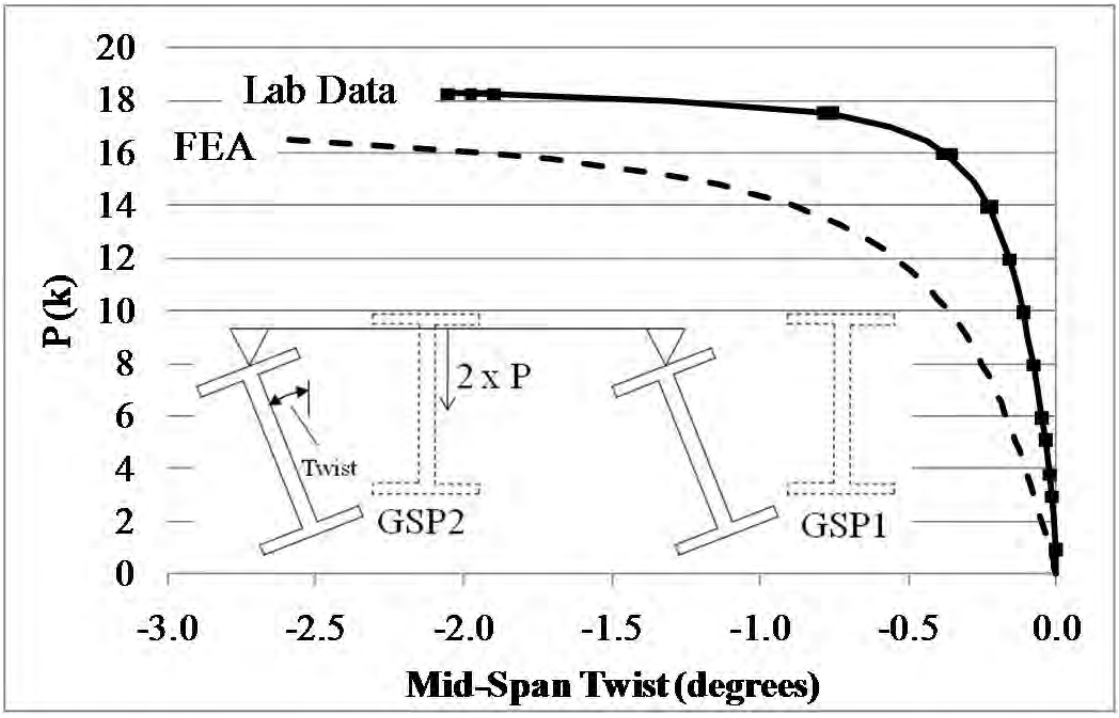

Figure B.22: GSP2 mid-span twist validation results

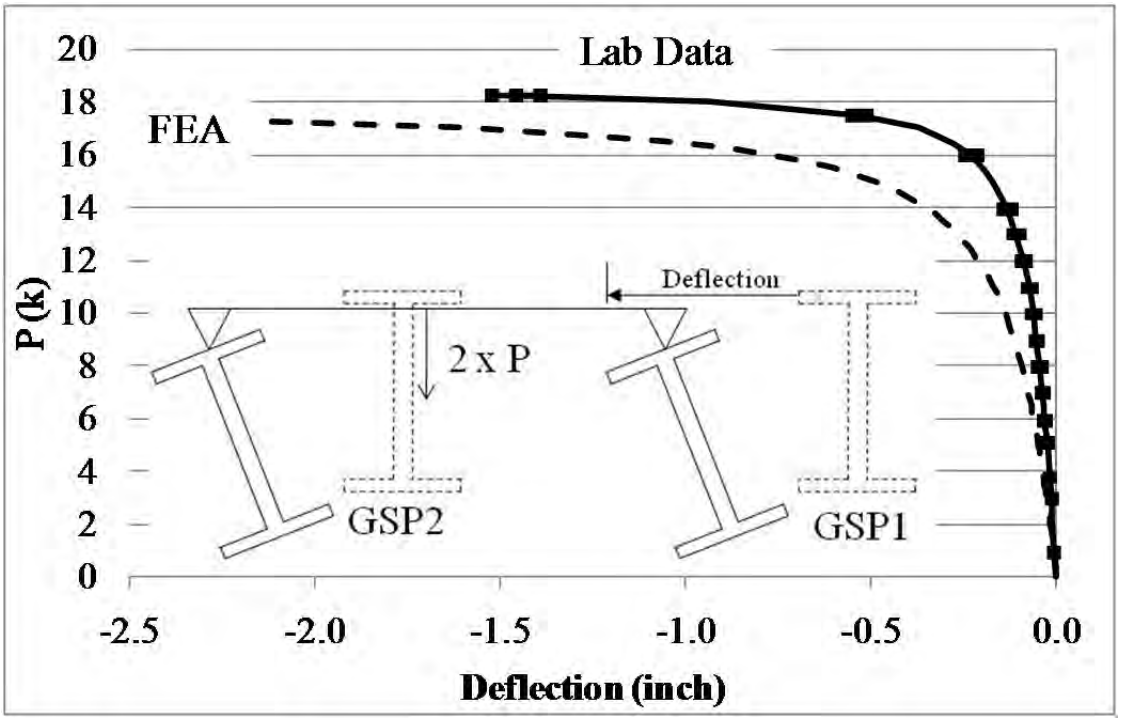

Figure B.23: GSP1 mid-span top flange lateral deflection validation results

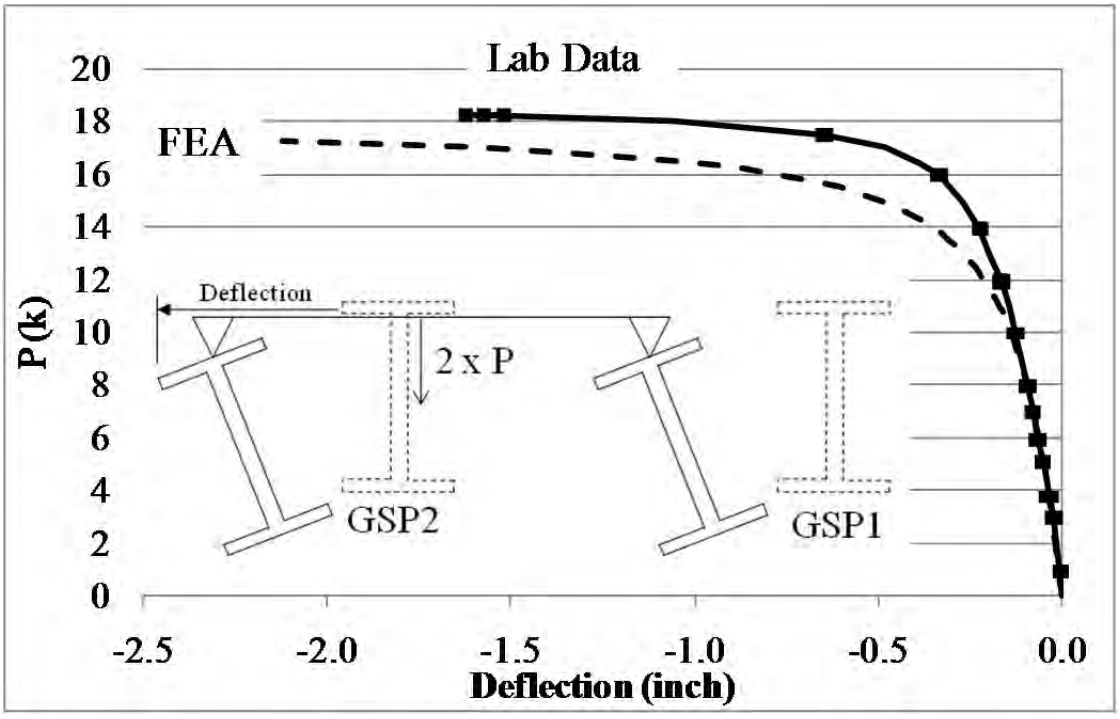

Figure B.24: GSP2 mid-span top flange lateral deflection validation results

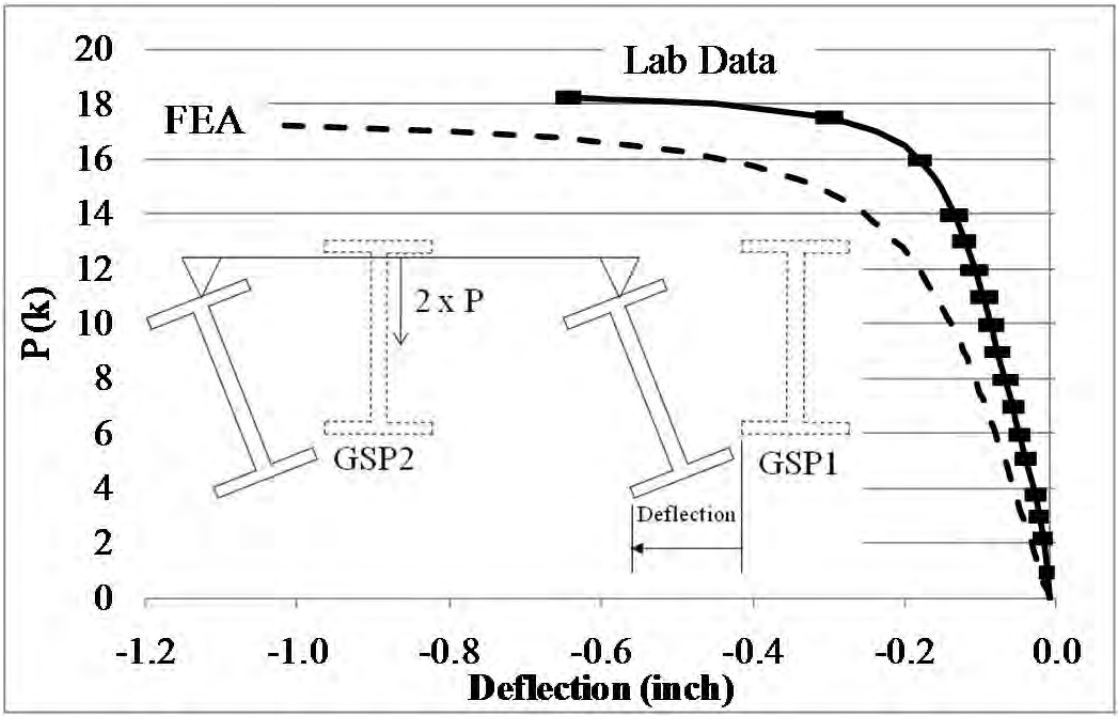

Figure B.25: GSP1 mid-span bottom flange lateral deflection validation results

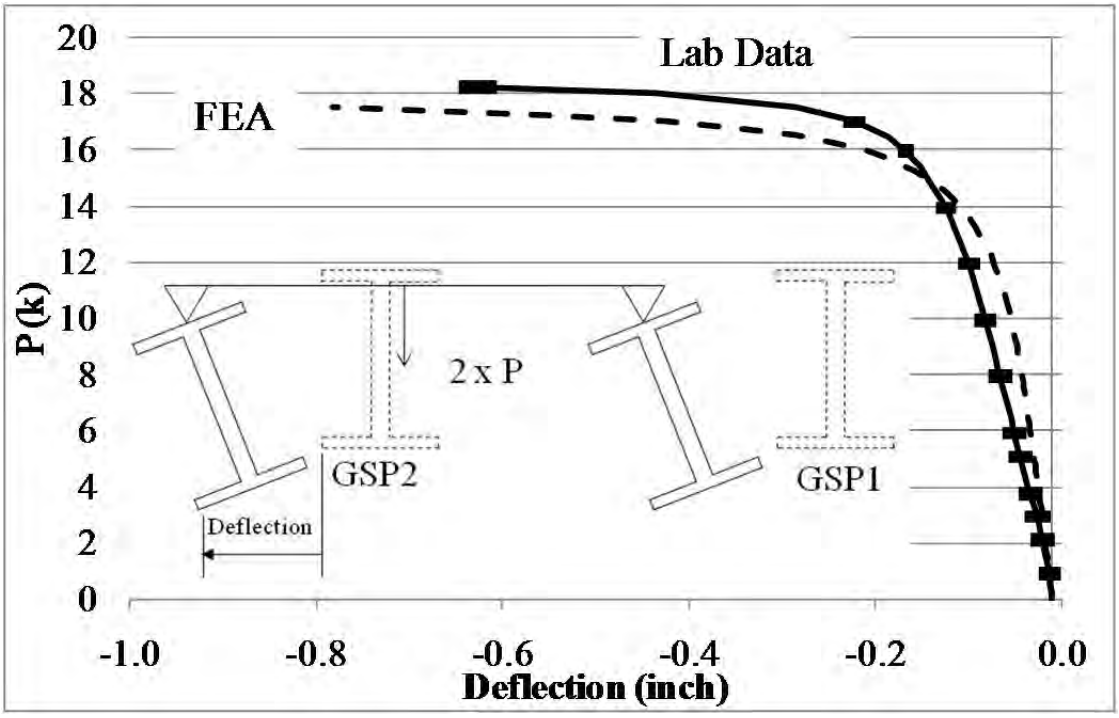

Figure B.26: GSP2 mid-span bottom flange lateral deflection validation results

B.3 THREE GIRDER PIPE-STIFFENER CROSS FRAME VALIDATION RESULTS

B.3.1 Thrust Washer Bearing with No Intermediate Cross Frames

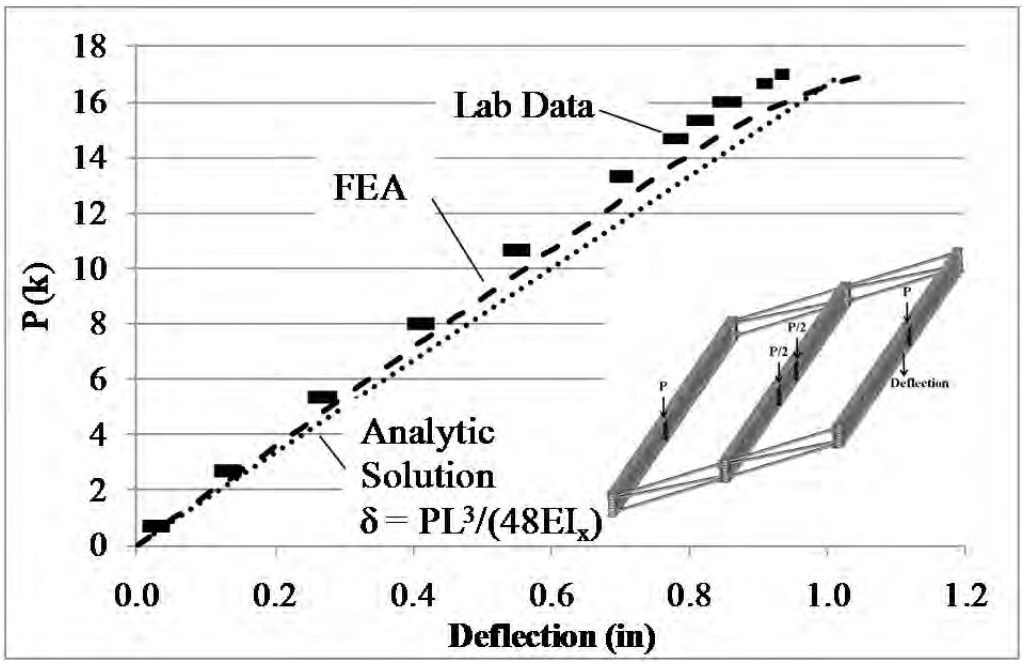

Figure B.27: GSP1 mid-span vertical deflection validation data

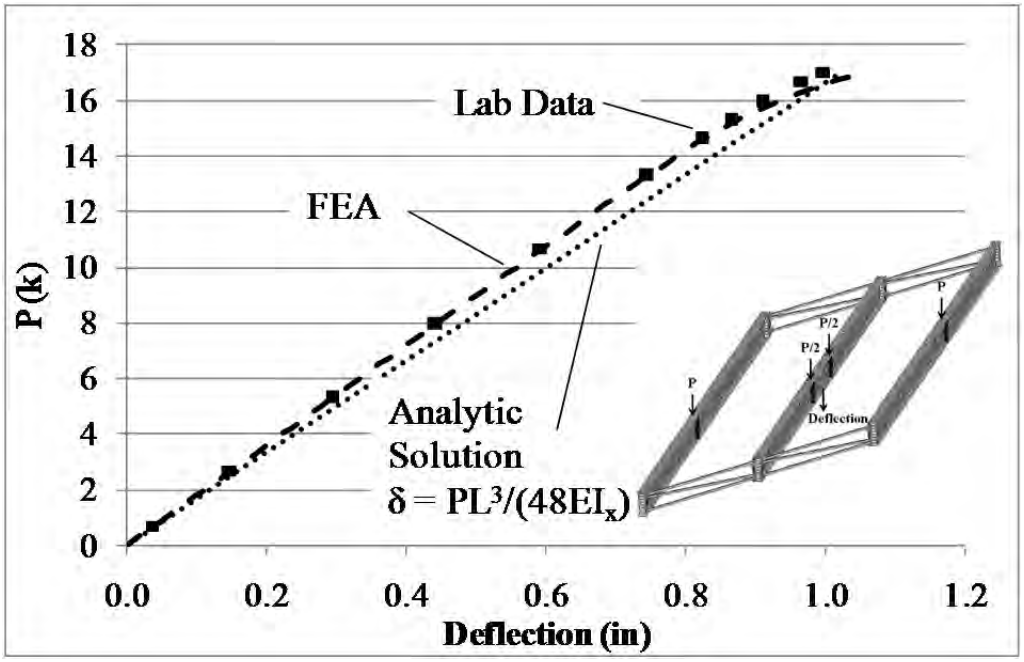

Figure B.28: GSP2 mid-span vertical deflection validation data

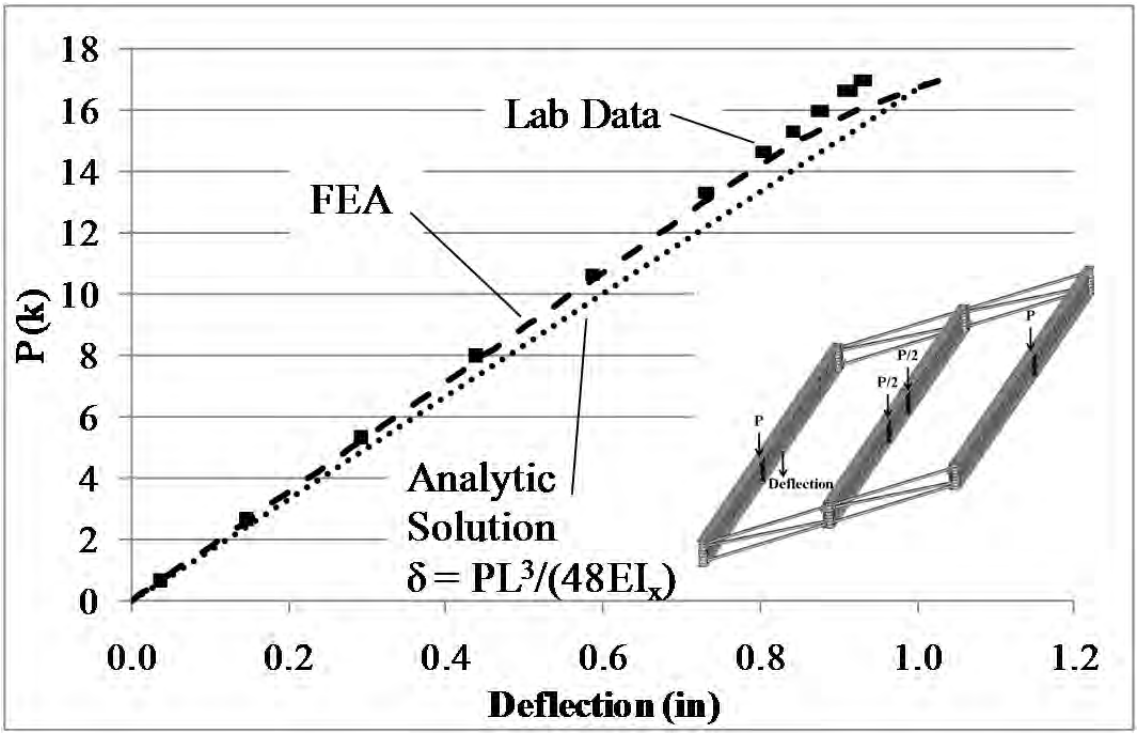

Figure B.29: GSP3 mid-span vertical deflection validation data

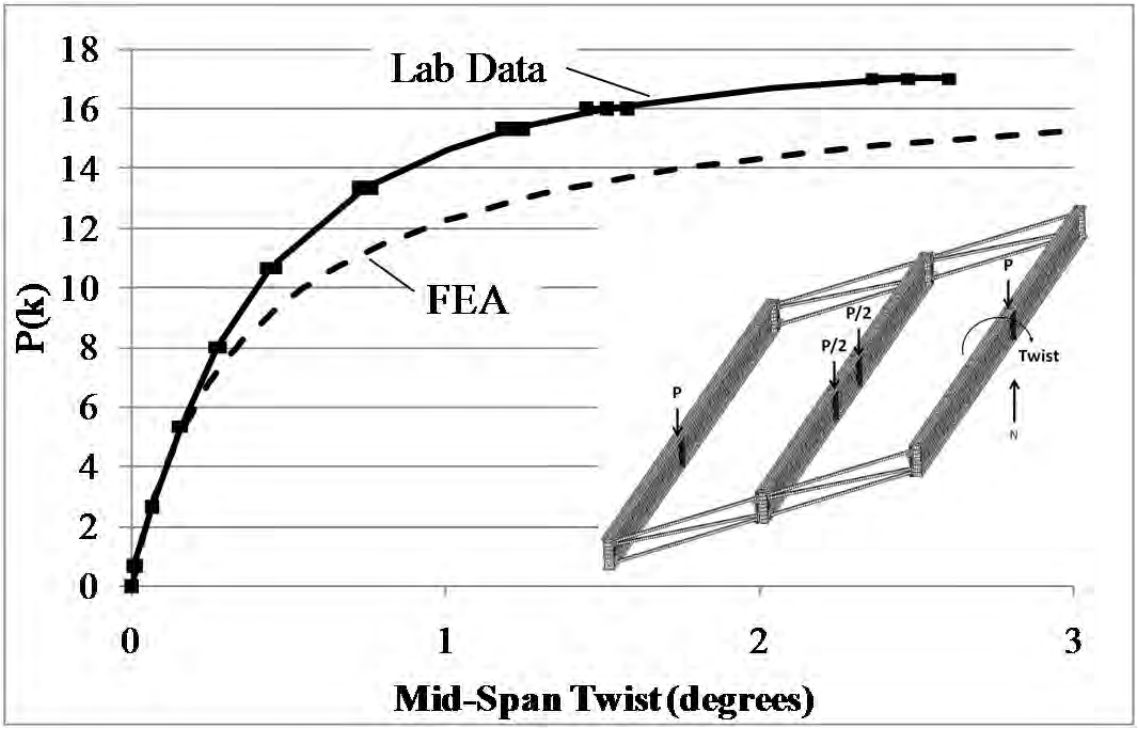

Figure B.30: GSP1 mid-span twist validation data

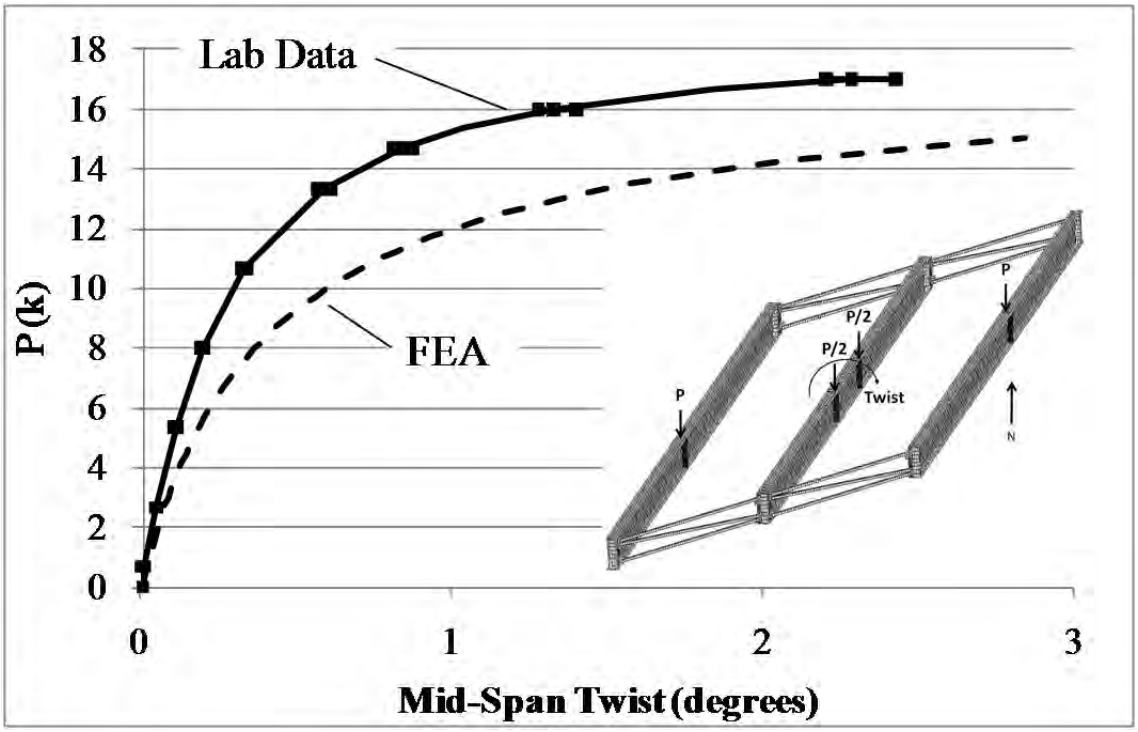

Figure B.31: GSP2 mid-span twist validation data

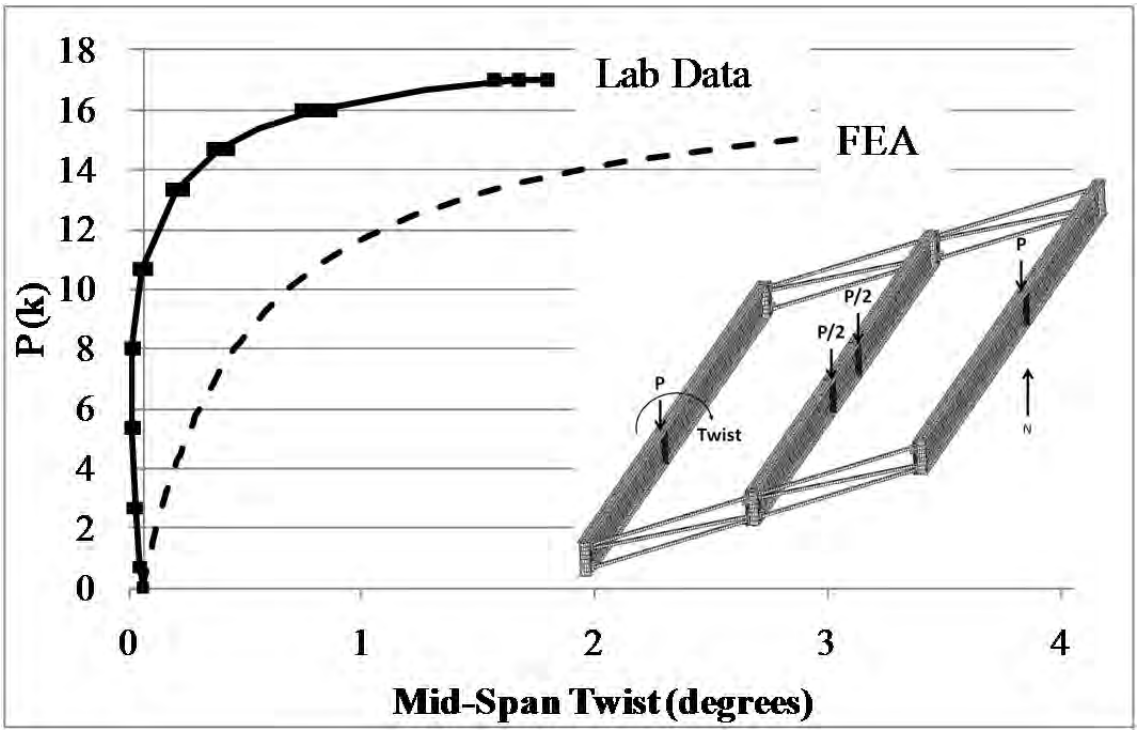

Figure B.32: GSP3 mid-span twist validation data

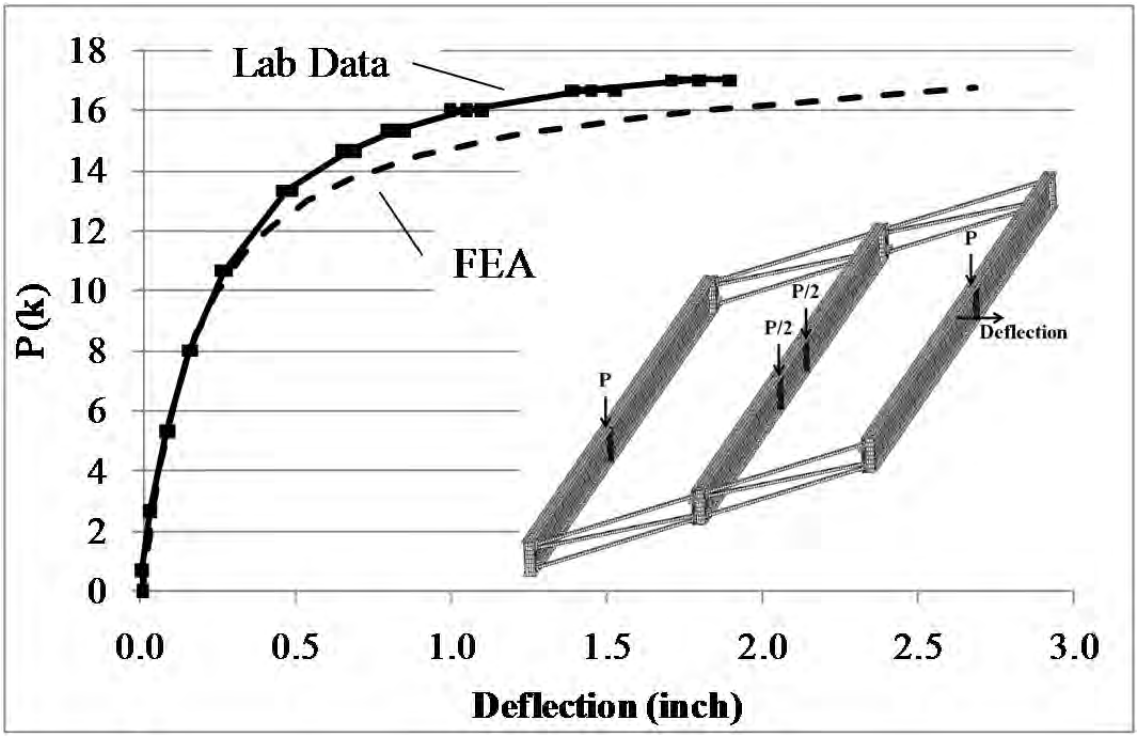

Figure B.33: GSP1 mid-span top flange lateral deflection validation data

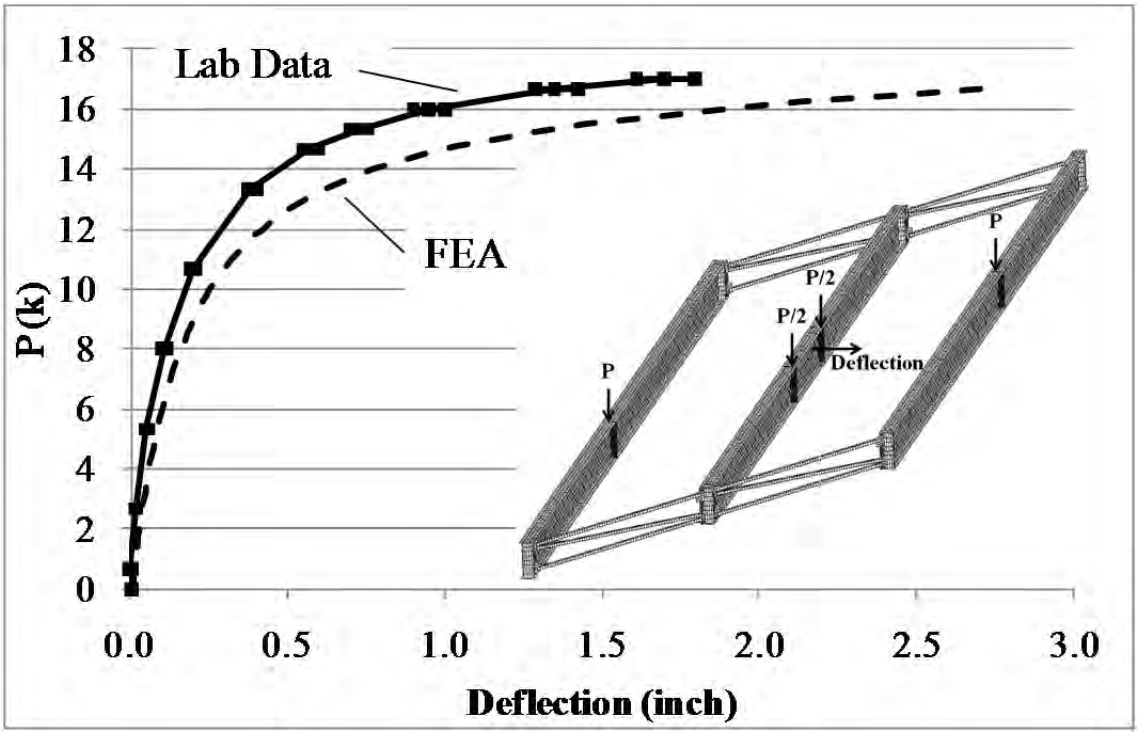

Figure B.34: GSP2 mid-span top flange lateral deflection validation data

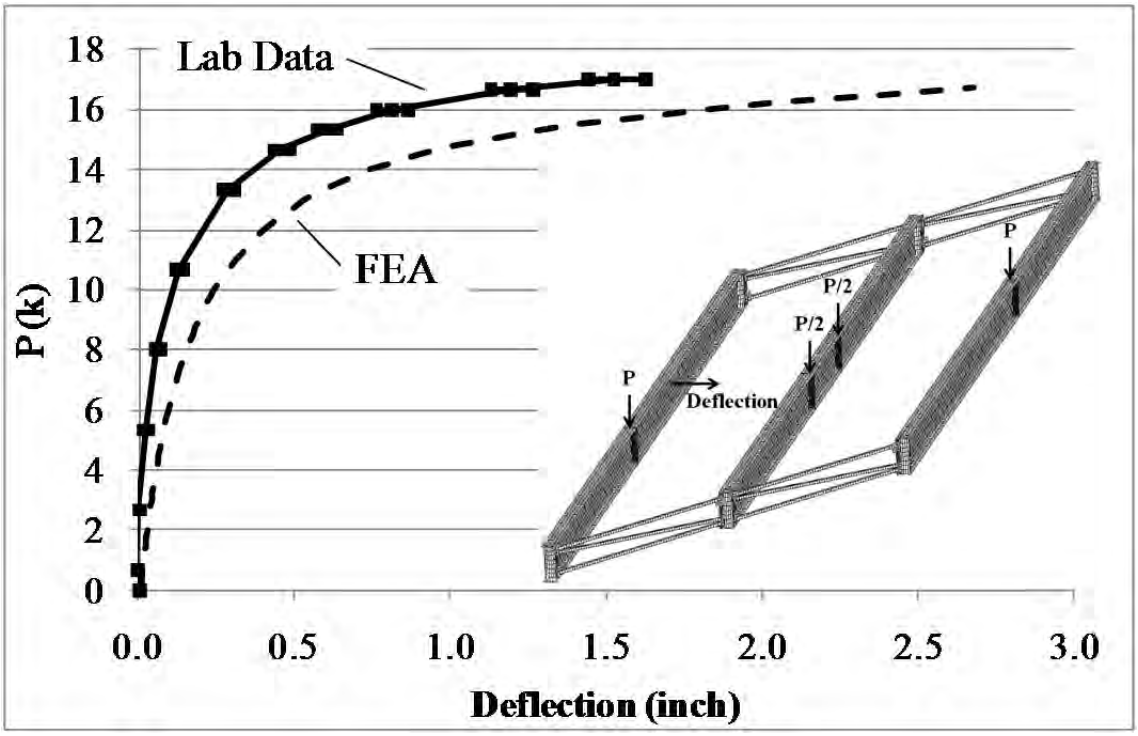

Figure B.35: GSP3 mid-span top flange lateral deflection validation data

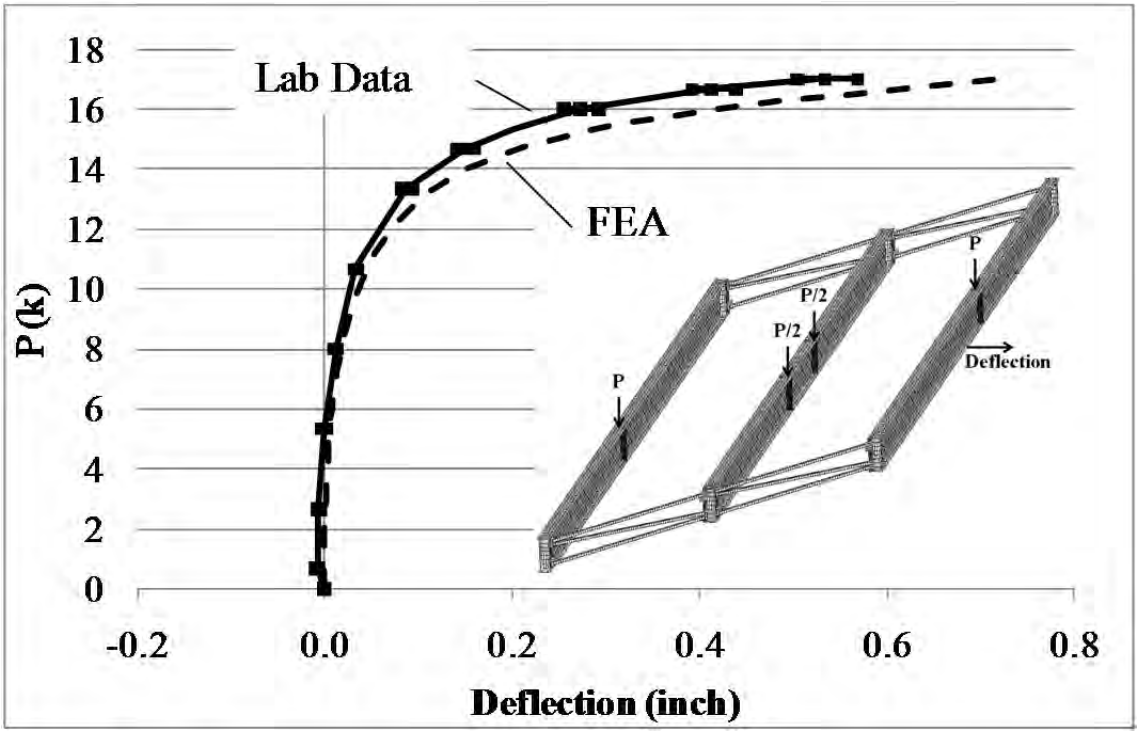

Figure B.36: GSP1 mid-span bottom flange lateral deflection validation data

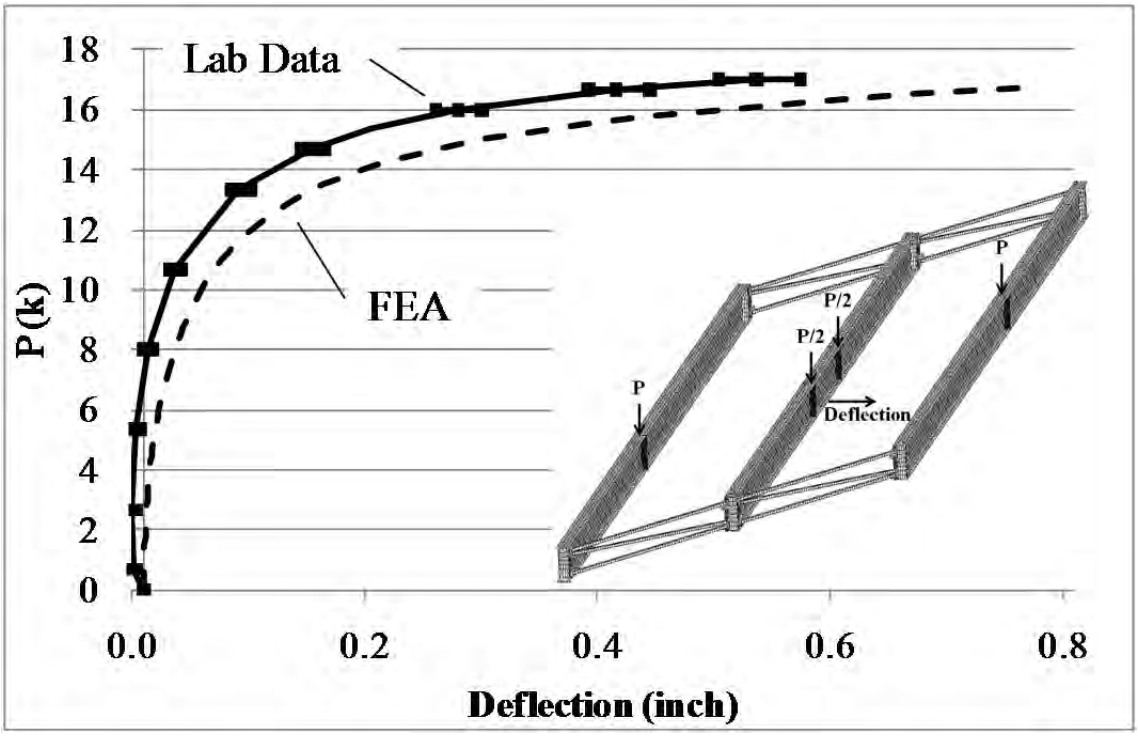

Figure B.37: GSP2 mid-span bottom flange lateral deflection validation data

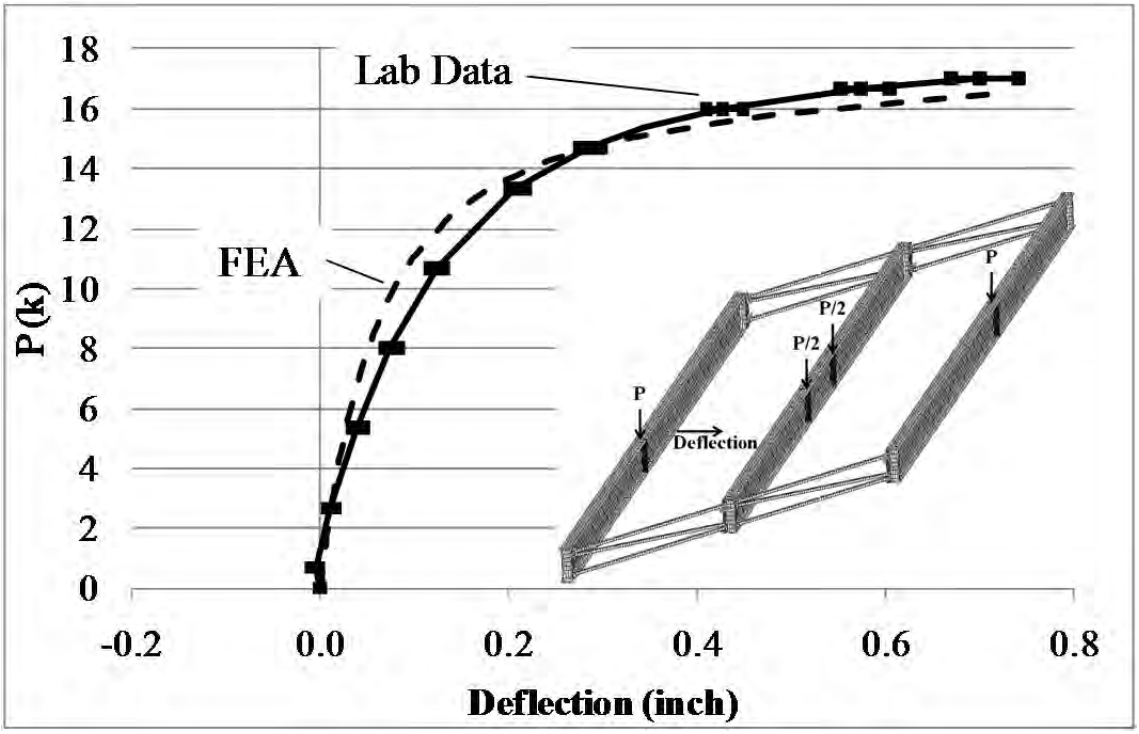

Figure B.38: GSP3 mid-span bottom flange lateral deflection validation data

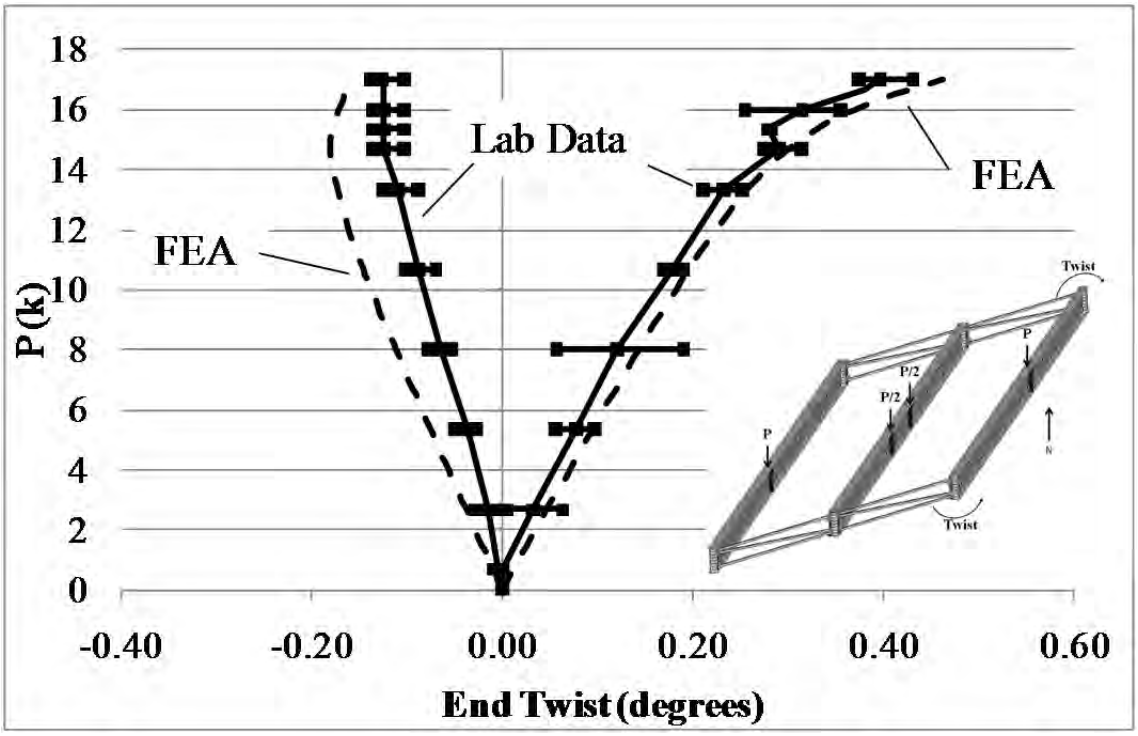

Figure B.39: GSP1 end twist validation data

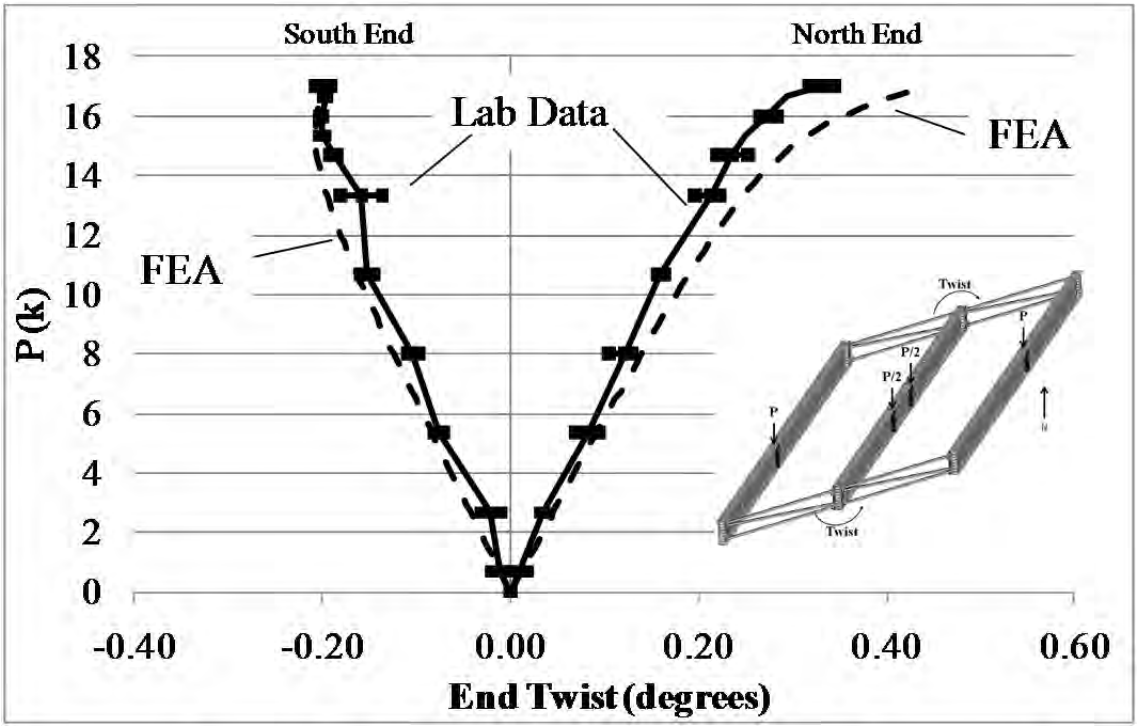

Figure B.40: GSP2 end twist validation data

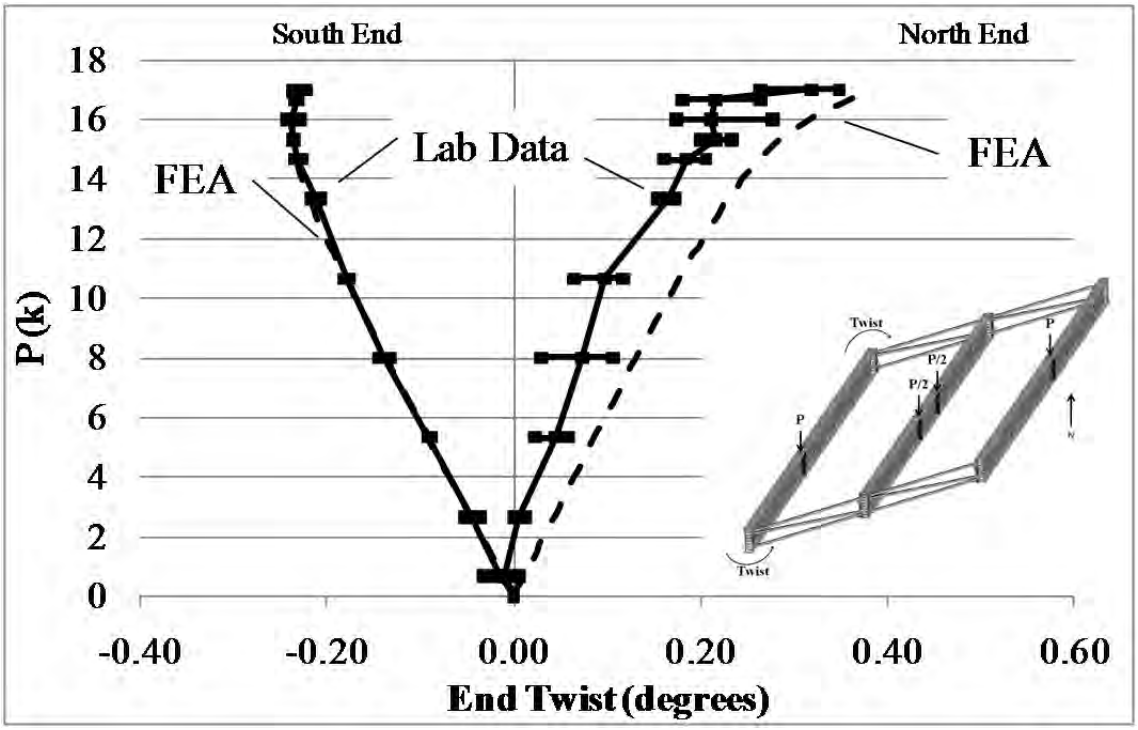

Figure B.41: GSP3 end twist validation data

B.3.2 Thrust Washer Bearing with Staggered Intermediate Cross Frames

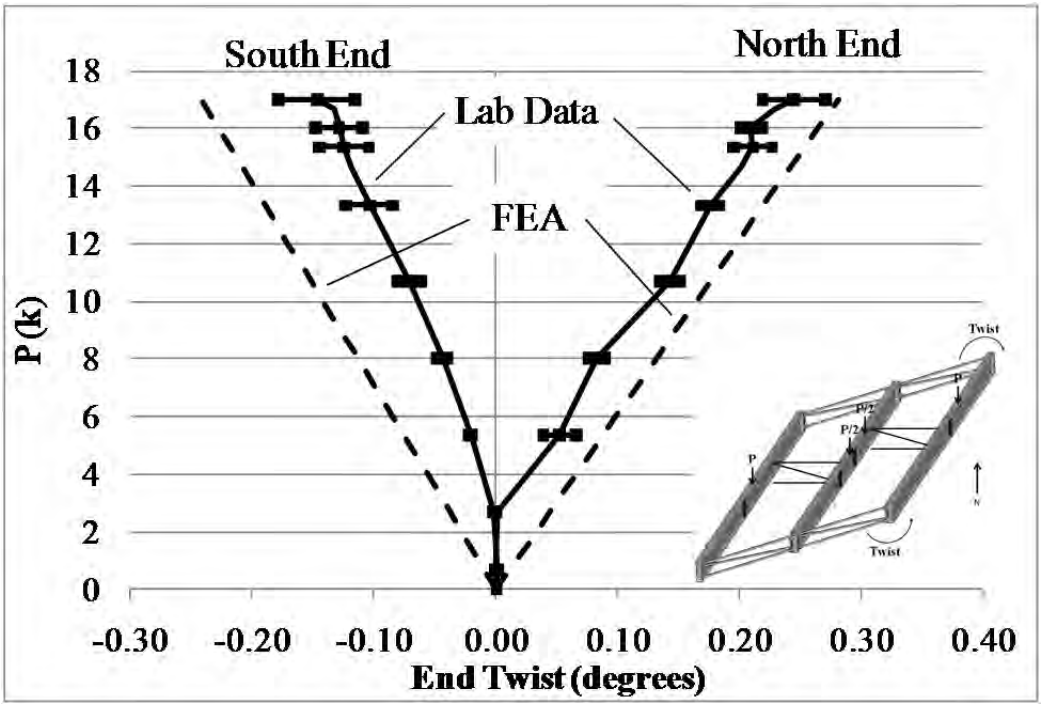

Figure B.42: GSP1 end twist validation data

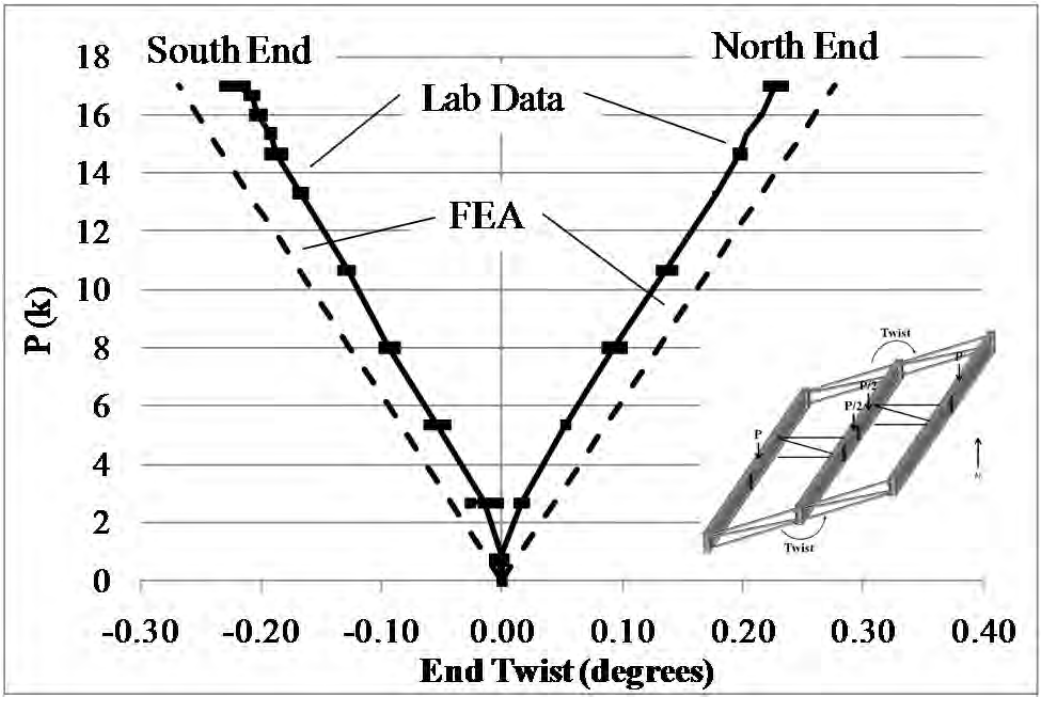

Figure B.43: GSP2 end twist validation data

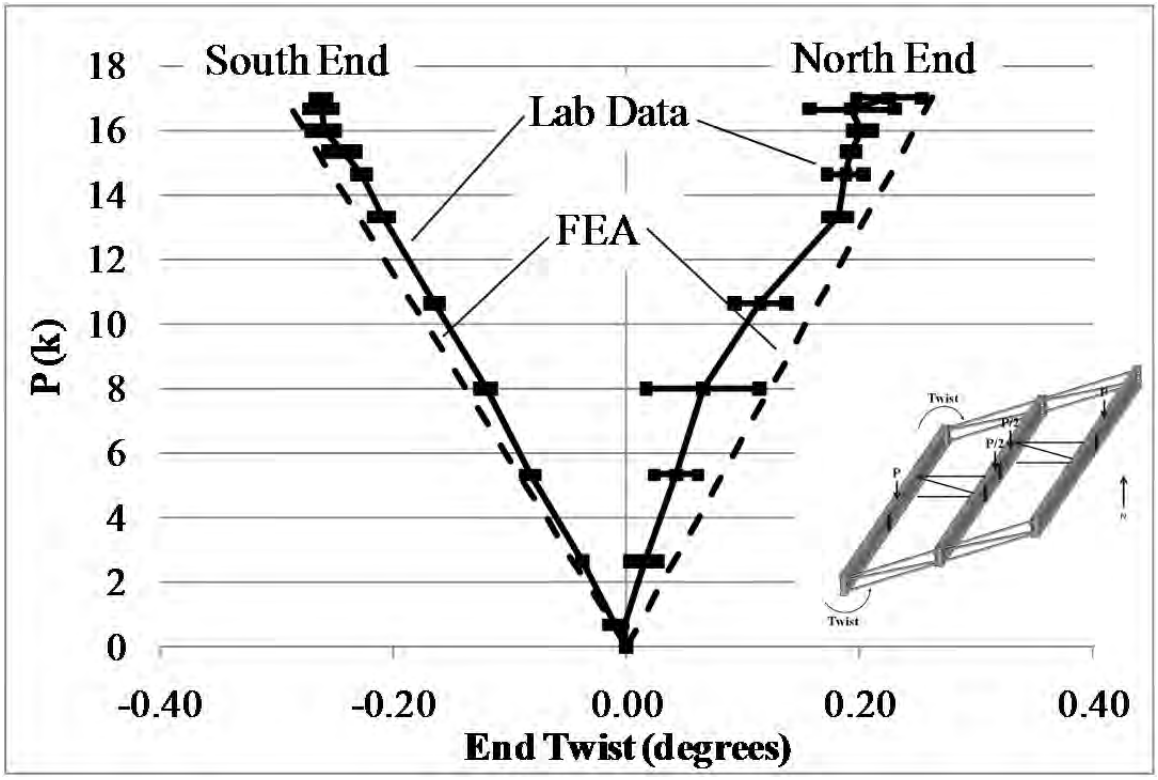

Figure B.44: GSP3 end twist validation data

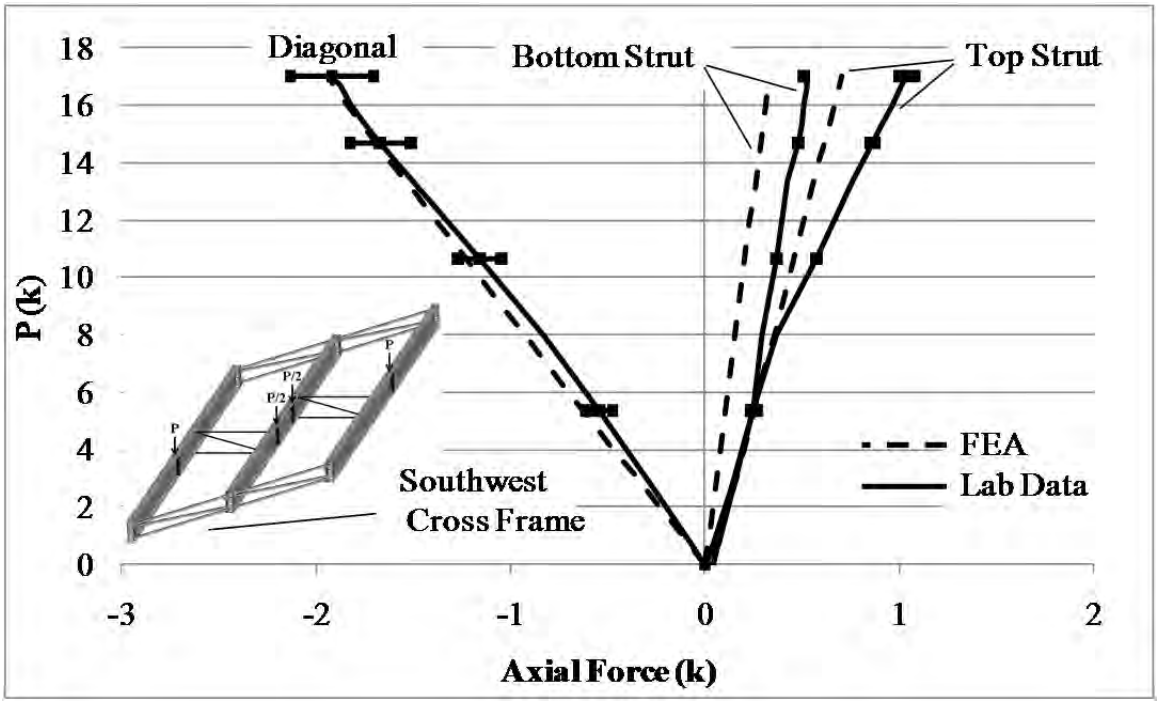

Figure B.45: SW end cross frame axial force validation data

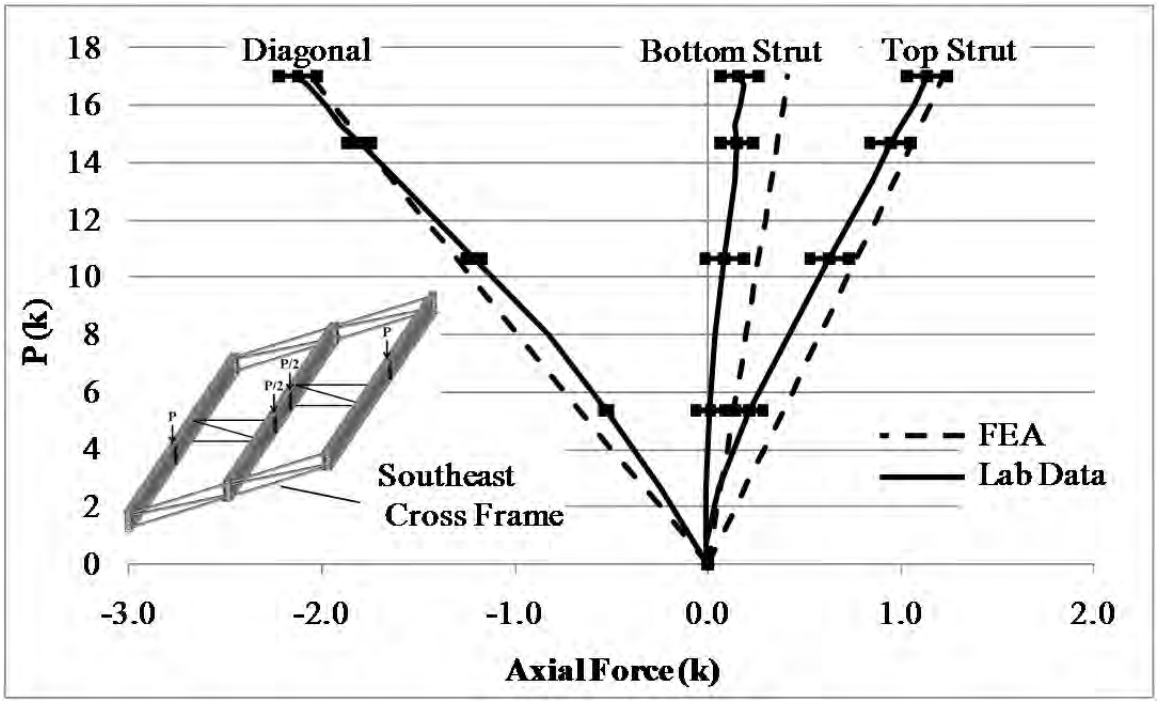

Figure B.46: SE end cross frame axial force validation data

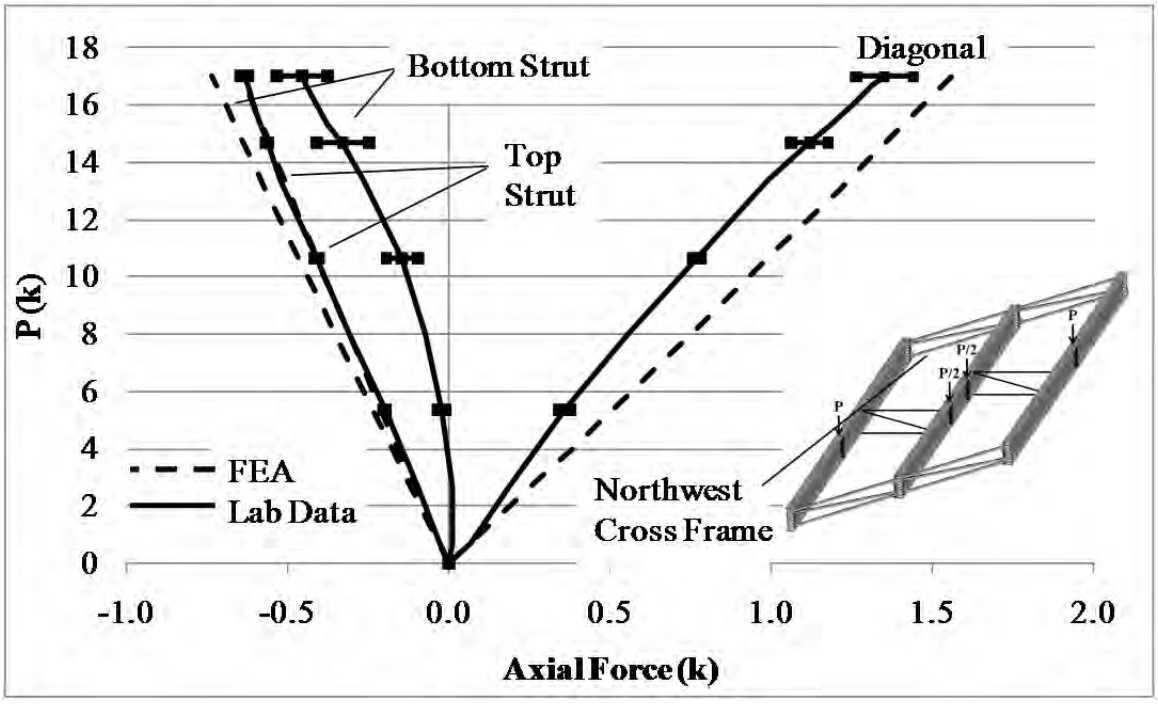

Figure B.47: NW end cross frame axial force validation data

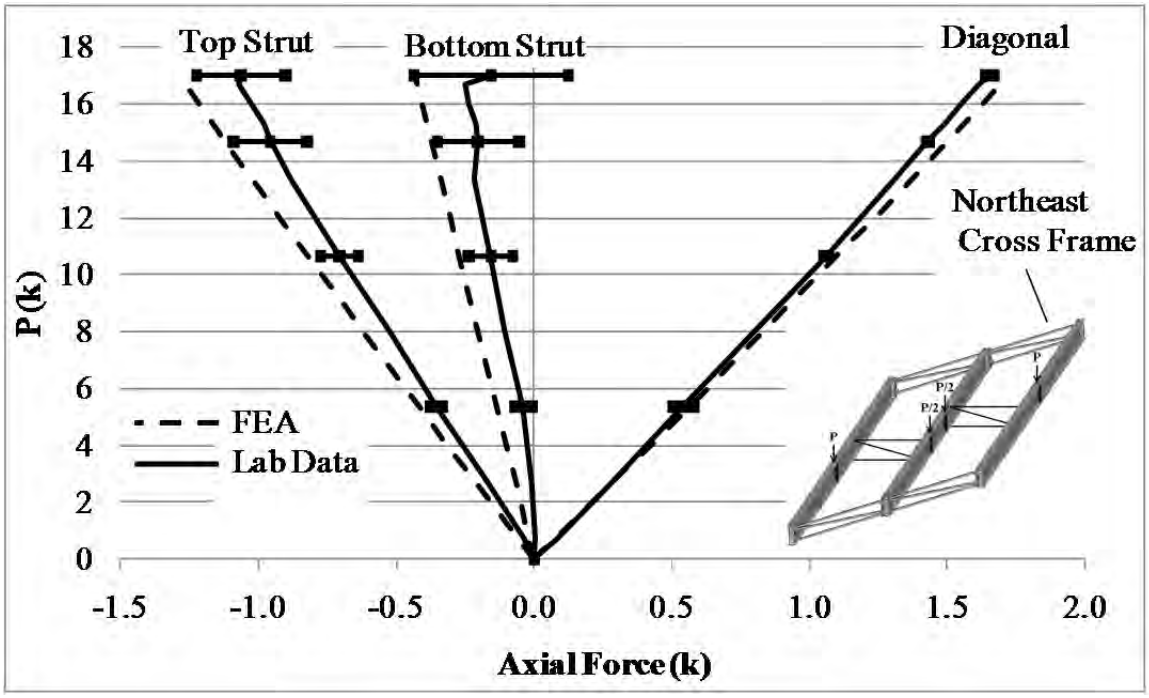

Figure B.48: NE end cross frame axial force validation data

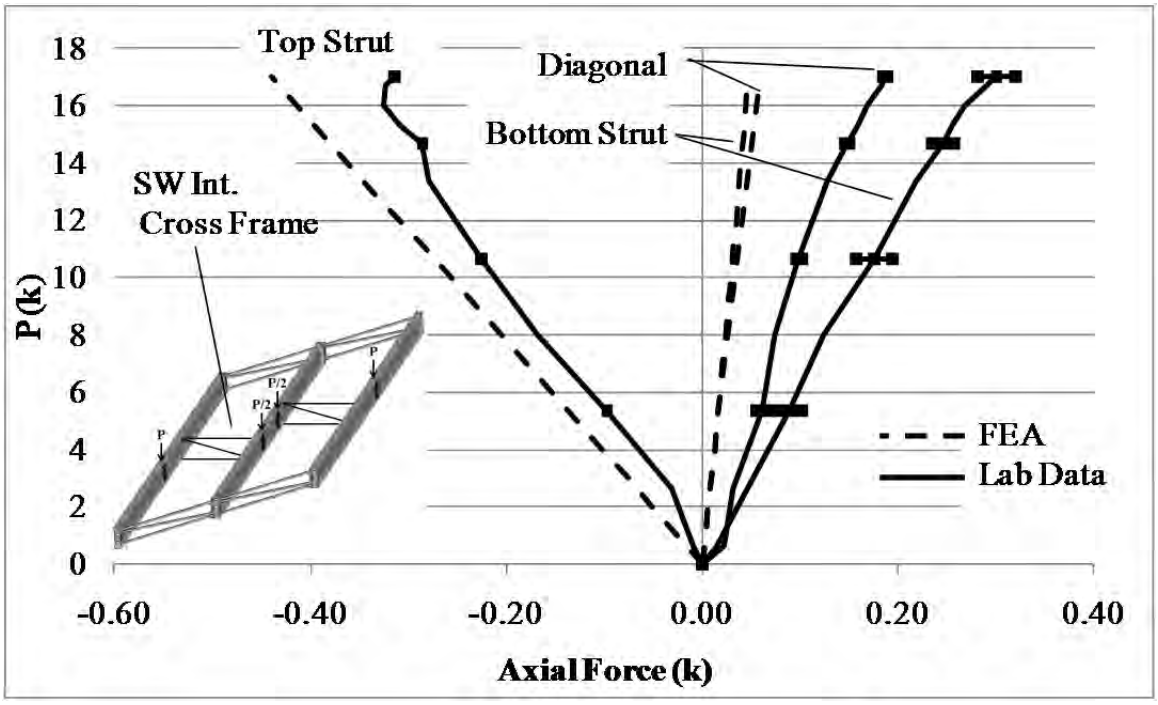

Figure B.49: SW intermediate cross frame axial force validation data

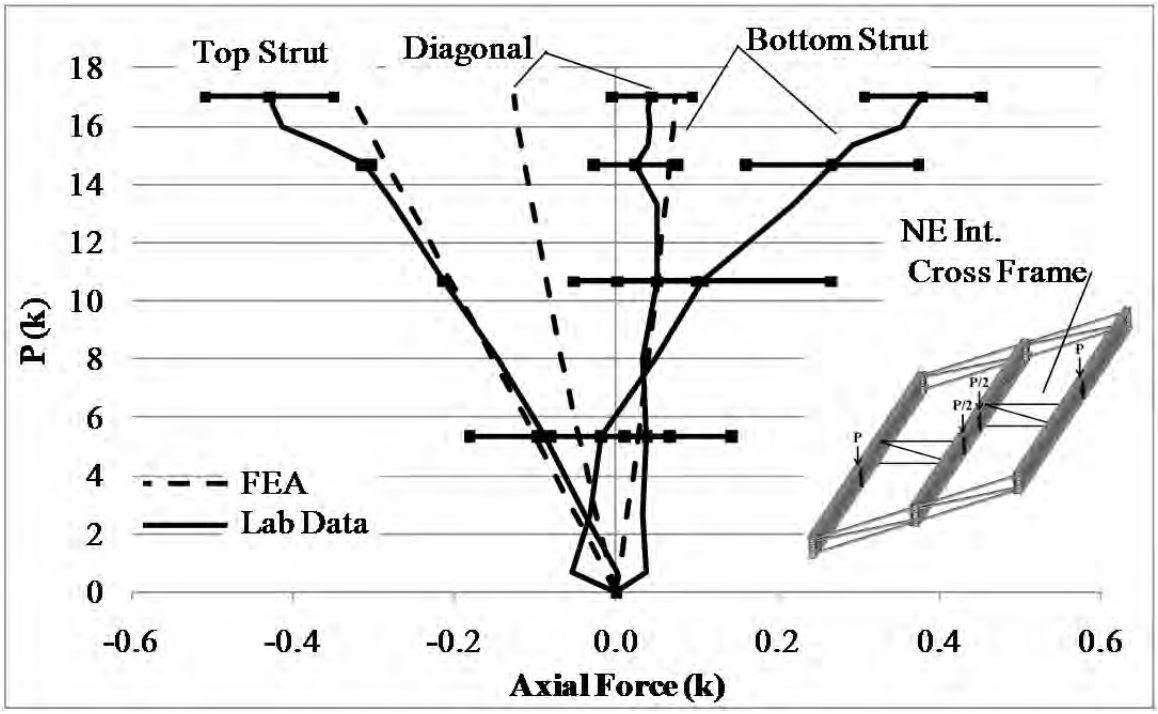

Figure B.50: NE intermediate cross frame axial force validation data

B.3.3 Thrust Washer Bearing with Continuous Intermediate Cross Frames

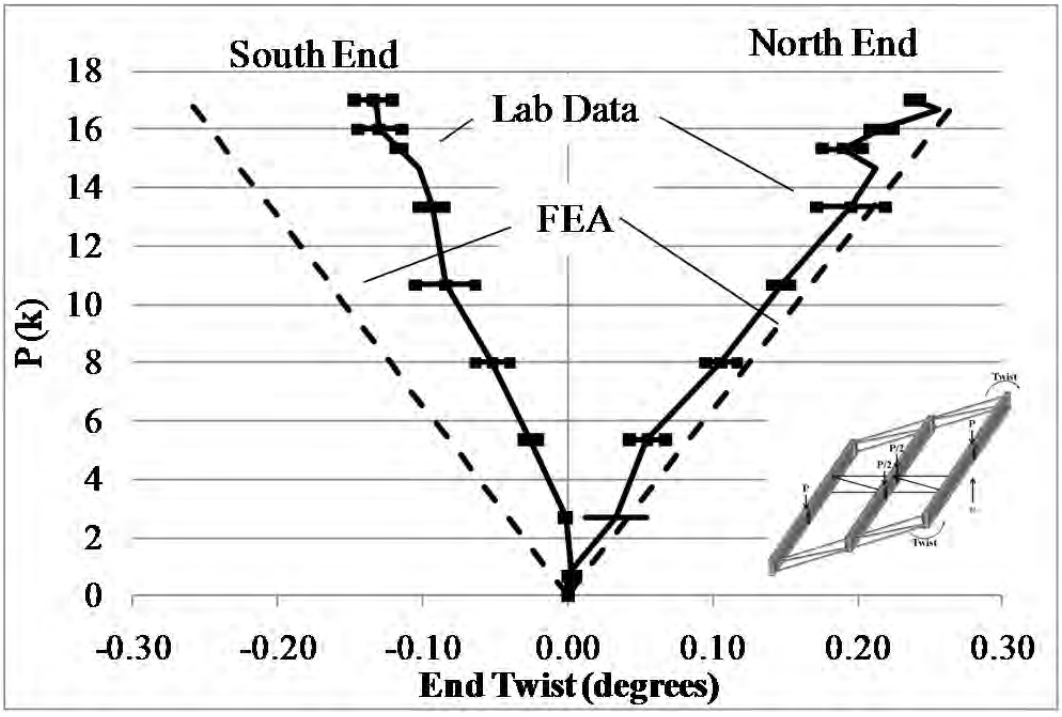

Figure B.51: GSP1 end twist validation data

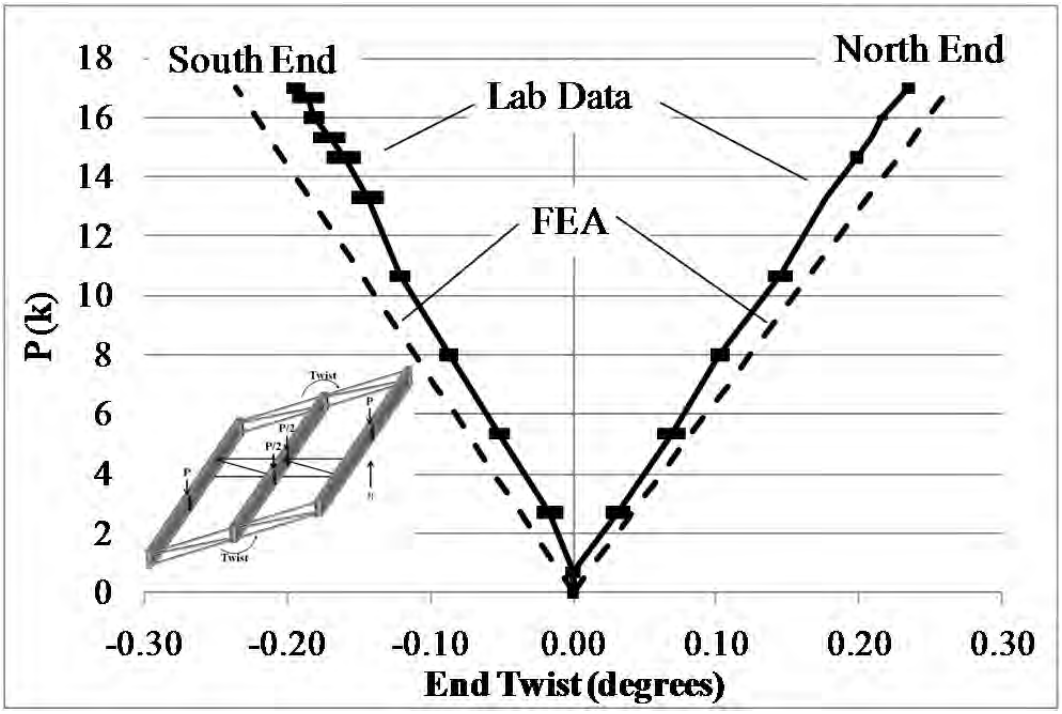

Figure B.52: GSP2 end twist validation data

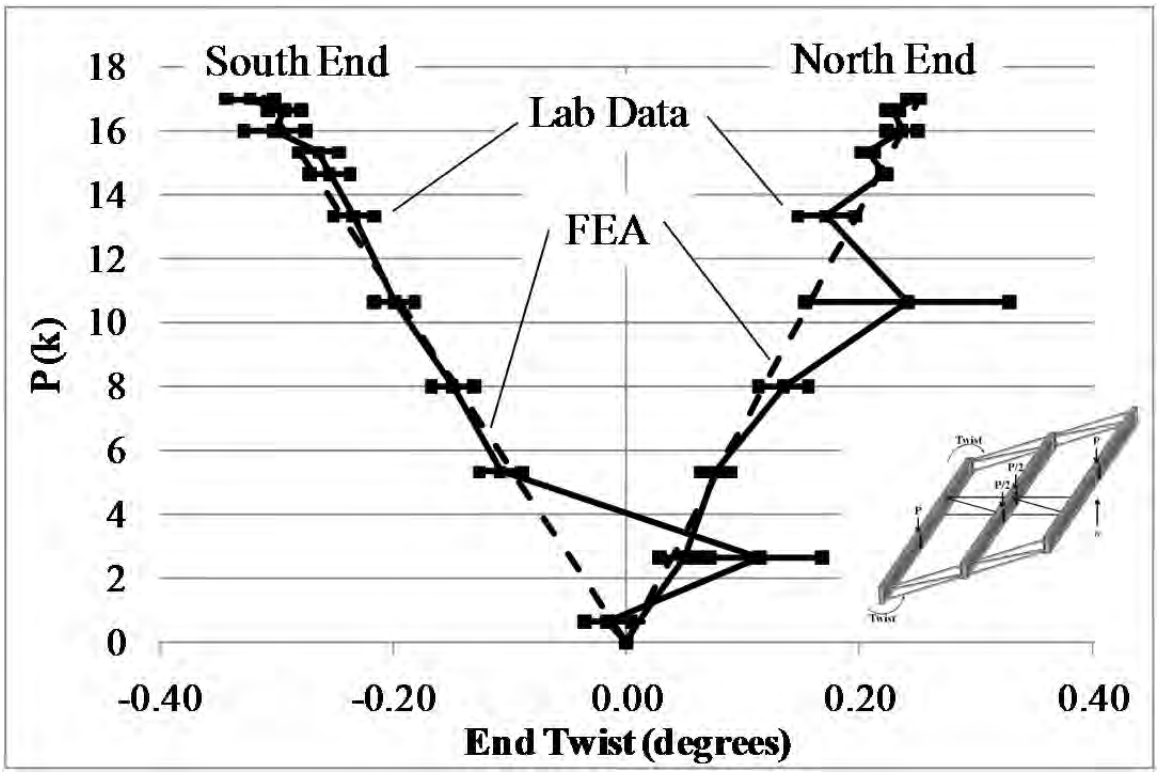

Figure B.53: GSP3 end twist validation data

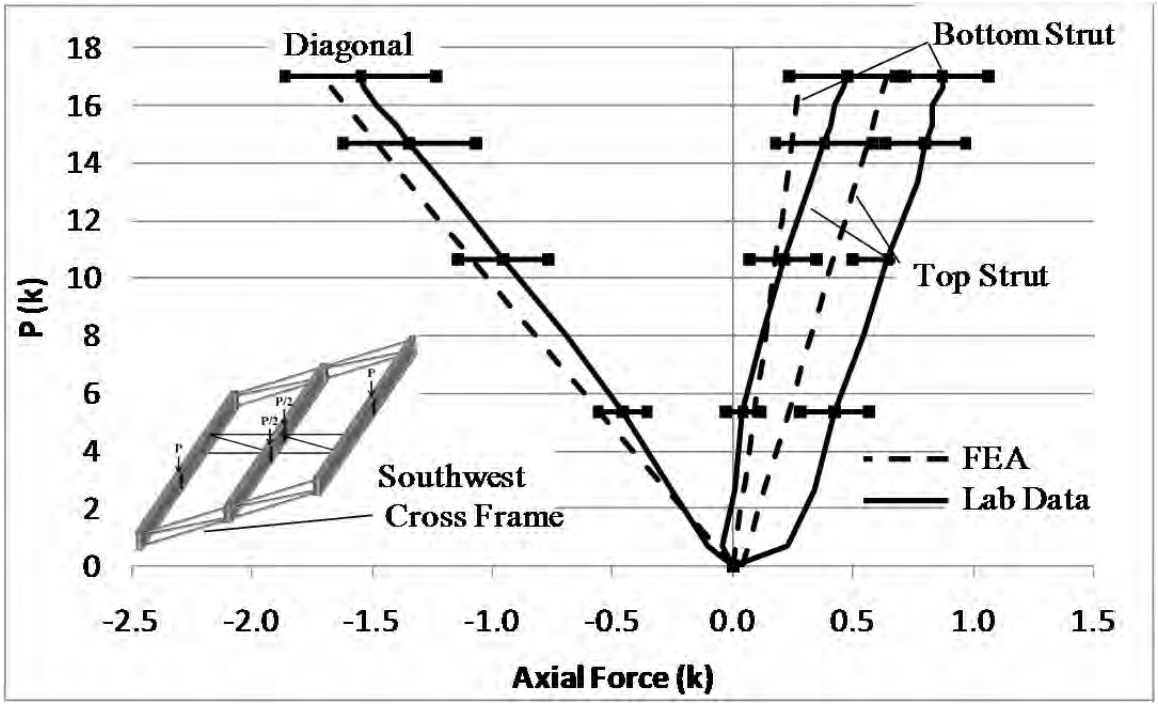

Figure B.54: SW end cross frame axial force validation data

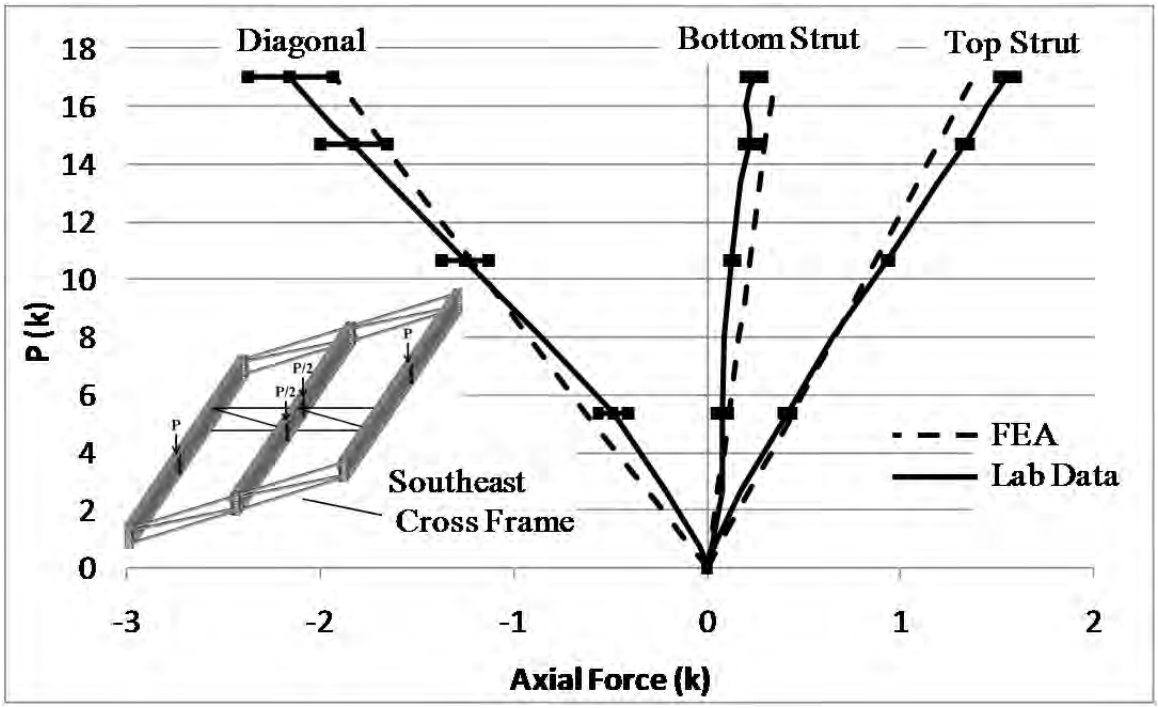

Figure B.55: SE end cross frame axial force validation data

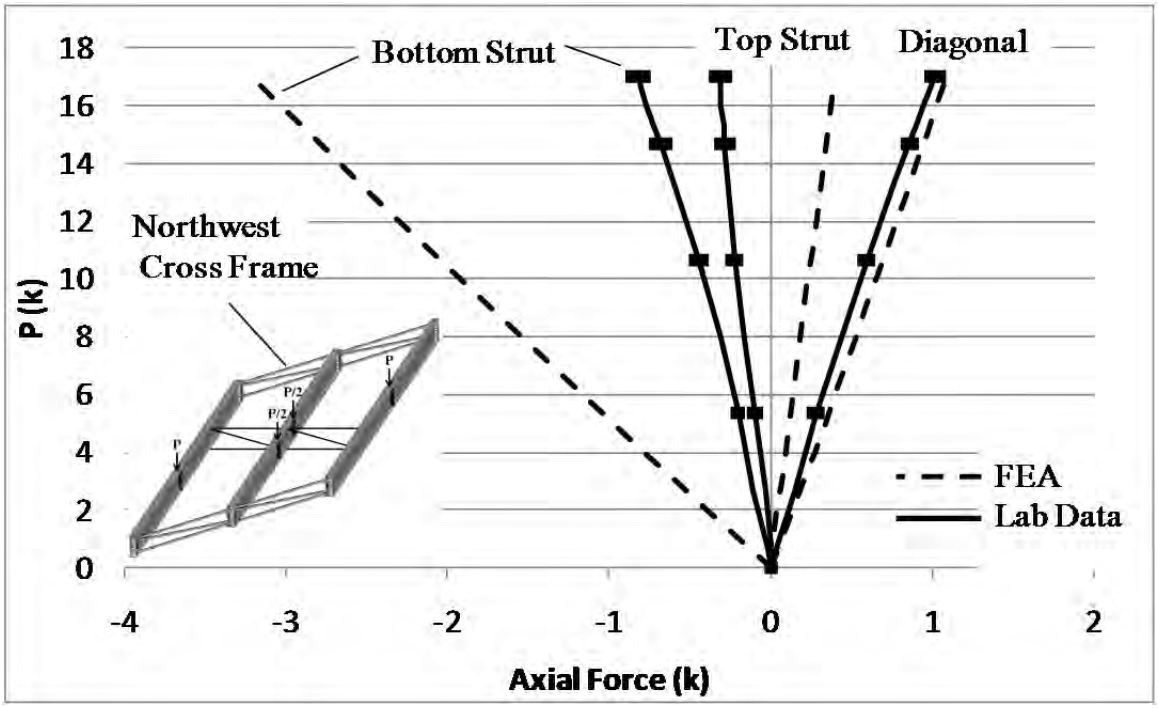

Figure B.56: NW end cross frame axial force validation data

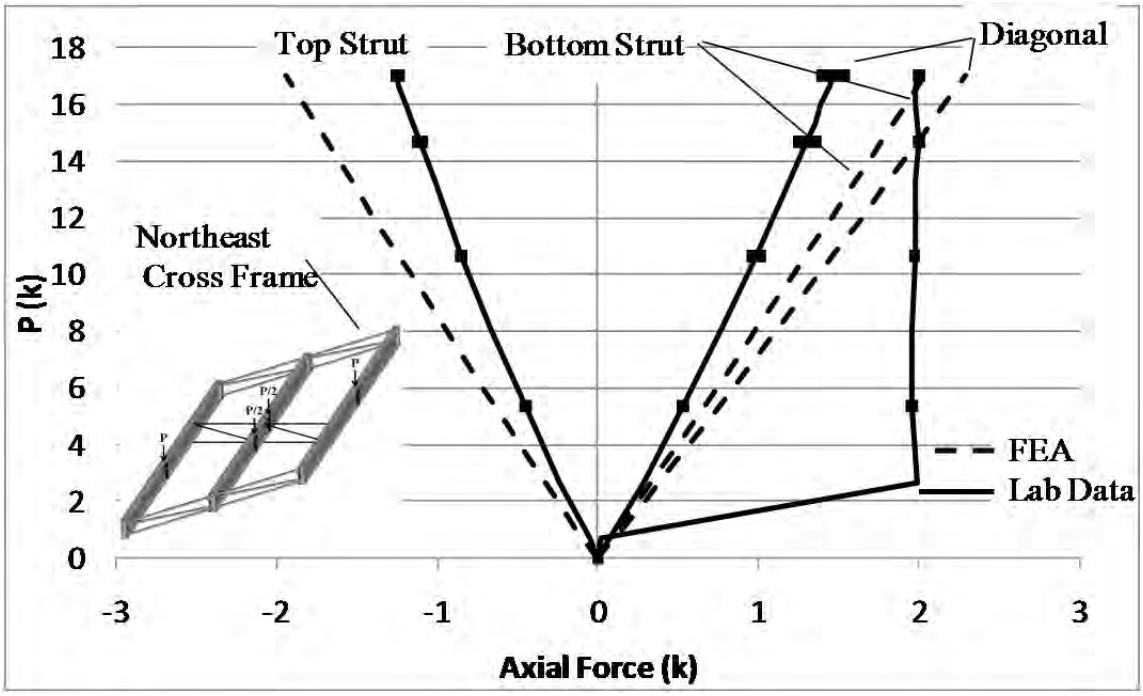

Figure B.57: NE end cross frame axial force validation data

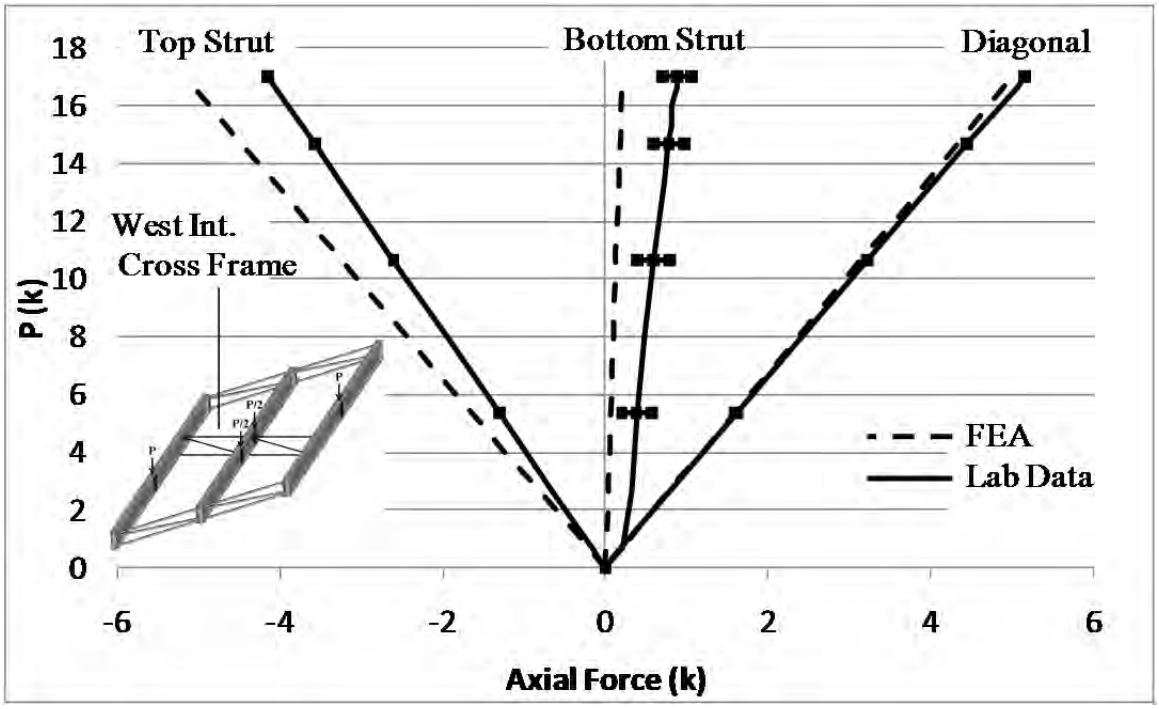

Figure B.58: West intermediate cross frame axial force validation data

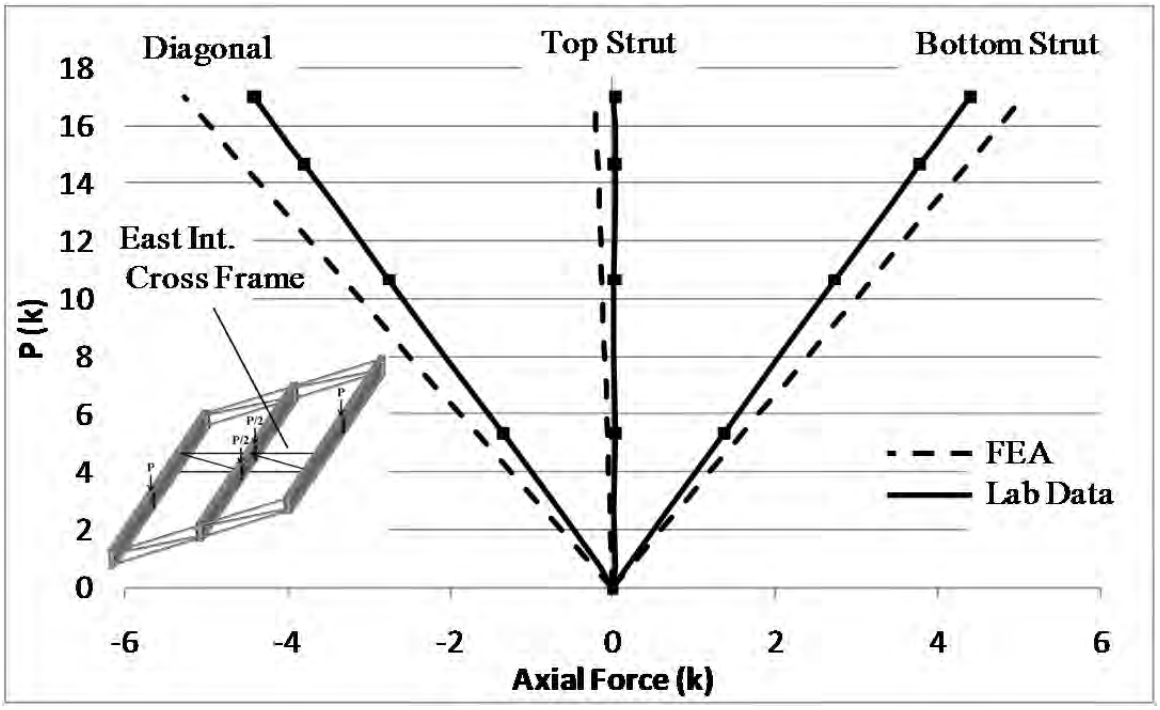

Figure B.59: East intermediate cross frame axial force validation data

B.3.4 Rubber Bearing with No Intermediate Cross Frames

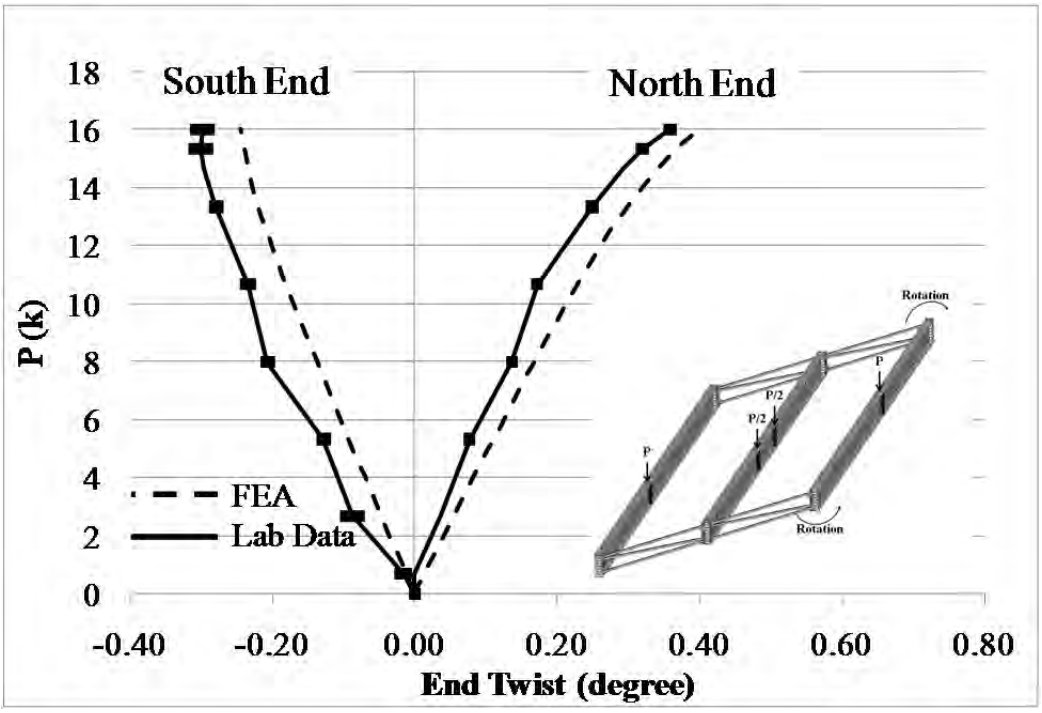

Figure B.60: GBP1 end twists

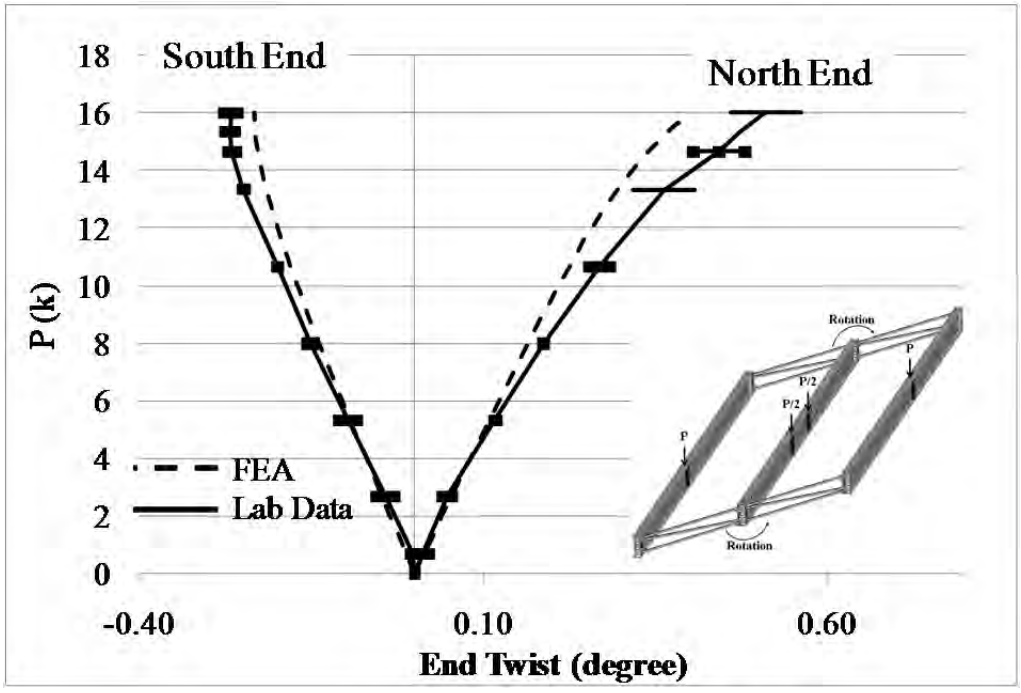

Figure B.61: GBP2 end twists

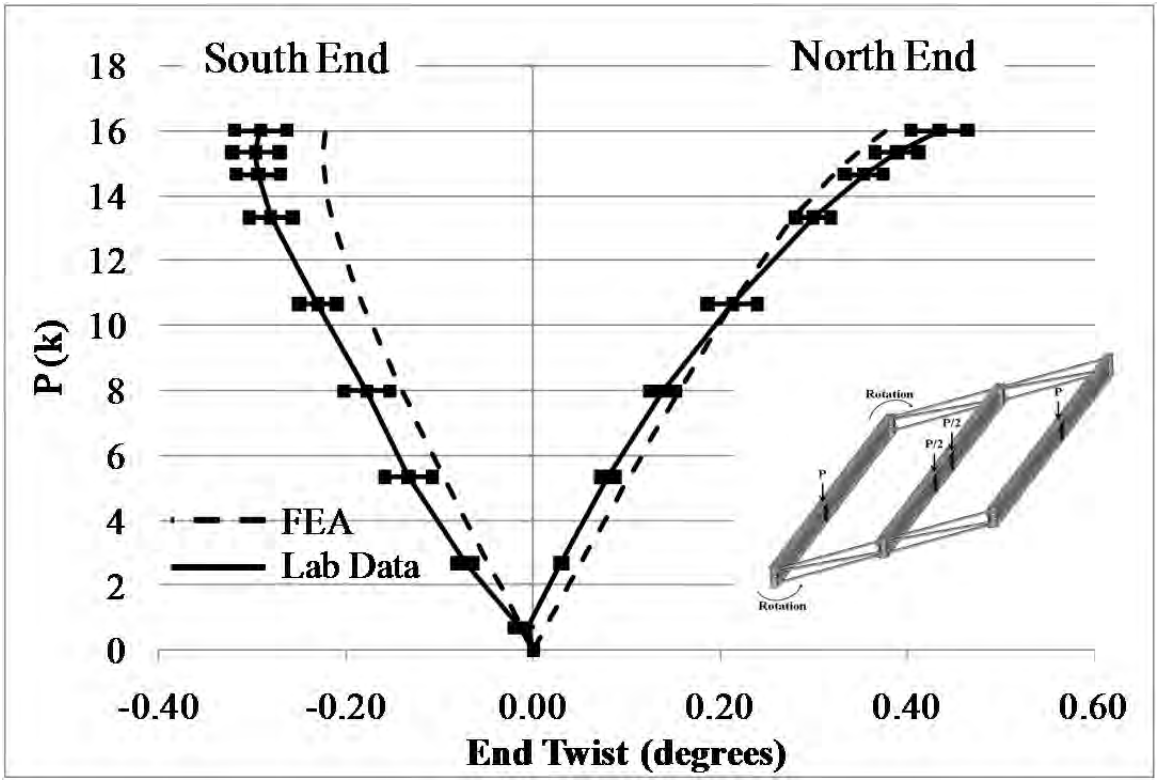

Figure B.62: GBP3 end twists

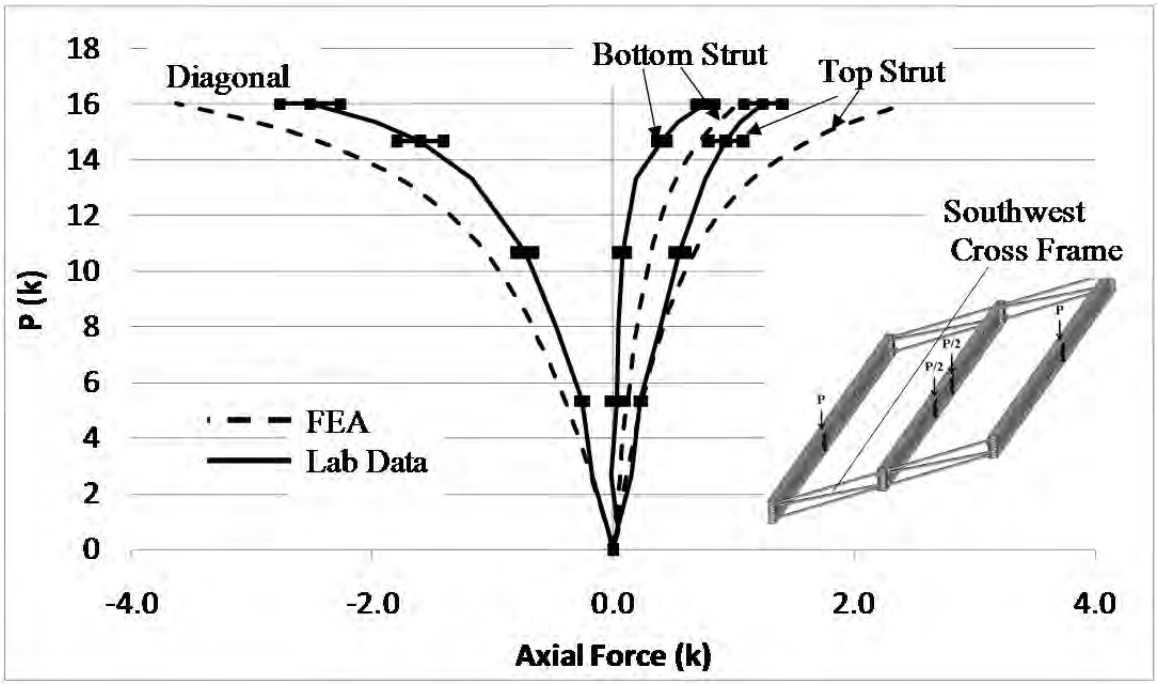

Figure B.63: SW end cross frame axial forces

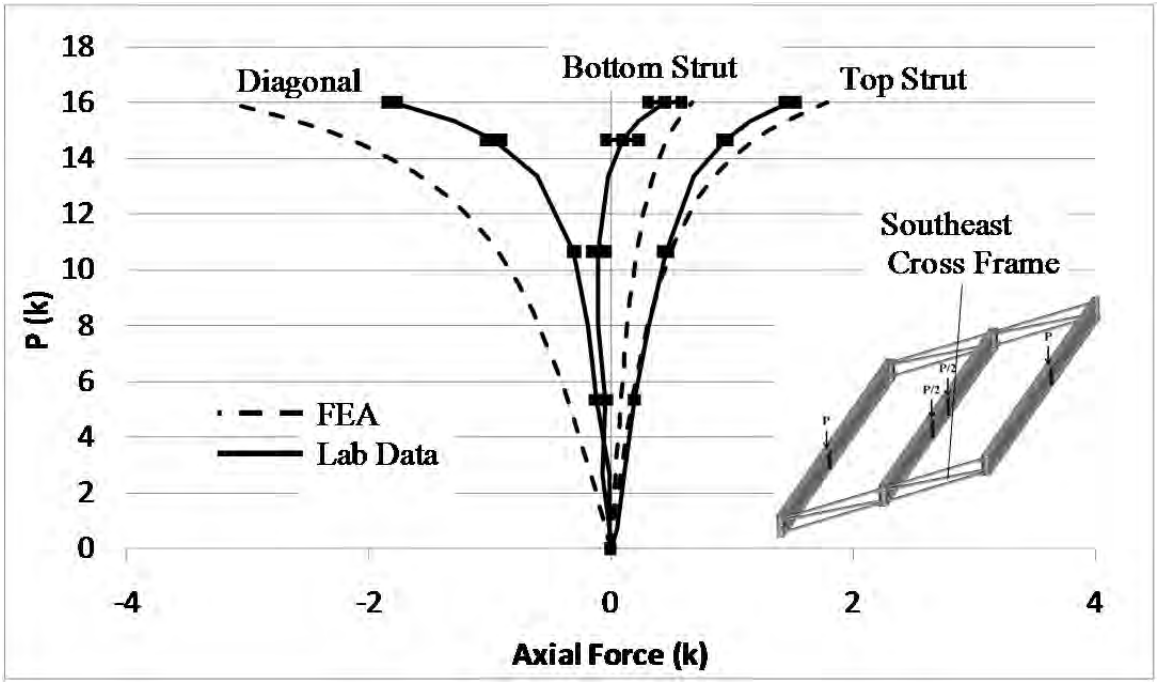

Figure B.64: SE end cross frame axial forces

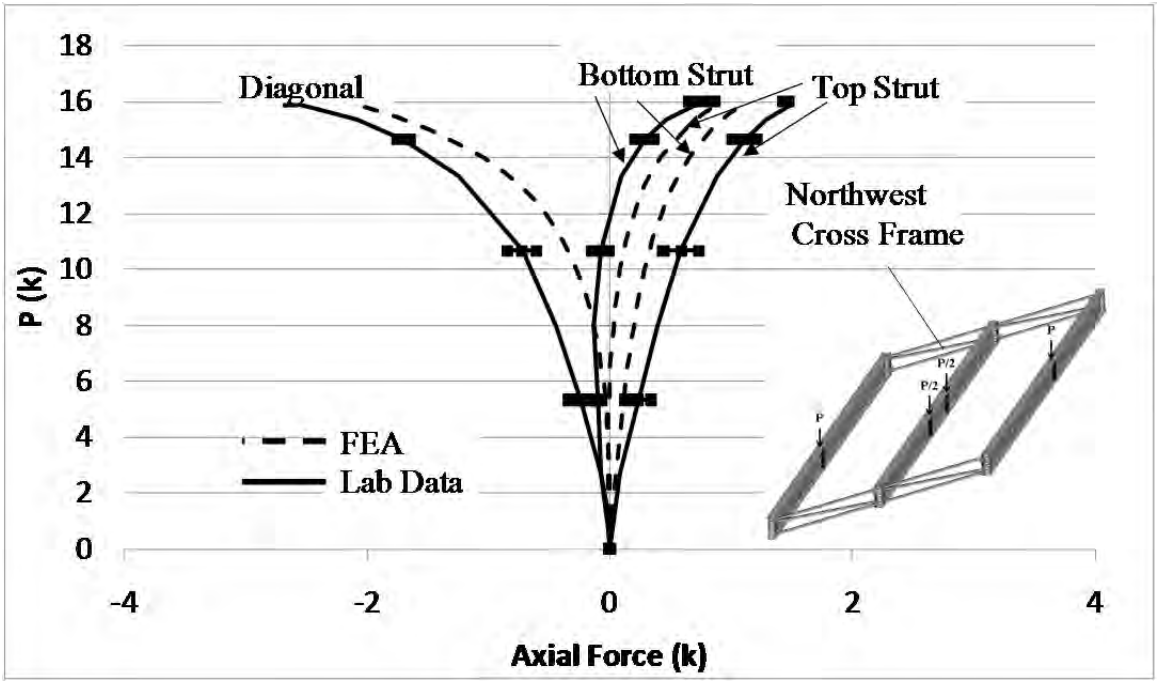

Figure B.65: NW end cross frame axial forces

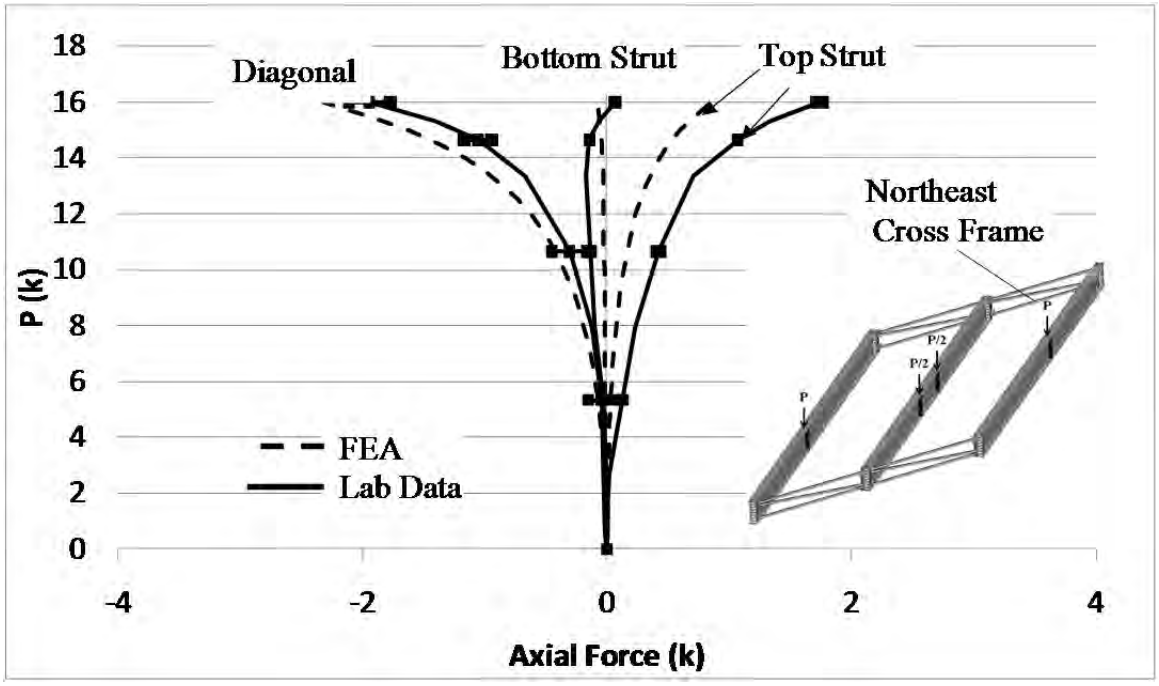

Figure B.66: NE end cross frame axial forces

B.3.5 Rubber Bearing with Shim with No Intermediate Cross Frames

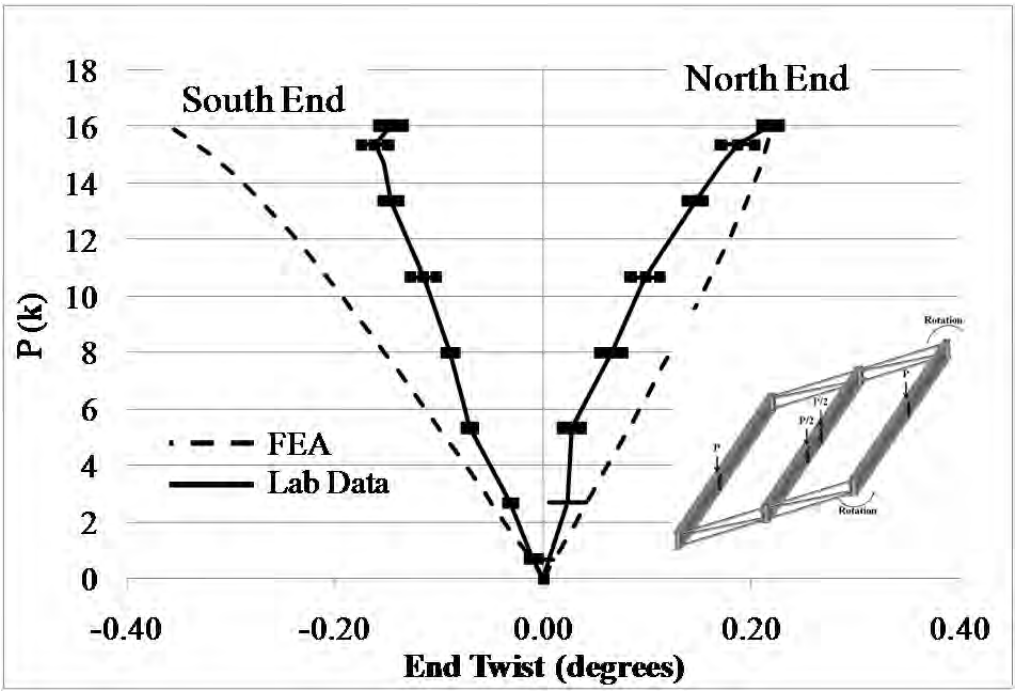

Figure B.67: GBP1 end twists

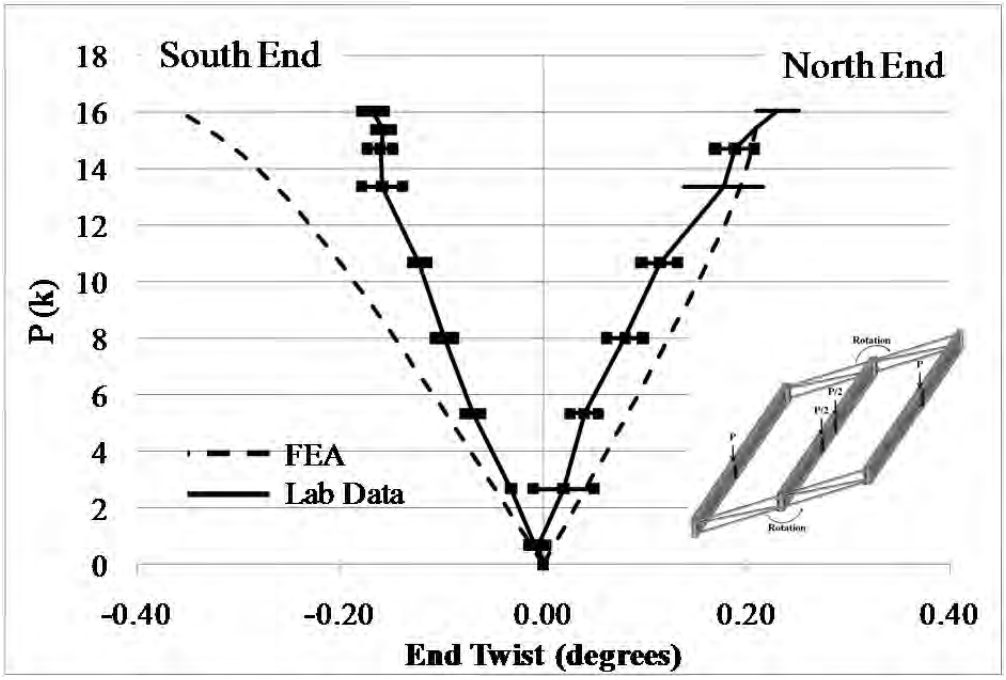

Figure B.68: GBP2 end twists

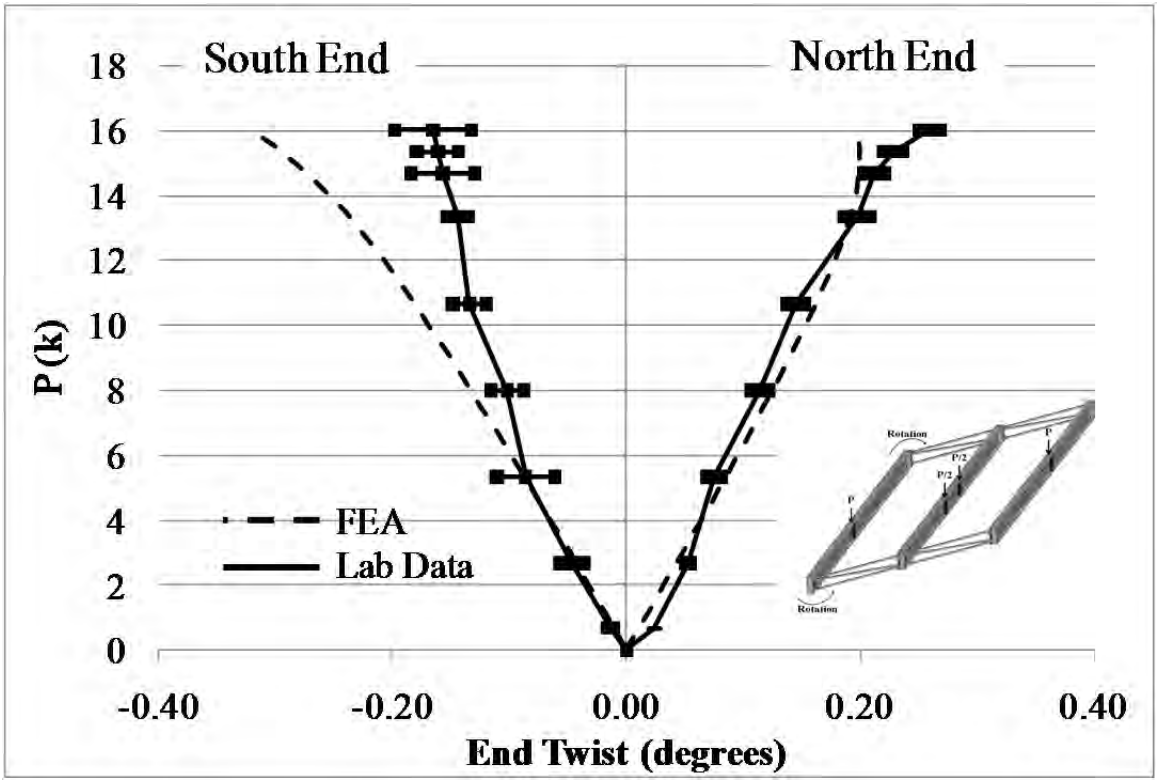

Figure B.69: GBP3 end twists

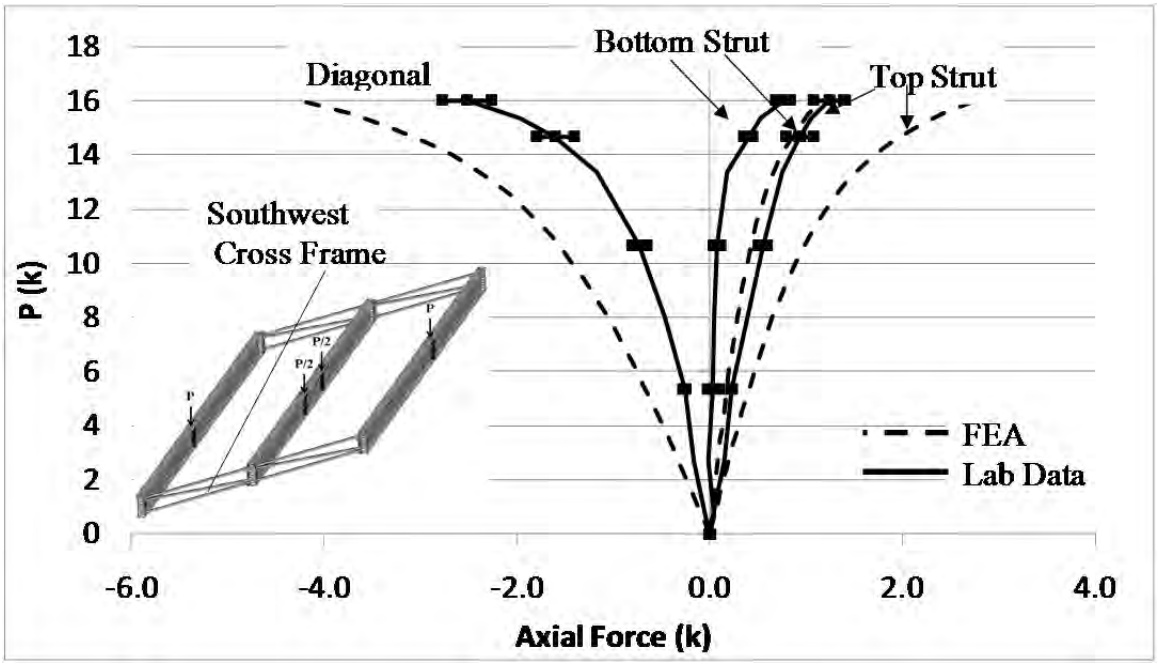

Figure B.70: SW end cross frame axial forces

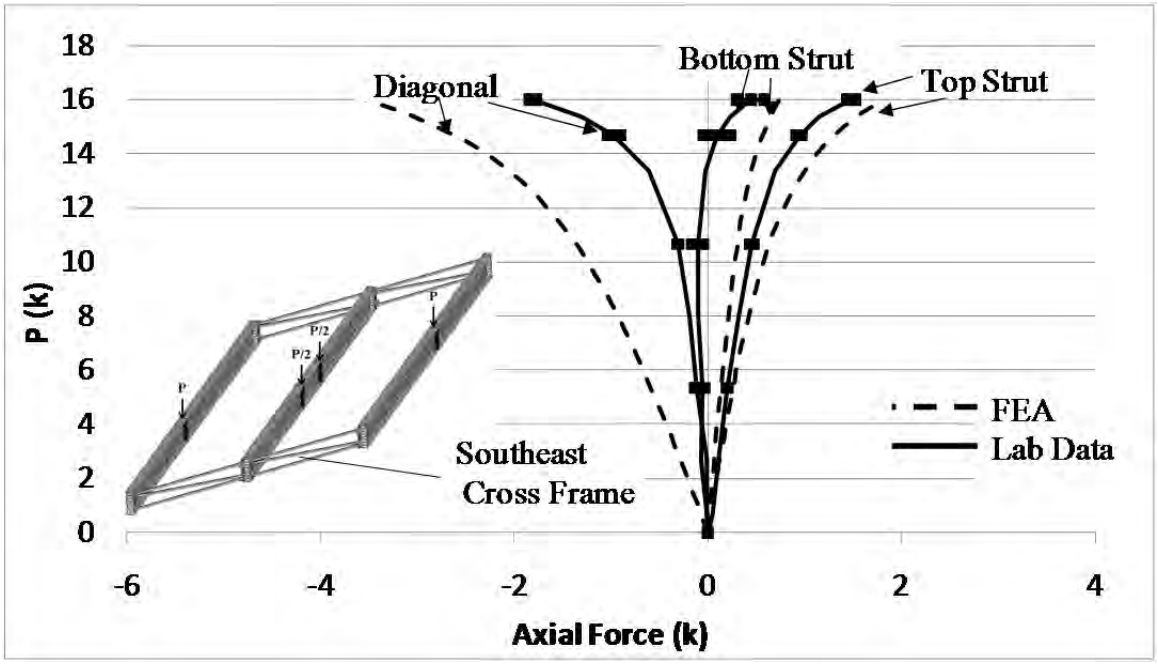

Figure B.71: SE end cross frame axial forces

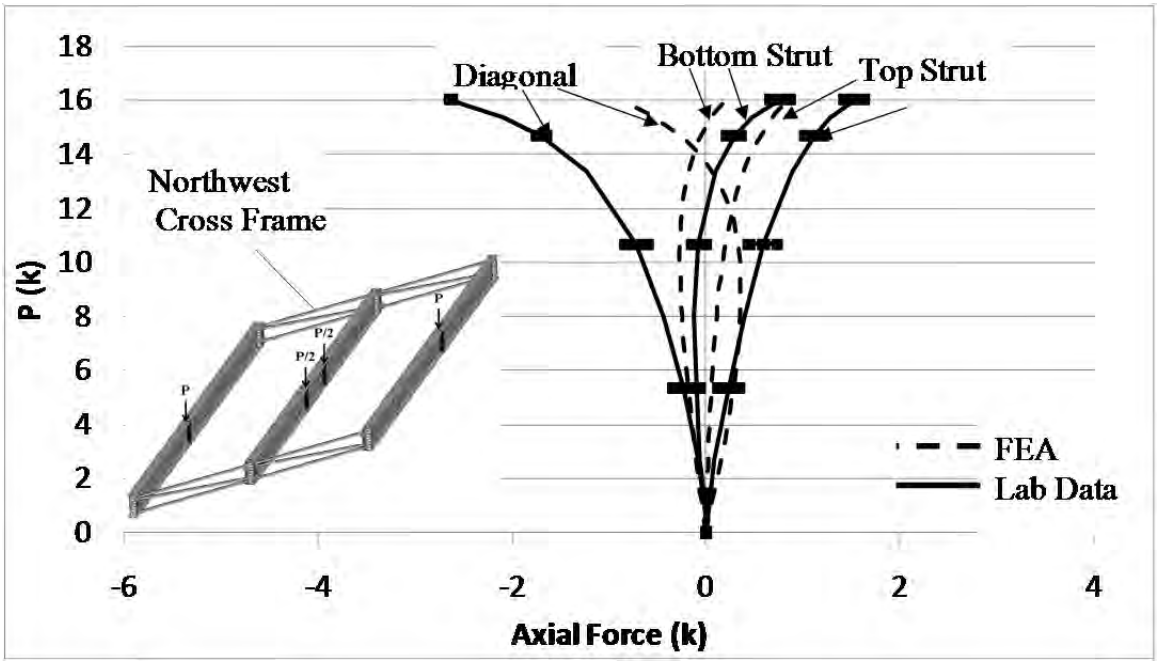

Figure B.72: NW end cross frame axial forces

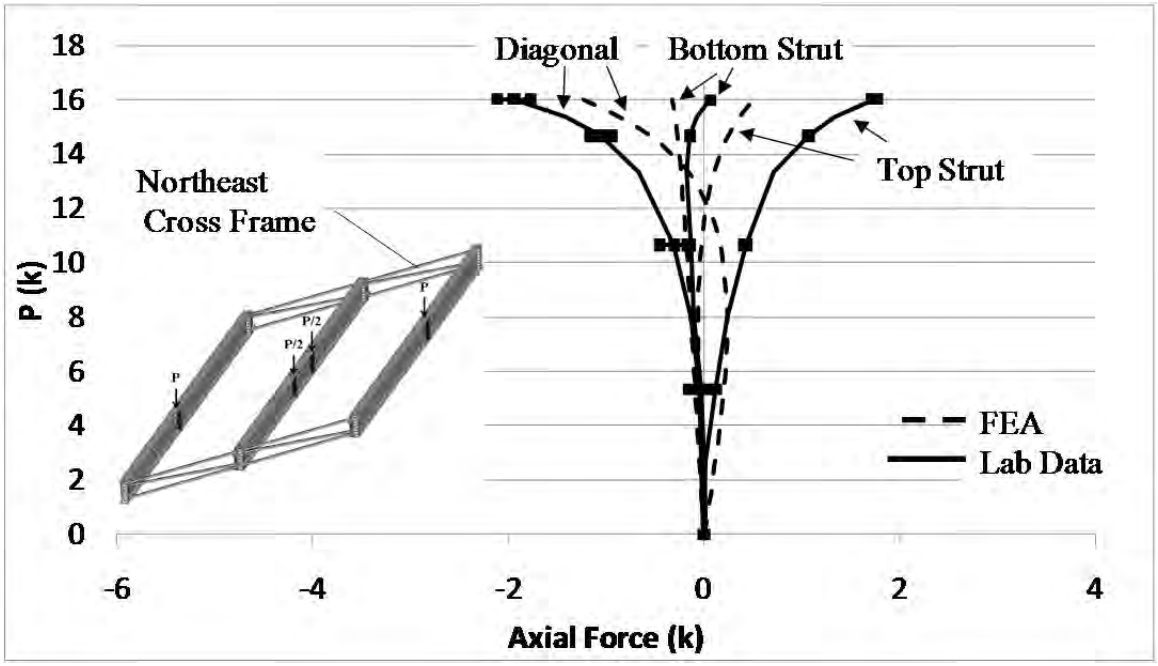

Figure B.73: NE end cross frame axial forces

B.4 THREE GIRDER BEND PLATE END FRAME VALIDATION RESULTS

B.4.1 Thrust Washer Bearing with No Intermediate Cross Frames

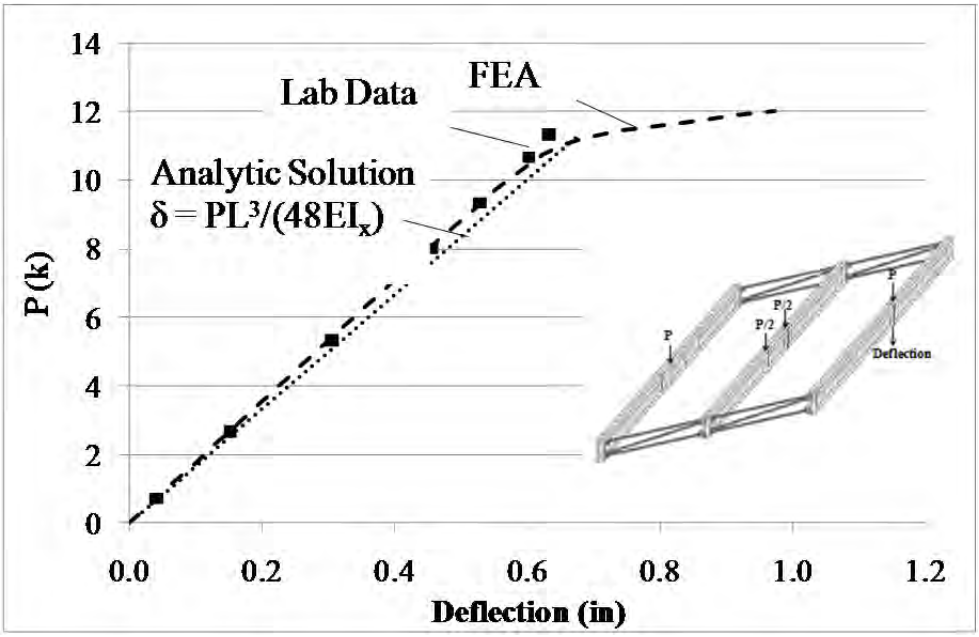

Figure B.74: GBP1 mid-span vertical deflection

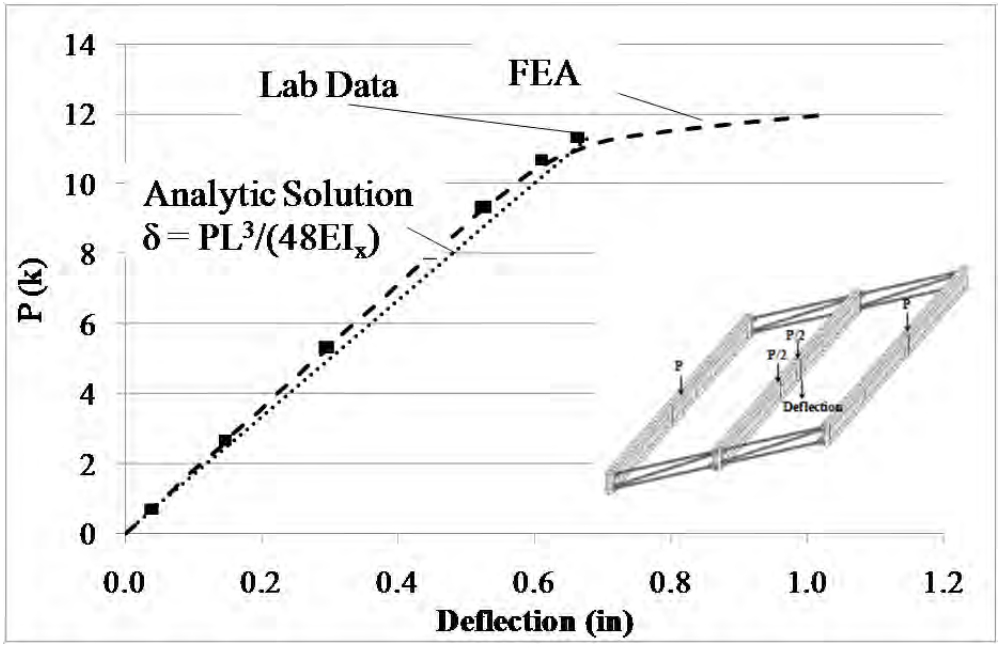

Figure B.75: GBP2 mid-span vertical deflection

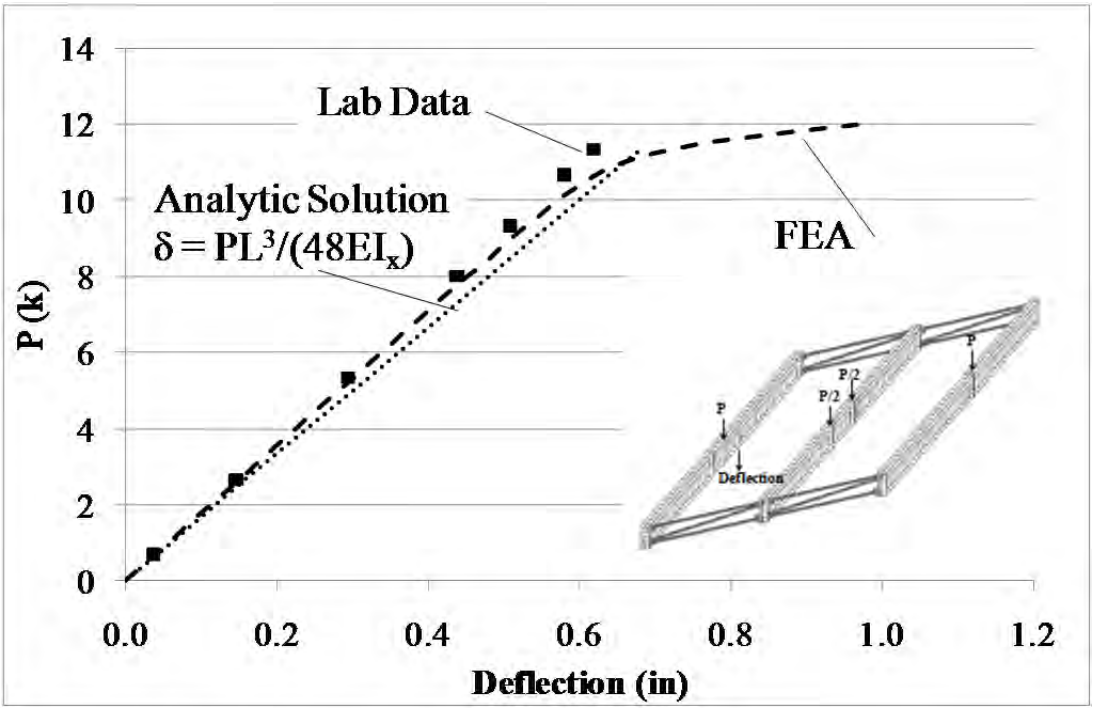

Figure B.76: GBP3 mid-span vertical deflection

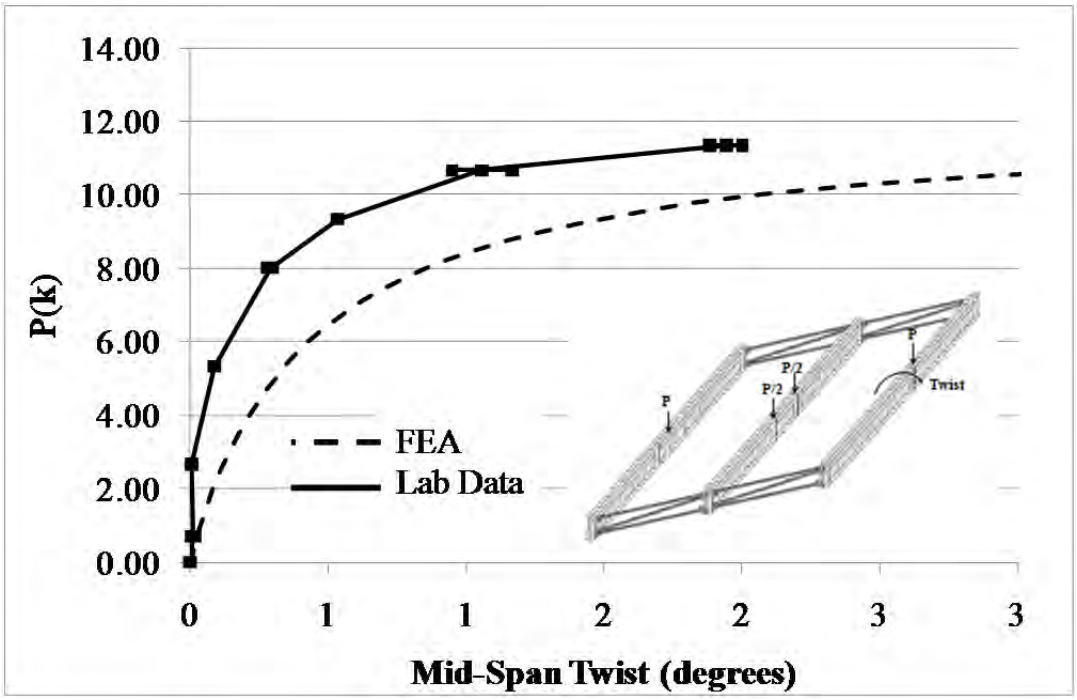

Figure B.77: GBP1 mid-span twist

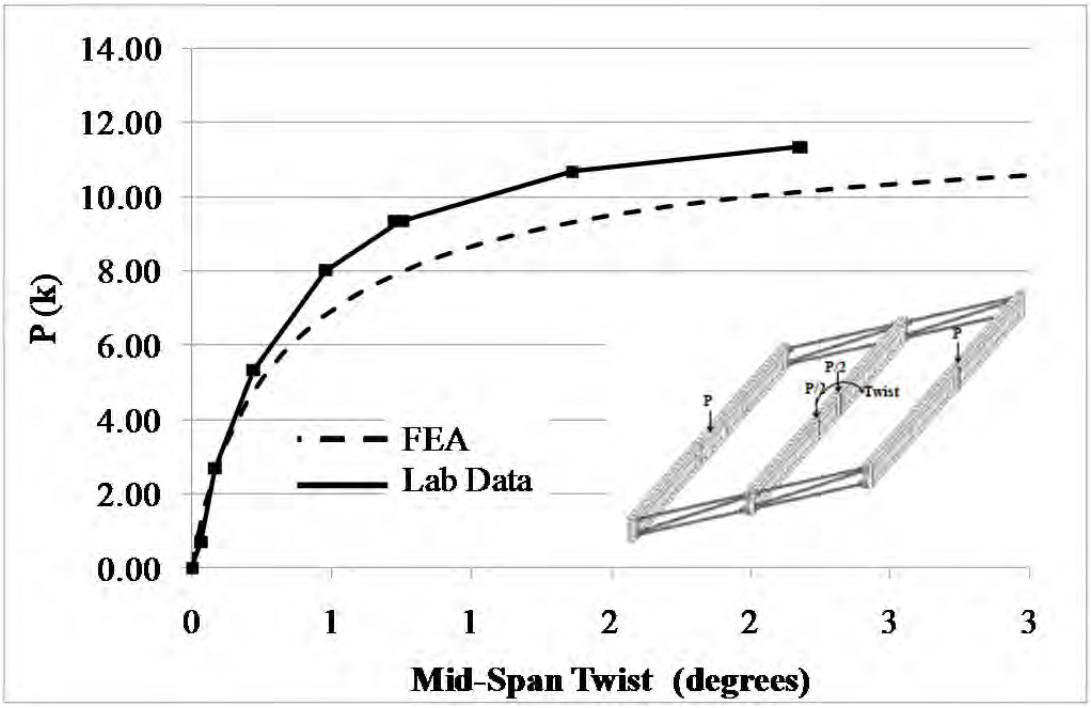

Figure B.78: GBP2 mid-span twist

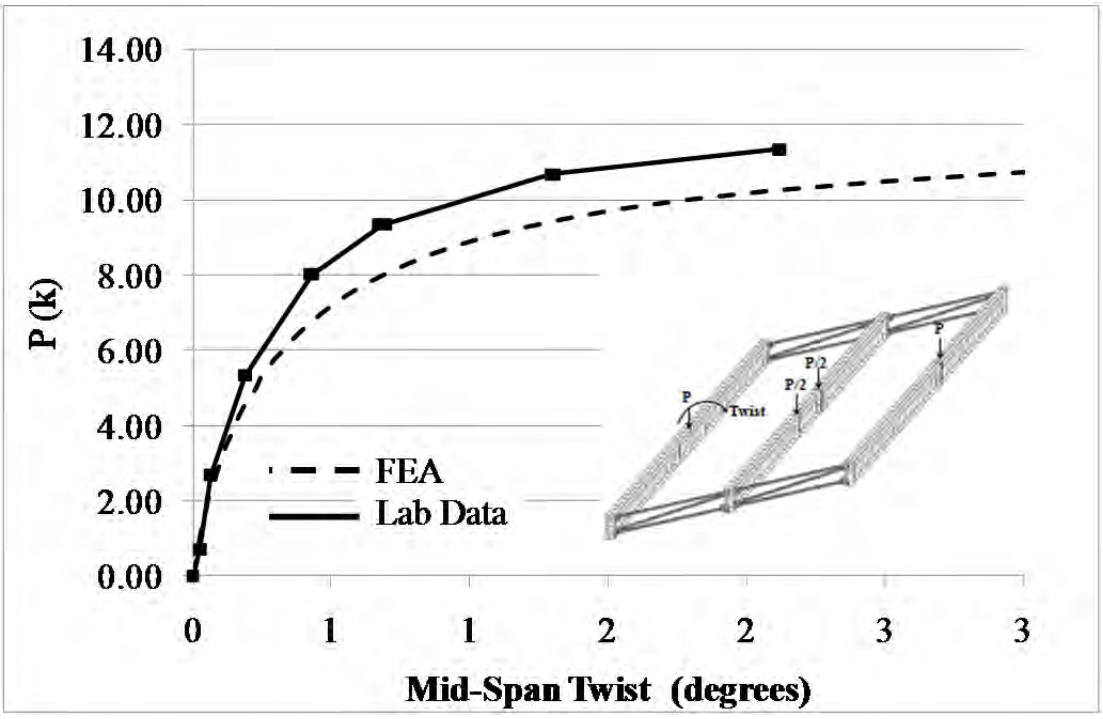

Figure B.79: GBP3 mid-span twist

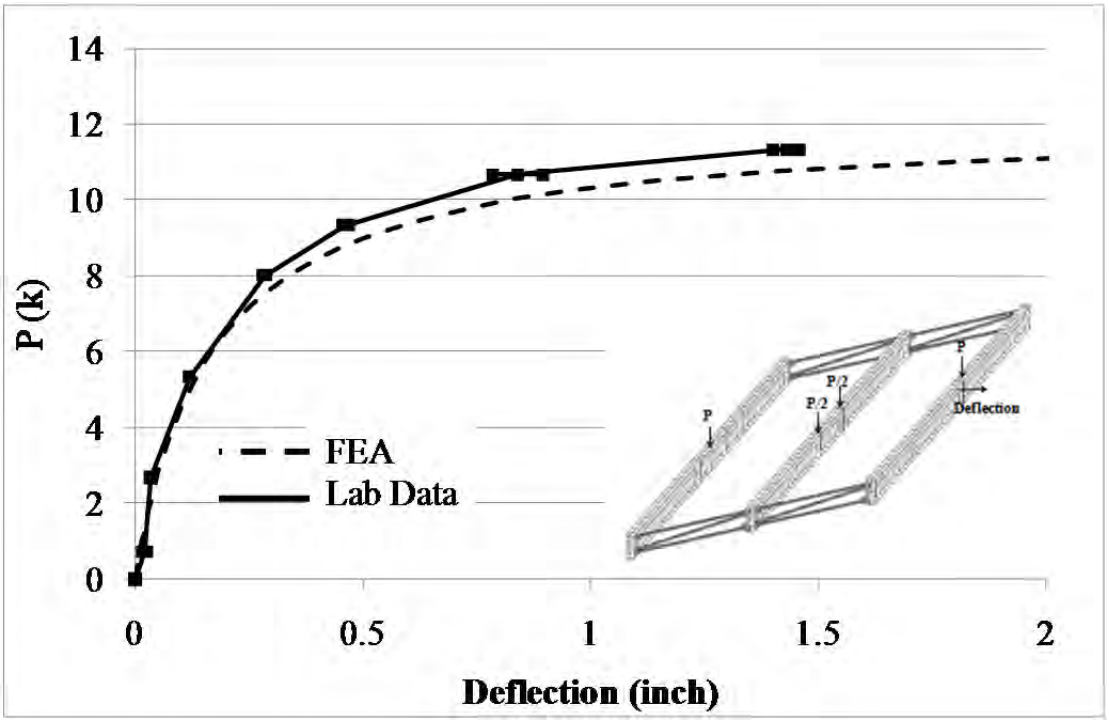

Figure B.80: GBP1 top flange deflection

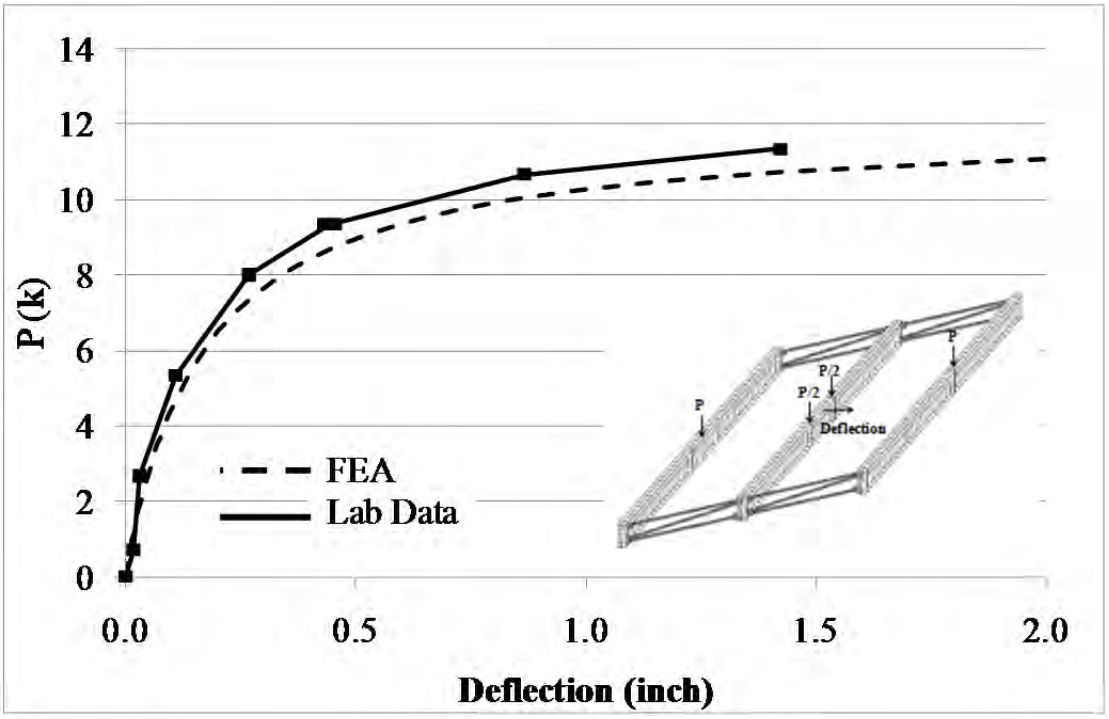

Figure B.81: GBP2 top flange deflection

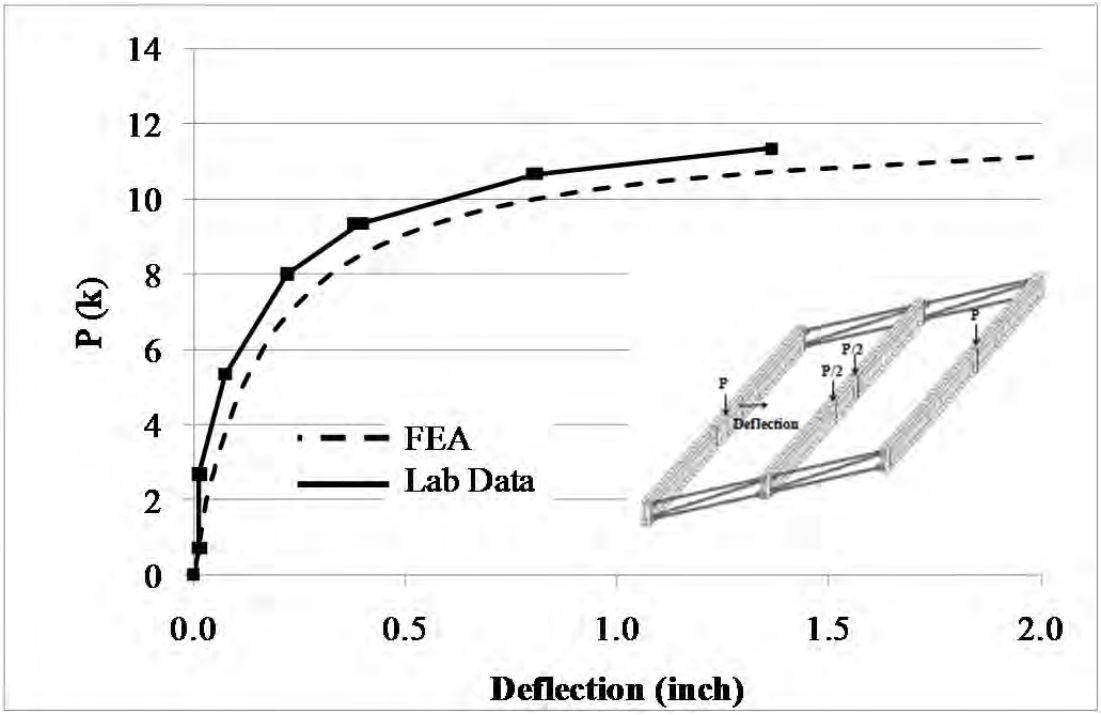

Figure B.82: GBP3 top flange deflection

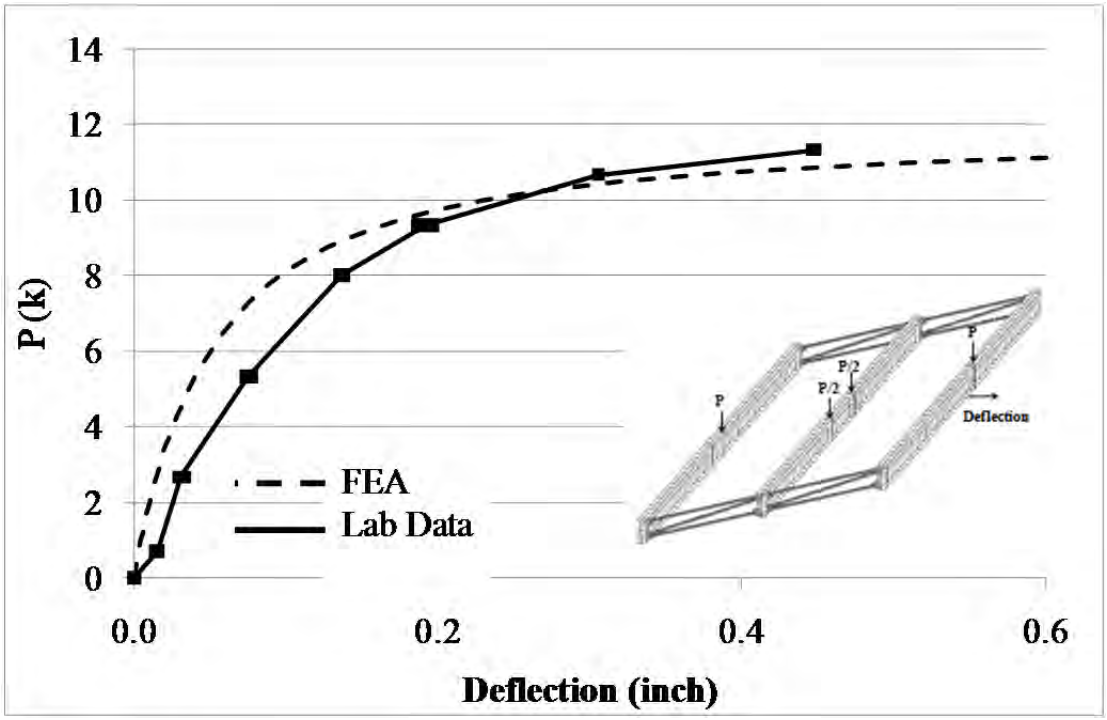

Figure B.83: GBP1 bottom flange deflection

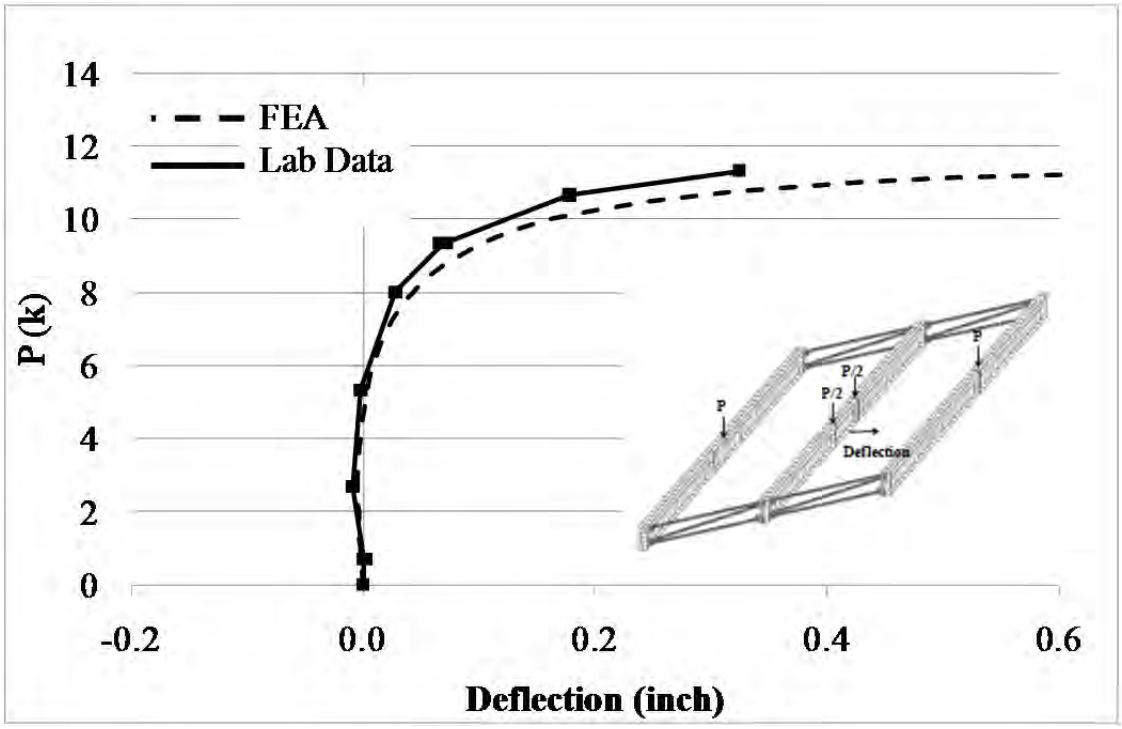

Figure B.84: GBP2 bottom flange deflection

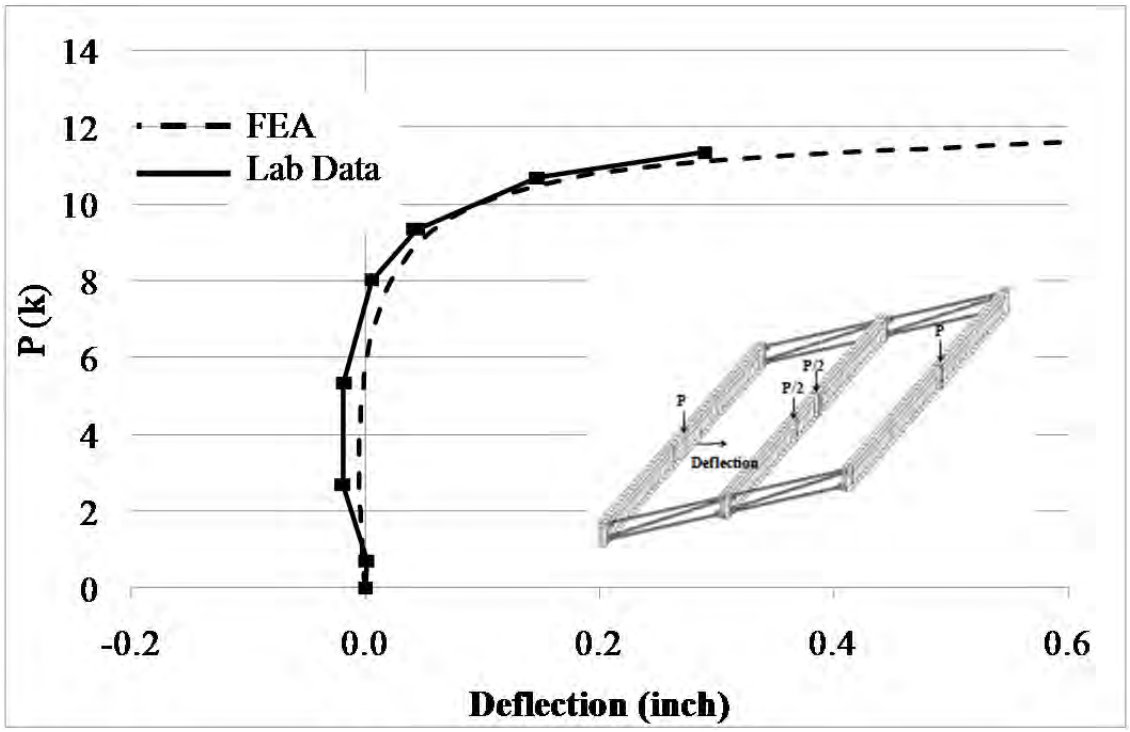

Figure B.85: GBP3 bottom flange deflection

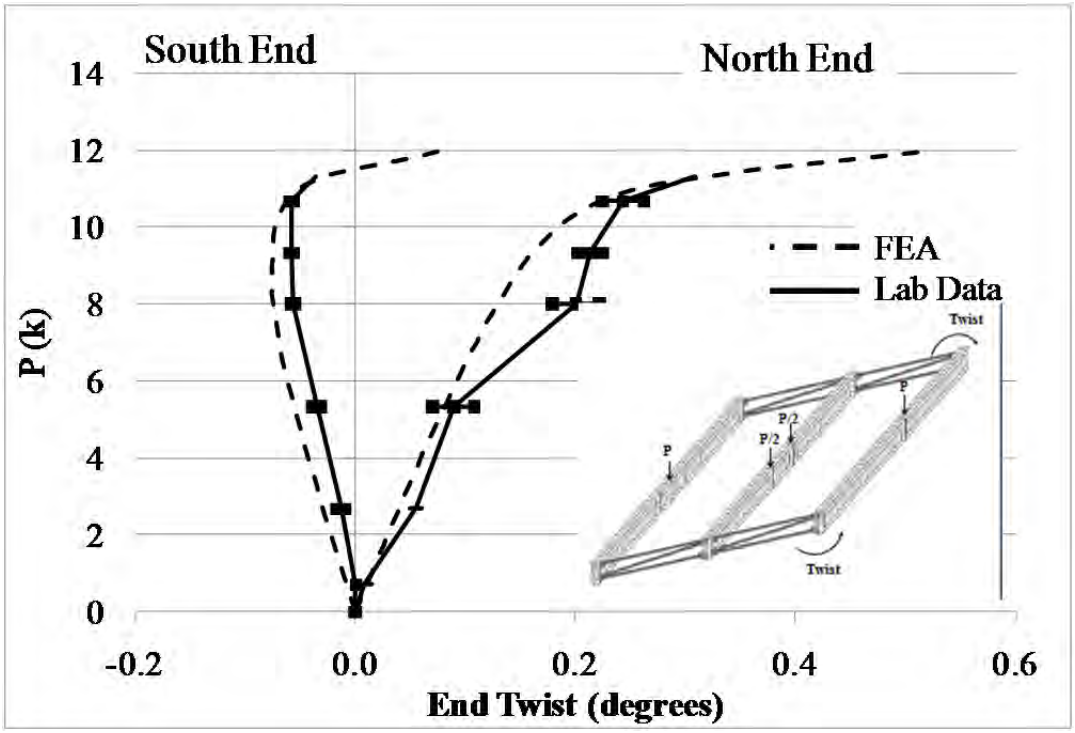

Figure B.86: GBP1 end twist

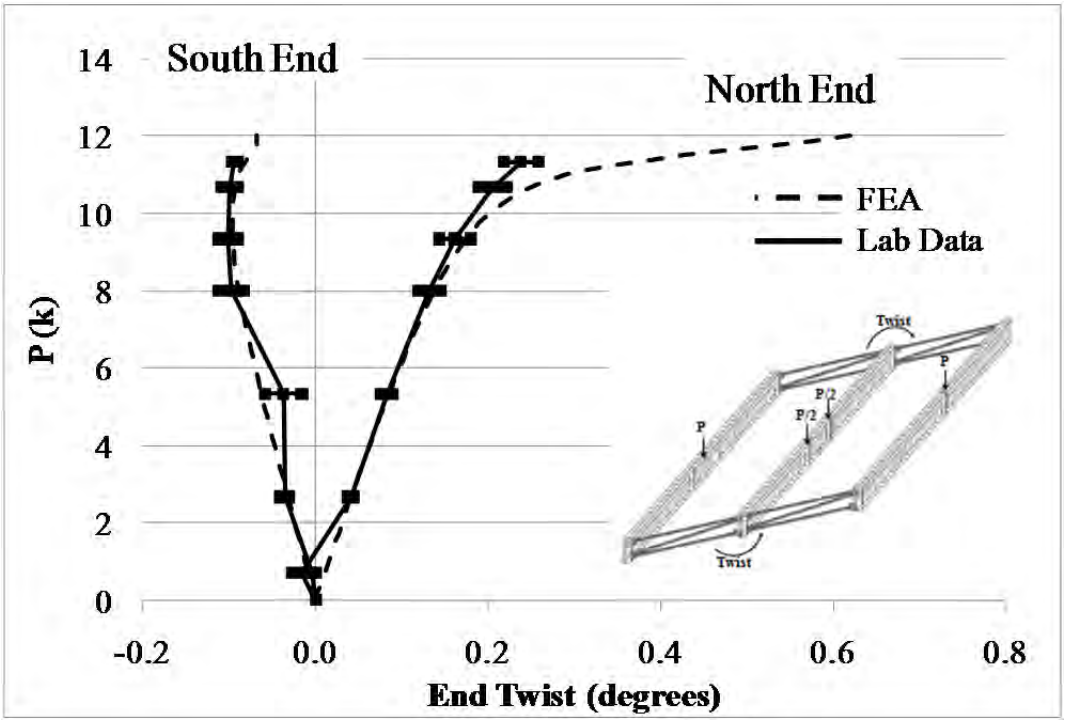

Figure B.87: GBP2 end twist

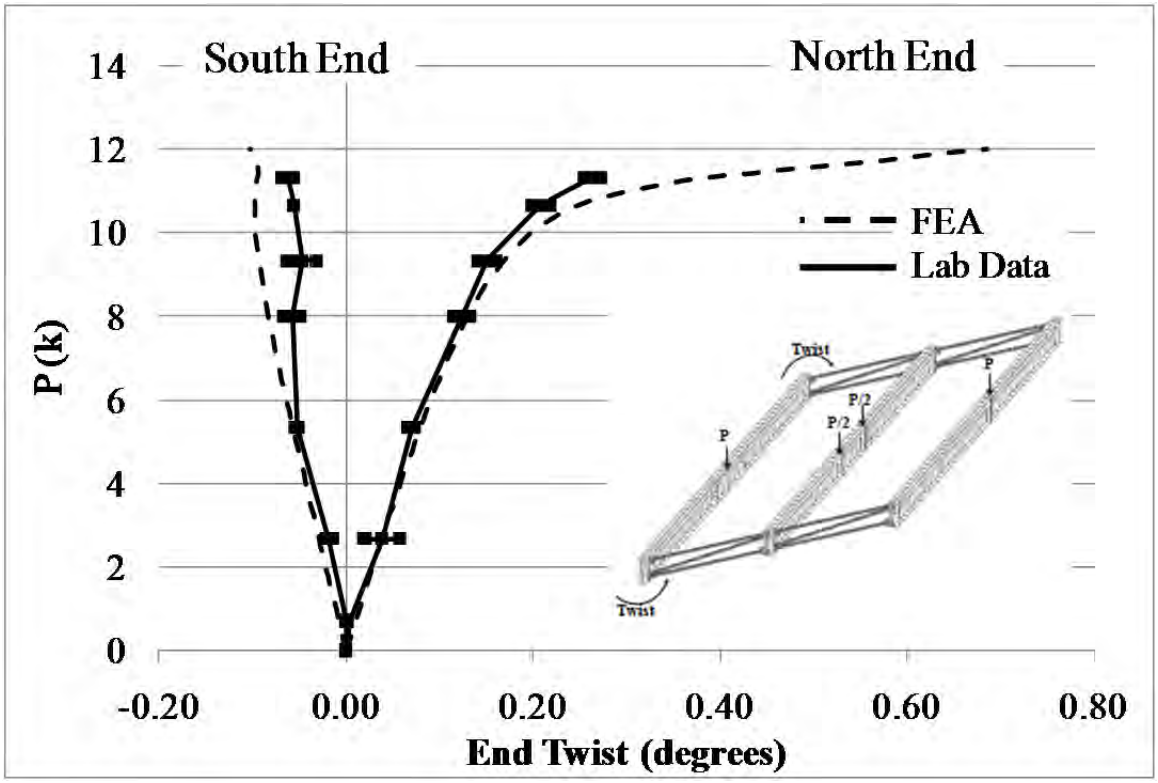

Figure B.88: GBP3 end twist

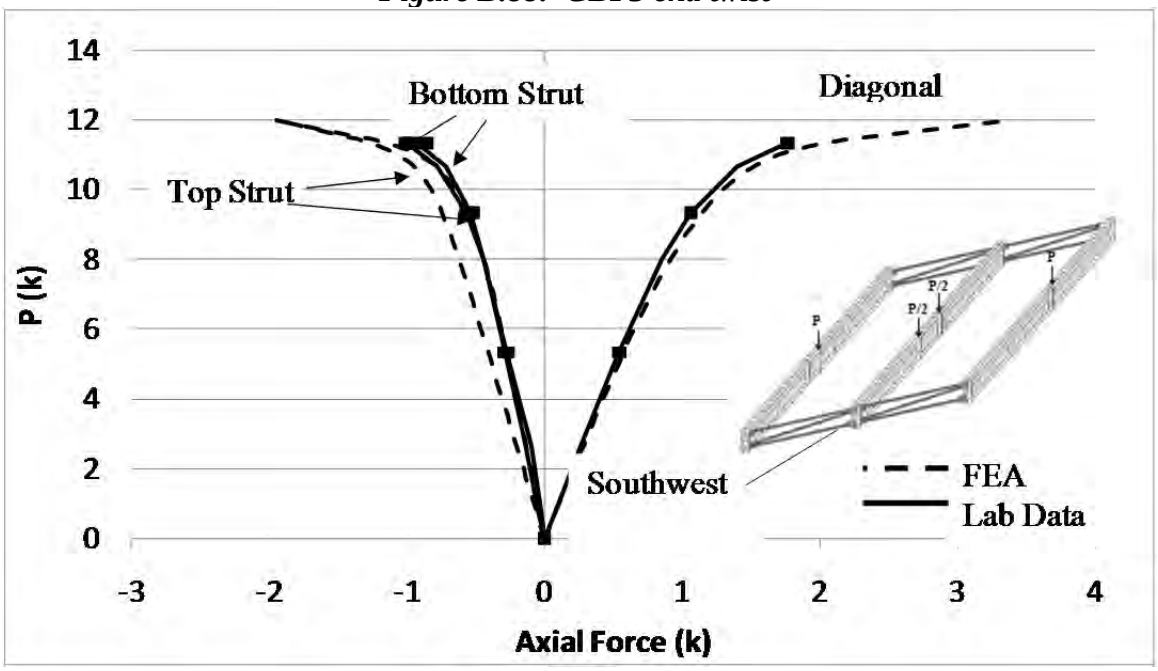

Figure B.89: SW end frame axial forces

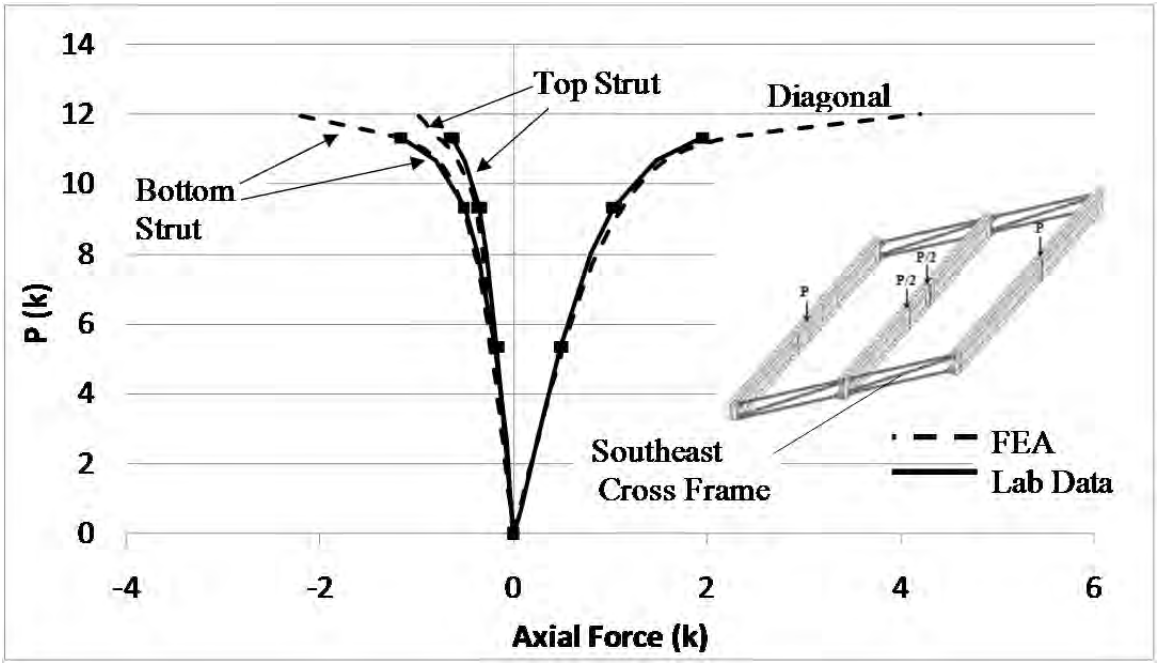

Figure B.90: SE end frame axial forces

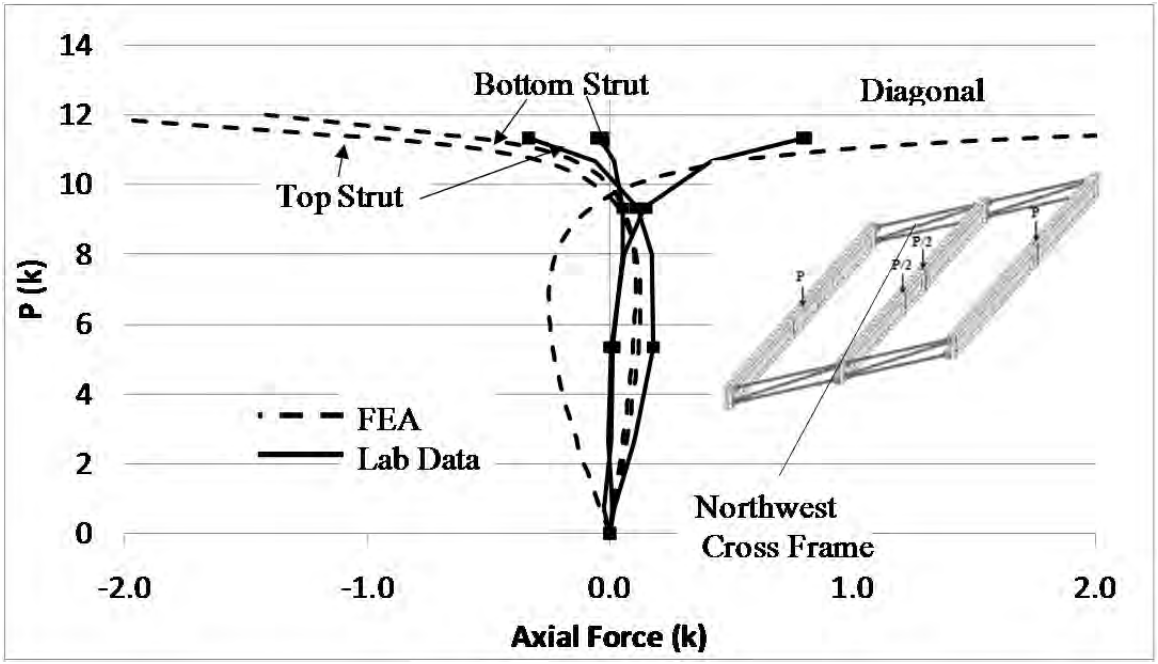

Figure B.91: NW end frame axial forces

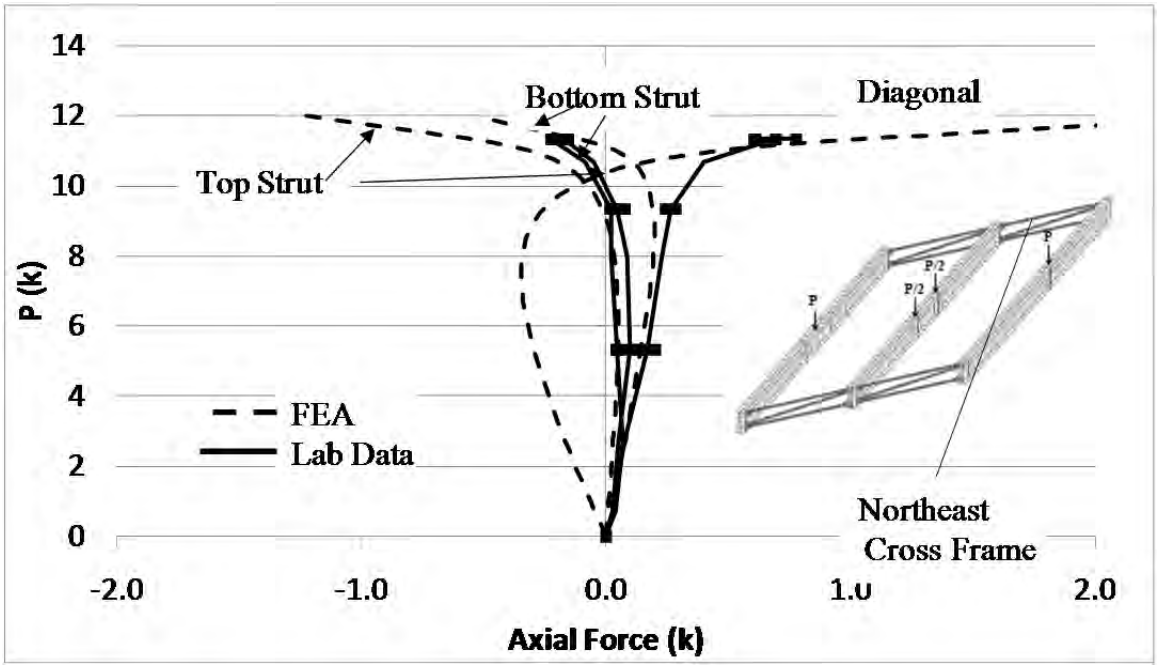

Figure B.92: NE end frame axial forces

B.4.2 Thrust Washer Bearing with Staggered Intermediate Cross Frames

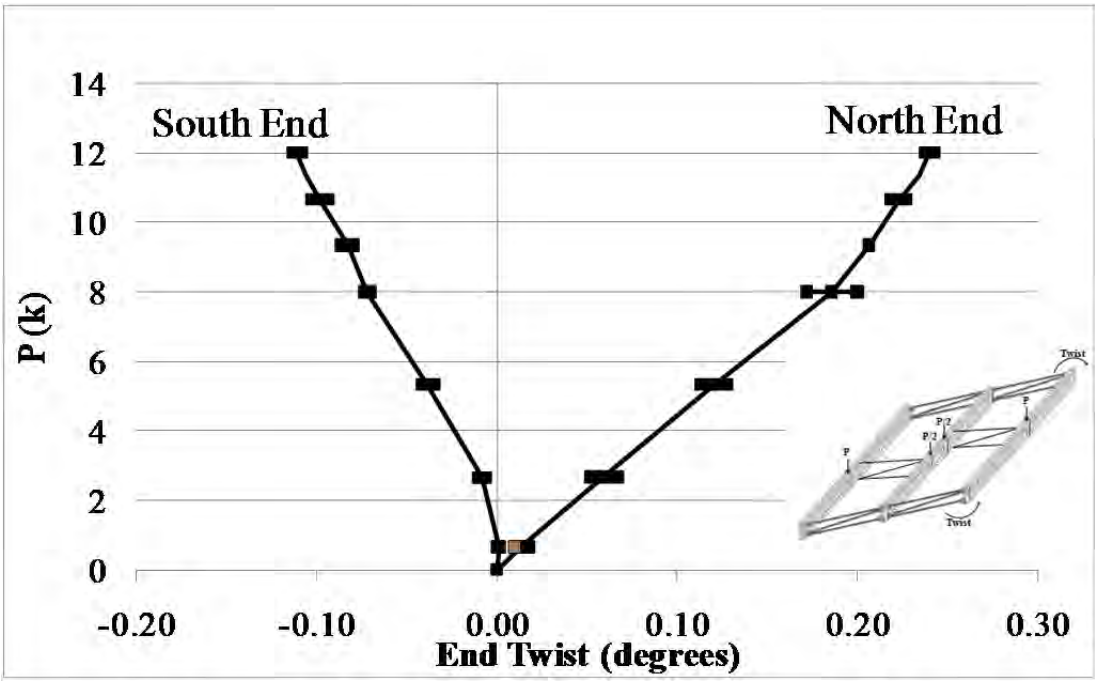

Figure B.93: GBP1 end twists

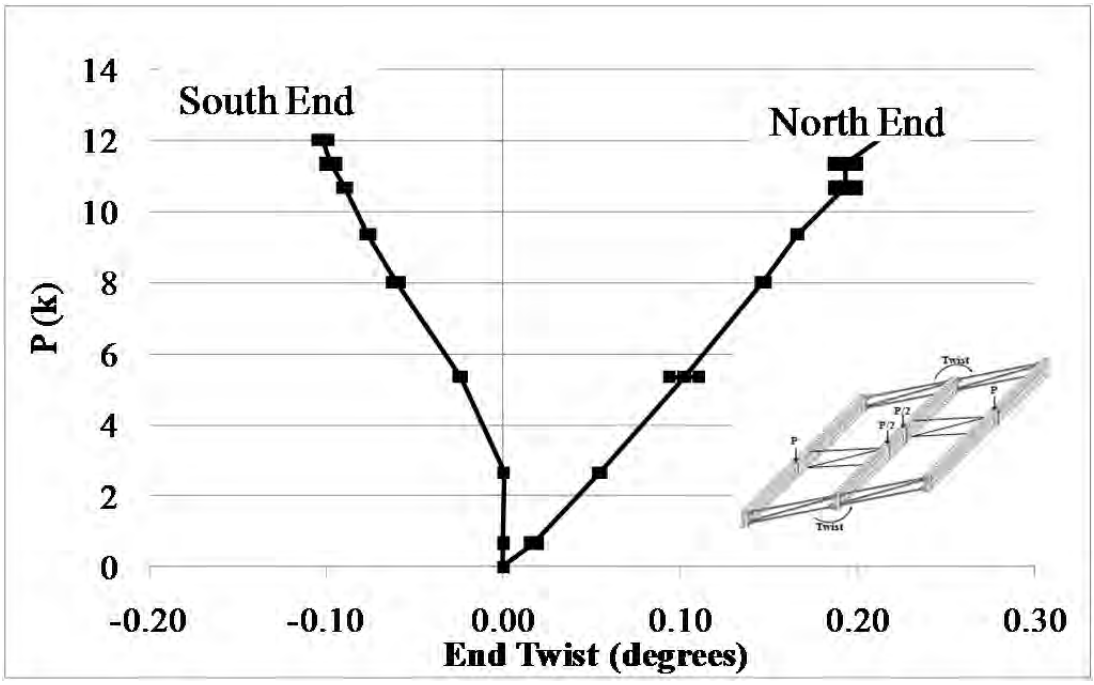

Figure B.94: GBP2 end twists

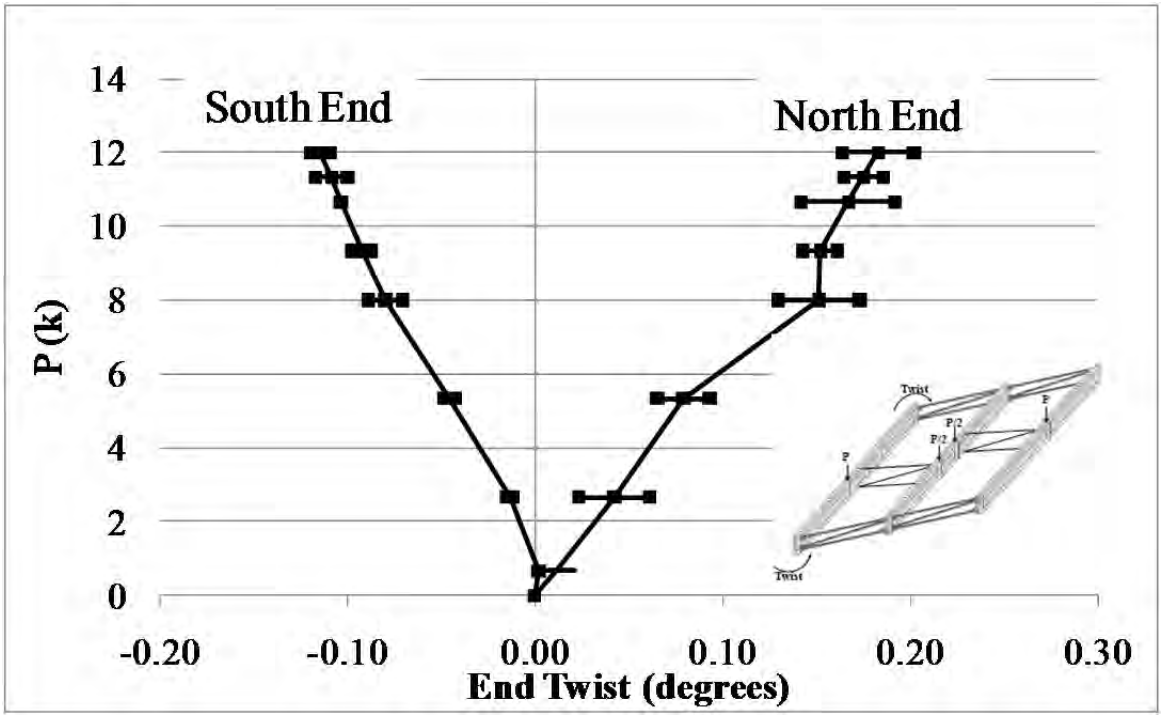

Figure B.95: GBP3 end twists

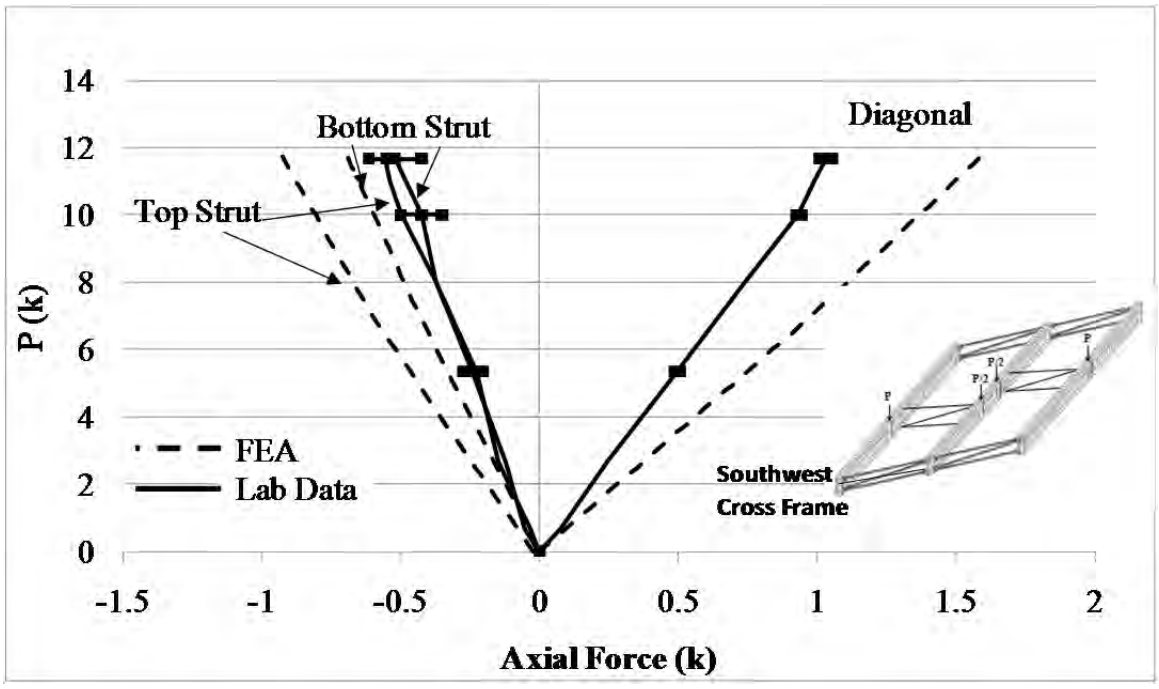

Figure B.96: SW cross frame axial forces

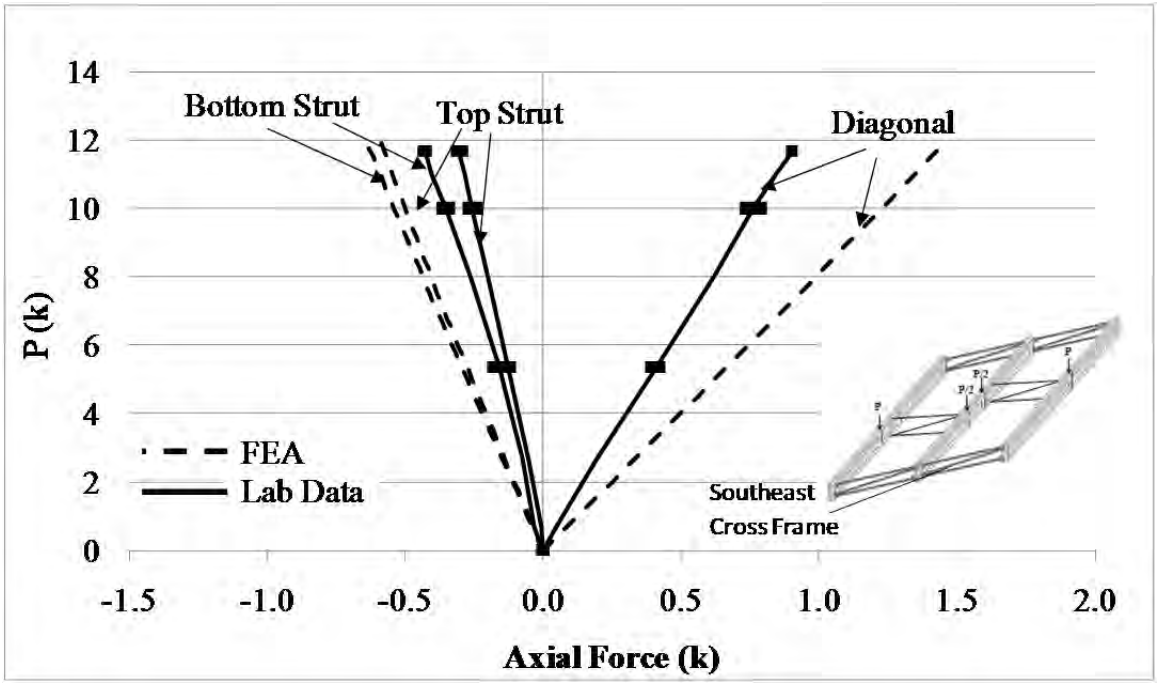

Figure B.97: SE cross frame axial forces

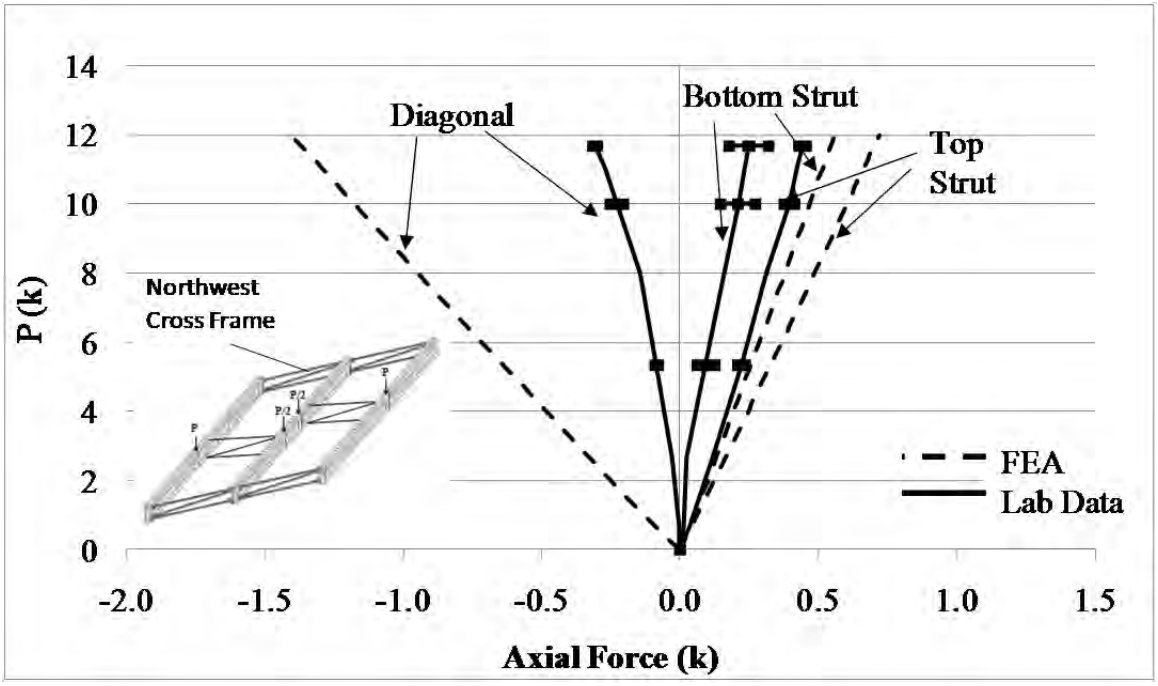

Figure B.98: NW cross frame axial forces

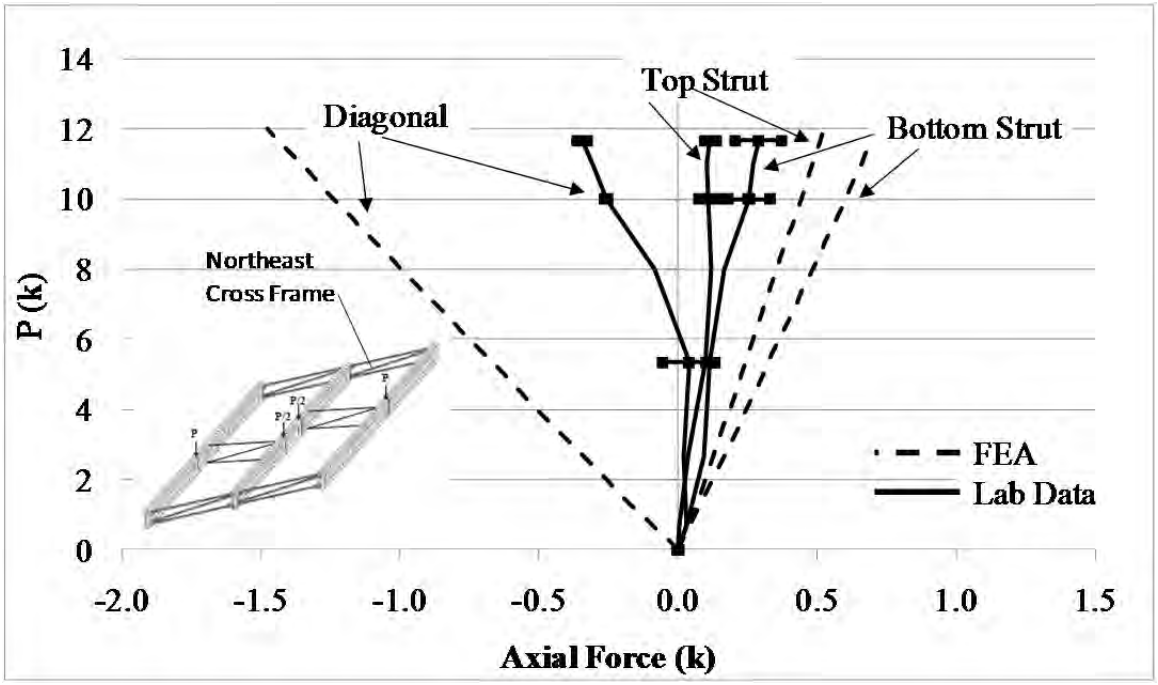

Figure B.99: NE cross frame axial forces

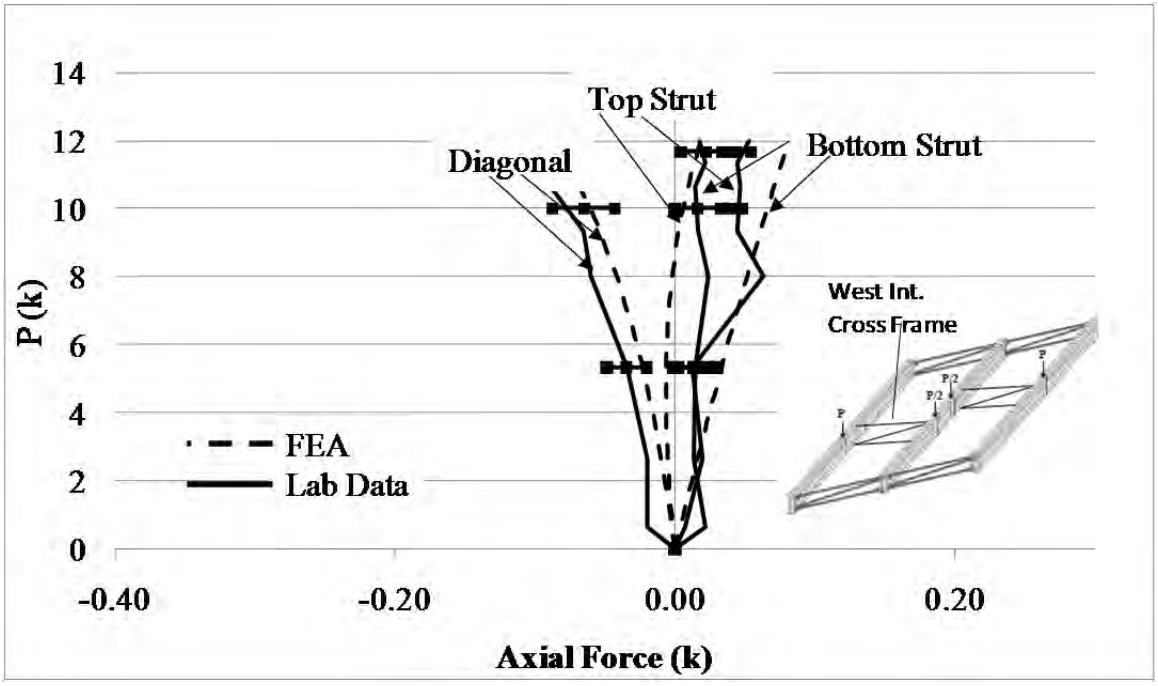

Figure B.100: West intermediate cross frame axial forces

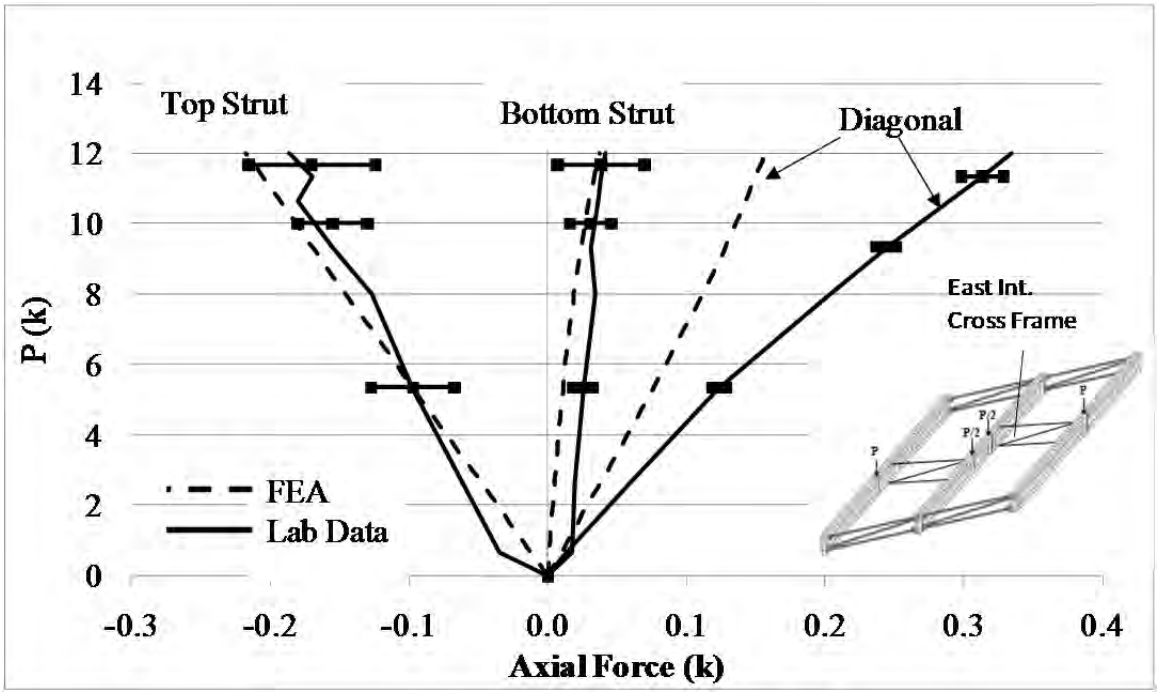

Figure B.101: East intermediate cross frame axial forces

B.4.3 Thrust Washer Bearing with Staggered Intermediate Cross Frames – Partial Loading

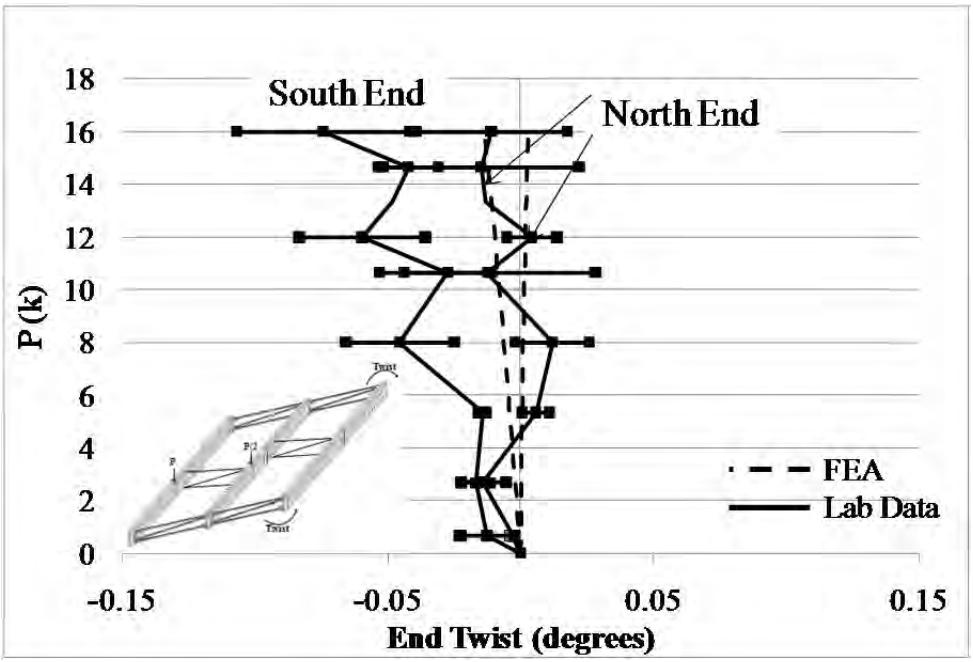

Figure B.102: GBP1 end twists

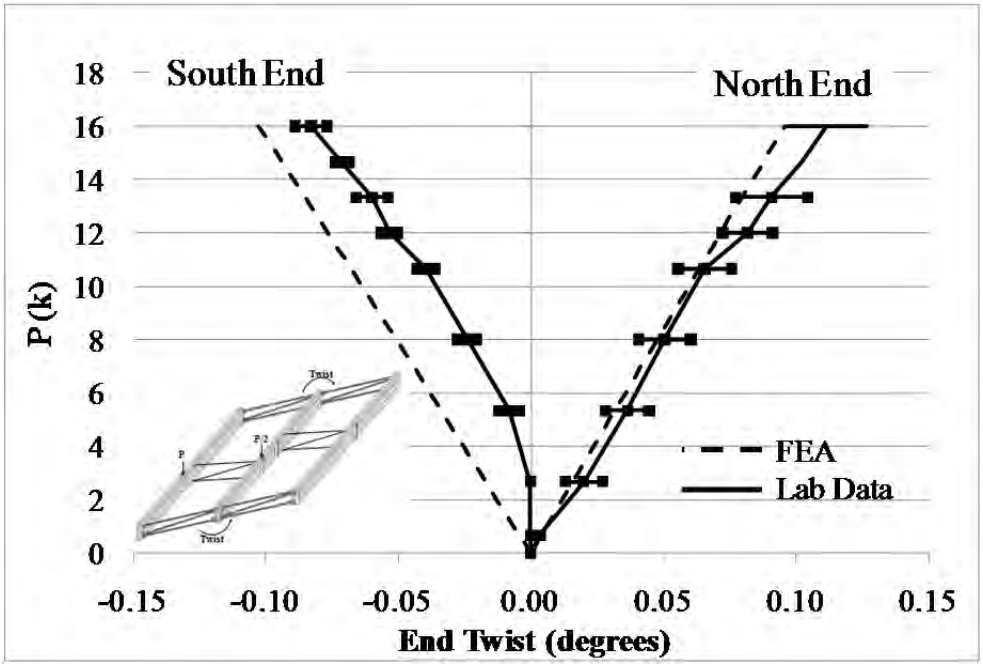

Figure B.103: GBP2 end twists

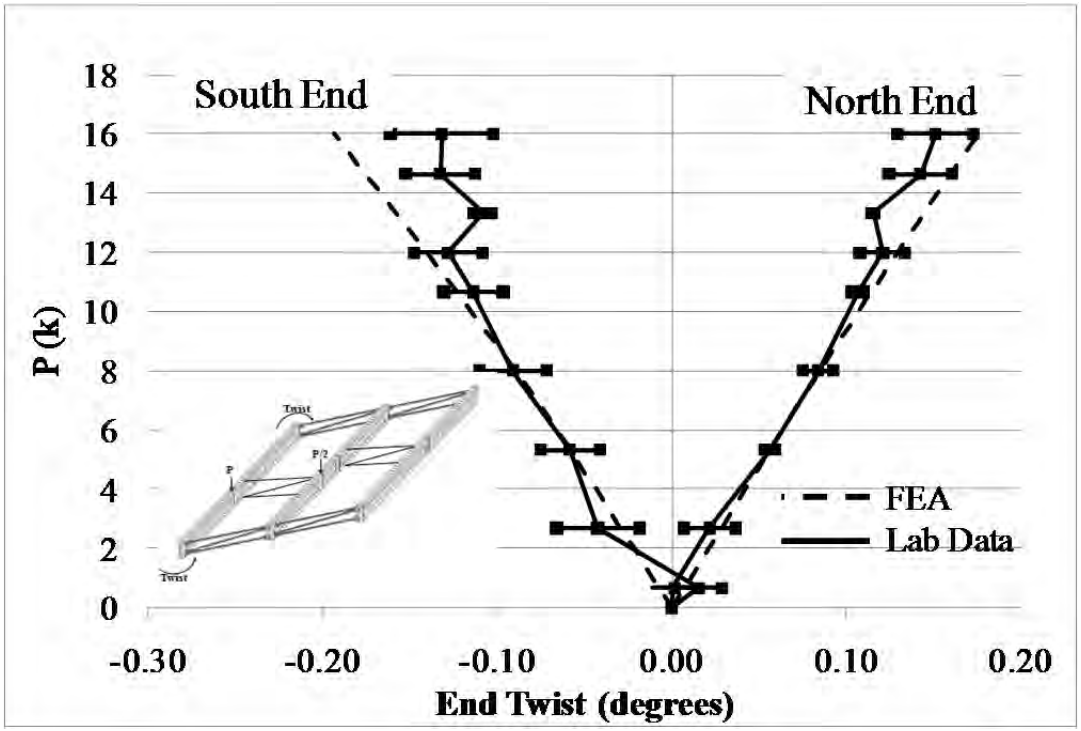

Figure B.104: GBP3 end twists

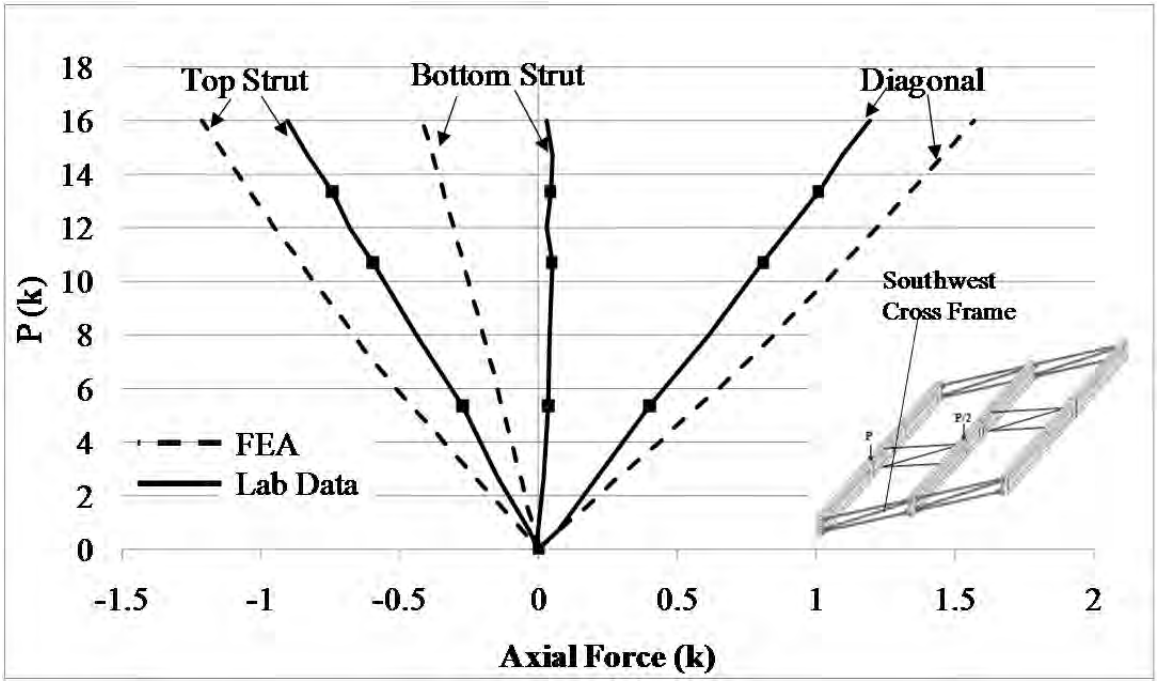

Figure B.105: SW cross frame axial forces

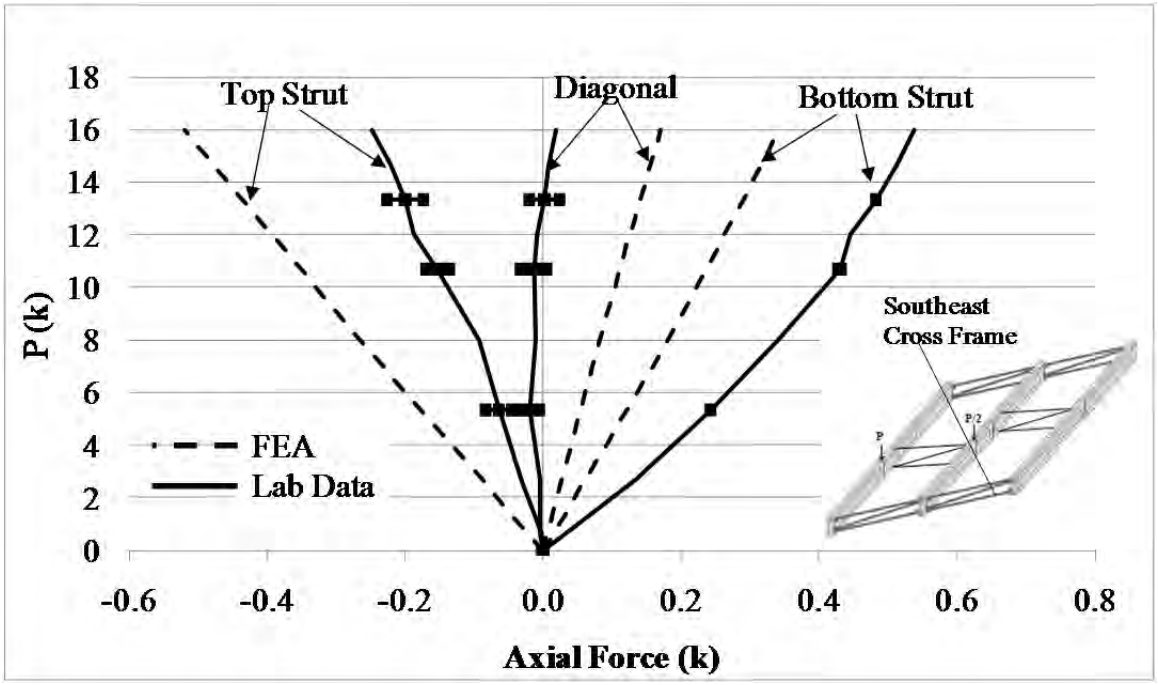

Figure B.106: SE cross frame axial forces

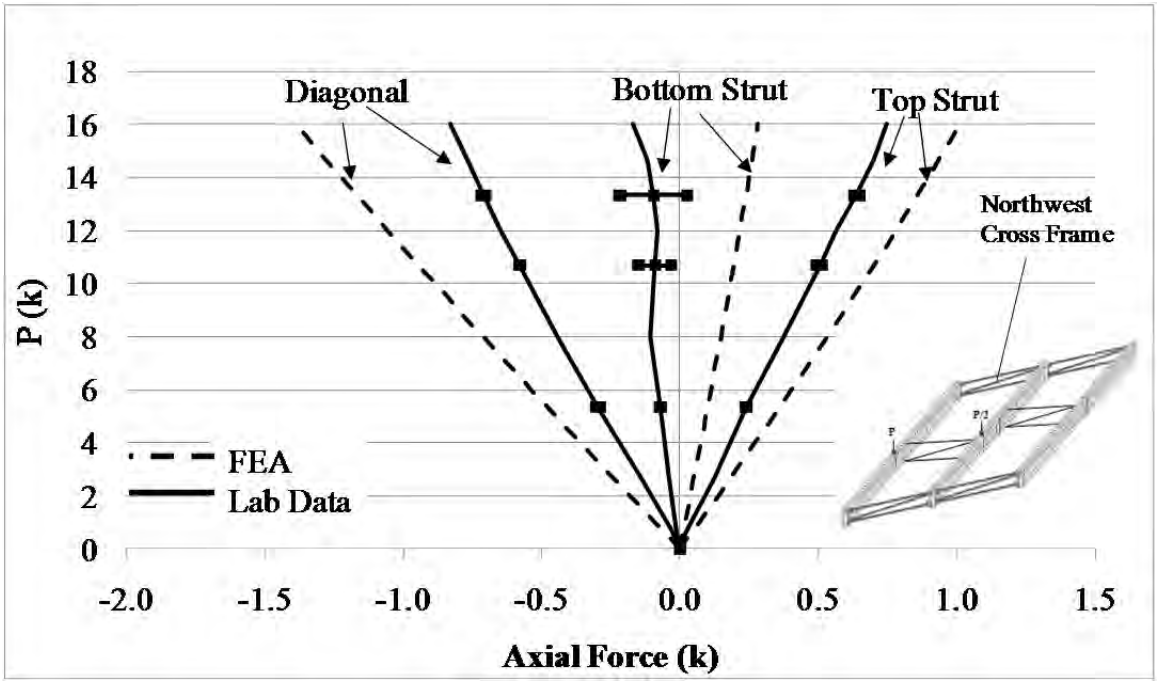

Figure B.107: NW cross frame axial forces

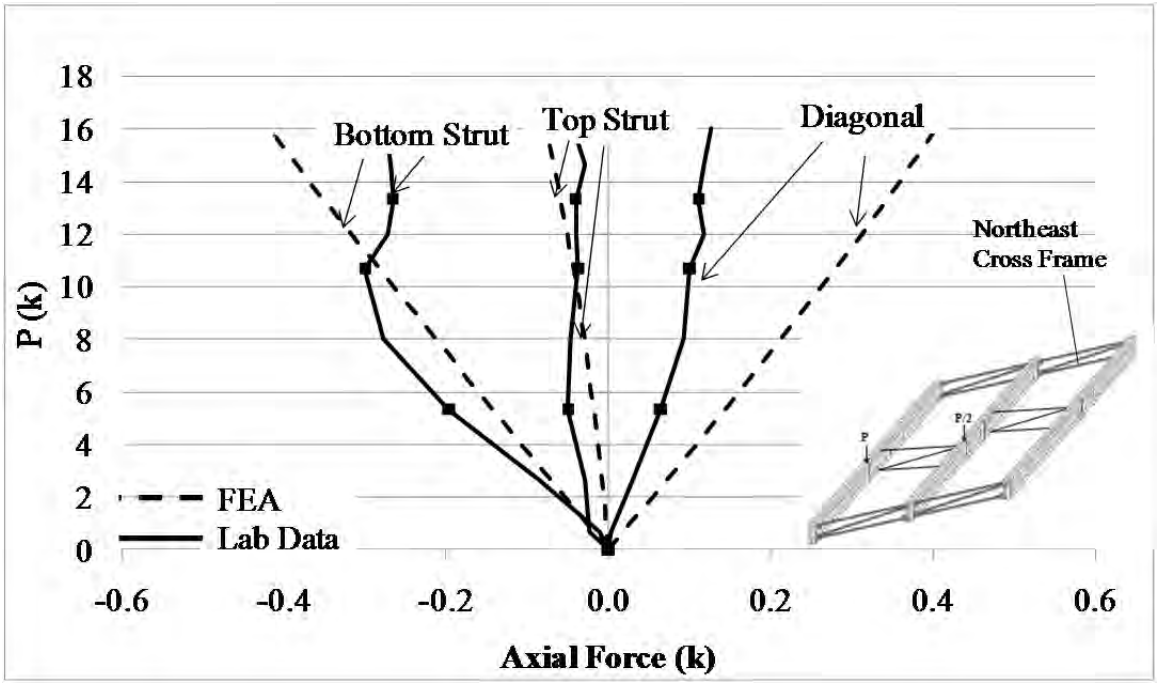

Figure B.108: NE cross frame axial forces

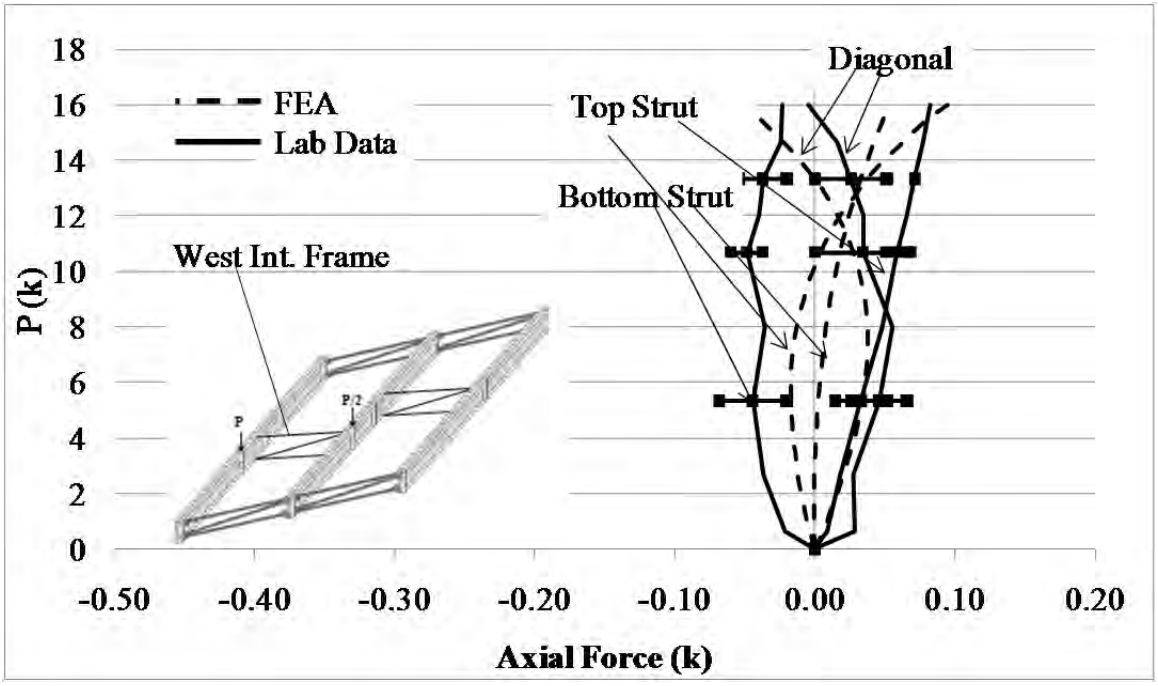

Figure B.109: West intermediate cross frame axial forces

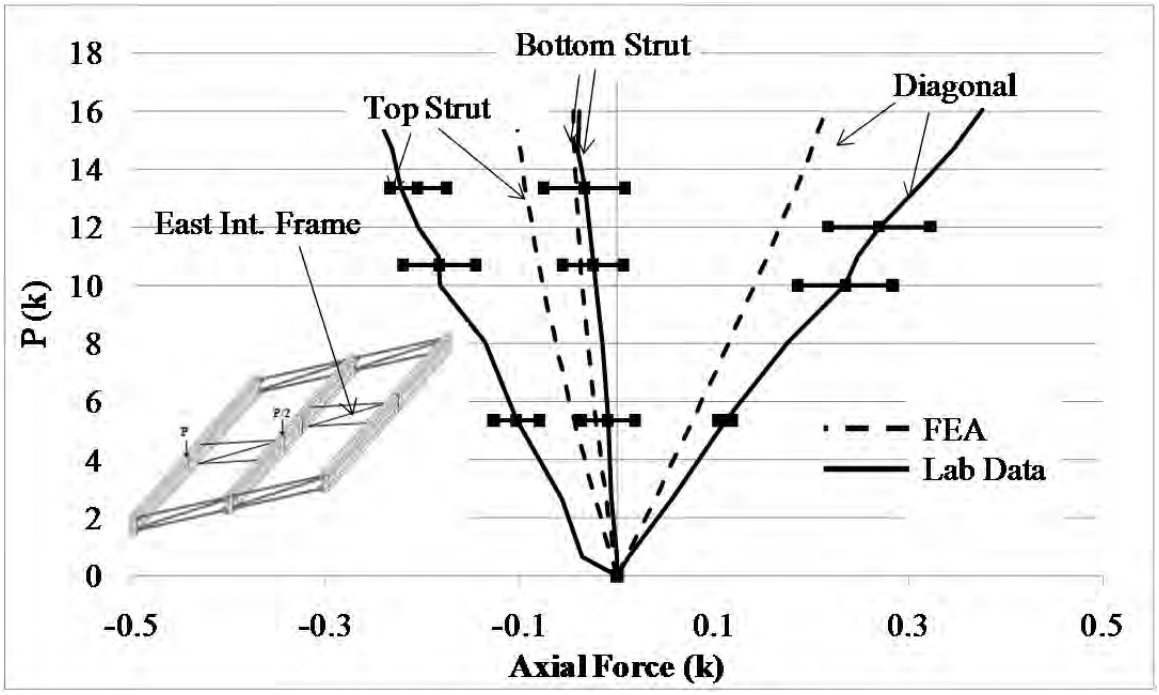

Figure B.110: East intermediate cross frame axial forces

B.4.4 Thrust Washer Bearing with Continuous Intermediate Cross Frames

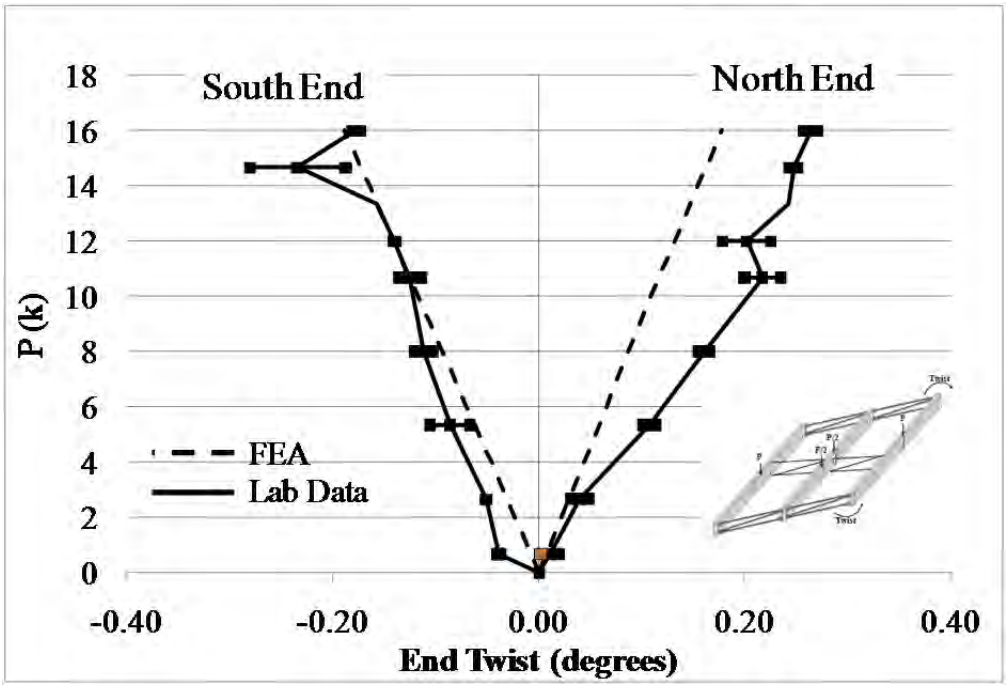

Figure B.111: GBP1 end twists

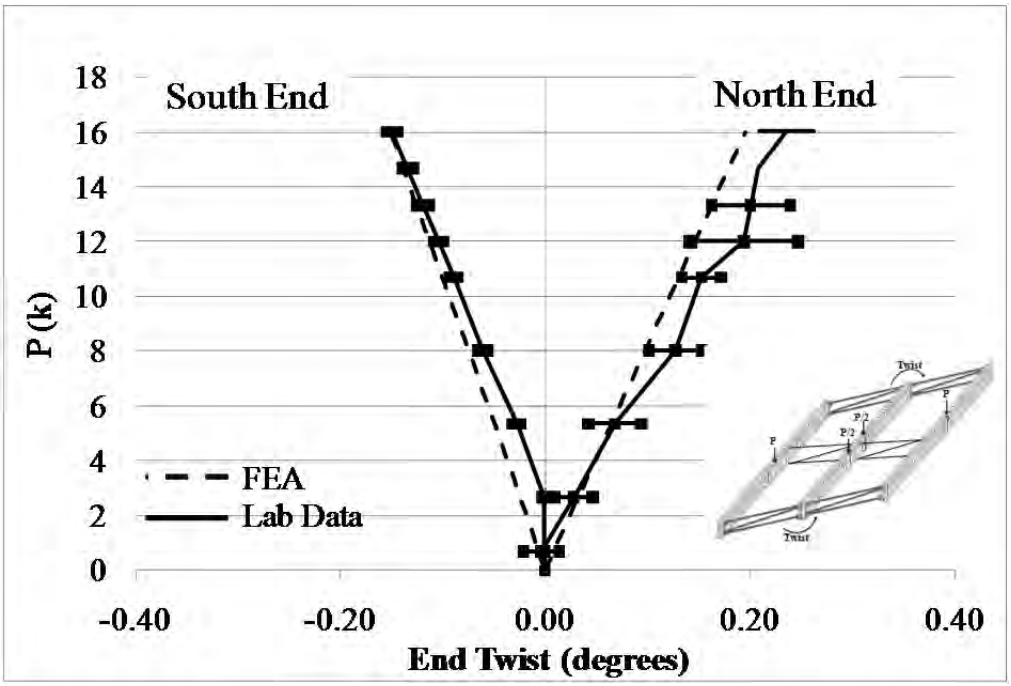

Figure B.112: GBP2 end twists

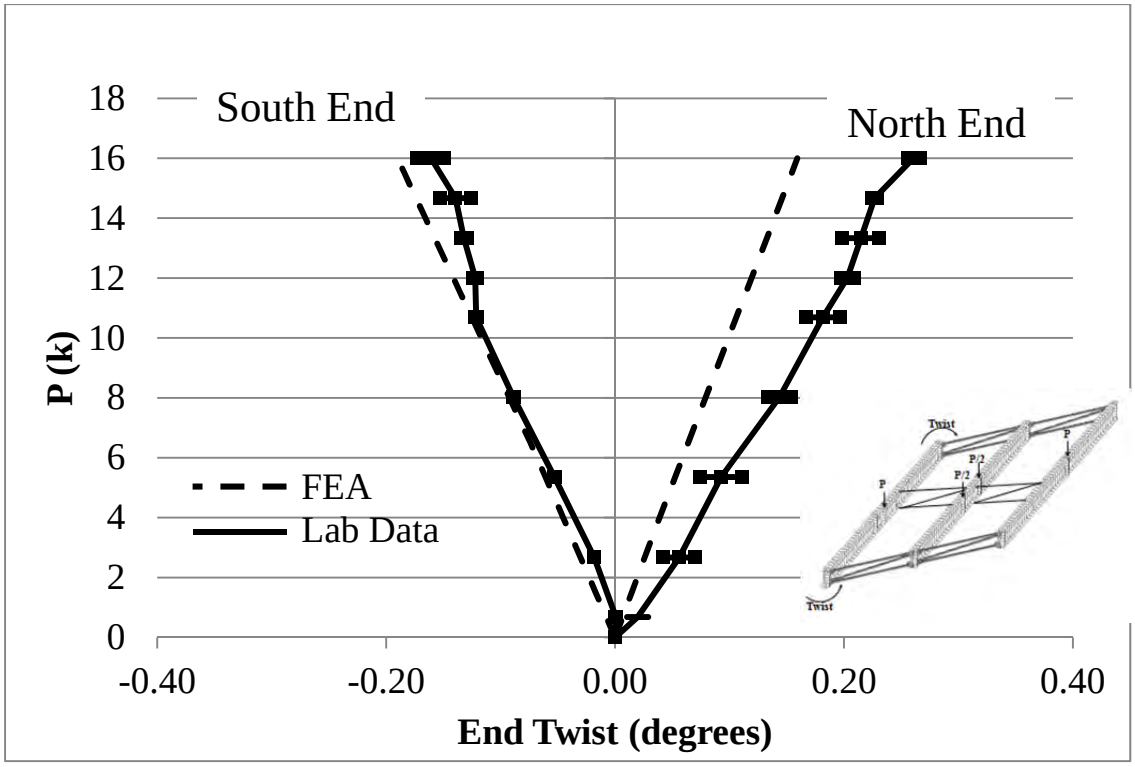

Figure B.113: GBP2 end twists

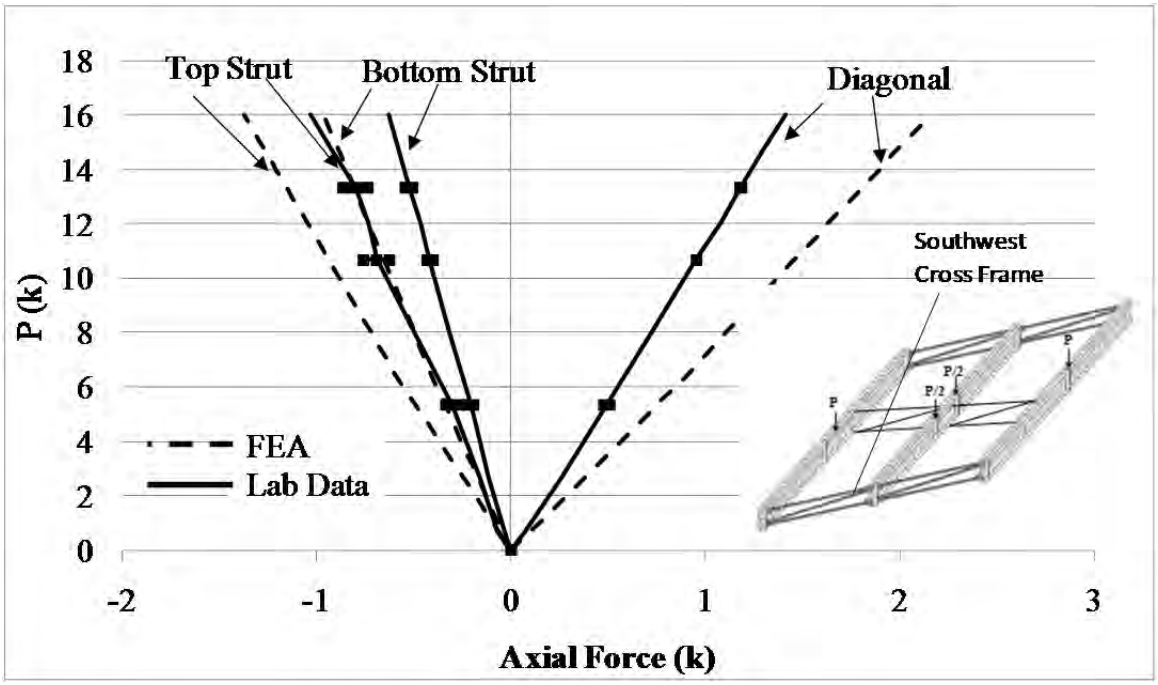

Figure B.114: SW end frame axial forces

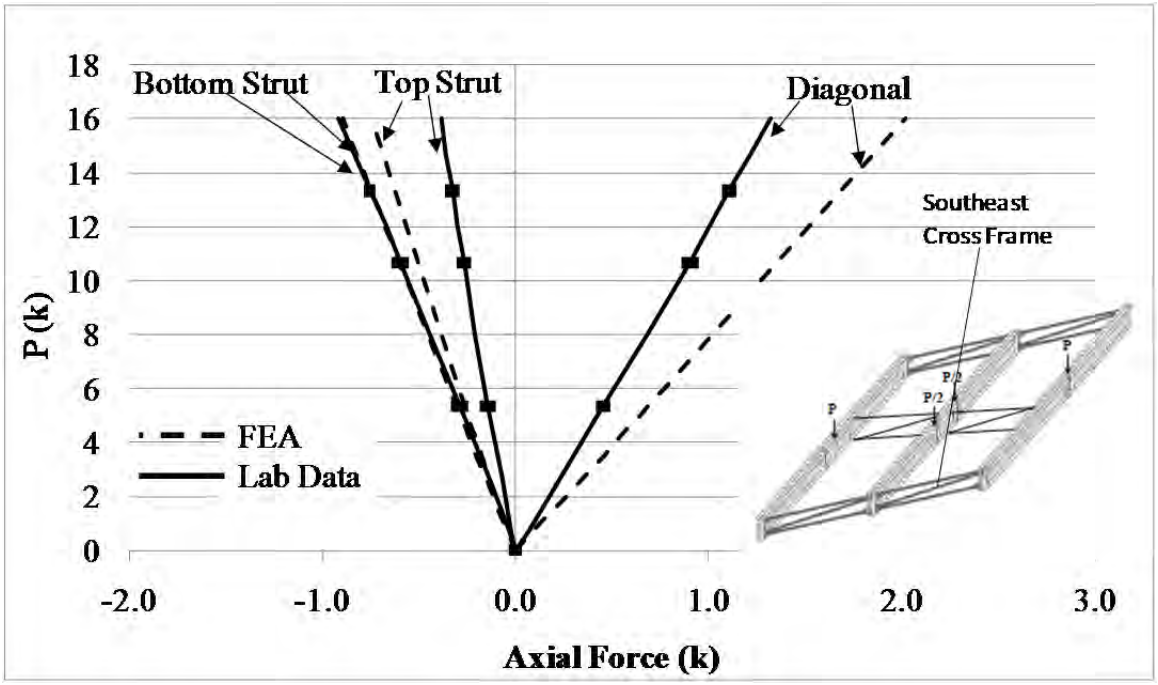

Figure B.115: SE end frame axial forces

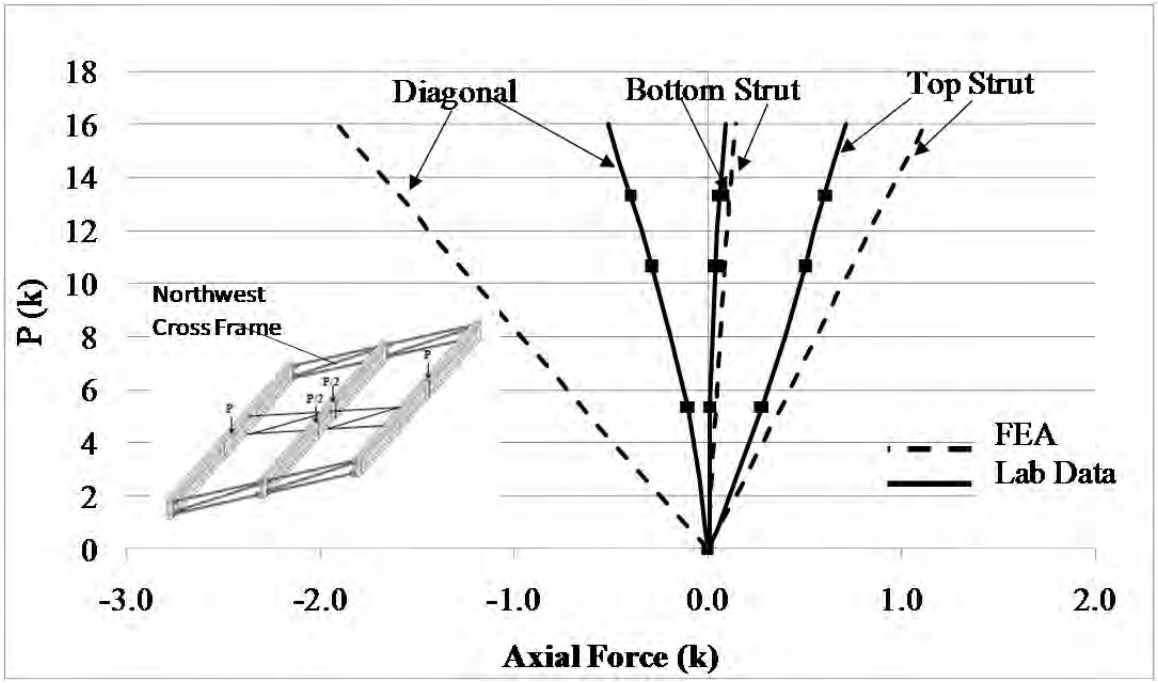

Figure B.116: NW end frame axial forces

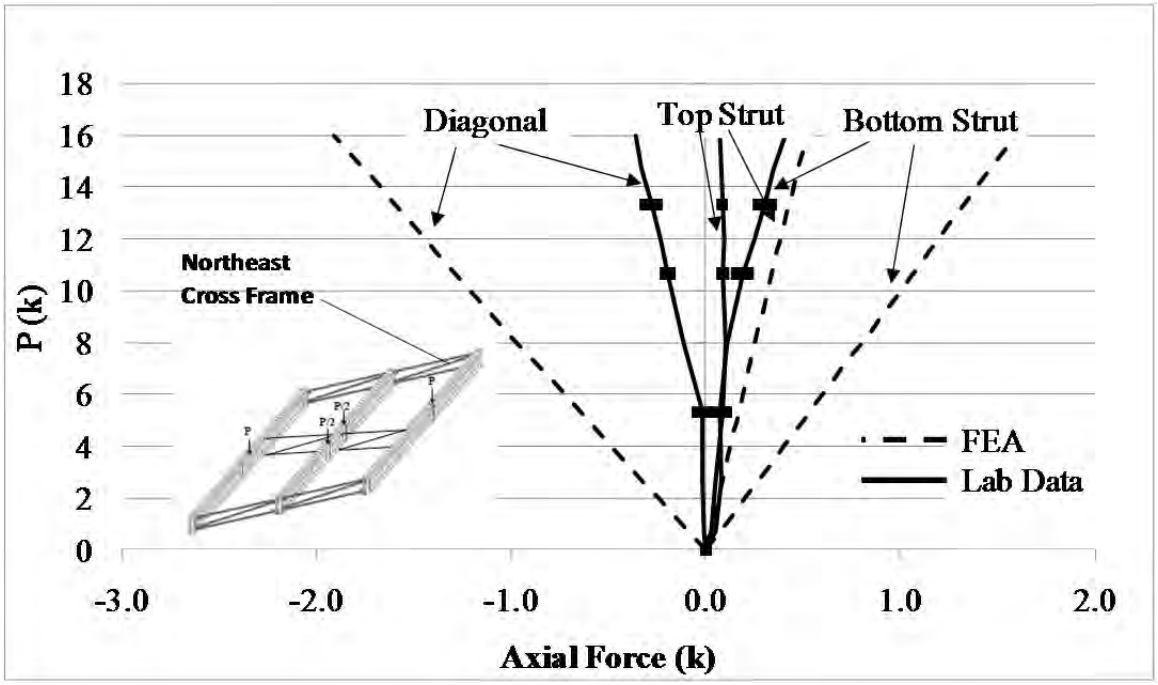

Figure B.117: NW end frame axial forces

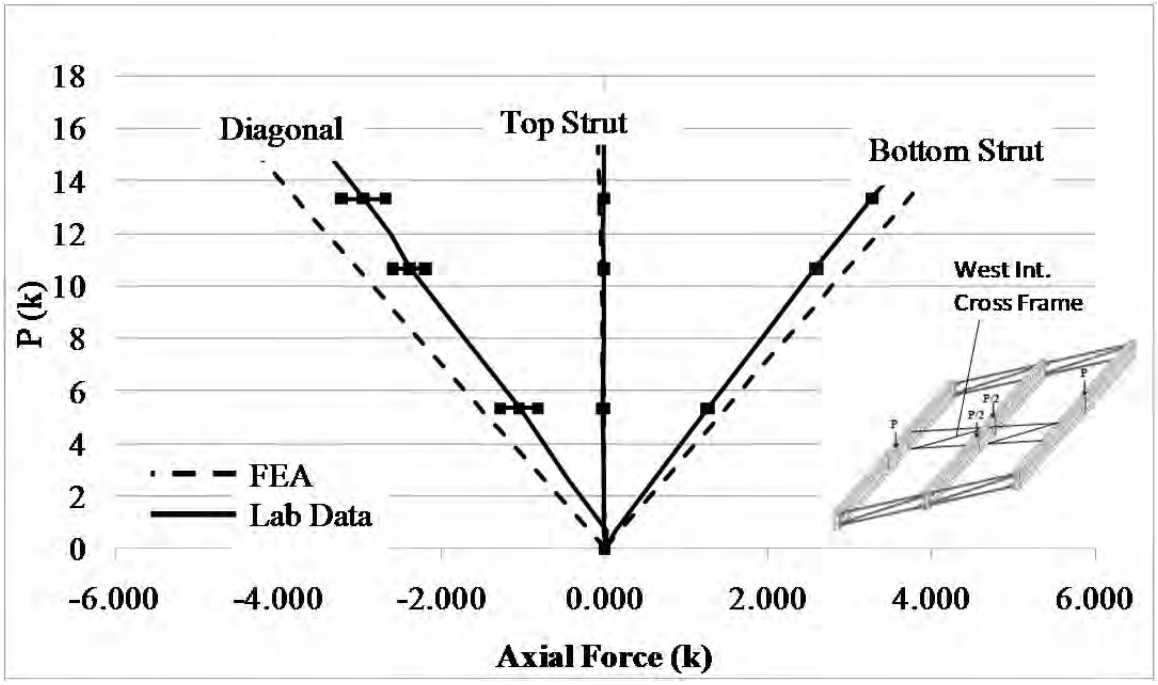

Figure B.118: West intermediate cross frame axial forces

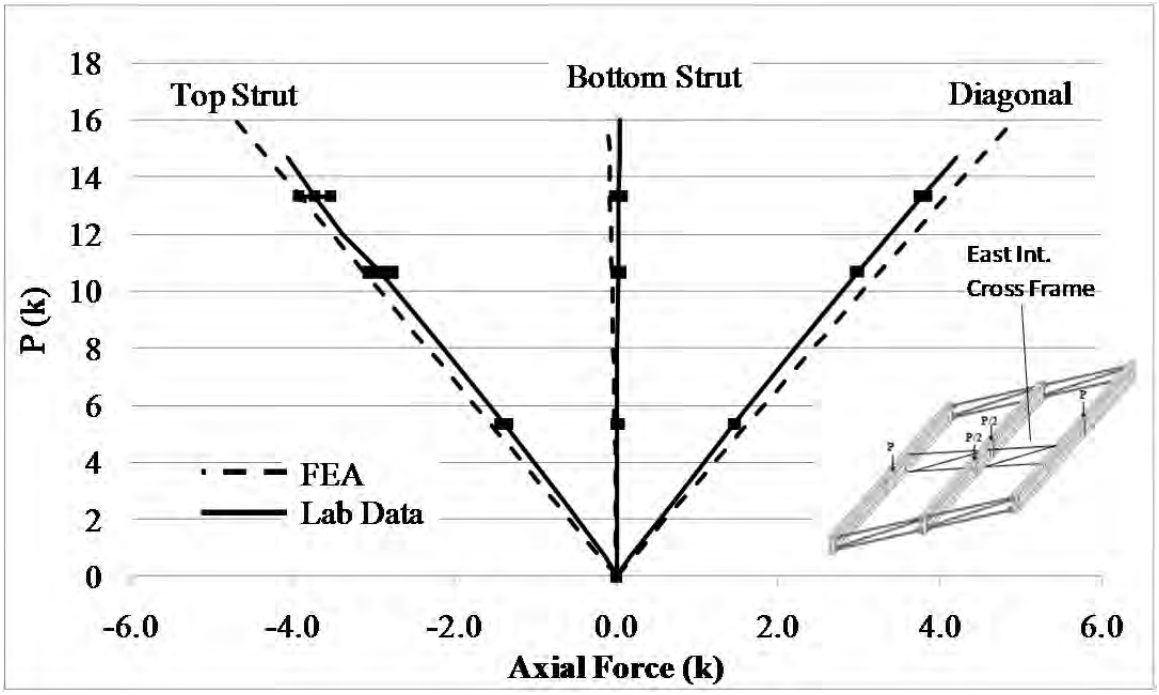

Figure B.119: East intermediate cross frame axial forces

B.4.5 Thrust Washer Bearing with Continuous Intermediate Cross Frames – Partial Loading

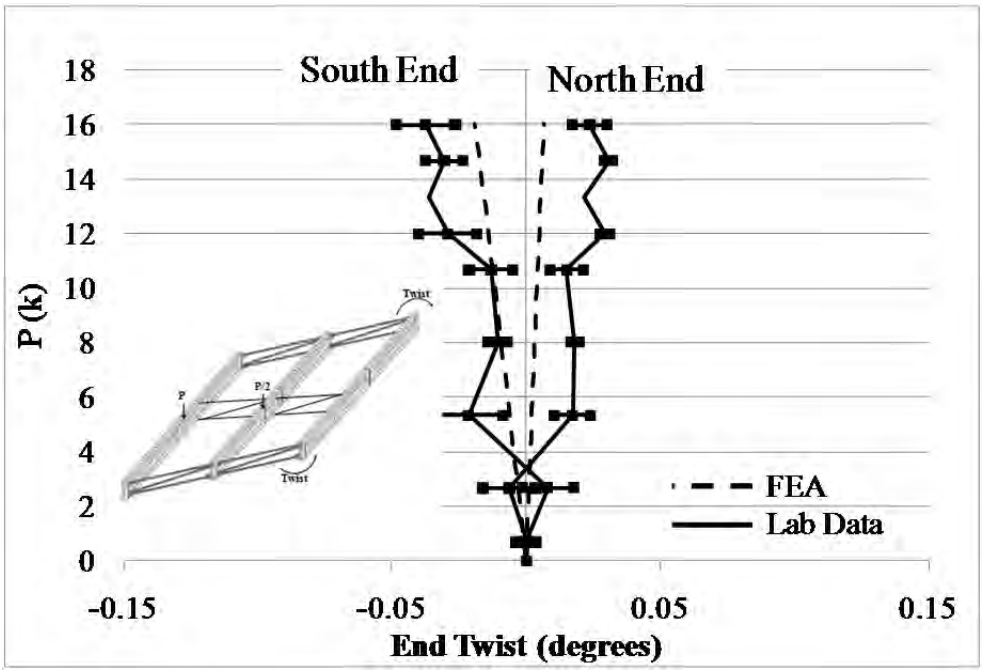

Figure B.120: GBP1 end twists

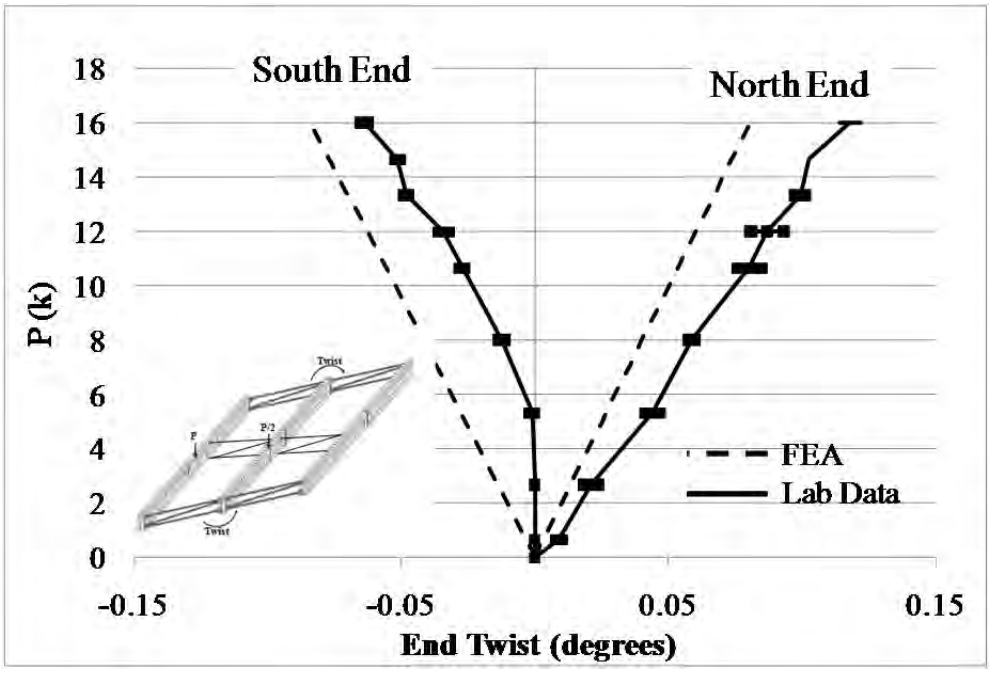

Figure B.121: GBP2 end twists

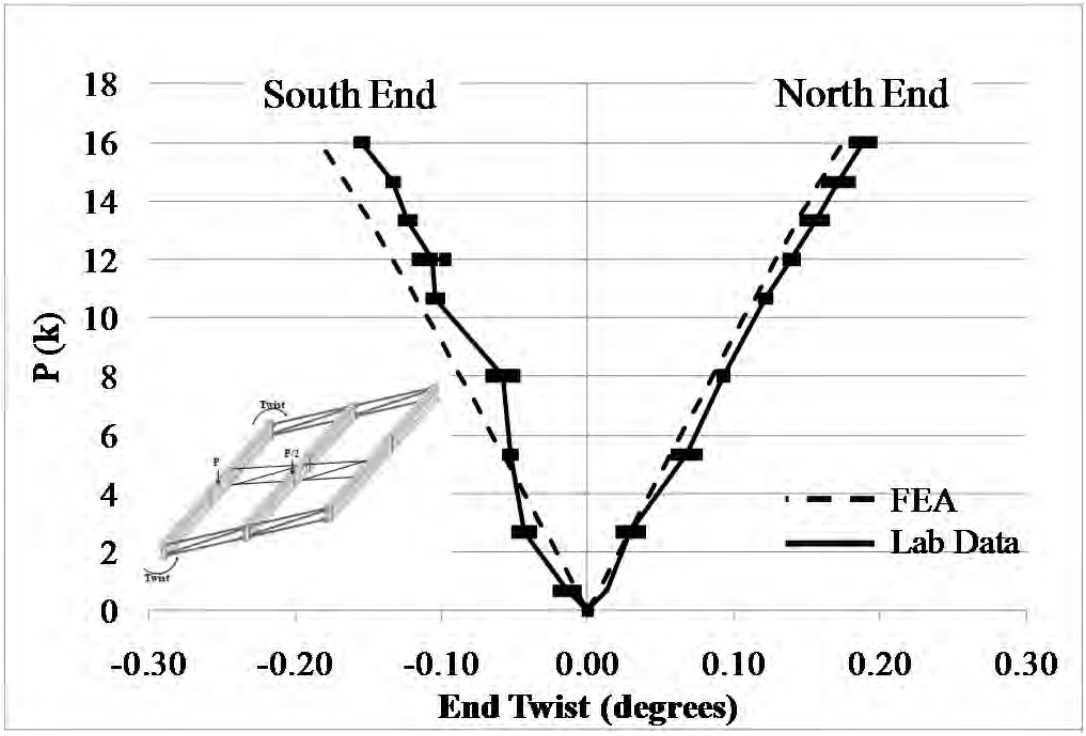

Figure B.122: GBP3 end twists

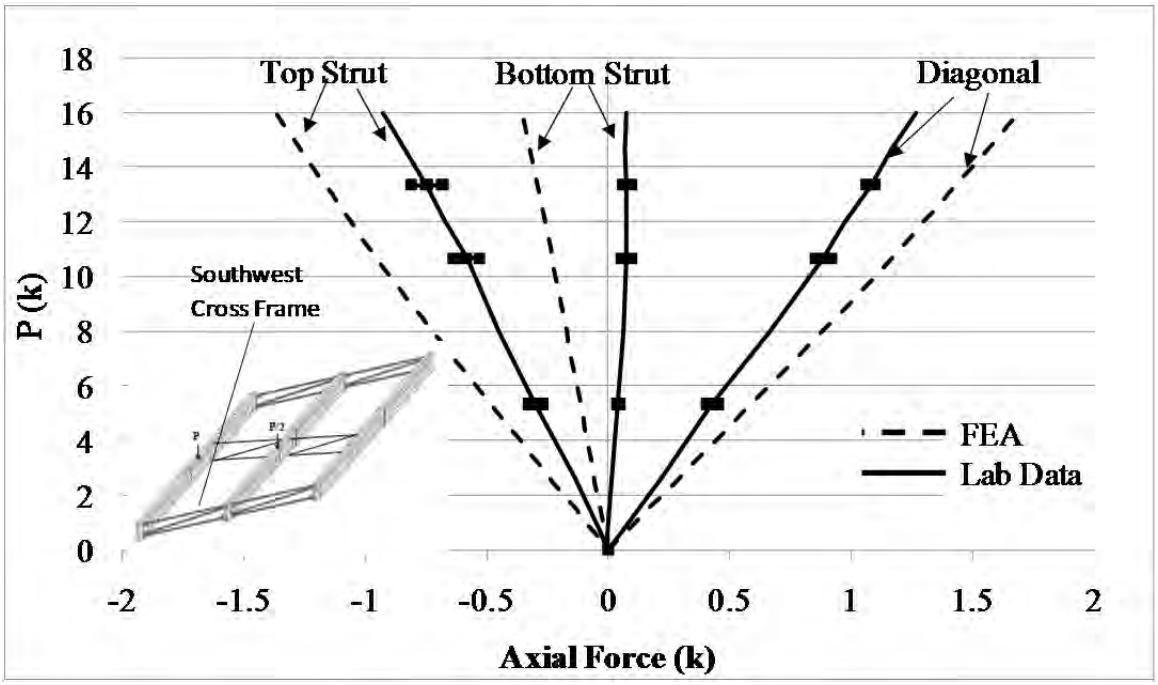

Figure B.123: SW cross frame axial forces

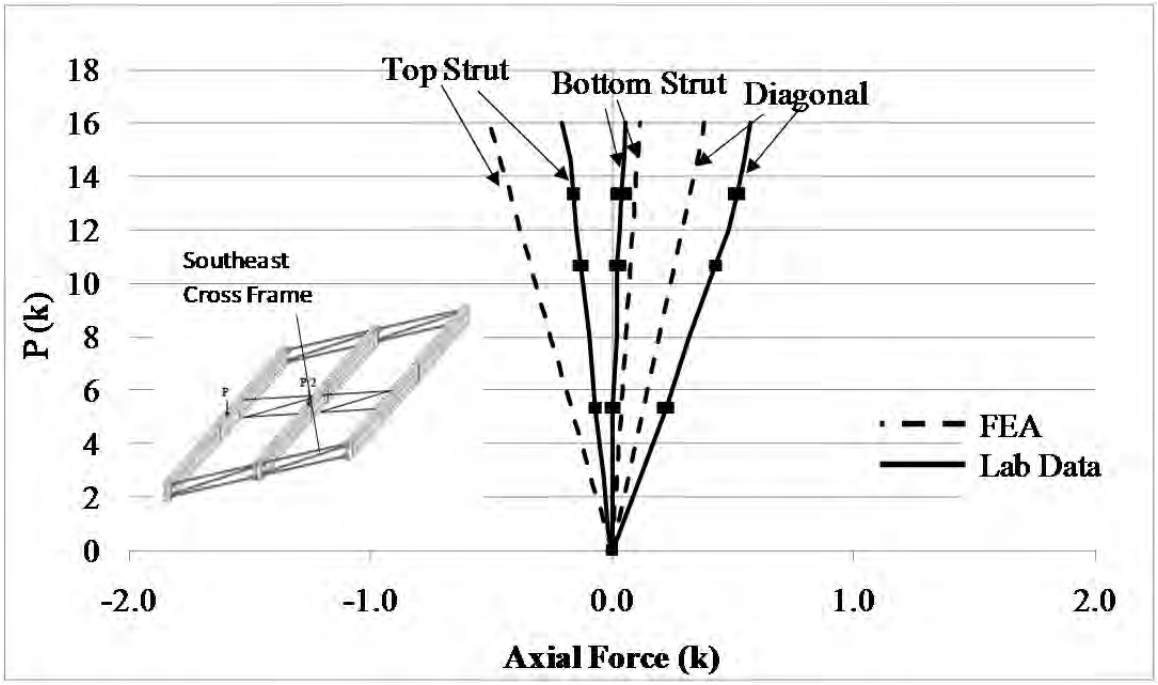

Figure B.124: SE cross frame axial forces

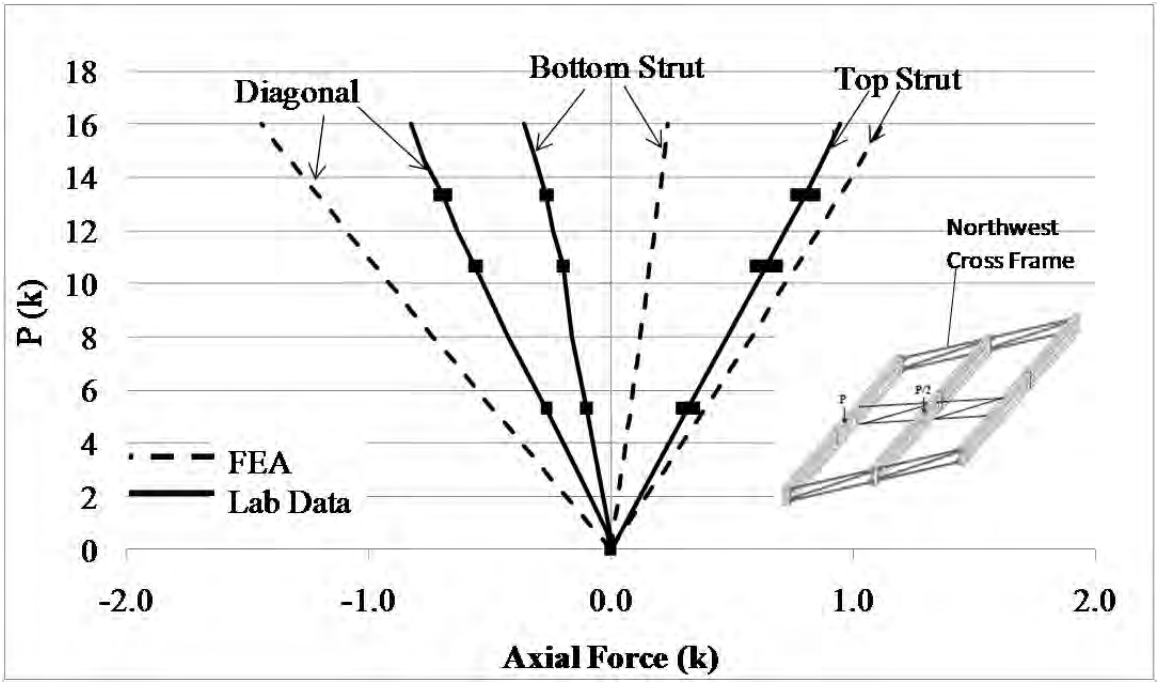

Figure B.125: NW cross frame axial forces

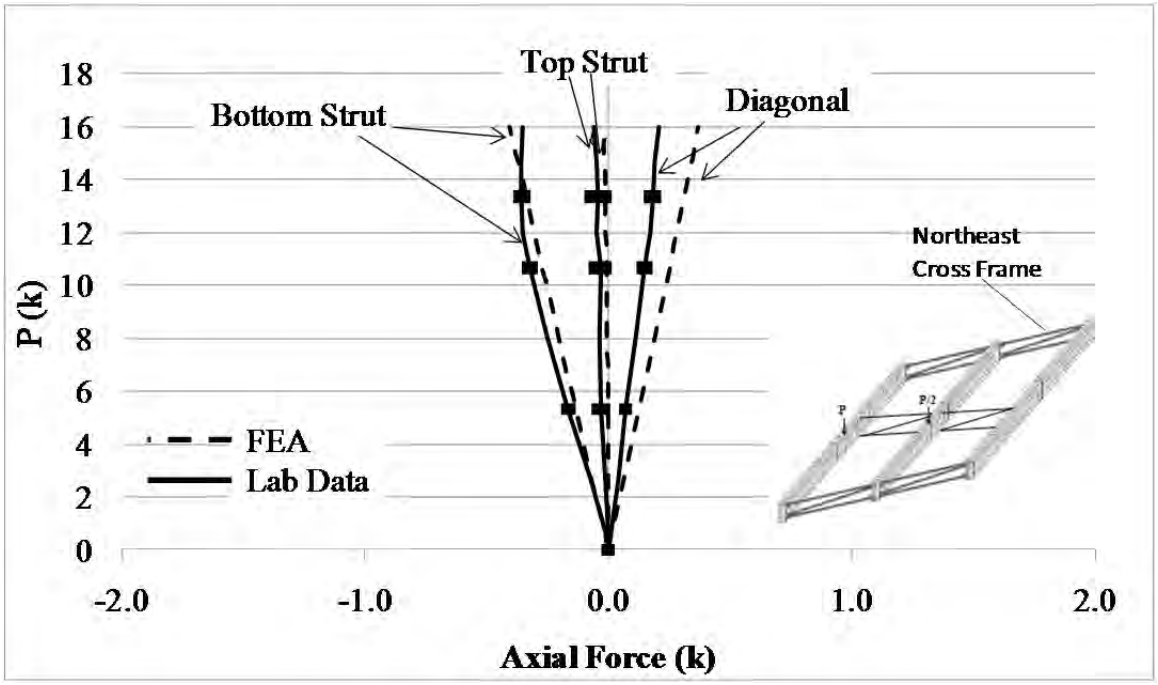

Figure B.126: NE cross frame axial forces

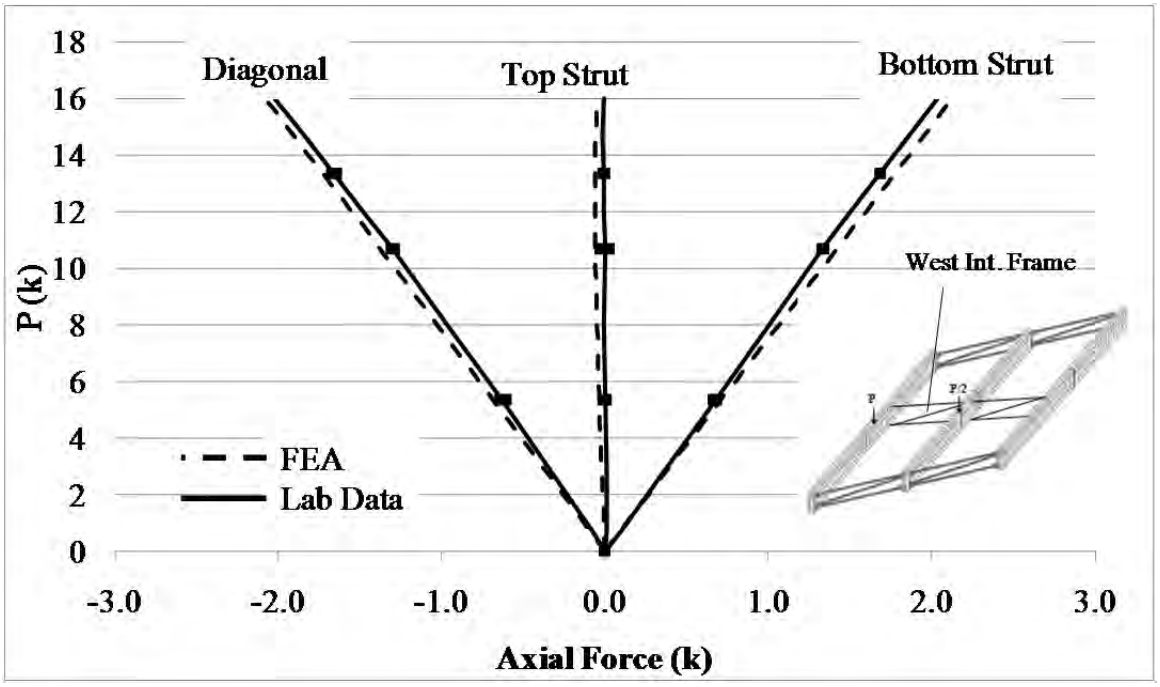

Figure B.127: West intermediate cross frame axial forces

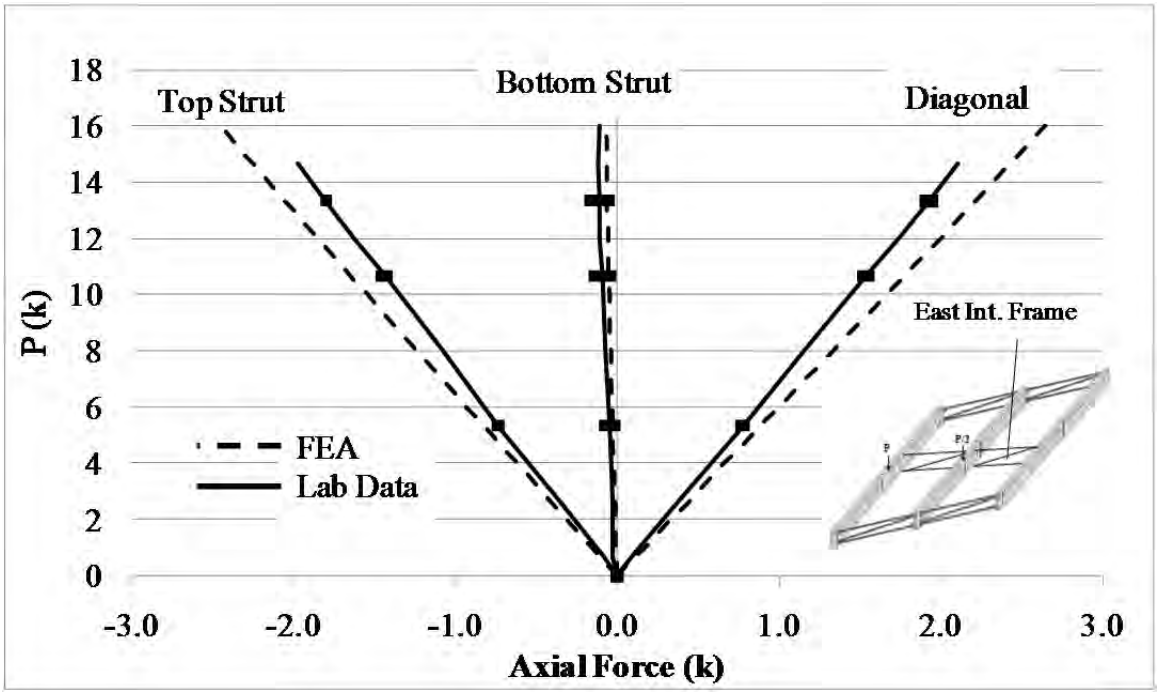

Figure B.128: East intermediate cross frame axial forces

B.4.6 Rubber Bearing with No Intermediate Cross Frames

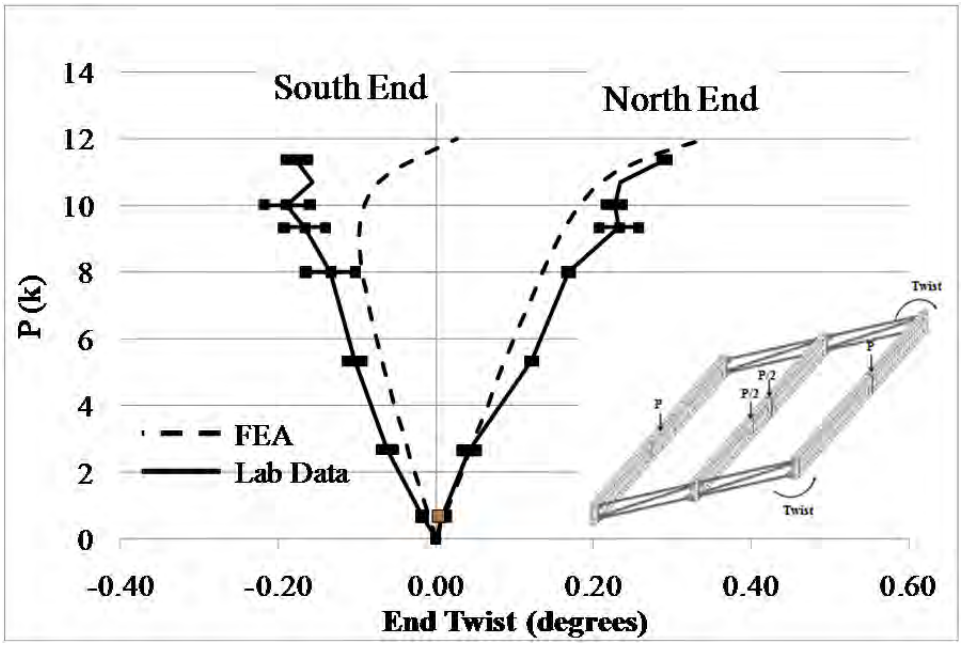

Figure B.129: GBP1 end twists

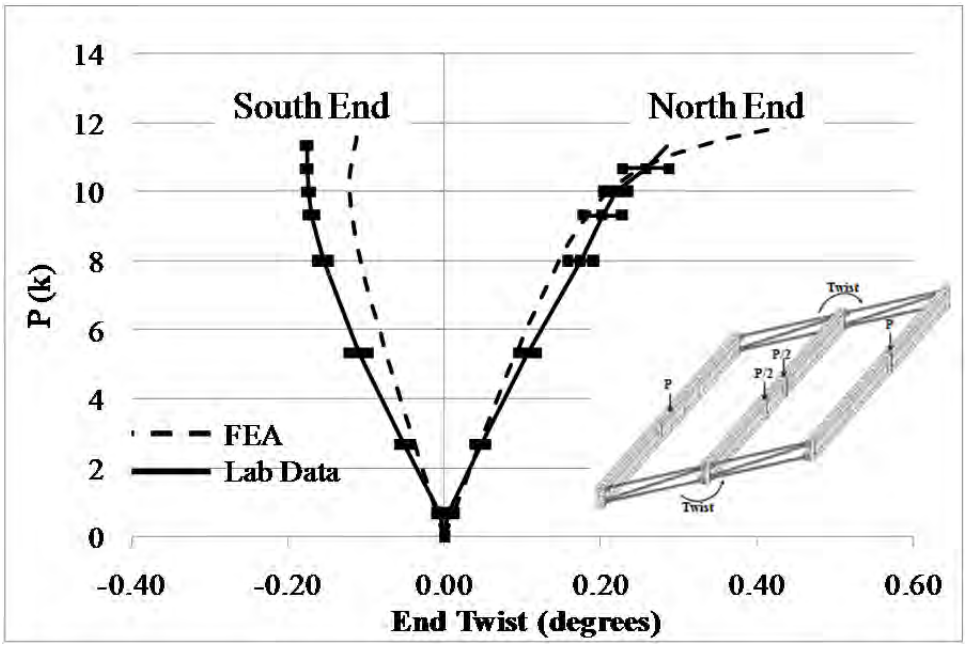

Figure B.130: GBP2 end twists

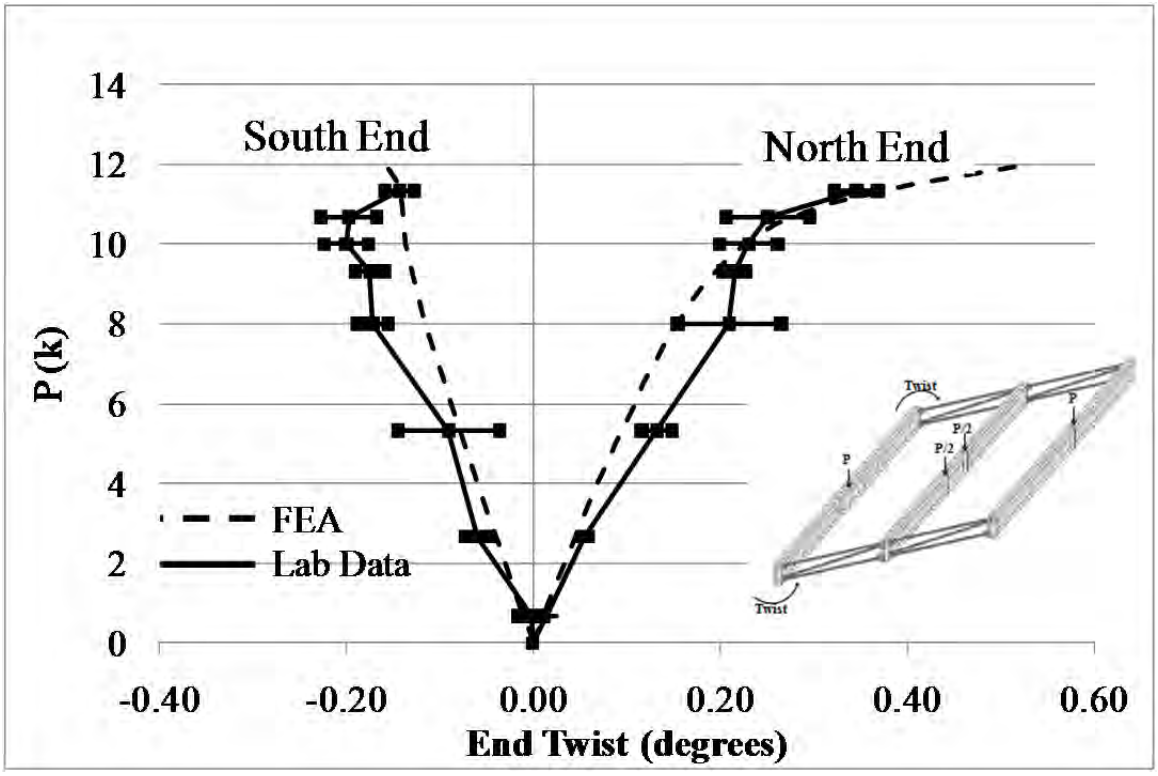

Figure B.131: GBP3 end twists

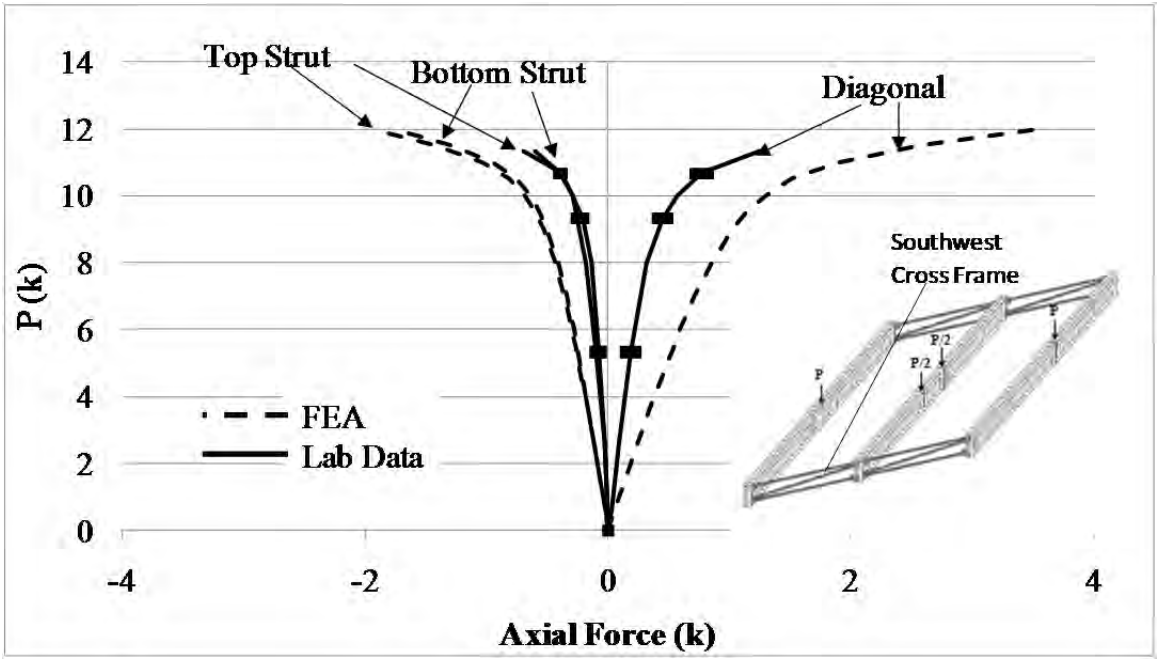

Figure B.132: SW end cross frame axial forces

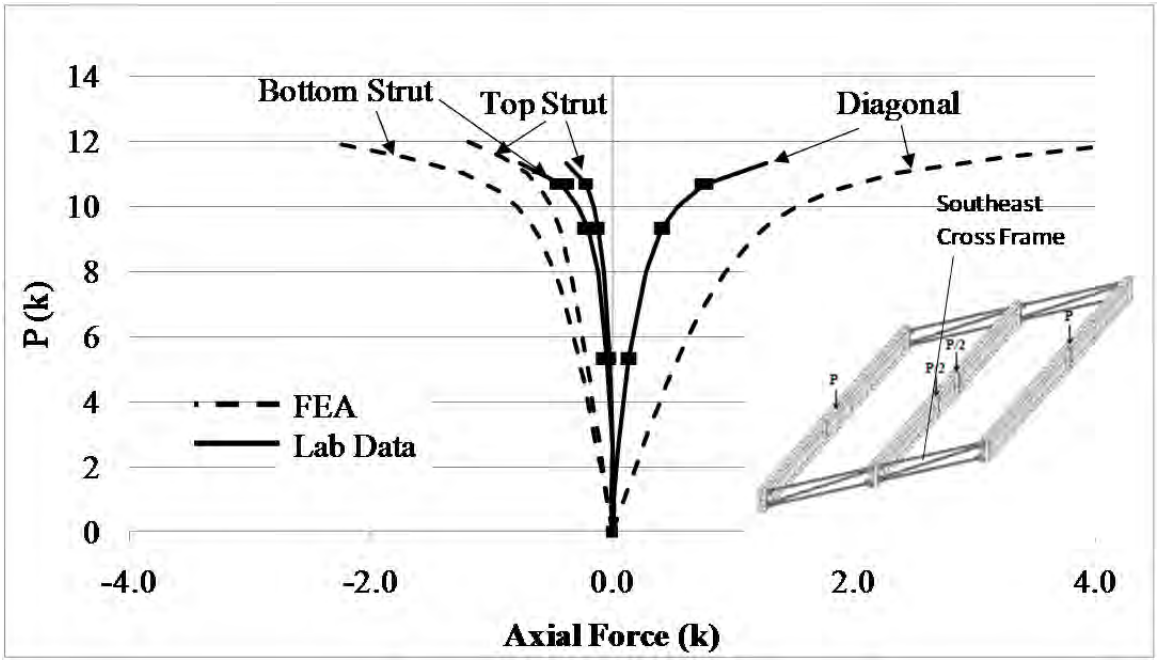

Figure B.133: SE end cross frame axial forces

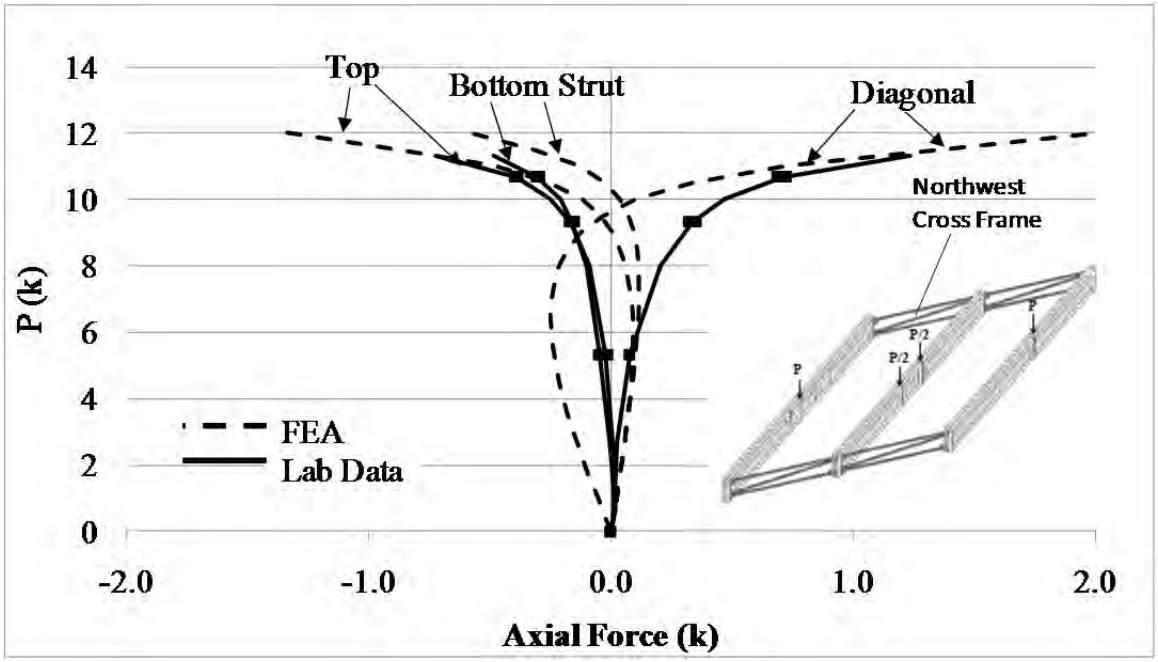

Figure B.134: NW end cross frame axial forces

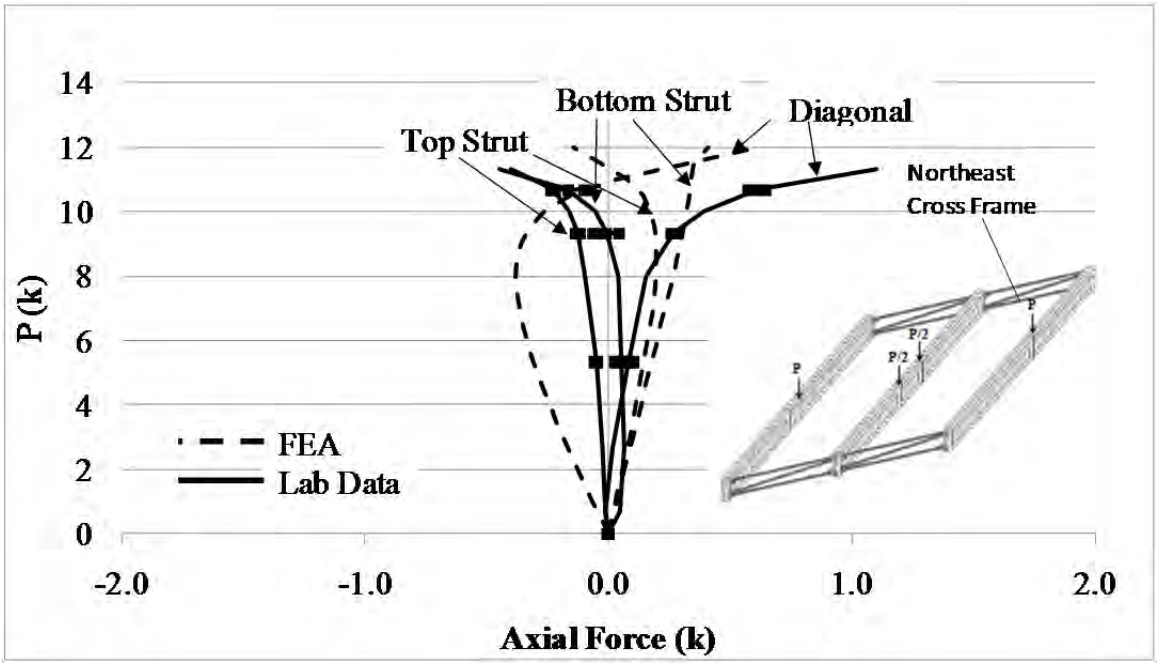

Figure B.135: NE end cross frame axial forces

B.4.7 Rubber Bearing with Shim with No Intermediate Cross Frames

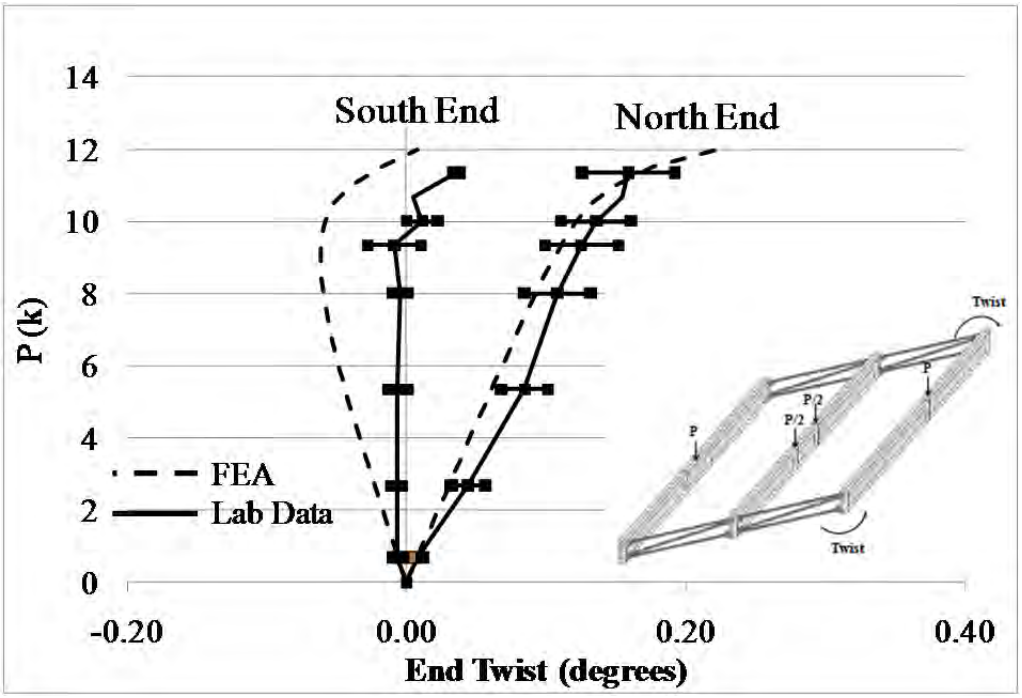

Figure B.136: GBP1 end twists

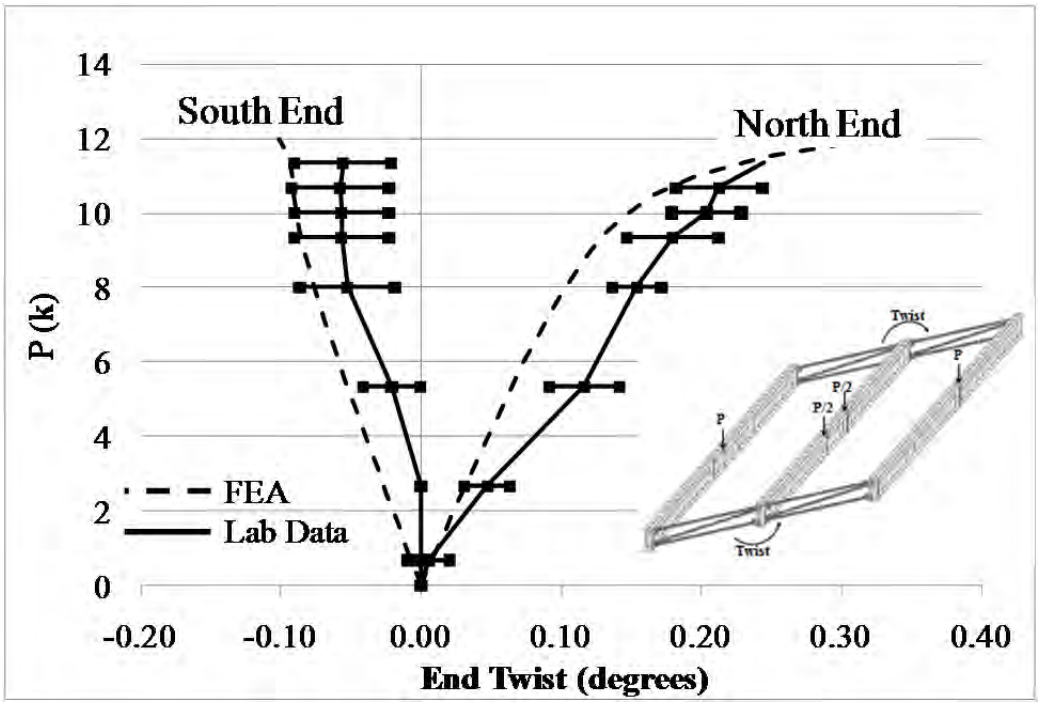

Figure B.137: GBP2 end twists

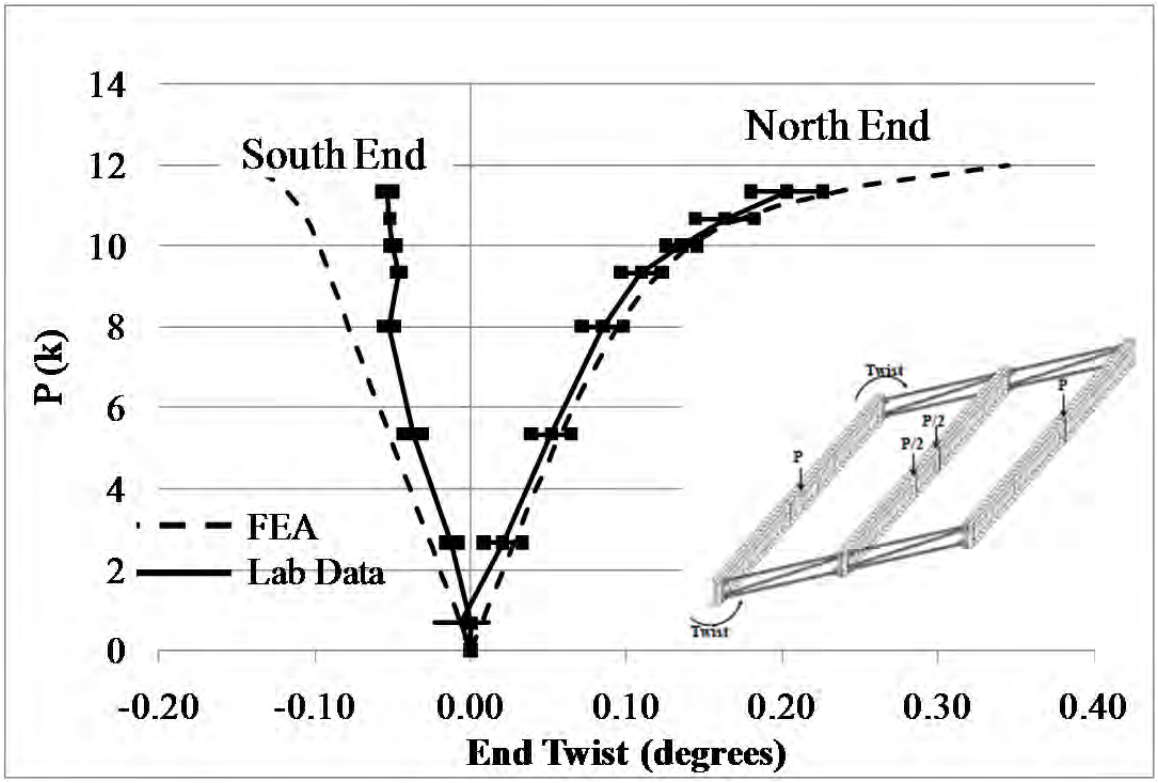

Figure B.138: GBP3 end twists

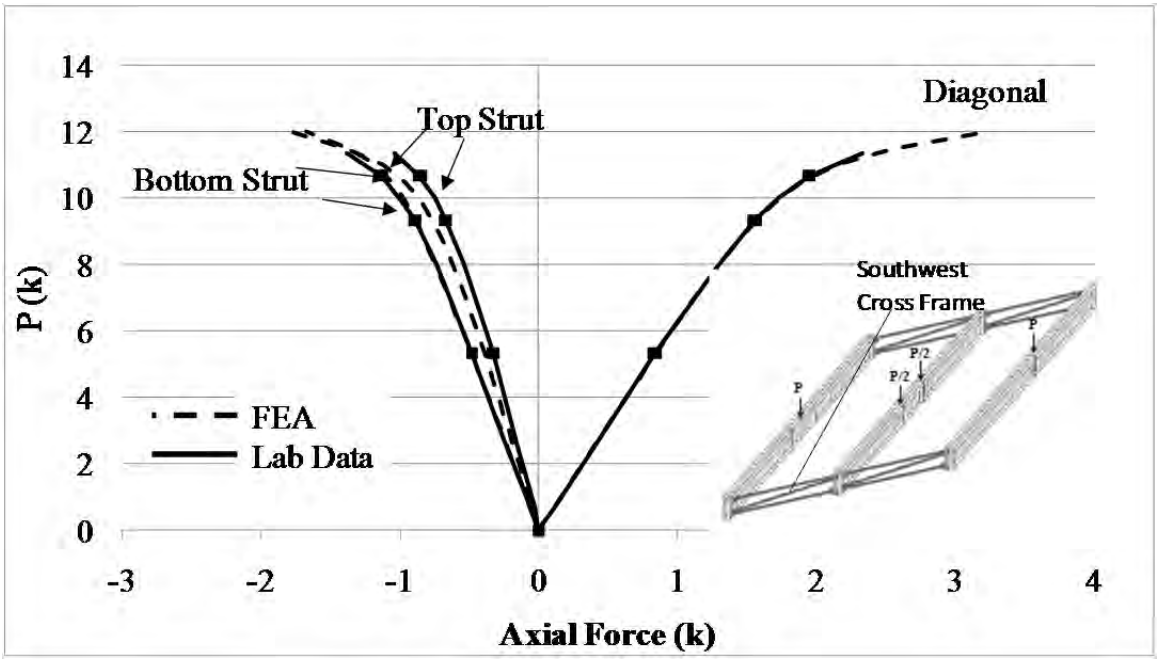

Figure B.139: SW end cross frame axial forces

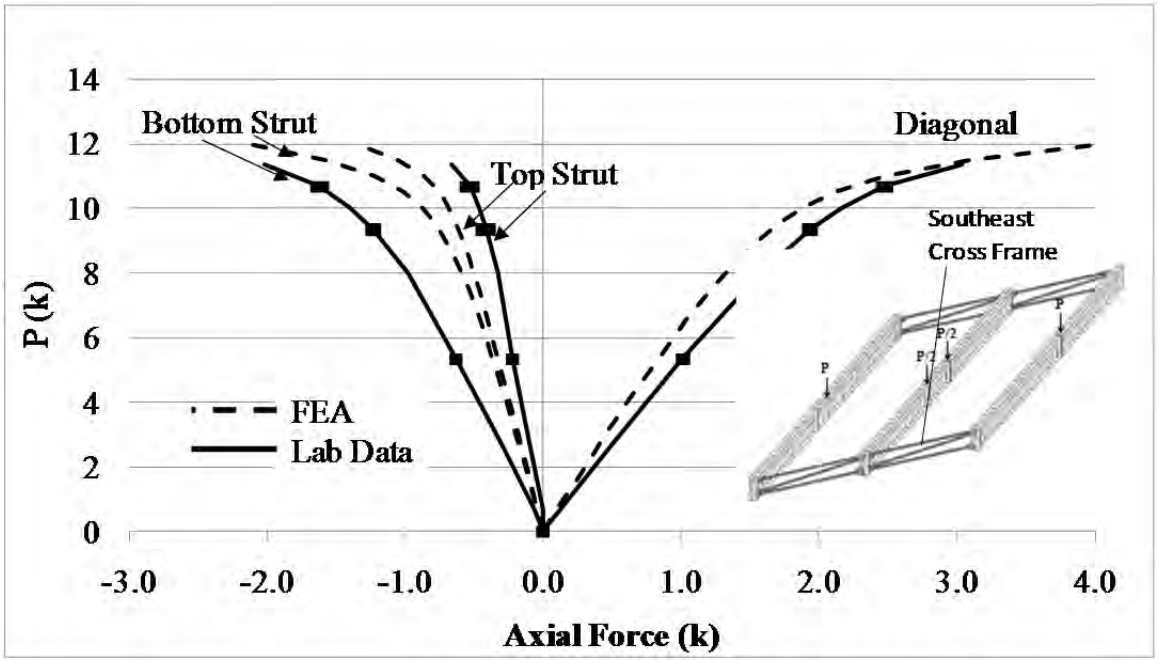

Figure B.140: SE end cross frame axial forces

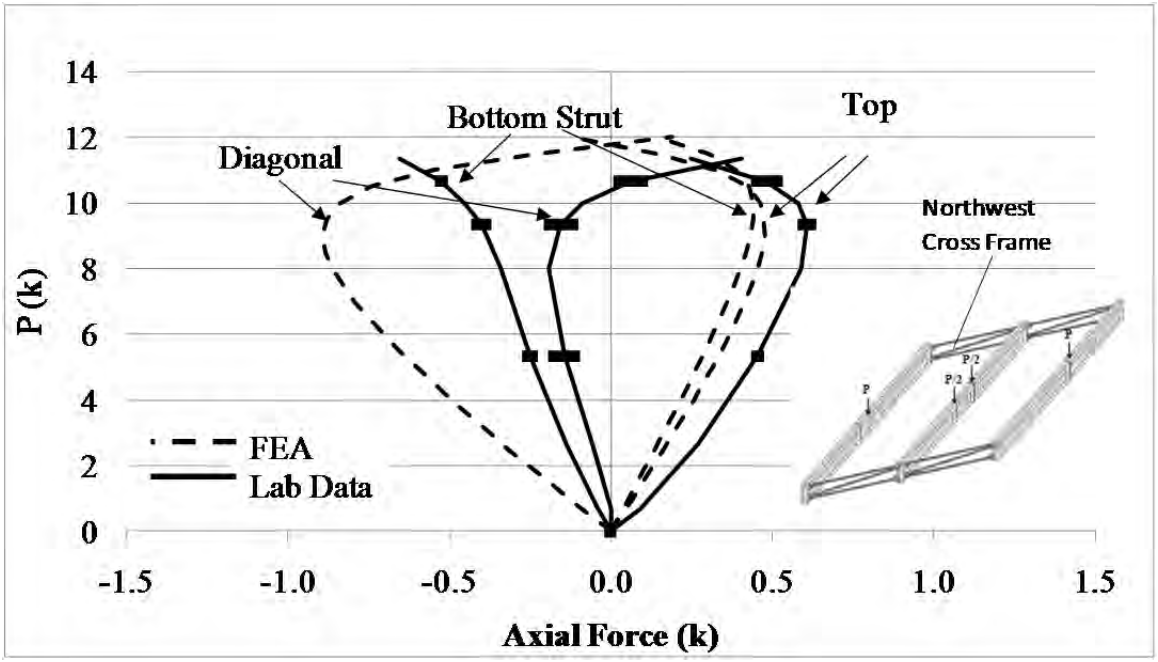

Figure B.141: NW end cross frame axial forces

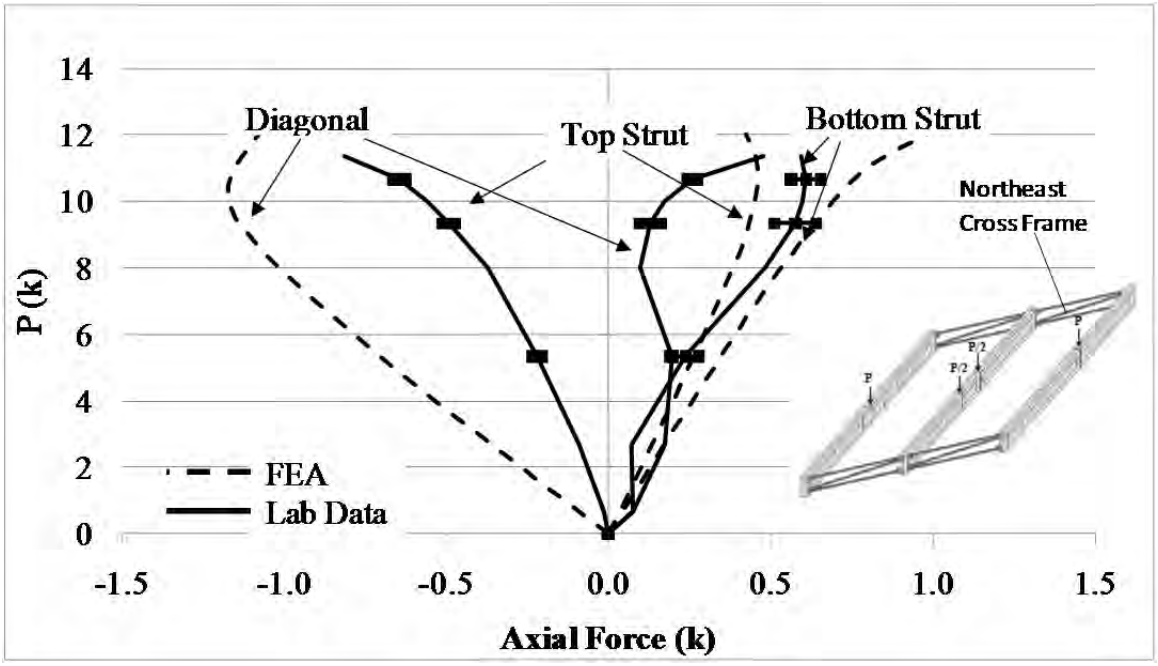

Figure B.142: NE end cross frame axial forces

APPENDIX C: Parametric Study Results

C.1 ANALYTIC TO FEA BENT PLATE CROSS FRAME STIFFNESS COMPARISON

C.1.1 8' Girder Spacing

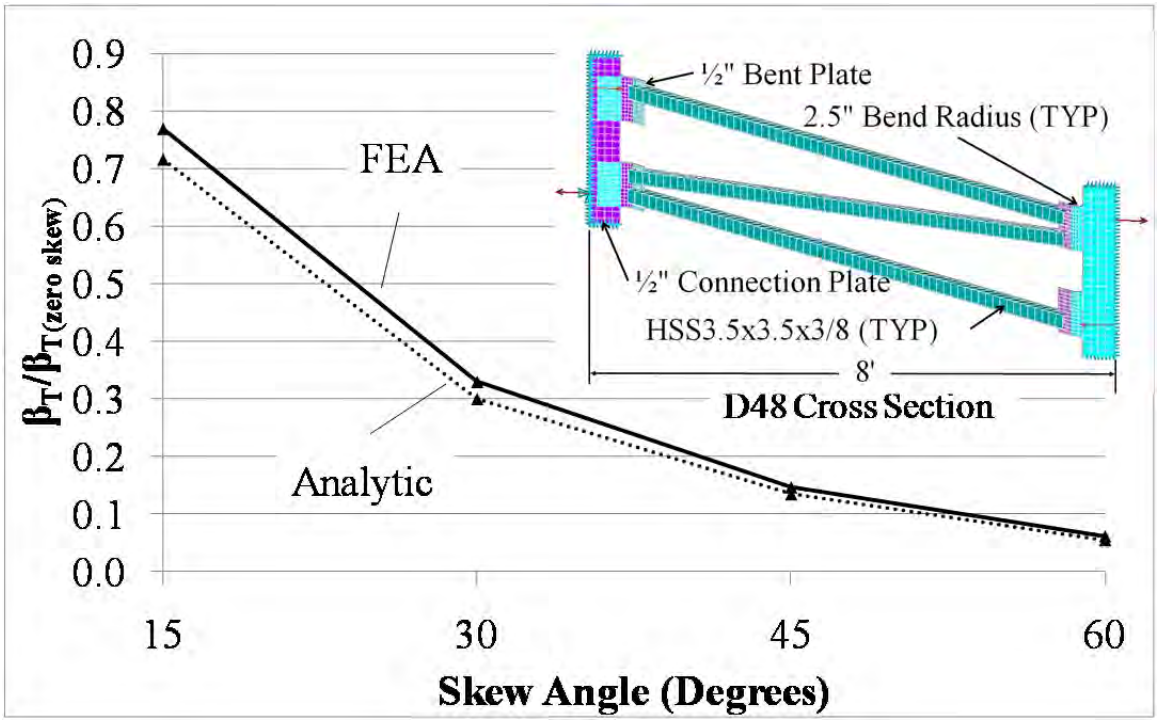

Figure C.1: D48 cross frame analytic to FEA comparison (S = 8')

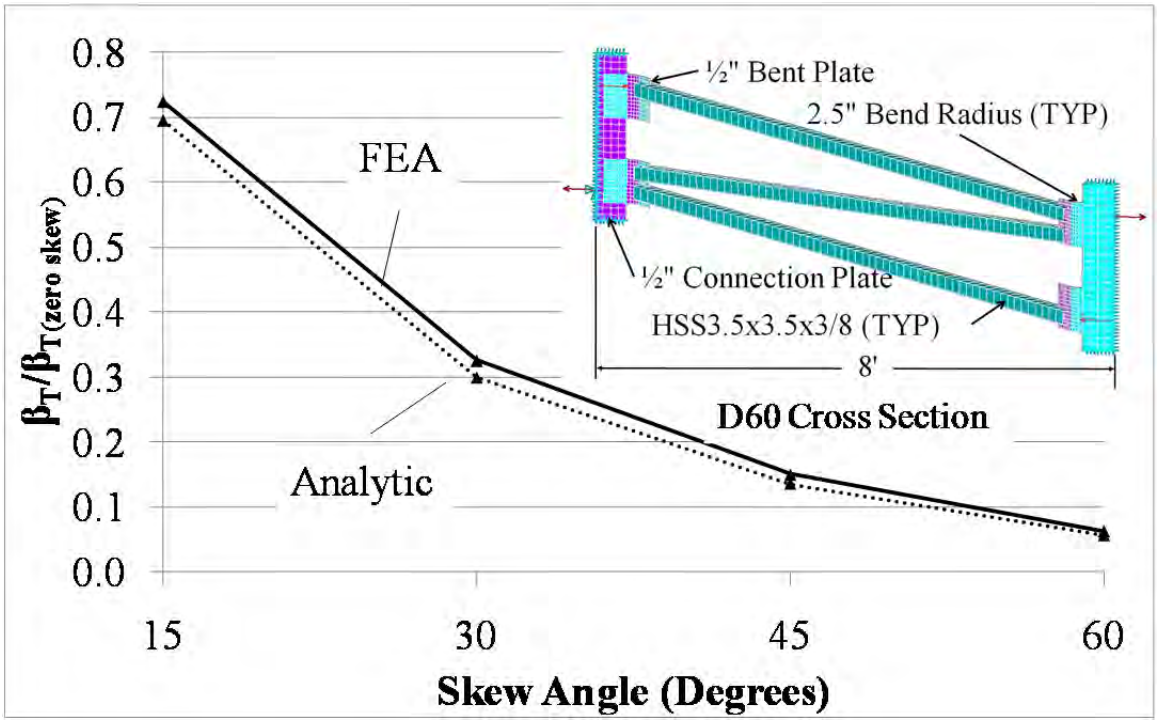

Figure C.2: D60 cross frame analytic to FEA comparison (S = 8')

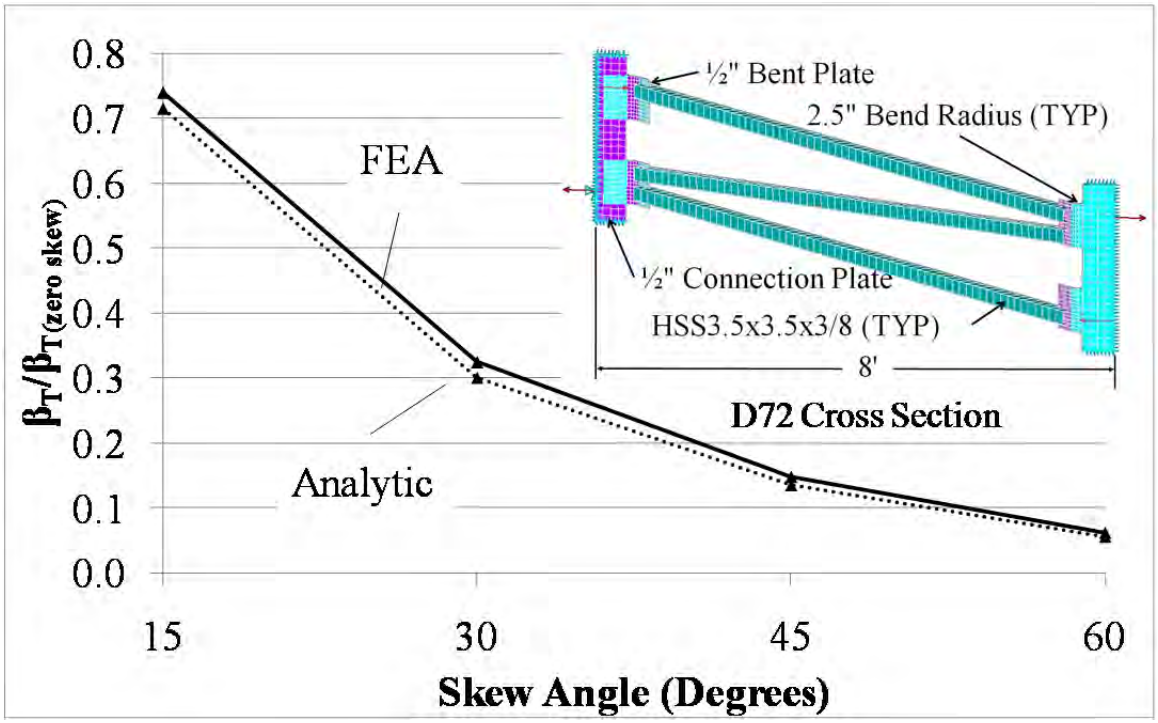

Figure C.3: D72 cross frame analytic to FEA comparison (S = 8')

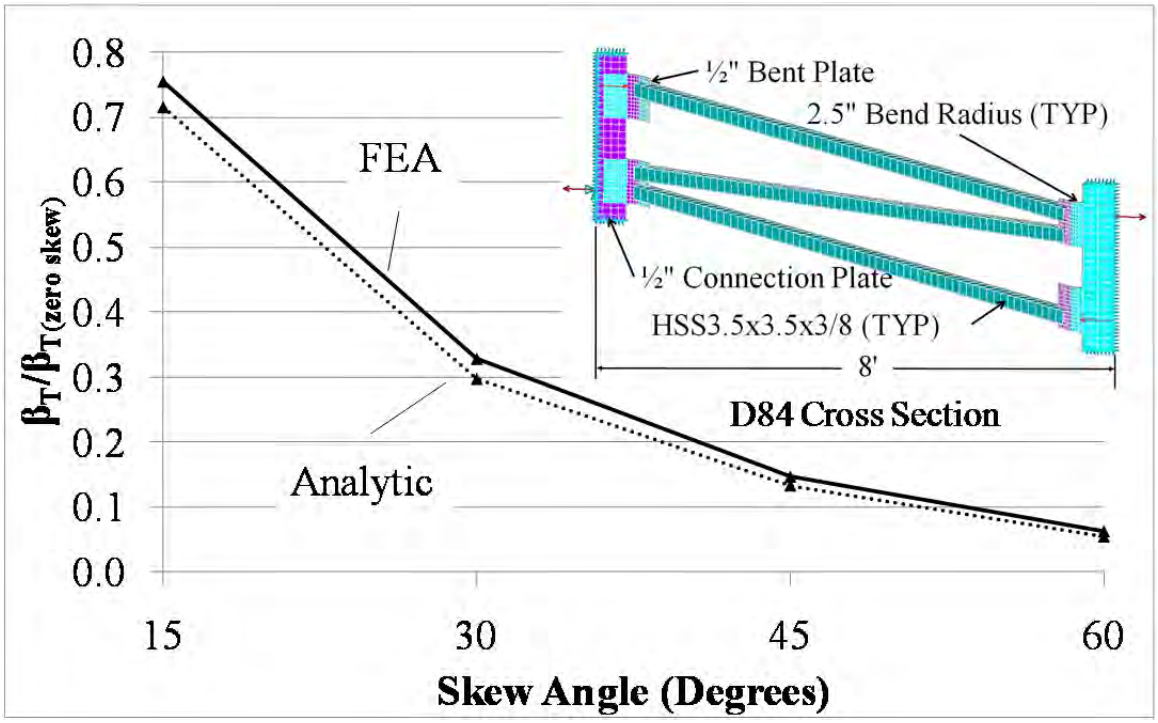

Figure C.4: D84 cross frame analytic to FEA comparison (S = 8')

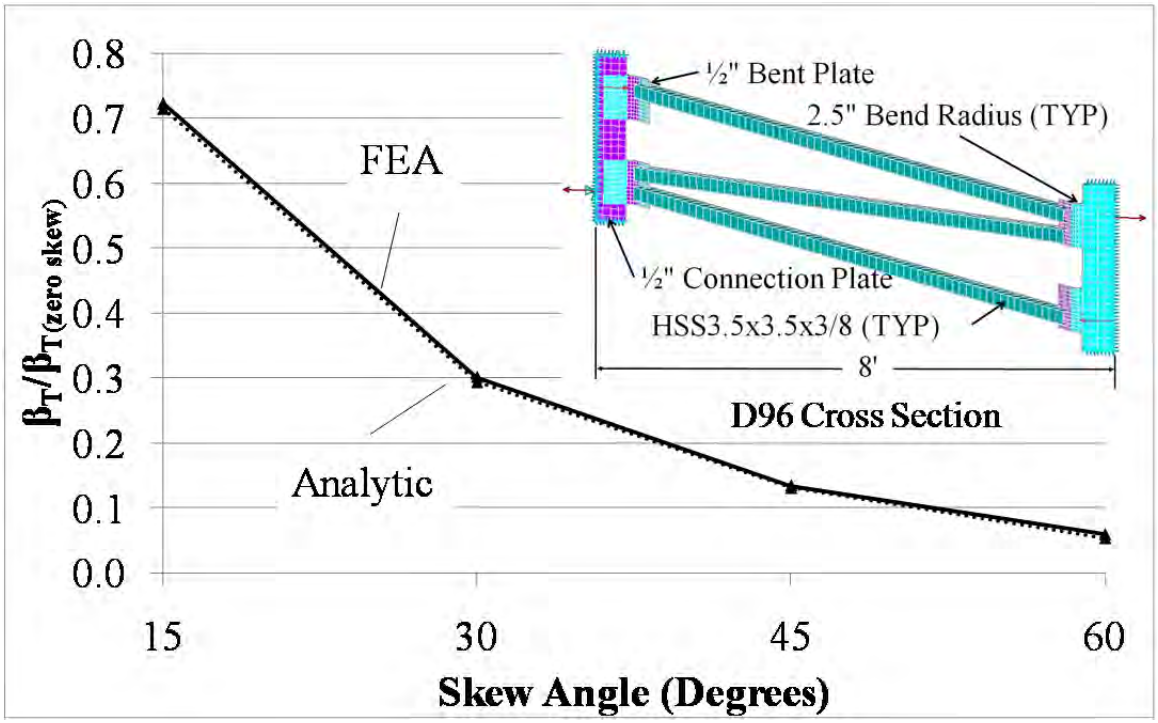

Figure C.5: D96 cross frame analytic to FEA comparison (S = 8')

C.1.2 10' Girder Spacing

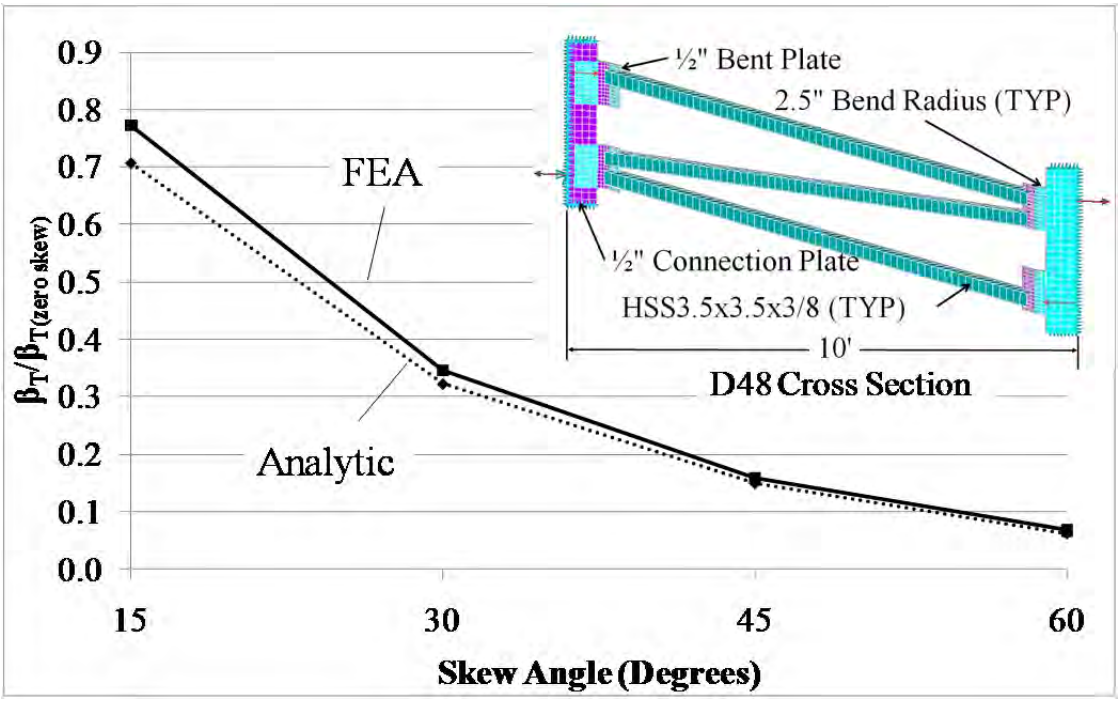

Figure C.6: D48 cross frame analytic to FEA comparison (S = 10')

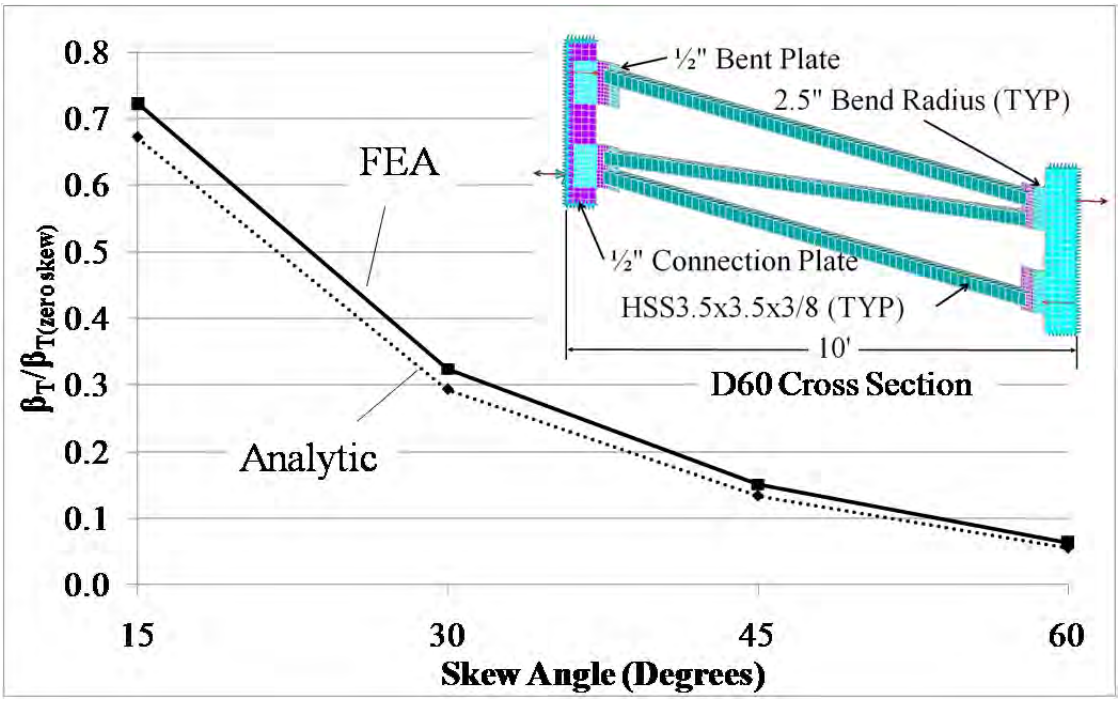

Figure C.7: D60 cross frame analytic to FEA comparison (S = 10')

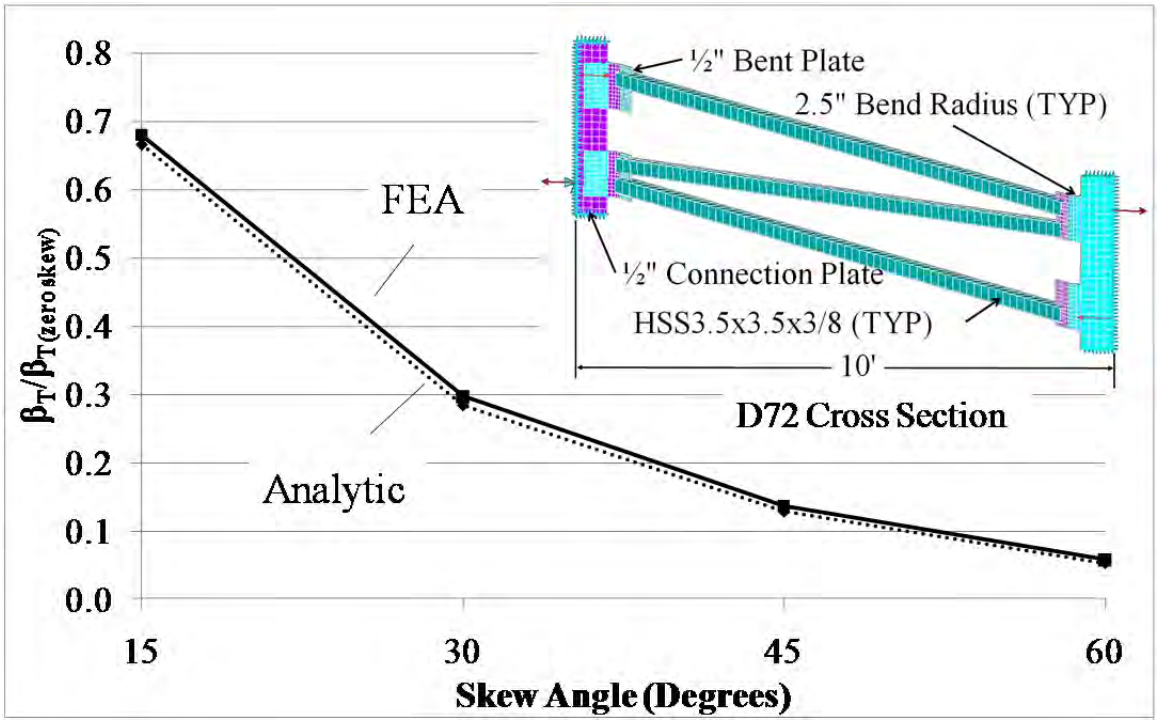

Figure C.8: D72 cross frame analytic to FEA comparison (S = 10')

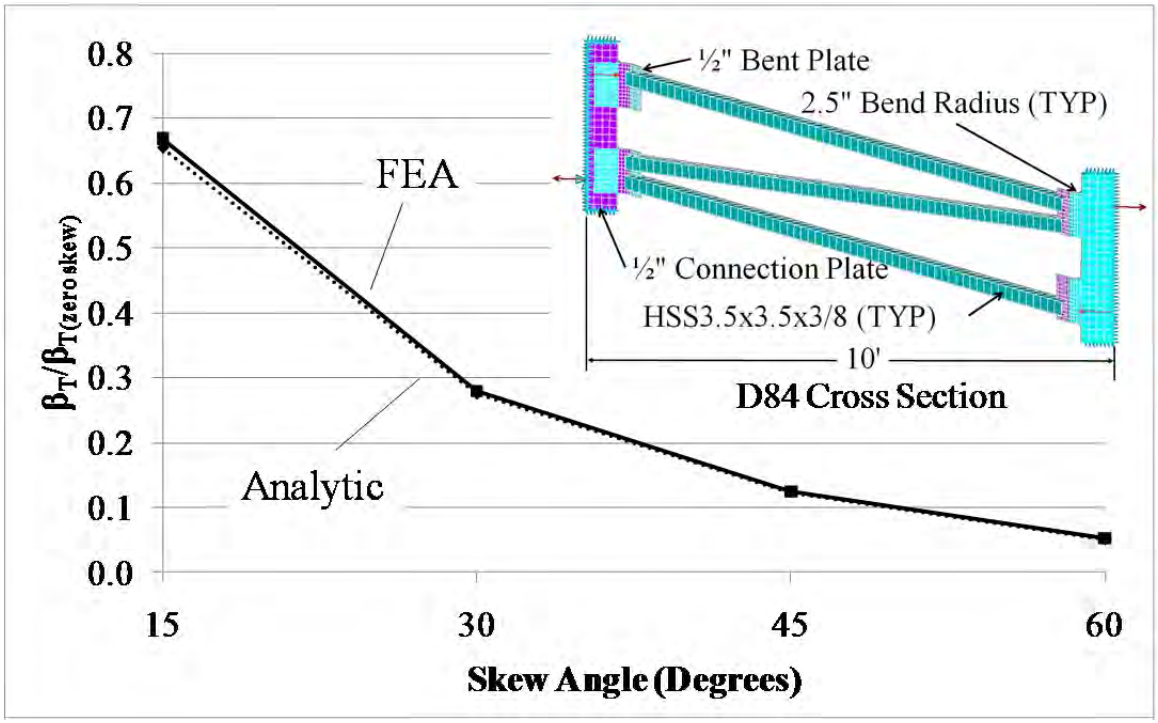

Figure C.9: D84 cross frame analytic to FEA comparison (S = 10')

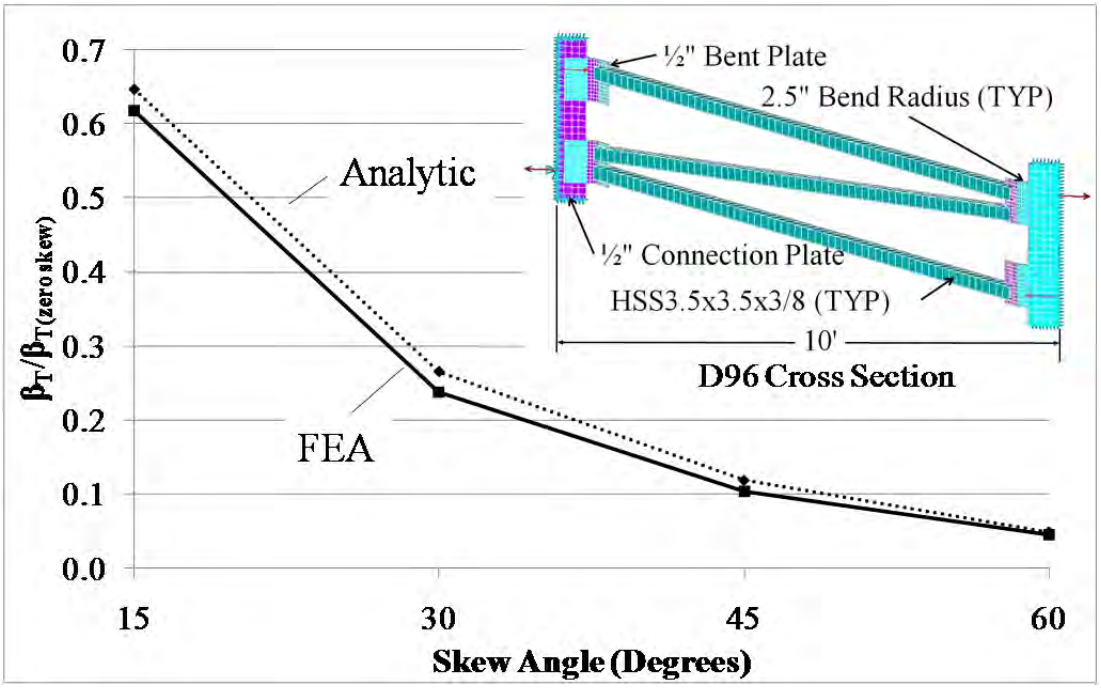

Figure C.10: D96 cross frame analytic to FEA comparison (S = 10')

C.1.3 6' Girder Spacing

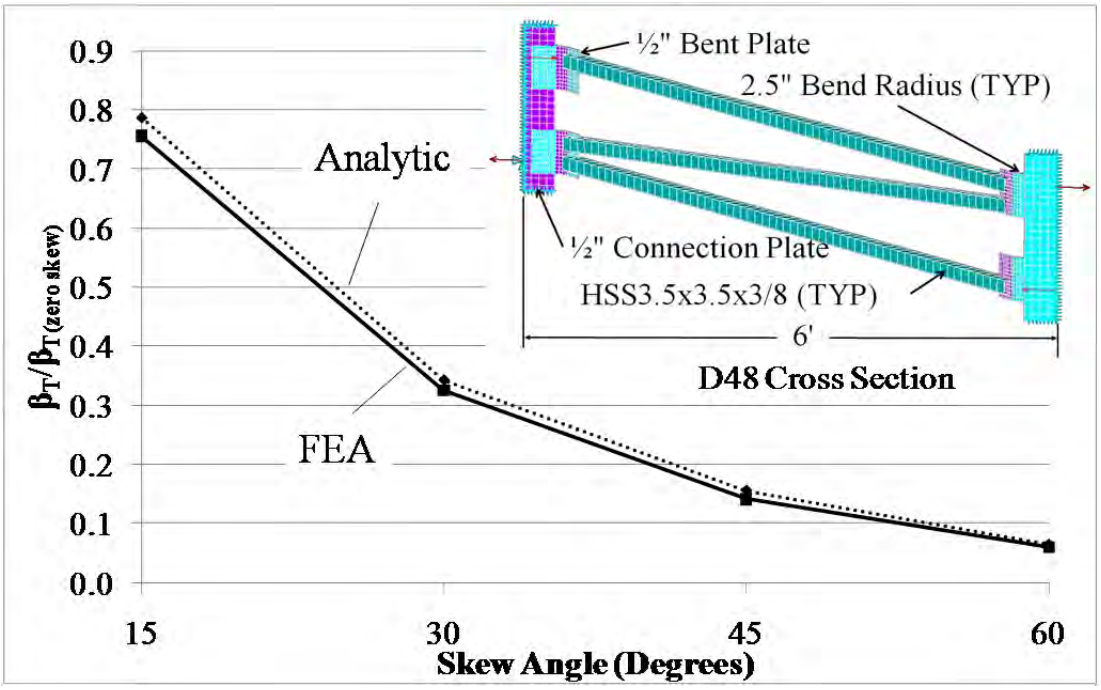

Figure C.11: D48 cross frame analytic to FEA comparison (S = 6')

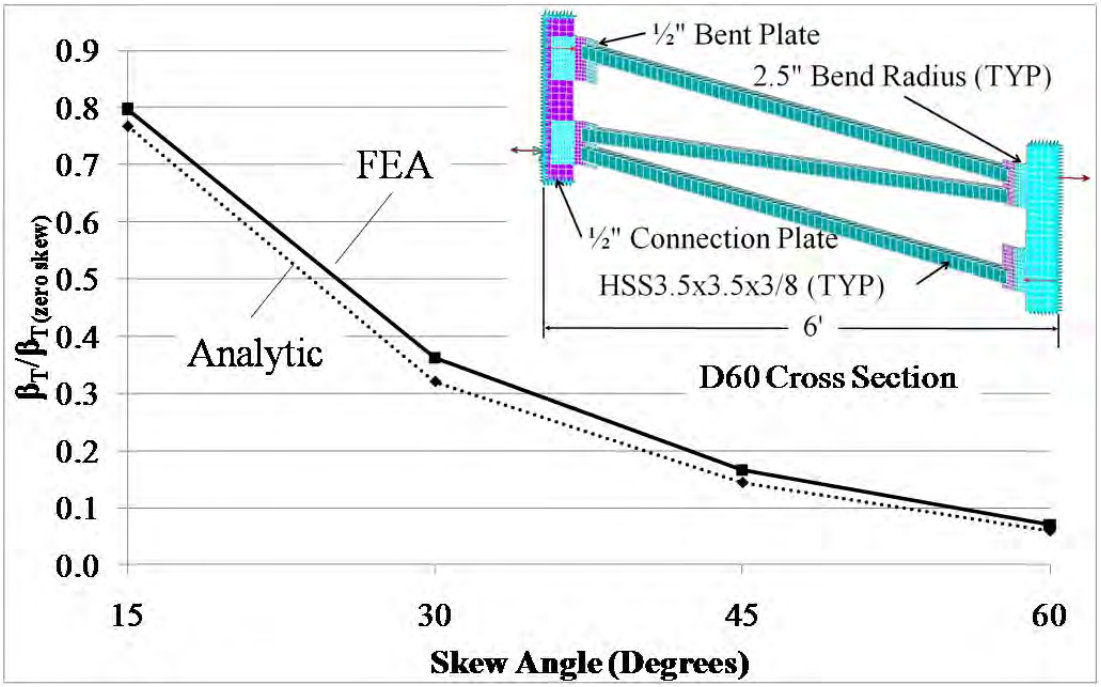

Figure C.12: D60 cross frame analytic to FEA comparison (S = 6')

C.2 Plate Thickness and Bend Radius Impact on Bent Plate Cross Frame Stiffness

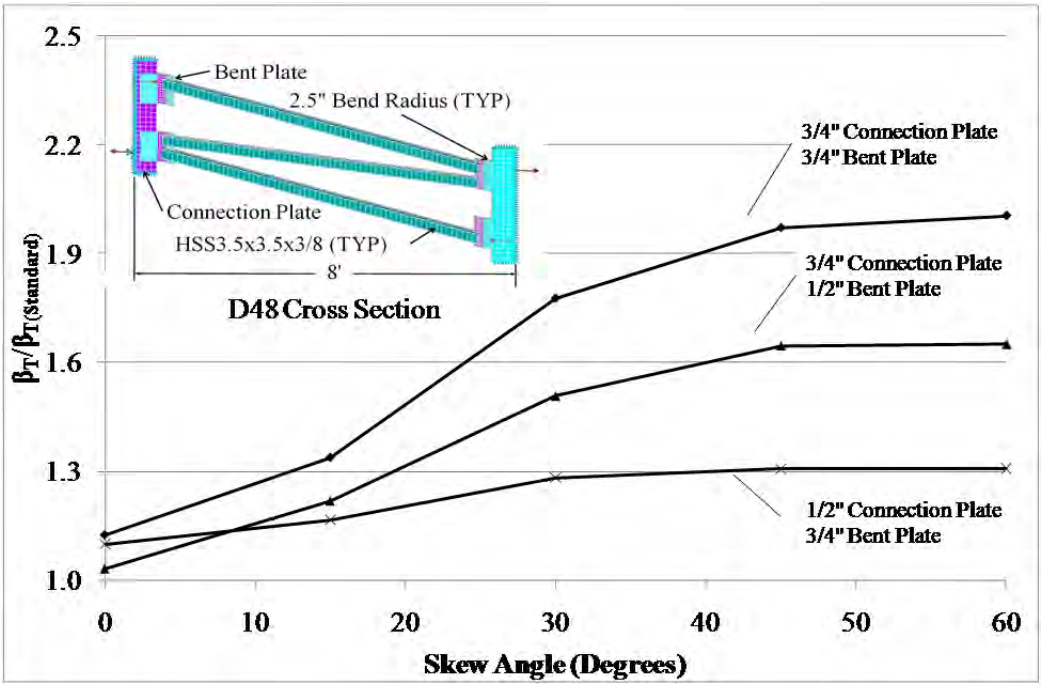

Figure C.13: D48 cross frame plate thickness impact on stiffness (2.5" bend radius)

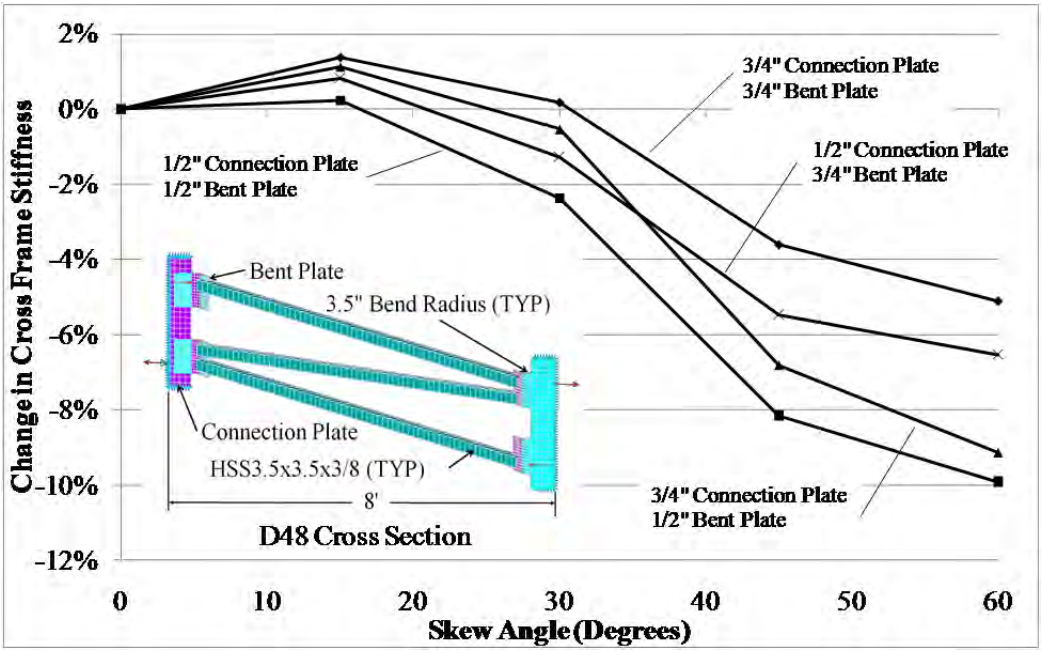

Figure C.14: D48 cross frame stiffness change (2.5" to 3.5" bend radius)

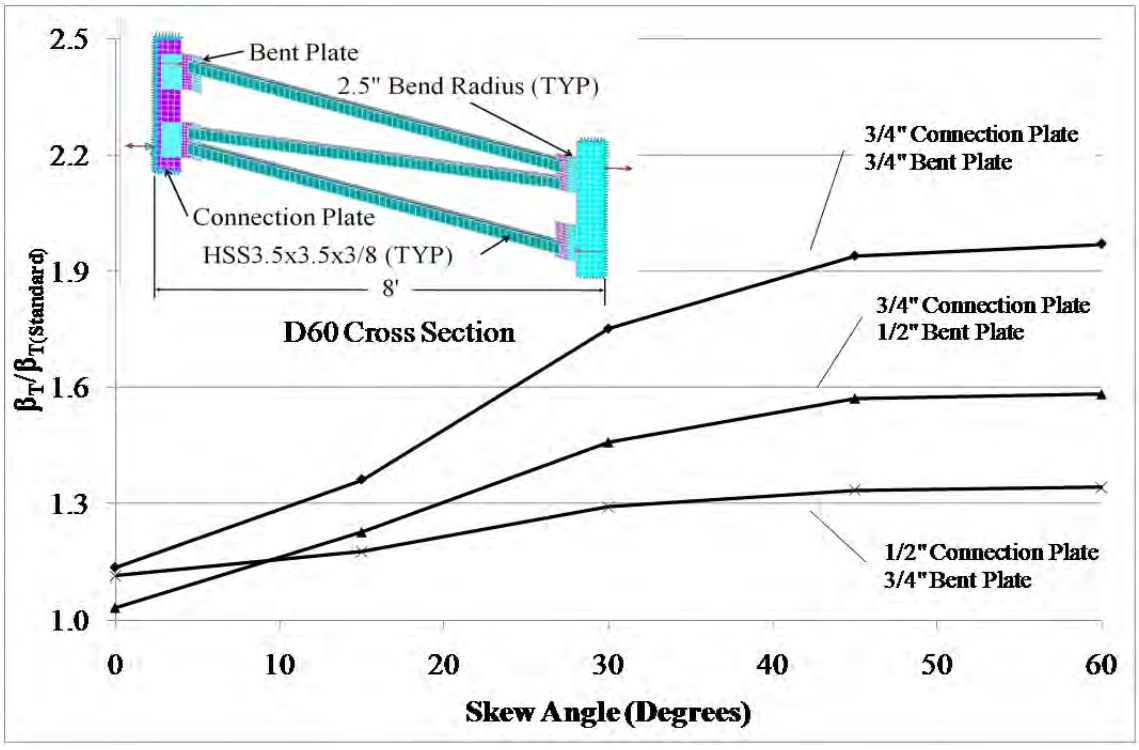

Figure C.15: D60 cross frame plate thickness impact on stiffness (2.5" bend radius)

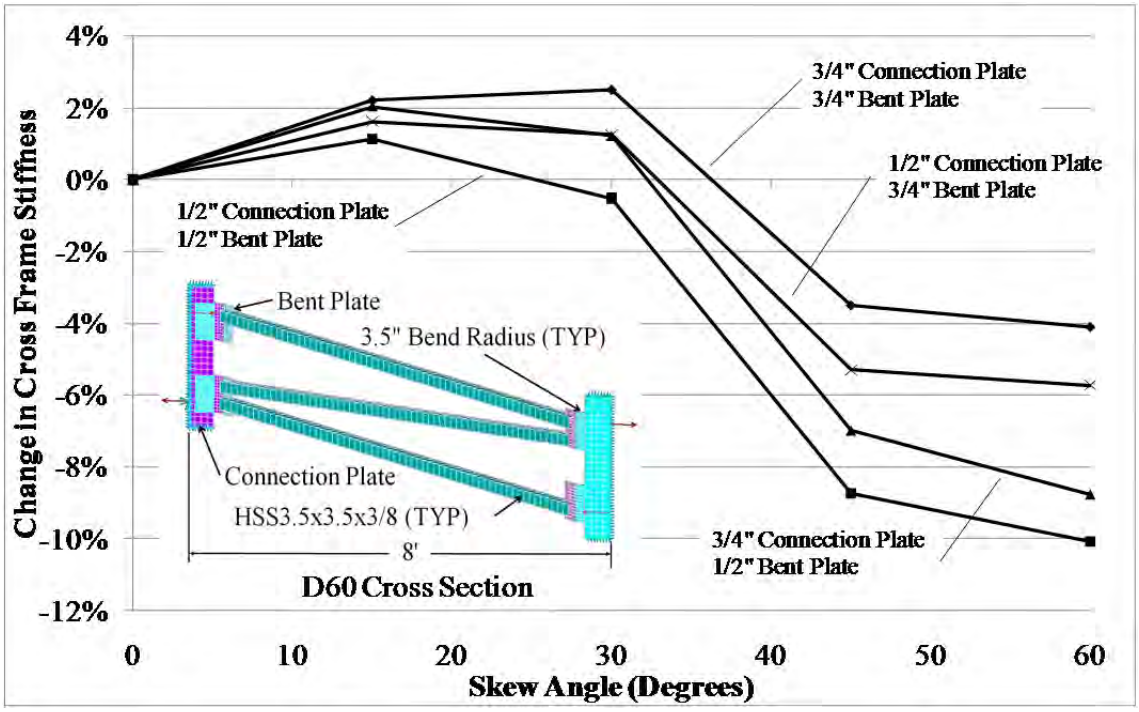

Figure C.16: D60 cross frame stiffness change (2.5" to 3.5" bend radius)

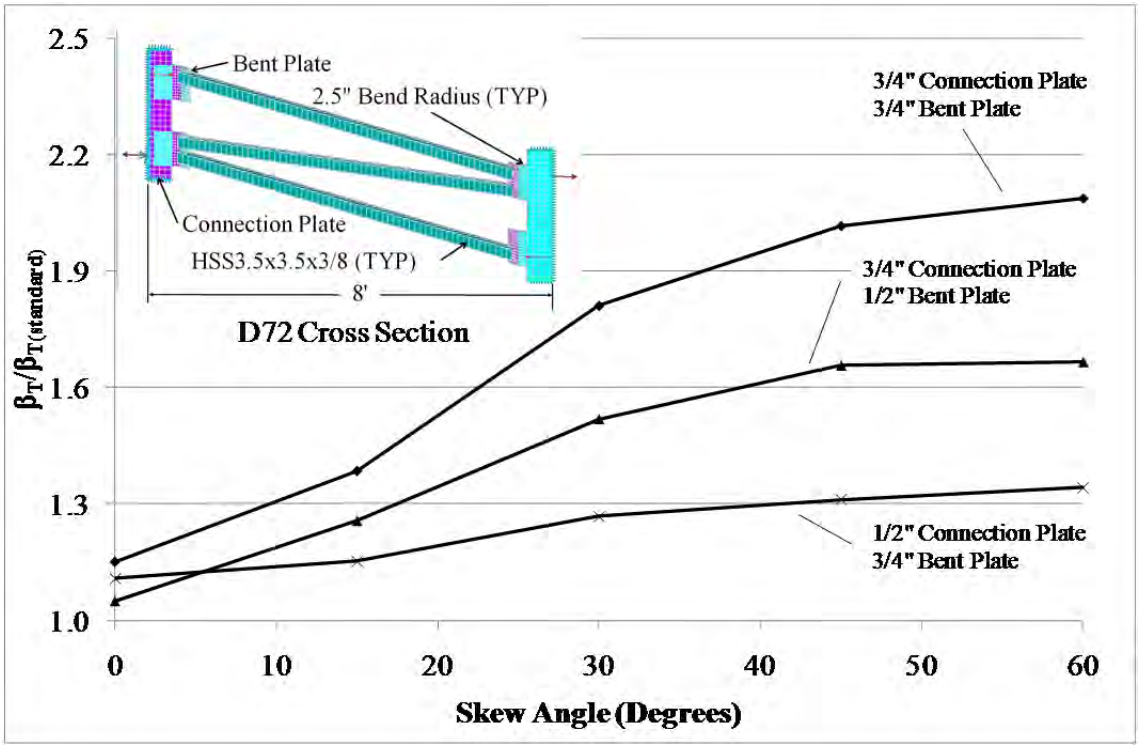

Figure C.17: D72 cross frame plate thickness impact on stiffness (2.5" bend radius)

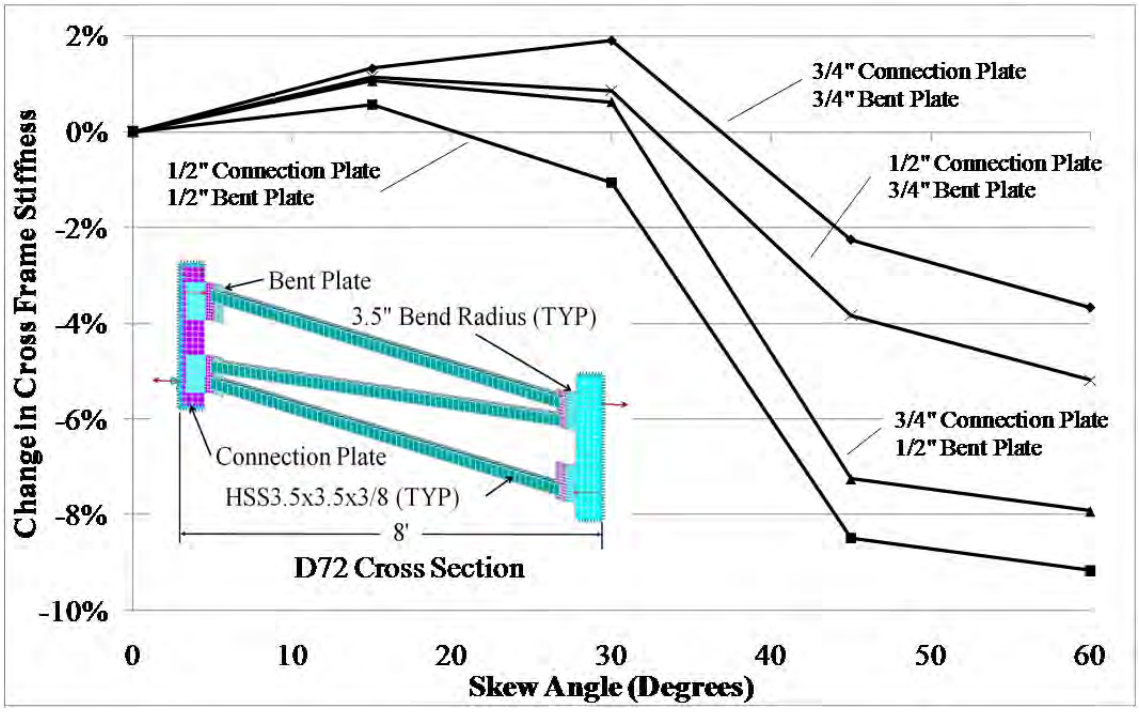

Figure C.18: D72 cross frame stiffness change (2.5" to 3.5" bend radius)

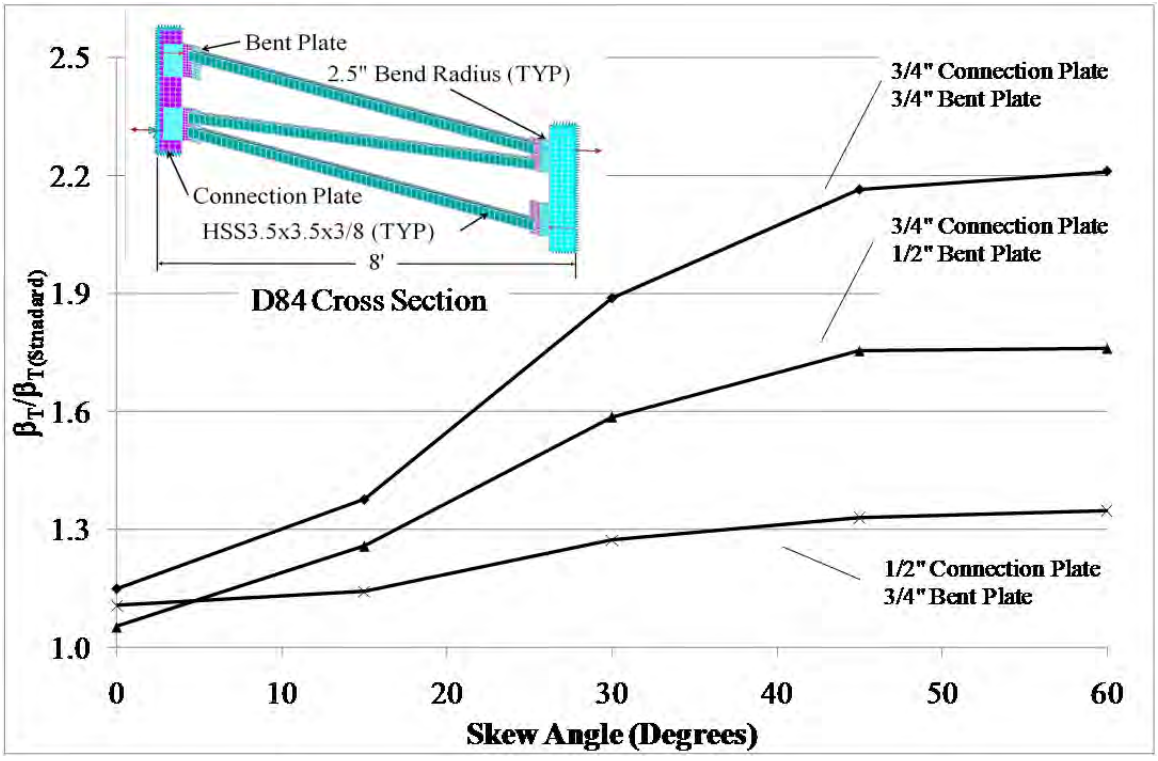

Figure C.19: D84 cross frame plate thickness impact on stiffness (2.5" bend radius)

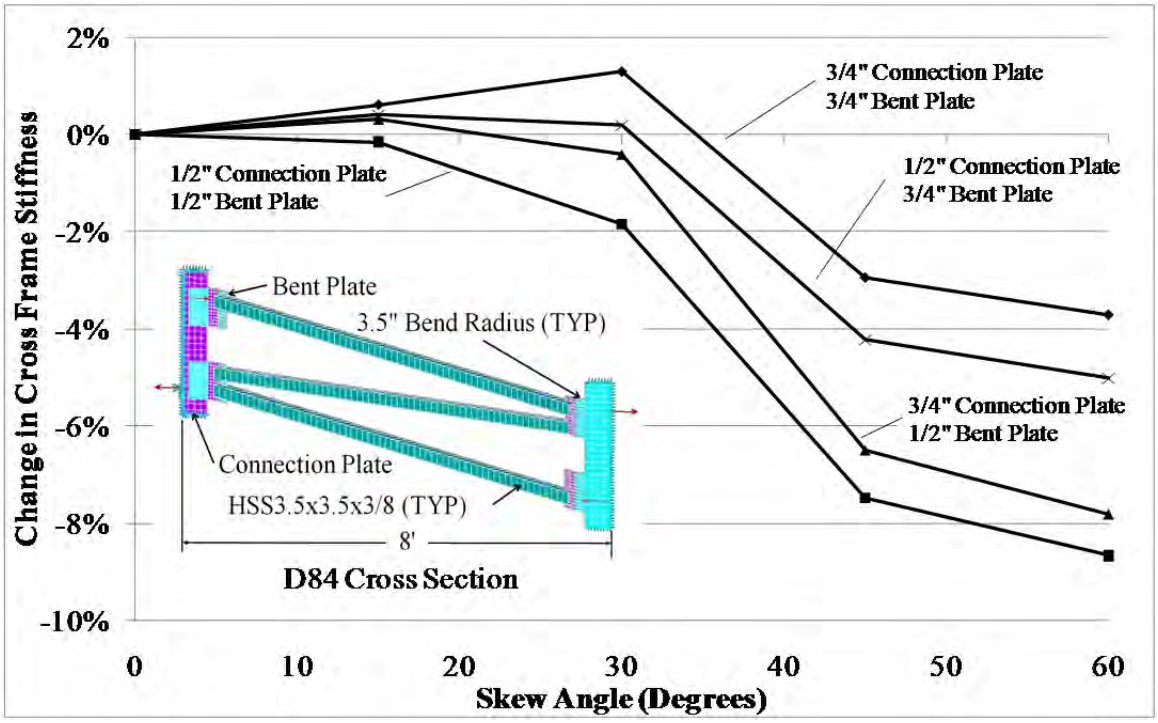

Figure C.20: D84 cross frame stiffness change (2.5" to 3.5" bend radius)

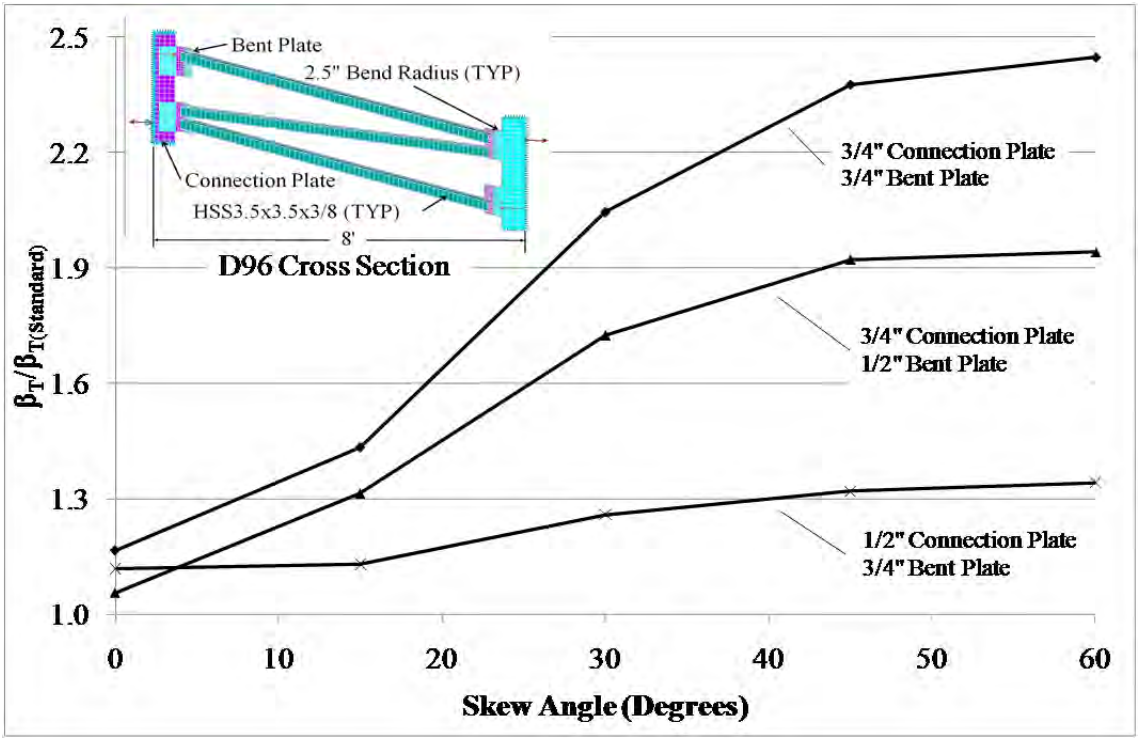

Figure C.21: D96 cross frame plate thickness impact on stiffness (2.5" bend radius)

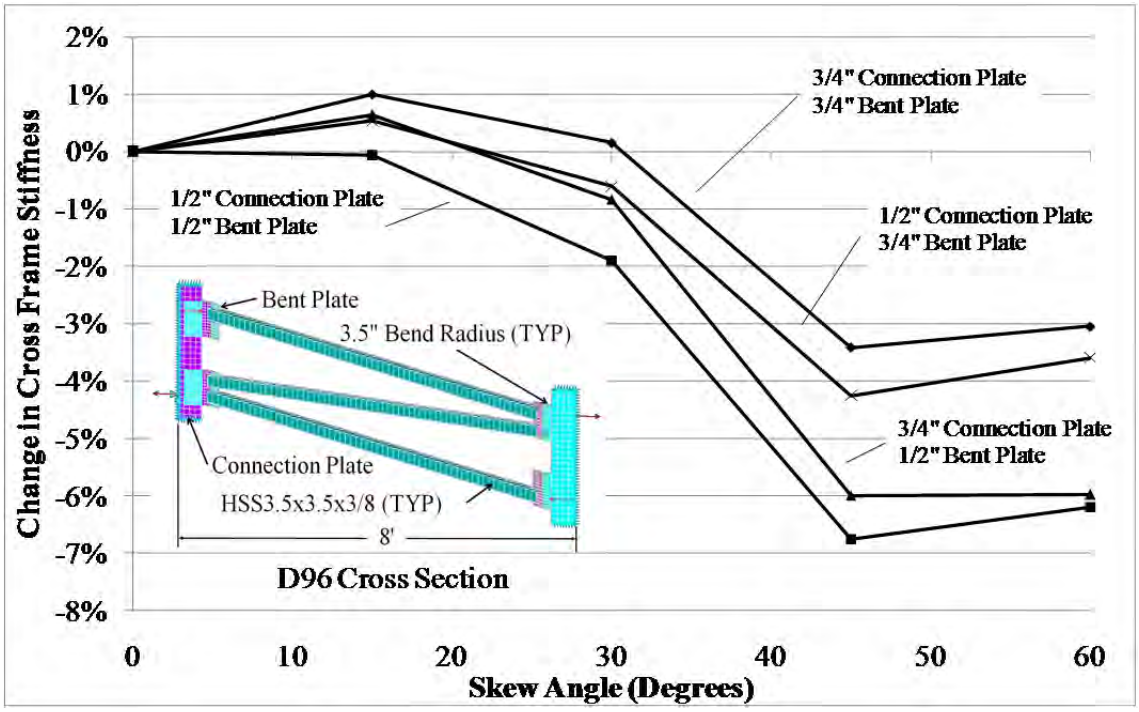

Figure C.22: D96 cross frame stiffness change (2.5" to 3.5" bend radius)

C.3 End Twist Impact on Girder Buckling Strength

C.3.1 Bent Plate Cross Frame Connection

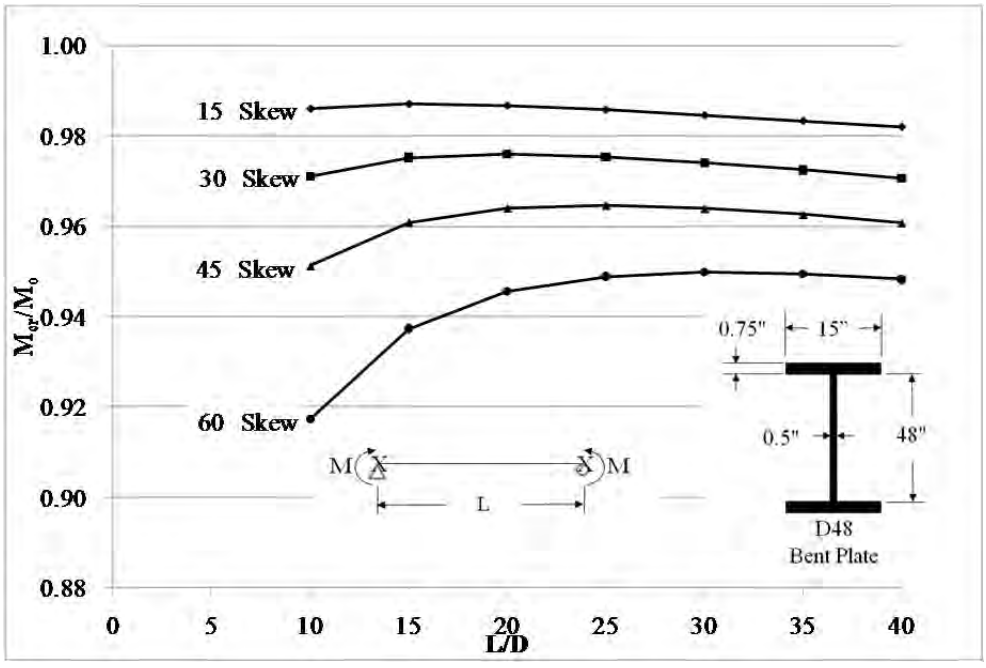

Figure C.23: D48 Cross section end twist affected buckling strength (bent plate)

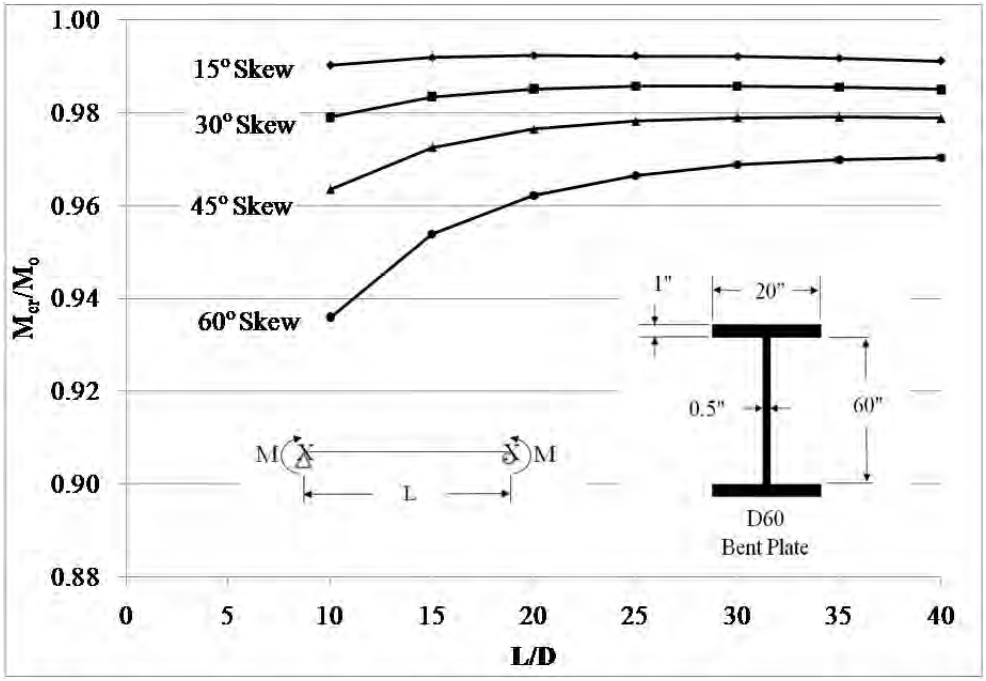

Figure C.24: D60 Cross section end twist affected buckling strength (bent plate)

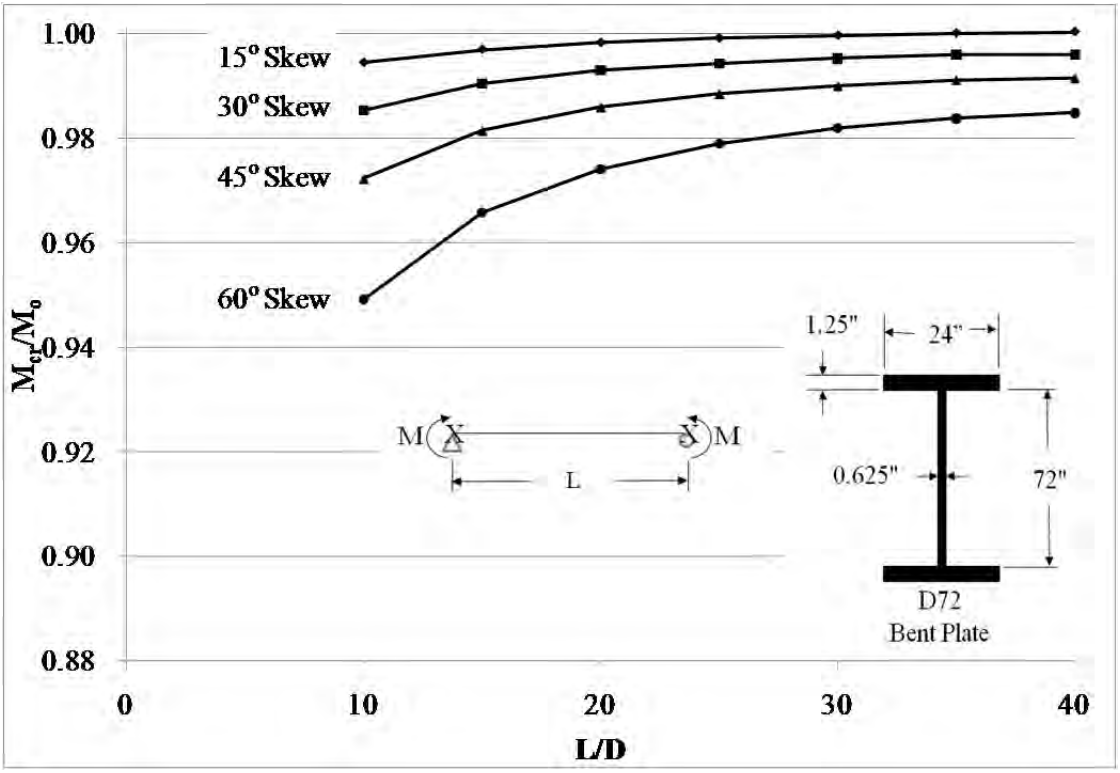

Figure C.25: D72 Cross section end twist affected buckling strength (bent plate)

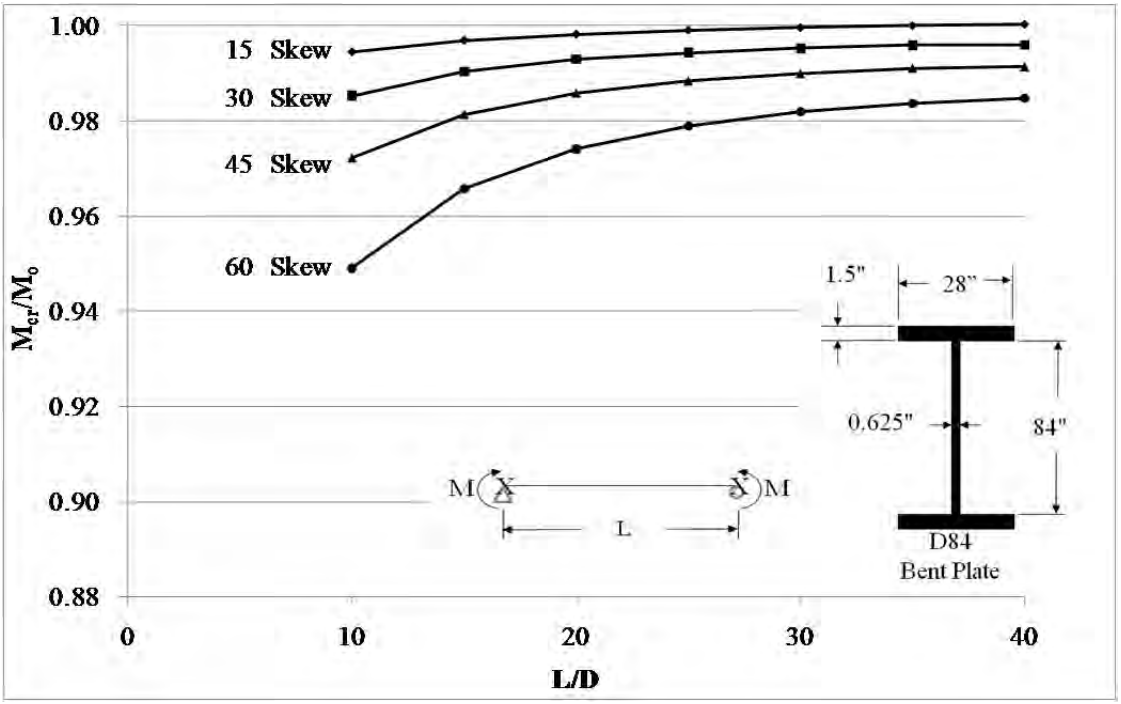

Figure C.26: D84 Cross section end twist affected buckling strength (bent plate)

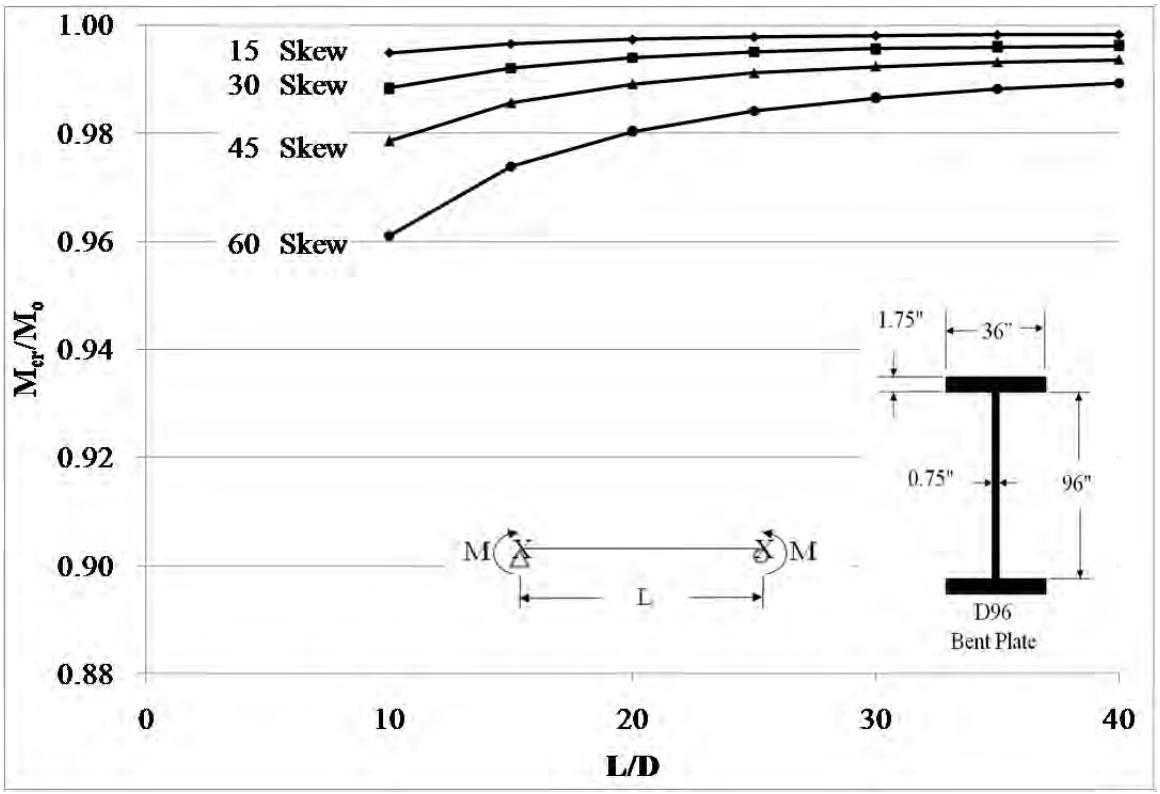

Figure C.27: D96 Cross section end twist affected buckling strength (bent plate)

C.3.2 Split Pipe Cross Frame Connection

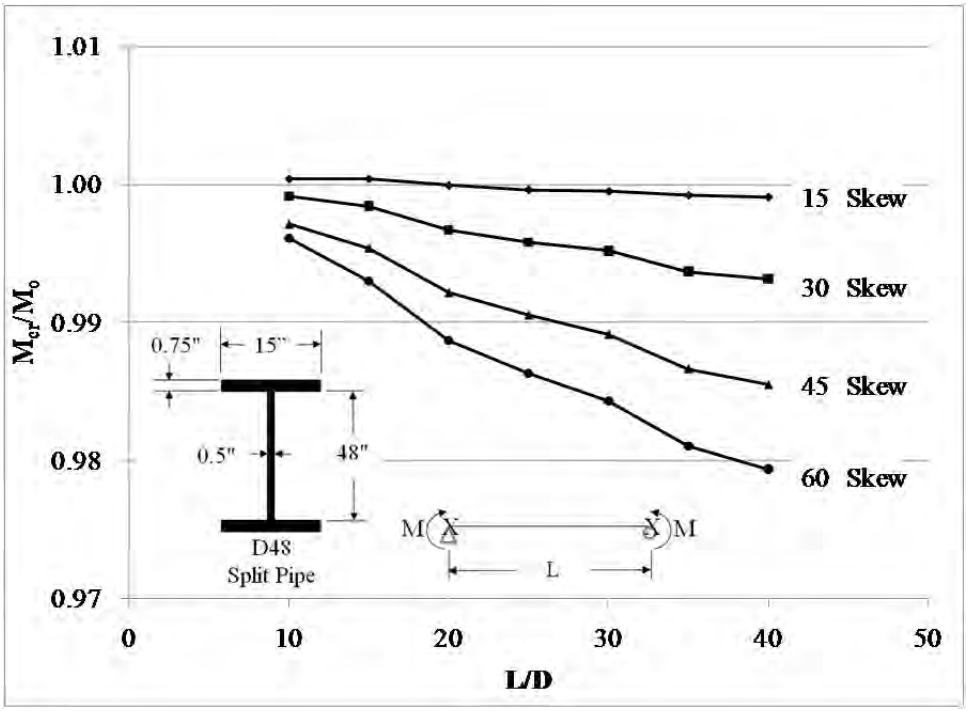

Figure C.28: D48 Cross section end twist affected buckling strength (split pipe)

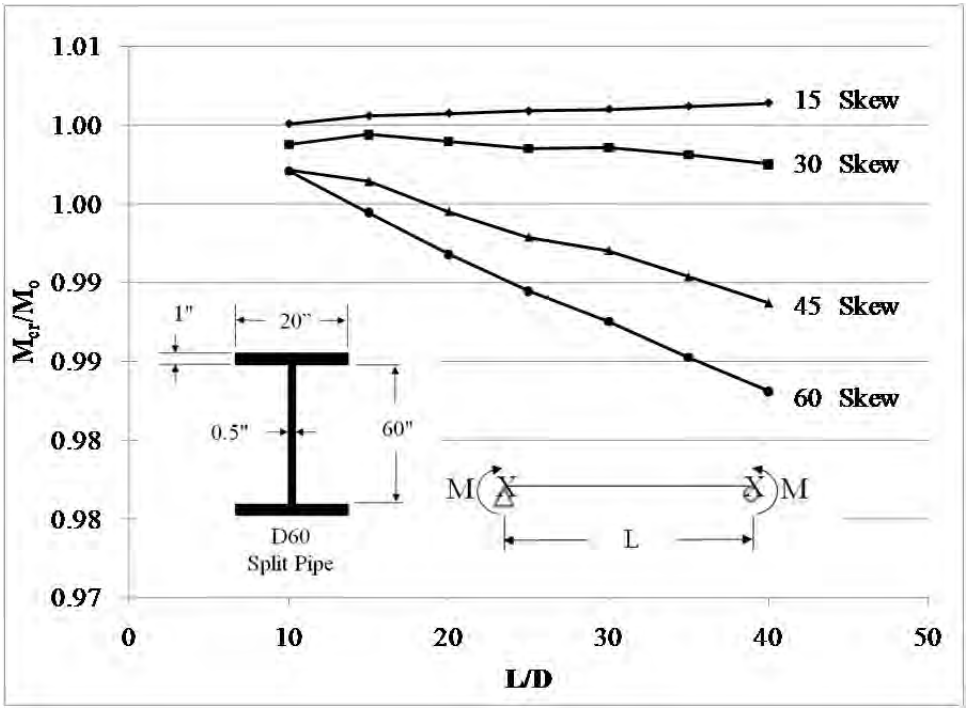

Figure C.29: D60 Cross section end twist affected buckling strength (split pipe)

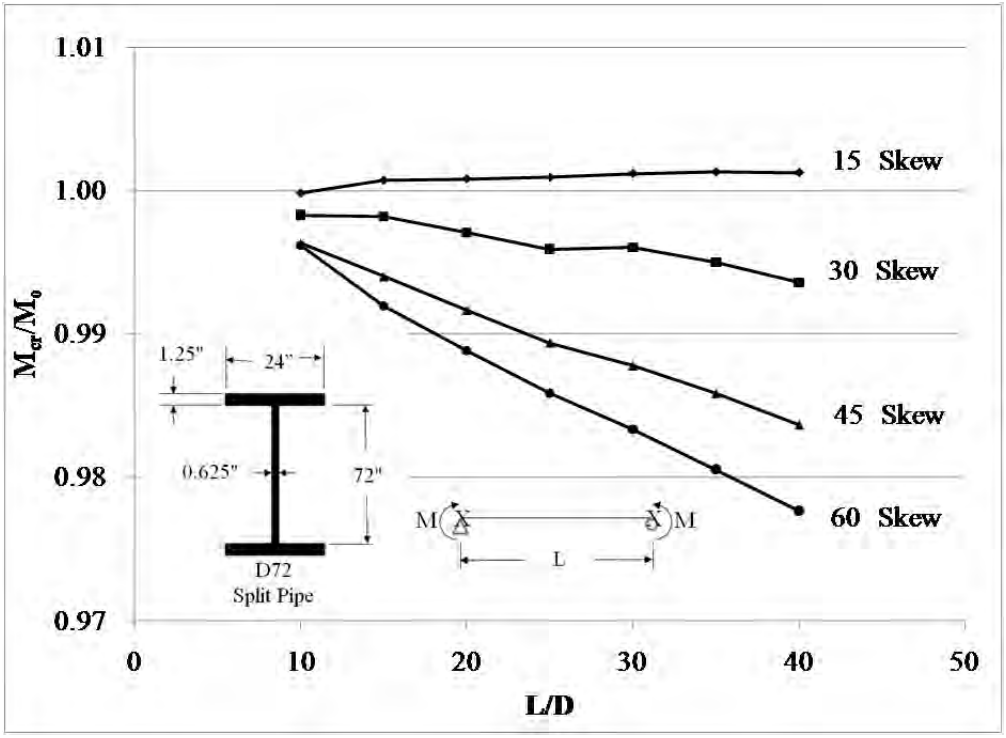

Figure C.30: D72 Cross section end twist affected buckling strength (split pipe)

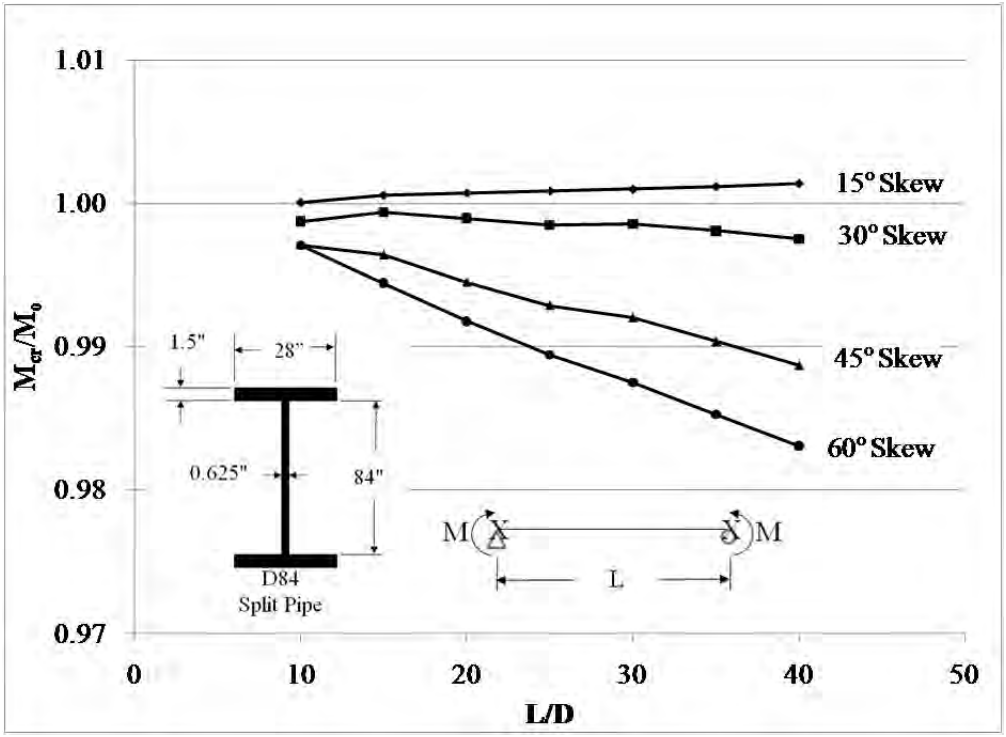

Figure C.31: D84 Cross section end twist affected buckling strength (split pipe)

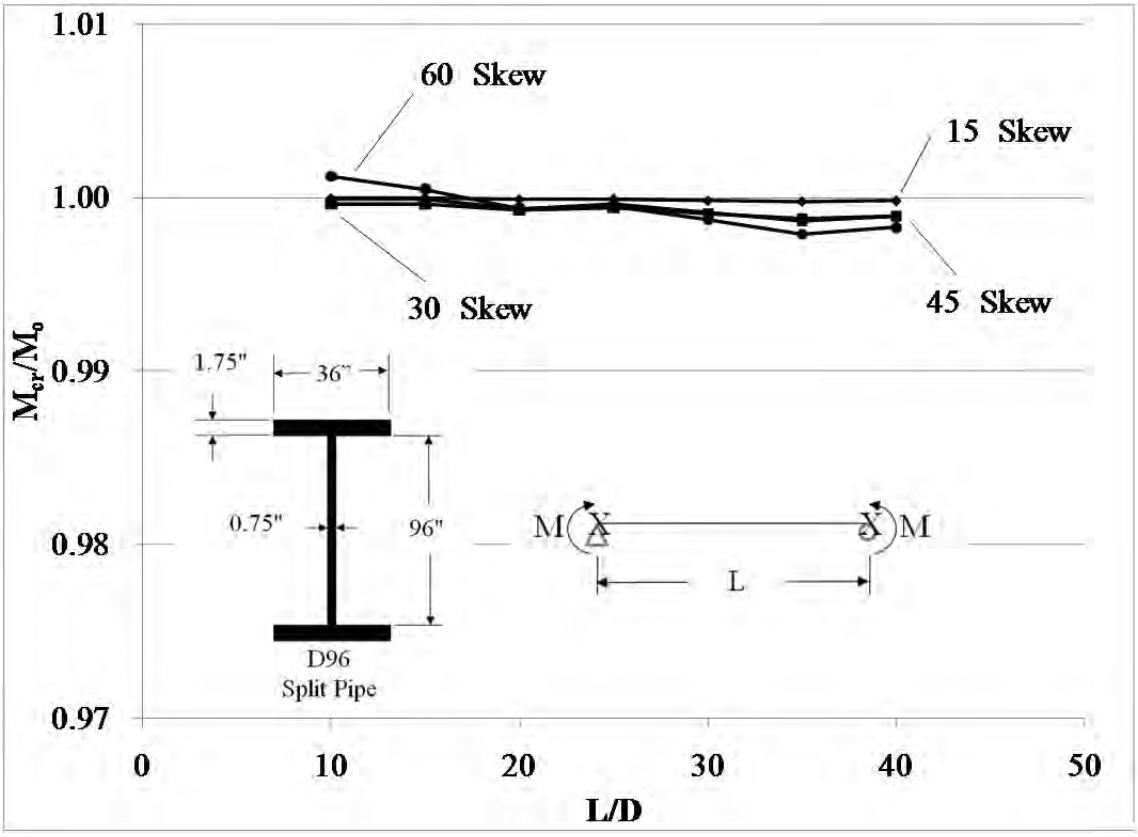

Figure C.32: D96 Cross section end twist affected buckling strength (split pipe)

C.4 PIPE STIFFENED GIRDER BUCKLING CAPACITY

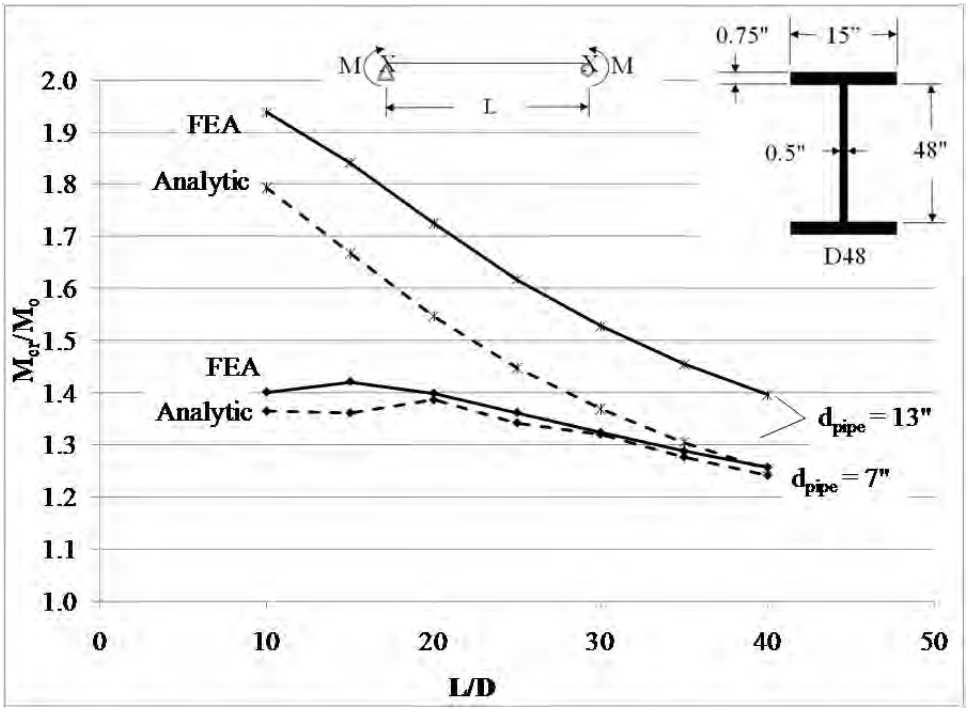

Figure C.33: D48 split pipe stiffened buckling capacity (uniform moment)

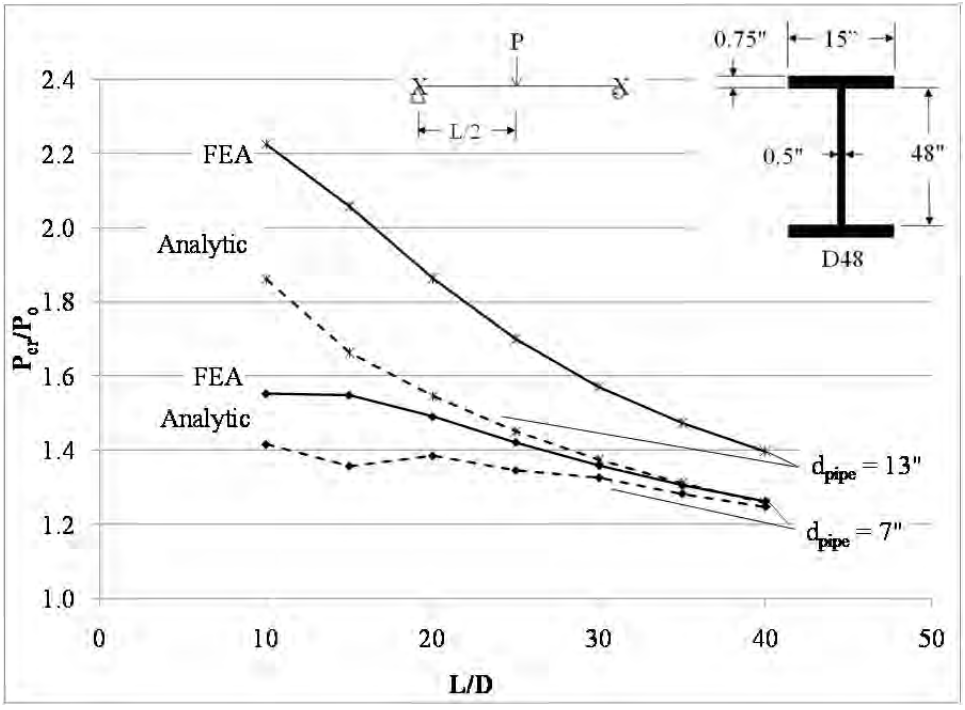

Figure C.34: D48 split pipe stiffened buckling capacity (mid-span point load)

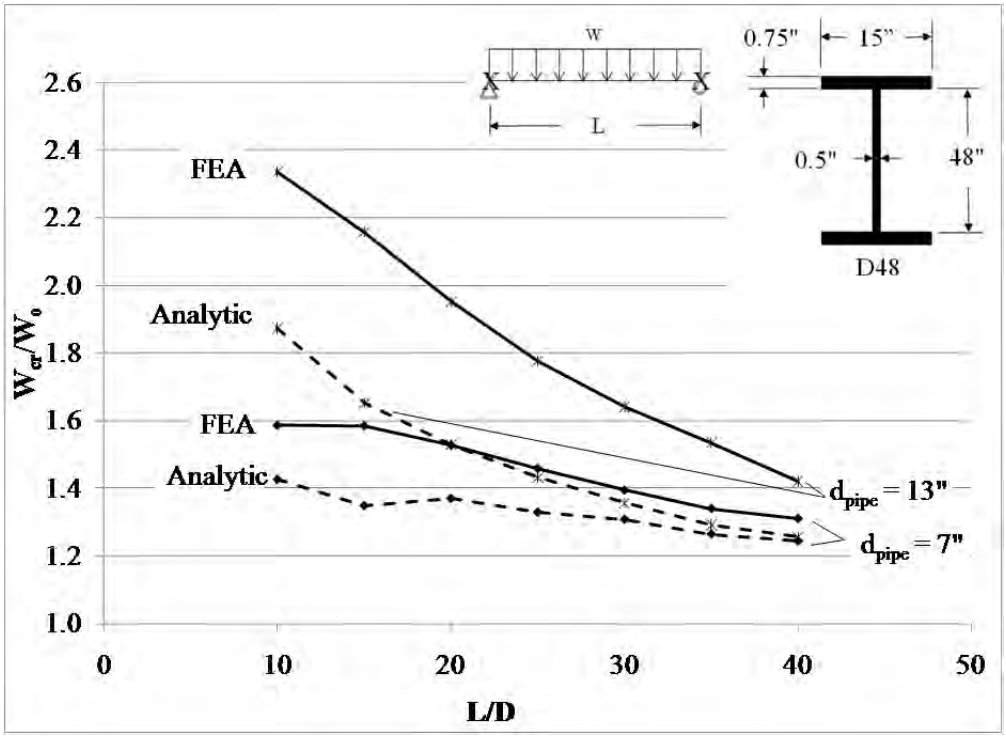

Figure C.35: D48 split pipe stiffened buckling capacity (distributed load)

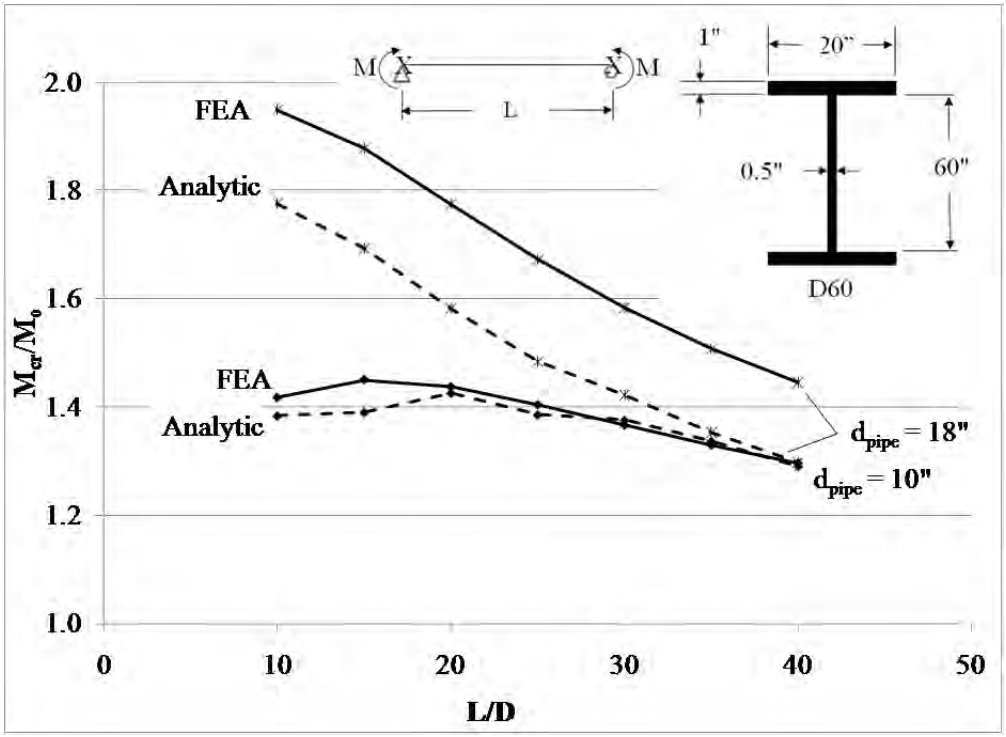

Figure C.36: D60 split pipe stiffened buckling capacity (uniform moment)

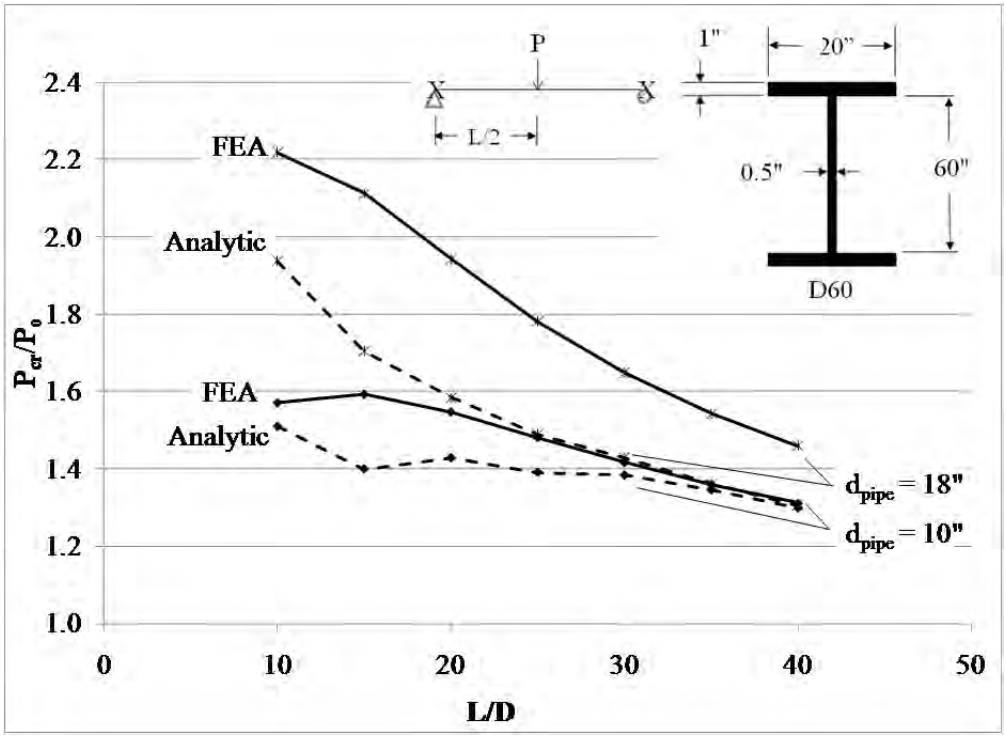

Figure C.37: D60 split pipe stiffened buckling capacity (mid-span point load)

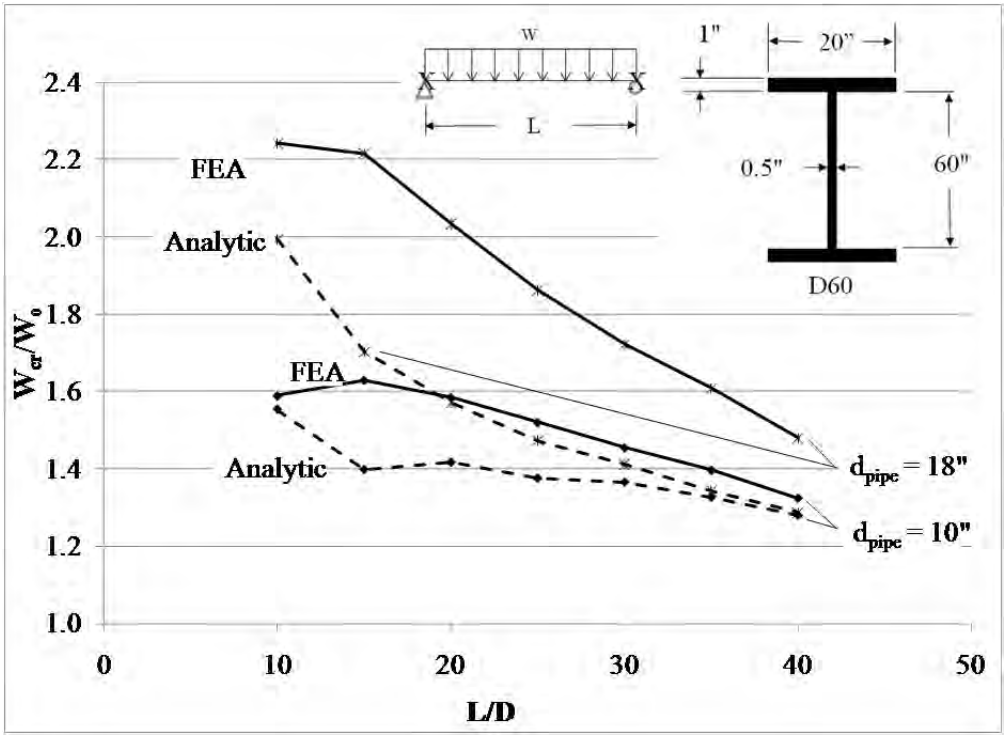

Figure C.38: D60 split pipe stiffened buckling capacity (distributed load)

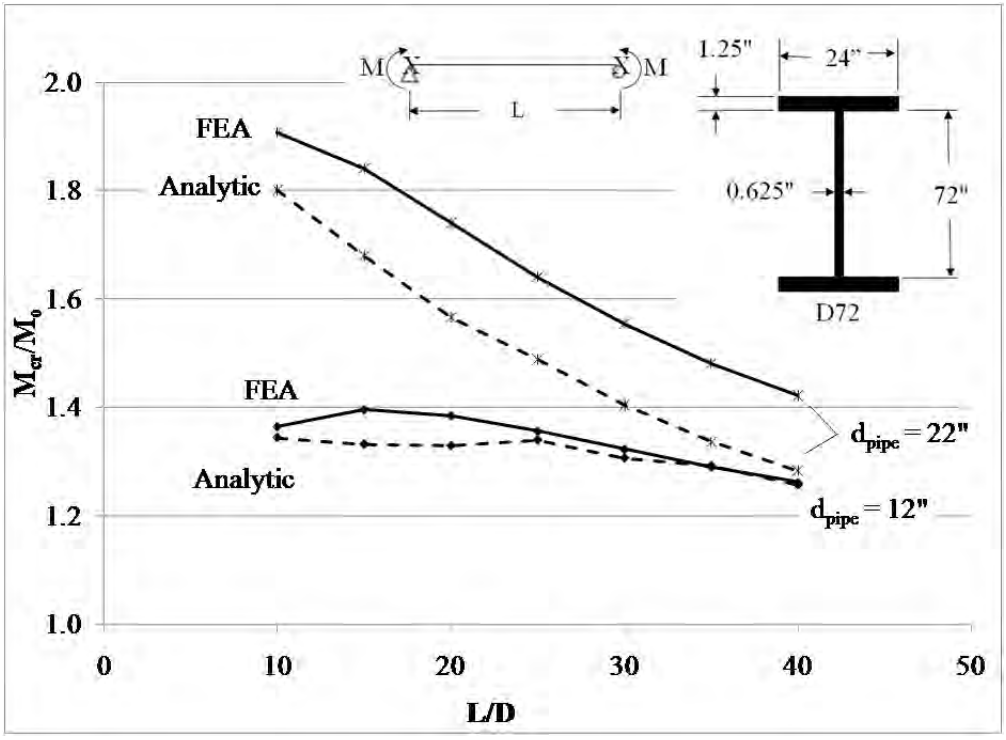

Figure C.39: D72 split pipe stiffened buckling capacity (uniform moment)

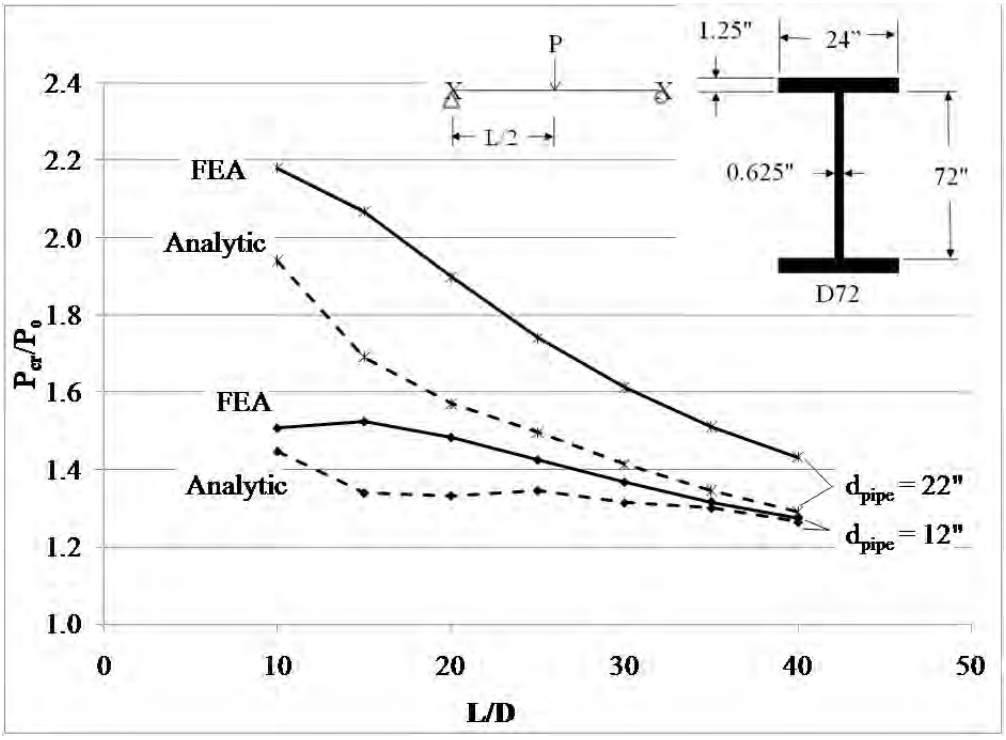

Figure C.40: D72 split pipe stiffened buckling capacity (mid-span point load)

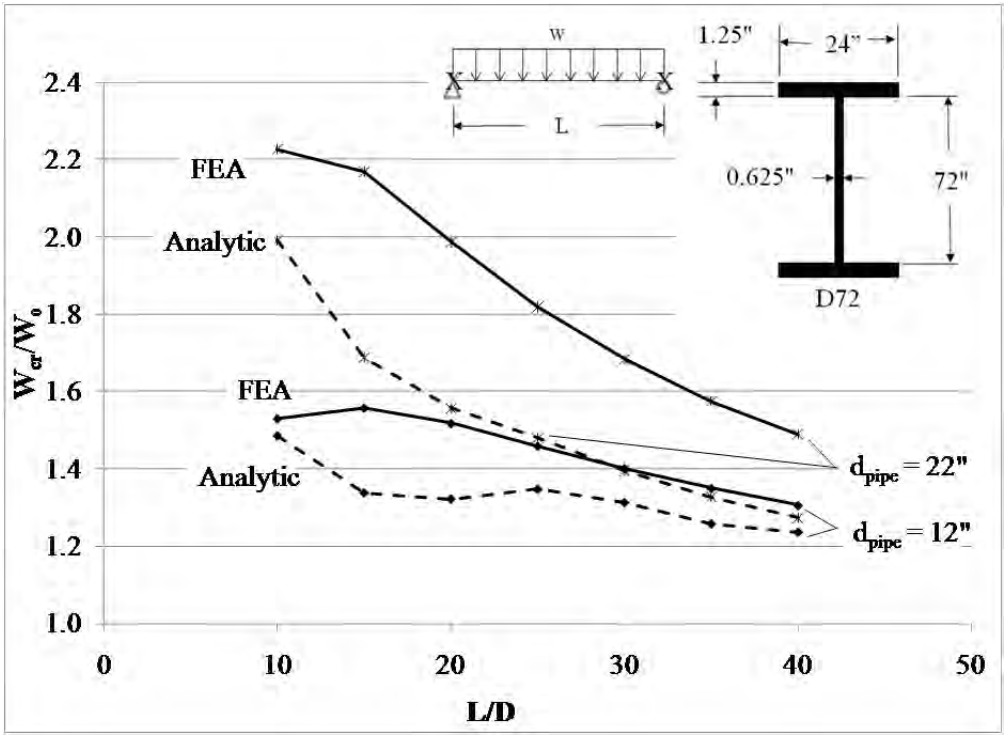

Figure C.41: D72 split pipe stiffened buckling capacity (distributed load)

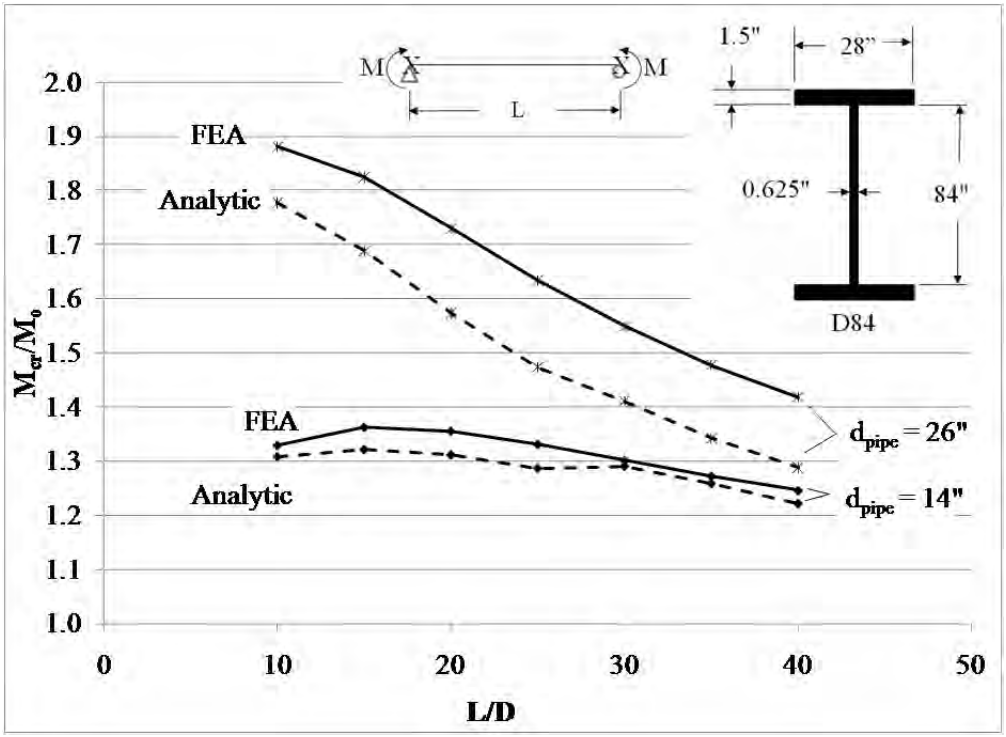

Figure C.42: D84 split pipe stiffened buckling capacity (uniform moment)

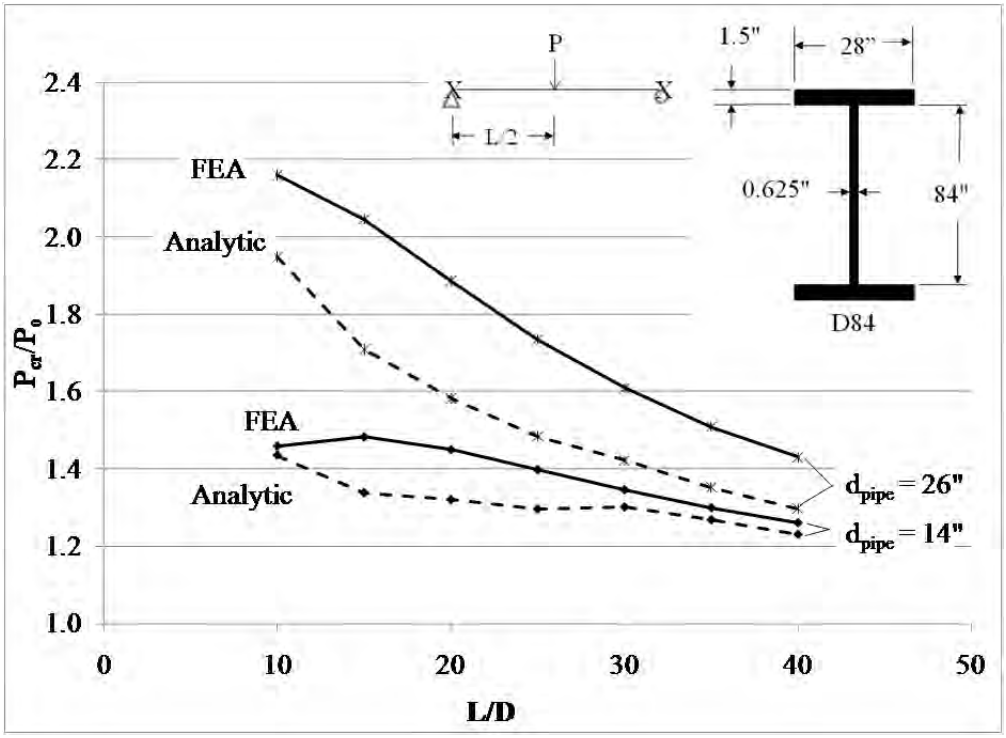

Figure C.43: D84 split pipe stiffened buckling capacity (mid-span point load)

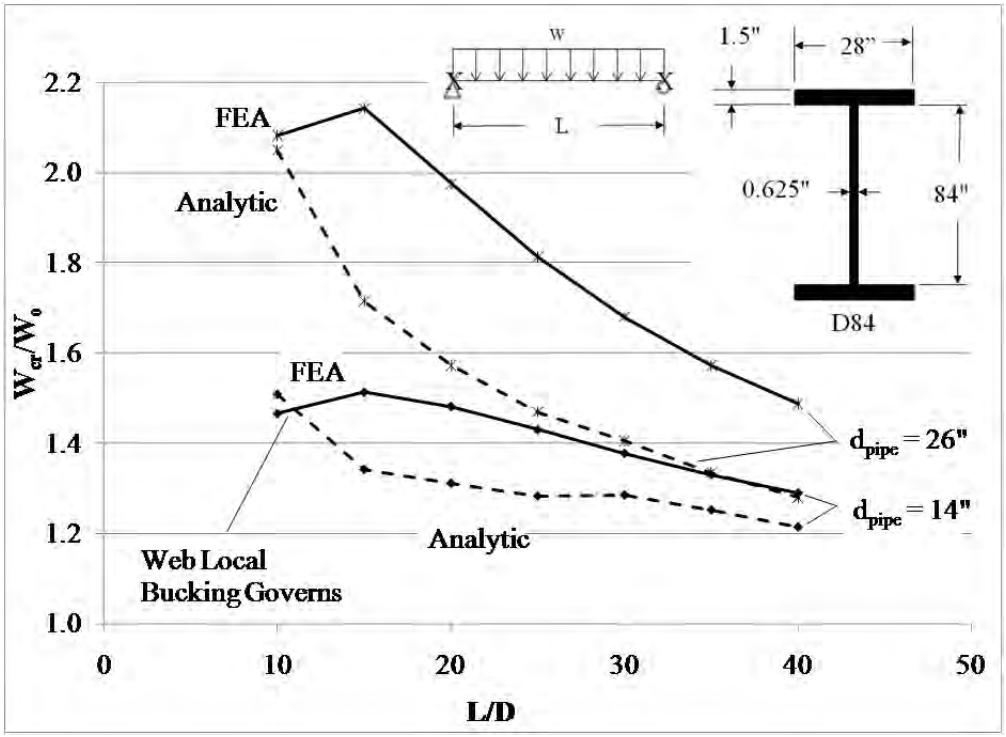

Figure C.44: D84 split pipe stiffened buckling capacity (distributed load)

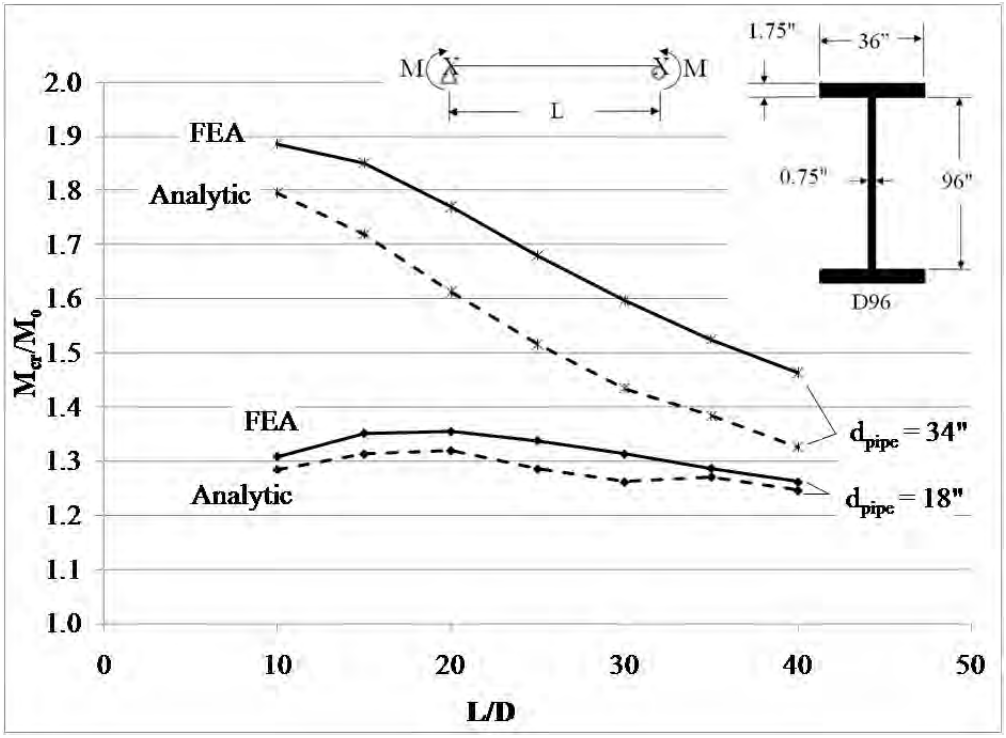

Figure C.45: D96 split pipe stiffened buckling capacity (uniform moment)

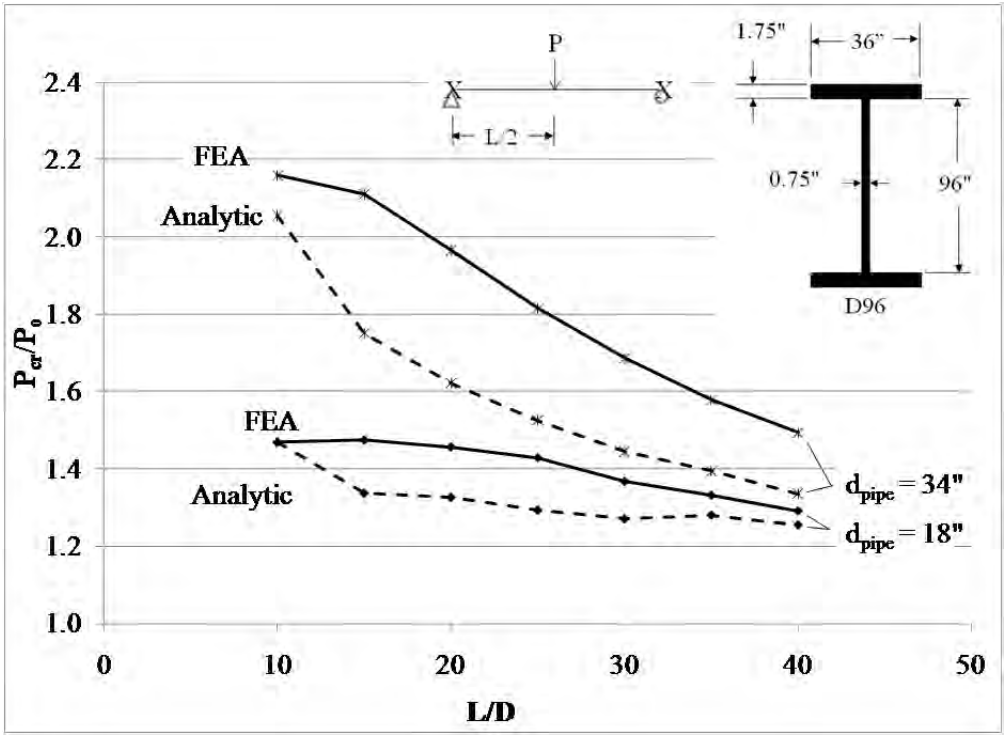

Figure C.46: D96 split pipe stiffened buckling capacity (mid-span point load)

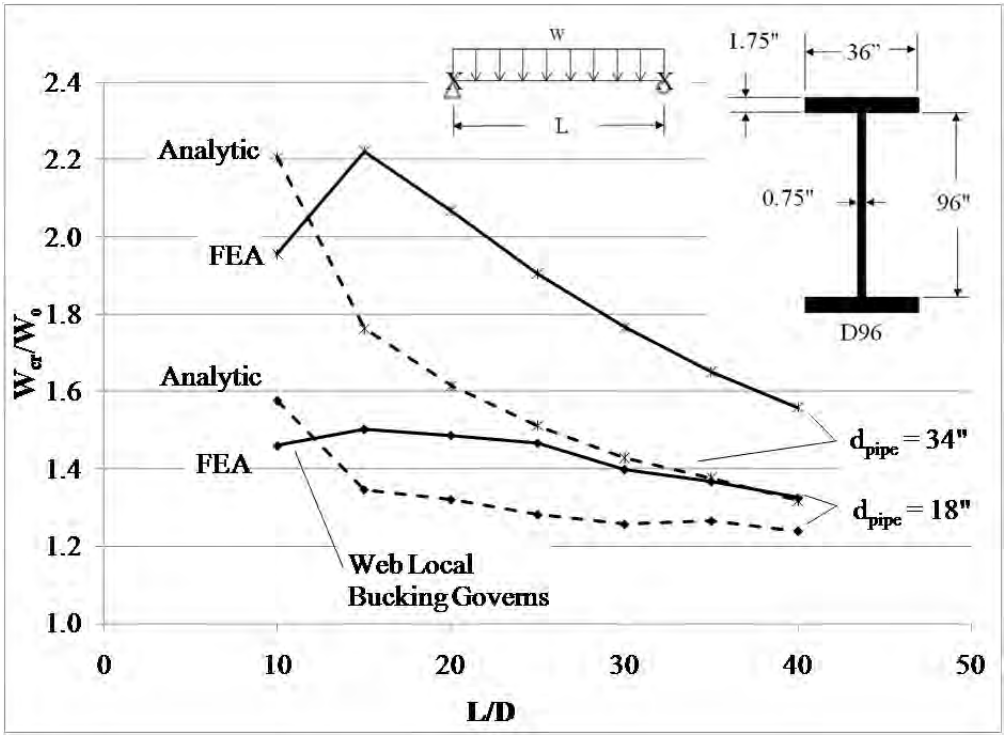

Figure C.47: D96 split pipe stiffened buckling capacity (distributed load)

Appendix D. Design Example

D.1 INTRODUCTION

The split pipe stiffener can increase the lateral torsional buckling strength of girders by providing warping restraint to the end of the girders, as discussed in Chapter 5 and Chapter 7. An example that demonstrates the procedure for determining the permissible unbraced length for girders with split pipe stiffeners and the resulting locations of intermediate cross-frames is presented in this appendix. To illustrate the benefits of the split pipe stiffener, cross-frame locations required to stabilize girders during the deck cast were determined for two cases. The first case was for girders with conventional plate stiffeners for attachment of end cross-frames, and the second case was for girders with split pipe stiffeners for attachment of end cross-frames.

D.2 DESIGN EXAMPLE

D.2.1 Bridge Layout

The example bridge is constructed using two span continuous I-girders, where each span is 200 ft. All supports for the bridge are skewed at an angle of 45 degrees. The bridge has an 8″ concrete deck with a 1.5″ concrete haunch. There are five girders at a 10 ft. spacing and the girders are Grade 50 steel. A plan view of the layout of the bridge is provided in Figure D.1 with a girder elevation view shown in Figure D.2. The girder section properties are listed in Table D.1.

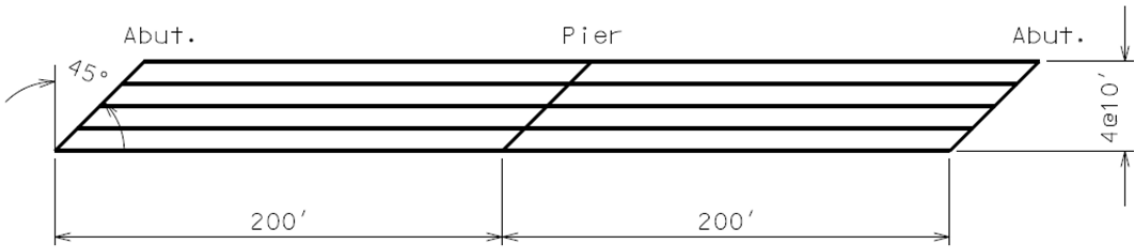

Figure D.1: Bridge layout

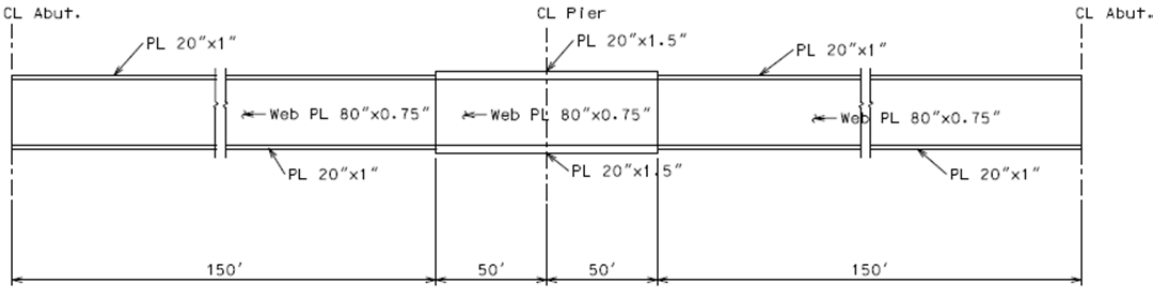

Figure D.2: Girder elevation

Table D.1: Girder section properties

Properties	***Positive Moment Region***	***Negative Moment Region***
A	100.0 in^2	120.0 in^2
d	82.0 in	83.0 in
I_x	97613 in^4	131645 in^4
I_y	1336 in^4	2002 in^4
J	24.6 in^4	56.3 in^4
C_w	2246000 in^6	3449000 in^6
r_t	4.7 in	5 in
S_x	2381 in^3	3172 in^3

D.2.2 Construction Design Loads

The service loads on the bridge during the deck cast are computed below.

Dead Loads:

Steel girder at positive moment areas:

$$w_s = 0.49k/ft^3 \times (100/144)ft^2 = 0.34k/ft$$

Steel girder at negative moment areas:

$$w_s = 0.49k/ft^3 \times (120/144)ft^2 = 0.41k/ft$$

Concrete deck:

$$w_s = 0.15k/ft^3 \times (8/12)ft \times 10ft = 1.00k/ft$$

Concrete haunch:

$$w_s = 0.15k/ft^3 \times (1.5/12)ft \times (20/12)ft = 0.031k/ft$$

Construction live load:

$$w_s = 0.03k/ft^3 \times 10ft = 0.3k/ft$$

The dead load factor of 1.5 and the live load factor of 1.6 for construction loads were taken according to AASHTO 2010.

Total Factored Load on Girders:

Positive moment areas:

$$w_T = 1.5 \times (0.34 + 1.00 + 0.031) + 1.6 \times (0.3)k/ft = 2.54k/ft$$

Negative moment areas:

$$w_T = 1.5 \times (0.41 + 1.00 + 0.031) + 1.6 \times (0.3)k/ft = 2.64k/ft$$

For the two-span continuous girders, the maximum positive moment is 7155 k-ft and the maximum negative moment is 12796 k-ft.

D.2.3 Unbraced Length for LTB of the Plate-Stiffened Girders

The required unbraced length for the plate-stiffened girders can be calculated by Equation (2.17) modified by moment gradient coefficient C_b. It is assumed that the girders are in the elastic buckling range. C_b can be evaluated using the methods described in AASHTO Section A6.3.3. By assuming an unbraced length of 40 feet, the following C_b values were obtained:

Abutment Areas: $C_b=1.45$

Pier Area: $C_b=1.58$

Maximum Positive Moment Area: $C_b=1$

(a) At the abutment areas, M_{cr} must satisfy:

$$\phi_f M_{cr} = (1.0)(1.45)\left(\frac{\pi}{L_b}\right)\sqrt{(29000)(1336)\,(11154)(24.6) + \frac{\pi^2(29000)^2(2246000)(1336)}{{L_b}^2}} \geq M_a$$

M_a is the moment at the location at a distance of L_b from the abutments. Through iteration, the maximum L_b is determined at 47.5 feet, where M_{cr} is 6234 kip-ft and M_a is 6200 kip-ft.

The resulted L_b should be checked with elastic limits (L_r) specified in AASHTO. Using AASHTO Equation A6.3.3-5:

$$L_r = (1.95)(4.7)\left(\frac{29000}{35}\right)\sqrt{\frac{24.6}{(2381)(81)}}\sqrt{1+\sqrt{1+(6.76)\left(\frac{(35)(2381)(81)}{(29000)(24.6)}\right)^2}}$$
$$= 434\ in = 36.2\ ft < 47.5\ ft = L_b$$

So the girders at the abutment areas are in the elastic lateral torsional buckling range.

(b) At the pier area:

$$\phi_f M_{cr}$$
$$= (1.0)(1.58)\left(\frac{\pi}{L_b}\right)\sqrt{(29000)(2003)(11154)(56.3\ ) + \frac{\pi^2(29000)^2(3449000)(2003)}{{L_b}^2}}$$
$$\geq 12796 kip - ft$$

L_b can be solved iteratively resulting in: $L_b \leq 42.0 ft$.
And then L_r can be calculated:

$$L_r = (1.95)(5.0)\left(\frac{29000}{35}\right)\sqrt{\frac{56.3}{(3172)(81)}}\sqrt{1+\sqrt{1+(6.76)\left(\frac{(35)(3172)(81.5)}{(29000)(56.3)}\right)^2}}$$
$$= 467\ in = 38.9\ ft < 42\ ft = L_b$$

So the girders at the pier area are in the elastic lateral torsional buckling range.

(c) At maximum positive moment areas:

$$\phi_f M_{cr}$$
$$= (1.0)\left(\frac{\pi}{L_b}\right)\sqrt{(29000)(1336)(11154)(24.6) + \frac{\pi^2(29000)^2(2246000)(1336)}{{L_b}^2}}$$
$$\geq 7155\ kip - ft$$

L_b can be solved iteratively resulting in: $L_b \leq 36.3 ft > 36.2\ ft$

So the girders at the maximum positive moment areas are in the elastic lateral torsional buckling range.

D.2.4 Brace Layout for Plate-Stiffened Girders

The first row of intermediate cross-frames near the supports were initially placed according to the minimum required unbraced lengths. The other cross-frames were then

placed to satisfy the required unbraced length for the positive moment area. The number of lines of intermediate cross-frames for one span is:

$N_{brace} = (200' + 40' \times tan45° - 42' - 47.5')/36.5' + 1 = 5.1$, use 6

The resulting layout of the bracing system for the plate-stiffened girders is presented in Figure D.3.

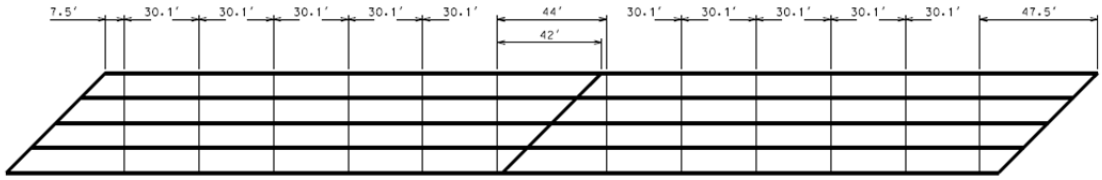

Figure D.3: Brace layout – girders with conventional plate stiffeners

D.2.5 Unbraced Length for LTB of Split Pipe-Stiffened Girders

This section outlines the evaluation of the brace layout for the girders to be stiffened at all support locations using split pipes with sizes recommended in Chapter 7. The plan view for one girder is shown in the Figure D.4.

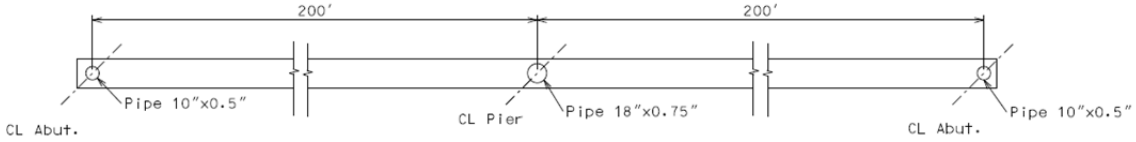

Figure D.4: Plan view – girders with split pipe stiffeners

(a) For the pipe stiffener at the pier

First, the effective unbraced length factor K is determined.

OD (Outside diameter) =18 in

t=0.75 in

J=3029.28 in^4

I_{flange}*=1000 in*^{4}

Preliminarily, L_b*=42 feet =504 in*

$$\left(\frac{GJ}{d_w}\right)_{pipe} = 11154ksi \times \frac{3029.28in^4}{80in} = 422350.8\ kips - in$$

$$\left(\frac{EI}{L_b}\right)_{flange} = 29000ksi \times \frac{1000in^4}{504in} = 57539.68\ kips - in$$

$$\left(\frac{GJ}{d_w}\right)_{pipe} / \left(\frac{EI}{L_b}\right)_{flange} = 7.3$$

From Table 5.1: m=3

$(G_Z)_A = \frac{57539.68}{3\times422350.8} = 0.045$

$(G_Z)_A = \infty$

From the alignment chart shown in Figure D.5:

K_z=0.72

To determine the required unbraced length, Equation (2.55) will be used.

$$\phi_f M_{cr}$$

$$= (1.0)(1.58)(\frac{\pi}{L_b})\sqrt{(29000)(2003)(11154)(56.2) + \frac{\pi^2(29000)^2(3449000)(2003)}{(0.72L_b)^2}}$$

$$\geq 12796kip - ft$$

Solve: $L_b \leq 49.5\ ft > 39\ ft = L_r$ (OK)

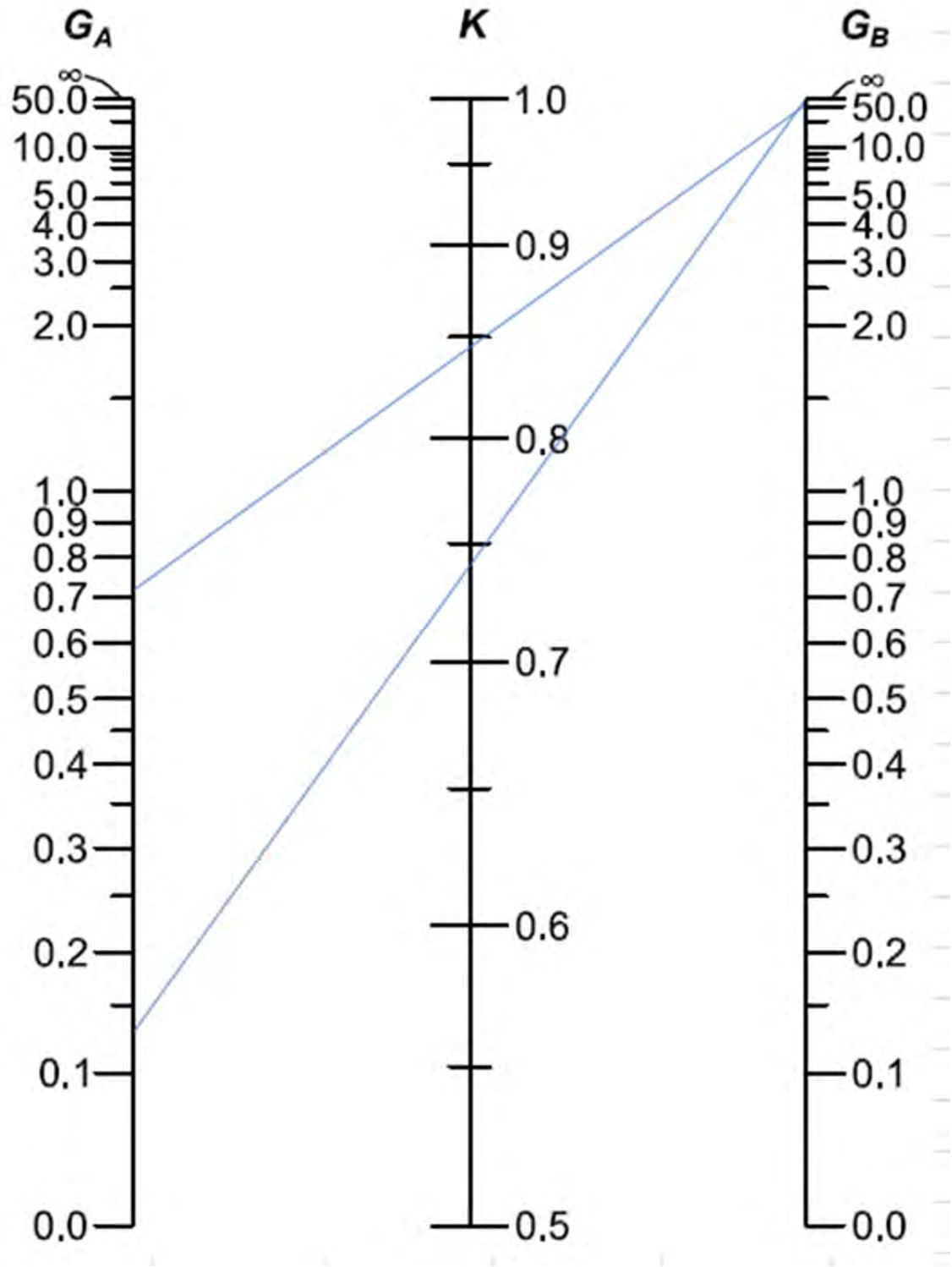

Figure D.5: Non-sway column alignment chart

(b) For the pipe stiffener at the abutments

Calculate the unbraced length factor K:

OD (Outside diameter) =10 in

t=0.5 in

J=337.62 in^4

I_{flange}=666.67in^4

Preliminarily, L_b=47.5 ft =570 in

$$\left(\frac{GJ}{d_w}\right)_{pipe} = 11154ksi \times \frac{337.62in^4}{80in} = 47072.4kips - in$$

$$\left(\frac{EI}{L_b}\right)_{flange} = 29000ksi \times \frac{666.67in^4}{570in} = 33918.1kips - in$$

$$\left(\frac{GJ}{d_w}\right)_{pipe} / \left(\frac{EI}{L_b}\right)_{flange} = 1.4$$

From Table 5.1, we get: m=1

$(G_Z)_A = \frac{33918.1}{1\times47072.4} = 0.72$ (from Equation 2.56)

$(G_Z)_A = \infty$

From alignment chart shown in Figure D.5, results in

K_z=0.84

Determine the required unbraced length:

$$\phi_f M_{cr}$$

$$= (1.0)(1.45)\left(\frac{\pi}{L_b}\right)\sqrt{(29000)(1336)\,(11154)(24.6) + \frac{\pi^2(29000)^2(2246000)(1336)}{(0.84L_b)^2}}$$

$$\geq M_a$$

Solve: $L_b \leq 50.5\,ft > 36\,ft = L_r$ (OK)

In this case the effective unbraced length factor K_Z is not highly sensitive to L_b. Consequently, the K_Z value was not iterated to get new L_b values.

D.2.6 Brace Layout for Split Pipe-Stiffened Girders

Similarly, the cross-frames can be located according to the unbraced length for the split pipe stiffened girders. The number of lines of intermediate cross-frames for one span is:

$N_{brace} = (200' + 40' \times tan45° - 49.5' - 50.5')/36.5' + 1 = 4.8$, use 5

The resulting layout of the bracing system for the plate-stiffened girders is presented in Figure D.6.

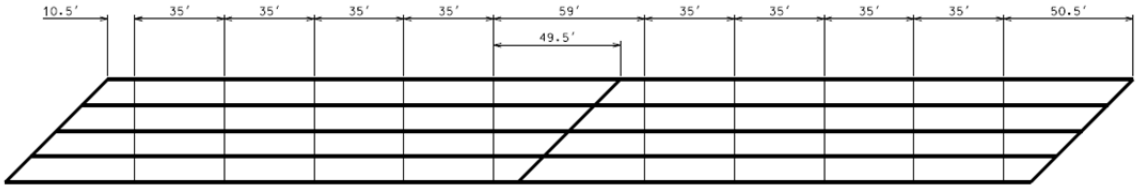

Figure D.6: Brace layout – girders with split pipe stiffeners

D.2.7 Eigenvalue Buckling Analysis

To verify the performance of the designed bridge, the validated Ansys bridge model was used to model the two proposed design options. Eigenvalue buckling analysis was performed to obtain the maximum buckling strength of the bridge girders. In addition to the two design options, a third analysis with conventional plate stiffeners and bent plate connections for end cross frames and with only ten bracing lines was performed to be compared with the pipe bridge with split pipe stiffeners. This analysis was done so that the two bracing details could be compared with a similar bracing layout. The details of the FEA modeling methods are discussed in the Chapter 4. A distributed load of 0.1 kips/in was applied at top of all girders as the reference load for buckling analysis. The results of the eigenvalue buckling analyses are presented in Figure D.7 through Figure D.9.

Figure D.7: Eigenvalue buckling analysis I – girders with conventional plate stiffeners

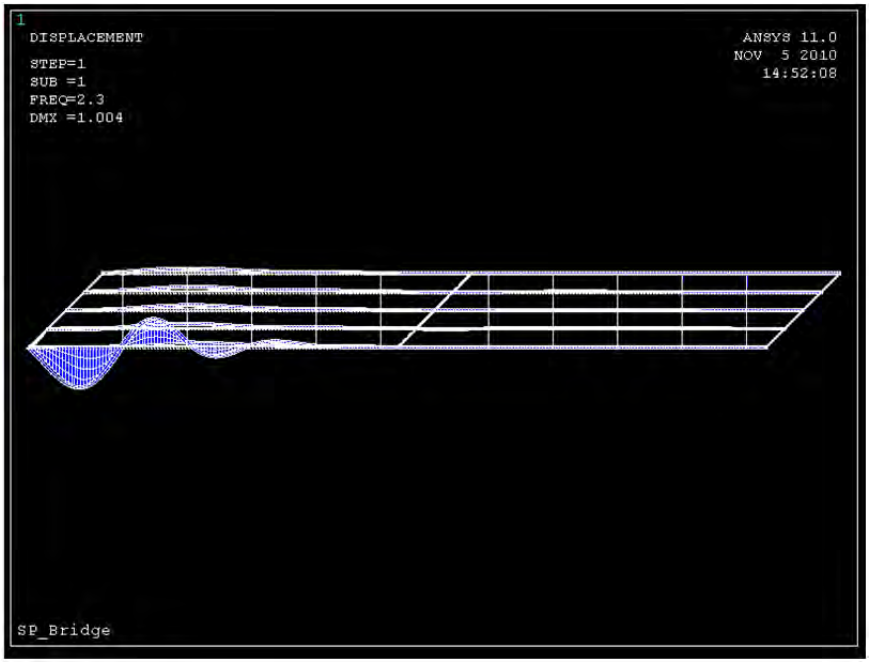

Figure D.8: Eigenvalue buckling analysis II –girders with split pipe stiffeners

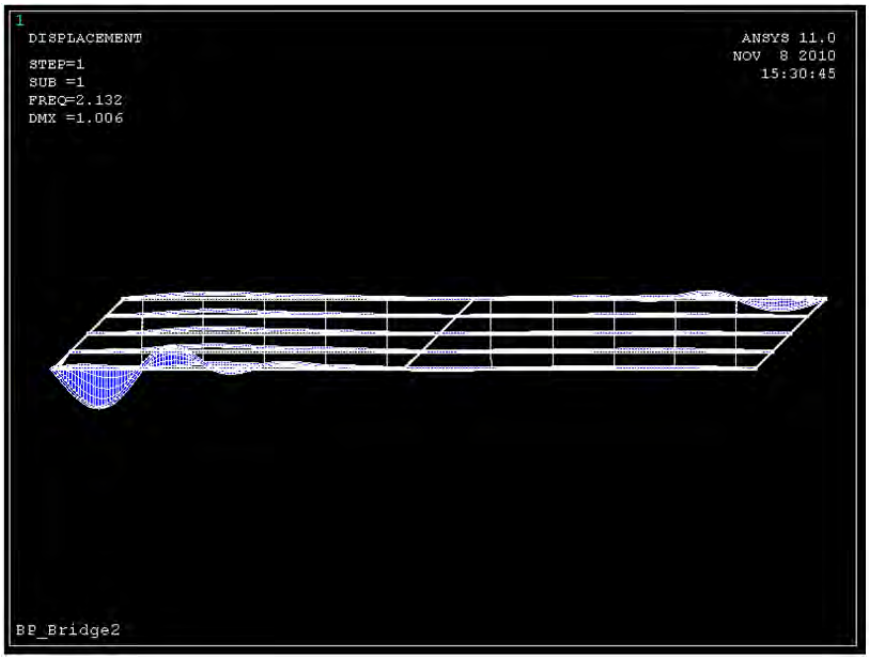

Figure D.9: Eigenvalue buckling analysis III – girders with conventional plate stiffeners and with 10 bracing lines

Based on the eigenvalue buckling analysis, the buckling strengths for the three cases are as follows:

Analysis I (plate stiffeners with 6 brace lines per span): *0.26 kip/in = 3.12 kip/ft*
Analysis II: (split pipe stiffeners with 5 brace lines per span): *0.23 kip/in = 2.76 kip/ft*
Analysis III: (plate stiffeners with 5 brace lines per span): *0.21 kip/in = 2.52 kip/ft*

As mentioned earlier, the maximum design service load is 2.61 kip/ft. So the girders with either conventional plate stiffeners and the girders with split pipe stiffeners are both stable during the deck casting. The girders with plate stiffeners showed a higher buckling strength because of the roundup of the number of bracing lines in the calculation gives shorter unbraced lengths than what is required. The comparison between Analysis II and Analysis III showed that if the same brace layout were to be used, the split pipe option will result in a safer bridge.

D.2.8 Conclusions

This example illustrated the steps using hand calculations for designing the bracing system layout for split pipe-stiffened girders. Compared with the conventional plate-stiffened girders, the use of the split pipe stiffeners allowed the first row of cross-frames to be moved farther away from the skewed supports. In this example, when plate-stiffened girders are used, the distance from the first row of cross-frames to the abutments is 7.5 feet and it is 2 feet to the interior pier. When the split pipe stiffeners are used, the distances are increased to 10.5 feet and 9.5 feet, respectively. Further, the use of the split pipe stiffeners allowed the total number of cross-frame in this bridge to be reduced from 48 to 40. And if the same layout is adopted, the use of split pipe stiffeners will result in a safer bridge compared to the bridge with conventional plate stiffeners and bent plate connections to the end cross frames. The split pipe stiffener will also be beneficial in increasing the torsional stiffness of the girders during lifting. This will increase safety during lifting, and will help minimize girder rotations during lifting, thereby facilitating making connections during air splicing.